

# **Miniature Wireless Deep-Brain Stimulator and EEG-Recording Device – Implications for the Treatment of Schizophrenia**

**Richard Charles Pinnell**

A thesis presented in fulfilment of the requirements for the degree of Doctor of  
Engineering

University of Strathclyde

Department of Biomedical Engineering


Strathclyde Institute of Pharmacy and Biomedical Sciences

2014

# Copyright Statement

This thesis is the result of the author's original research. It has been composed by the author and has not been previously submitted for examination which has led to the award of a degree.

The copyright of this thesis belongs to the author under the terms of the United Kingdom Copyright Acts as qualified by University of Strathclyde Regulation 3.50. Due acknowledgement must always be made of the use of any material contained in, or derived from, this thesis.

Signed:   
Date: 16/08/2014

# Acknowledgements

First and foremost, I would like to express my love and gratitude to my parents, for always telling me that I could succeed. I probably wouldn't be here otherwise, so thanks very much for that. Also thanks to my brothers for being the most supportive friends I could ask for, and also for keeping me sane during the write-up period. And cheers to my friends for making the last few years a genuine joy.

To my supervisors Judy and John, I would like to express deep gratitude for being patient, inspirational, and for providing me with the freedom to approach tasks my own way. You've been great mentors, and I couldn't have asked for better.

I would also like to extend a special thanks to Mark, Nadine and Neil, who were more than willing to give up their time to provide vital assistance, training and advice on various matters. Thanks also to the staff of the BPU for their hard work and support, which ultimately made this research project possible.

# Contents

<b>Abbreviations</b> .....	<b>xii</b>
<b>Abstract</b> .....	<b>xvii</b>
<b>1 - General Background</b> .....	<b>1</b>
1.1 Introduction .....	1
1.2 Aims and Objectives .....	2
1.2.1 Overview .....	2
1.2.2 Aims .....	3
1.3 Deep Brain Stimulation .....	4
1.3.1 DBS Mechanisms of Action .....	5
1.3.1.1 Functional Deactivation / Inhibition .....	5
1.3.1.2 Activation .....	7
1.3.2 Stimulation Parameters .....	9
1.3.2.1 Effect of Stimulation Frequency .....	10
1.3.2.2 The Need for Constant Current Stimulation .....	13
1.3.2.3 Effect of Stimulation Intensity and Pulse-Width .....	15
1.3.2.4 Monophasic vs. Biphasic Stimulation .....	18
1.3.3 Applications of DBS for Non-Motor Related Neuropsychiatric Disorders .....	19
1.3.3.1 Obsessive-Compulsive Disorder .....	20
1.3.3.2 Tourette's Syndrome .....	22
1.3.3.3 Treatment-Resistant Depression .....	24
1.3.3.4 Minimally Conscious States .....	25
1.3.3.5 Cluster Headaches .....	25
1.3.3.6 Schizophrenia .....	26
1.4 Working Memory .....	28

1.4.1	Medial Prefrontal Cortex .....	29
1.4.2	Hippocampus.....	30
1.4.3	Working Memory Relies on Connectivity of Hippocampus and Prefrontal Cortex.....	31
1.4.4	Neurophysiological Mechanisms of Working Memory .....	35
1.4.4.1	Theta Oscillations .....	36
1.4.4.2	Synchronisation of Brain Regions with Hippocampal Theta .....	36
1.4.4.3	Prefronto-Hippocampal Phase-Locking .....	38
1.4.4.4	Gamma Oscillations .....	40
1.4.4.5	Gamma Activity and Cross-Frequency Coupling.....	41
1.5	Schizophrenia .....	43
1.5.1	Working Memory Deficits in Schizophrenia .....	44
1.5.2	Medial Prefrontal Cortex in Schizophrenia.....	45
1.5.2.1	Functional Changes in PFC Activity.....	45
1.5.2.2	Reduced Somal Size and reduced Density of Dendritic Spines .....	48
1.5.2.3	Role of GABAergic Interneurons in Working Memory – and Evidence for Disruption .....	49
1.5.2.4	Reduction in Parvalbumin and Neuron Count .....	49
1.5.3	The Hippocampus in Schizophrenia.....	50
1.5.4	The Thalamus in Schizophrenia .....	51
1.5.4.1	Diminished Frontal Connectivity with the Mediodorsal Thalamic Nucleus... ..	52
1.5.5	EEG Changes in Schizophrenia .....	53
1.5.6	Candidate Brain Regions for DBS in Schizophrenia.....	55
1.5.6.1	Thalamic Reticular Nucleus (TRN).....	56
1.5.6.2	Mediodorsal Thalamic Nucleus (MD) .....	59
1.5.6.3	Anterior Thalamic Nucleus .....	64
1.5.6.4	Fimbria-Fornix (FF) .....	67
1.5.6.5	Summary of Brain Regions Selection.....	71
<b>2 - Wireless Device Technologies for Recording and Stimulation .....</b>		<b>74</b>
2.1	Introduction.....	74

2.2	Background.....	75
2.2.1	Need for Wireless Recording.....	76
2.2.2	Species under Study and System Size.....	77
2.2.3	Placement of System on Animal.....	78
2.2.4	Signal types.....	80
2.2.5	Standard Design Variations.....	81
2.2.5.1	Analogue/Digital System.....	81
2.2.5.2	Technology.....	82
2.2.5.3	System Control Centre.....	84
2.2.5.4	Channel Count.....	86
2.2.5.5	Input Stage.....	87
2.2.5.6	Analogue to Digital Converter (ADC).....	89
2.2.5.7	Wireless Telemetry.....	90
2.2.5.8	Transmission Range.....	92
2.2.5.9	Power Consumption.....	93
2.2.5.10	Inductive Powering.....	95
2.2.5.11	Low-Power Modes.....	96
2.2.5.12	Bi-directional Communication and Feedback.....	96
2.2.5.13	Deep-Brain-Stimulation.....	97
2.2.6	Additional Design Features.....	98
2.2.7	Summary.....	99
2.3	Aims and Rationale.....	101
2.3.1	Rationale.....	101
2.3.2	Aims.....	101
2.4	Methods.....	102
2.4.1	Systems Overview.....	102
2.4.2	Wireless EEG-DBS System and Receiver Summary.....	104
2.4.3	EEG-DBS System Design.....	105
2.4.3.1	MCU Programming.....	105
2.4.3.2	EEG Recording Circuitry.....	108
2.4.3.3	DBS Circuitry.....	110

2.4.3.4	Printed Circuit Board (PCB) Design.....	110
2.4.4	RCVR Design for EEG-DBS System .....	117
2.4.4.1	Main MCU and Buffer Programming.....	117
2.4.4.2	RS232 Transceiver .....	119
2.4.4.3	Additional Circuitry .....	119
2.4.4.4	Printed Circuit Board Design.....	119
2.4.5	Transceiver for EEG-DBS and RCVR Systems .....	124
2.4.6	Data Handling and Commands 1 .....	125
2.4.6.1	EEG-DBS to RCVR Information: LFP and Status Bytes .....	126
2.4.6.2	Commands for Controlling the Wireless System.....	127
2.4.6.3	RCVR to EEG-DBS Information: Commands.....	128
2.4.7	Wireless M-DBS System and Receiver Summary .....	130
2.4.8	M-DBS System Design.....	132
2.4.8.1	MCU-1 and MCU-2 Programming .....	132
2.4.8.2	DBS Circuitry .....	134
2.4.8.3	Printed Circuit Board Design.....	135
2.4.9	RCVR Design for M-DBS System .....	141
2.4.9.1	MCU-M and MCU-B Programming.....	141
2.4.10	Transceiver for M-DBS and RCVR Systems.....	142
2.4.11	Data Handling and Commands 2 .....	142
2.4.12	Assembly Techniques for Wireless Systems and Receiver .....	144
2.4.13	Modifications of the Wireless systems.....	145
2.4.14	Electrode Design.....	147
2.4.14.1	Local-Field Potential Electrodes .....	148
2.4.14.2	Deep-Brain Stimulation Electrodes .....	148
2.4.14.3	Attachment of the Guide Cannula.....	149
2.4.14.4	Electrode Testing.....	152
2.4.15	Headstage Design.....	152
2.4.16	Battery Connector.....	153
2.4.17	Basic System Tests .....	154
2.4.17.1	EEG-DBS Battery-Life Measurements.....	154

2.4.17.2	Basic Noise Test.....	157
2.4.17.3	ECG Measurements .....	160
2.4.17.4	DBS Pulses in Saline.....	160
2.5	Discussion .....	164
2.5.1	Alternative Design Choices / Future Work.....	170
<b>3 - Proof of Concept Experiment for the EEG-DBS System .....</b>		<b>173</b>
3.1	Introduction.....	173
3.2	Aims and Rationale.....	174
3.2.1	Rationale.....	174
3.2.2	Aims .....	174
3.3	Materials and Methods.....	176
3.3.1	Overview .....	176
3.3.2	Selection of Stimulus Parameters .....	177
3.3.3	Surgery .....	179
3.3.4	Recovery and Habituation .....	185
3.3.5	Arena Configuration.....	185
3.3.6	Analysis of Results .....	187
3.3.6.1	Power and Coherence Spectrograms .....	187
3.3.6.2	Power to Coherence/Velocity Scatterplots .....	187
3.4	Results.....	188
3.4.1	Raw LFP Recordings.....	188
3.4.2	Power Spectral Density in the mPFC and dCA1 Brain Regions.....	190
3.4.3	Theta-Coherence between mPFC and dCA1.....	194
3.4.4	Effect of Stimulation at High Currents upon Behaviour in the Open Field.....	196
3.4.5	Correlations Between dCA1 Theta, and Coherence/Velocity.....	198
3.5	Discussion .....	200
3.5.1	Implications for the Next Experiment.....	203
<b>4 - Investigation of DBS on Rodent Working Memory Performance.....</b>		<b>205</b>
4.1	Introduction.....	205
4.2	Background.....	206
4.2.1	T-Maze Task .....	206



4.3	Aims and Rationale.....	208
4.3.1	Rationale.....	208
4.3.2	Aims.....	209
4.4	Materials and Methods.....	210
4.4.1	Experimental Outline.....	210
4.4.2	Rat Groups and Experiment Organisation.....	210
4.4.3	T-Maze Task.....	212
4.4.4	Task Summary.....	213
4.4.4.1	Handling.....	214
4.4.4.2	Surgery.....	214
4.4.4.3	Recovery.....	215
4.4.4.4	T-Maze Sessions.....	215
4.4.4.4.1	Habituation.....	216
4.4.4.4.2	Acquisition of Task +/- DBS.....	216
4.4.4.4.3	Testing.....	216
4.4.5	Perfusion, Craniotomy and Tissue Staining.....	217
4.4.6	Brain Imaging and Electrode Coordinates.....	218
4.4.7	Equipment Setup.....	222
4.4.7.1	Placement of Equipment.....	222
4.4.7.2	Equipment Configuration.....	224
4.4.7.3	Video Tracking.....	224
4.4.7.4	LFP Recording and System Programming.....	225
4.4.8	Analysis of Results.....	228
4.4.8.1	Data Organisation.....	229
4.4.8.2	Artefact Removal.....	230
4.4.8.3	Power Spectral Density and Coherence.....	233
4.4.8.4	Spectrograms/Coherograms.....	234
4.4.8.5	Task-Phase PSD and Coherence Changes.....	236
4.5	Results.....	239
4.5.1	Rat Performance in the T-maze Task.....	239
4.5.2	PSD Changes in the mPFC.....	242

4.5.3	PSD Changes in dCA1 .....	246
4.5.4	Prefrontal-Hippocampal Coherence Changes.....	250
4.5.5	Summary of PSD and Coherence Changes .....	254
4.6	Discussion .....	255
4.6.1	Theta and Gamma Frequency PSD Changes .....	255
4.6.2	Coherence Changes .....	257
4.6.3	Effect of DBS on Behavioural Performance.....	258
4.6.4	Experimental Design .....	259

## **5 - Investigation of DBS in a Rodent Model Relevant to Schizophrenia .....265**

5.1	Introduction.....	265
5.2	Background.....	266
5.2.1	PCP to Model Aspects of Schizophrenia.....	266
5.2.2	PCP Administered to Rats in a T-Maze Task.....	268
5.3	Aims and Rationale.....	270
5.3.1	Rationale .....	270
5.3.2	Aims .....	270
5.4	Materials and Methods.....	272
5.4.1	Rat Groups and Experiment Overview.....	272
5.4.2	Analysis of Results .....	273
5.4.2.1	PSD Changes at the T-maze Choice Point.....	273
5.4.2.2	Hippocampal Theta-Frequency Changes.....	274
5.5	Results.....	276
5.5.1	Rat Performance in the T-Maze Task.....	276
5.5.1.1	Comparison of Behavioural Performance between the Saline and PCP-Treated Groups .....	277
5.5.2	Gamma-Power Increases in mPFC Following PCP Injection .....	278
5.5.3	Gamma-Power Increases in dCA1 Following PCP Injection.....	283
5.5.4	Summary of PSD Changes .....	286
5.5.5	Prefrontal-Hippocampal Coherence Reductions in PCP-Treated Rats .....	287
5.5.6	Cortical Gamma Hyper-Synchrony.....	291
5.5.7	Summary of Coherence Changes.....	294
5.5.8	Comparison of LFP findings between the Drug- and Saline-Treated Groups of Rats .....	295

5.5.8.1	Comparison mPFC PSD Changes in the T-Maze .....	295
5.5.8.2	Comparison of dCA1 PSD Changes in the T-Maze .....	297
5.5.8.3	Comparison of mPFC-dCA1 Coherence Changes in the Holding Pen....	299
5.5.9	Stimulation–Induced Theta-Power Increases.....	301
5.5.9.1	Habituation T-maze Central Arm PSD Changes.....	301
5.5.9.2	PSD Changes at the T-Maze Choice-Point during the Drug/Saline Test Days – Differences between T-Maze Run Types .....	303
5.5.9.3	Washout Test Day T-maze Central Arm PSD Changes.....	306
5.5.9.4	Summary of PSD Changes at the T-maze Choice Point.....	309
5.5.10	Peak Hippocampal Theta-Frequency Changes during Different Phases of the Behavioural Task.....	310
5.6	Discussion .....	316
5.6.1	Gamma Frequency PSD Increases at the T-Maze Choice-Point, and with Acute PCP Treatment.....	316
5.6.2	Coherence Changes in the T-Maze Task.....	321
5.6.3	Theta-Frequency PSD Observations during Drug and Washout Test Days ....	326
5.6.4	Effect of Deep-Brain Stimulation .....	329
5.6.5	Effect of PCP on Behavioural Performance .....	334
5.6.6	Hippocampal Theta-Frequency Changes .....	335
5.6.7	Summary of Results .....	337
<b>6</b>	<b>Conclusions .....</b>	<b>341</b>
	<b>References.....</b>	<b>346</b>
	<b>Suppliers .....</b>	<b>387</b>
	<b>Appendix.....</b>	<b>390</b>

# Abbreviations

AC	anterior commissure
ADC	analogue to digital converter
AMPA	$\alpha$ -Amino-3-hydroxy-5-methyl-4-isoxazolepropionic acid
ASIC	application-specific integrated circuit
ATN	anterior thalamic nucleus
BASE-A	T-maze task pre-injection period (15 minutes)
BASE-B	T-maze task post-injection period (5 minutes)
CA1	Cornu Ammonis area 1 (hippocampus)
CMOS	complementary metal-oxide semiconductor
CM-Pf	centromedian-parafascicular complex
CMRR	common mode rejection ratio
CPU	central processing unit
CRC	cyclic redundancy check
DBS	deep-brain stimulation
DC	direct current
dCA1	dorsal Cornu Ammonis area 1 (hippocampus)
DG	dentate gyrus
DIP	dual in-line package

dIPFC	dorsolateral prefrontal cortex
DNMS	delayed non-match to sample (task)
DPDT	double pole, double throw (switch)
DTI	diffusion tensor imaging
ECG	electrocardiogram
ECoG	electrocorticogram
EEG	electroencephalogram
EEG-DBS	wireless multichannel EEG recording and DBS device
EMG	electromyogram
ERP	event-related potential
FA	fractional anisotropy
FF	fimbria-fornix
FM	frequency-modulation
fMRI	functional magnetic resonance imaging
FPGA	field-programmable gate array
FSK	frequency-shift keying
GABA	$\gamma$ -Aminobutyric acid
GFSK	Gaussian frequency-shift keying
GP	globus pallidus
GPI	internal globus pallidus
HDRS	Hamilton depression rating scale
HFS	high-frequency stimulation

IC	integrated circuit
IR	infra-red
ITN	intralaminar thalamic nuclei
JTAG	joint test action group
LED	light-emitting diode
LFP	local-field potential
LFS	low-frequency stimulation
LTD	long term depression
LTP	long term potentiation
MCS	minimally conscious states
MCU	microcontroller
MCU-1	M-DBS system master MCU
MCU-2	M-DBS system slave MCU
MCU-B	RCVR system buffer MCU
MCU-M	RCVR system main MCU
MD	mediodorsal thalamic nucleus
M-DBS	multimode DBS device
MEMS	micro-electro-mechanical system
mPFC	medial prefrontal cortex
MRI	magnetic resonance imaging
MSK	minimum-shift keying
NMDA	<i>N</i> -Methyl- <i>D</i> -aspartate

OCD	obsessive compulsive disorder
OOK	on-off keying
PC	posterior commissure
PCB	printed circuit board
PCP	phencyclidine
PEN-C	T-maze task intra-trial delay (30 seconds)
PEN-F	T-maze task inter-trial delay (45 seconds)
PET	positron emission tomography
PFC	prefrontal cortex
PPI	prepulse inhibition
PPN	pedunculopontine nucleus
PSD	power spectral density
RCVR	receiver module for the EEG-DBS or M-DBS systems
RF	radio-frequency
RMS	root mean square
SMD	surface mount device
SNr	substantia nigra pars reticulate
SOiC	system-on-chip
SPDT	single pole, double throw (switch)
SPI	serial peripheral interface bus
STN	subthalamic nucleus
TM	T-maze task central arm recording duration (1 second)

TRN	thalamic reticular nucleus
TRX	transceiver
TS	Tourette's syndrome
UART	universal asynchronous receiver/transmitter
USB	universal serial bus
VIM	nucleus ventralis intermedius
WCS	Wisconsin card sort test
WOR	wake-on-radio
Y-BOCS	Yale-Brown obsessive-compulsive scale



# Abstract

Deep-brain stimulation (DBS) is increasingly being pursued as a treatment option for a range of neuropsychiatric disorders. When assessing its potential for the treatment of schizophrenia, related animal studies are often limited by the range of measurements that the equipment is capable of. In animals, the combination of DBS with various recording modalities such as local-field potential (LFP) recording has traditionally required complex and time-consuming laboratory setups. Furthermore, the elucidation of neural activity underpinning rodent behaviour has traditionally been hampered by the use of tethered systems and human involvement. Taken together, novel tools and techniques are required to drive forward DBS research in this area.

In this study, two miniature wireless devices were developed for electrophysiological recording and stimulation in freely-moving rodents. The performance of one of these devices was verified in an open-field chamber, in which high-frequency (100Hz) stimulation was delivered bilaterally into the anterior thalamic nucleus at a range of current intensities (20 $\mu$ A, 100 $\mu$ A) and pulse-widths (25 $\mu$ s, 100 $\mu$ s, 200 $\mu$ s). LFP recordings were made bilaterally in the fronto-hippocampal brain regions. Not only was the recording/stimulation device able to successfully correlate electrophysiological recording and stimulation with animal behaviour (via video tracking), but a transient velocity increase of the animals was observed following stimulation at the higher current setting (100 $\mu$ A).

The effect of fimbria-fornix (FF) DBS (at 130Hz, 30 $\mu$ A, 90 $\mu$ s) was then studied in a rodent disease model relevant to schizophrenia, using a spatial working memory paradigm inside a T-maze. Fronto-hippocampal LFP was recorded bilaterally, and was subsequently correlated to the rat's position using synchronised video-tracking. Notably, rat gamma-frequency LFP was found to be increased in all brain regions following an acute administration of the NMDA receptor antagonist phencyclidine

(PCP; 3 mg.kg<sup>-1</sup> i.p.), which had persisted throughout the duration of the recording session. Furthermore, rat hippocampal theta-frequency activity was transiently elevated following a 30-second period of FF-DBS, which was carried out during the intra-trial delay period of the task. Finally, the use of FF-DBS throughout the task training sessions highlighted a (non-significant) tendency for rats to reach criterion performance faster than their sham-stimulated counterparts, highlighting the FF as a potential DBS target to consider with regards to disorders that affect learning and memory.

The data presented in this study highlights a) the successful design and application of novel device technologies for enhancing the range of measurements in animal-related DBS studies, and b) the effects of FF-DBS in a rodent model relevant to schizophrenia, and its implications in the treatment of this disorder.

# Chapter 1

## General Background

### 1.1 Introduction

Deep-brain stimulation, working memory and schizophrenia are three major themes addressed in this project. This chapter provides a concise review of the literature surrounding these topics, where relevant to this study. The deep-brain stimulation literature looks at the proposed mechanisms by which it achieves a therapeutic effect, as well as the effects observed when modifying the stimulus parameters. Also an overview of DBS in non-motor related neuropsychiatric disorders including schizophrenia is presented. A discussion on working memory focuses on the coordination between the prefrontal cortex and hippocampus, and how this has been observed to change during working memory. Particular attention is given to some of the observed electroencephalogram (EEG) changes that take place between these brain regions. Finally a discussion on schizophrenia describes some of the pathological and functional changes that patients undergo, which can serve to disrupt working memory. In addition a number of brain regions are proposed as potential targets for DBS, with regards to ameliorating working memory deficits in schizophrenia.

## 1.2 Aims and Objectives

### 1.2.1 Overview

One of the core neural deficits in schizophrenia is a reduced ability to utilise working memory in cognitive tasks. A dysfunction in the signalling properties of the GABAergic interneurons in frontal and temporal structures are believed to play a key role in this, as revealed by a plethora of pathological and functional studies in both human and nonhuman species. Specifically, these problems result in a diminished coordination and synchronisation between the hippocampus and the prefrontal cortex in schizophrenia – two structures known to be crucial for working memory function.

Deep-brain stimulation (DBS) is a unique form of treatment which can provide neuromodulatory effects on neuronal populations at a specific target in the brain. It has so far proven itself to be an effective form of treatment for movement-related disorders, and investigation into non-motor related application areas, particularly schizophrenia, is relatively new. Nonetheless in spite of an incomplete understanding of the mechanisms by which it ameliorates symptoms, it remains an intriguing tool for exploratory research in disorders for which pharmacological treatment options has thus far proven ineffective.

As such, DBS remains a potentially powerful yet incompletely understood tool for exploring novel therapies in a range of central nervous system disorders. Working memory forms one of the core cognitive deficits in schizophrenia; which is indeed well documented in the literature with regards to the behavioural, pathological and functional observations made in both humans, and in animal models relevant to schizophrenia. Local-field potential recordings provide a valuable insight into the functional workings of neural networks, and when combined with DBS, can offer a unique insight into its effects. Thus, the future of DBS research can benefit from novel experimental approaches that combine these two modalities. A major obstacle to overcome in this regard is based on the technological limitations in the currently available equipment, which when overcome, can expand the range of experiments and research avenues that can be pursued.

### 1.2.2 Aims

The aims of this project are twofold:

- Investigation of DBS in an animal model relevant to schizophrenia; specifically in rats undergoing a working memory task, with behavioural observations and local-field potential recordings as experimental outcomes,
- Development of the technology to allow experiments of this type to take place.

As such this project details the design and development of novel technological solutions for carrying out wireless LFP recording and DBS in freely-moving rodents. Subsequently, this technology is tested in freely-moving rodents; both for the purposes of verifying the capabilities of the technology as well as to study the effects of DBS in a rodent model relevant to schizophrenia.

## 1.3 Deep Brain Stimulation

Deep brain stimulation (DBS) is the delivery of pulsed electrical current into brain regions of patients with neurological disorders, with the goal of ameliorating their symptoms. Needle-like electrodes are implanted into brain regions through which electrical pulses are delivered, which are generated from an implantable pulse-generator similar to a cardiac pacemaker. This idea evolved from traditional neurosurgeries whereby stimulation was carried out through the lesion probes prior to lesioning, as part of the targeting procedure.

The modern form of DBS emerged in the late 1980's through a pioneering study which combined lesion surgery with DBS for the treatment of Parkinson's disease (Benabid et al., 1987). In this case a lesion of the thalamic nucleus ventralis intermedius (VIM) in one hemisphere was combined with high-frequency DBS of the same structure in the opposite hemisphere, making it the first study utilising chronic DBS in a patient with a portable stimulator. The initial observations were promising, showing the same marked reduction in tremors associated with a lesion, but through a novel treatment that is reversible, adjustable, and which doesn't rely on the destruction of brain regions.

Nowadays DBS has virtually replaced lesion procedures, and is evolving into an accepted treatment for various movement-related disorders such as Parkinson's disease (Kalia et al., 2013), dystonia (Yianni et al., 2003), essential tremor (Koller et al., 1997) and cerebellar outflow tremor (Montgomery et al., 1999). Furthermore, its application has since been studied in a plethora of non-motor related neural disorders, with clinical trials having taken place in neuropsychiatric disorders such as Obsessive Compulsive Disorder (OCD) and treatment-resistant depression (e.g. Nuttin et al., 1999, Aouizerate et al., 2004); two disorders for which functional lesion procedures also previously existed. With the vast majority of DBS research unsurprisingly centred on the basal ganglia, researchers have gained a lot of ground in understanding the mechanisms by which DBS reduces symptoms. However a complete understanding how DBS works is far from complete, owing perhaps to the

complexity of the environment in which DBS acts, and the limited understanding of the underlying neural systems involved.

Research has been since carried out on its application in a wide range of neurological disorders (see Gubellini et al., 2009, Larson, 2008). With its initial application in movement-related disorders, the vast majority of DBS research is centred around structures in the basal ganglia, from which a great deal of information on its mechanisms of action have been explored. This section of the background focuses on the mechanisms of action of DBS from the point of view of basal-ganglia stimulation studies, before considering effects of altering the various DBS parameters. Finally a brief overview of DBS in non-motor related neuropsychiatric disorders including schizophrenia is presented (see 1.3.3: Applications of DBS for Non-Motor Related Neuropsychiatric Disorders).

### **1.3.1 DBS Mechanisms of Action**

Despite the successes of DBS in motor-related neurological disorders, its precise mechanism of action remains elusive and is widely debated in the literature (Breit et al., 2004, Deniau et al., 2010, McIntyre and Hahn, 2010, Garcia et al., 2005a, Montgomery and Gale, 2008, Gubellini et al., 2009). The environment in which the electrode is inserted is a highly complex, anisotropic and incompletely understood medium which varies based on the brain region, and the duration of electrode implantation. With variation in the electrode size and type, stimulating frequency, intensity, pulse-width, pulse-mode, shape and duration, all capable of modifying the effectiveness of the treatment, the challenge exists to find a mechanism(s) through which DBS exerts its actions.

#### **1.3.1.1 Functional Deactivation / Inhibition**

A lot of the earlier work on DBS led researchers to believe that its main effects were similar to a functional lesion, in which the activity of the target structure would be effectively inhibited. The clinical similarities between DBS and ablation of basal

structures were striking, and backed up with strong experimental evidence pointing to an inhibition of the target structure (Boraud et al., 1996, Wu et al., 2001, Dostrovsky et al., 2000, Beurrier et al., 2001). This became collectively known as the “inhibition hypothesis”, and a number of individual hypotheses were put forward to explain these effects.

One of these hypotheses is that stimulation of the neuronal membranes of the target results in a “depolarisation block”, whereby the membranes of the stimulated cells become so depolarised that their action potentials can no longer be evoked; due to the inactivation of the voltage-gated sodium current (Benazzouz et al., 1995, Bikson et al., 2001, Beurrier et al., 2001). This depolarisation is presumed to be a result of increased extracellular potassium following high-frequency stimulation (Bikson et al., 2001, Benazzouz et al., 1995). This idea has gained support from *in vivo* studies using rat subthalamic nucleus (STN) slices, showing that the L- and T-type calcium currents are also blocked in addition to sodium currents (Beurrier et al., 2001). This hypothesis however has been rejected by a number of researchers on the basis that in many studies the spike firing rates and amplitudes of stimulated neurons were reduced but not completely blocked (Dostrovsky and Lozano, 2002, Tai et al., 2003, Filali et al., 2004).

Other researchers proposed that the inhibitory effect of DBS could be caused by activation of GABAergic presynaptic terminals of the pyramidal neurons, resulting in inhibition of action potential firing (Dostrovsky et al., 2000). This is plausible considering the abundance of inhibitory pre-synaptic terminals in the STN and the internal globus pallidus (GPI; Lee et al., 2004). The GABA inhibition hypothesis has gained support from Pahapill et al., (1999), who were able to show that chemically-induced inhibition of the thalamus by GABA receptor agonist was shown to stop tremors as equally well as DBS.

Another popular hypothesis looked at the effects of neuronal “jamming” in the network, whereby erroneous or malfunctioning signals are reset through the use of high-frequency stimulation, which acts as a blank noise signal to ‘jam’ the abnormal signals (Benabid et al., 2002, Garcia et al., 2005a). In this case the ‘blank noise’ signal



was suggested to reduce the ability of downstream neurons in the brain circuit to 'lock-on' to an otherwise erroneous signal, effectively removing its influence in a malfunctioning brain loop (Benabid et al., 2002). This idea was derived from the assumption that thalamotomy removed the brain region causing the malfunctioning signal and hence the main cause of tremors, and stimulation overrides the malfunctioning structure with a signal of its own which is propagated through the basal ganglia. However it has been noted that this effect doesn't hold for all movement disorders, such as Parkinson's disease without tremors (Benabid et al., 2002).

### **1.3.1.2 Activation**

As already mentioned, the complexities involved in electrical stimulation of a target structure are varied and incompletely understood, and many of the attempts at elucidating its mechanisms of action rely on observing common effects and consistent patterns. When one approaches this problem from an electrochemical perspective, it's easy to understand that when passing an electrical pulse through a bipolar electrode immersed into the brain, the resultant electrical field will affect everything inside it to some degree, whether it's the presynaptic terminals, axons, somata, dendrites, extracellular fluid and the membranes of the stimulated neurons. Medium with higher conductivities such as large myelinated axons will become more influenced by the electrical field (Ranck, 1975, Nowak and Bullier, 1998), and so it would be expected to contribute significantly to the overall effect that DBS has. Axons in this case have higher conductivities owing to their basic ability to effectively propagate action potentials. The excitation of efferent axons casts doubt on the inhibition hypothesis, and when one considers that the axons under stimulation may project to distal brain regions, it becomes clear that DBS has effects extending beyond a local inhibition of cells.

Given the susceptibility of efferent projections to DBS, a number of studies have looked at the effects DBS has on efferent structures to the stimulation site. By stimulating neurons and recording the responses at a number of distal projection

sites, researchers have shown responses in distal neurons that are time-locked to the stimulation pulses in sites such as the globus pallidus, (GP; Benazzouz et al., 1995, Windels et al., 2003, Windels et al., 2000, Hashimoto et al., 2003a) and substantia nigra pars reticulata (SNr; Benazzouz et al., 1995, Windels et al., 2000, Windels et al., 2003, Maurice et al., 2003, Tai et al., 2003). Interestingly regarding the latter case, earlier reports indicated an inhibition in the SNr, which was hypothesised to occur through an inactivation of the STN-SNr glutamatergic pathways (Benazzouz and Hallett, 2000), and thus giving further strength to the inhibition hypothesis. Upon closer inspection Maurice and colleagues (2003) demonstrated that whilst 79% of SNr cells are inhibited, 21% of them were activated, pointing to glutamatergic intervention. This has been backed up with intercerebral microdialysis studies which revealed an increased glutamate levels in the SNr and GPi (Windels et al., 2003, Windels et al., 2000) following STN stimulation, along with increased GABA in the SNr. A number of reasons were put forward to explain the increased inhibition in the SNr following STN stimulation, such as GABAergic activation of the SNr through the pallido-nigral (Maurice et al., 2003) or striatal-nigral (Smith and Grace, 1992) fibres that are reported to run in close proximity to the STN. Or perhaps the variation in conduction velocities between fibres of relevant connected nuclei (Maurice et al., 2003). For example, axons passing through the STN are thicker than that originating from subthalamo-nigral neurons, which allow them to be more easily activated (Ranck, 1975). Either way this particular case serves to highlight the complexities involved in deducing the effect of stimulation on efferent nuclei, as it seems to depend highly on the architecture of the brain region under stimulation and the positions and orientation of interconnected fibres.

By combining some of the ideas put forth in the inhibition hypothesis, with the realisation that stimulation of efferent axons generates effects in connected structures, a more recent hypothesis combines a local inhibition with a more widespread pattern of activation and inhibition (Garcia et al., 2005a, McIntyre et al., 2004b, Birdno and Grill, 2008). Thus stimulation could have a dual effect of suppressing the soma through either a depolarisation block and/or activation of GABAergic inhibitory inputs (as previously discussed), as well as activation of the

axons projecting from the stimulation site (figure 1.1). In this case inactivation of the soma would not stop action potentials being propagated through the more easily excitable axon through direct stimulation of the axon hillock. In a sense the ‘processing state’ of the neuron produced by the integration of dendritic signals in the soma would become irrelevant (McIntyre et al., 2004b), since a new pattern of activity is being imposed directly on the stimulated neuron’s outputs (Garcia et al., 2005a), thus decoupling the activity in the axon and the cell body. Interestingly this decoupling effect has been predicted through finite-element models (McIntyre et al., 2004a), which also shown a complex pattern of activation and inhibition of neighbouring cells around the stimulating electrode.

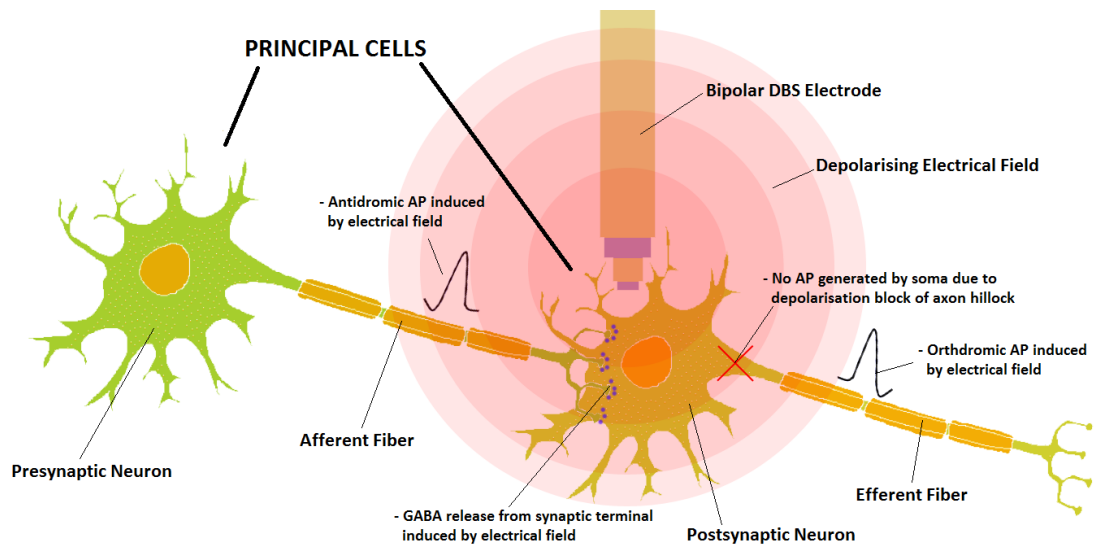


Figure 1.1 – An illustration of some of the effects believed to occur through DBS, on pre- and post-synaptic principal cells. The application of a DBS pulse results in a depolarising electrical field, which affects everything inside it. GABA release is stimulated from the post-synaptic terminals, and a depolarisation block prevents the soma from generating an AP. However the depolarising electrical field can cause action potentials to generate at the hillock, thereby overriding the local processing state of the neuron, and imposing a new DBS-driven network activity. Picture adapted from <http://webspace.ship.edu/cgboer/theneuron.html>.

### 1.3.2 Stimulation Parameters

DBS has a large number of adjustable parameters, all of which will have an effect on the outcome of stimulation. When considering a DBS study, one will have to consider the stimulating frequency, the pulse width, intensity, pulse mode and shape,

the electrode types and electrode materials, in addition to the selection of the brain region to be stimulated. One of the major benefits of DBS is that some of these parameters can be adjusted after the surgery has taken place. This of course depends on the system being used and how versatile it is. In human patients clinicians can typically adjust the pulse frequency, width, intensity, type and the active electrode contacts used (given that most modern systems used in humans utilise systems with quadripolar tetrodes; e.g. Soletra model 7426), through wireless telemetry. Some of the other parameters such as the electrode type and electrode material must be decided beforehand alongside the location of stimulation. This section provides an outline of the different effects gained by varying these parameters, some of which are better understood than others. Figure 1.2 provides a diagram showing representations of the most commonly adjusted DBS parameters.

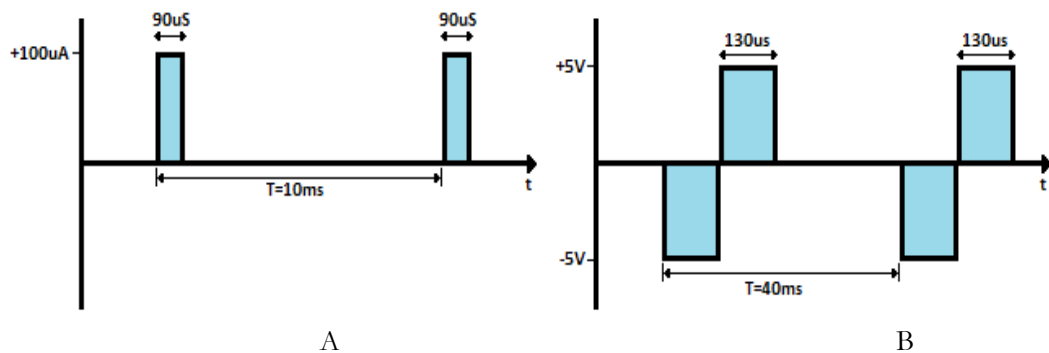


Figure 1.2 – Two examples of adjustments made to the frequency, intensity, pulse-width and pulse type of DBS pulses. (A) depicts a 100Hz, 100µA constant-current monophasic pulse-train with a pulse-width of 90µs, whereas (B) depicts a 25Hz, +/- 5V constant-voltage biphasic pulse-train with a pulse-width of 260µs.

### 1.3.2.1 Effect of Stimulation Frequency

Regarding the frequency at which stimulation pulses are delivered into the brain, there's no strict definition for the terms high-frequency stimulation (HFS) and low-frequency stimulation (LFS); two terms which see widespread use in the literature. Roughly speaking HFS refer to frequencies above 80Hz, whereas LFS refer to frequencies below 20Hz. Frequency values in-between these don't see much clinical use, and experiments over the previous two decades have shown profound

differences between HFS and LFS. Interestingly one of the most common frequencies in use for Parkinson's disease is 130Hz, a value which was used in the first modern DBS trial simply because equipment limitations prevented the researchers from reaching their target of 200Hz (Benabid et al., 1987). The exact role that stimulation frequency has in DBS is not completely understood, and many studies have a tendency to utilise multiple stimulation settings prior to selecting the most effective one. These settings often follow that which has shown success in related studies, with further reasoning behind their selection remaining vague. A reason behind this is an on-going and constantly evolving theory on how stimulation frequency changes affect a response. Notably in all procedures involving implantation of DBS electrodes into human patients, the stimulation parameters including frequency, pulse-width, duration, electrodes and polarity are often adjusted on an individual basis, for maximum clinical effect.

It has long been observed in Parkinson's disease that LFS (e.g. 5-10Hz) worsens symptoms, whereas HFS (e.g. >100Hz) improves symptoms (Moro et al., 2002, Rizzone et al., 2001). Furthermore Wu et al., (2001) found through variation of DBS frequency in patients that stimulation in the globus pallidus showed no effect on dyskinesias below 80Hz. LFS has proven to be clinically effective also, for example in the pedunculopontine nucleus (PPN) for movement disorders (Stefani et al., 2007). Where the STN is concerned, many researchers believe that LFS causes excitation, whilst HFS causes inhibition. Both *in vivo* (Benazzouz et al., 2000, Tai et al., 2003) and *in vitro* (Beurrier et al., 2001, Magarinos-Ascone et al., 2002) studies have demonstrated a transient silencing of the STN following high-frequency stimulation. Furthermore in both experimental types this effect was seen to depend highly on the frequency of stimulation (Tai et al., 2003, Beurrier et al., 2001), with higher stimulating frequencies producing more inhibition. In particular these findings mirrored that seen clinically, in which case frequencies at or above 130Hz were seen to largely inhibit or block STN activity completely, as opposed to LFS which had little effect. Interestingly a later study observed the effects of stimulation of STN slices derived from an acute rat model of Parkinson's disease (Garcia et al., 2005b, Garcia et al., 2003). In this case whilst LFS at 10Hz shown little change in

STN neuron activity, HFS between 50-80Hz resulted in a replacement of the spontaneous activity with a stimulation-driven activity, at the frequency of stimulation. Whilst data from these *in vitro* studies provide a useful insight into the mechanisms of DBS frequency changes, the parameters used are not representative of that used in anaesthetised rats (Tai et al., 2003) or human patients (Welter et al., 2004). Nonetheless the proposed mechanisms behind the silencing of STN neurons with HFS can be explained by the temporal summation of individual stimulation pulses. In this case whilst an individual pulse has been seen to reset the probability at which a neuron generates an action potential to zero, a train of pulses would in theory permanently inactivate the soma (Meissner et al., 2005).

The periodic nature of pulses is important, as a recent study found when introducing randomness into the inter-pulse timing of DBS pulses for patients with tremor (Birdno et al., 2007, Birdno et al., 2008). In this case they found that introducing irregular pulse periods between HFS pulses worsened symptoms, thus highlighting the importance of a periodic signal. An interesting recent hypothesis regarding the effectiveness of HFS revolves around the response time of neurons following an individual stimulation pulse (in a train of pulses delivered at high-frequency). In this case Montgomery and Gale (2008) explains that when pulses are delivered at 130Hz (giving an inter-pulse interval less than 8ms), there is insufficient time for the inhibited neuron to return to abnormal activity. Another recent hypothesis by the same researchers looked at resonance effects in the network, showing that the delivery of a pulse (in a high-frequency pulse train) coincided with neural activity resulting from the previous pulse, resulting in a resonance effect. Interestingly they note in particular that the average intrinsic oscillation frequency of the networks implicated in motor-related disorders is around 130Hz (Gale, 2004). Should this resonance hypothesis hold true, at least in some shape or form, it may go a long way in helping to deduce the most appropriate frequencies to use in a given neural disorder.

### 1.3.2.2 The Need for Constant Current Stimulation

Pulses delivered through stimulation devices are generated either using a “constant current” or a “constant voltage”. The majority of devices available clinically utilise a constant voltage source (Cheung and Tagliati, 2010) on the basis of previous success, but that is not to say constant current mode is lacking in any way (e.g. Okun et al., 2012). In fact, the benefits offered by a constant current mode include a stabilisation of DBS intensity parameters, resulting in a finer control over the generated electrical field. Explaining the differences between these two modes require a basic introduction to Ohm’s Law, as given by equation (1.1).

$$V = I \times R \quad \text{equation (1.1)}$$

Where  $V$  = Voltage

$I$  = Current

$R$  = Resistance

In this simple equation the voltage of the electrical field is equal to the current flow multiplied by the resistance of the medium. In this case the resistance is determined by the medium in-between the electrodes, i.e. the brain. At all instances, the voltage is directly proportional to the current flow, hence both stimulation modes essentially do the same job in that they provide an electrical field for which charged ions may flow. At all times for both modes, increasing  $V$  increases  $I$ , and vice-versa. The differences between the two become apparent when one considers that in the brain the resistance property  $R$  is not a straight-forward constant, but a complex function of (at least) time and voltage, given as an impedance  $Z(v,t)$ . This impedance is made up of many components, including the capacitance of the electrode, the charge-transfer resistance, electrolyte impedance, and a myriad of known and unknown effects based on the brain medium. Thus the ‘resistance’ in equation (1.1) is no longer a static variable but fluctuates under a number of conditions with time. As such for a constant-voltage device with the voltage held constant, the current flow varies. Similarly if the current were held constant, the voltage would vary to maintain a constant flow of charged particles (figure 1.3). Keeping the current constant as

opposed to voltage is important, since the desired clinical effect of DBS depends on a stable electric field spread over the brain regions of interest, which can only be achieved with a constant current flow over these regions. Should the current otherwise fluctuate because of say, transient electrochemical interactions at the electrodes, then the tissue in-between the electrode contacts would see an electrical field that varies with the current flow, making an otherwise constant-voltage parameter a much more complicated affair with regards to its predicted effects. These fluctuations can ultimately lead to unpredictability in clinical responses and side-effects (Cheung and Tagliati, 2010).

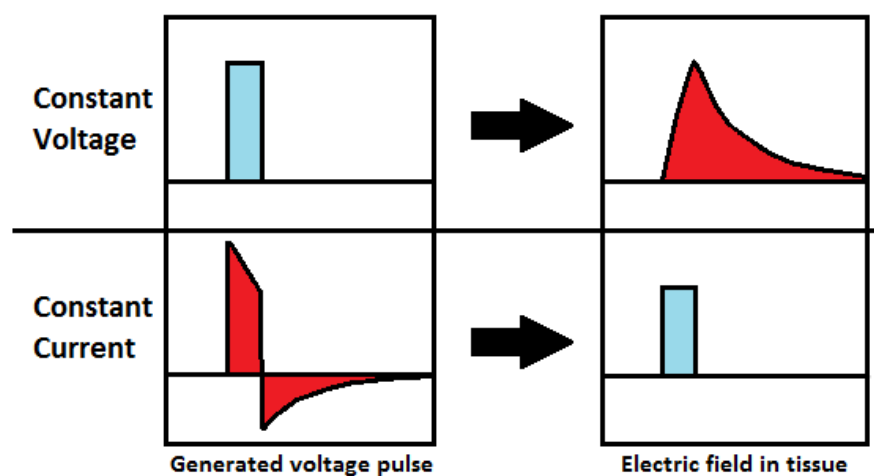


Figure 1.3 – The generated electric field in tissue (right panel) is directly proportional to the current flow, hence constant-current stimulation (bottom of figure) can directly specify the electrical field shape, by dynamically modulating the electrode voltage. With a constant-voltage device (top of figure) the user specifies the electrode voltage directly, resulting in a current field shape that is dependent on a number of known and unknown variables. Figure adapted from Gimsa et al., (2005).

The question to ask is what kind of brain impedance changes occur and how do they relate functionally to what is happening in the stimulated tissue? It is well accepted that the majority of changes relate to the tissue-electrode interface itself, which is subject to mechanical movement, morphology changes, and electrochemical changes on the electrode itself (e.g. through electrolysis; Merrill et al., 2005). Impedance increases following implantation have been reported (Lempka et al., 2010, Merrill et al., 2005), which have been shown to decrease upon application of stimulation in a



time-dependent manner (Lempka et al., 2010). The increases following implantation makes sense considering the well-known morphological changes that occur around the electrode, such as the formation of microglial cells (Griffith and Humphrey, 2006), which have a lower conductivity than that of the surrounding extracellular fluid. The benefits and drawbacks of microglial cell formation in this case have been debated based on its ability to repair injured tissue following electrode implantation (Trendelenburg and Dirnagl, 2005). These are some of the changes that occur over the period of hours or days. Given that the brain impedance is a function of the stimulus voltage itself, the impedance also decreases upon application of a constant-voltage pulse. The result of this is that the region of interest sees an electric field which progressively increases in strength as long as the pulse is in the 'on' state. Conversely with constant-current pulses, the region of interest sees a uniform electrical field throughout the duration of the pulse.

Ultimately, a constant-current stimulation source bypasses most if not all of the problems associated with current intensity fluctuations arising due to physiological changes in the tissue surrounding the electrode, resulting in a reduced need to a) reprogram the systems with time, and b) alter the system settings on a patient-by-patient basis.

### **1.3.2.3 Effect of Stimulation Intensity and Pulse-Width**

The stimulation intensity refers to the amplitude/magnitude of either the voltage or the current that is used in a particular study, and in the literature is seen to vary massively (for a comprehensive review see Gubellini et al., 2009). Different effects between high and low current have been observed, e.g. Maurice et al., (2003) observed inhibition in the SNR following low-intensity stimulation (4V) of the STN, which reversed at higher intensities (8V). On the other hand Hamani et al., (2010) shown through anterior thalamic nucleus (ATN) stimulation that activation occurred at low-current stimulation (100 $\mu$ A), whereas inhibition was observed at higher intensities (500 $\mu$ A). In any part of the brain it's clear that increasing the current/voltage leads to an increase in the size of stimulating field, and a greater

flow of charged particles passing between the electrode contacts. The increased size of the electrical field could activate pathways that couldn't be reached by the field during low-intensity stimulation.

Too much current or voltage would of course result in tissue damage through mechanisms such as heating or electrode corrosion. At a high enough current one could in theory turn the DBS probe into a lesion probe. A manufacturer of stimulation devices – Medtronic – provides a limit for 'safe' charge density at  $30\mu\text{C}/\text{cm}^2$  for individual pulses. This limit isn't standard however, as variations in brain region, stimulus frequency, and overall duration of stimulation can alter this safe recommended limit. This particular quoted safety limit is given as a charge density since it depends heavily on the geometry of the electrode. The smaller the diameter of the anode or cathode, the higher the current density will be at these regions. In theory most stimulus intensities can cause tissue damage given a small enough electrode contact, and Merrill et al., (2005) takes this into account by providing information based on the total charge vs. total charge density. Equation (1.2) shows the maximum constant current that can be utilised given an upper charge-density limit:

$$I_{max} = (C_{limit} \times A_{electrode})/PW \quad \text{equation (1.2)}$$

Where  $I_{max}$  = maximum safe current

$C_{limit}$  = maximum safe charge-density limit

$A_{electrode}$  = surface area of smallest electrode contact (in square cm)

$PW$  = pulse-width

Should this safe limit be applied to rodents, then given a typical surface area for a rodent DBS electrode as  $0.08\text{mm}^2$ , with a pulse-width set to  $100\mu\text{S}$ , the maximum current based on this limit is  $240\mu\text{A}$ . Note that by this logic one could halve the pulse-width and double the current intensity for the same effect. If a constant-voltage device were used, the current in the above equation would be replaced with  $(V/Z)$ , where  $V$  = voltage limit and  $Z$  = impedance. In this case if the impedance

were to increase then so would  $V$ , which could potentially result in a higher voltage being administered than that based on the recommended safe charge density limit. Studies in rodents have shown severe side-effects for stimulation currents in-between 150-200 $\mu$ A, such as involuntary movements and rotational behaviour (Meissner et al., 2002, Boulet et al., 2006).

With the safe limit taken into account, the level of stimulus intensity could be set based on the required electrical field strength. If one were to approximate the conductivities of different brain regions e.g. grey matter  $\sim 0.2$ S/m (Ranck, 1963), white matter  $\sim 0.1$ -1S/m (depending on orientation; Nicholson, 1965), the electrical field propagating around the electrode could be modelled. The derivative of the electrical field gives the magnitude of the activating function for neuronal excitement (Rattay, 1998; also see Kuncel et al., 2008 for an example of modelling of the activating function based on human DBS studies using tetrodes).

Unfortunately at present more practical information regarding the appropriate stimulation intensity to use depends on knowledge of the anatomy and functionality of the site undergoing stimulation, as well as the desired effect. The above serve as useful guidelines in selecting a stimulus parameter and importantly, help to avoid unwanted lesion effects. The safe limit described above however doesn't take into account degradation of the electrodes, which is itself property of the material being used. Electrochemical reactions take place at the electrode surfaces which can have adverse consequences for the surrounding tissue (besides the electrode track lesion), depending on the material used. Platinum-iridium is the material of choice for human and/or chronic studies, because of its inert nature and low damage to surrounding tissues for a variety of charge densities (Harnack et al., 2004). Stainless-steel on the other hand can result in iron deposits, thermo-necrosis, haemorrhages and cell death, with the affected volume proportional to the charge density (Harnack et al., 2004), despite being cheaper and easier to fabricate electrodes with. In fact previous studies assessing tissue damage have revealed permanent iron deposits in rats following short-duration stimulation currents as low as 1 $\mu$ A (Fung et al., 1998).

A vital question for any study involving DBS is: how does one decide which current intensity and pulse-width to use? Rizzone et al., (2001) observed for a range of frequencies that increasing the pulse-width allows for the same clinical effect to be realised with a lower current intensity, resulting in an intensity/pulse-width curve. In this curve the largest therapeutic window between the desirable and undesirable effects (with regards to stimulus intensity) was found at shorter pulse-widths. Earlier studies indicated that shorter pulses result in an increased threshold difference between activation of nerve fibres with differing diameters (Gorman and Mortimer, 1983). Finally, the pulse-width, current intensity (and frequency) affects the power utilisation in any particular DBS device, which may affect the length of certain studies (or the frequency of battery changes and animal handling). Furthermore, devices often have their own technical limits with regards to pulse intensity, width and frequency, which of course must encompass that required by a particular experiment.

#### **1.3.2.4 Monophasic vs. Biphasic Stimulation**

Not to be confused with bipolar electrodes (which have two electrode contacts - forming the anode and cathode), biphasic pulses are simply electrical pulses that have a positive and a negative voltage/current swing, as shown in figure 1.2. Depending on the direction of current (whether it's anodal or cathodal), monophasic stimulation is more effective than biphasic stimulation at activating cells or axons (McIntyre and Grill, 2000). One of the major advantages however with biphasic pulses are reduced tissue damage and electrode corrosion (see Merrill et al., 2005 for an in-depth review of the electrochemical processes that occur), and is thus well-suited to chronic studies. Biphasic pulses consist of a reversal of the current/voltage phase, which reduces the net build-up of charge present following an otherwise monophasic pulse. This removal of net charge can be beneficial for simultaneous electrophysiological recordings in any part of the brain.

### **1.3.3 Applications of DBS for Non-Motor Related Neuropsychiatric Disorders**

Following the unprecedented success of DBS for various neurological disorders such as Parkinson's and dyskinesias, the past 10 years have seen a movement of this treatment into various non-movement based neurological/neuropsychiatric disorders. The neural basis of these disorders are varied, as are the clinical effectiveness of the different studies that have taken place, and many of the rationales for stimulus sites are strongly linked to the existing and extensive research that have been carried out through stimulation of the basal ganglia. Cortical, particularly motor structures are involved in the treatment of Tourette's, and various parts of the limbic system play a role in depression and OCD. In schizophrenia the normal operation of multiple brain regions are believed to be diminished, including the medial prefrontal cortex, hippocampus and various regions of the thalamus (see 1.3.3.6: Schizophrenia).

Most of the literature discussed here is derived from studies involving patients who are considered to be 'treatment resistant'. As the exact definition of this varies between studies and country where the research takes place, it typically involves ineffective attempts of usually three pharmacotherapy treatments (varies with disease), electroconvulsive therapy, as well as behavioural treatment such as cognitive behavioural therapy. Patients must meet a strict requirement for inclusion in each study, and exclusion factors could include, other predominant neural disorders, dementia, history of severe head trauma, previous lesioning/neurosurgery treatment, a previously implanted electronic device, pregnancy, suicidal intentions, and others that are disease-specific. The severity of the patients underlying disease would also have to be severe enough to be considered for inclusion, as measured with scales such as HDRS (Hamilton Depression Rating Scale) scale for depression or Y-BOCS (Yale-Brown Obsessive-Compulsive Scale) for OCD.

One of the key differences between the studies performed here and those described earlier in animal models to understand the mechanisms of DBS, is that these studies allow for a much greater variability. As patients are typically implanted with these

devices for time periods up to several years, their stimulation parameters may be adjusted individually for maximum clinical effect. Patients are generally allowed concurrent pharmacotherapy and/or behavioural therapy, and in addition various other psychological/pathological events/situations in their lives may affect the outcome of long-term studies. However the majority of long-term studies are preceded by a battery of neuropsychological tests which are usually carried out double-blinded. An example of these could be the activation of any of the four electrode contacts on any of the bilaterally implanted electrodes (as almost every study described here uses quadripolar tetrodes), or perhaps the sudden and complete inactivation of electrodes - such that experimenters may observe acute and usually negative effects. During this time period patients typically record their day-to-day progress, make regular visits to their hospital/clinic, and are not allowed drug changes.

#### **1.3.3.1 Obsessive-Compulsive Disorder**

Obsessive-compulsive disorder (OCD) is an anxiety-related condition characterised by the presence of repeated time-consuming thoughts and compulsive behaviours that would seem meaningless to the unaffected. Affecting approximately 1-3% of the population, current treatment options include pharmacological agents such as antipsychotic drugs and serotonin-reuptake inhibitors, as well as behavioural techniques such as cognitive behavioural therapy. Approximately 30% of patients have been found to be resistant to these treatments (Bjorgvinsson et al., 2007). For patients with particularly severe cases of OCD, psychosurgery procedures including anterior capsulotomy and subcaudate tractomy cingulotomy (Lippitz et al., 1999) is an option. In a similar manner to that of Parkinson's disease, the idea of DBS for OCD emerged through stimulation of the same sites used in functional ablation (Nuttin et al., 1999), and to date modest but significant improvements have been reported in the Yale-Brown Obsessive Compulsive Scale (Y-BOCS), along with refinements to the technique such as location and stimulus parameters.

The first study involving DBS for OCD was carried out by Nuttin and colleagues (1999), which involved chronic bilateral stimulation of the anterior limb of the internal capsule for 4 patients with severe OCD. This particular site lies immediately rostral to the anterior commissure, extending into the adjacent ventral capsule / ventral striatum. The selection of stimulation targets was in this case identical to that used in anterior capsulotomy (Lippitz et al., 1999). Significant improvements were seen in 3 of the 4 patients, with further improvements gained through refinement of the stimulation technique (in which case larger voltages of 4.7V were used). Subsequent studies based on the same region shown similar beneficial effects, whereby slight refinements to the target location and stimulus parameters were made (Greenberg et al., 2006, Abelson et al., 2005, Gabriels et al., 2003, Aouizerate et al., 2004). Interestingly a number of these studies reported decreases in depression and anxiety, in addition to reductions in OCD symptoms.

In an attempt to elucidate the mechanisms behind stimulation of the ventral capsule / ventral striatum, Rauch and colleagues (2006) carried out a combined positron-emission tomography (PET) and stimulation study on OCD patients. By observing the blood flow changes in the white matter tracts of the anterior internal capsule, they observed that HFS of this area caused a functional override of the local circuitry, effectively modulating the 'abnormal' circuitry implicated in OCD. In this case stimulation would be relayed to the efferent targets of these tracts, including the medial prefrontal cortex, as well as basal structures such as the ventral globus pallidus and thalamus. However, the functional implications of this are unclear regarding the clinical effectiveness of OCD-DBS. Sturm and colleagues (2003) postulated that stimulation of the nucleus accumbens shell would block abnormal information flow from the amygdaloid complex, which would otherwise cause OCD symptoms. High-frequency unilateral stimulation in this case was shown to cause significant reductions in OCD symptoms in three of the four patients as recorded between 24-30 months after implantation (an electrode displacement was found in the fourth patient, however). Despite many of the successes in treatment around the ventral capsule area, a trend arising from these studies revolve around the high

pulse-width and intensities required to achieve therapeutic benefit. This has negative implications for the battery life of the system used for stimulation.

Some work has been done investigating nucleus accumbens stimulation using a rat model of OCD, looking particularly at spontaneous alternation behaviour (van Kuyck et al., 2003), and schedule-induced polydipsia (a model for OCD where rats excessively drink when presented with food; see van Kuyck et al., 2008). Both experiments produced positive results, despite the lack of a well-validated animal model for OCD (Larson, 2008).

Stimulation of the STN – an area already treated for movement disorders - has also been looked at for the treatment of severe cases of OCD. This emerged initially for patients suffering from both Parkinson’s disease and OCD (Mallet et al., 2002, Fontaine et al., 2004), whereby STN stimulation has already proven to be a safe and effective procedure. Whilst both of these cases revealed dramatic reductions in OCD symptoms for the patients involved, it was not immediately clear how STN stimulation achieves the therapeutic benefits. Later studies focussed on stimulation of the anterior (limbic) region of the STN in both a primate model (Baup et al., 2008) and in human patients (Mallet et al., 2008), the latter showing significant reductions in Y-BOCS scores, in spite of a series of adverse effects which were reported.

### **1.3.3.2 Tourette’s Syndrome**

With regards to clinical outcome, there has been an unprecedented level of success arising from the application of deep-brain stimulation to Gilles de la Tourette’s syndrome (TS). The dysfunction in TS is widely believed to involve the cortico-striato-pallido-thalamo-cortical loop (Mink, 2001), and all of the studies presented here involve stimulation in these regions. Once again treatment for TS has previously been attempted with surgical lesioning procedures for a variety of brain targets in this region (Temel and Visser-Vandewalle, 2004). However, DBS of targets in the thalamus and GPi have been shown not only to consistently reduce or remove



tics, but has also shown improvements in other disorders such as depression, anxiety and OCD.

Many of the studies for TS involve either stimulation of regions of the thalamus (Vandewalle et al., 1999, Visser-Vandewalle et al., 2003, Maciunas et al., 2007), the GPi (Diederich et al., 2005), or both (Welter et al., 2008, Houeto et al., 2005, Ackermans et al., 2006). Either way the studies are focussed on disrupting the loop known to cause tics as seen in Tourette's, and researchers are attempting to determine the most effective location for stimulation. As such it is not uncommon to see researchers make adjustments to electrode locations in the left and right hemisphere, as seen with Vandewalle et al., (1999) for example, who places electrodes 5mm in the left hemisphere and 3mm in the right hemisphere lateral to the anterior commissure-posterior commissure (AC-PC) line. In this case stimulation of the left side produced a reduction in tics whilst the right target produced an increased feeling of well-being. This study reported that tics were reduced to almost being "non-existent" after 4 months of stimulation. Similarly Maciunas and colleagues (2007) stimulated the same region with reports of reduced tics, anxiety, depression and even obsessive-compulsive behaviours.

Stimulation in the GPi is showing equally if not more promising clinical effects; with one study reporting a 73% decrease in tics over 14 months, along with significant reduction in anxiety and depression (Diederich et al., 2005). Comparisons between GPi and stimulation in the centromedian-parafascicular complex (CM-Pf) of the thalamus shows a trend towards improved responses in the GPi, particularly in one study where a patient with electrodes implanted in both locations in both hemispheres experienced a 96% reduction in tics via GPi stimulation as compared to 30% with CM-Pf stimulation (Welter et al., 2008). Houeto et al., (2005) however had found similar results through stimulation in either location, where in both cases tic severity was improved by 70%.

### 1.3.3.3 Treatment-Resistant Depression

There have only been a small number of depression studies to date with regards to DBS, although the effects of patient depression and/or mood elevation has been studied; and varies in nearly all DBS studies for neuropsychological disorders. Electrode locations have varied between studies, including structures in the limbic system, basal ganglia and anterior cingulate cortex.

One of the earlier studies looked at stimulation of the ventral caudate nucleus with the hopes of alleviating both depression and OCD (Aouizerate et al., 2004), but ultimately found the treatment more effective at alleviating depression and anxiety, with clinical effects showing near remission after 6 months. However it was acknowledged that the area of stimulation in this case lies just dorsal to the nucleus accumbens, an area well known for its role in pleasure and fear. Based on this idea, Schlaepfer and colleagues (2008) carried out bilateral stimulation of the nucleus accumbens over several months, revealing marked reductions in depression, which also correlated with changes in PET imaging. Given the modulatory role played by the nucleus accumbens, it was the researcher's intent to modulate various parts of the brain through HFS as opposed to blocking or jamming dysfunctional signals – as is the case in the majority of DBS studies.

Stimulation to alleviate depression has also been carried out in the ventral striatum, below the level of the anterior commissure (Malone et al., 2009), in close proximity to the ventral caudate nucleus as stimulated by Aouizerate et al., (2004). This study demonstrated modest improvements, with reduction in depression seen in 7 patients out of 15, measured using the Hamilton Depression Rating Scale (HDRS). It is of note that in this case the largest changes in depression took place between 3 and 6 months, a time course similar to that seen by Aouizerate and colleagues (2004). Researchers have also looked into stimulation of the subgenual cingulate region for treatment of depression (Mayberg et al., 2005). Based on the theory that chronic stimulation reduces the over-activity seen in the subgenual cingulate in severely depressed patients (as verified by increased blood flow through PET scans), stimulation of the white matter tracts adjacent to the subgenual cingulate gyrus was seen to produce “a striking and sustained remission of depression in 4 of 6 patients”.

More recently, the same group has evolved this idea into a multi-site stimulation paradigm, where not one but multiple white matter tracts of the subcallosal cingulate are stimulated to produce a more effective electrical field profile in the brain with regards to therapeutic outcome (Lujan et al., 2013).

#### **1.3.3.4 Minimally Conscious States**

Minimally conscious states (MCS) is a disorder characterised by the failure of brain mechanisms resulting in a minimal preservation of self or environmental conscious awareness (Giacino et al., 2002), usually following traumatic brain injury. Whilst there is currently no effective treatment for this disorder (Lombardi et al., 2002) Schiff and colleagues (2007) investigated bilateral central thalamic DBS on a patient who had been suffering MCS for 6 years prior to implantation. The anterior intralaminar thalamic nuclei (anterior ITN) were targeted as an attempt to modulate the forebrain arousal regulation system that is thought to be dysfunctional in MCS (Van der Werf et al., 2002). This study produced promising results, including an increase in the frequency of both cognitively mediated behaviours and limb control, suggesting activation of neural networks centred round the thalamus, although consciousness was not fully restored in the patient.

#### **1.3.3.5 Cluster Headaches**

Cluster headache is a disorder that results in an immense period of pain for the patient, often lasting from 15 minutes up to 3 hours. Its symptoms are believed to involve the activation of the hypothalamus, along with areas associated with pain modulation and perception, such as the anterior cingulate cortex and insulae and contralateral thalamus, as verified through PET imaging (May et al., 1998) and local-field potential (LFP; Brittain et al., 2009) studies. Treatment generally involves prophylactic verapamil and intravenous magnesium, both of which produce improvements in some but not all patients. Abortative treatments are also commonplace upon the onset of an attack, including intake of pure oxygen and lidocaine as a nasal spray. Based on the inhibition hypothesis of DBS, hypothalamic

high-frequency stimulation was introduced as a way of directly attenuating the intensity of attacks, and has generally been met with some success (Leone et al., 2001, Sillay et al., 2010, Leone et al., 2004), with some patients reporting a complete remission seen in the hemisphere ipsilateral to stimulation. In an effort to improve the success rates using this technique, much work is being done in assessing the role the hypothalamus plays during the course of a cluster headache (Leone et al., 2010). Although described as a safe procedure, there has been a fatality associated with the implantation of electrodes into this region following intercerebral haemorrhage (Schoenen et al., 2005).

#### **1.3.3.6 Schizophrenia**

The use of DBS as a treatment option for schizophrenia has only recently been explored. Ambiguities regarding the nature of the disease and its underlying pathology don't allow for a straight forward identification of a viable stimulus target, particularly when the mechanisms of action of DBS themselves are not well elucidated. Nonetheless the field can benefit from exploratory approaches with regards to the stimulus target selection, with each test helping to expand the knowledge of the effects of DBS and how it interacts with the core schizophrenia pathology. A recent investigation looked at the stimulation of a variety of candidate structures at varying stimulus parameters in a rat model of relevance to schizophrenia (Klein et al., 2012). They found that in a poly I:C model prepulse inhibition (PPI) deficits were reversed through stimulation in the mediodorsal thalamic nucleus (MD), medial prefrontal cortex (mPFC), and GP; however the results here were highly selective to stimulus parameters, highlighting that an adequately chosen anatomical location is not enough to guarantee a promising outcome.

A number of recent studies have focussed on stimulation in the ventral hippocampus in both humans (Mikell et al., 2009) and in rat models of relevance to schizophrenia (Ewing and Grace, 2013, Perez et al., 2012). The underlying hypothesis in this case is based on the hyperactivity of the ventral hippocampus,

which causes an abnormal regulation of dopamine through its efferent outputs to the nucleus accumbens (Lodge and Grace, 2007). So far this has shown to normalise brain signals arising from dopamine neurons (Perez et al., 2012) and those in the medial prefrontal cortex and mediodorsal thalamic nucleus which are related to auditory evoked potentials (Ewing and Grace, 2013). Interestingly Perez and colleagues (2012) demonstrated that ventral hippocampal stimulation could affect a normalisation of deficits in reversal learning and extra-dimension set-shifting in MAM-treated rats; thus indicating that stimulation of this structure may see therapeutic benefit against the cognitive symptoms in schizophrenia.

## 1.4 Working Memory

Working memory is one of the core functions in the brain that has repeatedly revealed to be disrupted in schizophrenia patients (Weinberger et al., 1986, Carter et al., 1998, Schroder et al., 1996, Potkin et al., 2002, Perlstein et al., 2001). It is the ability of the brain to maintain and manipulate information, which is retrieved from the environment or from long-term storage (Baddeley, 2003). Functioning as the ‘blackboard’ of the brain, working memory has a central role in cognitive function with regards to processing information and guiding decisions. Abstract thought, creative thinking, language, planning and learning all rely on working memory. An example of its practical use could involve asking an individual to calculate “ $2 + 3 + 5 + 7$ ” in their heads, which would require them to simultaneously hold those numbers in thought whilst processing each step of the result. A number of theories have been developed based on the functional aspects of working memory, with perhaps that by Baddeley being one of the more popular ones (Baddeley, 1992). Baddeley in this case divides working memory into four components: the central executive – which is an attentional-controlling system, the visio-spatial sketch pad, which processes and manipulates visual information, the phonological loop, which stores and rehearses auditory and speech information (Baddeley, 1992), and later added the episodic buffer, that integrates information into distinct representations (Baddeley, 2003). Although this model has gained popularity due to its correlations with human working memory studies, it cannot completely be applied to working memory in nonhuman primates due to, for example, the reduced need for a phonological loop. Whilst most of the working memory studies have been performed in nonhuman species such as monkeys and rats, parallels can still be made between experimental findings and existing models for working memory.

By its very nature, working memory relies on the activation and coordination of multiple structures located around the brain, including the prefrontal, temporal, entorhinal, premotor, supplementary and parietal cortices (see Constantinidis and Wang, 2004, for a review). The prefrontal cortex and the hippocampus in particular have central roles in working memory (Eichenbaum, 2004), and a vast body of research has been attributed to the network, functional, cellular and

electrophysiological aspects of both regions under a plethora of controlled working memory conditions. For example, functional magnetic resonance imaging (fMRI) studies have demonstrated simultaneous PFC and hippocampal activation during working memory tasks (Schon et al., 2008). The following sections outline some of the relevant pathology regarding these structures, before approaching some of the experimental findings in rats regarding electrophysiological measurements.

### **1.4.1 Medial Prefrontal Cortex**

The medial prefrontal cortex (mPFC) is a major centre in the brain for the integration and manipulation of information, allowing for complex functions such as planning, decision making, selective attention and working memory (Kolb, 1990, Neafsey, 1990, Vertes, 2004). Although the rat mPFC is ~1000 fold smaller than its human counterpart, it contains striking anatomical and functional correlates including reciprocal connectivity with the mediodorsal thalamic nucleus (MD; Krettek and Price, 1977), dopaminergic input from the ventral mesencephalon (Heidbreder and Groenewegen, 2003), and is heavily implicated in executive functions such as working memory (Kolb, 1990). As such this region has been heavily studied in order to better understand the causes and treatments of various cognitive disorders.

The medial prefrontal cortex in the rat consists of the following cytoarchitecturally distinct areas: the medial precentral area, the anterior cingulate area, the prelimbic area, and the infralimbic area (Heidbreder and Groenewegen, 2003; see also figure 1.4). Afferent and efferent connectivity in each of these regions is widespread, including the thalamus, amygdala, hypothalamus, striatum, brainstem nuclei as well as various cortico-cortical connections (see Heidbreder and Groenewegen, 2003, for review). Based on the connectivity and observed functionality of these regions, the infralimbic cortex has been implicated in visceral/autonomic functions, whilst the prelimbic cortex is seen to be analogous to the dorsolateral prefrontal cortex in primates due to its role in limbic-cognitive functions (Vertes, 2004). Damage to the mPFC in either rats or primates have

shown to result in various working memory deficits (Kolb, 1990, Fuster, 1997, Stuss and Alexander, 2000, Zola-Morgan and Squire, 1985, Goldman and Rosvold, 1970).

### **1.4.2 Hippocampus**

The hippocampus is a major structure in the limbic system and is believed to have central roles in learning and memory. Its basic structure, connectivity, and functionality are similar throughout most mammalian species, whereby extensive literature exists for the human, rodent and primate hippocampus (figure 1.4). Some of the main functions implicated in the hippocampus include the consolidation and retrieval of spatial and episodic memories (Squire, 1992, Burgess et al., 2002), the formation of cognitive maps (i.e. using ‘place cells’ for navigation, see O’Keefe and Conway, 1978), as well as working memory (e.g. Yoon et al., 2008, Wang and Cai, 2006, Floresco et al., 1997). In addition the hippocampus has seen extensive studies based on neuronal plasticity (e.g. Laroche et al., 2000), which directly relates to relevant theories on the formation of memories.

The hippocampus consists of four main subdivisions: *Cornu Ammonis* areas 1-3 (CA1-CA3), and the dentate gyrus (DG). The organisation of the sub regions are such that information largely flows uni-directionally with much of the main connectivity to cortical and subcortical structures occurring through the entorhinal cortex via the perforant pathway (Andersen, 2007). The CA1 region receive inputs from the entorhinal cortex via the perforant path as well as CA3 Schaffer collaterals, and in rats is mainly involved in spatial working memory (Moser et al., 1993).



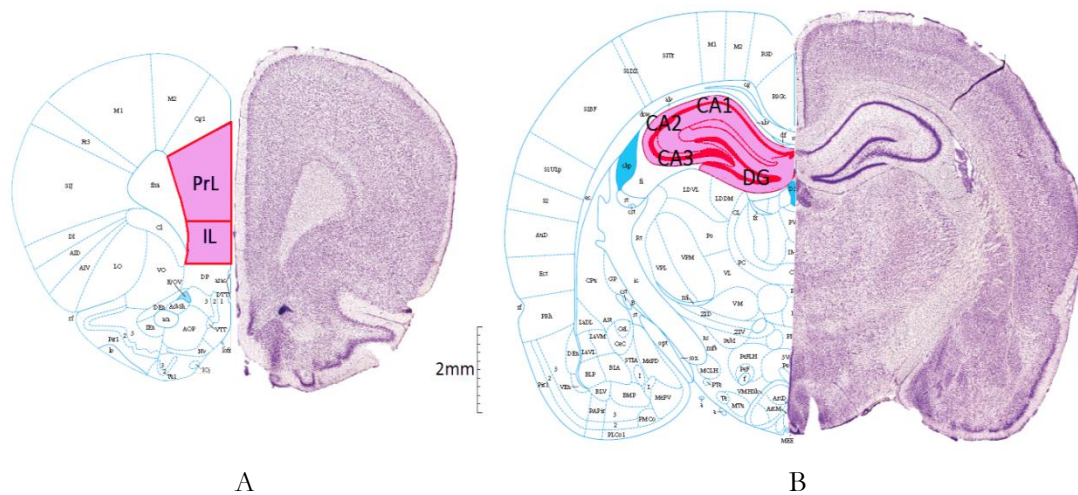


Figure 1.4 – Coronal views of the rat medial prefrontal cortex (A) and hippocampus (B). Images are adapted from “The Rat Brain in Stereotaxic Coordinates” by Paxinos and Watson, (2007).

Coordinates for the coronal sections are shown from Bregma at: mPFC = +3.24mm,  
hippocampus = -3.00mm.

### 1.4.3 Working Memory Relies on Connectivity of Hippocampus and Prefrontal Cortex

Much of what is known about the mPFC and hippocampus regarding working memory have been derived from early lesion studies in human patients. Selective ablation of the prefrontal cortex has revealed profound short-term memory deficits (Jacobsen 1936; Milner 1963; Goldman-Rakic 1987), whilst removal of the hippocampus can result in an inability to store new information (Scoville and Milner, 1957). To date a large number of combined mPFC and hippocampus lesion/disconnection studies have taken place under controlled conditions to examine the contributions made by both structures in working memory. Wang and Cai et al., (2006) and later Yoon et al., (2008) demonstrated spatial working memory deficits in rats which were infused with muscimol (a  $GABA_{\alpha}$  receptor agonist) in either the mPFC or the dCA1 region. Wang and Cai et al., (2006) noted that these deficits remained following a unilateral mPFC and contralateral hippocampal inactivation, mirroring an earlier study by Floresco et al., (1997), who reported the same impairments with temporary inactivation using lidocaine infusions. Interestingly whilst Yoon et al., (2008) noted that the spatial working memory deficits were delay-independent following mPFC lesions, an earlier study by Porter

et al., (2000) showed that these lesions resulted in delay-dependent deficits (for the longer delays) when extra-maze spatial cues were supplied. Similarly, (Lee and Kesner, 2003) reported delay-dependent deficits in spatial working memory following hippocampal lesions, although in their case additional training sessions were provided after surgery.

Taken together, the evidence presented here highlights the necessity for an intact mPFC and an ipsilateral hippocampus in order to effectively mediate spatial working memory in rats. In an effort to observe differences between bilateral hippocampal and mPFC inactivation, Sloan and colleagues (Sloan et al., 2006) tested rats on a delayed-match-to-position (DMTP) task and a water maze task. In this case rats with mPFC lesions displayed delay-dependent impairments on the retention part of the DMTP task (the longer delays produced impairments), whilst their performance on the water-maze task did not change from control levels. Conversely hippocampal-lesioned rats had shown deficits in the water-maze task, but no impairments on the DMTP task, thus highlighting the different roles played by each structure.

All of this reveals that working memory requires not only an intact hippocampus and mPFC, but they need to work together. A monosynaptic, ipsilateral connection links these two, projecting from the ventral CA1 hippocampal region to the medial prefrontal cortex; and its existence has been well established in rats (Ferino et al., 1987, Jay and Witter, 1991, Jay et al., 1989) and monkeys (Goldman-Rakic et al., 1984). Specifically in the rat this pathway passes through the fimbria and fornix to the nucleus accumbens, lateral septum, and the infralimbic, prelimbic and medial orbital cortices (Laroche et al., 2000). The dorsal CA1 (dCA1) region of the hippocampus – an area heavily implicated in spatial working memory (Moser et al., 1993), does not directly project to the mPFC, has instead is thought to interact with the mPFC through the ventral CA1/subiculum (Jay and Witter, 1991). Furthermore there are no known reciprocal connections that project from the mPFC to CA1 (Sesack et al., 1989).

The hippocampo-prefrontal pathway connecting these structures is known to be glutamatergic (Jay et al., 1992), forming asymmetric synapses on the dendritic spines

of pyramidal cells in the prelimbic cortex (Carr and Sesack, 1996) as well as parvalbumin-containing interneurons (Gabbott et al., 2002). It's well known that infusion of NMDA receptor antagonists in the mPFC cause spatial working memory deficits (e.g. Aura and Riekkinen, 1999), and numerous studies have thus focussed on the excitatory hippocampo-mPFC pathway by generating single-stimulus pulses in the hippocampus and recording the intracellular action potentials that are evoked in the mPFC. Early studies revealed that the latency of response in the mPFC following a single stimulation pulse was  $\sim 16\text{ms}$ , which is compatible with the conduction velocity of these fibres, as well as the latency of antidromic spikes recorded in the CA1 cells following prelimbic stimulation (Ferino et al., 1987). More recently Degenetais et al., (2003) carried out a study on anaesthetised rats whereby the intracellular activity in the medial prefrontal cortex was recorded following single-pulse stimulation of the hippocampus. They noticed that 91% of pyramidal cells located in layers 2 to 6 received a complex synaptic influence from the hippocampus, which was revealed through measurements on the recorded excitatory post-synaptic potential that resulted. They also noticed a prolonged IPSP that followed the EPSP, which they suggested may be due to simultaneous engagement of pyramidal and non-pyramidal neurons. In this case the evoked IPSPs may be due to the involvement of the GABAergic interneurons, as a direct activation of the GABAergic interneurons which synapse on the soma and proximal dendrites of mPFC pyramidal cells (Gabbott et al., 2002). Indeed Tierney et al., (2004) noticed that hippocampal stimulation resulted in the interneurons being activated before the pyramidal cells in most cases. The lowered latency of activation for the interneurons can be explained by the increased excitability of the interneurons as compared to the pyramidal cells, which again can be explained in part by the differential expression of  $\text{K}^+$  channels and an increased density of  $\text{Na}^+$  channels (Du et al., 1996, Martina et al., 2000). These findings mirror studies in pyramidal cells that receive monosynaptic excitatory inputs on the same type of pathway, in which case the interneurons was shown to always fire first (Buzsaki, 1984).

One of the roles of the GABAergic interneurons are to dynamically adjust the conductance's of the pyramidal cell network (Woo et al., 2008). GABAergic

interneurons provide powerful inhibitory control to the pyramidal neurons throughout the PFC layers 3 and 5 (Giguere and Goldman-Rakic, 1988), which in turn receive feedback excitatory modulation via local recurrent excitatory projections (Barbas, 1995, Melchitzky et al., 2001). The subclasses of interneurons in the PFC are based mainly on the variation of the calcium-binding proteins within them (DeFelipe, 1997), as well as distinct morphological and electrophysiological characteristics (Lund and Lewis, 1993). The monkey PFC for example has <50% GABAergic interneurons containing calretin, which are predominantly located in layers 1 to 3, whereas parvalbumin-containing interneurons are more localised to deep layers 3-4 (Conde et al., 1994), making up <25%. Given much of the findings regarding hippocampal-mPFC innervations, it is interesting that this pathway has been shown to synapse exclusively onto the parvalbumin-containing interneurons, rather than the calbindin or calretin interneurons (Gabbott et al., 2002). Many of the executive function deficits in schizophrenia including working memory are argued to be specific to prefrontal inhibitory circuits (Akbarian et al., 1995a, Benes et al., 1996, Lewis, 1998, Lewis, 2000), particularly those involving signalling deficits due to dysfunctional parvalbumin interneurons in these regions (Beasley and Reynolds, 1997, Reynolds and Beasley, 2001, Hashimoto et al., 2003b).

The preferential activation of inhibitory interneurons in the hippocampo-mPFC pathway as previously mentioned mediates a feed-forward inhibition mechanism. This essentially manifests as a temporal and spatial inhibition of widespread PFC pyramidal cells, which can help to explain the prolonged IPSPs as observed by Degenetais and colleagues (2003) following single-pulse hippocampal stimulation. This mechanism does not require prior activation of local pyramidal neurons, and can lead to precise widespread synchrony of inhibitory control in the network (Swadlow, 2003), which can perhaps explain the generation and synchronisation of mPFC to hippocampal theta rhythm (Tierney et al., 2004). This mechanism has also been suggested to help establish cognitive 'memory fields', allowing information to be held during the delay periods of working memory tasks (Goldman-Rakic, 1996, Tierney et al., 2004).

An interesting consequence of sending electrical stimulation pulses through the hippocampus is that tetanic or high-frequency stimulation has shown to induce long-term potentiation (LTP) in the PFC pyramidal cells. This has been demonstrated in the mPFC *in vitro* (Hirsch and Crepel, 1990), in anaesthetised rats (Laroche et al., 1990), and later in freely-moving rats (Degenetais et al., 2003). LTP induces a lasting enhancement of synaptic potentials, and is widely believed to be one of the main mechanisms by which learning and memory works. Similarly long-term depression (LTD) – a reduction in synaptic strength – has been observed through low-frequency paired-pulse stimulation *in vivo* (Thiels et al., 1994, Doyere et al., 1996). These studies reveal that synapses on the hippocampo-prefrontal pathway can be subjected to long-lasting synaptic changes based on the hippocampal activation pattern.

#### **1.4.4 Neurophysiological Mechanisms of Working Memory**

Local-field potentials are extracellular recordings in the brain that represent the synchronised firing activity of a population of neurons (Steriade et al., 1990). The characteristics of an LFP signal can be assessed in tandem with pathological and behavioural studies to help explain the functional workings of the neural systems generating them. Their temporal fidelity allows for them to be acquired during behavioural tasks, where changes can be tracked for the different task phases with millisecond precision. LFP signals are often characterised by the frequency composition of the signals, which is illustrated in figure 1.5 using an example recording from the rat dCA1 hippocampal region.

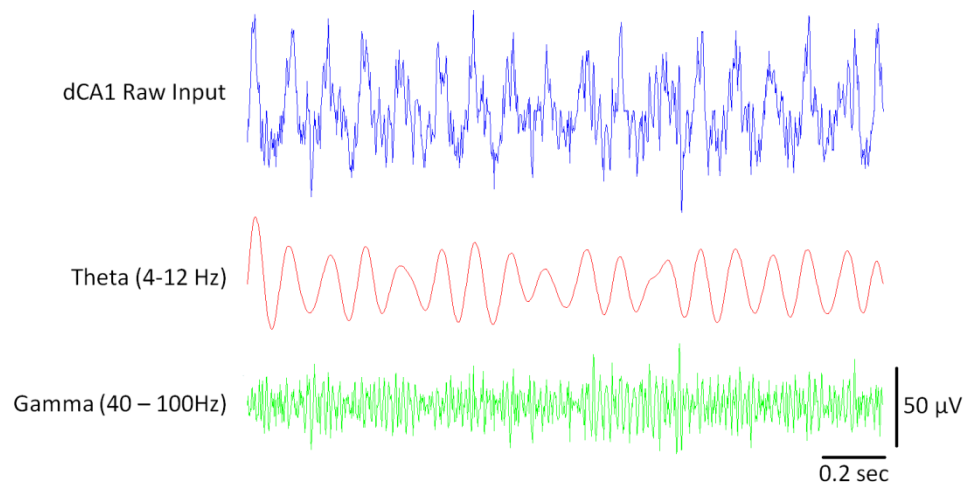


Figure 1.5 – Raw rat hippocampal LFP (blue) can be decomposed into its theta-frequency (red) and gamma-frequency (green) waveforms. These signals were extracted from rats that took part in the behavioural task described in Chapter 4.

#### 1.4.4.1 Theta Oscillations

The theta-band of activity encompasses the 4-12Hz frequency range, and in rodents is most prominently observed in the hippocampus; particularly in the str. lacunosum-moleculare of the CA1 region which feature the largest amplitude theta-waves (Buzsaki, 2002). Theta activity generally arises during mnemonic processing and decision making activities, and in the rodent is particularly prevalent during locomotion, spatial exploration, and learning-related behaviours such as attention to behaviourally relevant stimuli (Green and Arduini, 1954, Vanderwolf, 1969). Whilst a number of brain regions are implicated in the generation of hippocampal theta, it's generally accepted that the medial septum constitutes the main 'pacemaker' of hippocampal theta (Hasselmo et al., 2002), through its reciprocal connections with parvalbumin-containing interneurons (Freund, 1989, Freund and Antal, 1988, Toth et al., 1993, Vertes and Kocsis, 1997). Indeed inactivation of this structure is known to abolish hippocampal theta (Stumpf et al., 1962).

#### 1.4.4.2 Synchronisation of Brain Regions with Hippocampal Theta

A large amount of studies to date have been attributed to discerning the role of LFPs in functional brain phenomena such as neuronal plasticity, as well as a variety

of behavioural events such as attention, sensorimotor gating, learning or working memory. They are believed to be a fundamental mechanism behind the conditioning of information in the brain regarding an efficient transfer of information (Buzsaki, 2004). One of the major ways in which LFP oscillations are believed to facilitate this is through the synchronisation of brain activities. The coupling of LFP oscillations to individual neurons as well as other LFP oscillations is well documented for many behaviours, whether at the local and network levels. A good example of local coupling is seen in the hippocampus, whereby every cell is known to be phase-locked to the local theta-rhythm (Bland et al., 1975, Buzsaki et al., 1983), thus allowing coherent cell ensembles to be formed (Harris et al., 2003), and arguably enhancing plasticity (Markram et al., 1997, Bi and Poo, 1998).

At the network level, communication between separate brain regions has been proposed to facilitate plastic changes that can effectively enhance or block inputs from another structure. Buzsaki, (2002), offers an interesting review on hippocampal-PFC plasticity as mediated by hippocampal theta. A number of studies based on electrical stimulation of the hippocampal-prefrontal cortex tract have found long-term plastic changes (Izaki et al., 2001, Hyman et al., 2003), particularly so when carried out using theta-frequency stimulation (Huang and Kandel, 2005). Theta-activity in particular is well suited for the coordination of brain activities over large distances, when one considers the period of theta oscillations (~100-170ms) and the conduction times of pathways in the brain (e.g. 16ms for the hippocampal-prefrontal cortex tract, Ferino et al., 1987; and 40ms for polysynaptic activation, Degenetais et al., 2003).

By measuring the electrical activity of separate brain regions, both at the neuronal or network level, the interactions between these regions during complex functions such as working memory can be better understood. As previously demonstrated through lesion studies, the involvement and connectivity of both the mPFC and the hippocampus in working memory tasks is essential, (e.g. Floresco et al., 1997, Wang and Cai, 2006, Yoon et al., 2008), with each structure purported to play a specific role (Sloan et al., 2006). The synchronisation of theta-frequency LFP during activities involving working memory between the prefrontal cortex and

hippocampus have been observed both in humans (Tesche and Karhu, 2000, Sauseng et al., 2004) and rodents (Jones and Wilson, 2005, Benchenane et al., 2010, Sigurdsson et al., 2010). Jones et al., (2005) demonstrated enhanced dCA1-mPFC coherence in freely-moving rats as they performed a spatial working memory task. They noted in particular that coherence between these structures increased at the point where the rats would make a decision to turn left or right, with one of these decisions leading to a reward. Later on, Benchenane and colleagues (2010) performed a similar task in a Y-maze, with recording electrodes positioned in the mPFC and ventral CA1 – the region from which a direct hippocampo-PFC glutamatergic pathway protrudes (Jay et al., 1992). They noted that, in addition to coherence increasing at the decision point, coherence in general was greatest when rats had learned the task rules, thus supporting views regarding learning-related neuronal plasticity on this pathway. In addition they noted that during periods of high coherence, mPFC theta amplitude had decreased, relative to periods of low coherence, which could perhaps be mediated by increased control of the mPFC inhibitory interneurons, which among pyramidal cells, is where the hippocampo-prefrontal cortex tracts terminate (Gabbott et al., 2002). Interestingly, mPFC-CA1 coherence was found to be reduced in a transgenic mouse model relevant to schizophrenia, during a working memory task (Sigurdsson et al., 2010), and this was correlated with working memory deficits.

#### **1.4.4.3 Prefronto-Hippocampal Phase-Locking**

Phase-locking is a term used to describe the preferential firing of neurons at a certain phase of a background LFP oscillation. For example, neurons which are phase-locked to the  $180^{\circ}$  portion of a theta wave fire preferentially at the trough of the waveform. The hippocampal theta rhythm has been shown to phase-lock neurons from a variety of brain regions, including the entorhinal cortex (Dickson et al., 1995), cingulate cortex (Colom et al., 1988) and the striatum (Berke et al., 2004). In addition to the findings reported regarding hippocampo-prefrontal coherence, numerous studies which combined LFP and single-unit nerve action potential recordings in the last decade have revealed correlations between hippocampal theta,



and the neuronal activity of pyramidal cells in the prefrontal cortex. In rats, the firing characteristics of the pyramidal neurons in the prefrontal cortex have shown correlations with almost all observed aspects of behaviour. For example, single-unit recordings in the prelimbic and infralimbic cortices in rats undergoing a variety of behavioural tasks have shown correlations related to the delay periods, selection of certain maze paths, and the start and end of trials (Jung et al., 1998).

The first group to demonstrate hippocampal-prefrontal cortex phase-locking carried out chronic multi-tetrode recordings in the mPFC and CA1 region of the hippocampus in rats (Siapas et al., 2005), finding that around 40% of mPFC neurons were significantly phase-locked to hippocampal theta rhythms with a latency of ~50ms. These rats however were freely-moving with no specific behavioural correlations made with the firing patterns and hippocampal theta phase. Two studies performed shortly after addressed this, showing that phase-locking was correlated to a specific behavioural context (Hyman et al., 2005), and more specifically, was associated with spatial working memory (Jones and Wilson, 2005, Benchenane et al., 2010). Jones et al., (2005) carried out recordings in the dCA1 and mPFC of rats as they performed a continuous alternation spatial working memory task, and observed that phase-locking of mPFC neurons was greatest during the choice phase where animals were about to make a correct choice. Incorrect choices in this case had shown phase-locking and theta coherence similar to that seen during the forced-run epochs. This finding mirrors a later study whereby mPFC cells had shown enhanced phase-locking to hippocampal theta during the correct-choice trials in a delayed non-match-to-sample task (Hyman et al., 2010). In this case 46% of mPFC cells were modulated to hippocampal phase just before the rat had made a correct choice, as opposed to 17% prior to making an incorrect choice. Given that these recordings were taken throughout the training as well as the test period, the researchers had noted that not only did the theta coherence increase with rule acquisition, but also that the phase of the mPFC pyramidal cells had shifted to fire more synchronously, which in this case was at the trough of hippocampal theta rhythm. Taken together these results are interesting because not only do they highlight specific functional interactions at the stage of these tasks where it is presumed animals are actively using

their working memory, but the presence of phase-locking or coherence can be used to predict the outcome of these tasks before the animal makes a decision. The inhibitory GABAergic interneuron has been proposed as a key mechanism in these findings of synchronised activity (Benchenane et al., 2010), and has been suggested as one of the reasons why mPFC-CA1 coherence seems to be unaffected by reductions and/or low mPFC theta amplitude (Benchenane et al., 2010, Hyman et al., 2005), particularly given a specific inhibitory control of mPFC pyramidal cells during synchronised oscillations. Of particular note is a recent study which identified mPFC parvalbumin-containing basket cells which fired phase-locked to hippocampal theta, thus providing further support for its role in feed-forward inhibition and thus recruiting only the most excitable prefrontal pyramidal cells during these synchronised states (Hartwich et al., 2009).

#### **1.4.4.4 Gamma Oscillations**

The gamma frequency band of neuronal oscillations are generally taken to lie between 25 and 150Hz (Fries et al., 2007), with various sub-bands e.g. slow gamma ~25-60Hz, medium gamma ~60-100Hz, etc. When observed in LFPs they are smaller in amplitude than lower-frequency oscillations such as delta or theta waves, and encompass a much broader range of frequencies. Functionally, they are believed to reflect the summated action potentials of local cell assemblies whereby their effects are mediated locally (Harris et al., 2003), rather than larger, lower-frequency waves such as hippocampal theta which as previously discussed can synchronise the activity of separate brain regions. In the hippocampus they are believed to arise both intrinsically via projections from the entorhinal cortex (Bragin et al., 1995), and play a role in sensory binding (Singer and Gray, 1995), selective attention (Jensen et al., 2007) and working memory (Jensen et al., 2007, van Vugt et al., 2010, Howard et al., 2003). The fast-firing activity of GABAergic interneurons are believed to play a key role in their generation (Cobb et al., 1995).

Gamma oscillations in awake mammals have traditionally been associated with sensory binding (Singer and Gray, 1995), selective attention (Jensen et al., 2007), and

more recently has been observed to be prevalent during working memory (Jensen et al., 2007, van Vugt et al., 2010, Howard et al., 2003). In human neurosurgical patients, electrocorticogram (ECoG) studies have revealed gamma-activity increases in both the cortical (Howard et al., 2003) and hippocampal (van Vugt et al., 2010) brain regions, which in both cases were correlated with working memory load. This gamma activity increase with working memory load mirrors widespread findings of increased cortical activation with working memory, as reported through various imaging studies (e.g. Callicott et al., 1999).

#### **1.4.4.5 Gamma Activity and Cross-Frequency Coupling**

Gamma activity is often studied with regards to its cross-frequency interactions with other brain waves. In this case cross-frequency interactions refer to the properties of one brain rhythm directly affecting a property of another. For example one of the most common findings refers to theta-gamma phase-amplitude cross-frequency interactions, which means that the amplitude of the gamma rhythm will change depending on the phase of the theta rhythm. Many of these cross-frequency interactions have been studied by comparing two frequency patterns in the same brain region. In the hippocampus the amplitude of gamma oscillations are known to be modulated by theta phase (Bragin et al., 1995). More recent studies noted the presence of two separate bands of gamma activity in CA1, that being a slow gamma range (25-50Hz) and a fast gamma range (65-140Hz) (Colgin et al., 2009). They observed that whilst both these bands were modulated by theta phase (at the early descending part and the trough of the theta cycle respectively), only one of them was modulated by theta at any single moment. Behavioural correlations have been made between cross-frequency interactions in both humans (Mormann et al., 2005) and rats (Tort et al., 2008). In this latter study Tort et al., (2008) observed the phase-amplitude couplings in the hippocampus and striatum for rats performing a T-maze task which required the rats to choose a goal arm based on an audio cue given at the beginning of the trial. They noted that in the maze, the theta-phase modulation of gamma amplitude peaked at the decision point, where it is presumed that the animals would choose a direction. A more recent study further noted phase-phase coupling

between hippocampal theta and gamma activity (Belluscio et al., 2012), where in this case the gamma oscillations up to 90Hz were shown to correlate in phase with theta-oscillations, as well as amplitude. Finally phase-amplitude interactions have been observed across brain regions, in particular regarding hippocampal theta and mPFC gamma (Dzirasa et al., 2009, Adhikari et al., 2010, Sirota et al., 2008), thus providing further proof that spatially distributed cell assemblies can be integrated with an underlying theta rhythm.

Cross-frequency interactions such as these are often regarded as forms of coding in the brain, whereby information can be transmitted with efficiency. A well-known model of this revolves around phase coding in hippocampal place cells whereby the firing of individual place-cells (represented as an individual gamma cycle) occurs earlier and earlier in the phase of theta-wave (phase-precession), as a rat moves about its place field (O'Keefe and Recce, 1993). With regards to working memory Lisman and Idiart (1995) proposes that each gamma sub-cycle in a single theta cycle makes up an active representation in working memory, which in this case is  $7 \pm 2$  gamma cycles. Indeed cross-modulation of theta-gamma has been seen to increase during working memory (see Jensen, 2006). When considering the mechanisms of cross-frequency interactions functionally, the perisomatic basket cells are suggested to be a major source by firing theta rhythmic trains of action potentials at gamma-frequencies (see Belluscio et al., 2012).

## 1.5 Schizophrenia

Schizophrenia is a neuropsychiatric disorder resulting from a number of widespread abnormalities in brain function, leading to a diminished social and occupational functionality in the individuals affected. Affecting approximately 1% of the population (Lewis and Lieberman, 2000), patients with schizophrenia are estimated to die between 12-15 years before the average population age through such causes as poorer diet, reduced exercise, and increased rate of suicide (Saha et al., 2007). As such there exists a considerable financial and social incentive to further the understanding of this disorder as well as treatment options. The exact cause of schizophrenia is unknown, but it is widely believe to be a neuro-developmental disorder related to an interaction between environmental risk factors and genetic susceptibility. Its symptoms vary with the individual patient; diagnosis is based on the individual's experiences, reported behaviour, and a clinical assessment by a health professional under the guidance of either the DSM-IV or the ICD-10. Generally speaking, the symptoms that individuals experience fall under the following categories:

- Positive symptoms – which add to normal experience, representing changes in behaviour or thought such as hallucinations or delusions.
- Negative symptoms – which subtract from normal experience, resulting in social withdrawal, poverty of speech, and a lack of motivation or pleasure with regards to ordinary activities.
- Cognitive symptoms – which result in an inability to sustain attention, an inability to absorb/interpret new information and make decisions based on that information, and poorer working memory.

Whilst there is no known cure for schizophrenia, it can be managed through the use of antipsychotic medications as well as psychological and social support (van Os and Kapur, 2009). Pharmacological treatment currently only works on the positive symptoms of the disorder, taking into account that a third of patients do not respond to treatment (Smith et al., 2010). In spite of this the cognitive and negative symptoms are considered to be implicated in the core pathology of this illness (Elvevag and Goldberg, 2000), whereby its symptoms are present throughout all

stages including adolescence (Davidson et al., 1999) and during the initial onset of psychosis (Saykin et al., 1994).

Whilst a comprehensive analysis of all the implicated brain regions and functional deficits in schizophrenia is beyond the scope of this review, this section focuses instead on the pathological and functional features surrounding some of the core cognitive symptoms such as impaired working memory. This review focuses on some of the pathological deficits surrounding the fronto-temporal brain regions that result in a reduced ability of these regions to transfer information both on a local and network scale, and its resulting implications in some of the primary cognitive symptoms of the disease.

### **1.5.1 Working Memory Deficits in Schizophrenia**

Working memory deficits in schizophrenia have long been observed in a wide range of cognitive tasks spanning the last 3 decades (for meta-reviews see Lee and Park, 2005, Forbes et al., 2009; see also Barch, 2005), and is widely considered to be one of the core neurological deficits of this disorder (Goldman-Rakic, 1994). Due to the heterogeneous nature of schizophrenia, as well as the variations in tasks that experimenters typically use to assess cognitive function, the exact nature and source(s) of these working memory deficits are yet to be elucidated. The first meta-analysis that specifically addressed this issue combined the results of 124 studies that focussed on working memory deficits in schizophrenia (Lee and Park, 2005). In this case whilst they had observed significant working memory deficits in all of the studies they assessed (across a wide range of experimental approaches), there was no significant prevalence of one particular working memory deficit over another (e.g. verbal vs. visuospatial). This suggested the possibility that a common mechanism to all working memory types may be implicated in schizophrenia. However they did observe that the visio-spatial working memory deficits were more consistent and robust than that of verbal working memory. A later meta-analysis which included a broader range of studies (187) also noted significant working memory deficits in 36 measures of phonological, visuospatial and central executive working memory.

However again, there were no clear differences between each of the working memory tasks or the working memory sub-domains, and the authors had noted in general a large heterogeneity across the results.

The lack of prevalence of one working memory deficit over another in schizophrenia suggests an aspect of the disorder which may be common to all working memory types; regardless of whether it is visio-spatial, verbal, etc. In the context of Baddeley's model of working memory (Baddeley, 1992; see also 1.4: Working Memory), the central executive component of working memory (involving manipulation and transformation of information in working memory) has been consistently and robustly implicated in these tasks (see Barch, 2005, Barch and Ceaser, 2012). The central executive functions in working memory have been linked to the activity patterns of the dorsolateral prefrontal cortex (dlPFC; Wager and Smith, 2003), which in turn have consistently shown abnormal activation patterns in schizophrenia (Callicott et al., 1999, Callicott et al., 2003, Weinberger et al., 1986, Barch et al., 2001, Wager and Smith, 2003; see also 1.5.2.1: Functional Changes in PFC Activity). Furthermore, numerous lines of evidence have found pathological changes in the prefrontal cortex of schizophrenia patients such as pyramidal and interneuronal cell changes (see 1.5.2.2 – 1.5.2.4) that can collectively serve to disrupt intra-cortical communication in this brain region. As such, the following sections highlight some of the findings that link pathological abnormalities with working memory deficits in schizophrenia.

## **1.5.2 Medial Prefrontal Cortex in Schizophrenia**

### **1.5.2.1 Functional Changes in PFC Activity**

There is perhaps no region more studied with regards to the negative and cognitive deficits than the prefrontal cortex (PFC). This is unsurprising, given its well-known role in executive functions. Executive function in this case refers to higher-order cognitive processes such as planning, attention, working memory, and task-switching. From a general perspective the results of this research to date suggest

extensive correlations between the cognitive/negative symptoms, and the pathology and functionality of the PFC.

In the past few decades a large number of experiments have looked at the activity of the dorsolateral prefrontal cortex (dlPFC) in schizophrenia patients during a working memory task. In healthy subjects, the activation of the dlPFC during a working memory task is well known (Callicott et al., 1999), and such tests to gauge working memory activity include the Wisconsin Card Sorting (WCS) test, the n-back test (at various levels), along with numerous forms of the Continuous Performance Task.

When schizophrenia patients are compared to healthy controls whilst performing a working memory task, a reduced activation in the dlPFC have been widely observed through a number of imaging modalities. An early study utilised Xenon Xe 133 inhalation procedures to study the regional cerebral blood flow in schizophrenia patients during a WCS test (Weinberger et al., 1986). Using 20 schizophrenia patients and 25 healthy controls, Weinberger and colleagues noted not only a reduced blood flow in the dlPFC of schizophrenia patients, but also that it was correlated with reduced cognitive performance on the task. This finding has been replicated repeatedly, with improvements in the techniques and variations in the tasks, e.g. [18F] fluro-deoxyglucose PET during an n-back working memory task (Carter et al., 1998). Successive refinements to these experiments have been made to allow for tighter control. For example Schroder et al., (1996) and later Potkin et al., (2002) grouped patients into separate clusters based on their symptoms subtypes, noting in both cases a reduced frontal metabolism in patients showing negative symptoms, whilst performing variations of the continuous performance task. Functional magnetic-resonance imaging (fMRI) has been used extensively to study cerebral blood flow changes between schizophrenia patients and healthy controls during working memory tasks. For example Barch and colleagues (2001) carried out an AX-continuous performance task using medication-naïve patients, showing a reduced activation of the dlPFC under conditions that required context processing, but also shown intact activation of the posterior and inferior PFC. Similarly, a reduced dlPFC activation was seen in medicated schizophrenia patients whilst performing multiple



levels of the n-back working memory task, noting in particular a deficit in the right dlPFC (Perlstein et al., 2001).

In many of the studies performed, the changes in dlPFC activation only became apparent at a certain threshold of working memory load. Furthermore, the correlation between task performance and activation of dlPFC is almost universal. There are however exceptions to this, as some studies have reported an increased activation in schizophrenia patients relative to controls during a working memory task. In two successive Steinberg Item Recognition Tasks utilising fMRI, Manoach and colleagues (1999; 2000), reported that not only did schizophrenia patients display an increased activation of the left dlPFC, but also that dlPFC activation was inversely correlated with task performance, in direct contradiction to (Weinberger et al., 1986). Despite their abundance, experiments of this nature have been subject to criticism based on their heterogeneity, as the subjects between each experiment often vary in age, sex, medication status, education, etc.; in addition to subtle test differences. Nonetheless, a later study attempted to probe this contradictory evidence further using a powerful 3T fMRI imaging modality – one which can discern finer cerebral blood flow changes than that used in the majority of experiments of this type. In this case Callicott and colleagues (2003) carried out an n-back working memory task using 14 schizophrenia patients and 14 matched controls. When the patients were grouped into high-scoring and low-scoring categories, they noted that whilst the low-scoring patients indeed displayed hypofrontality in the dlPFC, the high-scoring patients displayed separate locales of high and low activity in the same region. On lower resolution scanners this change would not be so apparent, leading the researchers to conclude that rather than working memory deficits manifesting strictly as a hypofrontality, it appears to display an overall altered neural activity pattern that points to a compromised ability of the dlPFC to handle information.

### **1.5.2.2 Reduced Somal Size and reduced Density of Dendritic Spines**

Imaging studies carried out using post-mortem schizophrenia subjects have revealed a reduction in the somal volume of dlPFC pyramidal neurons in deep-layer 3c (Rajkowska et al., 1998, Pierri et al., 2001). In particular, Pierri et al., (2001) noted that a 9.2% decrease in mean somal volume was not associated with either antipsychotic medication or treatment history. Interestingly reductions in the density of dendritic spines – a marker for the number of excitatory inputs to pyramidal neurons (DeFelipe and Farinas, 1992) has also been found in this same region (Garey et al., 1998, Glantz and Lewis, 2000, Broadbelt et al., 2002). Glantz and Lewis (2000) compared the basilar dendrites of Golgi-impregnated pyramidal neurons in the superficial and deep portions of dlPFC layer 3 using a 15 schizophrenic, 15 healthy, and 15 non-schizophrenic psychosis subjects. They observed a 23% reduction in dendritic spine density in the schizophrenia subjects compared to controls, which was significant in the deep but not superficial layer 3 of the dlPFC. Similar to the findings of Pierri et al., (2001) regarding mean somal volumes, this effect did not differ between medicated and non-medicated schizophrenia subjects either. Similarly in a later study Broadbelt et al., (2002) shown a significant decrease in the number of both primary and secondary basilar dendrites in layers 3 and 5 of the dlPFC.

Given the findings regarding abnormalities in layer 3 of the dlPFC, one would expect a deficit in cortico-cortical and thalamocortical communication, given its abundance of widespread excitatory connections with the rest of the dlPFC (Kritzer and Goldman-Rakic, 1995, Levitt et al., 1993). A reduced somal size highlights a reduction in afferent and efferent connectivity, since a neuron's size is correlated with the extent of the neuron's axonal and dendritic arbour (Jacobs et al., 1997). A loss of dendritic spines has been suggested to account for the loss of cortical volume in schizophrenia patients without the loss of neurons (Garey et al., 1998). Such a loss would have the effect of reducing the synaptic surface area of the neurons, effectively reducing its ability to transmit and receive information in a normal manner (Broadbelt et al., 2002).

### **1.5.2.3 Role of GABAergic Interneurons in Working Memory – and Evidence for Disruption**

When taking a closer look at the regions implicated in the working memory deficits in schizophrenia, a dysfunction of the GABA ( $\gamma$ -aminobutyric acid) system is seen to underlie many of the problems associated with the disease. Inhibition in the prefrontal cortex is largely mediated by the GABAergic interneurons that control and synchronise the firing of pyramidal cells. This regulation of pyramidal cell activity gives rise to the cortical oscillations and synchrony of brain regions that have been widely associated with proper working memory function. GABAergic interneurons have been shown to be directly responsible for task-related neuronal firing as well as spatial tuning during working memory tasks (Rao et al., 2000). In addition, working memory performance has been shown to be impaired by disrupting the GABA regulation by injection of bicuculline into the dlPFC of macaque monkeys (Sawaguchi et al., 1989).

There are many different types of GABAergic interneurons in the prefrontal cortex, but when looking at schizophrenia two in particular fall under the spotlight. Chandelier and basket interneurons both express the calcium-binding protein parvalbumin (Lewis and Lund, 1990, Conde et al., 1994), and inhibit pyramidal cells through fast-spiking action potentials (Gonzalez-Burgos et al., 2005). These fast spiking properties are widely believed to be the cause of gamma-band LFP in the prefrontal cortex. Chandelier cells synapse onto the axon initial segments of pyramidal cells (Somogyi, 1977), whereas basket cells project widespread terminals which synapse on the proximal dendrites and cell bodies of pyramidal cells (Lewis and Lund, 1990). In this way both types of interneurons are ideally placed to regulate the output firing of pyramidal cells.

### **1.5.2.4 Reduction in Parvalbumin and Neuron Count**

Numerous studies have revealed reductions in the prefrontal cortex of schizophrenia patients of mRNA which encodes for a GABA synthesizing enzyme, GAD67. An initial study by Akbarian et al., (1995b) used cell-counting methods which

demonstrated reductions in GAD67 of between 30-50% throughout the prefrontal cortex in schizophrenic post-mortem subjects, although the number of neurons expressing this mRNA had not reduced in number (Woo et al., 1997, Akbarian et al., 1995b). This finding has been consistently replicated (e.g. Volk et al., 2000, Guidotti et al., 2000) with reports of similar reductions in the GABA synthesizing enzyme. Volk et al., (2000) showed that whilst the expression level of GAD67 mRNA per neuron did not differ between schizophrenic and control subjects, the mRNA was indeed undetectable in 25-30% of GABA neurons. This led to further investigation by Hashimoto and colleagues (2003b) which revealed that GAD67 mRNA was undetectable in around 50% of parvalbumin-expressing interneurons. In addition to these findings parvalbumin-expressing mRNA itself was also found to be reduced in patients suffering from schizophrenia, again without a reduction in density of parvalbumin-expressing neurons (Hashimoto et al., 2003b). To summarise, this data points not to a reduction in the number of interneurons in the areas implicated in schizophrenia, but to a diminished ability of these neurons to express proteins vital for normal signalling functions. This reduction in interneuron functionality would ultimately reduce the inhibitory control over the pyramidal cell network, leading to a reduction in the coordination of neural networks.

### **1.5.3 The Hippocampus in Schizophrenia**

Many of the earlier reports regarding the hippocampus in schizophrenia highlight a reduction in volume, as observed with MRI techniques (Nelson et al., 1998), which is more often reported in the left hemisphere in first-episode schizophrenic patients (Velakoulis et al., 2006). This latter study pointed out that structural changes in the hippocampus were not evident in patients with an ultra-high risk of psychosis, suggesting that the changes were mediated at the onset of psychosis. The shape of the hippocampus however has seen contradictory evidence in the literature, with MRI studies pointing to significant abnormalities in the tail (Styner et al., 2004), and the head (Csernansky et al., 2002) region in schizophrenic patients, although the latter study suggests that a deformation of the head may correlate with abnormalities in the neurons that project to the frontal cortices.

Hippocampal neurons are generally found to be smaller in varying regions across the structure, with no clear pattern emerging throughout the studies (Arnold et al., 1995, Benes et al., 1991). However the pyramidal neurons in the CA1 area seem to be affected in all studies, which is itself a subfield of the hippocampal region that maintain the afferent and efferent connections between the hippocampus and cortical and subcortical structures. Benes et al. (1991) further notes a reduction in pyramidal neurons in this same region when compared to healthy controls, although generally speaking neuronal density studies have so far been largely equivocal, as this evidence is contrary to more recent studies (Walker et al., 2002). Likewise conflicting reports are also seen in the literature with regards to cell neuronal orientation, with studies showing a presence of cell disorganisation (Conrad et al., 1991), and those that suggest otherwise (Benes et al., 1991).

Deficits in the GABAergic interneurons are present in the hippocampus, as revealed by a reduction in parvalbumin containing interneurons (Konradi et al., 2011, Eyles et al., 2002, Torrey et al., 2005). A recent study highlighted that whilst the levels of parvalbumin-positive interneurons were reduced in the CA1 and CA4 regions, parvalbumin mRNA shown significant reductions in the CA2 region (Konradi et al., 2011).

#### **1.5.4 The Thalamus in Schizophrenia**

The thalamus is a brain structure that is situated between the cortex and midbrain, and consists of several anatomically and functionally distinct regions, each of which are implicated in various roles. Although it has been traditionally difficult to measure the activity of individual regions in human studies, the thalamus has nonetheless become of great interest in the study of schizophrenia. It acts to relay signals to a variety of brain structures including the prefrontal, cingulate and temporal cortices - all areas in which abnormalities are observed in schizophrenia. Whilst metabolic reductions and volume changes are widely observed in the thalamus, the confounding interpretation of thalamus size can only perhaps illustrate the heterogeneous nature of the disease, as suggested by various researchers. Decreases

in the total thalamic volume (Chua et al., 2007, Andreasen et al., 1994) have been seen, as well as significant increases (Corey-Bloom et al., 1995). In addition combined MRI and PET studies have found metabolic reductions in the thalamus (Buchsbaum et al., 1996), particularly shown in the right thalamus.

#### **1.5.4.1 Diminished Frontal Connectivity with the Mediodorsal Thalamic Nucleus**

One nucleus in the thalamus of particular interest is the mediodorsal thalamic nucleus (MD), both for its pathological changes observed in schizophrenia and its known involvement in thalamocortical circuits. This structure receives afferents from the prefrontal and limbic system, and in turn projects back to the frontal regions. Although the volume of the MD have been reported to be significantly decreased (Shimizu et al., 2008, Young et al., 2000), reports of reduced number of neurons are conflicting (see Dorph-Petersen et al., 2004 for a review). Metabolic rates as measured using  $^{18}\text{F}$ -deoxyglucose PET and MRI imaging modalities in schizophrenia patients reveal a significantly lower glucose metabolism compared with healthy controls, which are correlated with both negative and positive symptoms (Hazlett et al., 2004, Andrews et al., 2006). Furthermore this same technique has revealed a metabolic disconnection in the left hemisphere of schizophrenia patients between the MD and fronto-temporal cortical regions (Mitelman et al., 2005).

Many of the thalamocortical connections originate in the MD and terminate in the PFC, particularly in the dlPFC. The connecting white matter has recently been looked at using fibre-tracking techniques, with the results suggesting a significant reduction in the cross-sectional area of the left anterior thalamic peduncle (Kito et al., 2009). A resulting reduction in the glutamatergic drive to the PFC supports the 'hypofrontality' hypothesis, which is derived from reports of reduced frontal metabolism in schizophrenia patients as previously discussed. A number of lines of evidence support this, firstly in studies in non-human primates which have demonstrated the necessity of thalamocortical connections that terminate in the

dIPFC during working memory tasks (Leichnetz, 1989). Second, the dPFC layer-3 pyramidal neurons are known to be located at the termination zone of axon projections that arise from the MD (Giguere and Goldman-Rakic, 1988), which in this case are glutamatergic efferents. As mentioned earlier many prefrontal cortex changes in schizophrenia such as a reduced density of dendritic spines focalise on this region.

### **1.5.5 EEG Changes in Schizophrenia**

Analysis of the electroencephalogram (EEG) in schizophrenia patients has shown widespread power and coherence changes in various frequency bands in multiple brain regions. Despite the abundance of information from studies utilising scalp EEG electrodes, a large amount of confounding information is present which perhaps results from the heterogeneous nature of these experiments, particularly regarding the myriad of variables such as age, symptoms and medication status. Nonetheless a recent meta-analysis combining over 50 of these studies suggested that an increased low-frequency EEG power during the resting state is a robust finding within medicated and non-medicated patients (Boutros et al., 2008). Indeed this finding has been suggested to a robust enough measure to qualify as one of the diagnostic criteria for schizophrenia (Boostani et al., 2009).

In schizophrenia patients, the gamma band of frequencies shows reductions in power spectral density, both during resting state (Rutter et al., 2009), and during working memory tasks (Haenschel et al., 2009, Schmiedt et al., 2005, Cho et al., 2006). Haenschel et al., (2009) for example carried out a delayed non-match to sample task using 14 early-onset schizophrenia patients and matched controls, and revealed abnormalities in multiple frequency bands during each phase of the task, including reduced theta and gamma power during retrieval (Haenschel et al., 2009). In addition, reductions in cortical gamma-band synchronisation have been observed during working memory tasks, and have been correlated with the negative (Lee et al., 2003, Spencer et al., 2004), and cognitive symptoms (Schmiedt et al., 2005, Cho et al., 2006) of schizophrenia. Given that the power of gamma band oscillations in the

prefrontal cortex is correlated with working memory load (Howard et al., 2003), it is of little surprise that many of the studies reporting gamma-band deficits in schizophrenia patients also show correlations with poor task performance.

The deficits in the power and synchrony of schizophrenia EEG activity can in part be attributed to the pathological deficits associated with the interneurons in the brains of schizophrenia individuals. Fast-spiking parvalbumin-containing basket cells are able to generate a narrow window for excitation, resulting in neural ensemble synchrony, and hence gamma oscillations (Bartos et al., 2002, Buzsaki et al., 1983, Whittington et al., 1995). An *in vitro* optogenetic study has demonstrated this relationship by amplifying gamma signals through activation of the parvalbumin-containing GABAergic interneurons (Sohal et al., 2009). This is loosely supported by evidence revealing that the decay period of currents produced by postsynaptic parvalbumin-containing basket-cell receptors are in line with the period of gamma oscillations (Gonzalez-Burgos and Lewis, 2008). Furthermore, basket cell firing in the hippocampus is strongly phase-locked to the local gamma oscillation (Gulyas et al., 2010).

Given the ability of GABAergic interneurons to synchronise neural networks, one would expect the functional connectivity between brain regions to be diminished, and several lines of evidence support this in studies using schizophrenia patients. Where global connectivity is concerned, many of the observed power changes in the EEG frequency bands are often accompanied by corresponding reductions in theta coherence (e.g. Koenig et al., 2001). Earlier reports combined recordings throughout the brain in first-episode schizophrenia patients and found increased EEG dimensionality and complexity (Koukkou et al., 1993; Saito et al., 1998) – which highlights an increased independence of activity in the measured brain regions. This evidence has given rise to a ‘disconnection hypothesis’, which supports the idea that a loss of synchronisation in the EEG of separate brain regions mirrors a diminished ability of neural networks to organise and synchronise information in schizophrenia (Liddle, 1996, Andreasen, 1997, Friston and Frith, 1995).



Lastly, some of the most well-known deficits in the EEG of schizophrenia patients revolve around event-related potentials (ERP's). These are transient deflections in the EEG signal which are produced in response to a certain event, such as a thought or perception that has been invoked directly by the experimental setup. By far the most researched ERP in schizophrenic EEG studies is the P300 component - a wave which is generated 300ms following an unusual target stimulus. Whilst this wave itself is made up of two components (smaller waves called P3a and P3b component signals or wavelets), the majority of studies have focussed on the P300 in its entirety. These experiments are often performed via the 'oddball' paradigm, in which the subject is required to discriminate the target stimuli from a random mix of target and non-target stimuli (e.g. a frequently occurring high-pitched tone with a background of medium-pitched tones; Picton, 1992, Polich, 1998). Whilst the stimulus in this case can take a number of different modalities, an audio stimulus through the 'oddball' paradigm has consistently produced the strongest P300 responses (Ford, 1999). Despite the large number of results showing methodological differences that could easily account for the discrepancies such as age, gender and drug treatment (Bramon et al., 2004), two meta-analysis performed within a year of each other confirm that the P300 wave shows both a reduction in amplitude, as well as an increased latency from the stimulus event (Bramon et al., 2004, Jeon and Polich, 2003). Furthermore, Jeon and Polich (2003) mentions that whilst the P300 latency effect is more pronounced with longer durations of schizophrenia, both its amplitude and latency are unaffected by psychopathology severity and antipsychotic medications. With this in mind, much of the current research focuses on locating the P300 wave locus, and commonly that of its P3b component, as well as its functional and pathological implications.

### **1.5.6 Candidate Brain Regions for DBS in Schizophrenia**

Deep-brain stimulation (DBS) is proving to be a promising alternative treatment option for neuropsychiatric disorders, particularly where other treatment options prove ineffective (see 1.3.3: Applications of DBS for Non-Motor Related Neuropsychiatric Disorders). Using this tool for the treatment of schizophrenia has

only recently been explored. The pathological and functional changes in schizophrenia are not so straight-forward or completely understood, with many brain systems purported to be affected to varying degrees. Nonetheless, one can integrate knowledge gained from the neural systems affected in schizophrenia, the mechanisms of action of DBS, and previous studies based on the stimulation of brain regions; to provide hints that can drive forward this research. The following literature examines a number of candidate brain regions which may be of interest for the treatment of schizophrenia using DBS.

#### **1.5.6.1 Thalamic Reticular Nucleus (TRN)**

The thalamic reticular nucleus (TRN) is a thin layer of parvalbumin-containing GABAergic cells that sits between the cortex and the thalamus, and acts to modulate thalamocortical information flow through its extensive GABAergic efferents to the thalamus and thalamocortical axons. It consists of 7 sectors (5 sensory, 1 motor, 1 limbic), which receives excitatory afferents from corresponding cortical and thalamic neurons, and projects back to the thalamic nuclei by which it's innervated, giving it an organised topographic structure (see Pinault, 2004, Ferrarelli and Tononi, 2011, for a review). Whilst the majority of cells in the TRN project to thalamocortical neurons, 10% of its cells are GABAergic interneurons, which act through a process known as lateral inhibition to amplify relevant inputs and suppress distractor stimuli (Deschenes et al., 2005; see also figure 1.6). This regulation of attention has been likened to an “attentional searchlight” (Crick, 1984), because of the ability of the TRN to rapidly move the centre of attention between external inputs, based on a decision made by the prefrontal cortex.

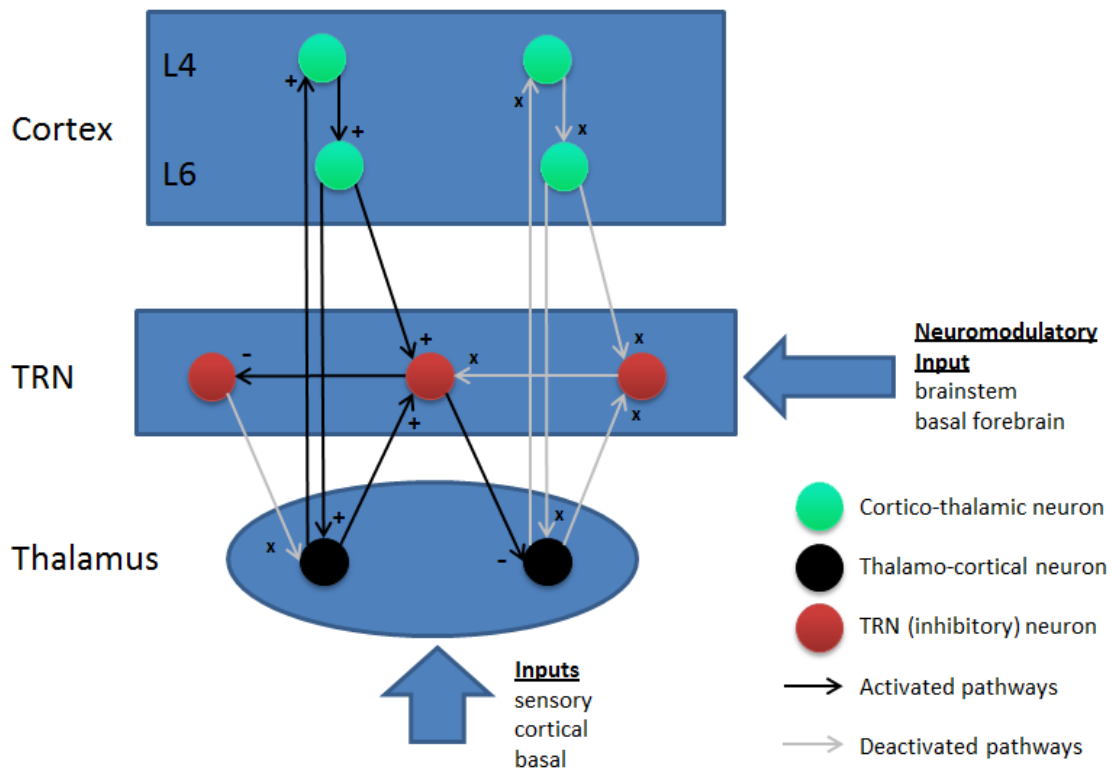


Figure 1.6 – A proposed function for the thalamic reticular nucleus (TRN), and how it is proposed to amplify thalamic inputs. Thalamo-cortical projection neurons may activate TRN inhibitory neurons, which in turn deactivates surrounding thalamocortical neurons, in a process known as “lateral inhibition” (Deschnes et al., 2005). Similarly TRN neurons are believed to influence each other via GABAergic synapses, which elicits a “disinhibition” of the activated thalamocortical neuron (Pinault, 2011). This effect ultimately leads to an increased contrast of thalamo-cortical communication, as relevant inputs are amplified and distractor inputs are suppressed. In the diagram inhibitory pathways are those originating from the TRN neurons, whilst all other pathways shown are excitatory. Diagram adapted from (Pinault, 2011, Ferrarelli and Tononi, 2011). See text for further details.

Inputs to the TRN from thalamocortical or corticothalamic afferents mediate a local effect of inhibition, whereas cholinergic inputs from neuromodulatory systems including the brainstem and basal forebrain (Hallanger et al., 1987, Morrison and Foote, 1986) have a more global effect (Guillery and Harting, 2003). Their effect is to hyperpolarise thalamocortical neurons (Kim et al., 1997). It has been noted that the thalamocortical and corticothalamic neurons that innervate the TRN outnumber the TRN neurons (Buzsáki, 2006), which perhaps allows it to perform tasks in an environment with competing sensory inputs.

Given its well-known functions in gating sensory inputs, the TRN has been hypothesized to play a major role in sensory processing and attention (Guillery et al., 1998, Mayo, 2009, McAlonan et al., 2008, Rees, 2009). Of particular note, the prefrontal cortex, which is an area crucial for attention (Zikopoulos and Barbas, 2007), differs with the other cortico-TRN projections in that its axons terminate in the anterior, central and posterior parts of the TRN, overlapping with projections from sensory association areas (Zikopoulos and Barbas, 2006). These projections include a significant proportion of large boutons (Zikopoulos and Barbas, 2006), which have been associated with driver inputs (Guillery and Sherman, 2002). Furthermore, the mediodorsal thalamic nucleus (MD) – which is the main thalamic nucleus which connects to the prefrontal cortex – has connections to the TRN which cover the anterior three quarters of the structure, at sites that also receive projections from area 46 (Zikopoulos and Barbas, 2006). Area 46 is known to have a key role in working memory, and this pattern of circuitry has been suggested to affect sensory processing at early stages throughout the thalamus (Zikopoulos and Barbas, 2007). Finally, the TRN is also known to be a pacemaker of sleep spindles, given its ability to generate these oscillations in isolation (Fuentelba and Steriade, 2005).

Changes in the rat TRN can be seen through the NMDA receptor antagonist phencyclidine (PCP; Cochran et al., 2002, Cochran et al., 2003, Olney et al., 1991, Sharp et al., 2001), the latter of which has also shown to produce attentional-set shifting deficits in rodents (Egerton et al., 2005). In addition, ketamine has been found to block thalamocortical rhythmicity (Buzsáki, 1991). Generally speaking an

NMDA receptor hypofunction occurs in schizophrenia; and in the TRN this may be predicted to have the effect of a decreased ability of the GABAergic reticulo-thalamic afferents to modulate thalamocortical neurotransmission (Sharp et al., 2001). In this sense, in addition to attentional deficits resulting from reduced inhibitory control, TRN hypofunction has been linked to psychotic symptoms via a resulting overactivity of the cortex (Ferrarelli and Tononi, 2011).

DBS of the TRN could mediate its actions through an inactivation of the target nucleus, along with activations of efferent targets of the TRN. The resulting increased global output of this structure could have an effect similar to that of its neuromodulatory inputs, which can perhaps counter the hypofunction that results in schizophrenia or NMDA receptor antagonists such as PCP. Indeed stimulus-induced activation of neuromodulatory systems in nearby regions of the thalamus (in rats) have been explored as a way of causing a global non-specific effect, resulting in cognitive enhancement (Mair et al., 2011). Low-frequency stimulation of this structure has been carried out in rats in a T-maze (Andrade et al., 2010), which had subsequently revealed reductions in 8-OH-DPAT-induced perseverative behaviours. Given that the TRN is a thin structure, there may inevitably be difficulties in successfully positioning DBS electrodes to a correct depth to mediate its effects, particularly when novel electrodes and surgical techniques are used. Furthermore, electrical stimulation is likely to mediate strong effects in adjacent nuclei, with different effects expected depending on the exact location of the electrodes in the TRN.

#### **1.5.6.2 Mediodorsal Thalamic Nucleus (MD)**

The mediodorsal thalamic nucleus (MD) is ideally placed in the brain to functionally connect a diverse array of cortical and subcortical structures. This structure has become of great interest to research into the cognitive deficits in schizophrenia, since it is the primary thalamic nucleus that projects to the prefrontal cortex. In humans and other primates, the majority of the MD glutamatergic output is projected reciprocally throughout the prefrontal cortex (figure 1.7; Akert and

Hartmann-von Monakow, 1980), whereby it acts as a relay station to functionally link multiple prefrontal regions (Groenewegen et al., 1990, McFarland and Haber, 2002). It also receives GABAergic innervation from the ventral pallidum through pathways that involve the prefrontal cortex, nucleus accumbens, and the thalamic reticular nucleus (see Pakkenberg et al., 2009). Whilst the MD can be split up into three distinct regions, of particular interest is the dorsolateral parvocellular region, because of its reciprocal connections with the dorsolateral prefrontal cortex and anterior cingulate cortex (see Pakkenberg et al., 2009); both areas of which are heavily implicated in the negative and cognitive pathology of schizophrenia.

The functions of the MD are varied and are thought to involve visual object recognition, and stimulus and reward mechanisms, as well as certain memory processes (see Alelu-Paz and Gimenez-Amaya, 2008 for a review). In humans and other primates, the MD shows an activation in tasks that tax memory and attention (Krasnow et al., 2003, Burgess et al., 2003, Buchsbaum et al., 1996, Clark et al., 2001), and has been suggested to be involved in the first phases of information processing for learning and memory (Jones, 2007). In rats, the role of the MD in spatial working memory has shown some correlations through lesion studies (Stokes and Best, 1988, Stokes and Best, 1990), but later studies have failed to support this (Hunt and Aggleton, 1998). In this latter case whilst spatial working memory wasn't affected directly by MD lesions, there were other processes related to task performance that were affected, such as a change in activity and exploration levels. The prefrontal cortex is well-known to be involved heavily in executive function, and lesions in the MD-PFC circuit has resulted in alterations in several higher cognitive functions (Cummings, 1995).

There have been confounding reports of anatomical alterations regarding the size of the primate MD using both neuroimaging (Hazlett et al., 1999, Byne et al., 2001, Kemether et al., 2003) and post-mortem material from the schizophrenia brain (Pakkenberg, 1992, Cullen et al., 2003, Young et al., 2000, Byne et al., 2002, Danos et al., 2003, Danos et al., 2005). One possible reason for the disparity may be the difficulties in establishing the neuroanatomical limits of the MD, as suggested by Alelu-Paz and Gimenez-Amaya (2008), in addition to the heterogeneous nature of

the disease. There have been reports of a reduced neuronal count (Pakkenberg, 1990, Pakkenberg, 1992, Young et al., 2000), although once again this is disputed, with some reports finding no significant change in cell number (Dorph-Petersen et al., 2004, Cullen et al., 2003). Generally speaking, even though the changes are small, the majority of evidence seems to point towards a reduced overall thalamic volume in schizophrenia relative to brain size (Cronenwett and Csernansky, 2010). A PET study in never-medicated patients shown a significantly lower [18F] deoxyglucose metabolism in the region of the MD when compared to controls, which was found to reduce with the increasing severity of the negative symptoms (Hazlett et al., 2004).

Given the dense thalamocortical projections originating from the MD and terminating in the PFC, much attention has been turned to the function of this circuit in schizophrenia patients. In fact imaging studies have revealed a physical disconnection, using magnetic-resonance-imaging (MRI; Kito et al., 2009), as well as PET (Mitelman et al., 2005), in the brains of schizophrenia patients when compared to healthy controls. Using diffusion tensor imaging (an MRI modality which measures diffusion of water molecules), a lower functional anisotropy has been found in the white matter connecting the dorsolateral PFC to the thalamus in both bipolar and schizophrenia patients as compared to healthy controls (Sussmann et al., 2009), thus providing further evidence of white-matter tract changes in this disease.

Hypofrontality is a widely reported feature of schizophrenia in which a reduced metabolism is seen across the frontal regions during working memory tasks, although this response appears to be dependent on task demands and is currently the subject of debate (Manoach et al., 1999, Manoach et al., 2000). One may postulate that a contributing factor to the hypothesised hypofrontality of cortical regions is a glutamatergic signalling deficit from the MD – the primary thalamic glutamatergic input to the PFC. Studies in non-human primates have revealed that working memory tasks require the use of the thalamocortical connections that terminate at the dlPFC. These thalamocortical axons terminate in layer-3 of the dlPFC, where pyramidal neurons are known to be located (Giguere and Goldman-Rakic, 1988). This termination site has shown to feature neuro-anatomical changes in schizophrenia patients including a reduction in the somal size (Pierri et al., 2001)

and the density of dendritic spines (Garey et al., 1998, Broadbelt et al., 2002, Glantz and Lewis, 2000; see also 1.5.2.2: Reduced Somal Size and Reduced Density of Dendritic Spines). The reduction in soma size can perhaps be attributed to a reduction in the synaptic density, and would support hypothesis suggesting that dlPFC dysfunction is attributable to both thalamocortical and cortico-cortical connections. Rajkowska and colleagues (1998) in particular noted that the greatest reductions occur in sub-layer 3c – the site of the otherwise largest cortico-cortical projection neurons.

Studies involving deep-brain stimulation of the MD have been carried out recently in a rat model of cortical seizure (Takase et al., 2009), and to study its effects on rats with schedule-induced polydipsia (van Kuyck et al., 2008), both of which found no significant differences with stimulation. Excitatory electrophysiological responses have been found in the prefrontal cortex following electrical stimulation of the mediodorsal thalamic nucleus (Pirot et al., 1995, Gigg et al., 1992, Ferron et al., 1984). These excitatory responses are suggested to arise from two mechanisms: direct stimulation of thalamocortical pathways, and through the recurrent collaterals of antidromically driven corticothalamic neurons (Pirot et al., 1995). Work which looks at the MD-stimulation-induced metabolism changes have only been done recently with promising results (Ewing et al., 2013b). In this case a significant increase in the immediate early gene *c-fos*-268 – a marker for neuronal activity – was found following acute stimulation of the MD. In addition, activation of the MD by microdialysis means have shown increases in *c-fos* activity in the prefrontal cortex (Bubser et al., 1998, Erdtsieck-Ernste et al., 1995). In both cases the GABA $\alpha$  receptor antagonist bicuculline-methyl chloride was injected into the MD, whereby a rapid *c-fos* increase in the frontal regions followed.



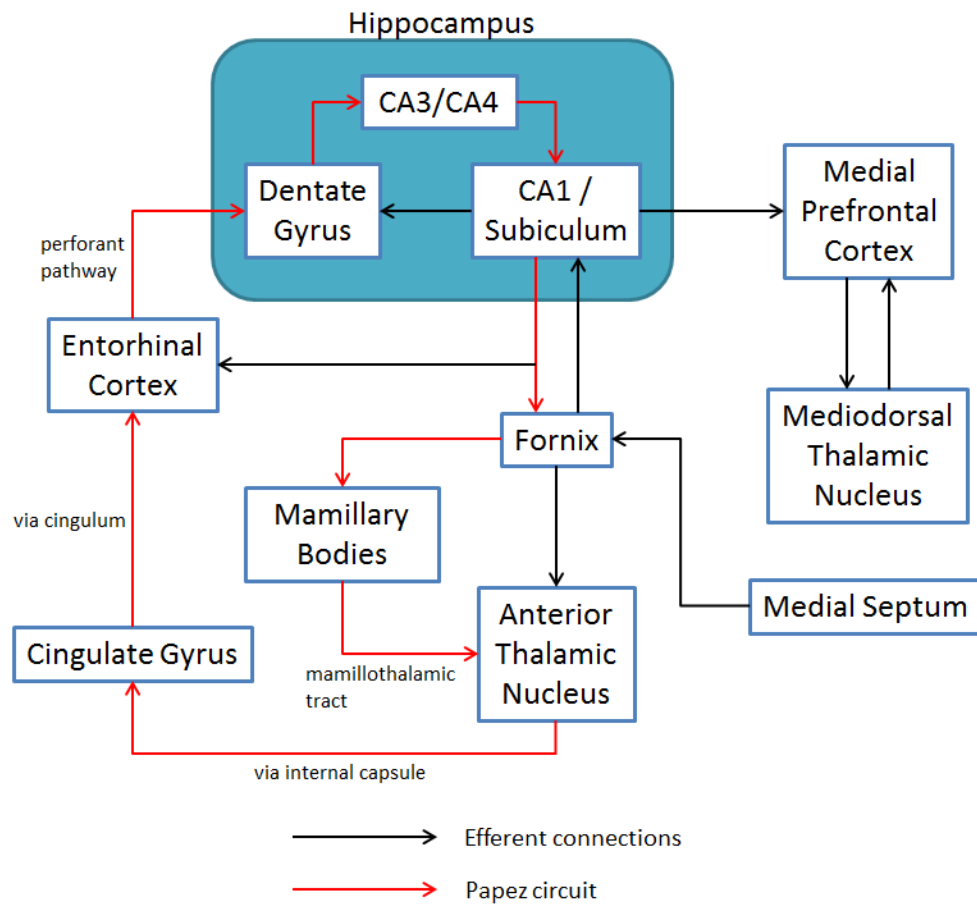


Figure 1.7 – Simplified interpretation of Papez’s circuit along with the medial prefrontal cortex, mediodorsal thalamic nucleus, and medial septum. Red arrows link various limbic structures described by Papez (1937) which have recently been suggested to have a significant involvement in mnemonic functions including spatial working memory. Many structures in this circuit have undergone investigation with their relevance to working memory, and a few recent stimulation studies have been promising. Diagram adapted from (Augustinack et al., 2010).

### 1.5.6.3 Anterior Thalamic Nucleus

The anterior thalamic nucleus (ATN) consist of the anteromedial, anteroventral, and anterodorsal nuclei, and collectively play important roles in learning and memory. In addition, it makes up a major structure in Papez's circuit – a limbic brain circuit strongly linked with memory and emotions (Papez, 1937; see also figure 1.7), and more recently, with mnemonic functions. The ATN is reciprocally connected with the cingulate and paracingulate gyri, and sends efferent tracts to the hippocampus. In turn it receives monosynaptic afferents from the hippocampus via the mammillary bodies (see Byne et al., 2009 for a review), thus forming the “extended hippocampal system”.

Lesions of the ATN have been found to result in spatial working memory deficits in the T-maze (Aggleton et al., 1996, Aggleton et al., 1995, Warburton and Aggleton, 1999), radial arm maze (Byatt and Dalrymple-Alford, 1996, Aggleton et al., 1996) and Morris water maze (Warburton and Aggleton, 1999). It has been noted that whilst tasks that use allocentric cues (external directional cues) are impaired, tasks which utilise egocentric cues (directional cues related to body position) remain relatively unaffected through ATN lesions (Aggleton et al., 1996, Sziklas and Petrides, 1999, Warburton et al., 1997). These effects are generally more pronounced for bilateral disconnections between the hippocampus and ATN, rather than unilateral (Warburton et al., 2000a). Activity of the immediate early gene *c-fos* has been shown to increase during spatial working memory tasks in rats in various structures including the ATN and the hippocampus (Vann et al., 2000). Following a lesion to the ATN, a hypoactivity has been shown in all structures linked to spatial working memory including the dorsal and ventral hippocampus, retrosplenial cortex, anterior cingulate cortex, as well as the prelimbic cortex (Jenkins et al., 2002). Furthermore blocking of *c-fos* expression in the CA3 region of the hippocampus – an area with extensive reciprocal ATN connections - has also been found to impair spatial working memory in the radial-arm maze (He et al., 2002).

Clearly the functional cooperation between the ATN and hippocampus, as well as other structures in Papez's circuit is essential for successful spatial working memory performance (Tsanov et al., 2011b, Ward-Robinson et al., 2002, Henry et al., 2004).

Electrophysiological recordings in the ATN have revealed that a large population of its cells oscillate in the theta-frequency range and is strongly synchronous with hippocampal theta (6-12 Hz; Vertes et al., 2001, Tsanov et al., 2011a). This same theta-oscillatory activity is seen in other structures in Papez's circuit, including the pacemaking cells of the medial septal nucleus (Bland, 1986, Vertes and Kocsis, 1997), and the mammillary bodies (Aggleton et al., 2010). This data combined suggests that a theta-rhythmic signal may resonate throughout Papez's circuit which is involved in the memory processing functions of this network. It has also been suggested that synchronization of brain regions with hippocampal theta facilitates the strengthening of memory traces (Tsanov et al., 2011b), similar to that seen between e.g. the hippocampus and amygdala during fear conditioning (Seidenbecher et al., 2003). One of the contributing features the ATN is thought to provide to spatial working memory processing is information based on the animal's heading through its so-called 'head-direction' cells (Blair and Sharp, 1995, Taube, 1995, Taube et al., 1996). These cells have been shown to fire rhythmically with ATN theta (Tsanov et al., 2011a), thus encoding the animal's directional heading in the horizontal plane (Taube et al., 1990).

Investigations into the morphological changes of the thalamus in schizophrenia have been confounding (e.g. Andreasen et al., 1994, Chua et al., 2007, Corey-Bloom et al., 1995), owing perhaps to the heterogeneity of the disorder. A better insight can be gained by looking at the individual thalamic regions and its sub-regions. Significant morphological abnormalities have been seen in the anterior thalamic nucleus of schizophrenia patients (Hazlett et al., 1999), as well as a reduced anterior thalamic area (Buchsbaum et al., 1996). Further insight into the changes in schizophrenia can be seen through histopathological studies, whereby a reduction in the total number of neurons in the anteroventral and anteromedial nuclei have been observed (Young et al., 2000). The anteroventral nucleus – which is reciprocally connected with the hippocampal region and the cingulate cortex (Amaral and Cowan, 1980) has shown a reduction in parvalbumin-containing thalamocortical projection neurons in antipsychotic-treated schizophrenia patients (Danos et al., 1998).

Measurements of mean diffusivity using MRI has revealed increases in both the MD and the ATN (Rose et al., 2006). It is well documented that signalling deficits occur in parvalbumin-containing GABAergic interneurons throughout the cortex in schizophrenia patients (see 1.5.2.3: Role of GABAergic Interneurons in Working Memory – And Evidence for Disruption), however in the anteroventral nucleus the parvalbumin-containing neurons are cortically-projecting relay neurons (Danos et al., 1998). Interestingly, Dixon and Harper (2004) noticed that the GABAergic interneurons of the ATN does not show a reduction in schizophrenia patients as compared to healthy controls. Unlike the interneurons of the prefrontal cortex, the GABAergic interneurons in the AT does not contain parvalbumin. This reduction in cortically projection neurons perhaps highlights a similar disconnection to the frontal cortices as is well documented with the MD (e.g. Kito et al., 2009, Mitelman et al., 2005). Finally, in schizophrenia patients a diminished thalamic metabolism in the anterior region of the thalamus has been observed (Buchsbaum et al., 1996, Katz et al., 1996), and a more recent study has found a reduced task-related activation in the same structure (Andrews et al., 2006).

Despite a clear role of the ATN in cognition, deep brain stimulation of the ATN has seen its biggest application in epilepsy (Lee et al., 2006, Hodaie et al., 2002), owing to its ability to reduce seizures. Given the role of the ATN in working memory, mixed results have been seen in patients that are assessed for cognitive performance. Whilst (Fisher et al., 2010) noted a transient memory dysfunction, Oh et al., (Oh et al., 2012) reported a cognitive improvement in verbal memory, a year after surgery. In the latter case this improvement was purported to be based on activation of the limbic “memory circuit” and the associated thalamo-cortical pathway. Indeed memory enhancement has been seen through stimulation of other limbic regions involved in working memory, such as the fornix (Hamani et al., 2008), medial septum (Lee et al., 2013), the entorhinal cortex (Suthana et al., 2012), (see also 1.5.6.4: Fimbria-Fornix) and the ventral hippocampus (Perez et al., 2012; see also 1.3.3.6 for a discussion on schizophrenia studies using DBS). One of the effects of DBS is believed to involve orthodromic and antidromic stimulation of fibres projecting to and from the target nucleus, resulting in a modulation in the activity of

surrounding regions (see 1.3.1: DBS Mechanisms of Action). Bilateral but not unilateral stimulation of the ATN in rats has been found to cause increases and decreases in the metabolism of several connected brain regions in rats (Gao et al., 2009). In this case high-frequency stimulation (100Hz, 100 $\mu$ S, 150-300 $\mu$ A) resulted in increases in glucose uptake in the ATN, thalamus and hippocampus, whilst showing reductions in the cingulate cortex and frontal cortex. Whilst this 'deactivation' of the frontal cortex is contradictory to the epilepsy study by Oh and colleagues (2012), it should be noted that in most DBS studies the outcome can vary widely with the stimulation parameters used. In attempting to elucidate this issue, Hamani et al., (2010) found that rats were impaired on a spatial memory task for high currents of 500 $\mu$ A, along with a 32% reduction in hippocampal dentate gyrus (DG) firing. Interestingly, these spatial deficits were not seen at 100 $\mu$ A, and a slight but significant (9%) increase in neuronal firing was reported at this intensity for the same brain region measured. The mechanism by which the behavioural impairments at high current were believed to occur was through a depolarisation block (Hamani et al., 2010). It is easy to imagine a brain region deactivating with a high current intensity, as this case is not only well documented throughout DBS studies but also forms one of the underlying rationales for DBS of subcortical structures in the treatment of Parkinson's disease.

#### **1.5.6.4 Fimbria-Fornix (FF)**

The fimbria-fornix (FF) is a system of white-matter tracts situated along the lateral and anterior edges of the hippocampus, and serve to provide a major route for afferent and efferent connections to and from the hippocampus (Andersen, 2007). The hippocampus is connected to various subcortical regions including the ATN, medial septum and mammillary bodies, via the FF (Amaral and Witter 1995; see also figure 1.7). Lesion studies dating back 30 years have consistently shown the FF to play a vital role in tasks that require spatial working memory (e.g. Buzsaki et al., 1982, van der Staay et al., 1989, Walker and Dolton, 1984, Galani et al., 2002). For example, Buzsaki et al., (1982) demonstrated that lesions to the FF in animals resulted in severe spatial working memory deficits.

Being a major conduit for information passage within limbic structures vital for working memory, numerous lesion studies in rats have focussed on the functional cooperation between various structures via the FF pathway. Notable examples of these have looked at fornix-dependent connectivity between the hippocampus, the ATN (Okada and Okaichi, 2006, Warburton et al., 2000b) and the medial septum (Okada and Okaichi, 2010). Warburton et al., (2000b) studied the effects of ipsilateral and contralateral FF/ATN lesions in rats that underwent object recognition, object location, and T-maze alternation tasks. Whilst the lesioned groups were not impaired in the object recognition tasks, animals featuring contralateral FF lesions had shown severe impairments in the T-maze task, with mild impairments shown for groups with ipsilateral and contralateral FF/ATN lesions. A similar study carried out later on had shown similar results, in which contralateral (but not ipsilateral) FF/ATN lesions resulted in deficits in spatial learning and spatial recognition tasks (Okada and Okaichi, 2006). The same group had later carried out ipsilateral/contralateral lesions in the medial septum and hippocampus, in rats that subsequently underwent unreinforced and reinforced learning tasks that required spatial working memory (Okada and Okaichi, 2010). Compared to the ipsilateral lesion groups, they had found that rats with contralateral medial-septum / hippocampus lesions were impaired on both types of tasks regardless of the presence of reward.

Much of this evidence suggests a vital role in the FF in mediating spatial working memory function by facilitating the functional connectivity between the hippocampus and other structures known to be involved in spatial working memory, such as the medial septum and anterior thalamus. The medial septum is known to be involved in the generation of theta activity in the hippocampus (Lee et al., 1994, Hasselmo et al., 2002), which in turn is correlated with behaviours such as locomotion, spatial exploration, and learning (Green and Arduini, 1954, Vanderwolf, 1969; see also 1.4.4.1 Theta Oscillations). Thus disconnecting the main connectivity between these structures can diminish performance in tasks that require the functional cooperation of these structures.

Changes that occur in the fornix in schizophrenia have only come to light in the past decade or so, following advances in MRI imaging modalities such as diffusion tensor imaging (DTI; Basser, 1995). This allows for an opportunity to study white matter features such as mean diffusivity and fractional anisotropy (FA), which together can highlight changes in the density and coherence of fibres, as well as water content and molecule movement. This, in turn can point to pathological changes such as axonal degradation or demyelination, in addition to information traditionally provided by MRI such as the volume of brain regions (see Kuroki et al., 2006, for further explanation). As such numerous studies which have employed this technique (or variants thereof) have highlighted reductions in the integrity of the fornix white-matter tracts, both in chronic (Kubicki et al., 2005, Kuroki et al., 2006, Nestor et al., 2007, Takei et al., 2008, Abdul-Rahman et al., 2011) and in first-episode (Luck et al., 2010) schizophrenia patients. Kuroki et al., (2006) used DTI to observe fornix integrity differences between chronic schizophrenia patients and healthy controls. They noticed that not only was the FA and cross-sectional area of the fornix significantly reduced in the schizophrenia group, but this also correlated with reductions in hippocampal volume. This in turn was shown to correlate with reduced scores on tests that measured declarative-episodic memory. Later on, studies by Luck et al., (2010) and Takei et al., (2008) were able to correlate significant fornix FA reductions in schizophrenia patients, with deficits in the Wisconsin Card Sort Test (WCS), and in a battery of verbal memory tests, respectively. More recent studies have been focussed on the regional abnormalities within the fornix, and obtaining more detailed information from refinements to the DTI technique (Abdul-Rahman et al., 2011, Kunimatsu et al., 2012). Kunimatsu et al., (2012) had noticed that not only was the FA significantly lower in both sides of the fornix in schizophrenia patients (as compared to healthy controls), but there was a significant correlation between negative symptom scores and the FA in the right fornix, for right-handed male schizophrenia patients.

Generally speaking, white matter abnormalities in schizophrenia are relatively well-known, and help to support the growing view that schizophrenia can manifest itself as a disconnection between brain regions. Given that the fornix is a vital interface

between the hippocampus and various subcortical regions involved in higher cognitive functions, it comes as no surprise that degradations to these connecting tracts are consistently correlated with deficits in tests of executive function. The implications of reduced FA in the fornix has been attributed to various effects including decreased myelination, decreased axonal density as well as increased axonal damage (Beaulieu, 2002, Kuroki et al., 2006).

Deep brain stimulation of the fornix is relatively recent and gained popularity following a study in 2008 where Hamini and colleagues (2008) were able to (unexpectedly) demonstrate a marked enhancement of memories in a patient undergoing DBS in the hypothalamic/fornix region. Interestingly subsequent analysis using EEG source localization revealed left or right increases in activity in the hippocampal and parahippocampal gyrus regions, and this had followed unilateral activation of the left or right electrodes, respectively. Furthermore these hippocampal activations correlated with improved memory recall in the patient, which led the authors to suggest that the increased hippocampal activation was in part responsible to the improved memory performance. This has since led to recent studies of its efficacy in Alzheimer's disease (Laxton et al., 2010, Smith et al., 2012). By stimulating in the same region of the fornix/hypothalamus, Laxton et al (2010) had demonstrated in 6 patients with mild Alzheimer's disease a cognitive improvement or slowing of anticipated decline between 6 and 12 months following DBS. In addition PET studies had shown a reversal of the impaired glucose utilization in the temporal and parietal lobes. In a subsequent analysis of this study, Smith et al., (2012) noted an increased functional connectivity between multiple brain regions connecting the hippocampus, including the fronto-temporal-occipital-hippocampal network, and the frontal-temporal-parietal-striatal-thalamic network, as observed a year after the onset of fornix DBS.

Given the findings in a recent number of studies, DBS in limbic structures relevant to learning and memory have shown to provide a potential avenue for the treatment of disorders which affect learning and memory. Suthana et al., (2012), for example was able to demonstrate a significant increase in spatial working memory performance in epileptic patients when stimulation of the entorhinal cortex



perforant pathway was applied during learning. More recently Lee et al., (2013) was able to demonstrate that theta-frequency stimulation in the medial septal nucleus could restore diminished spatial working memory in rodents who underwent prior brain injury using a fluid percussion method. Interestingly this study also demonstrated a transient increase in hippocampal theta activity, directly following stimulation. Numerous theories exist based on the reported memory/cognitive increases following stimulation of limbic structures, such as increased activation of the hippocampus (Hamani et al., 2008), and even hippocampal neurogenesis (Toda et al., 2008). Nonetheless activation of various structures in this circuit has at least seen beneficial effects with regards to spatial working memory, perhaps through a widespread activation of structures in Papez circuit (Papez, 1937), of which the fornix is a vital node.

The fimbria-fornix is known to connect various brain regions crucial for spatial working memory, and it has been seen to undergo degradation in schizophrenia patients. Stimulation of these remaining connecting white-matter tracts could therefore offer a means of enhancing the activation of various structures in this circuit (including the hippocampus) which would otherwise show a diminished performance due to their diminished connectivity, in schizophrenia. In light of promising recent results from the activation of various limbic structures in this circuit with DBS, the fornix may provide an interesting avenue for stimulation studies that enhance mnemonic functions that are impaired in schizophrenia.

#### **1.5.6.5 Summary of Brain Regions Selection**

Selection of an appropriate target for DBS in schizophrenia relies on an in-depth understanding of the underlying pathology of the disease, and the mechanisms by which DBS effects its actions. At present this knowledge is incomplete, meaning that researchers often try out numerous stimulation sites each with their own underlying hypothesis (e.g. Klein et al., 2012, Mikell et al., 2009). There have been some recent studies involving DBS in rodent models of relevance to schizophrenia, which were aimed at targeting the positive symptoms of the disease (e.g. Ewing and Grace, 2013,

Perez et al., 2012). In both of these cases the ventral hippocampus was targeted as a stimulation site in an attempt to normalise its aberrant output activity; which is believed to result in a dysregulation of dopamine through its efferent outputs to the nucleus accumbens (Lodge and Grace, 2007). Interestingly Perez and colleagues (2012) demonstrated that ventral hippocampal stimulation could affect a normalisation of deficits in reversal learning and extra-dimension set-shifting in MAM-treated rats; thus indicating that stimulation of this structure may see therapeutic benefit against the cognitive symptoms in schizophrenia (see also 1.3.3.6: Schizophrenia; for a more in-depth discussion on previous studies investigating DBS and its implications in the treatment of schizophrenia). Generally speaking there has been comparatively little in the study of DBS with regards to ameliorating the cognitive symptoms of schizophrenia.

The anterior and mediodorsal thalamic nuclei, thalamic reticular nucleus and fimbria-fornix have all been suggested as possible sites for stimulation with regards to improving some of the executive function deficits that occur in schizophrenia. These candidate brain regions have all been considered with regards to their functional characteristics, the pathological and functional changes they undergo in schizophrenia, and the mechanisms by which DBS of these structures may provide a therapeutic benefit. Of particular interest are the FF and ATN, for a number of reasons. First, they form vital nodes in a brain circuit which is known to play a significant role in working memory (e.g. Okada and Okaichi, 2006, Warburton et al., 2000b). Second, they undergo pathological changes in schizophrenia, for which DBS may provide a therapeutic solution. Finally these sites are directly adjacent to each other in the rat (Paxinos and Watson, 2007), and until the effects of DBS are properly characterised it cannot be ruled out that stimulation in one structure may affect the other, given the spread of the depolarising electrical field. The fornix shows degradations in integrity in schizophrenia patients (Kubicki et al., 2005, Kuroki et al., 2006, Nestor et al., 2007, Takei et al., 2008, Abdul-Rahman et al., 2011), which has been demonstrated to correlate with deficits in declarative-episodic memory (Kuroki et al., 2006), and measures of negative symptoms (Kunimatsu et al., 2012). Indeed a damage to these tracts can result in a diminished communication

between the hippocampus and various other brain regions (e.g. Okada and Okaichi, 2006, Warburton et al., 2000b, Okada and Okaichi, 2010), which can in part be attributed to the “disconnection syndrome” hypothesis in schizophrenia. Electrical stimulation of the fornix in humans (Hamani et al., 2008, Laxton et al., 2010, Smith et al., 2012) has consistently revealed activation in limbic structures linked to Papez’s circuit, which in turn has been correlated with cognitive improvement. The FF in this case is the region of the fornix which forms a major conduit for information transfer between the hippocampus and various limbic structures in Papez circuit including the anterior thalamus, medial septum, and mammillary bodies. In schizophrenia patients, the anterior thalamus shows a reduced metabolism (Buchsbaum et al., 1996, Katz et al., 1996) and task-related activation (Andrews et al., 2006), as well as pathological deficits (Rose et al., 2006, Amaral and Cowan, 1980). Furthermore, the ATN features a strong theta rhythm that is highly synchronous with that of the hippocampus (Vertes et al., 2001, Tsanov et al., 2011a), which is itself linked with mnemonic functions (Green and Arduini, 1954, Vanderwolf, 1969). Activation of these structures via DBS may therefore facilitate an increased activity throughout this “memory” circuit, which in turn may have therapeutic benefit in the neural networks that otherwise rely on a strong functional cooperation for learning and memory functions.

## Chapter 2

# Wireless Device Technologies for Recording and Stimulation

### 2.1 Introduction

This chapter is based on the design and development of two novel wireless embedded systems for local-field potential (LFP) recording and deep-brain stimulation (DBS), for use in freely-moving rodents. Given the current state of commercially sold wireless solutions, or prototype systems as described in the literature, experimenters are still faced with financial and technological barriers to overcome when realising novel paradigms that mix DBS and LFP recording modalities. Starting with a background review of wireless device technologies for recording and stimulation, this chapter considers many of the key system design characteristics to be considered with regards their application in behavioural experiments. The first system described is capable of performing simultaneous multichannel LFP recording with 2-channel DBS in freely-moving rodents, whereas the second system described performs 4-channel DBS in freely-moving rodents. These systems have been designed to provide a high level of performance, functionality and simplicity for their relatively small sizes, at 8.5g each (including batteries).

## 2.2 Background

As the field of deep-brain stimulation gains momentum, there exists the growing need for researchers to have access to the tools and equipment that can drive future studies. Being able to combine DBS with neural recordings in a practical manner presents itself as a powerful means of furthering study in this area, but there currently exists challenges in designing experiments of this type; mainly concerning the hardware/technology involved. Many researchers are looking towards wireless telemetry to alleviate many of the problems inherent with traditional tethered recording systems. Numerous system solutions are available commercially for a wide range of animals (e.g. Data Sciences International, Triangle Biosystems, Multichannel Systems, Alpha Omega, Pinnacle Technology), but their high costs are often seen as a barrier for inclusion in many studies.

This section outlines many of the design characteristics that have to be considered when designing such a system, from the practicalities of attaching a system to an animal, to the technological options that are available in each of the design stages. To date a large number of wireless systems have been described for either recording neural signals or performing DBS, but relatively few which combine these two modalities. The vast majority of these recording/stimulation systems are non-commercial prototypes developed to forward research for a particular group. Taken together, they represent a highly diverse set of solutions that can be employed in a wide range of animals and experimental situations. This section outlines many of the key design characteristics and possibilities present in these systems, whilst drawing examples from the literature. Since the progression of technology plays a major factor in the performance of these systems, newer systems are discussed in preference of older systems.

Generally speaking the design of these systems require a careful balance between a large set of parameters, including the system size, weight, battery life, number and quality of recording channels, functionality, transmission type and transmission range. The necessity to compromise between these particular aspects of a design is ultimately dictated by the strict design requirements, set by the experiment itself.

### **2.2.1 Need for Wireless Recording**

Up until around 15 years ago the use of a cable tether for recording and/or stimulating in awake animals was the norm. A cable tether in this case is a physical cable connection between the animal and the recording system. Typically this involves a headstage implant which acts as an interface, between the implanted electrodes and the recording cable. The recording cable subsequently interfaces directly with amplification / signal-processing hardware. The use of the cable tether allowed only limited movement for small animals inside a small cage or holding arena, which itself was often tailored to whatever behavioural task the study demands. Larger animals such as primates were traditionally confined to a head-restraint (e.g. Kojima and Goldman-Rakic, 1982, Aston-Jones et al., 1997), halting any locomotion-based movement and causing additional stress.

The obvious advantage of using a tethered system is that chronic recordings can take place using high-quality signal processing hardware. The hardware is not carried by the animal (as is the case with portable systems), thus the power consumption of the circuitry and the amount of components it uses is not limited. However despite the enhanced signal processing, the recording cable itself can be subject to noise, primarily mains interference. The main disadvantages of this recording method revolve around the mechanical aspects of having a physical cable tether. The animals can potentially chew the cable, the cable can get caught or twisted, and in the worst cases – the headstage implant can come free with enough force. Numerous innovations have been utilised to enhance the animal's range of motion using this recording method for both small and large animals. Ludvig and colleagues, (2001) developed a 1.5 x 1.5 m test-chamber for recordings in monkeys, with an elaborate cable tether made up of rods, swivels, counterweights, straight and rigid recording cables. Similarly Bertram et al., (1997) utilised a custom electrical swivel connector for tethered rat recordings inside a 25cm diameter holding pen. More recently Lin et al., (2006) attached a helium-filled balloon to the headstage portion of a cable-tether in mice, in order to alleviate some of its weight. Generally speaking any attempt at circumventing some of the mechanical issues associated with a cable tether had to be incorporated into the design of the test chamber, often with creative but complex

solutions. Each solution would be specific to a particular test chamber, thus a T-maze and open-field arena for example would require different tethered system solutions. In addition cable tethers are not possible for some arenas, such as 3D mazes, or those requiring a lot of space (e.g. recordings in birds). Finally, the presence of recording cables can act as a visual distraction to the animals.

### **2.2.2 Species under Study and System Size**

Perhaps the most significant constraint on a system's performance and functionality is the animal species for which it is designed. This is entirely due to practical limitations on what the animal can carry, which is in turn affected by the size, shape and weight of the wireless system. Designers of larger systems have more freedom regarding the amount of components that can be included, and can provide more channels, larger batteries, higher-power transceivers and more intricate amplification and filtering stages. At one end of the scale are systems that can be carried by relatively large non-rodent animals such as cats (Sherk and Wilkinson, 2008) and monkeys (Mavoori et al., 2005, Obeid et al., 2004). Obeid and colleagues (2004) for example, describe a 16-channel preamplifier-multiplexer-digitizer circuit; and despite forming only half of a complete wireless system solution it weighs over 50g and features multiple amplification and active filtering stages for each channel. The non-telemetry portable system described by Sherk and Wilson (2008) also features a high-quality signal conditioning stage, whilst taking advantage of a novel microdrive design that can incrementally advance the recording electrodes to an optimum depth in the brain following surgery. At the other end of the scale are some of the smallest systems that can be physically designed, and are used in insects such as moths (Ando et al., 2002), locusts (Fischer et al., 1996) and cockroaches (Takeuchi and Shimoyama, 2004). These systems weigh between 0.1-0.55g, feature one or two channels, and comparatively basic signal amplification/filtering strategies. Furthermore they are entirely analogue; utilising miniature FM transmitters fabricated from a handful of transistors.

Simply put, systems designed for small animals such as mice and rats are subjected to a greater number of compromises and limitations compared to those designed for larger animals such as cats and monkeys. When designing a system for a small animal, an optimum balance between the design specifications is important due to the compromises that will inevitably be made. For example, if the system had to have a battery-life of at least 24 hours (non-inductively powered), the designer would have to a) make the system consume as little power as possible, or b) give it a large battery – two choices which will compromise the other aspects of the particular design. For a given technology, efficiency in wireless system design can only be taken so far. As a result of this a large number of innovations and creative solutions have been seen in wireless systems designed for small animals, as researchers attempt to sidestep many of the technical hurdles involved with system size and weight. The majority of systems subsequently discussed in this section are that used for small animals such as rats or mice; although where relevant the design features of systems designed for larger animals are discussed also.

### **2.2.3 Placement of System on Animal**

If designed properly, wireless systems can circumvent many of the issues inherent with traditional cable tethers including reducing animal stress, whilst enhancing system portability and animal freedom of movement. A large number of wireless systems developed for small animals are based on a 2-part headstage/backpack combination. The headstage interfaces with the implanted electrodes, and an external recording cable. This short cable plugs into a backpack module which houses the system's battery, along with the main signal processing, control and telemetry circuitry. Example of these designs are used for a wide variety of animals, including owls (Nieder, 2000), monkeys (Grohrock et al., 1997), cats (Sherk and Wilkinson, 2008) and rats (Hawley et al., 2002, Ye et al., 2008, Hampson et al., 2009, Chen et al., 2008, Xu et al., 2004). Quite often the headstages in these designs includes pre-amplification circuitry (e.g. Hawley et al., 2002, Hampson et al., 2009, Ye et al., 2008), which amplifies brain signals prior to them being sent through the short connecting cable to the backpack, where the rest of the signal processing and



telemetry takes place. This pre-amplification step is necessary because any external noise which is picked up by the connecting cables can interfere with the micro-volt sized neural signals (since the cables act as an antenna). It is also advantageous for any system of this type to keep these cables as short as possible and preferably shielded.

A more optimal configuration is to place the amplification and filtering circuitry as close as possible to the site of recording, which in this case is on the head of the animal itself. Since in rats the head generally is capable of supporting less weight than the back, a head-mounted system is typically smaller than that carried on the back of an animal. Such examples of these systems are seen in zebra finch (Schregardus et al., 2006), primates (Grohrock et al., 1997, Roy and Wang, 2012) and rodents (Fan et al., 2011). The majority of commercial systems utilise head-mounted designs (e.g. Triangle Biosystems, Pinnacle Technology, Multichannel Systems).

Another alternative is to make the system implantable. Examples of these systems for rodents have been seen both independently (Irazoqui-Pastor et al., 2003, Lapray et al., 2008) and commercially (e.g. Data Sciences International). Implantable systems have a number of pros and cons with regards to those previously described. Animals can use these devices in water-based tasks such as the Morris water maze, assuming the previous devices haven't been treated with a waterproof coating. The wound site is less susceptible to infection, although arguably the process of implanting a system into the animal can itself cause surgical complications (e.g. Williams et al., 2006). In addition implantable devices allow the animal greater comfort with regards to natural behaviours such as grooming. The downsides are based mainly on the devices technical limitations. The device has to be small with an acceptable shape relevant to the animal, and fully bio-compatible. Also, the device lasts as long as the battery does, unless an induction link is used (e.g. Irazoqui-Pastor et al., 2003) to supply power. Also the transmission range of the system is attenuated by the animal's overlying skin. Implantable devices must be controllable from outside the body, in order to be able to switch the device off, which necessitates either a bi-directional transmission link (Lapray et al., 2008), or a simpler mechanism such as a magnetic on/off switch (see implantable range; Data Sciences International).

The location of the device dictates its size, which in turn places a practical limit on its performance and functionality. Head-mounted and implantable devices are often sold commercially (but not exclusively), since the companies that develop them are likely to have the resources to develop application-specific integrated circuits (see 2.2.5.2: System Technology), which are typically lower power and more space-conscious than those using ‘off the shelf’ components. As an example of this a 1-channel implantable EEG recorder by Lapray et al., (2008) using off-the-shelf components is 40mm long, weighs 4g, and lasts for 14h. By comparison the HD-X11 telemetry system by DataSciences International is 2.2g and lasts for 1 month, although with a vastly inferior transmission range.

Taken together the placement of the system must be carefully considered in tandem with the experimental requirements, since the design solution for one problem may not be satisfactory for all circumstances.

#### **2.2.4 Signal types**

There are a number of different bioelectric signals which a wireless system can be configured to record, including electrocardiogram (ECG), electromyogram (EMG), single unit nerve action potential, local-field potential (LFPs), electrocorticogram (ECoG) and also in rare cases, scalp-electroencephalogram (EEG). Wireless systems that record any of these signals share the same basic hardware stages consisting of signal acquisition, amplification, filtering, (optional digitisation), and telemetry. The differences between each signal type lie mainly in the amplification and bandwidth characteristics of these systems. For example, brain-recorded signals are at least an order of magnitude lower in amplitude than ECG and EMG, and thus require higher amplification in order to be adequately detected. Similarly ECoG signals require higher amplification than LFP, since the brain signals are attenuated by the skull by the time they reach the ECoG electrodes. Whilst EEG, LFP and ECoG recordings typically require a sampling rate of a few hundred Hz, single-unit recordings require a sampling rate of several KHz in order to adequately detect action potentials and spikes. Generally speaking most of the systems reviewed here

are capable of detecting only electrical signals from the brain in some form, although sometimes a system may sometimes have separate channels devoted for ECG or EMG measurements (e.g. Data Sciences International). Interestingly recent systems by Mollazadeh et al., (2008a) and Zanos et al., (2011) feature adjustable parameters on their system's input stage; including gain, ADC resolution, and filters for selective acquisition of different neural signals.

## **2.2.5 Standard Design Variations**

### **2.2.5.1 Analogue/Digital System**

Every system that is based on the recording of neural signals is made up either completely using analogue components, or a mixture of analogue and digital components. Analogue components in this case are necessary to construct the amplifiers and filters that extract and condition the neural signals. However after that there is the choice of whether to transmit the analogue signal directly, or to digitise it into a digital data stream prior to transmission. The choice of how to proceed depends on several trade-offs, including the system size, lifetime, performance and complexity.

Generally the analogue systems are reserved for those which need to be ultra-small, with the expense of greatly reduced accuracy, precision and functionality. Analogue-only systems can be made from a handful of active components (requires power - e.g. operational amplifiers) and discrete components (e.g. resistors, inductors, capacitors), with basic amplification and analogue radio transmission such as frequency-modulation (FM). Examples include small systems for use with insects (Takeuchi and Shimoyama, 2004, Ando et al., 2002) and birds (Schregardus et al., 2006). These types of systems, although small, are highly susceptible to noise in all parts of the design. In a digital system, the opportunity for noise to interfere with the signal is negligible when the signal is digitised. Digital transceivers are far more accurate than their analogue counterparts, as their transmission is much less susceptible to interference and distortion, and can be enhanced with error-checking codes (see 2.2.5.7: Wireless Telemetry). Most systems that convert the signal from

analogue to digital incorporate an analogue-digital converter, and a digital control unit in the form of a microcontroller (MCU), system-on-chip (SOiC), or a custom-designed control module incorporated into an application-specific integrated circuit (ASIC), or a field-programmable-gate-array (FPGA) chip. In addition to enhanced signal quality, typically the benefits of digital systems over analogue also include the multiplexing and organisation of a large number of recording channels, the ability to configure system settings, bi-directional communication, spike-detection and digital signal processing, and low-power modes to preserve battery-life during periods of inactivity. The downsides mainly revolve around the additional space and power taken up by digital components.

### **2.2.5.2 Technology**

The technology used for a wireless system depends on a number of factors, including the system design requirements, cost, development time, and in some cases the need for the system to be replicated by others. Systems built using commercial, off-the-shelf components in conjunction with custom-designed printed-circuit-boards (PCB's), are attractive options for their low cost and ability to be reproduced with only a basic working knowledge of surface-mount PCB design (figure 2.1A). Systems built entirely with these components are often diverse in their nature, from miniature analogue-only systems designed with a handful of components (Takeuchi and Shimoyama, 2004, Ando et al., 2002), to multichannel digital systems featuring programmable control units (e.g. Ativanichayaphong et al., 2008, Ye et al., 2008, Chen et al., 2008, Cieslewski et al., 2006). The size of these systems and the power they consume are often dependent on the choice and placement of components, of which there are millions of potential combinations. Developing these systems to fit into a small space presents a challenge in efficient design, with some of the smallest of these systems suffering severe penalties in functionality, such as an implantable system by Lapray et al., (2008), which features only a single recording channel.

Application-specific-integrated-circuits (ASIC's) are custom-designed integrated circuits whose functionality is focussed entirely on the system for which they are

designed. These are typically produced using a complementary-metal-oxide-semiconductor (CMOS) process (or variants thereof), in which transistors are physically etched and/or deposited onto a silicon substrate (figure 2.1B). With this, all of the parts that can be built using commercial components can be replicated in an ASIC, albeit on a much smaller substrate that consumes lower power. As such, systems that utilise ASICs typically benefit from a reduced size and power consumption (e.g. Mollazadeh et al., 2008b, Moosung et al., 2008, Harrison et al., 2007). Some interesting designs mix ASIC circuitry with off the shelf components, such as a recent system by Hampson and colleagues (2009), which utilises an ASIC for the headstage connector to perform 16-channels of amplification and band-pass filtering. Whilst these systems can be produced to a high standard, their costs and development time are considerably high compared to off-the-shelf components, with typically longer production time scales. ASICs are sometimes designed alongside micro-electro-mechanical-system (MEMS) electrodes that can be integrated with the device. A wireless system developed by Mojarradi and colleagues (2003), for instance includes all the circuitry required for signal processing and transmission, which is placed on top of a 100-microelectrode MEMS array, although this particular system is designed for neuro-prosthesis applications in humans.

Finally field-programmable-gate-array (FPGA) technology is relatively new and seldom seen in these applications, but can nonetheless offer remarkable benefits (figure 2.1C). FPGA's are integrated circuits with field-programmable transistor connections, which are arranged into a micro-circuit based on a computer-based design. Essentially they can be considered as low-cost programmable ASICs that offer comparable levels of performance and functionality.

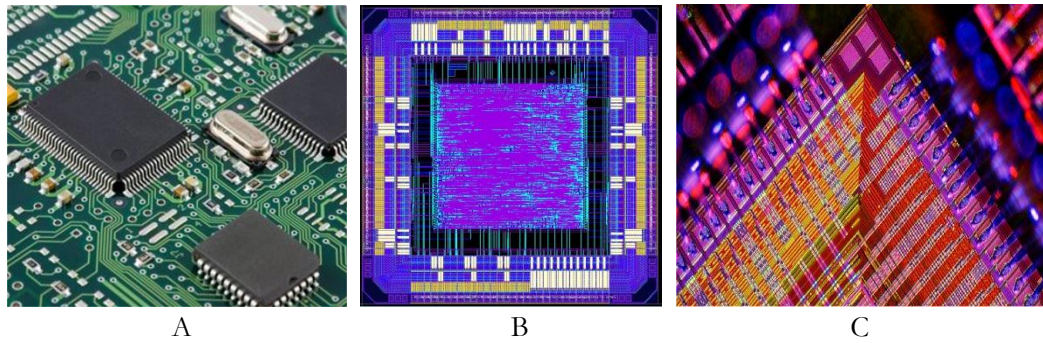


Figure 2.1 – Examples of the different technologies that can be utilised when designing a miniature wireless recording and stimulation device, including surface-mount PCB technology using off-the-shelf components (A), application-specific integrated circuit (ASIC; B), and field-programmable-gate-array (FPGA; C). Images taken (from left to right) from [www.electronicsarena.co.uk](http://www.electronicsarena.co.uk); [www.bo.infn.it](http://www.bo.infn.it); [www.fpga.synth.net](http://www.fpga.synth.net).

### 2.2.5.3 System Control Centre

Digital systems are based around a central control unit, which has diverse functions including managing digital data, communicating with the transceiver, controlling other peripherals and adjusting the system's operating mode based on commands. Systems developed using off-the-shelf components typically utilise microcontrollers (MCUs) or system-on-chips (SOiCs). An MCU is a miniature computer complete with a processor, clock generator, RAM, code memory and programmable input/output peripherals (see figure 2.2 for a functional block diagram of the Texas Instruments MSP430 MCU). The choice of MCU is based on trade-offs between its size, power-usage, number of input/output pins, additional peripherals (such as SPI/UART communication modules and in-built analogue-digital converters), and the amount of processing and memory. Popular choices for miniature wireless systems include the MSP430 range (Texas Instruments; e.g Cieslewski et al., 2006), and the PIC range (Microchip Technology Inc.; e.g Vyssotski et al., 2006, Chen et al., 2008, Hampson et al., 2009). These particular MCU's are chosen for their low power consumption, and all come with in-built analogue-digital converters (ADC; see 2.2.5.6: Analogue to Digital Converter). An interesting PIC variant (dsPIC30F6010; Microchip Technology Inc.) chosen by Hampson et al., (2009) contains advanced signal-processing functions which are used to perform real-time waveform detection on the recorded signals as soon as they are digitised.

SOiCs are a step up in complexity from MCUs, and are created as complete programmable system solutions. These typically combine several chips onto one integrated circuit; including central processing, code memory, RAM, transceiver, crystal oscillator, an ADC, communications peripherals including RF transmission, and input/output peripherals. One of the more popular choices for SOiCs in miniature wireless systems are those by Nordic Semiconductor, as used in systems that perform wireless EEG recording (Xin and Xiaoguang, 2005), stimulation (Song et al., 2006b), and both (Song et al., 2006a). The 8051 processors that these devices use process 8-bits of data at a time (as opposed to most MCU's which feature 16-bit instructions), which can potentially make the programming more difficult. Furthermore when implemented they are typically larger in size and consume more power than their MCU counterparts. In addition, the combination of a transceiver onto the same PCB substrate can make the device very susceptible to noise, particularly if the low-amplitude brain signals are anywhere in the vicinity.

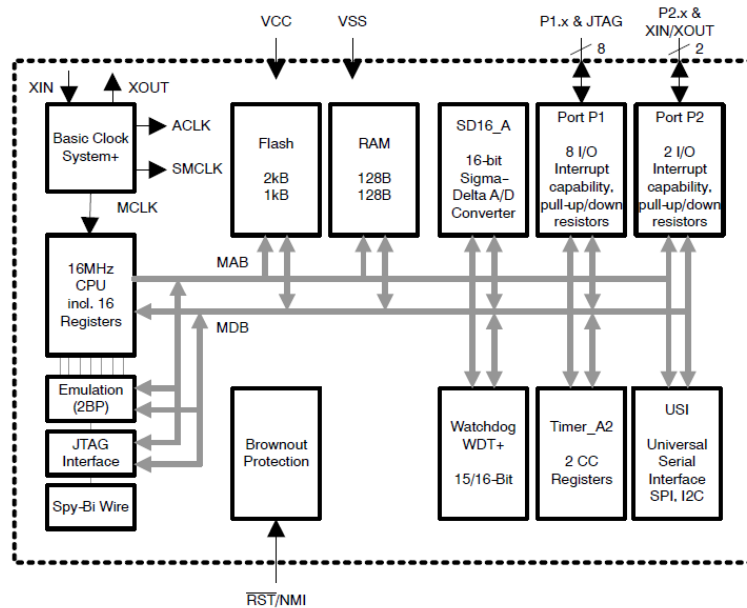


Figure 2.2 – Functional block diagram of the MSP430f2013 microcontroller (Texas Instruments). This 16-bit device features a 16 MHz processor, in-built clock oscillator, code and program memory, an analogue-digital converter, 10 input/output pins, timers, communication modules, and a programming/debug interface. Taken from MSP430x20x3 datasheet (Texas Instruments, 2007).

#### 2.2.5.4 Channel Count

Given an adequate placement of electrodes, more channels generally equates to more and better overall information. Additional channels can make heavy demands on the systems size and power consumption, particularly where commercial off-the-shelf components are concerned. The sensitive input stage with the input amplifiers and filters must be replicated for each channel. As an extreme example, a system by Cieslewski et al., (2006) utilises 8 channels, but consumes 106mW. A more recent device by Chen et al., (2008) contains the same number of channels but has a battery life of 2 hours. Vyssotski and colleagues (2006), on the other hand has an 8-channel system made from commercial components with a battery life of over 2 days; but they sacrificed the wireless telemetry in favour of an on-board memory to allow this to happen. Even with the most efficient design, there is a practical limit in the number of recording channels for a given system size. The use of ASICs however can allow for relatively more channels since the input signal conditioning circuitry can be replicated many times over a small space (e.g. Hampson et al., 2009).



### 2.2.5.5 Input Stage

The input stage of the design consists of the components necessary to extract the neuronal signal and convert it to a form suitable for further processing. This includes mainly amplifiers to increase the magnitude of the signal, and filters to remove unwanted signals/noise/artefacts, whilst keeping the frequencies of interest. The signal in its untreated form is of very small magnitude and thus susceptible to noise and distortions. The choice of components at the input stage can determine not only the signal accuracy, but also the systems overall physical limitations. Often the analogue circuitry is separated from the digital/telemetry circuitry using a separate headstage and backpack combination (e.g. Hawley et al., 2002, Hampson et al., 2009, Ye et al., 2008, Sherk and Wilkinson, 2008), which serves the dual purpose of keeping the neural signal – preamplifier distance short, and physically isolating the ground plane of the sensitive analogue circuitry.

The properties of the input preamplifier or buffer stage is crucial for determining the overall signal quality. As a general rule, the input amplifiers should have a high impedance differential input and a high common-mode-rejection-ratio (CMRR). High impedance (preferably  $> 100\text{M}\Omega$ ) reduces the influence of a parasitic voltage drop across the recording electrodes which would otherwise distort and attenuate the signal of interest. A high CMRR (preferably  $> 70\text{dB}$  – depending on required voltage resolution) improves the system's ability to reject unwanted noise signals that are common to both channels, by preferentially amplifying the desired differential signals. Further desirable properties include low offset voltage, low bias currents (preferably less than a few nA), as well as low input noise (ideally no greater than  $50\text{nV}/\sqrt{\text{Hz}}$ ). There are many high-quality input amplifiers available commercially that satisfy these requirements, and preferred ones are instrumentation amplifiers - devices that combine multiple operational amplifiers in one IC for increased precision. Finally, the feedback components in the operational amplifiers can themselves be a source of noise, which is why pre-amplifiers are generally set to a low gain (or even configured as a unity-gain impedance-matching buffer), with a separate subsequent main amplification stage.

Signals are filtered to remove frequency components above and below a predetermined range, e.g. filtering between 1-100Hz is sufficient for capturing EEG signals up to low- and medium-gamma. In addition low-pass filtering removes the possibility of aliasing artefacts occurring in the recorded signal when it gets sampled by the ADC. Often a trade-off exists between PCB board space and the quality of filtering. Most devices contain a band-pass filter (which is often manifested as a low- and high-pass filter placed in series), though their quality differs widely, which ultimately determines its frequency-spectrum profile (shape of its frequency-response curve), as well as the number of poles it contains. More poles allow for a more rapid attenuation of unwanted signals beyond the filter's set cut-off frequency, thus rejecting the unwanted signals better. The simplest low-/high-pass filters consist of only a resistor and capacitor each (e.g. Schregardus et al., 2006), which may be integrated into the amplification stage to form active filters (e.g. Lapray et al., 2008). These filter stages may even be cascaded in series to double the number of poles, as seen with designs by Parthasarathy et al., (2006) and Sherket al., (2008), which contain for each input a 4-pole Butterworth low-pass filter followed by a 4-pole Butterworth high-pass filter. In this case 'Butterworth' refers to the frequency spectrum profile of the filter, which has an extremely flat pass-band. This is commonly used for neuronal signal recording devices, although at the cost of increased component count and power usage. However other filter profiles can be used instead, including Bessel filters, which are renowned for producing little phase distortion. Notch filters are entirely optional in designs, and remove 50Hz noise which is commonly generated from power supplies (as the mains power supply runs at 50Hz). However because notch filters also degrade low-gamma at 50Hz, it is preferable to make the system less susceptible to 50Hz noise in the first place by careful design of the input stage.

As part of the input stage, the majority of systems that use more than one channel employ the use of a multiplexer. A multiplexer is a rapid switch that routes the amplified signals from each channel into one ADC input, thereby allowing for a reduction in circuitry. The type of multiplexer that is required is one that is capable of switching its output signal fast enough to keep up with the system sampling rate.

Desirable characteristics for a multiplexer in these systems include low switching noise (a parasitic property of high-speed switching), and low power usage.

A good input stage is not just dependent on the components that are used, but also their placement. When designing the PCB, ground planes must be set up appropriately to a) isolate the analogue and digital signals, b) avoid ground-loops that can attract noise (by working like an antenna), and c) avoid parasitic resistances/capacitances/inductances that can degrade the quality of the signal. Keeping the analogue circuitry close to the signal source, as well as physically and electrically isolated from the digital and transceiver circuitry can offer improved signal quality.

#### **2.2.5.6 Analogue to Digital Converter (ADC)**

The voltage resolution at which signals are sampled affects not only the signal's bandwidth, but also the size of the signal in data terms. For example an 8-bit ADC converts each sample into an 8-bit binary number, for which there are  $2^8$  (or 256) discrete voltage levels between the ADC's input range. Similarly a 16-bit ADC can resolve  $2^{16}$  (65536) voltage levels, allowing for a much higher voltage resolution. For signal quality higher resolutions are therefore better than lower resolutions, but there is a practical limit. A 16-bit resolution for an ADC input voltage range of 1.2V equates to a voltage resolution of approximately 18.3 $\mu$ V. If the system's (amplified) noise magnitude is significantly higher than 18.3 $\mu$ V, then this resolution is unnecessary. Nonetheless higher resolutions are favourable since the input signal doesn't have to undergo such large amplification in order to retain its accuracy. Higher-resolution analogue-digital converters (such as a sigma-delta converter) often operate at lower speeds than their lower-resolution counterparts, meaning there is often a trade-off between voltage and temporal signal resolution. When considering a high ADC resolution, the other components in the system have to be fast enough to keep up. The potential bottlenecks here include a) the processing speed of the system's control unit, b) the transmission speed of the transceiver, c) the receiver processing speed, and d) the choice of computer port for which to transmit data. A

serial port transmits data at a maximum of 115.2Kbaud, whereas a modern USB 3.0 port can handle data speeds of at least 5000Mbaud. Two examples in the literature show multichannel systems where the ADC resolution was deliberately reduced in order to sustain a high data communication rate (Perelman and Ginosar, 2007, Harrison et al., 2007).

The second parameter that determines the performance of the ADC is the sampling frequency. This is the number of ‘snapshots’ of a signal per second, and for complete signal restoration a sample frequency of at least double the highest frequency component is required (via. the Nyquist theorem). In practice a sampling rate of at least 2.5-3x the maximum input frequency allows for an acceptable margin of error, accounting for low-pass filters with imperfect characteristics (cut-off frequencies). Thus a signal with a bandwidth between 1-100Hz should ideally be sampled above 250Hz. Sampling rates for spikes and action potentials however must be at least an order of magnitude higher than that used for LFP recordings; somewhere in the region of 5 KHz upwards will suffice.

#### **2.2.5.7 Wireless Telemetry**

All wireless telemetry devices feature some medium of transmission, with infra-red (IR) and radio-frequency (RF) being by far the two most popular. Most devices in the literature employ the use of RF telemetry, due to its range, power consumption, small PCB footprint (space taken up by the components) and ability to transmit through obstacles.

RF telemetry can be broken down into two types: analogue and digital transmission. Analogue transmission is where the radio carrier wave is amplitude, frequency or phase modulated by an analogue signal, and in general is highly susceptible to distortion. Digital transmission uses only two discrete carrier wave variations (representing binary 1 and 0), thus making digital telemetry many times more resistant to distortion and interference. This is extremely important for preserving the fidelity of the received signal, especially where the device is operated in

electrically noisy environments such as laboratories; where electromagnetic radio fluctuations from lab equipment, can be found all over the place.

The most widely used analogue transmission scheme is frequency-modulation (FM), owing to its simplicity, and ease of implementation. FM oscillators can be made with only a few components including a single transistor, making it an extremely popular choice for small devices (e.g. Takeuchi and Shimoyama, 2004, Fischer et al., 1996, Schregardus et al., 2006, Chien and Jaw, 2005). It is also seen in ASIC designs (e.g. Fang-Ren et al., 2004) due again, to its small size. An interesting variation is seen in a system by Nieder, (2000), where 2 signals are superimposed onto one using an FM technique called suppressed-sideband double-carrier. Because FM signals are highly susceptible to noise and distortion, preserving the quality of brain recording is a problem. For example in a wireless (FM) system designed to record high-frequency spikes and action potentials, the filter bandwidth was limited to 3.8KHz as a trade-off between signal fidelity and noise (Chien and Jaw, 2005), thus resulting in a loss of high-frequency signal features.

Digital transmission schemes are generally more varied, one of the reasons being that commercial transceivers often come with several programmable transmission options such as the CC2500 (Texas Instruments), which provides frequency-shift-keying (FSK), Gaussian FSK (GFSK), minimum-shift-keying (MSK), as well as on-off-keying (OOK). These forms of telemetry revolve around a carrier signal being modulated by digital '1s' and '0s', either varying the amplitude, frequency, phase, a combination of those, or in the case of OOK, switching the carrier signal on and off repeatedly. Differences between these formats are superficial when compared with analogue transmission, and researchers that employ digital transmission seldom point out these details, perhaps for this reason. One of the key benefits of digital transmission is that its transmission can be made more reliable with numerous digital data processing steps such as forward-error correction, data whitening, interleaving, and error-detection codes. Low-power digital transceivers are employed on a large number of wireless systems (e.g. Lapray et al., 2008, Chestek et al., 2009, Song et al., 2006a, Cieslewski et al., 2006, Xin and Xiaoguang, 2005) owing to their flexibility and quality.

More advanced digital transmission schemes employ the use of transceivers, which use a 2.4GHz, frequency-hopping spread-spectrum transmission format (e.g. Hampson et al., 2009, Ye et al., 2008, Chen et al., 2008). Data sent this way conforms to a specific standard for which there is an established infrastructure in place, making the data relatively easy to handle, (i.e. the data can be transmitted directly to pre-programmed Bluetooth enabled devices). Generally speaking they offer an excellent transmission range for the power they consume. Another protocol used is the IEEE 802.11b wireless protocol (Parthasarathy et al., 2006), although this is primarily designed for high-throughput data transmission between multiple networked devices such as computers and smartphones, and thus consumes a lot of power (i.e. this particular system weighs 87g without the battery, and consumes 2.7W of power).

Moving away from radio telemetry, infra-red (IR) transmission is another option (Mavoori et al., 2005, Tsuchida et al., 2004). The benefits of this stand out in situations where RF telemetry cannot be used. For example Tsuchida et al., (2004) developed a system for use in crayfish underwater, where RF telemetry cannot be used because the high conductivity of the water severely attenuates the RF signal. Unlike RF, IR light is not susceptible to electronic noise or electromagnetic radiation, thus making it a highly secure transmission medium. However to operate properly it requires a finite transmission distance that must be in line-of-sight, with an LED that must be pointed almost directly at the receiver photodiode. The components on an IR system typically have a smaller PCB footprint than their RF counterparts, but take up more power, which results in a larger overall space due to the increased battery size. As such a more efficient use of this technology is for non-continuous reliable transmission of data such as stimulation parameters to a wireless stimulation system (Mavoori et al., 2005).

#### **2.2.5.8 Transmission Range**

Perhaps the single largest drain of power in wireless systems is the transmitter circuitry. Power is required to convert an electrical signal to a RF signal by sending a

current through an antenna. The required transmission range has an effect on the size of the system (via the battery) and its operational lifetime. Systems equipped with a digital transceiver often come with several programmable transmission options; e.g. the CC2500 (Texas Instruments) has an adjustable transmit power from -30 to +1 dBm, which consumes currents from 8.4 to 21.5 mA, respectively. Consequently, the maximum range of the transceiver must be tightly matched with that required for the experiment, to allow for maximum efficiency. The transmission range used by wireless system prototypes are varied, and have been seen to range from 0.5m using an integrated FM transmitter (Mohseni et al., 2005) to 100m as seen with a Bluetooth device (Ye et al., 2008). A recent device by Ativanichayaphong and colleagues (2008) in particular transmits over 300m, which is impractical and inefficient for most purposes. Many commercially sold wireless systems target the transceiver power consumption as a means of improving the system operational lifetime, by employing novel receiver solutions to keep the transmit power as low as possible. For example, devices by Data Sciences utilise receiver-plates which sit directly below the recording arena, thus prolonging the battery life on their implantable systems for months.

#### **2.2.5.9 Power Consumption**

The amount of power consumed by the system is one of the most important parameters in the design of miniature wireless EEG recorder/stimulator devices, and affects virtually every design choice made in the system. The use of digital components, additional channels, comprehensive amplification and filtering strategies, large transmission ranges and noise-reduction circuitry all cause power consumption to increase. All devices face a trade-off between operational lifetime, battery size and range of features used in the device. Systems designed for large animals such as monkeys and cats can get away with consuming a lot of power, but this becomes increasingly important as the animal size and system size is reduced.

As far as non-ASIC systems are concerned, at one of these extremes is a wireless EEG recording device for rats with high-quality amplification and filtering in each of

its 4 input channels, along with a high-powered IEEE 802.11b Ethernet module and wireless router (Parthasarathy et al., 2006). This device weighs 87g and consumes 2.7W - over 500 times greater than by Hampson et al., (2009), which performs 1-channel implantable EEG recording. ASIC systems are even more impressive, with a system by Mollazadeh et al., (2008b) offering 1.8mW power consumption for 16-channels of simultaneous neuronal data.

Unfortunately whilst most forms of technology have evolved rapidly over the past few decades, battery technology has progressed at a relatively slow pace. Miniature coin and button cell batteries are the ideal size for these wireless systems (figure 2.3), but they are typically designed for long-life, low-current applications such as calculators and watches, which consume current in the micro-amp range. Most of the devices described here operate at least in the milli-amp range, meaning that using a coin-/button-cell battery with these devices results in their capacity being reduced to a fraction of its quoted manufacturer's value. These types of batteries are nonetheless seen in a large range of devices (e.g. Ando et al., 2002, Schregardus et al., 2006, Lin et al., 2008, Cieslewski et al., 2006, Lapray et al., 2008). Larger batteries have also been seen (Hawley et al., 2002, Ye et al., 2008, Xu et al., 2004). Rechargeable batteries are by far the most cost-effective solution and are increasingly seen in newer devices (e.g. Chen et al., 2008, Roy and Wang, 2012, Ewing et al., 2013a) as the market for them expands with in line with consumer electronics. However these produce typically the least amount of power per volume, resulting in a trade-off between device cost (via replacement batteries) and operational lifetime. Given the proliferation of portable consumer electronics these batteries exist in a large range of types, and their performance is expected to improve.



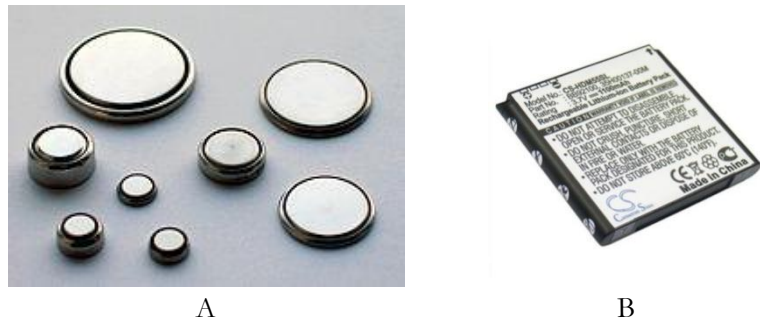


Figure 2.3 – Coin and button-cells (A) come in many shapes and sizes, and are made with different compositions such as silver-oxide, and lithium-ion. Rechargeable battery packs can save money on batteries, but typically have a low volume-power efficiency compared to disposable batteries (B). Images taken from en.wikipedia.org; smorainternational.com.

### 2.2.5.10 Inductive Powering

Inductively-powered devices remove the power problem completely by making it wireless. Wireless power can be supplied over an inductive link, but this comes with steep limitations. In addition to the low power provided by these links, wireless power has the inherent requirement of a large primary coil (around the device) placed into close proximity of a secondary coil (which supplies the power). The maximum distance between these coils depend on (among other aspects) the size of both coils, and is seldom greater than a few centimetres. Nonetheless researchers have explored this option, such as an implantable stimulation system by Peng et al., (2004) which requires the primary coil be attached to the animal during operation. These coils must remain parallel to each other at all times in order for transmission to work – which renders it unsuitable for rat experiments where the rat stands up altering the coil orientation. However researchers have attempted creating ‘rotating’ magnetic fields to cover all implant orientations and lift this restriction (Winter et al., 1998). This latter solution required that the animal cage be covered in coils covering the x, y, and z planes; thereby limiting the physical space these experiments can operate with. For most systems only the low-power warranted by ASIC technology would practically justify attempting an inductive link (e.g. Harrison et al., 2007, Mollazadeh et al., 2008b).

### **2.2.5.11 Low-Power Modes**

With power management being a critical issue that directly relates to the size of the system via the battery, it's beneficial to be able to power-down parts of the system that are not in use. Most MCUs are equipped with various low-power modes that be used to switch off certain peripherals whilst leaving others on, e.g. an MCU may be instructed to switch off its internal clock, ADC, CPU, etc., and be instructed to 'wake up' to full-power mode after receiving an external RF signal (Lapray et al., 2008). Other systems such as that by Vyssotski and colleagues (2006) contain multiple modes of operation, where certain features (in this case a GPS receiver) may be optionally switched off to preserve battery. Powering down parts of the system can even occur many hundreds of times a second, e.g. powering down parts of the system as it waits for wireless transmission to process.

Being able to remotely activate/deactivate the system allows for prolonged studies to take place, without directly handling the animal. This is of crucial importance in implantable systems (e.g. Lapray et al., 2008, Chung-Chiun et al., 2006), where the only option to power the system up/down is remotely. Many implantable systems of this type revert to a simple hall-effect sensor, which powers the device up/down when a magnet is placed nearby (e.g. Chung-Chiun et al., 2006).

### **2.2.5.12 Bi-directional Communication and Feedback**

Bi-directional communication between the wireless system and its receiver increases the system versatility, as parameters and operating modes can be adjusted. Numerous examples of 2-way communication include commands being sent to the wireless system for changing the sampling rate and number of channels (Chen et al., 2008), changing the system's active state (Lapray et al., 2008), and transmission of commands related to DBS (Ye et al., 2008). An interesting recent system uses bi-directional communication to mediate closed-loop feedback (Ativanichayaphong et al., 2008). In this case the optimum DBS parameters that are transmitted to the wireless system are dependent on the occurrence of neural spikes, which are recorded and transmitted to the computer. Whilst this example demonstrates closed-

loop feedback, the calculation of DBS parameters is performed at the computer end, which adds a transmission delay between the input (spikes) and the response (stimulation). Restricting these calculations to the portable stage reduces this delay (e.g. Mavoori et al., 2005) at the expense of increased processing power (and therefore reduced battery life). As more knowledge is gained in both the fields of neural signal recording for psychiatric diseases and DBS, one can expect more prototype systems in the future that employ closed-loop feedback in this manner.

#### **2.2.5.13 Deep-Brain-Stimulation**

There have to date been a large number of wireless systems developed specifically for DBS in various animals such as primates (Mavoori et al., 2005), rabbits (Peng et al., 2004), mice (de Haas et al., 2012), and rats (Ativanichayaphong et al., 2008, Xu et al., 2004, Ye et al., 2008, Song et al., 2006b, Ewing et al., 2013a, Xing et al., 2011, Sheng-Fu et al., 2010). Systems whose only function is DBS are typically (though not exclusively) made with fewer components than their EEG recording counterparts, and less importance is required regarding the effects of noise or component layout. Furthermore devices which employ wireless telemetry for real-time control require only a transient communication arrangement, thus negating the requirement (otherwise present in neural signal recorders) for a constant transmission which heavily reduces battery life. These systems vary not just in their size and power usage, but also in their DBS parameters and operating modes. Constant-voltage pulses (e.g. Xu et al., 2004, Song et al., 2006b) are easier to generate than constant-current pulses (e.g. Ewing et al., 2013a, de Haas et al., 2012), since they can be driven directly from microcontroller or timer outputs, without the need for additional constant-current circuitry.

Some prototypes combine neural signal recording and DBS into one system (Sheng-Fu et al., 2010, Ativanichayaphong et al., 2008, Ye et al., 2008, Song et al., 2006a, Mavoori et al., 2005), in some cases for the purpose of providing closed-loop feedback (Ativanichayaphong et al., 2008, Mavoori et al., 2005, Sheng-Fu et al., 2010). Devices of this type are a step-up in complexity from separate neural signal

recorders and DBS devices, since they must be able to perform both functions well. Combining a neural recorder and stimulator into one device will inevitably result in a larger device with reduced battery life. Also, the effect that these systems have on each other must be carefully considered. For instance, the high-voltages required to generate a constant current must be electrically isolated from the sensitive neural signal recording circuitry. Also the digital processing module on the system must efficiently divide its time between generating pulses and recording neural signals, whilst maintaining low power. Many wireless neural recorders and stimulators currently described are either large in size (Ativanichayaphong et al., 2008, Ye et al., 2008, Mavoori et al., 2005) or feature limited functionality (Song et al., 2006a). For example a system described by Song et al., (2006a) features only one recording channel and constant-voltage pulses. A recent system for use in rats is actually implemented as a separate recording and separate stimulation system, which can operate together with computer-based closed-loop control, or independently (Zuo et al., 2012), complete with their own batteries.

### **2.2.6 Additional Design Features**

At its core, all wireless EEG recorders and DBS systems work by the same principles, and thus have the same types of components/modules. However many of the different experiments performed in various animals have focussed on more than just neural signal recording and/or stimulation, resulting in a range of peripheral attachments to these devices as seen in the literature.

A common addition is the use of a head-mounted LED to allow for position tracking via video cameras and tracking software (e.g. Fan et al., 2011, Chen et al., 2008, Hawley et al., 2002). This is easy and cost-effective to implement, since it requires only an LED and resistor which can be connected to the system's main power line. These are often used in conjunction with video-tracking systems to enable the animal's position to be determined, e.g. in studies observing rat location with recordings of hippocampal place cells (Chen et al., 2008, Hawley et al., 2002). Cameras have also been seen affixed to the head of monkeys to track its eye

positions (Mavoori et al., 2005), although in this case the system weight is described as 800g. Devices that record the skull vibrations in monkeys have been used alongside dual-channel neuronal signal recording (Grohrock et al., 1997, Jürgens and Hage, 2006), and even a miniature GPS device has been used on homing pigeons (Vyssotski et al., 2006). This latter device was shown to reduce the battery life from 2days 5hrs to just 3hrs 30mins when GPS was activated, highlighting a point that is essential when considering the attachment of any peripheral device to the existing system – that it must balance well with the other performance requirements in the system.

Not all prototypes make use of wireless telemetry; some systems store the EEG data into on-board memory for subsequent uploading and analysis with a computer (Sherk and Wilkinson, 2008, Mavoori et al., 2005, Vyssotski et al., 2006). Whilst this dramatically cuts down on the system size and power consumption that would otherwise be reserved for a wireless telemetry attachment, the signals cannot be displayed in real-time, thus providing no visible feedback on the recorded signals. This is nonetheless an attractive option given the current technological trend of higher amounts of memory being cost-effectively packed into increasingly small sizes.

### **2.2.7 Summary**

Wireless systems for recording and stimulating have proliferated in the past 15 years as an alternative to tethered recording, and have already shown a large diversity. Systems between 0.1g and 800g have been described in a large range of applications from insects to primates, rodents and birds; all of which share the goal of stimulating, and/or recording neural data free from the confines of a cable tether. These systems have been seen to differ widely not just in their cost and core technology, but also in their functionality, performance and specificity to a particular application. There are a myriad of design choices to make when designing either a neural recorder or stimulator, which must be carefully balanced with the experimental requirements for maximum efficiency. A successful system is ultimately

one which fulfils the objective to which it is intended, whilst being a better overall solution than existing available techniques such as tethered recording. Generally speaking commercial systems offer more efficient solutions than many of the prototypes seen, but often at a high cost.

## 2.3 Aims and Rationale

### 2.3.1 Rationale

Despite the diversity in many of the prototypes seen, there still exist plenty of applications for which a novel system is required, such as multichannel DBS or combined EEG recording and DBS in a miniature system. Although numerous systems exist commercially, these are often high in cost due to the small market in which they are sold. Furthermore to the author's knowledge there are no commercially sold wireless system that offers the combined functions of recording and stimulation. Prototype systems which combine wireless recording and stimulation is relatively new, and has been met with several examples that are either large in size (Ativanichayaphong et al., 2008, Ye et al., 2008, Mavoori et al., 2005) or have a functionality that is insufficient for the current investigation (Song et al., 2006a). To maximise the range of experiments that can be performed, innovative enhancements to this field are thus required. A prototype device of this nature can form a necessary milestone towards the development of a commercial-ready system. Given the increasing interest in combining EEG recording with DBS *in vivo*, such a device may prove an attractive option to researchers who wish to expand their experimental designs involving either DBS or EEG recording.

### 2.3.2 Aims

The goal of this study was to develop 2 miniature wireless system solutions that took part in 2 separate experiments; the current study which required simultaneous multichannel LFP recording and DBS in a rodent model of relevance to schizophrenia, and an external study which required chronic 4-channel DBS in freely-moving rodent Parkinson's disease models (Gut and Winn, 2012). The core design requirements for these systems are simplicity, portability and functionality, whilst being cost-effective and easy to replicate by future researchers. As such two wireless systems were developed to perform multichannel recording and stimulation, whilst weighing only 8.5g (including battery).

## 2.4 Methods

### 2.4.1 Systems Overview

This section outlines the design and development of two miniature wireless systems for neural recording and stimulation. The first system described performs multichannel EEG recording and DBS (figure 2.4A), whereas the second performs multichannel DBS only, though with an increased selection of stimulation parameters. Both systems have a number of operating modes and parameters that can be adjusted in real-time through a bi-directional transmission link. Two of the main design criteria for these systems are portability and simplicity, allowing them to be used in a myriad of experimental paradigms with little set-up times. Simply plugging the system into the headstage implant and switching them on is all that is required for instant EEG recording and/or DBS. Their versatility is enhanced by their ability to be reprogrammed, allowing them to integrate further into a particular experimental design (e.g. Chapter 4 – 4.4.7: Equipment Setup; describes how the systems are reprogrammed to facilitate synchronisation between the recorded LFP and external video-tracking data). A summary of the main design features of both systems is given in table 2.1. For the remainder of this chapter the wireless EEG recorder / DBS device is referred to as EEG-DBS, whereas the multichannel DBS device is referred to as M-DBS. Both systems share the same receiver (RCVR) hardware (figure 2.4B), but they are uploaded with different programs and therefore function differently.

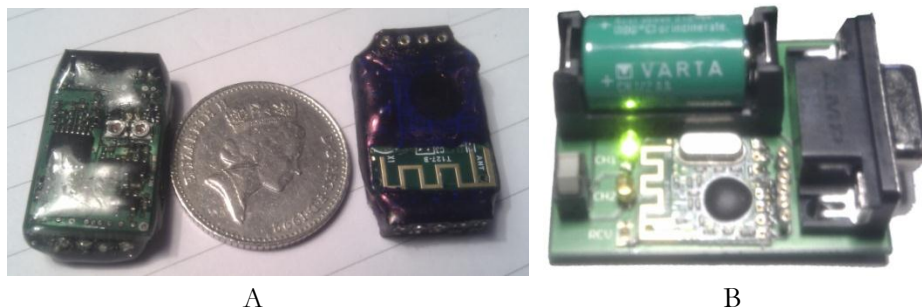


Figure 2.4 – The EEG-DBS system (A), and the RCVR system (B).



	EEG-DBS	M-DBS
<b>Stimulation</b>		
No. of Channels	2	4
DBS Type	Constant current	Constant current
Pulse-Modes	Monophasic	Monophasic (selectable direction), charge-balanced biphasic
Frequency Range	0.1Hz – 5KHz	0.1Hz – 5KHz
Current Intensity Range	30uA–1.5mA, (up to 15V)	30uA– 1.5mA (up to 15V)
Pulse-Width Range	10uS– 500mS	10uS– 500mS
<b>EEG Recording</b>		
No. of Channels	4	N/A
Resolution	16-bit	N/A
Amplification	520	N/A
Filtering	1.5Hz - 100Hz	N/A
Sampling Rate	500 Hz	N/A
Input CMRR	90 dB (input amplifier)	N/A
<b>General</b>		
Operating Modes	low-power, EEG, DBS, EEG + DBS	low-power, DBS-1, DBS-2, dual DBS
Battery Life	5-8h	48-72h
Max. Transmission Range	3-5m	8-10m
Transmission Type	2.4GHz MSK	2.4GHz MSK
Dimensions	28 x 17 x 7 mm	28 x 17 x 7 mm
Weight (inc. battery)	8.5g	8.5g
Software Control	WinEDR	DB Stimulator

Table 2.1 – Overview of the functions and parameters in both wireless systems. Note that the transmission range and battery life shown reflect typical usage, whilst the systems are in an active state (recording EEG or generating stimulus pulses). These parameters are highly dependent on transmission power, system operating mode, stimulation parameters, and ultimately the type of battery used. WinEDR and DB Stimulator were created by Strathclyde University (J. Dempster, Strathclyde University).

## 2.4.2 Wireless EEG-DBS System and Receiver Summary

The EEG-DBS and the RCVR system perform the functions of wireless recording and stimulation in freely-moving animals. The EEG-DBS system contains a 10-pin headstage connector that is designed to plug into a custom-built headstage implant (which is surgically implanted onto the head of the animal). Through this headstage interface signals are detected, and stimulus pulses are injected. The RCVR system is designed to facilitate a bi-directional communication link between the EEG-DBS system and the computer. As such LFP information is transmitted to the computer from the EEG-DBS system, and commands are sent the opposite way whenever the user wishes to change the system's operation mode or parameters. Control options available allow the user to activate/deactivate DBS, change the DBS pulse-width and frequency, reset the system, put it into a low-power state (which deactivates EEG recording), and subsequently put the system back into active operation. The DBS constant-current intensity may also be adjusted by turning a small screw built onto the side of the device, with the assistance of an oscilloscope (TDS 3032B; Tektronix) and a custom-built intensity-changer circuit. The software WinEDR (J. Dempster, Strathclyde University) is used to display and record real-time EEG (figure 2.5A), as well as control the wireless system through its DBS Stimulator control panel (figure 2.5B).

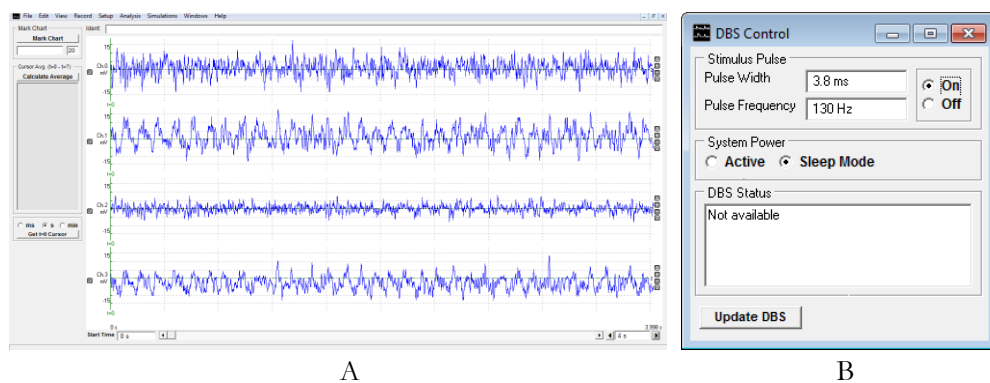


Figure 2.5 – WinEDR is used for displaying/recording real-time multichannel LFP information (A), and for controlling the EEG-DBS system through its DBS Control module (B). WinEDR was created by Strathclyde University (J. Dempster, Strathclyde University).

The EEG-DBS system can be considered as three hardware modules connected to a central control hub (figure 2.6). The central control hub in this case is the microcontroller (MCU; MSP430f2013; Texas Instruments), and the three modules are the EEG recording circuitry, DBS circuitry, and transceiver module (DSQFM-TRX-2; Quasar UK). The programmable MCU controls and coordinates the exchange of information between the three modules; using the transceiver as a means of communicating with the RCVR system. The receiver contains the same combination of MCU and transceiver, which again acts as the control hub and communications exchange, respectively. The receiver features RS232 circuitry necessary to send and receive communications from the computer via its serial port, and also a buffer which stores wireless commands from the computer until they're ready to be transmitted to the EEG-DBS system.

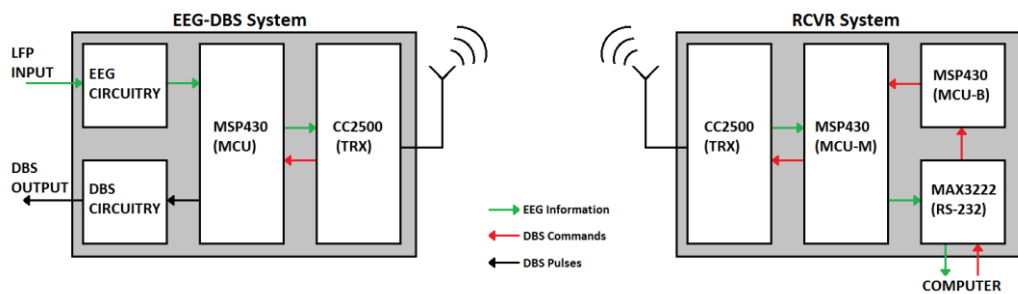


Figure 2.6 – Block diagram of the EEG-DBS and RCVR systems. A 2-way communication link facilitates the transfer of EEG information in one direction, and the transfer of DBS commands/pulses in the other.

## 2.4.3 EEG-DBS System Design

### 2.4.3.1 MCU Programming

The MCU is essentially a miniature programmable computer that can manipulate any hardware connected to it through its input/output ports. Specifically its functions involve organising, digitizing and forwarding EEG to the transceiver module, generating DBS pulses, and altering the system's DBS parameters and operational modes based on the content of wirelessly received commands. The MSP430 MCU was chosen because it balances various low-power modes of operation with a

relatively high-degree of functionality, such as an in-built 16-bit analogue-digital converter which it uses to sample incoming EEG.

The software architecture used in the EEG-DBS systems MCU is based on a custom-design which integrates two timed control loops with interrupts (see figure 2.7 for a functional block diagram of the MCU software). One timed control loop is used during the systems active (power-on) state involving sampling/transmitting EEG and checking for commands, whilst the other operates during the system's sleep-mode state, which involves periodically checking for a "power-up" command.

When the system is first powered on, the MCU's software follows an initialisation sequence in which its ports/peripherals are configured prior to use. During this step, the CC2500 transceiver is programmed by the MCU to the desired transmission settings (see 2.4.5: Transceiver for EEG-DBS and RCVR Systems – for an overview of the transmission configuration used). Next the MCU enters the default (active-state) control loop, which is a cycle of sampling EEG, forwarding the digitised content to the transceiver module (which is subsequently transmitted wirelessly), and checking the transceiver's receive buffer for any incoming commands that may have been received. EEG in this case is sampled by the MCU at 500Hz per channel, with a 16-bit voltage resolution. Any incoming commands that are sent from WinEDR (via the RCVR system) are checked following the transmission of EEG data. If a command has been received, the MCU momentarily halts the operation of the main control loop, whilst it adjusts its parameters/operation based on the content of the received command.

Commands for adjusting the DBS frequency or pulse-width result in the appropriate system settings being adjusted, after which the system resumes its normal operation of sampling/transmitting EEG. A "wake/reset" command given during the system's active-mode simply resets the MCU, which has the effect of switching off DBS and resetting its pulse-width and frequency parameters to the default programmed value. If the command is to activate DBS, pulses are then generated by the MCU using a timer-controlled interrupt to adjust the voltage on one of its port pins. This timer-controlled interrupt can run concurrently with either the default or power-down

control loops, meaning that DBS can operate during either active or sleep mode. A command for deactivating DBS simply deactivates this timer-controlled interrupt routine, thus halting DBS.

A command for powering down the system causes EEG recording to stop, as the MCU powers down most of its own in-built peripherals including the analogue-digital converter, prior to entering the sleep-mode control loop. At this point the transceiver enters a low-power wake-on-radio (WOR) state whereby it activates for approximately 4.4ms every second to detect a possible power-up command (see 2.4.5: Transceiver for EEG-DBS and RCVR Systems). DBS may be active during this power-down state for a longer period of time than it would during active-mode, since the transceiver and MCU are operating with greatly reduced currents. During the low-power state the MCU will only respond to a wake/reset command, at which point it will resume normal operation in sampling and transmitting EEG. Note that during each cycle of the active-mode control loop, the MCU regularly powers up/down its own in-built peripherals (timers, ADC, etc.) in order to conserve battery life and maximise MCU efficiency.

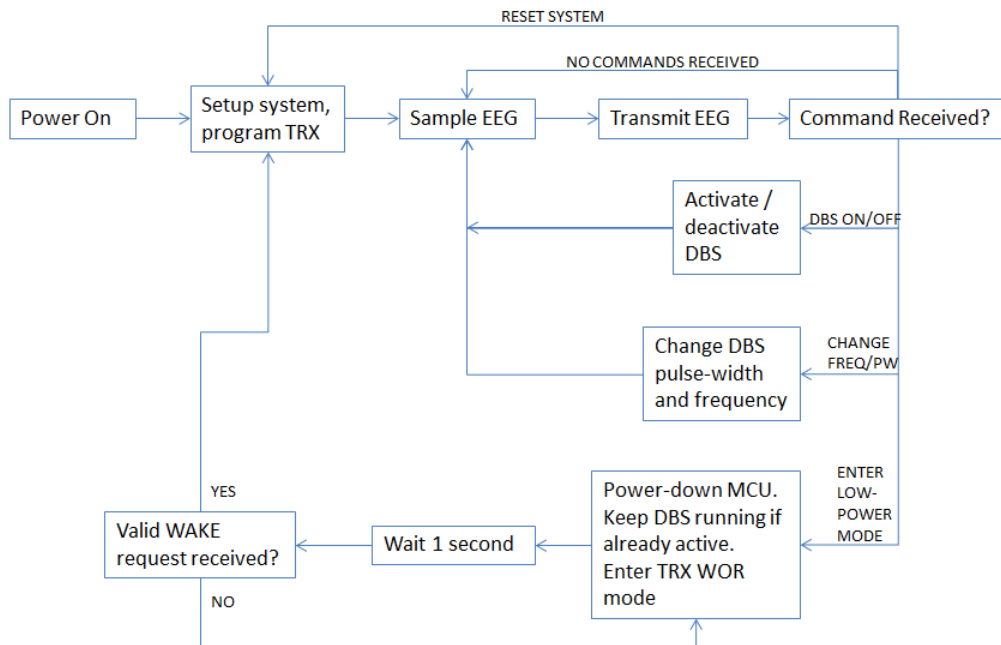


Figure 2.7 – Flowchart for the software loaded onto the EEG-DBS MCU. By default the system samples and transmits EEG, whilst checking for incoming commands for altering its parameters and operating modes.

A custom architecture was necessary for the system's MCU, because of a) its code memory and peripheral limitations, and b) the necessity for the system to adhere strictly to accurate timing with regards to EEG sampling and DBS pulse generation. During the main (active-state) control loop, the transmission and reception functions are separated into their own time slots, in order to avoid a condition whereby the receiver is being written to and read from at the same time. In order to preserve the timing accuracy of EEG sampling/transmission, interrupts that are related to the analogue-digital converter and transceiver are set at a higher priority than those which are used in the DBS interrupt routines, meaning that samples will always be taken at 500Hz regardless of the active state of DBS is active or not. Prior to use in animal studies, the EEG-DBS system was repeatedly tested in all of its operating modes and stimulus parameter ranges and subsequently refined until it could operate reliably and robustly.

Generally speaking, altering the programming of the MCU can completely alter the way the system functions. The sampling rate, number of channels and DBS default parameters can be adjusted, along with a myriad of transmission options such as transmit power, frequency and modulation type. The transceiver can be reprogrammed (via the MCU) to operate on a variety of frequency channels, allowing multiple wireless systems to operate together. The EEG-DBS system is reprogrammed via its 4-pin battery connector, which contains a 2-pin Spy-Bi-Wire JTAG interface. This interface allows the MCU's flash memory to be rewritten and debugged with a new program. Programs are written and edited in C on a desktop/laptop computer using the compiler software IAR Embedded Workbench IDE (IAR Systems). Compiled programs are uploaded to the DBS-EEG system using an MSP430 USB debug-interface module (MSP-FETU430IF; Texas Instruments), connected to a custom-built circuit board for reprogramming.

#### **2.4.3.2 EEG Recording Circuitry**

Information from the LFP electrodes are passed through several levels of signal conditioning prior to being transmitted wirelessly (figure 2.8). Each electrode

interface is coupled to an instrumentation amplifier input via a  $10\mu\text{F}$  capacitor, which prevents DC brain/electrode potentials from saturating the input amplifiers. A  $47\text{K}\Omega$  resistor is placed immediately after this to provide a DC return path for the instrumentation amplifiers input bias currents (since it features an extremely high input impedance, bias currents must be dealt with in this way to prevent the output from saturating at the voltage rails). These components result in the first of two high-pass filters, which cuts-off frequencies below  $0.34\text{Hz}$ . Signals then pass through the instrumentation amplifiers INA2126 (Texas Instruments), which provides buffering of the signals and an initial pre-amplification of 10. The INA2126 amplifier was chosen for its low quiescent current of  $175\mu\text{A}$  per channel, low noise ( $35\text{nV}/\sqrt{\text{Hz}}$ ), common-mode-rejection ratio of  $90\text{dB}$ , and extremely high input impedance ( $> 1\text{G}\Omega$ , which is important for capturing brain signals). For each channel of pre-amplified LFP, the reference electrode is used as the common reference. Following pre-amplification a second high-pass filter is configured with a cut-off frequency of  $1.5\text{Hz}$ , which filters the signal prior to the main amplification. The main amplifier in this case is the AD8609 quad operational amplifier (Analog Devices), with each channel configured with a gain of 52, thus giving the system a total amplification of 520 per channel. The AD8609 was chosen for its low input offset currents (at  $50\mu\text{V}$  maximum), low noise performance ( $35\text{nV}/\sqrt{\text{Hz}}$ ) and low quiescent current ( $50\mu\text{A}$  maximum). Following amplification signals are passed through a low-pass filter configured to cut-off frequencies above  $100\text{Hz}$ . Finally amplified and filtered signals are passed to a 4-N-1 high-speed multiplexer (AD604; Analog Devices), which is controlled directly by the MCU. The MCU samples incoming multiplexed LFP through a single 16-bit analogue-digital converter input, and switches the multiplexer output (via 2 control pins) immediately after taking the current sample, which allows the multiplexer's output to cycle from one LFP signal to the next. To this effect each LFP channel is sampled at a rate of  $500\text{Hz}$ . The input range of the ADC is  $\pm 600\text{mV}$ , which when combined with the  $\times 520$  gain and 16-bit quantisation gives the signals a theoretical resolution of  $35.2\text{nV}$ . Lastly, a charge-pump (TPS60400; Texas Instruments) is included in the circuitry to provide a  $-3\text{V}$  supply for all of the EEG signal-conditioning integrated circuits.

### **2.4.3.3 DBS Circuitry**

The DBS circuitry consists of a DC voltage amplifier, constant current generator, and virtual ground generator (figure 2.8). The pattern of DBS pulses (which is variable in frequency and pulse-width) is generated entirely by the MCU, based on either its pre-programmed default setting, or a command that has been wirelessly received. The DBS pulse-pattern passes through one of the MCU's standard output ports, which in turn drives a transistor switch and gates the flow of constant current. The design of the constant-current generator was adapted from a previous 2-channel wireless DBS device (Ewing et al., 2009). The current flow in this case is held constant by a pnp-pnp transistor pair configured as a constant current source, and its magnitude is set by configuring a variable resistor. This has a base value of  $50\text{K}\Omega$ , which when varied can change the current intensity from  $30\mu\text{A}$  to over  $1.5\text{mA}$ . However in practice the maximum voltage available for this is  $15\text{V}$ , which limits the actual current based on the impedance between the DBS electrode terminals depending on the electrode geometry (see 2.4.17.4: DBS Pulses in Saline). The maximum voltage provided for this is set by the DC voltage amplifier, which amplifies the system voltage by 6 times (meaning a  $2.5\text{-}3\text{V}$  battery level is amplified to  $15\text{-}18\text{V}$ ; see 2.4.17.1: EEG-DBS Battery Life Measurements). If a higher voltage is required then an alternative battery (e.g. a  $3.3\text{V}$  cell) can provide for an increased DBS voltage amplification. The voltage amplifier consists of two voltage doublers (MAX1682; Maxim Integrated Products) connected in series; the second of which is configured to triple the voltage by inclusion of a Schottky diode – capacitor rectifier. Finally a virtual ground was inserted as the reference for each DBS electrode contact to isolate DBS ground from the recording circuitry ground. This was done by placing two miniature operational amplifiers (OPA347; Texas Instruments), in a unity gain configuration.

### **2.4.3.4 Printed Circuit Board (PCB) Design**

The EEG-DBS system consists of two separate printed circuit boards (PCBs) sandwiched together; the transceiver module (with its crystal oscillator swapped for an SMD version), and the rest of the system circuitry which is housed on the main



board (figure 2.9). The main board was fabricated by PCB-Pool, and was designed as a 21x16x1.6mm 4-layer PCB using the design software Eagle (CadSoft), with surface-mount (SMD) components distributed on both sides. Each layer consists of a ground plane which fills all of the spaces between the circuit tracks, pads and vias. PCB tracks for the power-line (Vdd) and DBS circuitry are 150um in width, whilst all other tracks are 125um. Power-line tracks are arranged in a 'star' pattern to ensure that parasitic signals from one device does not flow into another (as it would with a 'bus' pattern), thus ensuring each device has a clear path to the main power battery connection (Vdd). Vias are used extensively throughout the design to connect circuit tracks and ground planes between the 4 layers, and are 200um in diameter. Vias configured for external connections are 300um in diameter (shown in red and yellow in figure 2.9C). The main PCB is split into 4 quadrants, containing the following:

- Input pre-amplification and high-pass filtering (top side, upper half),
- Input coupling, main amplification, and low-pass filtering (bottom side, upper half),
- DBS voltage amplification, charge-pump, and constant-current generators (bottom side, lower half),
- MCU and multiplexer (top side, lower half).

The ground planes of the analogue circuitry (up to the multiplexer stage) are physically isolated from the rest of the circuitry, with only two vias in inner-layer 2 connecting them to the main system ground (figure 2.9E). This ensures that little current from the digital and transceiver circuitry flows into the analogue ground plane. In addition the EEG ground connector is isolated from the rest of the system (including the rest of the analogue circuitry) using a via on inner-layer 2 to connect it. Having the noisy RF circuitry housed on a separate PCB isolates it further from the rest of the system. In this case the ground connector of the TRX module is placed in close proximity to the main system ground connector, thus minimising current flow into the main PCBs ground plane. Generally speaking the positioning of all components has been considered with respect to the direction of current flow in the ground plane – as such narrow points in the ground plane are avoided to reduce the chance of current building up in these regions. The positioning of all components has also been considered with respect to parasitic impedances and

capacitances; tracks and components from the analogue plane are separated from the digital plane. Finally, all active integrated circuits have power supply decoupling capacitors placed in close proximity to the power pins (Vdd or Vss); 10uF is used for the main power-line decoupling, and 1uF is used for each individual IC.

External connections on the left-side of the board are made to the system's 10-pin headstage connector. Connections on the right-side of the board connect the transceiver module, and the 4-pin battery/programming connection. For convenience in system assembly, the transceiver module's external pins line up with their relevant connections on the system's main PCB.

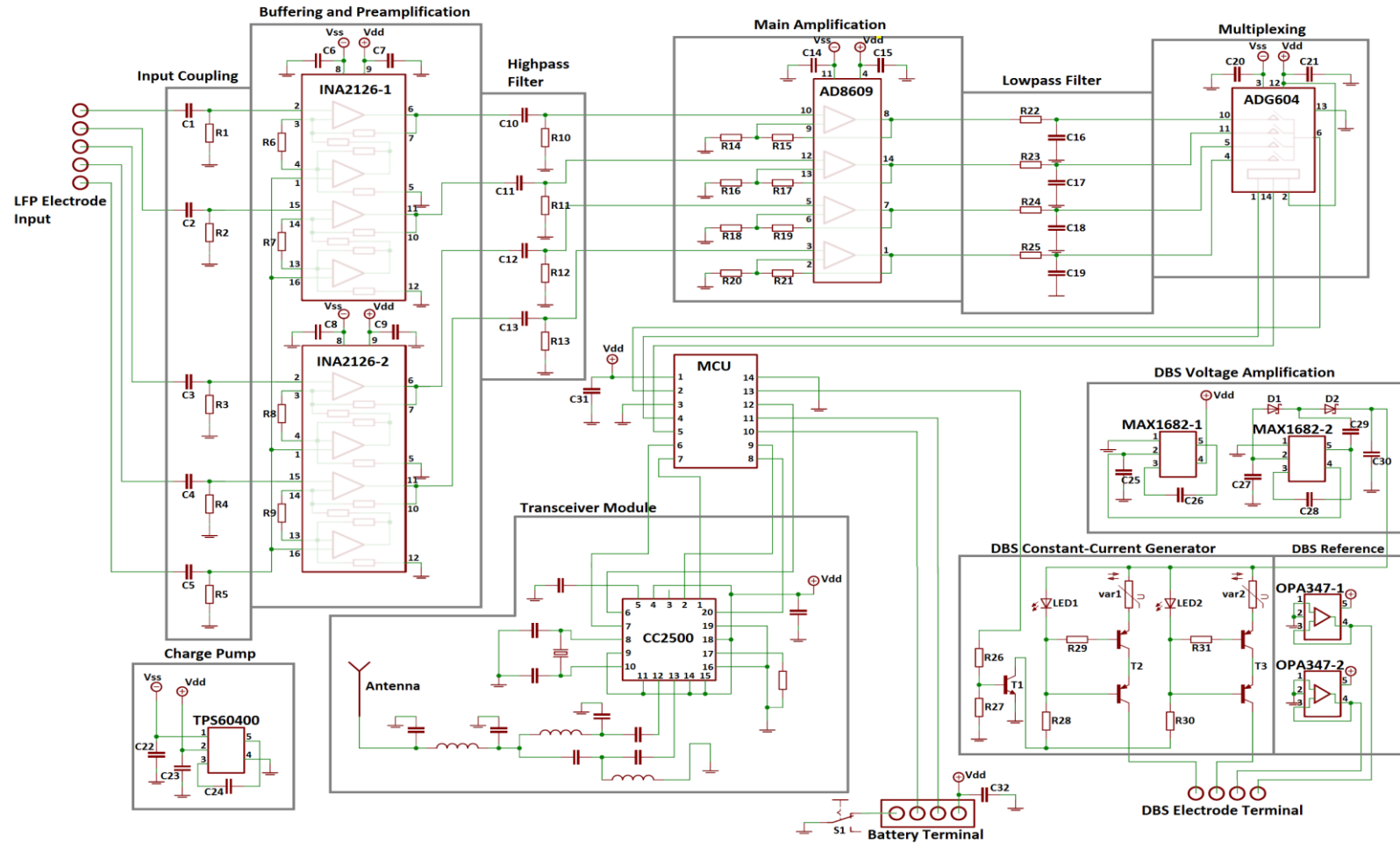


Figure 2.8 – Circuit diagram for the EEG-DBS system. The numbers on the integrated circuits represent their physical pin connections with external tracks.

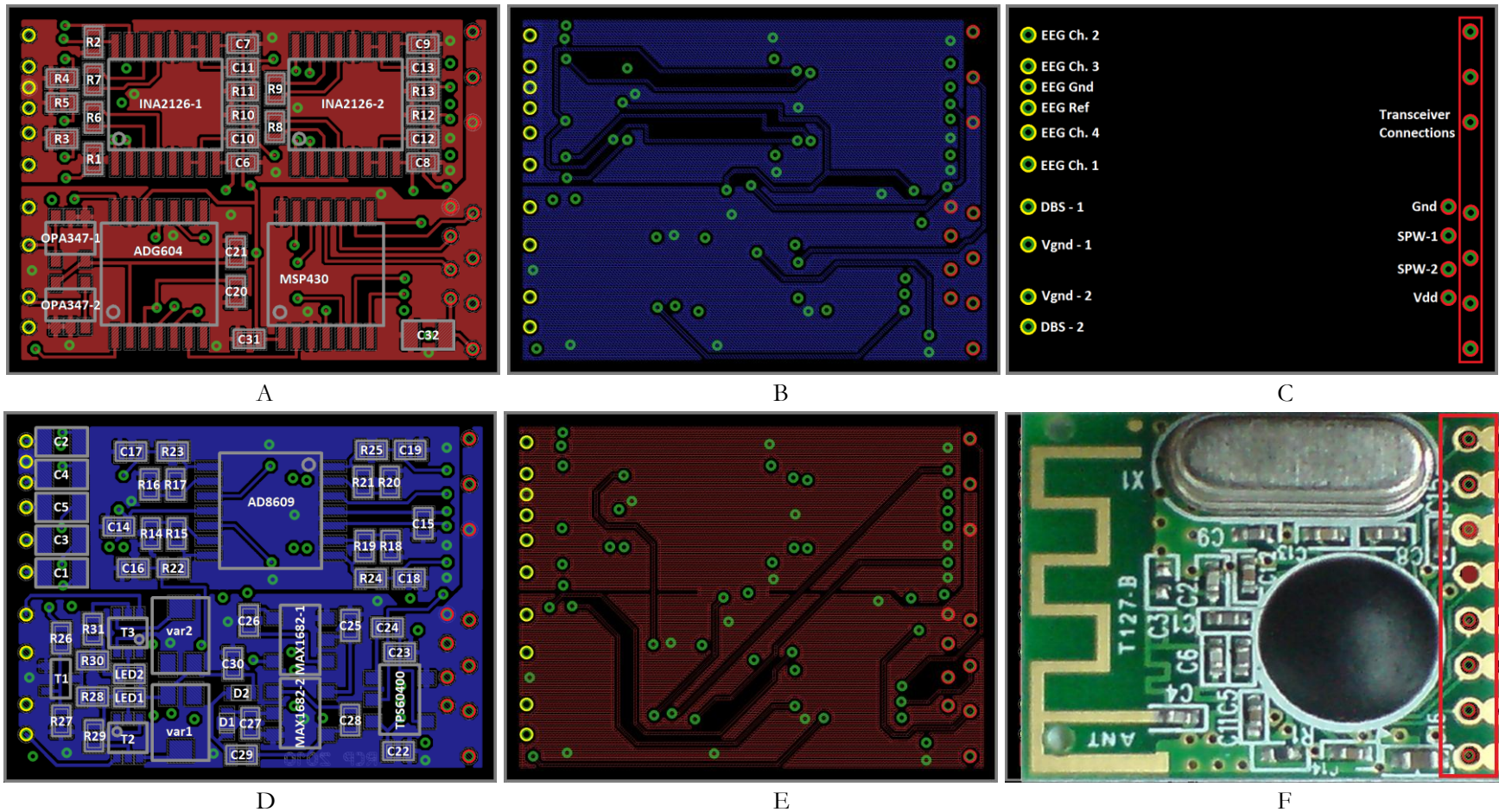


Figure 2.9 – PCB design for the EEG-DBS system showing the placement of tracks, pads, vias and components on the top (A), bottom (D) and inner (B,E) layers. The external connectivity with the headstage, battery/programmer and transceiver module are shown in (C), with connections to the animal (via headstage) shown in yellow, and transceiver/battery/programming connections shown in red. The transceiver sits on top of the PCB and aligns with the relevant connections (F).

In Circuit Diagram	Description	Value	Amount Used in Design	Package	Manufacturer	Manufacturer Part Number	Supplier
<b>Integrated Circuits</b>							
MCU	MSP430 Microcontroller	n/a	1	TSSOP-14	Texas Instruments	MSP430F2013IPW	Farnell
ADG604	4-channel Analog Multiplexer	n/a	1	TSSOP-14	Analog Devices	ADG604YRUZ	RS Components
TPS60400	Charge-Pump Inverter	n/a	1	SOT-23	Texas Instruments	TPS60400DBVT	Farnell
INA2126-1, INA2126-2	Dual Instrumentation Amplifier	n/a	2	SSOP-16	Texas Instruments	INA2126EA/250G4	RS Components
AD8609	Quad Operational Amplifier	n/a	1	TSSOP-14	Analog Devices	AD8609ARUZ	Farnell
OPA347-1, OPA347-2	Single Operational Amplifier	n/a	2	SC-70	Texas Instruments	OPA347SA/250G4	RS Components
MAX1682-1, MAX1682-2	Voltage Doubler	n/a	2	SOT-23	Maxim Integrated Products	MAX1683EUK+	RS Components
<b>Discrete Components</b>							
C1-C5, C32	Capacitor	10uF	6	0603	AVX	06036D106MAT2A	Farnell
C10-C13	Capacitor	2.2uF	4	0402	AVX	04026D225KAT2A	Farnell
C16-C19	Capacitor	100nF	4	0402	AVX	0402YC104KAT2A	Farnell
C6-C9, C14, C15, C20, C21, C22-C31	Capacitor	1uF	17	0402	Multicomp	MCCA000500	Farnell
R1-R5	Resistor	47K $\Omega$	4	0402	Susmu	RG1005P-473-B-T5	Farnell
R6-R9, R22-R25	Resistor	16K $\Omega$	8	0402	Welwyn	PCF0402-R-16K-B-T1.	Farnell
R10-R13	Resistor	499K $\Omega$	4	0402	Multicomp	MC0402WGF4993TCE	Farnell
R14, R16, R18, R20	Resistor	100 $\Omega$	4	0402	TE Connectivity / NEOHM	CPF0402B100RE1	Farnell
R15, R17, R19, R21	Resistor	5.1K $\Omega$	4	0402	Welwyn	PCF0402-R-5K1-B-T1.	Farnell
R26, R28, R30	Resistor	10K $\Omega$	3	0402	Welwyn	PCF0402PR-10KBT1	Farnell
R27	Resistor	100K $\Omega$	1	0402	Welwyn	PCF0402-R-100K-B-T1.	Farnell
R29, R31	Resistor	4.7K $\Omega$	2	0402	Susmu	RG1005P-472-B-T5	Farnell
D1, D2	Diode, Schottky	n/a	2	SOD-923	On Semiconductor	NSR0130P2T5G	Farnell
LED1, LED2	LED	Red	2	0402	VCC	VAOL-S4GT4	Farnell
T1	Transistor, NPN	n/a	1	SOT-523	Diodes Inc.	BC847CT-7-F	Farnell

In Circuit Diagram	Description	Value	Amount Used in Design	Package	Manufacturer	Manufacturer Part Number	Supplier
T2, T3	Dual Transistor, PNP	n/a	2	SOT-666	NXP	BC857BV	Farnell
var1, var2	Trimmer Resistor	50K $\Omega$	2	n/a	Bourns	3312J-1-503E	Farnell
Other							
Transceiver Module	2.4 GHz Transceiver Module	n/a	1	n/a	Quasar	QFM-TRX2-24G	Quasar
XOSC-1	Crystal Oscillator	26MHz	1	n/a	Epson Toyocom	FA-128	Farnell
S1	SPDT Switch	n/a	1	n/a	Multicomp	MCS2S-A15F	Farnell
Battery	Battery, Lithium, 170mAh	3V	1	CR1/3N	Varta	6131101501	Farnell
System Sockets	28-way DIP sockets	n/a	(see methods)	n/a	E-TEC	POS-328-S001-95	RS Components
Nylon Nut	Nylon Nut	M2	1	n/a	Duratool	1110020	Farnell

Table 2.2 – Information for each of the components used in the EEG-DBS system.

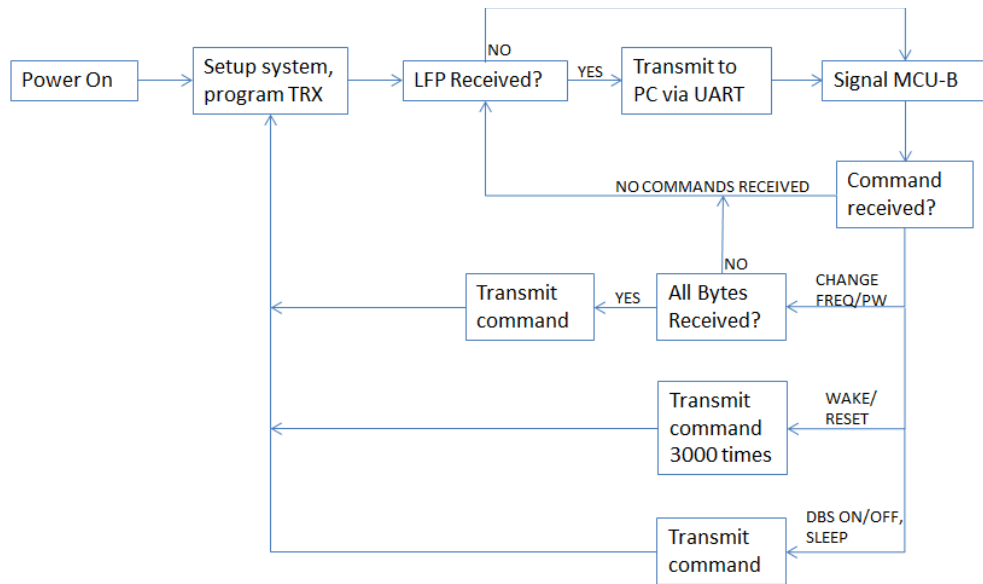
## 2.4.4 RCVR Design for EEG-DBS System

### 2.4.4.1 Main MCU and Buffer Programming

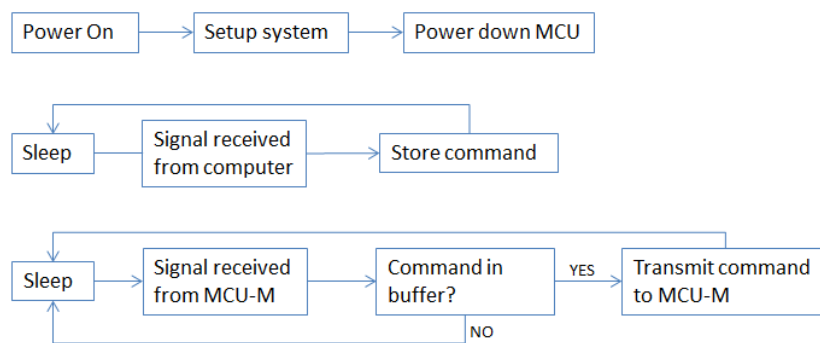
There are two MCU's (MSP430f2013; Texas Instruments) in the RCVR system, one of which acts as the control hub of the system (MCU-M), and the other which acts as a memory buffer (MCU-B) for incoming commands sent from the computer. The main cycle of operation for MCU-M consists of a) listening to incoming LFP data from the wireless system, b) transferring any received LFP data to the computer (via RS232 interface), and c) signalling MCU-B to see if any commands from the computer have arrived (figure 2.10A). Sampled EEG information arrives at the RCVR MCU via the transceiver module, and is subsequently forwarded to the computer via the RS232 interface. Commands arriving from the computer, on the other hand are sent directly to MCU-B (via RS232 interface), where it waits until requested by MCU-M. A second MCU was used as a memory buffer because MCU-M cannot simultaneously listen to incoming transmissions from both the transceiver module and the computer – owing to resource limitations on that particular MCU model. As such during each cycle of operation MCU-M signals MCU-B to check if any commands have arrived. If so MCU-B transfers this command to MCU-M (figure 2.10B). Commands to activate/deactivate the DBS, or power the system up/down require only a single byte and are forwarded to the transceiver immediately. Commands for changing the DBS pulse-width or frequency however are 4-bytes in length and in this case MCU-M will wait for the entire command sequence before transmitting (see 2.4.6: Data Handling and Commands 1). If the command is to reset/wake the system, MCU-M transmits this 3000 times over approximately 1 second, because when the EEG-DBS system is powered down, its transceiver module is active for only 4.4ms each second. When not receiving any commands or communicating with MCU-M, MCU-B spends its time in a low-power state; awakening only when a) a command is sent from the computer via the RS232 interface, and b) signalled by MCU-M to check for commands.

Communication between MCU-M, MCU-B, the RS232 interface and the computer are all based on an 8-N-1 UART transmission protocol. This is an asynchronous transmission mode used for transmitting data to/from a computer's serial port, and

in this case the data rate between all devices is 115.2Kbaud. All data is transmitted as single bytes; commands for changing the pulse-width and frequency are transmitted as four separate bytes in rapid succession (see 2.4.6: Data Handling and Commands 1).



A



B

Figure 2.10 – Flowchart for the software loaded onto the RCVR system’s MCU-M (A) and MCU-B (B). By default MCU-M is responsive for incoming LFP data, which it forwards to the computer via the RS232 interface (A). MCU-B operates entirely in sleep-mode, and is only responsive to commands transmitted from the computer, or from requests for commands transmitted from MCU-M (B).



#### **2.4.4.2 RS232 Transceiver**

Communication between MCU-M/MCU-B and the computer requires an interface to account for the different voltages used by each. The RCVR system operates with a standard 3V battery, with an active voltage range of 0-3V. Data input/output with the serial port utilises a voltage range of +/- 5V. The RS232 transceiver (MAX3222; Maxim Integrated Products) was used in conjunction with several 100nF loading capacitors to form this interface.

#### **2.4.4.3 Additional Circuitry**

The RCVR system has a DPDT (double-pole, double-throw) switch in addition to three LEDs (figure 2.11). The DPDT switch is connected to an input pin of MCU-M as well as the green and blue LEDs. Toggling this switch selects one of two frequency channels for the RCVR system to pick up transmissions from, with the green and blue LED reflecting which channel is selected. The red LED is connected directly to an output port of MCU-M and lights whenever valid transmissions are being received.

#### **2.4.4.4 Printed Circuit Board Design**

The RCVR system components are distributed onto both sides of a 2-layer PCB designed in Eagle (Cadsoft) and manufactured by PCB-Pool, and measures approximately 50x36x1mm (figure 2.12). The top layer houses the transceiver module, battery holder, DPDT switch, LED's (with resistors), and the 9-pin D-SUB connector for connecting to the serial port. The bottom side houses the main and buffer MCU's, the RS232-transceiver (with loading capacitors), and power-supply decoupling capacitors. The pins on the transceiver module line up with the relevant connections on the PCB, thus simplifying connection of the two. Unlike the EEG-DBS and M-DBS systems, the RCVR system is designed to be programmed only once. As such 0.6mm vias are placed next to the transceiver module where temporary wire-connections are attached for programming the main and buffer MCU's. Once programmed, these connections are discarded, and the vias are

soldered to the main power-line (Vdd), which runs parallel to these pins (on the top side).

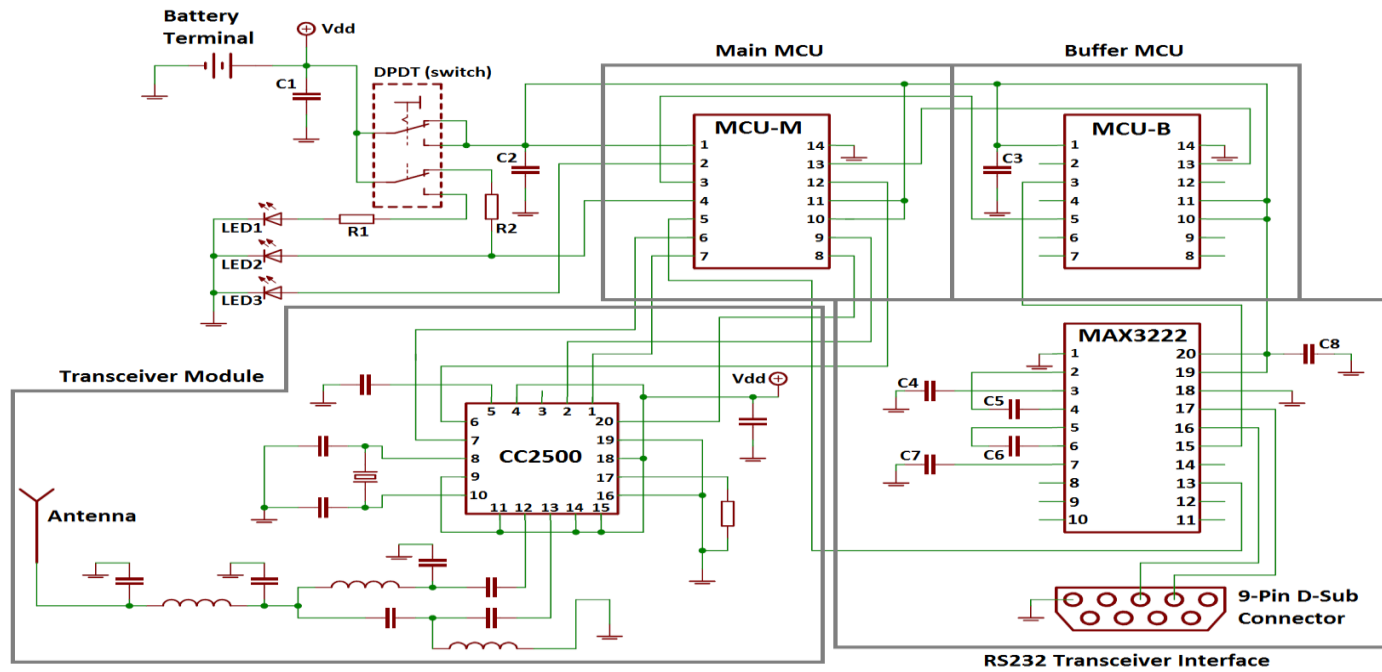


Figure 2.11 – Circuit diagram for RCVR system. Numbers in the integrated circuits correspond to their external pin connections.

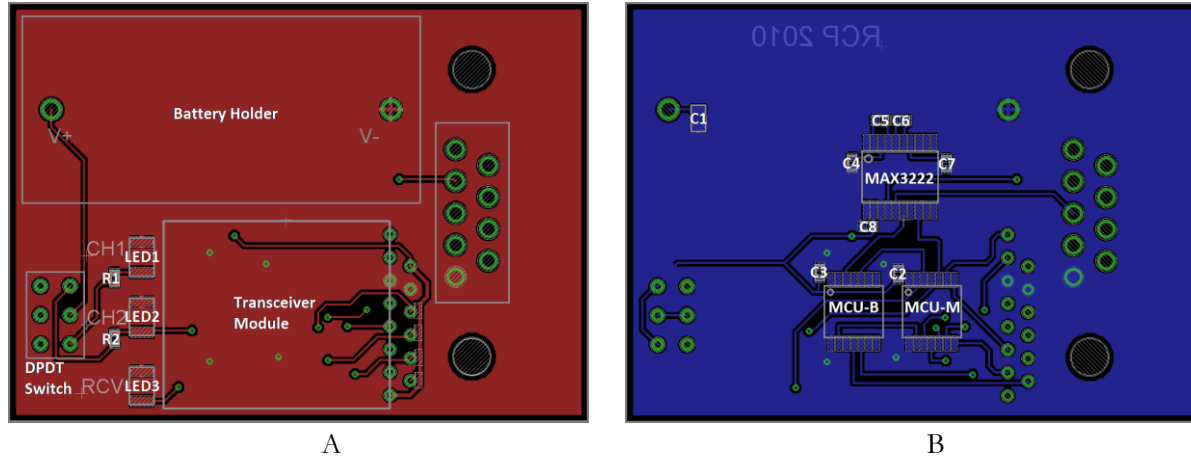


Figure 2.12 –PCB design for the RCVR system showing the placement of tracks, pads, vias and components on the top (A) and bottom (B) layers.

In Circuit Diagram	Description	Value	Amount Used in Design	Package	Manufacturer	Manufacturer Part Number	Supplier
<b>Integrated Circuits</b>							
MCU-M, MCU-B	MSP430 Microcontroller	n/a	2	TSSOP-14	Texas Instruments	MSP430F2013IPW	Farnell
MAX3222	Transceiver, RS232	n/a	1	TSSOP-20	Maxim Integrated Products	MAX3222ECUP+	Farnell
<b>Discrete Components</b>							
C1	Capacitor	10uF	1	0603	AVX	06036D106MAT2A	Farnell
C2, C3, C8	Capacitor	1uF	3	0402	Multicomp	MCCA000500	Farnell
C4 - C7	Capacitor	100 nF	4	0402	AVX	0402YC104KAT2A	Farnell
R1, R2	Resistor	150 $\Omega$	2	0402	Vishay Draloric	CRCW0402150RFKEAHP	Farnell
LED1	LED	blue	1	SMD	Avago Technologies	ASMT-BB20-NS000	Farnell
LED2	LED	red	1	SMD	Avago Technologies	ASMT-BR20-AS000	Farnell
LED3	LED	green	1	SMD	Avago Technologies	ASMT-BG20-AS000	Farnell
<b>Other</b>							
Transceiver Module	2.4 GHz Transceiver Module	n/a	1	n/a	Quasar	QFM-TRX2-24G	Quasar
S1	Rocker Switch, DPDT	n/a	1	n/a	NKK Switches	GW22RHP	Farnell
Battery Holder	Battery Holder	n/a	1	1/2AA	Keystone	108	Farnell
9-Pin D-SUB Connector	Connector, D-SUB	n/a	1	n/a	TE Connectivity / AM	1734354-1.	Farnell
Battery	Battery, Lithium, 950mAh	3V	1	1/2AA	Varta	6127101301	Farnell

Table 2.3 – Information for each of the components used in the RCVR system.

### 2.4.5 Transceiver for EEG-DBS and RCVR Systems

The transceiver module (TRX; DSQFM-TRX-2; Quasar UK) is a ready-made transceiver circuit based on the CC2500 chipset (Texas Instruments), complete with all of the necessary passive components for operation, and an in-built meandered inverted 'F' PCB antenna. The passive components in this system consist of power supply decoupling capacitors, a crystal oscillator complete with loading capacitors, a current bias resistor, and several inductors and capacitors that make up RF filtering and antenna impedance matching circuitry. The CC2500 transceiver itself is a miniature computer, which runs a program uploaded by the MCU when the system is switched on. In all systems the MCU and transceiver are tightly integrated together with 5 dedicated communication lines; 4 of which constitute a fast synchronous SPI (serial peripheral interface) bus. This module performs the wireless transmission/reception functions on all wireless and receiver systems, and enables a 2-way link both with the controlling MCU and another transceiver via the wireless link. Furthermore it can operate in a low-power 'wake-on-radio' (WOR) mode when instructed to do so by the MCU. In this state the TRX powers down, and activates for approximately 4.4ms every second to detect a possible 'wake' command, thus conserving battery life whilst remaining responsive to incoming commands.

The digital format for wireless transmission used between all systems is 2.4 GHz minimum-shift keying (MSK; see also CC2500 datasheet; Texas Instruments, 2010). Data sent from the MCU to the TRX consists of an address byte for identifying the receiving TRX, and a series of content organised into a data-stream called a payload (figure 2.13). The address byte that is transmitted matches the same unique address byte which is programmed into the receiving MCU. The payload contains either the LFP information and DBS status bits (EEG-DBS to RCVR transmission), or DBS commands (RCVR to EEG-DBS transmission; see 2.4.6: Data Handling and Commands 1). The TRX takes the address and payload, and incorporates them into a larger data-stream called a packet (figure 2.13), which is sent as a discrete burst transmission. In the EEG-DBS system, burst transmissions are sent at 500Hz, meaning each transmission corresponds to a single sample of LFP data from each of the 4 channels. Packets contain additional overhead which is added by the

transmitting TRX, and removed from the receiving TRX. This additional overhead consists of the preamble bits, a synchronisation word, and a 16-bit cyclic-redundancy check (CRC) code (figure 2.13). The preamble bits and sync words allow the receiving TRX to detect the presence of a data packet being broadcast. The CRC is a 16-bit code which is appended to all transmission packets, and checks the validity of the received data. The CRC code is calculated based on the contents of the payload and address byte, and is transmitted along with the rest of the packet. This calculation is performed again by the receiver, and the two CRC codes are checked to see if they match. Packets which fail either the address check or CRC check are discarded, and the data is not subsequently passed to the receiving MCU. Lastly all packets undergo a signal whitening procedure using a pseudorandom PN9 sequence, which has the effect of distributing the signal’s output power over its transmission bandwidth – thereby improving transmission performance.

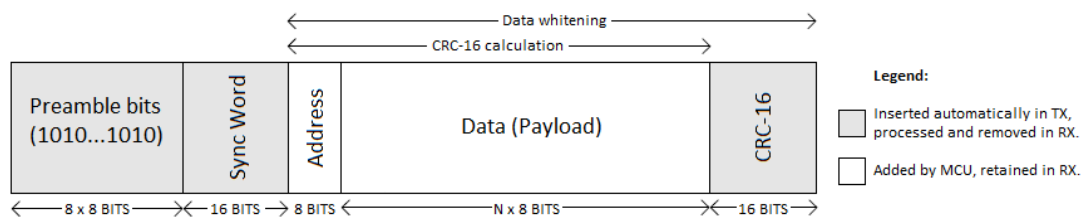


Figure 2.13 – Structure of a data packet sent wirelessly from the transceiver module. Adapted from CC2500 datasheet (Texas Instruments, 2010).

## 2.4.6 Data Handling and Commands 1

Given that communication between the wireless system and its receiver is bi-directional, there are two opposite paths for which data is passed. Recorded EEG originates in the brain and ends up being displayed on the computer in WinEDR. Commands to control the wireless system on the other hand begin at the computer in WinEDR and end up in the EEG-DBS MCU. This section outlines how data is handled and formatted at each step of these two pathways.

### 2.4.6.1 EEG-DBS to RCVR Information: LFP and Status Bytes

Communication from the EEG-DBS to the RCVR system is made through burst transmissions involving 12-byte payloads (figure 2.14). Transmissions are made after the 4 multiplexed LFP channels have been sampled once, at a rate of 500Hz. The 12 bytes in the payload are separated into four sets of three bytes, with each set corresponding to an individual LFP channel. Each set contains: byte identifier bits, channel identifier bits, 16-bits of EEG, and 3 DBS status bits. The byte identifier bits tell WinEDR where the start and end of this three-byte sequence is. In this case the first bit of the first byte is '1' and the first bit of the subsequent two bytes are '0'. The channel identifier bits are two bits following the first byte identifier bit (1), which identifies which channel the sample of EEG belongs to. In this case these bits are 00 (channel 1), 01 (channel 2), 10 (channel 3) and 11 (channel 4). The 16 bits of each EEG sample is spread out over the three-byte set. Lastly the final three bits in the last byte are either 000 when DBS is off or 111 when DBS is on. EEG information arriving at the RCVR system is forwarded directly to WinEDR via the RS232 interface and serial port.

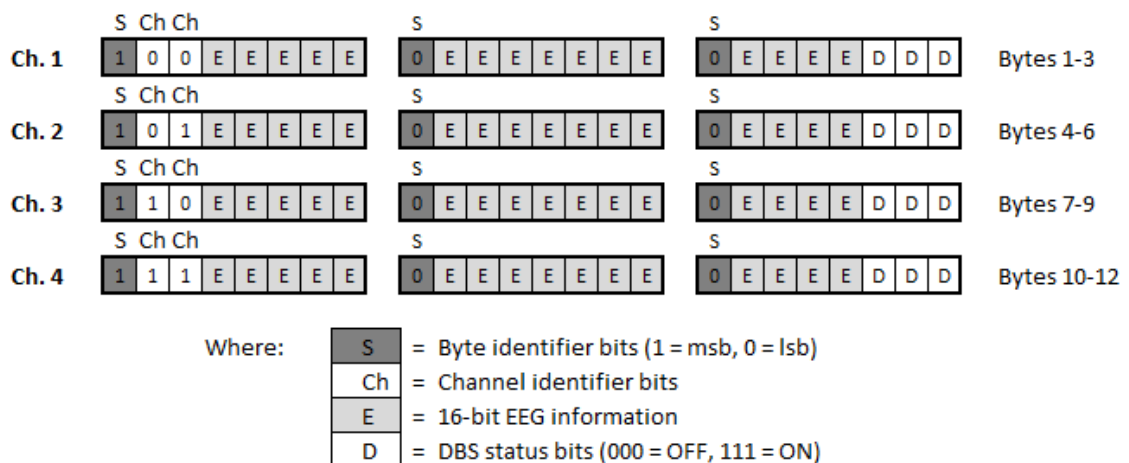


Figure 2.14 – 12-byte transmission payload from the EEG-DBS to RCVR system, containing sampled LFP, DBS status information, and channel/byte identifier information.



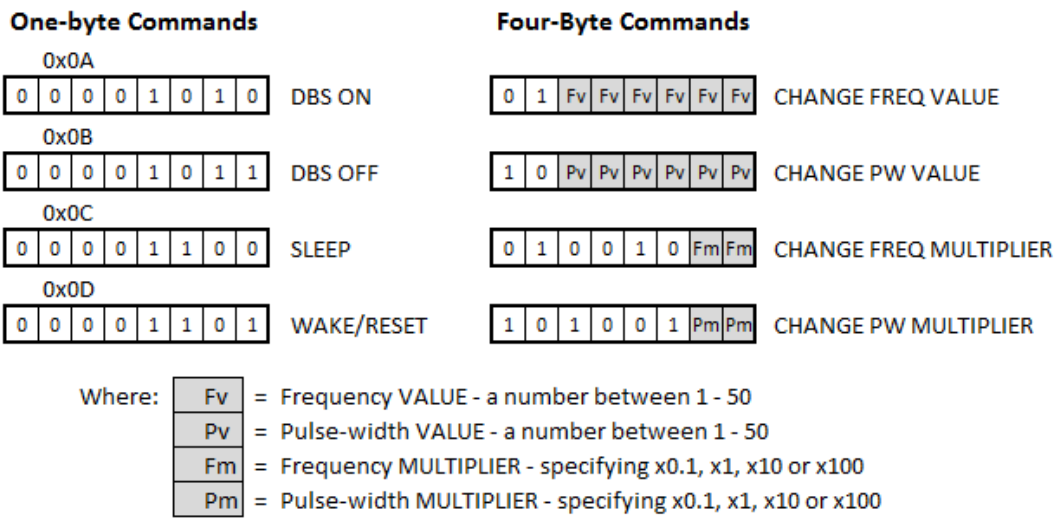
#### 2.4.6.2 Commands for Controlling the Wireless System

Commands are sent from WinEDR through the serial port and to the RCVR system via the RS232 interface one byte at a time, and fall into two categories: single-byte commands, and four-byte commands. Single-byte commands have a fixed value and are used for activating/deactivating DBS, powering down the wireless system, or for waking/resetting it, and four-byte commands are used for changing the DBS pulse-width and frequency (figure 2.15A). The values used in single-byte commands are static, e.g. the code for activating DBS is always 0x0A, and the code for putting the system to SLEEP mode is always 0x0C. The content of 4-byte commands change based on the desired pulse-width and frequency the user wishes to send.

The 4-byte commands for changing the DBS pulse-width and frequency have been arranged in such a way that a large range of parameters are possible using a minimum number of bytes. The 4-byte commands for changing the DBS pulse-width and frequency can be broken down into 2 bytes for changing the pulse-width, and 2 bytes for changing the frequency (figure 2.15B). Each DBS parameter requires a byte specifying a VALUE, and a byte specifying a MULTIPLIER. The VALUE is a number ranging from 1-50, and the MULTIPLIER specifies x0.1, x1, x10 or x100. These two properties are multiplied together with a pre-defined BASE frequency/pulse-width (which is set at 1Hz/100 $\mu$ s respectively), to arrive at the final parameter used for stimulation. For example, given a pulse-width VALUE of 20 and a MULTIPLIER of x10 (as specified with 2 bytes), the final pulse-width used for stimulation is 20mS:

$$\text{BASE} * \text{VALUE} * \text{MULTIPLIER} = 0.0001 \times 20 \times 10 = 20\text{mS}.$$

Using this arrangement, the resolution of each parameter depends on what the MULTIPLIER is set to. For example if the pulse-width multiplier is set to x0.1, its VALUES can support a range between 10-500 $\mu$ s, in 10 $\mu$ s steps. If this MULTIPLIER is increased to x10, its VALUES will support a range of 1-50ms, in 1ms steps. WinEDR automatically determines the most appropriate VALUE/MULTIPLIER command to send based on the specified stimulation settings.



A

	MULTIPLIER, Pm/Fm			
	X 0.1	X 1	X 10	X 100
Frequency (BASE = 1Hz)	0.1Hz – 5Hz (0.1 Hz steps)	1Hz – 50Hz (1Hz steps)	10Hz – 500Hz (10Hz steps)	100Hz – 5000Hz (100Hz steps)
Pulse-Width (BASE = 100µS)	10µS – 500µS (10µS steps)	100µS – 5mS (100µS steps)	1mS – 50mS (1mS steps)	10mS – 500mS (10mS steps)

B

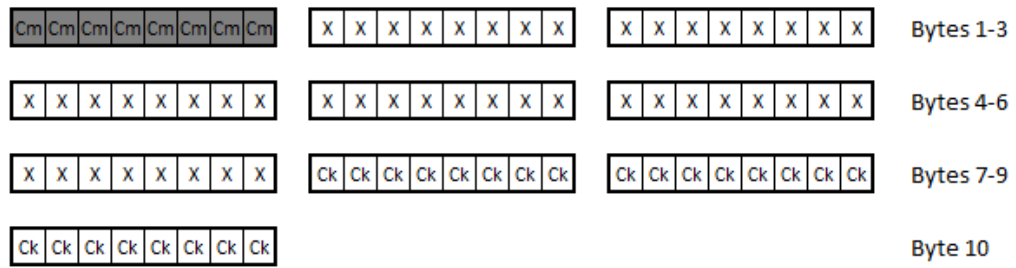
Figure 2.15 – Single-byte commands are fixed in value, as opposed to four-byte commands whose contents change depending on the desired stimulation parameters (A). The range of frequency and pulse-width values are set by the VALUE and MULTIPLIER information contained in the 4-byte commands, and is summarised in (B).

### 2.4.6.3 RCVR to EEG-DBS Information: Commands

All transmissions from the RCVR system utilise 10-byte payloads, which are assembled by MCU-M (figure 2.16). The content of this payload changes depending on whether a single- or multi-byte command has been issued. For single-byte commands, the RCVR system places the command byte into the first byte in the payload, and forwards it to the TRX. When a four-byte command is issued, MCU-M waits until all four bytes has been received before assembling a payload. Unlike the single-byte commands, the four-byte commands must be translated to a form that can be directly utilised by the EEG-DBS MCU. In this case the VALUE and MULTIPLIER information for each parameter is converted into variables that configure the timing peripherals built into the wireless system’s MCU. These transformations require a series of calculations on the VALUE and MULTIPLIER

information, and to balance processing resources evenly, these calculations are carried out in both the EEG-DBS and RCVR systems. The VALUE information is converted by the EEG-DBS system MCU; hence the commands specifying frequency/pulse-width VALUE are placed directly into the second and third bytes of the RCVR payload. The MULTIPLIER information is converted by the RCVR system, in which case it is translated into 4 bytes that occupy the 4<sup>th</sup> – 7<sup>th</sup> bytes in the payload. The first byte in the payload for four-byte commands is a unique identifier which tells the EEG-DBS system that the command specifies a DBS frequency/pulse-width change. In both single- and four-byte payloads, the final three bytes are manual ‘check’ bytes, which add further verification on the received data. Like the address check and CRC code check, payloads which fail this additional check are discarded by the EEG-DBS system.

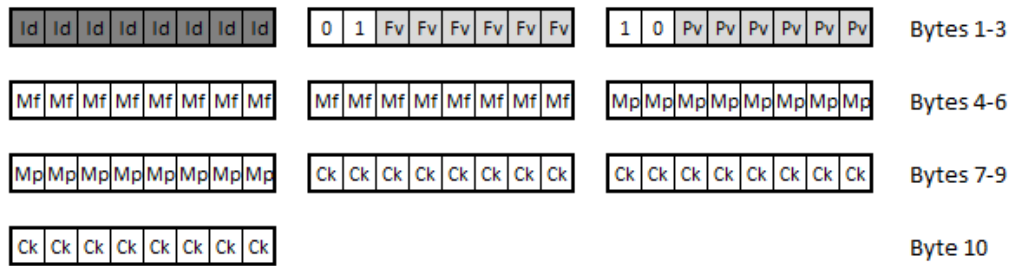
For both single- and four-byte commands, the 10-byte payload is forwarded once to the RCVR TRX. The only exception is when a WAKE/RESET command is issued, in which case this process occurs 3000 times. This repeated transmission ensures that the EEG-DBS TRX can detect the command when in WOR mode.



Where:

Cm	= One-byte command
Ck	= Manual check bits
X	= Not used

A



Where:

Id	= Command identifier bits
Fv	= Frequency VALUE
Pv	= Pulse-width VALUE
Mf	= Transformed frequency MULTIPLIER information
Mp	= Transformed pulse-width MULTIPLIER information
Ck	= Manual check bits

B

Figure 2.16 – 10-byte transmission payload from the RCVR to EEG-DBS system, which takes a different format depending on whether a single byte (A) or multi-byte (B) command is issued.

### 2.4.7 Wireless M-DBS System and Receiver Summary

The multimode DBS system (M-DBS) was adapted from the EEG-DBS system design, with EEG recording functionality swapped for an additional 2 DBS channels with enhanced control options. The 2 DBS channel pairs can be independently controlled with regards to its stimulation frequency, pulse-width, and pulse mode. Pulse mode options allow the user to utilise biphasic pulses, as well as specifying the direction of monophasic pulses (positive or negative). Like the EEG-DBS system, the current intensity for each DBS channel can be adjusted by turning a small screw

on the side of the device. Because the transceiver isn't transmitting a constant stream of EEG with this system, it operates entirely in a low-power mode; activating only the peripherals/circuitry that is required. Similarly both MCU's in the system operate almost entirely in a low-power mode, with the DBS generation algorithms running. Furthermore low-power mode is enhanced in this system with a digitally-controlled switch that cuts power to the DBS circuitry when not in use. The RCVR system is the same as that used with the EEG-DBS system with regards to its circuitry, but it was programmed differently. Its built-in DPDT switch was reassigned to accommodate a safety feature, which when toggled causes the system to prevent any transmissions of DBS parameters that specify a stimulus duty cycle of over 5%. Furthermore the default 'power-on' state of this system can be changed to specify any stimulus parameters for either channel. Because many aspects of this system are based on its EEG-DBS predecessor, this section will assume an understanding of many of the concepts introduced in the previous section; explaining EEG-DBS system design.

The M-DBS system consists of 2 MSP430f2013 (Texas Instruments) microcontrollers, which each independently configure their own DBS circuitry (figure 2.17). The master microcontroller (MCU-1) deals with communication between itself and the transceiver module, and forwards any received commands on to the slave microcontroller (MCU-2). Furthermore it controls a digital power-switch (TPS22945; Texas Instruments), which is used to cut power to the voltage amplification circuitry and constant-current generators, when DBS is not in use. Wireless transmission is unilateral, and performed through repeated burst transmissions, since the M-DBS TRX operates entirely in WOR mode. Commands arrive through the computer to the RCVR system and are checked for validity. This system is controlled using DB Stimulator (J. Dempster, Strathclyde University).

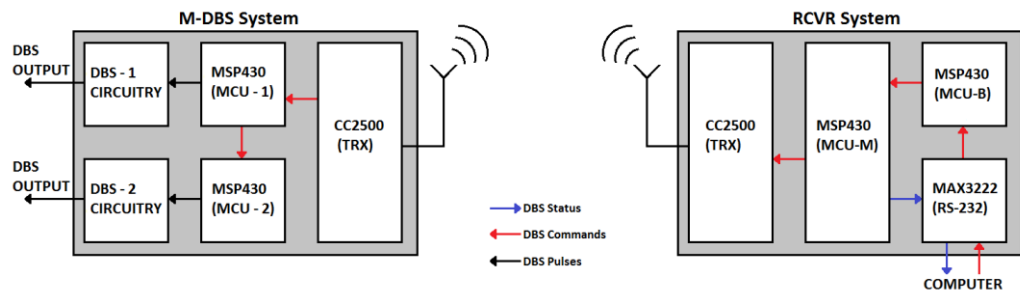


Figure 2.17 – Block diagram of the M-DBS and RCVR systems. The M-DBS system contains two separate MCU’s which each configure a DBS channel pair.

## 2.4.8 M-DBS System Design

### 2.4.8.1 MCU-1 and MCU-2 Programming

Two MCUs are used in the M-DBS system in order to allow for independent control of two DBS channel pairs. The software architecture used in both MCU’s is timed-control loops with interrupts, whereby each MCU operates in a timed low-power control-loop whilst periodically checking for incoming commands. When the system is switched on, both MCU-1 and MCU-2 configure their settings and DBS parameters before entering a low-power state (figure 2.18). At this point MCU-1 also programs the TRX to permanently operate in a WOR mode. The default pre-programmed DBS parameters for each channel will determine the behaviour of the systems when power is switched on. At all times MCU-1 monitors the DBS status; if neither MCU-1 nor MCU-2 is generating DBS pulses, MCU-1 powers down the DBS circuitry via the digital power switch. DBS pulses for each MCU are generated in the same way as that of the EEG-DBS system (see 2.4.3.1: MCU Programming), in which case a timer-controlled interrupt is used to alter the voltage levels on a single MCU port.

Commands are 5-byte sequences which configure all DBS parameters; DBS pulse-mode, active state, frequency and pulse-width, and can be issued to either DBS channel pair (see 2.4.11: Data Handling and Commands 2). Upon receiving this command its contents are checked for validity by MCU-1 (in addition to the TRX-mediated address and CRC checks). Should any received data fail this additional check, its contents are changed to a ‘DBS-OFF’ command. At this point if the

command is for MCU-1, then the appropriate changes are made. If the command is for MCU-2, the data is passed on via 8-N-1 UART transmission at 115.2 Kbaud.

The M-DBS system has a 6-pin battery connector (as opposed to 4-pin on the EEG-DBS system), to accommodate the positive and negative battery terminals, and 2 Spy-Bi-Wire JTAG interfaces for reprogramming each of the MCU's. In this case both MCU's can be reprogrammed with default stimulation parameters, which it will assume when the system power is switched on. A special 'reprogrammer' circuit board was constructed for this device to quickly reprogram both MCU's. As with the EEG-DBS system, programs were written and edited in C, and uploaded to the M-DBS system using an MSP430 USB debug-interface module (MSP-FETU430IF; Texas Instruments) connected to a custom-built reprogrammer circuit.

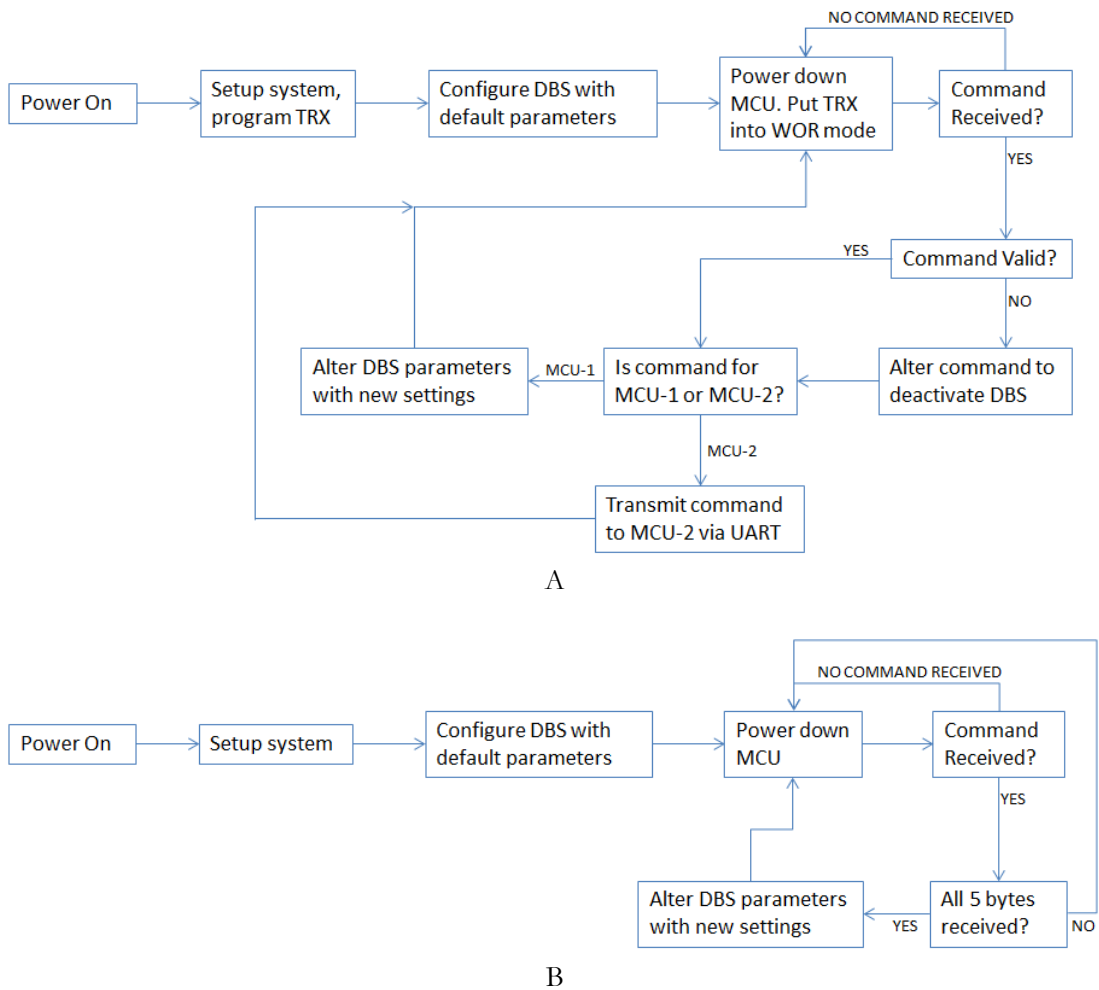


Figure 2.18 – Flowchart for the software loaded onto the master (MCU-1; A) and slave (MCU-2; B) MCU’s in the M-DBS system. Both MCU’s operate entirely in a low-power state, and awoken whenever commands are received from the transceiver module. Any commands destined for MCU-2 are transferred by MCU-1 via UART.

### 2.4.8.2 DBS Circuitry

The DBS circuitry in this system is altered from the EEG-DBS system to provide 2 independently controllable channel pairs, as well as circuitry that change the direction of DBS current (figure 2.19). Like the EEG-DBS system, a DC voltage amplifier circuit provides the x6 amplification of the DC battery voltage, which in turn drives the constant current generators. Each MCU interfaces directly with its own constant current generator via a transistor switch; allowing a variable constant current for each channel to be set using a 50K $\Omega$  variable resistor. In addition, a



virtual ground generator provides a reference point for each of the 4 DBS channels, using a quad operational amplifier (OPA4347; Texas Instruments). In this system the virtual ground points and the constant-current outputs for each channel pair are interfaced directly with a quad single-pole double-throw (SPDT) high-speed digital switch (ADG333; Analog Devices). These switches are controlled directly by the MCU's and alternate the direction of current flow. When biphasic pulses are enabled these switches change the output direction during the centre of each stimulus pulse, thus providing a reversal of constant current flow.

### **2.4.8.3 Printed Circuit Board Design**

Like the EEG-DBS system, the M-DBS system consists of two separate printed circuit boards (PCB's) sandwiched together; the transceiver module (with its crystal oscillator swapped for an SMD version), and the rest of the system circuitry which is housed on the main board (figure 2.20). The main board is designed as a 4-layer PCB in Eagle (Cadsoft), fabricated by PCB-Pool, and measures approximately 21x16x1.6 mm with SMD components distributed on both sides. Each of the 4 layers contains a ground plane which fills any spaces between the tracks, vias and pads. Most of the tracks in this system are 150 $\mu$ m in width, owing to the extensive DBS circuitry used. The remaining control-line tracks that don't carry as much current are set to 125 $\mu$ m. Also, like the EEG-DBS system the main power-line (Vdd) tracks are arranged in a 'star' pattern to allow for an optimal passage of current without inducing unnecessary noise. Vias are used extensively in this design to connect the tracks and ground planes of the 4 layers together, and are 200 $\mu$ m. Connecting vias however are set to 400 $\mu$ m diameter.

The top side of the board consists of the two MCUs and the high-speed SPDT switches, and the bottom side consists of the rest of the circuitry including the DBS voltage amplifier, constant-current circuitry, digital switch and virtual ground generator. The arrangement of most of the DBS circuitry is based on an optimal pattern used in the EEG-DBS system, only in this system it is replicated on the upper and lower halves of the bottom side of the PCB, to create 4 DBS channels.

All integrated circuits (except for the SPDT switches) contain 1 $\mu$ F power-supply decoupling capacitors, and a 10 $\mu$ F capacitor is placed next to the main power supply (Vdd) pin which connects to the battery. External vias are used for connections on both sides of the board; the left side contains the DBS output pins, and the right side contains a) the transceiver connections, and b) the 6-pin battery/reprogrammer connection. The external pins on the transceiver module line up with the external transceiver connections on the main PCB, to assist with assembly.



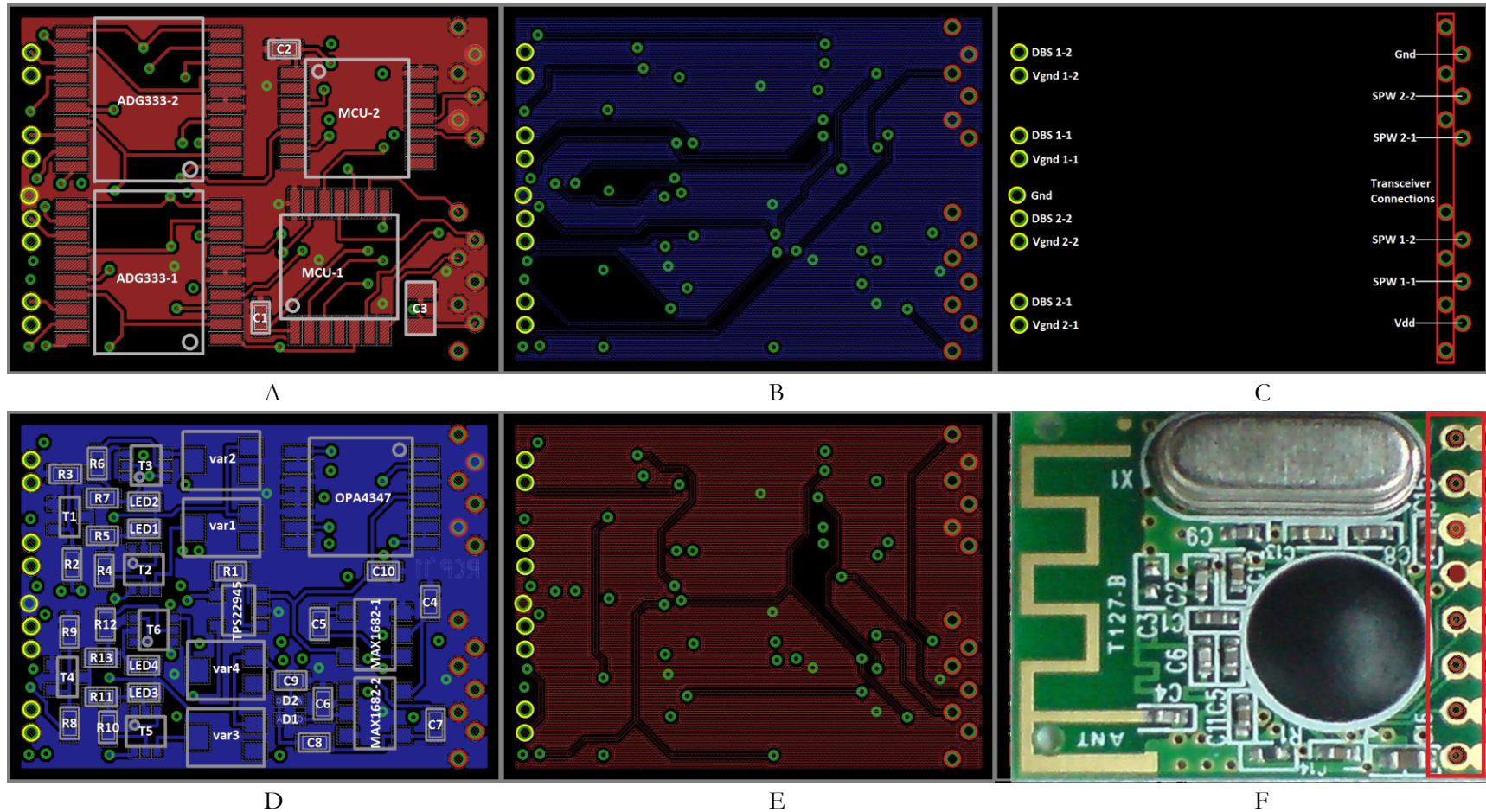


Figure 2.20 – PCB design for the M-DBS system showing the placement of tracks, pads, vias and components on the top (A), bottom (D) and inner (B,E) layers. The external connectivity with the headstage, battery/programmer and transceiver module are shown in (C), with connections to the animal (via headstage) shown in yellow, and transceiver/battery/programming connections shown in red. The transceiver sits on top of the PCB and aligns with the relevant connections (F).

In Circuit Diagram	Description	Value	Amount Used in Design	Package	Manufacturer	Manufacturer Part Number	Supplier
<b>Integrated Circuits</b>							
MCU-1, MCU-2	MSP430 Microcontroller	n/a	2	TSSOP-14	Texas Instruments	MSP430F2013IPW	Farnell
ADG333-1, ADG333-2	Quad SPDT Switch	n/a	2	SSOP-20	Analog Devices	ADG333ABRSZ	Farnell
OPA4347	Quad Operational Amplifier	n/a	1	TSSOP-14	Texas Instruments	OPA4347EA/250	Farnell
MAX1682-1, MAX1682-2	Voltage Doubler	n/a	2	SOT-23	Maxim Integrated Products	MAX1683EUK+	RS Components
TPS22945	Digital Power Switch	n/a	1	SC-70	Texas Instruments	TPS22945DCKR	Farnell
<b>Discrete Components</b>							
C1-C3, C5-C10	Capacitor	1uF	8	0402	Multicomp	MCCA000500	Farnell
C4	Capacitor	10uF	1	0603	AVX	06036D106MAT2A	Farnell
R1, R3, R5	Resistor	100 K $\Omega$	3	0402	Welwyn	PCF0402-R-100K-B-T1.	Farnell
R2, R4, R7, R9, R11, R13	Resistor	10 K $\Omega$	6	0402	Welwyn	PCF0402PR-10KBT1	Farnell
R6, R8, R10, R12	Resistor	4.7 K $\Omega$	4	0402	Susmu	RG1005P-472-B-T5	Farnell
D1, D2	Diode, Schottky	n/a	2	SOD-923	On Semiconductor	NSR0130P2T5G	Farnell
LED1-LED4	LED	red	2	0402	VCC	VAOL-S4GT4	Farnell
T1, T4	Transistor, NPN	n/a	1	SOT-523	Diodes Inc.	BC847CT-7-F	Farnell
T2, T3, T5, T6	Dual Transistor, PNP	n/a	2	SOT-666	NXP	BC857BV	Farnell
var1 - var4	Trimmer Resistor	50 K $\Omega$	4	n/a	Bourns	3312J-1-503E	Farnell

In Circuit Diagram	Description	Value	Amount Used in Design	Package	Manufacturer	Manufacturer Part Number	Supplier
Other							
Transceiver Module	2.4 GHz Transceiver Module	n/a	1	n/a	Quasar	QFM-TRX2-24G	Quasar
XOSC-1	Crystal Oscillator	26 MHz	1	n/a	Epson Toyocom	FA-128	Farnell
S1	SPDT Switch	n/a	1	n/a	Multicomp	MCS2S-A15F	Farnell
Battery	Battery, Lithium, 210mAh	3V	1	2032	Multicomp	CR2032	Farnell
System Sockets	28-way DIP sockets	n/a	(see methods)	n/a	E-TEC	POS-328-S001-95	RS Components
Nylon Nut	Nylon Nut	M2	1	n/a	Duratool	1110020	Farnell

Table 2.4 – Information for each of the components used in the M-DBS system.

## **2.4.9 RCVR Design for M-DBS System**

The circuitry in the M-DBS receiver is the same as that used for the EEG-DBS receiver (refer to 2.4.4: RCVR Design for EEG-DBS System). However it is programmed differently and thus cannot be used with the EEG-DBS system.

### **2.4.9.1 MCU-M and MCU-B Programming**

Communication between the M-DBS and the RCVR systems is carried out in a similar way to that of the EEG-DBS system. In the RCVR system one MCU is used as a memory buffer (MCU-B), and the other as the control hub (MCU-M). Programming of MCU-B is the same as that used for the EEG-DBS system (see 2.4.4.1: Main MCU and Buffer Programming). MCU-M is not receiving a constant stream of EEG data this time, and so it remains in a low-power mode, periodically signalling MCU-B to see if any incoming commands have arrived. Incoming commands are all 5-bytes in length (see 2.4.11: Data Handling and Commands 2), and upon receiving the first byte the RCVR system waits until the set are collected (figure 2.21). The next course of action depends on which way the RCVR system's built-in DPDT switch is toggled. If toggled one way, a check will be performed on the 5-byte command to see if the stimulus duty cycle exceeds a pre-programmed limit (5%). If this is the case, the transmission does not take place, and an error signal is transmitted to the software DBStimulator via the RS232 interface. Valid commands that satisfy this check are transmitted 3000 times because the M-DBS TRX is operating in WOR mode. Following this the 5-byte command is sent back to the computer via the RS232 interface.

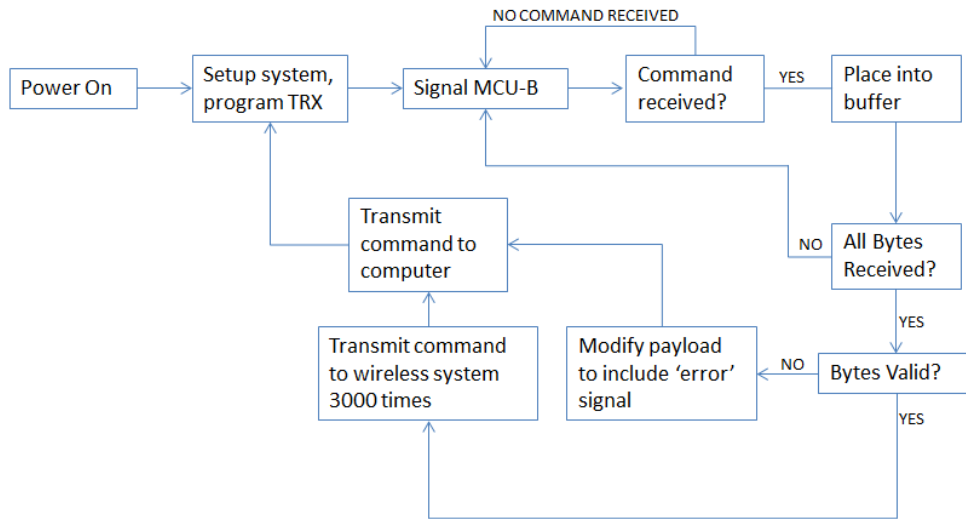


Fig. 2.21 – The RCVR MCU-M spends most of its time in a low-power state, periodically signalling MCU-B for incoming commands. Upon reception of the first byte, the MCU waits for the remainder to arrive. Once all bytes have arrived, they are checked, and transmitted to the M-DBS system if valid.

#### 2.4.10 Transceiver for M-DBS and RCVR Systems

The transceiver module used on the M-DBS and RCVR systems are configured in almost exactly the same way as that with the EEG-DBS system and its RCVR. In this case transmission occurs at 2.4 GHz MSK with address checks, data-whitening and a 16-bit CRC code (see 2.4.5: Transceiver for EEG-DBS and RCVR Systems). The only difference in the configuration is that the MCU-M TRX operates entirely in WOR mode, thus conserving system battery life.

#### 2.4.11 Data Handling and Commands 2

All commands sent from the RCVR to the M-DBS system occurs through 5-byte instructions, which are organised into 10-byte payloads (figure 2.22). The first byte in this set is used for specifying the DBS channel pair to modify, and subsequently activating/deactivating it, and for changing the pulse-mode. This byte is split into two sets of 4 bits (characters), with the first character specifying a change in MCU-1, and the second character specify change in MCU-2. The subsequent 4 bytes configure the pulse-width and frequency in exactly the same way as it does in the

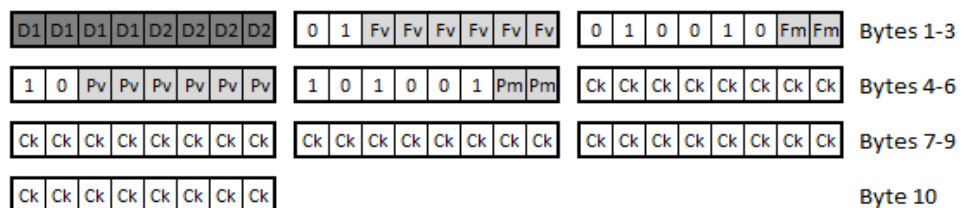


EEG-DBS system (see 2.4.6.2: Commands for Controlling the EEG-DBS System). The difference here is that all of these commands are transmitted directly to the M-DBS system without undergoing any transformations; M-DBS MCU-1 and MCU-2 processes the data directly. The subsequent 5 bytes in the payload are static values used for extracting the right information from the M-DBS TRX receive buffer by acting as a reference data sequence. Since instructions are transmitted 3000 times in 1 second, the M-DBS TRX's receive buffer is being read from (by MCU-1) and simultaneously written to (via wireless transmission). This 5-byte sequence a) acts as an additional validation on the data (in addition to the address check and CRC code), and b) allows the MCU-1 to identify the correct commands in the buffer by looking for this sequence. If MCU-1 is not able to find this sequence, or if the bytes are different to that expected, the first byte of the incorrect data is replaced with a 'DBS OFF' signal, and both DBS channel pairs deactivate as a safety precaution.

D1	D1	D1	D1	D2	D2	D2	D2	<b>DBS CONTROL</b>		<b>DBS Control Characters</b>				
0	1	Fv	Fv	Fv	Fv	Fv	Fv	CHANGE FREQ VALUE		1	1	0	0	Activate DBS, FORWARD Pulses
0	1	0	0	1	0	Fm	Fm	CHANGE FREQ MULTIPLIER		0	0	1	1	Activate DBS, BACKWARD Pulses
1	0	Pv	Pv	Pv	Pv	Pv	Pv	CHANGE PW VALUE		0	1	1	0	Activate DBS, BIPHASIC Pulses
1	0	1	0	0	1	Pm	Pm	CHANGE PW MULTIPLIER		0	0	0	0	Deactivate DBS

Where D1 = MCU-1 Command, D2 = MCU-2 Command

A



Where:

D1, D2	= DBS MCU-1/MCU-2 Command Identifier
Fv, Pv	= Frequency/Pulse-width VALUE
Fm, Pm	= Frequency/Pulse-width MULTIPLIER
Ck	= Manual check bits

B

Figure 2.22– Commands sent from the computer to the RCVR system are 5-bytes in length (A). In this case the first byte specifies an activation/deactivation of either channel pair, and the next 4 bytes specify a change in the pulse-width or frequency in the same way that it does for the EEG-DBS system. Payloads are sent in 10-byte sequences (B), with 5 bytes dedicated to packet-alignment checking at the M-DBS system.

#### **2.4.12 Assembly Techniques for Wireless Systems and Receiver**

Electrical components were soldered onto both sides of the EEG-DBS, M-DBS and RCVR PCB's (figure 2.23) using a 50W temperature-controlled soldering iron (Antex Electronics) with 0.1mm pointed tips (Antex Electronics), a pair of fine tweezers (Lindstrom; Farnell) and a dissection microscope (SMZ645; Nikon) along with assistance of a fibre-optic lamp (KL 1500 LCD; Schott). All solder used in this process was 0.2mm diameter extra-fine lead-free silver solder (Edsyn; Farnell). The connections made throughout soldering were routinely checked under the microscope with a digital multi-meter. The only modification made to the transceiver module was a replacement of its 'can' style 26MHz crystal oscillator with a miniature SMD-profile version (FA-128; Epson Toyocom; Farnell) in all wireless systems, to reduce the overall system size. The TRX2 transceiver module was connected to the main PCB (for wireless and receiver systems) by lining up its external pin connectors with those on the PCB, and connecting them together with an insulated copper wire, which was soldered to both connectors. In this case prior to soldering the copper wire used for each connection was cut to ~20mm and stripped at either end using a scalpel blade.

The external connectors on the wireless systems consist of a 10-pin headstage connector, and a 4-pin battery/programming connector (6-pins for the M-DBS system). Standard gold plated DIP contacts (Assmann Electronics; RS Components) were cut into rows of 4, 5 and 6-pins, with the male ends crimped using a pair of pliers. 30mm stripped copper wires were soldered to each of these contacts, and connected to the relevant external connections provided on the EEG-DBS and M-DBS PCB's. In this case two rows of 5 pins were used to form the 10-pin headstage on both systems, and a row of 4 or 6 pins were used as the battery/programming connector on the EEG-DBS or M-DBS systems, respectively. In both wireless systems a miniature SPDT switch (Multicomp; Farnell) was connected in-between the system's ground connector and the negative battery terminal, which formed the on/off switch.

At this point the wireless systems consist of a main PCB, 2 rows of 5 DIP headstage connectors, a 4-pin battery/programming connector, and a switch; all held together

with copper wire. All of this is then affixed into place using Araldite (Farnell), a 2-part clear epoxy adhesive. Care is taken at this point not to put excess glue on either side of the transceiver's PCB antenna, since this attenuates the transmission range. With the glue settled, an M2 nylon nut (Duratool; Farnell) is attached to the front of the headstage connector using high-viscosity superglue (Bondloc; Maplin) with bicarbonate of soda sprinkled onto it, creating a hardened connection.

During assembly of the RCVR system, a temporary four-wire connection is made for the purposes of programming the main and buffer microcontrollers (MCU-M and MCU-B). Once reprogrammed, the wires are taken out, and solder is applied between these wire connectors and a circuit track which was deliberately left exposed for this purpose.



Figure 2.23 – Top and bottom layers of the EEG-DBS PCB's after surface-mount components have been soldered onto them.

#### **2.4.13 Modifications of the Wireless systems**

The EEG-DBS system underwent a number of major revisions, before arriving at the final design presented in this chapter. The actual system used in subsequent experiments (in Chapters 3 and 4) utilised an older PCB design, and was subsequently modified to include all of the features seen in the final design. Relevant portions of the circuitry were accessed by carefully peeling away the Araldite layer using a soldering iron and a pair of fine-tip tweezers, and modifications involved

cutting PCB tracks with a scalpel blade, inserting components or copper-wire connections.

The original EEG-DBS system had a digital power-switch (TPS22945; Texas Instruments) and a J/K flip-flop (SN74AUP1G80; Texas Instruments), which were both disconnected with a system redesign. The digital power switch was the same as that used with the M-DBS system, and its function was to cut power to the EEG recording and DBS circuitry when not in use. The J/K flip-flop was used to allow the multiplexer to be controlled by the MCU with only one control line; the first multiplexer control signal fed into the flip-flop, which produced the second multiplexer control signal by dividing its clock rate. This feature worked until the system was awakened from SLEEP mode; at which point the flip-flop's output would swing randomly to either an active '1' or '0' state. This ultimately led to LFP channels 1+3 and 2+4 sometimes being swapped round in WinEDR whenever the system was brought out of SLEEP mode. As such the control line from the MCU to the digital power switch was reassigned to function as the second multiplexer control signal, where the MCU could directly ensure the correct control signals were being sent.

The original system did not feature input coupling or DC-return path resistors. These were carefully inserted at the rear end of the system, next to the headstage-PCB pin connectors. Also, the original DBS ground was simply connected to the system ground. This was changed to a virtual ground for each channel by soldering copper wires to miniature SC-70 sized single operational amplifiers (OPA347; Texas Instruments), and connecting them to the relevant portions of the PCB. This change was made to prevent the EEG-recording circuitry's reference/ground from being influenced by an additional two ground points present on the DBS electrodes. Finally in the system redesign the positions of the external PCB-transceiver connections were adjusted slightly to allow them to line-up with the transceiver's connectors. This arrangement could potentially speed-up the attachment of the transceiver to the main PCB.

Two modifications were made to the original RCVR system design. First the original ½ AA-sized battery housing was swapped for dual-AA battery housing. This was done simply because AA batteries were cheaper, more accessible, and lasted longer than the original battery used. The new battery compartment was fixed underneath the PCB using Araldite (Farnell). The second modification was the introduction of a power switch. Simply a SPDT toggle switch (Multicomp; Farnell) was connected along the main power line extending from the battery compartment, and held in place using Araldite. These modifications are not present on the PCB's previously presented, because they don't directly affect the performance of the system, since the ½ AA battery can be rapidly changed anyway.

#### **2.4.14 Electrode Design**

Two types of electrodes are used with the wireless systems: DBS electrodes (EEG-DBS and M-DBS systems), and LFP electrodes (EEG-DBS system only). The monopolar LFP electrodes are made from stainless-steel, whilst the bipolar DBS electrodes are tungsten-cores threaded through a stainless-steel cannula, in a concentric design. Both electrode types feature a wire connector which attaches to the headstage implant, and a removable cannula guide. The cannula guide allows the electrodes to be positioned in the stereotaxic frame (David Kopf Instruments) and implanted, and is subsequently removed once the electrode is secured to the skull (see Chapter 3 – 3.3.3: Surgery). Given the small sizes of the electrodes, most fabrication steps took place under a dissection microscope (SMZ645; Nikon) with the assistance of a fibre-optic lamp (KL 1500 LDC; Schott). All solder used in this process was 0.2mm diameter extra-fine lead-free silver solder (Farnell), with the assistance of phosphoric acid as a flux. When soldering to either stainless-steel or tungsten materials, the phosphoric acid was used to remove the oxide layer, allowing a solder joint to be made.

#### **2.4.14.1 Local-Field Potential Electrodes**

The core conductor for LFP electrodes are polyimide-coated stainless-steel wires (Plastics One), with a coated diameter of 230 $\mu$ m. Wire segments are cut to a length of 1mm + electrode brain-depth, using a pair of pliers (Knipex; Farnell). Cutting it this way provided the electrode tip with a bevelled edge. Polyimide insulation was stripped from both ends of the wire; 100 $\mu$ m at the electrode tip and 500 $\mu$ m at connector end (figure 2.24A). A 30mm length of insulated copper wire (stripped 500 $\mu$ m at both ends) was soldered at the connector end of the electrode (figure 2.24C). A single DIP pin (Assmann Electronics; RS Components) was removed from its plastic housing and cut in half using a pair of pliers. The end of the 30mm copper wire (the part that is not soldered to the electrode) was threaded inside the DIP pin and soldered in place (figure 2.24D). This joint was reinforced with a small amount of high-viscosity superglue (Bondloc; Maplin) to provide mechanical support, thus helping to prevent the connection from breaking during attachment to the headstage during surgery.

#### **2.4.14.2 Deep-Brain Stimulation Electrodes**

The outer conductor of a DBS electrode is a 28-gauge stainless-steel cannula, pre-cut to a length of 7mm (Plastics One). A 30mm length insulated copper wire was stripped at both ends, with one of the exposed copper conductors soldered to the end of the cannula. The other end of the copper wire was soldered to a DIP pin (Assmann Electronics; RS Components) which was cut in half, and reinforced with a drop of high-viscosity superglue (Bondloc; Maplin).

Next, a 40mm length of 180 $\mu$ m diameter Teflon-coated tungsten wire (A-M Systems, Inc) was stripped of its insulation at one end by 500 $\mu$ m. This exposed end was soldered to a DIP pin which had been cut from its plastic housing, in the same way as that done with the LFP electrode connectors. This formed the second DBS connection, and was reinforced with a small drop of superglue. The tungsten wire was then threaded through the stainless-steel cannula, until the other (insulated) end protruded from the cannula by 200 $\mu$ m (figure 2.24B). The tungsten wire was held in

place at the connector end of the cannula by folding it back along the end of the cannula and holding in place with a small drop of superglue (figure 2.24E). A small amount of superglue was also placed at the electrode tip where the tungsten wire protrudes from the cannula. Some of the glue was drawn into the cannula via capillary action, with the rest settling around the tungsten wire at the end of the electrode. This held the tip into place. Once the glue had dried, a heated soldering iron tip was placed in close proximity to the electrode tip, allowing the first 100 $\mu$ m of Teflon insulation to be melted away from the protruding tungsten wire, leaving the exposed tungsten conductor.

The stainless-steel cannula was then sheathed in an ultra-thin Polyolefin heat-shrink (Smallparts USA), which was contracted around the cannula by placing a heated soldering iron tip into close proximity with it. The heat-shrink in this case was cut to a length that allowed 100 $\mu$ m of the stainless-steel cannula to remain exposed at the tip.

#### **2.4.14.3 Attachment of the Guide Cannula**

The process of attaching the removable guide cannula was the same for both LFP and DBS electrodes. An 'alignment' stencil was created by cutting a piece of cardboard into a square, and attaching two 1mm rectangular glass slides (VWR International) onto it using Blu-Tack. These slides were placed down touching each other, with one slide slightly higher than the other. A 26-gauge stainless-steel cannula (Plastics One) was cut to a length of  $\sim$ 80mm, and positioned along the gap between the two slides with the electrode, at a space of 1mm apart. Both were held in place with Blu-Tack. A low-viscosity dental cement was mixed up by filling a small glass crucible with Simplex Rapid™ (Kemdent) powder and mixing it with a small amount of Simplex Rapid™ (Kemdent) liquid using a fine-tip spatula. Once mixed, the cement was applied at the junction between the cannula and the electrode connection point. Once the cement has begun to harden, excess bits were cut away using a scalpel blade, resulting in a rectangular shape covering the junction and wire-electrode connection (figure 2.24F). Once the cement had hardened fully, the

electrode plus cement was removed, and the electrode was secured onto the glass-block upside down. A small amount of cement was then placed on the other side of the electrode junction (figure 2.24F), without covering the other side of the cannula. Doing it this way intentionally made the cannula weak against lateral forces, allowing it to be ‘snapped’ away from the electrode during surgery. In practice a dental burr (Royem Scientific Limited) was used to assist with this (see Chapter 3 – 3.3.3: Surgery). Once the dental cement had hardened, electrodes were cleaned by gently rubbing a small piece of Blu-Tack along it – which picked up small debris particles.



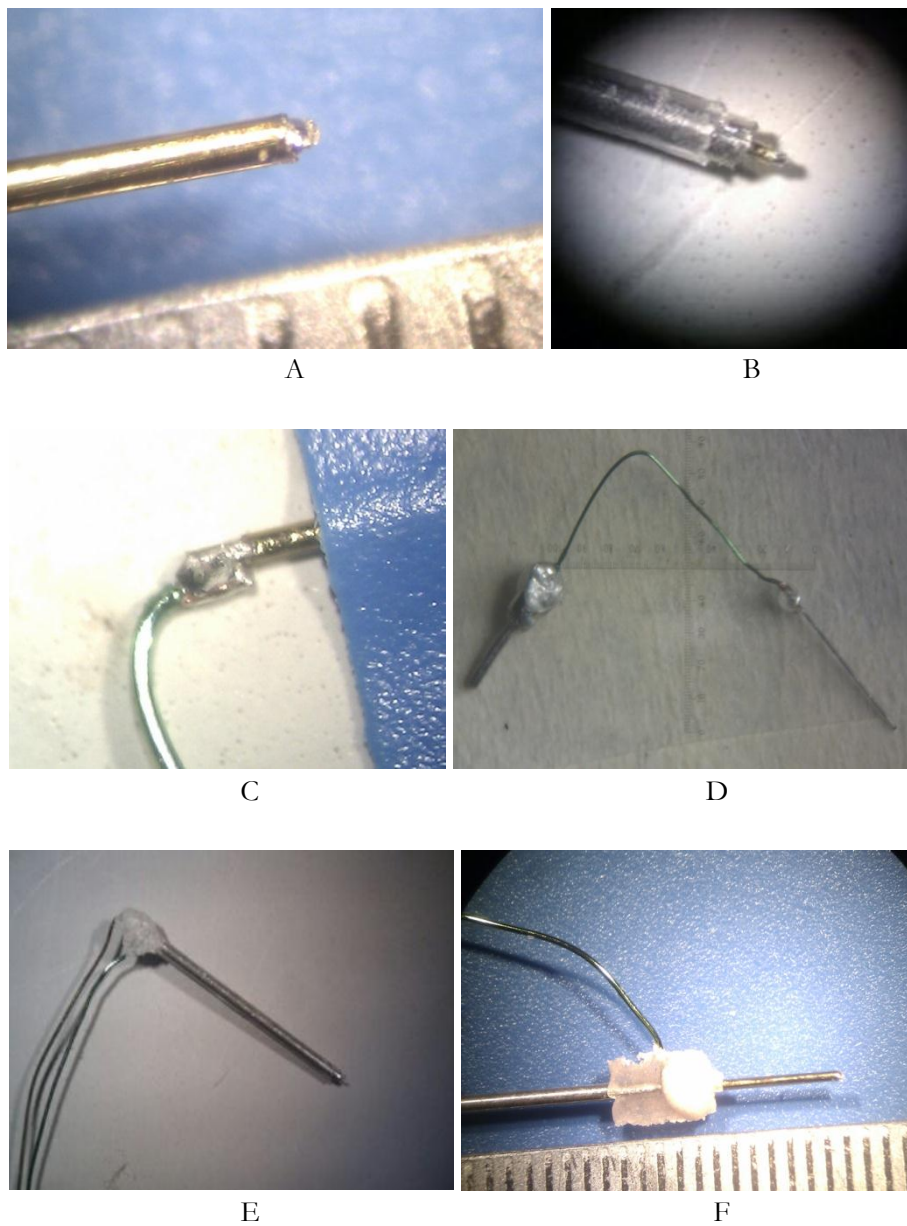


Figure 2.24 – Design steps for the LFP and DBS electrodes, showing the electrode tips for the LFP (A) and DBS (B) electrodes, attachment of the connecting wire to an LFP electrode (C), the LFP (D) and DBS (E) electrodes without a cannula guide, and a completed LFP electrode with a cannula guide (F).

#### **2.4.14.4 Electrode Testing**

All electrodes were electrically tested to see if a) a current could be passed through them, and b) if there were any breaches in the insulation. LFP electrodes were connected in series with a 10 K $\Omega$  resistor and a 6V lithium battery, and immersed into a beaker filled with saline (0.9% w/v; TPS Healthcare). An electrical current flowed between the resistor and the LFP electrode tip. Electrons at the tip of the electrode combined with hydrogen ions in the saline to form a stream of H<sub>2</sub> bubbles which floated to the surface. The presence of these bubbles anywhere along the electrode indicated an exposed connector, and breaches in the electrode polyimide insulation could be detected this way.

DBS electrodes were tested in a similar way, by connecting the electrode in series with a 6V lithium battery and a 10 K $\Omega$  resistor. The electrode was immersed into the saline solution, and bubbles formed at the electrode tip as current passed between the electrode contacts. Once again any breaches in the outer polyimide layer could be identified by the presence of bubbles flowing from the breach.

LFP and DBS electrodes that passed these tests were sterilised by immersing them briefly into a 70% ethanol solution. Electrodes that failed this test were discarded.

#### **2.4.15 Headstage Design**

The headstage is a 10-pin connector that was implanted onto the animal's skull during surgery (figure 2.25). The bottom side interfaced directly with the electrodes, which were connected during surgery. The top side interfaced with the wireless system, which was 'plugged in' prior to testing. For each headstage, two rows of 5 gold-plated DIP pin sockets (Assmann Electronics; RS Components) were attached on all sides to small pieces of plastic using Araldite (Farnell). The plastic in this case was from a standard polypropylene video-game/DVD jewel case – chosen for its combination of weight, rigidity and ability to be easily cut. One side was shaped to accommodate an M2 nylon nut (Duratool; Farnell), which matched that placed on the wireless systems. This latter piece was attached whilst the partially-completed headstage was connected to the wireless system, to ensure that the M2 nuts on the

system and headstage lined up. Once the glue had dried, the plastic sides of the headstage (including the front of the M2 nut) were smeared with dental cement to reinforce its stability. When the system was attached to the headstage, an M2 nylon screw (Duratool; Farnell) secured them into place. Headstage implants were sterilised by briefly immersing them in 70% ethanol.

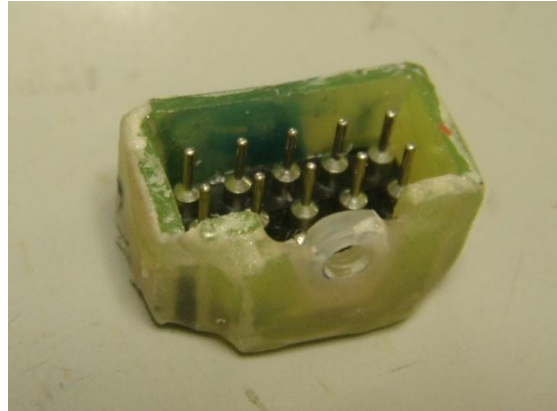


Figure 2.25 – The headstage connector was implanted onto the skull of the animal during surgery. The bottom (female) connectors interfaced with the implanted electrodes and the top (male) connectors interfaced with the wireless system, which was plugged in and screwed tight prior to testing.

#### 2.4.16 Battery Connector

The choice of battery used for the two systems was based on a trade-off between their size and performance. A large range of coin and button cell batteries were tested for each system, including silver-oxide, alkaline, lithium-ion and zinc-air. The EEG-DBS system requires a constant transmission link during active operation, and therefore consumes several times more current than the M-DBS system. A lithium-ion 170mAh CR1/3N button-cell (Varta; Farnell) was selected for use with the EEG-DBS system, since it offered a relatively high current density for a battery of its size, and was the smallest battery tested that allowed for constant EEG recordings lasting over 8 hours (figure 2.26). For the M-DBS system a lithium-ion 210mAh 2032 coin-cell (Multicomp; Farnell) was selected. This battery provided over 2 days of constant DBS (with all channels configured to bipolar pulses, 130Hz, 100 $\mu$ S, 100 $\mu$ A; test results not shown). Because this particular system was designed

for chronic recordings, the flat 2032 coin shape allowed it to be placed flat along the back of the M-DBS system.

Batteries for both systems were connected to a 4- or 6- pin DIP connector, for the EEG-DBS and M-DBS system, respectively. DIP connectors were cut into rows of 4 or 6 from standard DIP sockets (Assmann Electronics; RS Components), and the end two pins of each row were connected to the positive and negative terminals of each battery via a small piece of insulated copper wire. To allow for soldering onto the battery, a drop of phosphoric acid was placed on the battery surface, and soldering was performed quickly to prevent the battery from heating up significantly. The ‘programming pins’ on each battery connector (2 for EEG-DBS; 4 for M-DBS) were each shorted to the positive battery terminal using a soldering iron, since during active operation the programming pins on each system must be shorted to Vdd. Finally for the M-DBS system battery, its connecting wires were reinforced with Araldite (Farnell) to provide it with additional strength for chronic operation.

#### **2.4.17 Basic System Tests**

A number of basic tests were carried out on the EEG-DBS system, prior to use in animals. These basic tests looked at the system operational lifetime, as well as its recording and stimulation capabilities.

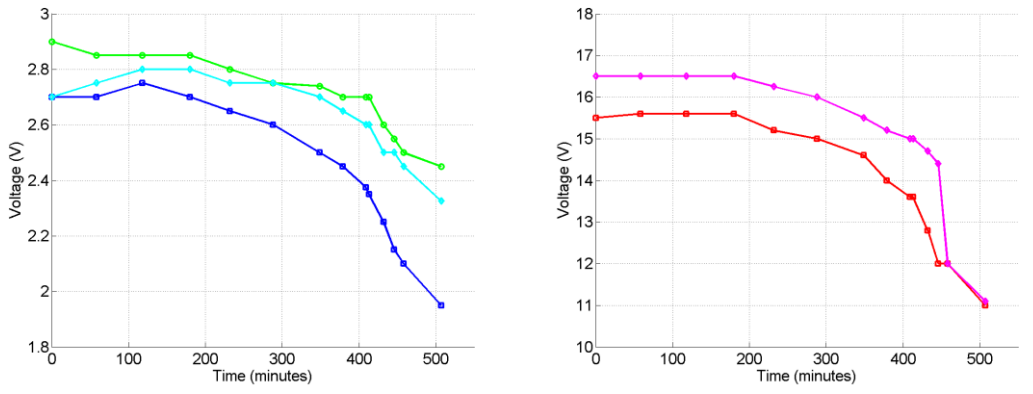
##### **2.4.17.1 EEG-DBS Battery-Life Measurements**

The operational lifetime of the EEG-DBS system was tested using the CR1/3N battery, based on the following system operational modes:

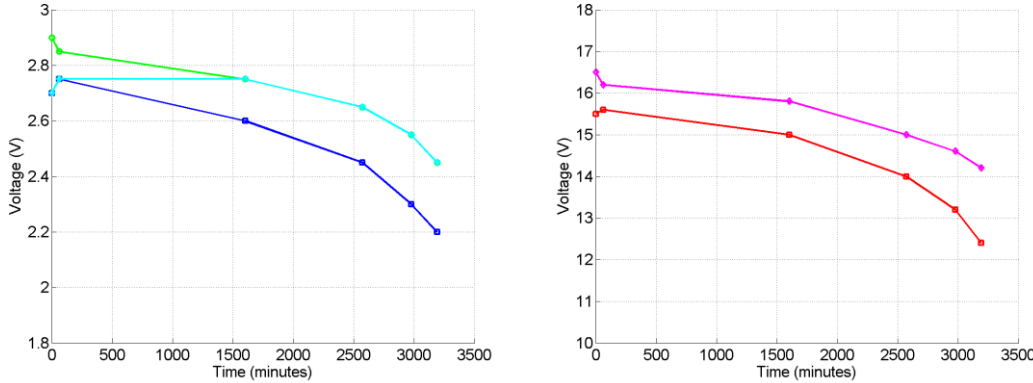
- Constant EEG recording/transmission
- Constant EEG recording/transmission with simultaneous DBS pulses
- DBS pulses only (system in low-power SLEEP mode)

In each case a fully charged battery was inserted and the test commenced until the battery was depleted. The final reading for each battery life measurement was taken as the final reading where the system performed properly (readings that coincided

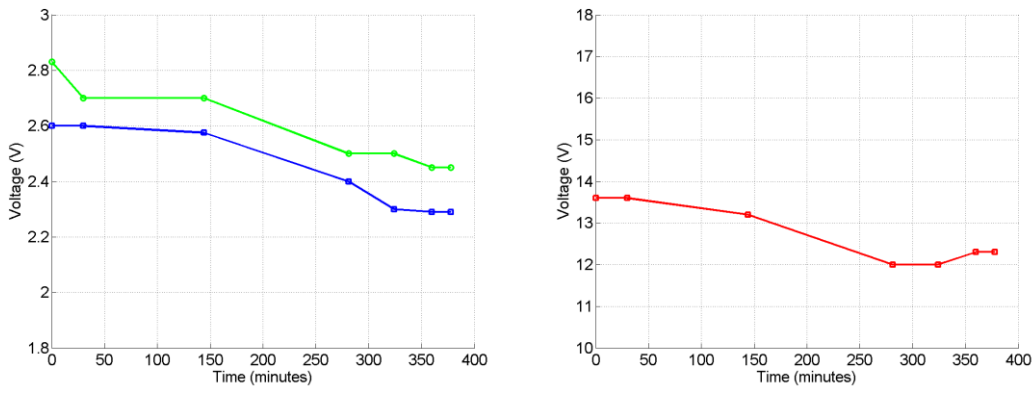
with transmission/recording/stimulation impairments are not included). Given that all of the integrated circuits on the system have minimum operating voltages between 1.8V – 2V, performance problems only began when the system voltage approached these levels. For tests involving constant DBS pulses, the parameters were set to 100 $\mu$ S, 130Hz, 100 $\mu$ A, with the pulses delivered through a 33K $\Omega$  resistor. Voltage measurements were made throughout each test using a digital oscilloscope (TDS 3032B; Tektronix). Several voltage measurements were made in each test, including the battery and system voltages, the system voltage during sleep mode, and the amplified voltage provided for DBS during active and sleep modes. Note that the DBS voltage amplification was measured in all tests regardless of whether DBS was activated. Similarly the sleep and active mode voltages were measured regardless of whether the system was tested in sleep or active mode. In these cases the system was transiently activated/deactivated in order to make a measurement. Measuring this way provided an insight into e.g. the level of DBS voltage following constant EEG recording only, or the system working voltage during sleep-mode DBS.



A



B



C

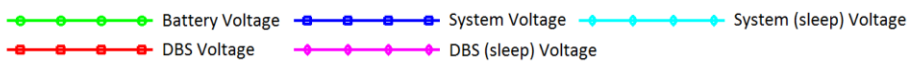


Figure 2.26 – Graphs showing the measured system voltages in the constant EEG recording (A), constant DBS (B), and constant EEG recording + DBS (C) tests. The left panel shows the battery and system voltages, and the sleep-mode system voltage. The right panel illustrate the DC amplified voltage available for stimulation during active and sleep-modes. Note the alternating voltage/time ranges in these plots.

The system is able to perform normally for a wide range of battery voltages, with problems only appearing when the system voltage drops below 2V. The amount of voltage available for DBS varies based on its operating mode; it is highest when EEG recording is deactivated and lowest when EEG recording is activated. This determines the maximum limit for constant-current, based on the impedance between the electrode terminals in the brain.

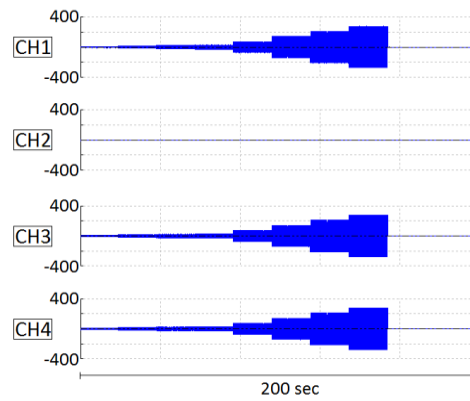
Several other batteries were tested with the EEG-DBS system. Two miniature 1.55V silver-oxide batteries (393; Renata) were an initial choice due to their small size and weight. Numerous tests had shown these to last an average of 1hr 26 minutes for constant EEG recording and transmission. Similarly a CR2032 battery was shown to give an average time of 1hr 42 minutes, despite having a capacity of 210mAh (as opposed to 170mAh with the CR1/3N). However when used in a constant-DBS (sleep-mode) test, the CR2032 gave an average lifetime of 52hrs 26 minutes, with the more current-intensive parameters of 130Hz, 100 $\mu$ A, 200 $\mu$ S through a 33K $\Omega$  resistor.

The average current consumption for the EEG-DBS system during constant EEG recording and transmission varied between 18.25 – 22.5 mA, depending on the programmed transmission power. Current consumption during constant DBS was several times lower than with constant EEG recording, but varied significantly with the stimulation parameters.

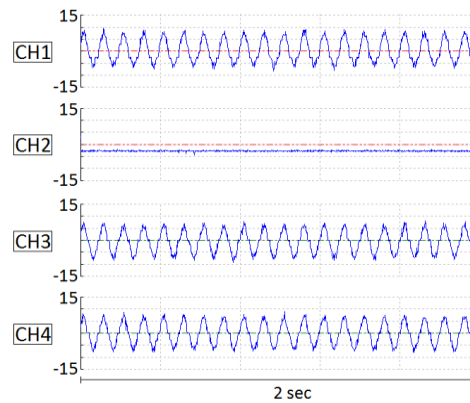
#### **2.4.17.2 Basic Noise Test**

A basic test was carried out on the EEG-DBS system to characterise its amplification and noise properties. A 10Hz sine-wave of varying magnitude was injected into three of the four system channels using a digital function generator (USB X Series; National Instruments) and a  $\div$  940 voltage divider, with one channel left unconnected/floating. This was repeated 4 times such that each channel was recorded floating, whilst the other three recorded the sine-waves (figure 2.27). In this case the input signal amplitude ranged from 0.027 – 1.06 mV. The EEG-DBS system and the function generator outputs were wrapped in foil to minimise the

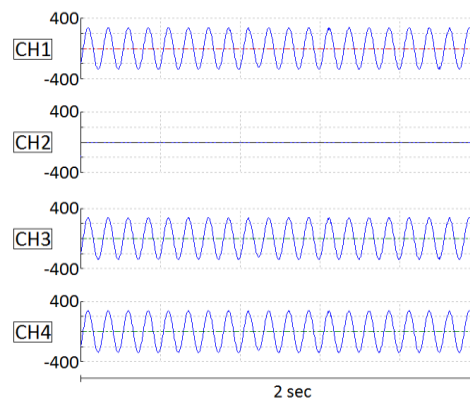
effects of noise, and recordings were made in WinEDR (J. Dempster, Strathclyde University).



A



B



C

Figure 2.27 – 10 Hz input sine waves were increased in magnitude from  $27\mu\text{V}$  to  $1.06\text{mV}$  (pk-pk), with one channel left unconnected/floating (A). The reproduced output waveforms are shown with the lowest (B) and highest (C) input amplitude. Note that noise is easily visible on the amplified  $27\mu\text{V}$  input signal (B). Numbers on the y-axis represent amplified voltage amplitude in mV.



Recorded signals were exported to Matlab (Mathworks) where they were extracted into their signal and noise components, using a custom-written de-noise algorithm which uses wavelet analysis (figure 2.28). The peak-peak voltages of the signal and noise were calculated using a custom-written script, and plotted as a function of the input signal amplitude (figure 2.28D). The signal to noise ratio was calculated as a ratio between the powers of the signal against the power of the noise component, and expressed in decibels plotted as a function of the input signal amplitude (figure 2.28E).

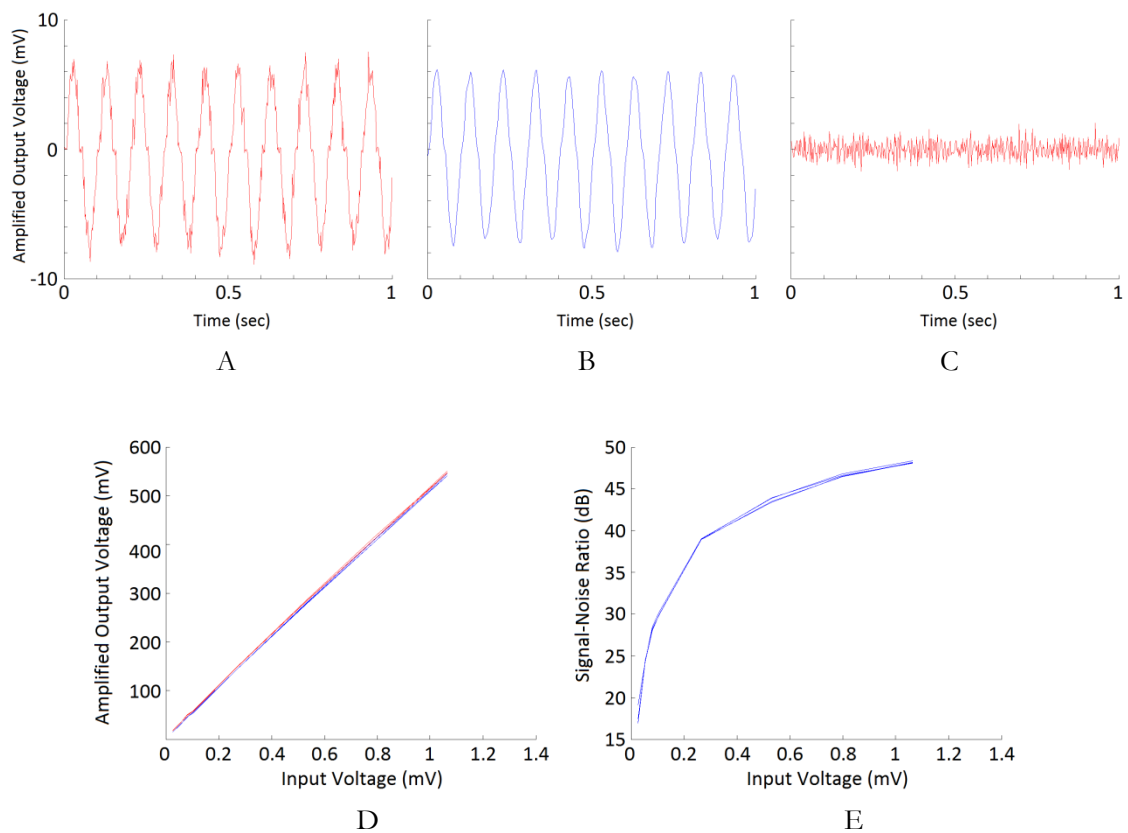


Figure 2.28 – The recorded output signal for a  $27\mu\text{V}$  input (A) was decomposed into its clean (B) and noisy (C) variants using wavelet analysis. The peak-peak amplitude was plotted against the input signal for each channel using the clean (blue curves) and noisy (red curves) signals. The voltage output (D) and calculated signal-noise ratio (E) are shown as a function of the input signal amplitude.

### 2.4.17.3 ECG Measurements

A measurement of electrocardiogram (ECG) was made on one of the channels to confirm its ability to record differential signals. Disposable ECG electrodes were attached to the left and right wrists of the subject, forming the two differential inputs of one system channel. A third electrode was attached to the ankle of the subject. Recordings were made in WinEDR (figure 2.29A), and later exported to Matlab where the power-spectral density was calculated (figure 2.29B). The QRS wave is shown to saturate at the +600mV level, which is expected since the systems gain was set for recording EEG and is thus too large for capturing ECG signals in their entirety. In addition 50Hz noise was quite prominent in the recording, notably appearing as a spike in the power spectral density (PSD) plot (figure. 2.29B). This noise was due to the long leads used between the subject and the system inputs.

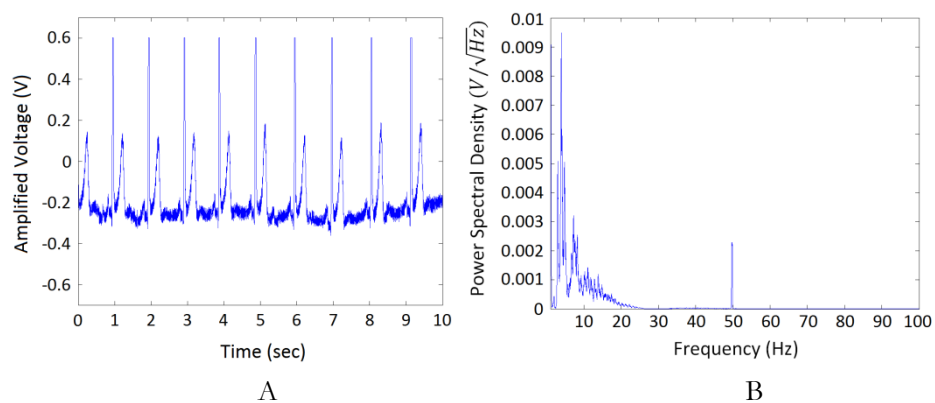


Figure 2.29 – Recording of ECG in both the time (A) and frequency (B) domains.

### 2.4.17.4 DBS Pulses in Saline

The maximum current range of the DBS system is dependent on the maximum voltage that is available for stimulation. High currents undoubtedly need a higher voltage to drive the pulses through the electrode-electrolyte interface, whilst maintaining a constant current (rectangular) pulse profile. However the impedance between the DBS electrode terminals in the brain are complex, and can be simplified by substituting brain matter for saline, and performing measurements on it. As such the system's ability to generate DBS pulses and its current range was tested by

connecting it to a DBS electrode immersed into a 0.9% NaCl solution, and using the EEG-DBS system to send pulses through it. This was only intended to give a basic idea of how the pulses behave at an electrode-electrode interface. 100Hz, 100 $\mu$ S pulses of varying magnitude were delivered through the electrode, and the voltage across the electrode contacts was observed using a digital oscilloscope (TDS 3032B; Tektronix). This was also carried out in an older system which had previously been used to perform wireless DBS in rodents (Ewing et al., 2009); using the same electrode and saline setup. Through a comparison of the oscilloscope output, the voltages across the electrodes on both systems were seen to be very similar in shape (figure 2.30). Under a constant current pulse, the electrode in NaCl was seen to rapidly polarise as shown by the rapid voltage rise time. When the constant current pulse had finished, the voltage waveform indicated a discharge featuring an initial fast phase, followed by a slow phase (figure 2.30).

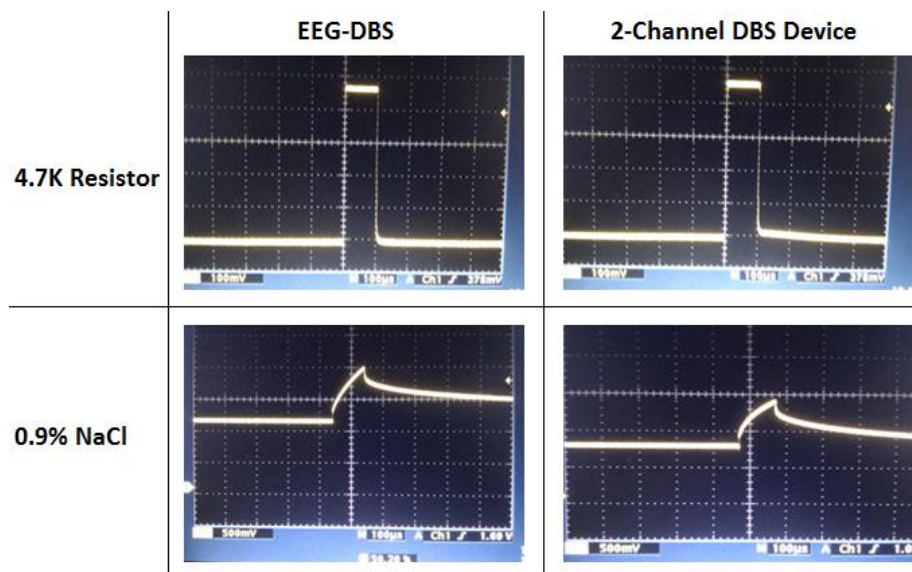


Figure 2.30 – Comparison between the stimulus pulses generated by the EEG-DBS system, and a 2-channel DBS device used in previous work (Ewing et al., 2009), as seen on the oscilloscope screen. Both devices were used to deliver 100 $\mu$ S, 100Hz, 100 $\mu$ A pulses through a 4.7K $\Omega$  resistor (top photographs), and 0.9% NaCl (bottom photographs).

The voltage across the DBS electrode was observed for a range of stimulus parameters, with current intensities from 100 $\mu$ A up to 1.5mA. This was done to

observe the voltage requirement for stimulation of high currents. Figure 2.31 shows the voltage waveforms obtained from stimulating at 100Hz, 100 $\mu$ s, with the current ranging from 100 $\mu$ A to 1.5mA. The fast/slow discharge phase is seen more clearly for waveforms in figure 2.31. Notably as the current increases, the voltage requirement for stimulation also increases, from  $\sim$ 2.75V (100 $\mu$ A) to  $\sim$ 9V (1.5mA).

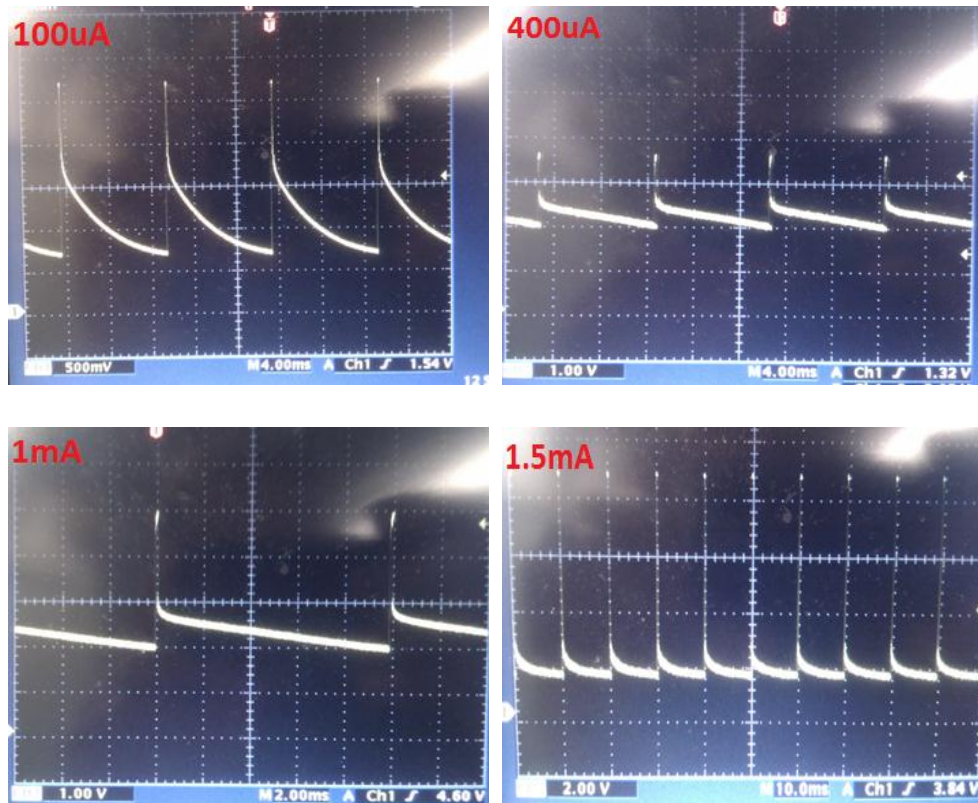


Figure 2.31 – Voltage waveforms across the DBS electrodes as observed with an oscilloscope, following the generation of 100Hz, 100 $\mu$ s pulses into 0.9% NaCl.

The voltage waveforms at 1.5mA were looked at more closely (figure 2.32A). At such a high current the electrode-electrolyte interface is seen to behave more like a resistance, with the voltage drop assuming a more rectangular shape. The shape of the constant current pulse was confirmed to be rectangular by placing a 10 $\Omega$  resistance in series with the electrode-saline setup, and measuring the voltage drop across it (figure 2.32B). In this case the 1.5mA pulse had successfully resulted in a 15mV drop across this resistance, thus confirming that 1.5mA was being driven through the electrode-saline interface.

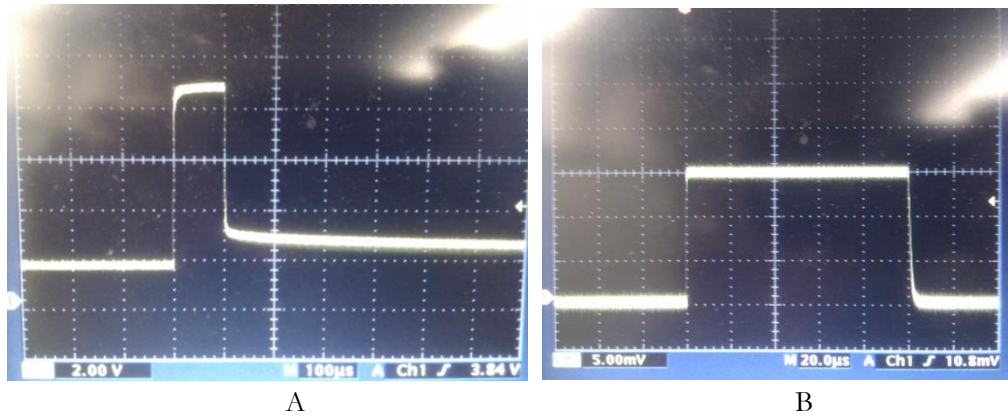


Figure 2.32 – A close-up of the 1.5mA stimulus pulse sent through saline shows it requires just less than 9V, with a square pulse-shape resembling the voltage drop across a resistance (A). The voltage measurement in (B) was taken across a 10Ω resistor which was connected in series with the DBS electrode. In this case a 15mV voltage drop across this confirmed that the 1.5mA current is being held constant across the electrode-saline interface.

## 2.5 Discussion

This chapter has outlined the design and development of two miniature wireless systems capable of EEG recording and DBS. The devices were developed to solve two specific problems related to neural recording and stimulation. One problem was based on the current study which required a system that can simultaneously perform EEG recording and DBS in freely-moving rodents. The other problem was an external study which required 4-channel chronic DBS in freely-moving rodents, with two independently controllable channel pairs (Gut and Winn, 2012). The initial EEG-DBS system tests have paved the way for its use *in vivo*, which is document in subsequent chapters.

Between commercially-sold devices and prototypes developed and described in the literature, there has been a proliferation of wireless system solutions for recording and stimulating in the past two decades. With no fixed standard for which any of these devices can adhere to, the diversity in the design choices made between these systems has been enormous; differing not just by the animals and applications for which the systems are designed, but also by the core technologies and design choices made at each step of the way. As such these prototype devices vary largely with regards to the system core technology, number of recording channels, signal bandwidth, noise performance and signal reproducibility, digital control options, wireless telemetry, use of stimulation and its parameters, as well as a plethora of novel features specifically related to a particular study. As such there exists a rich pool of data from which to develop a wireless system solution, taking into account the aspects of a design that works and aspects that can be made more efficient. Nonetheless there are relatively few devices that can either perform 4-channel DBS, or combined EEG recording and DBS. The devices that do exist are either relatively large and/or have limited functionality, such as single channels, constant-voltage pulses, and limited parameter selection (see table 2.5 for a comparison). For its small size of 8.5g the EEG-DBS system is able to outperform these devices in many key design criteria, whilst offering a battery life that is adequate for the current studies. Furthermore these devices are built for versatility, allowing them to be reprogrammed to adapt to a particular experimental design.

	Ativanichayaphong et al., 2008	Ye et al., 2008	Song et al., 2006	Mavoori et al., 2005	Zuo et al., 2012	Zanos et al., 2011	EEG-DBS	M-DBS
Species	Rats	Rats	Rats	Primates	Rats	Primates	Rats	Rats
System Type	Back-mount	Back-mount	Back-mount	Head-mount	Back-mount	Head-mount	Head-mount	Head-mount
Dimensions (mm)	25x50x27mm	36x22x3.5mm + headstage	-	-	27x20mm (cylinder)	66x63x30mm	28x17x7mm	28x17x7mm
Weight (g)	> 20g	43g	14g	56 g	27g	145g	8.5g	8.5g
Battery Life (hours)	6h	2h	10h	~ 60h	39h (rec) > 100h (stim)	48h	5-8h (rec) 50h (stim)	48h
Recording Channels	1	2	1	1	1	3	4	0
Sample rate	10KHz	12KHz	8KHz	11.7KHz	10KHz	adjustable (256Hz - 24KHz)	500Hz	n/a
ADC	N/A	12-bit	8-bit	8-bit	8-bit	8-bit	16-bit	n/a
Signal Bandwidth	0.3 - 10KHz	< 4.5KHz	100Hz - 10KHz + 50Hz notch	0.5 - 5KHz (4-pole filters)	300Hz - 5KHz	adjustable (10Hz - 7.5KHz)	1.5-100 Hz	n/a
Transmission Type	914 MHz FM	2.4 GHz Bluetooth	2.4 GHz	57.6 Kbps (IR), local data storage	2.4 GHz	Local data storage	2.4 GHz MSK	2.4GHz MSK
DBS Type	Voltage	voltage, current	voltage	current	voltage	current	current	current
DBS Channels	-	4 pairs (only 1 active)	1	1	1	3	2	4
DBS Intensity Range	+/- 18V, 4 levels	1-10V, 35-120 $\mu$ A	3.3V only	up to 100 $\mu$ A	0-6 V	10-200 $\mu$ A	30 $\mu$ A-1.5mA (+/- 15V)	30 $\mu$ A-1.5mA (+/- 15V)
DBS PW Range	-	-	50 $\mu$ s - 10ms	-	0.5 - 100ms	-	10 $\mu$ S - 500mS	10 $\mu$ S - 500mS
DBS Freq Range	-	-	0.1Hz - 255Hz	-	dc - 1KHz	-	0.1Hz - 5KHz	0.1Hz - 5KHz

Table 2.5 – Summary of the features in modern neural recorder/stimulator prototype systems. For comparison the EEG-DBS and M-DBS system features are also shown.

The final design for the EEG-DBS system is a product of several iterations, in which its components were refined and adjusted in light of lab and *in vivo* test data. The M-DBS system was created as a modification of the EEG-DBS system, based on parts of the design that had shown to function well. In this case the EEG-recording circuitry was substituted for an additional two channels, as well as digital switches that could facilitate biphasic pulses – a feature which was left out of the EEG-DBS system due to space considerations.

The EEG-DBS system was originally intended to be implantable, but this idea was rejected for several reasons. The system would have to be smaller than its current form, with significant consideration given to biocompatibility. To the author's knowledge, there are no prototype wireless stimulators and recorders that are smaller than the current system, and some indeed weigh over 40g (see table 2.5). The transmission distance would have been shorter since signals would have to pass through the animal's overlying skin. The battery for the system would have been fixed onto the device also (with no possibility of changing it), limiting the available time for recording and stimulating. Finally the act of implanting the system would potentially have added to the list of potential surgical complications, particularly if it remained at its current size. The next consideration was to have the system mounted onto the back of the animal, with a wire connecting it to an implantable headstage. At 8.5g (including the battery) the system can easily be carried on the animal's head, and so placing the system on the animal's back would only have served to introduce noise problems in the headstage-backpack connecting cable. In the current configuration, signals from the brain only have to travel a very short distance (~30mm) prior to reaching the input pre-amplification and buffering stage, with no external cables to pick up noise. However the current system can easily be configured to be worn on the back of a rat, should one wish to operate the system for a longer period of time with a larger battery. For example a 20g 3.7V 1120mAh lithium-ion rechargeable battery pack (CA5L; Energizer), would theoretically provide over 50 hours of constant EEG recording (based on the system average current consumption of 20mA), and over a week for DBS (with typical parameters).



The choice of battery to use with the system was a decision which was heavily influenced by the overall shape, size and weight of the system. As such the CR1/3N button-cell was selected as the ideal battery for the EEG-DBS system, and the CR2032 coin-cell was selected as the ideal battery for the M-DBS system. These batteries are roughly equivalent in weight (at  $\sim 3\text{g}$  each), but the CR1/3N is more suited for delivering higher currents, and the CR2032 is a better shape for chronic use. Despite having a lower capacity than the CR2032, the CR1/3N can last over 4 times longer for constant EEG recording, owing to its ability to deliver higher currents. However constant DBS pulses require much less current, and can last for over 50 hours with either battery (on both systems), with typically used DBS parameters. These battery lifetimes were adequate, considering that the EEG-DBS system was operated for a maximum of 2 hours for any given session.

Custom software architectures were used for both the EEG-DBS and M-DBS systems, which in each case had involved a combination of timed control loops and interrupts. Interrupts were used extensively in both systems, due to the necessity of these systems to respond to timed events (such as the activation/deactivation of a stimulus pulse, communication between system microcontrollers, or the timed transmission of EEG data). One limiting factor of the MSP430 MCU was its code-memory size. During the development of this system the code memory of the MCU had reached its maximum on a few occasions, resulting in a redesign of the code to suit. Furthermore the EEG-DBS system uses all of the MSP430's input/output pins, as well as most of its in-built hardware modules (analogue-digital converter, timers, SPI module, etc). Whilst the EEG-DBS system was tested repeatedly and has proven to work reliably using its custom software architecture, the process of developing this software could have been greatly simplified by using an MCU with a higher-specification (e.g. one with more code memory, more timer modules, etc.). However given that both the physical size and power consumption of the MCU must be as low as possible, the challenge therefore exists in selecting an appropriate MCU that can be programmed robustly and efficiently, without being an over-engineered solution. Nonetheless, every change in either the EEG-DBS or M-DBS MCU programming was followed by an extensive battery of tests based on all of the

systems operating modes and parameters. No software bugs or issues were observed using these systems during any of the experiments in which they had participated in (which weren't the result of physical system damage or battery depletion).

The input stage in the EEG-DBS system underwent numerous revisions during the course of the systems development, with the final revision occurring after a T-maze pilot study (unreported). In this case the gain, filtering and input-coupling characteristics were altered to suit a final specification. Initially the system's high-pass filter was set to 0.14Hz, which meant that any significant deflections in the EEG (e.g. from the system being knocked against a wall generating a movement artefact) took several seconds to recover; owing to the filter's long time constant. This was subsequently increased to 1.5Hz, which provided a much faster recovery of the LFP signal from abrupt signal deflections. Regarding the characteristics of the analogue filters, potential issues may have arisen due to their single-pole filtering characteristics. These filters were configured to provide a shallow roll-off in their frequency response curve, specifically at -20dB per frequency decade. When considering the low-pass filter, this shallow roll-off provides a theoretical signal attenuation of approximately 75.9% at 400Hz, and 80.5% at 500Hz. Given that the sample-rate of the system is 500Hz, this would have resulted in aliasing artefacts in the recorded data. In this case, 500Hz sampling would have resulted in a harmonic repetition of the filtered 400-500Hz signal component being superimposed onto the recorded data at 0-100Hz. The size of aliasing artefacts in this case would be between 20-25% of the amplitude of (un-sampled) EEG at 400-500Hz.

Regarding the amplification properties of the EEG-DBS system, the gain of the main amplification stage was adjusted throughout the different recording scenarios (it was set initially at 3000 for scalp-EEG measurements). The final gain was settled at a fixed value of 520 for each channel. This gain provided a good balance between amplification and signal resolution for rat LFP. Of particular note regarding wireless system prototypes, is that many of them offer sampling rates of several KHz. While this is appropriate for the detection of spikes and action potentials, LFP recordings only need a few hundred Hz. Indeed many recordings of LFP made at several KHz were down-sampled to a few hundred Hz for memory saving and data-processing

purposes (e.g. Jones et al., 2005). The EEG-DBS system takes advantage of this by utilising a 16-bit ADC (built into the MCU), which is inherently slow since it trades temporal resolution for voltage resolution.

Another potential issue with the system is based on its transmission characteristics. Each individual transmission from the EEG-DBS system consists of a single sample of EEG data from each recording channel, plus additional overhead data. Whilst the transmission link has proven to be robust, there is the possibility of individual EEG samples to not being detected by the RCVR system due to, for example, the system being out of range, or the transmission packet failing an error-check. Given that there is no time-stamp or index associated with these samples, missing samples are not logged by the receiver. This can lead to the LFP data being misinterpreted in WinEDR. As an example, if 5 samples out of 505 were not detected by the RCVR system, WinEDR would represent 1.01 seconds of real-world LFP data as 1-second of recorded data. Another consequence of transmitting each sample separately is that the battery life of the system is reduced due to the increased number of repeated transmissions, as opposed to a single transmission containing, for example 500 samples of LFP. This is a consequence of the memory limitations on the MCU, which prohibited more than 4 samples of EEG being stored at any one time.

The DBS feature has been shown to reliably generate a continuous train of pulses which matches the performance of a previous system which had been used for DBS (Ewing et al., 2009). Through an interface built into WinEDR, the user is able to successfully alter the DBS pulse-width and frequency. Furthermore, the constant current can be adjusted from  $30\mu\text{A}$ , up to  $1.5\text{mA}$  in saline, although this must be treated with caution given the differences in dynamics between saline and brain tissue. Nonetheless the impedance of the electrode-electrolyte interface in the brain is known to decrease with increasing current (Ewing et al., 2013a), which is in part why  $1.5\text{mA}$  pulses require  $\sim 9\text{V}$ , and  $100\mu\text{A}$  pulses require  $\sim 2.75\text{V}$ . The voltage available for DBS on the EEG-DBS system averages at around  $15\text{V}$ , which decreases when EEG recording is active, and increases during sleep mode. In reality,  $1.5\text{mA}$  would cause a lesion under most conditions, thus showing that these systems can handle what is considered low and large ranges of constant current.

### 2.5.1 Alternative Design Choices / Future Work

Some potential alterations to the EEG-DBS system are based on some of the reported issues as previously described. A better method of signal filtering could be achieved by replacing the single-pole RC filters with active-filter designs. By making use of the frequency roll-off characteristics of the main amplifier, resistors and capacitors can be arranged to form a second-order bandpass filter which has better signal attenuation properties than that which is currently implemented. A high-frequency roll-off of -40dB per frequency decade would significantly reduce the presence of aliasing artefacts that occur through 500Hz sampling.

Given the complexity of the software used in the EEG-DBS system, an MCU with enhanced capabilities (increased code memory, more timers, etc.) can give the designer more freedom in their choice of system architecture and software design. An interrupt-driven system (using timed subroutines in a main loop) will suffice, if it is designed in such a way as to provide accurate timing of all of the core system functions (EEG sampling, DBS, transmission, etc). An alternative is to use a pre-emptive multi-threading architecture, whereby an interrupt-controlled timer can switch between the core system functions at discrete time points (e.g. transmission and reception being coordinated by a timer which runs in the background). Using the MSP430 MCU, DBS pulses were generated in a separate timer interrupt routine. More sophisticated MCUs generally have the ability to adjust the voltage level on their output pins directly from their timer modules (i.e. without having to resort to manually altering the output voltage through a timer interrupt). Thus the enhanced capabilities of more sophisticated MCU's could simplify the software design whilst reducing the number of potential software issues that can arise during system operation. By enhancing the capabilities of the MCU, system designers also have the scope and flexibility to upgrade their system, in the event that software modifications are later required. Indeed the EEG-DBS and RCVR system software were themselves modified to allow for synchronisation with a video-tracking system, as described in Chapter 4. Finally, by using an MCU with an enhanced memory, a large number of LFP samples for each channel can be stored and transmitted together. This would circumvent issues that arise from transmission packet loss, as

well as increasing the battery life of the system via a reduced number of individual transmissions. However in this case if one transmission fails, then many samples would be lost (as opposed to just one sample per channel with the current system).

Reductions in the overall system size and power utilisation can be made by transferring all or part of the design to a low-cost FPGA chip, which are increasingly available as cost-effective alternatives to ASIC technology. FPGA technology has the potential to largely increase the number of recording channels on the EEG-DBS system whilst taking up less space than its current off-the-shelf components. Given the rapid advancement of off-the-shelf technology, more efficient versions of the currently used components are expected to increase in number with time; such as lower-power transceivers and microcontrollers.

A larger range of devices are possible through minor modifications to the current wireless systems. For example a micro-sized 2-channel DBS device could be developed with a fraction of the volume and weight as the current EEG-DBS system. In this case the 2-channel DBS circuitry from the current EEG-DBS system (which takes up less than  $\frac{1}{4}$  of its volume) would be retained, and the wireless functionality swapped for programmable settings, thus greatly increasing the system's battery life whilst reducing its size. Modifications to the M-DBS system could see it augmented with circuitry that alter the shape of stimulus pulses (e.g. charge-imbalanced biphasic), or perhaps a wirelessly-controlled voltage select facility. The existing EEG-DBS system itself can be enhanced with some of these more sophisticated DBS settings, albeit with a more sophisticated MCU to handle the enhanced functionality.

The current system is deliberately configured to sample at 500 Hz in the interests of capturing LFP signals. However higher-frequency brain signals such as spikes or action potentials require much higher sampling rates. The ADC voltage and temporal resolution is largely limited by the data-rate of the system. Whilst a sample rate of several KHz is compatible with many of the components used in the EEG-DBS system, two crucial changes would have to be made to facilitate it. First, the MCU would have to change to a version with a faster ADC (many MCU's in the

MSP430 range have fast 12-bit ADC's; Texas Instruments). Second, the receiver-computer communication would have to change from serial transmission to USB transmission. Serial transmission was used for its simplicity with regards to the programming and circuitry involved, and crucially, it was adequate for the transmission of 4-channel, 16-bit data at 500Hz along with commands. However this transmission format approached the limit of its 115.2 Kbaud maximum data-rate, meaning that more channels and/or a higher sampling rate would require the receiver to be converted to USB communication, which offers speeds of over 5000Mbaud.

Finally, an interesting design choice seen in various designs of novel systems is the storage of EEG data into on-board memory (e.g. Sherk and Wilkinson, 2008, Mavoori et al., 2005, Vyssotski et al., 2006). In line with the ever-growing consumer electronics markets, the cost of miniature high-capacity memory modules is continuously decreasing, thus opening up a low-power solution to wireless recording of neural data that bypasses the power-consumption bottleneck involved with wireless telemetry. Wireless telemetry is a large drain on the system power, and perhaps the reason why commercial systems often utilise large, expensive receiver systems, such as the receiver plates used by Data Sciences International. The use of a miniaturised, low-power memory module could potentially bypass these issues at the expense of real-time system control. A miniature hall-effect (magnetic) sensor and miniature LED's could be used to activate the system and let the user know when recording is taking place, respectively.

## Chapter 3

# Proof of Concept Experiment for the EEG-DBS System

### 3.1 Introduction

This section serves to bridge the gap between the wireless technology described in Chapter 2, and the *in vivo* behavioural task described in Chapter 4, by validating the EEG-DBS system in freely-moving rats. This is the first experiment in the study which features simultaneous local-field potential (LFP) recording and deep-brain stimulation (DBS), and the implications and practicalities of using both modalities are explored here. The site for stimulation – the anterior thalamic nucleus (ATN) – is chosen based on its relevance to schizophrenia and in particular, the cognitive deficits (see Chapter 1 – 1.5.6: Candidate Brain Regions for DBS in Schizophrenia; for a discussion of the various optional sites for DBS). In this experiment, rats undergo DBS and LFP recording sessions using a variety of stimulus parameters, inside an open-field arena.

## 3.2 Aims and Rationale

### 3.2.1 Rationale

Prior to undertaking a larger-scale experiment involving the EEG-DBS system, an intermediary approach can be explored to address two issues. The first is based on the verification of the EEG-DBS system *in vivo*. Given the large number of novel techniques employed with this device and its novel electrode design, any issues flagged up in this experiment can be addressed and refined for future studies. The second issue is the exploration of the effects of bilateral ATN stimulation in freely-moving rats. Given its nodal presence in brain circuits related to learning and memory, as well as the pathological changes it undergoes in schizophrenia; stimulation of this structure at high-frequency has been proposed to effect a modulation of some of the brain circuits implicated in the cognitive deficits in schizophrenia (see Chapter 1 – 1.5.6: Candidate Brain Regions for DBS in Schizophrenia).

### 3.2.2 Aims

The aims of this experiment were twofold:

- a) Validate the operation of the EEG-DBS system in freely-moving rodents, by integrating DBS, LFP recording, and video-tracking into one experiment.
- b) Explore the effects of ATN stimulation in freely-moving rodents, by observing changes in the rat mean velocity and LFP under a variety of stimulus parameters.

The following experiment utilised the full features of the EEG-DBS system, including 4-channel LFP recording in both hemispheres of the medial prefrontal cortex (mPFC) and dCA1 region of hippocampus, and bilateral DBS of the ATN. The interactions between the mPFC and hippocampus are of great interest in this study because of their relevance to learning and memory (see Chapter 1 – 1.4.3: Working Memory Relies on Connectivity of Hippocampus and Prefrontal Cortex). Bilateral stimulation was carried out in the ATN using a variety of stimulation



parameters, which varied in their pulse-width and constant-current intensity. The outcomes of this study were used to refine the practicalities involved both in using the EEG-DBS system, as well as designing the subsequent working-memory experiment in Chapter 4.

## 3.3 Materials and Methods

### 3.3.1 Overview

This experiment involved the simultaneous recording and deep-brain stimulation of freely-moving rodents using the EEG-DBS system. Bilateral DBS was carried out in the anterior-thalamic nucleus (ATN), with bilateral recording in the medial prefrontal cortex (mPFC) and dCA1 region of hippocampus (dCA1). Note that although these locations were targeted with recording/stimulation electrodes, electrode verification was not available in this experiment due to limitations imposed by the Home Office licence at the time of testing. 4 rats each underwent 5 separate 2-hour recording and stimulation sessions, where they were free to roam about an open-field arena. Each session consisted of a 30-minute baseline recording period, followed by 60 minutes of constant DBS, followed by 30-minutes of local-field potential (LFP) recording (figure 3.1), with video-tracking of their movement made throughout. The stimulation parameters varied by pulse-width ( $25\mu\text{s}$ ,  $100\mu\text{s}$ ,  $200\mu\text{s}$ ) and intensity ( $20\mu\text{A}$ ,  $100\mu\text{A}$ ), with a fixed frequency of  $100\text{Hz}$  (table 3.1). Note that in this study there was no sham-stimulation control group (i.e. rats which had electrodes implanted but received no DBS). As such this experiment was focussed on observing differences between the stimulus parameters used.

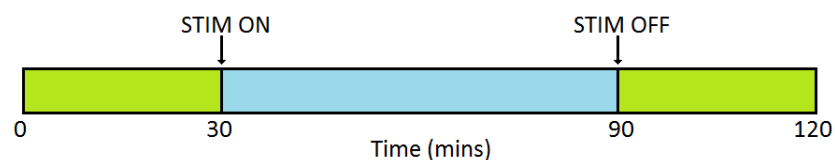


Figure 3.1 – LFP recording takes place for the full 120 minutes in each recording session, with stimulation activated between 30 and 90 minutes.

STIM Parameters	Frequency	Pulse-Width	Current
A	100Hz	100 $\mu$ S	20 $\mu$ A
B	100Hz	100 $\mu$ S	100 $\mu$ A
C	100Hz	200 $\mu$ S	20 $\mu$ A
D	100Hz	200 $\mu$ S	100 $\mu$ A
E	100Hz	25 $\mu$ S	20 $\mu$ A

Table 3.1 – 5 stimulation settings were used, each of which varied in its pulse-width and current, with a fixed frequency of 100Hz.

For each recording/stimulation session, rats were pseudo-randomly assigned 1 of 5 stimulation parameters (table 3.1), until they underwent stimulation with each of the 5 parameters by the final recording session.

### 3.3.2 Selection of Stimulus Parameters

The choice of stimulus pulse-width, frequency and intensity that were used in this study were determined based on a) a calculated maximum ‘safe’ current limit based on the geometry of the DBS electrodes used, b) a current understanding of the mechanisms of action of DBS from previous studies, and c) the outcomes of various related DBS studies through which uses similar DBS parameters. Given the incomplete knowledge of the effects DBS has on the brain, researchers typically employ a range of stimulus settings for use in their studies. Portable stimulators used in patients are often adjusted by clinicians for maximum therapeutic effect. For example, Greenberg et al., (2006) carried out DBS in the anterior limb of the internal capsule for patients with severe OCD, and varied the stimulus frequency from 100 to 130Hz, varied the stimulus intensity from 2-6V, and the pulse-width was set to either 90 or 210 $\mu$ s. Similarly in the study of treatment-resistant depression in humans, Malone et al., (2009) utilised exactly the same parameters for DBS in the ventral capsule/ventral striatum region. In rodents, Klein et al., (2012) performed DBS in one of a number of brain regions in a poly I:C model relevant to the prepulse-inhibition deficits in schizophrenia, and found that its effect was highly selective to not just the brain region, but also to the stimulus parameters used. To date there has been a high degree of ambiguity regarding the selection of appropriate

stimulus parameters, and indeed the rationale for the selection of stimulus parameters used in many studies has been based primarily on the outcome of similar related studies.

Generally speaking high-frequency stimulation (HFS) parameters ( $> 100\text{Hz}$ ) have been utilised in the majority of DBS studies to date, with its origins based in the treatment of motor-related neurological disorders such as Parkinson's disease. Typically in these motor-related disorders it has been observed that HFS improves symptoms, whereas low-frequency stimulation (LFS; e.g. 5-10Hz) worsens symptoms (Moro et al., 2002, Rizzone et al., 2001). This use of HFS in these studies has perhaps resonated throughout the various fields of DBS research, whilst the current mechanisms behind this are still being debated (see Chapter 1 – 1.3.2.1: Effect of Stimulation Frequency, for further details). An investigation into the effects of stimulation of *in vitro* STN slices derived from an acute rat model of Parkinson's disease (Garcia et al., 2005b, Garcia et al., 2003), revealed that whilst LFS at 10Hz had shown little change in STN neuron activity, HFS between 50-80Hz resulted in a replacement of the spontaneous activity with a stimulation-driven activity, at the frequency of stimulation. One possible mechanism behind this is based on the average intrinsic oscillation frequency of these neural networks, which in motor-related disorders has found to be around 130Hz (Gale, 2004; see also Chapter 1 – 1.3.2.1: Effect of Stimulation Frequency, for further discussions and theories).

In the study of working memory, high-frequency stimulus pulses in the fornix of humans (at 130Hz) has been found to result in an activation of hippocampal networks (Hamani et al., 2008, Laxton et al., 2010, Smith et al., 2012). Furthermore a recent study revealed an activation of the prefrontal cortex in rats, through stimulation of the mediodorsal thalamic nucleus at the same frequency of 130Hz (Ewing et al., 2013). In the current study the desired effect of stimulation is to facilitate an activation of hippocampal-dependent networks associated with learning and memory. Thus given that high-frequency stimulus signals have previously been observed to facilitate activation in neural networks, this study utilised stimulus frequencies at or above 100 Hz.

The current intensity and pulse-width used in this experiment was varied between low and high values; in which case the current intensity was set to either 20 $\mu$ A or 100 $\mu$ A, and the pulse-width was set to 25 $\mu$ s, 100 $\mu$ s, or 200 $\mu$ s. This range of parameters was selected as an exploratory approach in order to observe any behavioural differences between them. The maximum current intensity and pulse-width (100 $\mu$ A and 200 $\mu$ s, respectively) used in this experiment were set based on a) the maximum 'safe' charge density limit of 30 $\mu$ C/cm<sup>2</sup> (for individual stimulus pulses), as suggested by Medtronic, and b) an equation described by Merrill et al., (2005) for calculating the maximum 'safe' current to use based on the electrode geometry, as well as a given charge density limit (which in this case is 30 $\mu$ C/cm<sup>2</sup>; see Chapter 1 – Equation 1.2 for further details). With a measured DBS electrode contact area of 0.08mm<sup>2</sup> and a pulse-width of 200 $\mu$ s, the theoretical maximum 'safe' current for use in this study was calculated to be 120 $\mu$ A.

### **3.3.3 Surgery**

All procedures were carried out in accordance with the Animals Scientific Procedures Act (1986). The instruments, gown and drape used during surgery were autoclaved the night before, and all surfaces and equipment were wiped down with 70% ethanol prior to handling of the animal. Male Lister Hooded rats (n=4; Harlan UK Ltd) weighing between 350-400g were individually transported to the surgery room in a separate transport cage, and then placed into a clear acrylic anaesthesia chamber. Animals were anaesthetised with a mixture of oxygen (0.3 l.min<sup>-1</sup>), nitrous oxide (0.7 l.min<sup>-1</sup>), and isoflurane (Isoflo®; Abbott Animal Health) set to a level of 5%, which was lowered through the subsequent surgery steps as appropriate; first to 3%, then to 1.5%. The level of anaesthesia was checked throughout the experiment via the tail and hind-paw reflex, as observed by pinching these areas with a pair of forceps. In addition checks for the eye-blink reflex were carried out for each rat prior to handling the autoclaved gown/instruments. Once the rat was anaesthetised with absence of reflex responses, the area on the scalp between the eyes to the back of the neck was shaved using a small set of clippers. Following this the anaesthesia was switched from the chamber to the stereotaxic frame (David Kopf Instruments),

and the rat was secured into the face-mask. Adjustments were made on the equipment for head elevation, and the rat was secured into place using atraumatic (blunt) ear bars (David Kopf Instruments). Once secured, the animals were given a subcutaneous injection of Rimadyl™ (Pfizer) administered at (1ml.kg<sup>-1</sup>), and wrapped in bubble-wrap to maintain core body temperature.

With the animal secured in the stereotaxic frame, the surgery table was covered with a sterile drape, and any non-sterile surfaces to be handled were covered with autoclaved tinfoil. The shaved area of the scalp was rubbed with an iodine-soaked cotton swab which removed loose hairs and cleaned the incision site. Throughout the surgery this site was regularly cleaned with saline-soaked sterile cotton buds to keep the area clear of blood and to help prevent infection. A single rostral-caudal incision was made from between the eyes to the back of the ears using a sterile scalpel blade, and the underlying skin was drawn back using small pairs of forceps clamped to the underlying muscle. The connective tissue over the skull was scraped away with sterile cotton buds, until the surface of the skull had been exposed encompassing the sites of interest.

An LFP electrode was mounted into the stereotaxic arm, and used to make fine adjustments on the apparatus to achieve a flat-skull, by measuring the relative heights of bregma and lambda (Paxinos and Watson, 2007). Bregma and lambda were both marked using a fine-tip permanent marker for future reference. Following this the locations of each electrode site was calculated, and then marked on the skull using a fine-tip permanent marker (figure 3.2A). Once all electrode locations had been marked, holes were drilled carefully around these points using a dental burr (Royem Scientific Limited) to accommodate the 2 different types of stainless-steel anchor screws. The larger 4 anchor screws have a 2mm shaft-diameter (Royem Scientific Limited), whilst the remaining three smaller screws (including the reference electrode) have a 1.2mm shaft-diameter (Plastics One). The anchor screws, including the reference electrode were affixed through the drilled holes using a small screwdriver (Plastics One). The reference electrode in this case was affixed directly above the cerebellum anterior to lambda, directly on the midline.

The next step involved implantation of the 4 LFP and 2 DBS electrodes. These electrodes followed a custom 2-part design consisting of the electrode itself and connector; along with a removable guide (see Chapter 2 – 2.4.14: Electrode Design). The electrodes were handled by gripping them into the stereotaxic arm by its removable guide. The following steps were repeated for each electrode, noting that they were implanted from anterior to posterior, i.e. mPFC electrodes first and dCA1 electrodes last:

1. LFP/DBS electrode was mounted securely into stereotaxic arm.
2. The coordinates of bregma and lambda were measured again, accounting for an offset in the electrode position in the stereotaxic arm.
3. The coordinates for the electrode site were calculated.
4. The electrode was moved into its medial/lateral, anterior/posterior position above the skull, and gently lowered until nearly touching the overlying skull region, to confirm the precise site for drilling.
5. Electrode was raised, and a hole was carefully drilled through the skull at this point. For LFP electrodes, a 0.8mm diameter drill piece was used, whereas DBS electrodes utilised a 1mm diameter drill piece. Once dura matter was visible, it was pierced using a small needle.
6. Electrode was slowly lowered into the brain, until it reached its calculated dorsal/ventral position.
7. The electrode hole was plugged with bone-wax (Ethicon) using a fine pair of tweezers and a fine spatula.
8. Low viscosity dental cement was mixed up by filling a small glass crucible with Simplex Rapid™ (Kendent) powder and mixing it with a small amount of Simplex Rapid™ (Kendent) liquid using a fine-tip spatula. When mixed, it was placed around the electrode site, making sure it covered the cemented part of the electrode, and an adjacent skull anchor. Care was taken at this point not to cover either bregma or lambda with cement, or any un-drilled electrode sites.
9. Once the cement had hardened, the stereotaxic arm was released from the electrode, leaving the electrode guide protruding from the newly cemented

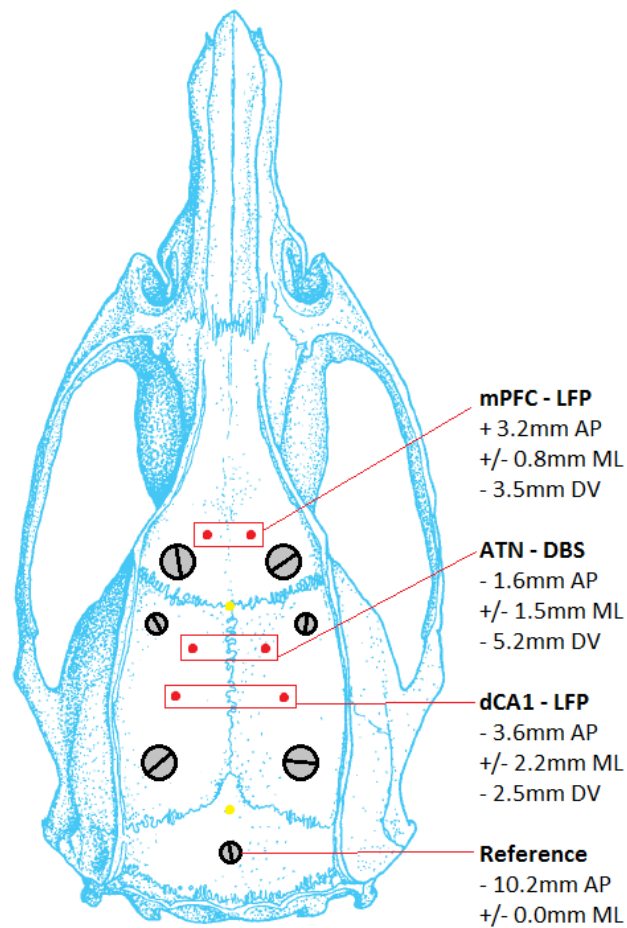
electrode. Note that premature removal of the guide (see Chapter 2 – figure 2.24F) at this point can potentially dislodge the electrode whilst inside the brain.

10. The guide was released from the rest of the electrode by gently using a 1mm dental burr to drill around the dental cement attaching it to the rest of the electrode.
11. A new electrode was picked up, and this process repeated from step 1.

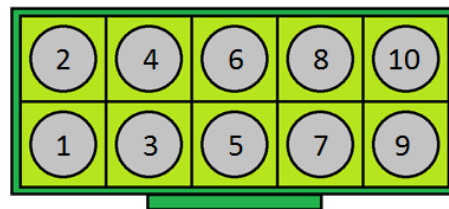
With all electrodes implanted, an additional layer of dental cement was placed on the skull, and any protruding or sharp bits of dental cement were removed using the dental burr. At this point the individual electrode pins were carefully attached to the headstage implant (figure 3.2B), with any excess wire folded underneath it. When all pins were connected, the headstage was adjusted to an ideal position, and dental cement placed around and under it. Subsequently, dental cement was layered around the implant and the skull surface, and care was taken to avoid either sharp protrusions in the dental cement, or dental cement which had stuck to the wound site. Addition of dental cement around the sides of the implant further reinforced its structural integrity.

With the headstage hardened and wound site cleaned, the animal was taken out of the stereotaxic frame, and given a 2.5ml intra-peritoneal injection of Hartmann's Solution (TPS Healthcare), which is a sodium chloride solution consisting of various salts and minerals. The animal was then placed belly-down into a recovery cage, which consisted of a paper lining and watered down food. The cage itself was placed onto a cage-size heat-pad prior to the surgery, allowing it time to warm up to provide the animal with a warm environment post-surgery. See figure 3.3 for photographs of a rat post-surgery with a headstage implant and attached EEG-DBS system.





A



- 1 - LFP: mPFC (left)
- 2 - LFP: mPFC (right)
- 3 - LFP: dCA1 (left)
- 4 - LFP: dCA1 (right)
- 5 - N/A
- 6 - Ref/Gnd
- 7 - DBS: ATN (left cathode)
- 8 - DBS: ATN (left anode)
- 9 - DBS: ATN (right cathode)
- 10 - DBS: ATN (right anode)

B

Figure 3.2 – The locations of the LFP, DBS and reference electrodes, along with the skull anchors is shown in (A). All electrode coordinates are given relative to bregma, with dorso-ventral measurements taken from the skull surface at these points. Bregma and Lambda are marked in yellow. The connectivity of the electrodes to the headstage is shown in (B) as viewed from above. The headstage is positioned such that its screw connector is facing to the left of the rat skull in (A). Image in (A) was adapted from “The Rat Brain in Stereotaxic Coordinates – 6<sup>th</sup> Edition” (Paxinos and Watson, 2007).



A



B



C

Figure 3.3 –Photographs of a male Hooded Lister rat with the 10-pin headstage implant (A), along with the wireless EEG-DBS system and battery attached (B,C). Although this particular rat is from the working memory task described in Chapter 4 (with T-maze shown in the background in B and C), rats in the proof-of-concept task underwent the same procedure regarding surgery, and device attachment. The mean weight of the system, battery, headstage implant, electrodes, dental cement and skull anchors is approximately 11.5g. Rats were able to move freely, whilst displaying all normal behaviours including running, jumping and grooming.

### **3.3.4 Recovery and Habituation**

Rats were given at least 7 days recovery following surgery. During this period, they were weighed daily and checked carefully for any post-operative complications such as loosening of the headstage or bleeding around the wound site. Of the 4 rats that underwent surgery, all 4 progressed to the experimental phase for DBS and LFP recording. Following recovery they each underwent 3 separate habituation sessions in which they are placed into the open-field arena and left alone to roam for 20 minutes. Throughout the course of the study animal were placed on an ad-libitum diet and were weighed daily.

### **3.3.5 Arena Configuration**

Two 60x60cm PVC plastic arenas were placed on top of an infra-red (IR) light source, and were positioned directly underneath a ceiling-mounted video camera (Sanyo). The camera interfaced with video-tracking software Ethovision XT (Nodulus Information Technology), which was configured to record and track the animal movements inside the arenas. Two EEG-DBS receiver (RCVR) systems were positioned close to the outside of each recording arena, with a serial cable connecting them to laptops positioned outside the recording room (figure 3.4). With this arrangement, stimulation parameters were delivered from outside the closed recording room, without disturbing the rats.

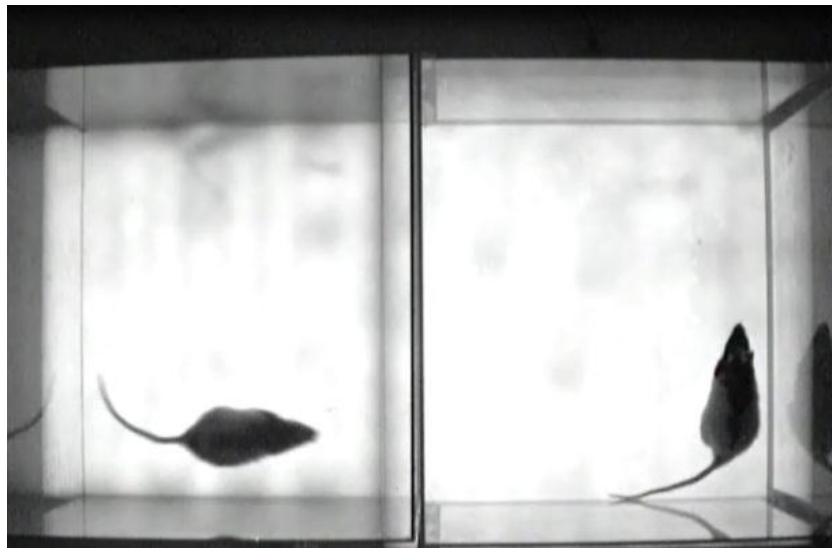
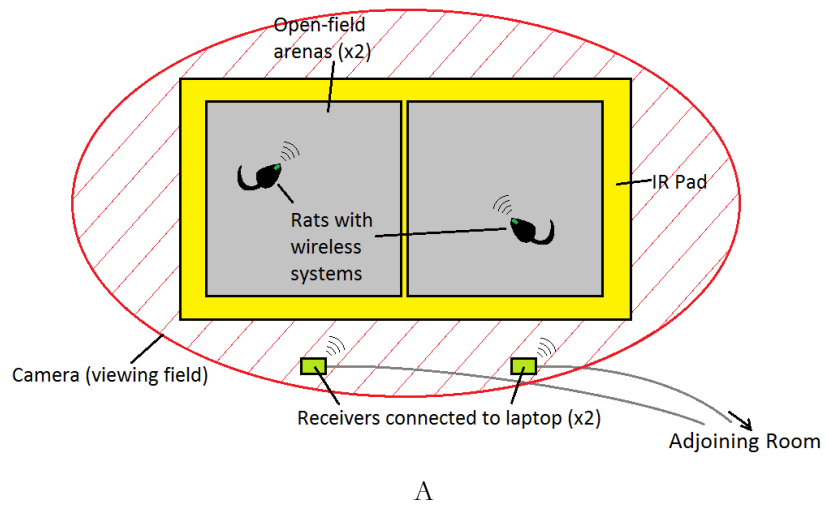


Figure 3.4 – Layout of the open-field arena, IR pad, wireless systems and receivers, and the camera viewing field are shown in A. Video still from the recorded data is shown in B.

### **3.3.6 Analysis of Results**

#### **3.3.6.1 Power and Coherence Spectrograms**

Recorded LFP and video-tracking data were imported into Matlab (Mathworks) for further analysis. The data was organised into 5 groups based on each of the 5 stimulation parameters, from which power and coherence spectrograms are calculated using scripts adapted from the Chronux library (<http://www.chronux.org>). Spectral power and coherence was calculated using multi-taper functions featuring 11 data-tapers, and a 4-second sliding window with 500ms overlap. For individual channels, power spectrograms were normalised by dividing by its root-mean-square (RMS), which was calculated over the non-stimulation periods of that particular channel. Data from each of the channels and channel pairs were subsequently combined with the rest of the recordings from each stimulation group.

#### **3.3.6.2 Power to Coherence/Velocity Scatterplots**

The values used to represent power and coherence in the scatterplots were derived directly from the spectrograms and coherograms as calculated for each stimulation group. In this case the peak power and coherence between 4-12Hz was extracted using a custom-written Matlab script.

Velocity information for each rat was exported from Ethovision XT as Excel files, and subsequently imported into Matlab. Sampling of the video information in the raw data file occurred at 25Hz. In Matlab the velocity information was averaged into 2-minute bins over the entire duration of the recording session, and displayed as a group average as bar plots. In the scatterplots the velocity information was placed through a smoothing filter several times to allow for a meaningful correlation to be made with dCA1 theta power. This type of averaging was carried out because in reality the rat mean velocity consisted of many discrete moments of starting and stopping, thus giving rise to spikes in the velocity plot.

## 3.4 Results

### 3.4.1 Raw LFP Recordings

The system was able to successfully perform 2 hours of constant LFP recording and DBS for each of the rats tested. Whilst the electrode verification data is not available, recorded LFP data is characteristic of that recorded from their respective brain regions; with dCA1 featuring a prominent theta-peak, and mPFC featuring a comparatively broader range of frequencies with a predominant theta-peak (figure 3.5).

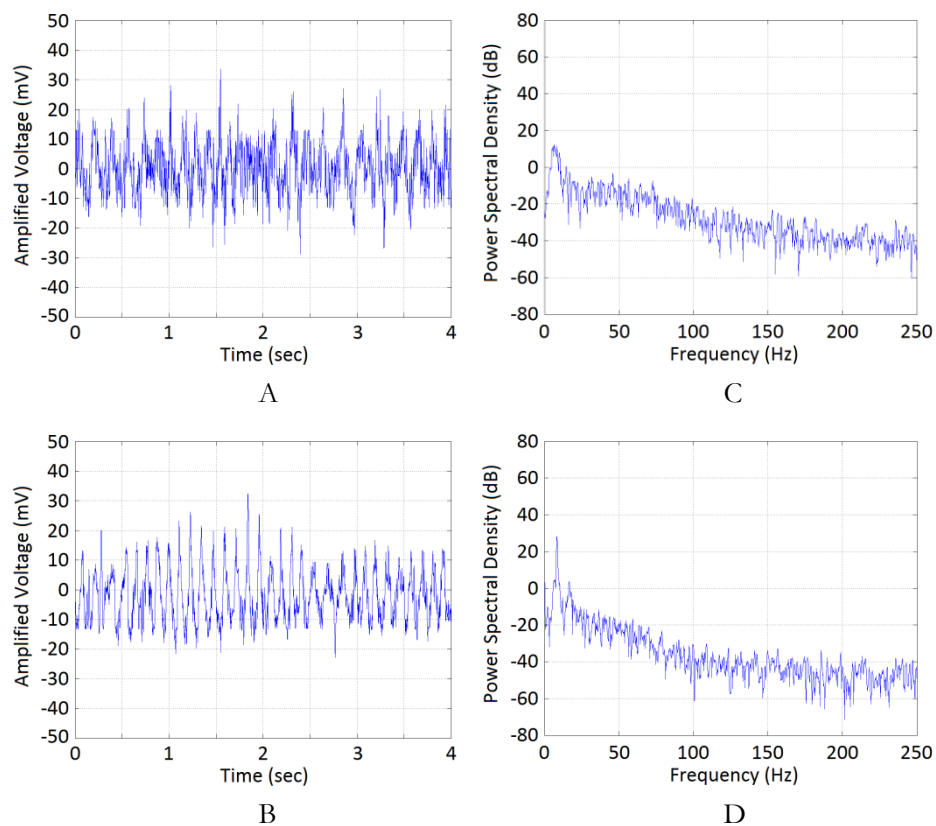


Figure 3.5 –Raw LFP recordings from mPFC (A) and dCA1 (B) and their respective power-spectral density plots (C and D, respectively).

Activating stimulation resulted in prominent stimulus artefacts that were superimposed onto the raw LFP recording (figure 3.6 – A and B). A power-spectral density measurement of this recording reveals a signal with multiple predominant

spectral components superimposed onto the raw LFP spectrum, with major stimulus artefacts featuring most prominently at 100Hz and 200Hz (figure 3.6 – C and D). Depending on the pulse-width and current intensity, these artefacts would sometimes exceed the maximum input voltage of the system, resulting in the saturation of these signals. Because of this, recordings made during stimulation were left out of the subsequent analysis, leaving only the recordings that were made during the first and final 30 minutes of the 2-hour test session (i.e. before and after stimulation).

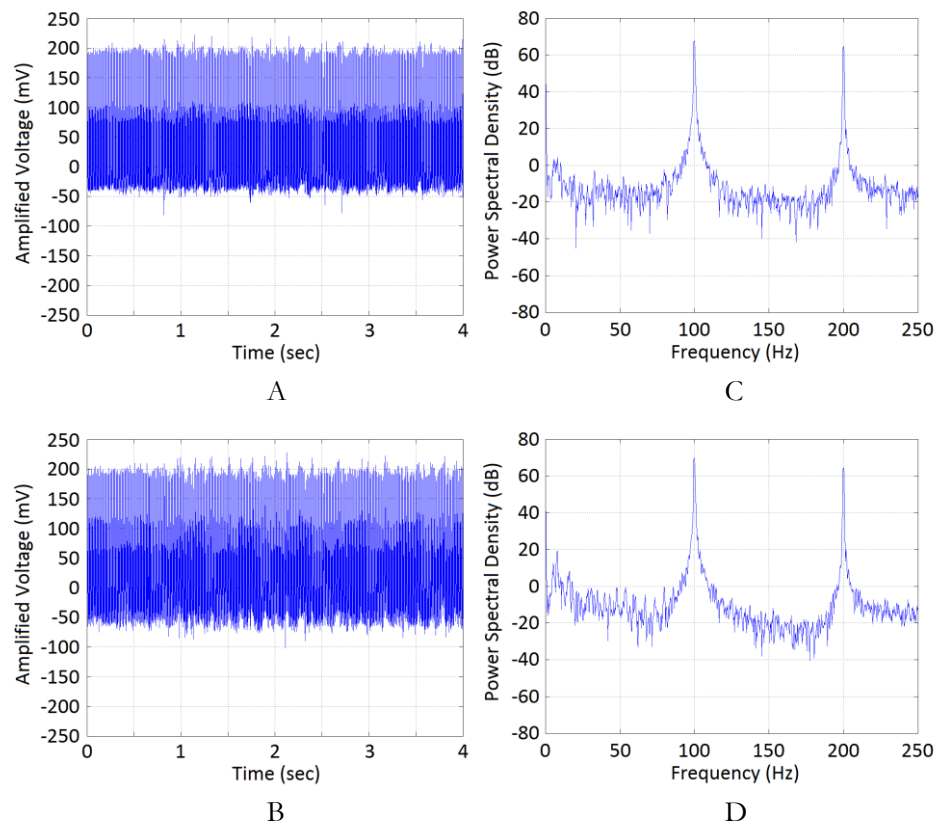


Figure 3.6 – Simultaneously recording and stimulating with the EEG-DBS system resulted in prominent stimulus artefacts which were superimposed onto the raw LFP signal for both the mPFC (A) and dCA1 (B) electrodes. The power-spectral density of these waveforms revealed a spectral pulse-train superimposed onto these raw signals, with pulses appearing most prominently at 100Hz and 200Hz (B and D).

An analysis of the *in vivo* noise level was not carried out in any of the LFP segments in this study, due to the impracticalities in devising a suitable measure for the noise

(e.g. establishing the difference between noise and LFP without knowing *a priori* the exact characteristics of either). Nonetheless 50Hz mains noise – a problematic feature in many wired and wireless systems – was not visible against the background signal at that frequency.

### **3.4.2 Power Spectral Density in the mPFC and dCA1 Brain Regions**

Averaged, normalised PSD estimates are shown for both the mPFC (figure 3.7) and dCA1 (figure 3.8) brain regions. These spectrograms reveal the time-domain PSD estimates for each of the 5 stimulation parameters (denoted A-E; see table 3.1), during the 30-minute periods before and after the 1-hour stimulation period. In the mPFC and dCA1 spectrograms, (figures 3.7-3.8) a theta-frequency peak can be observed as a yellow/orange horizontal band in each of the recordings at ~9Hz. One of the most consistent findings in this study revealed reductions in theta-band (4-12Hz) PSD in dCA1 recordings (figure 3.8) during the post-stimulation period, as compared to the pre-stimulation period (see also the histograms representing dCA1 theta activity before and after stimulation in figure 3.9). No clear pattern can be observed between the different stimulation parameters used. Generally speaking theta-power in dCA1 is seen to be at its highest at the beginning of the recording session, which diminishes gradually throughout the pre- and post-stimulation periods.



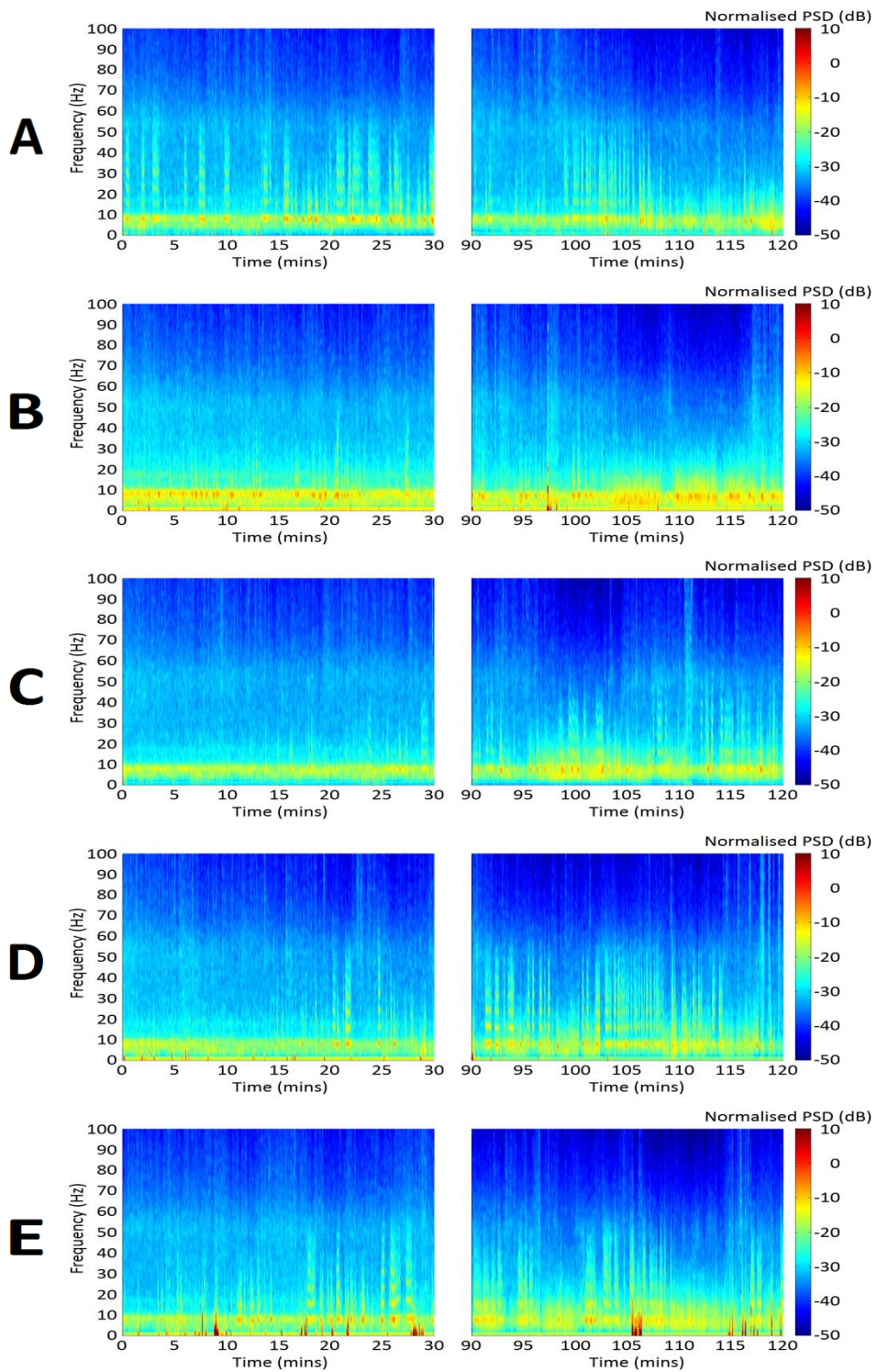


Figure 3.7 Spectrograms of mPFC power in each of the stimulation groups, with the pre-stimulation period shown on the left, and the post-stimulation period shown on the right. Stimulation parameters were A:  $100\mu\text{s}$ ,  $20\mu\text{A}$  ( $n=4$ ); B:  $100\mu\text{s}$ ,  $100\mu\text{A}$  ( $n=4$ ); C:  $200\mu\text{s}$ ,  $20\mu\text{A}$  ( $n=4$ ); D:  $200\mu\text{s}$ ,  $100\mu\text{A}$  ( $n=3$ ); E:  $25\mu\text{s}$ ,  $20\mu\text{A}$  ( $n=4$ ). All stimulation parameters utilised a stimulus frequency of  $100\text{Hz}$ . Note that artefacts are more prominent in the mPFC recordings than in dCA1 (figure 3.8). The horizontal yellow band towards the bottom of the spectrograms (at close to  $10\text{Hz}$ ) represent theta activity, which is the most predominant brain frequency observed in this recording.

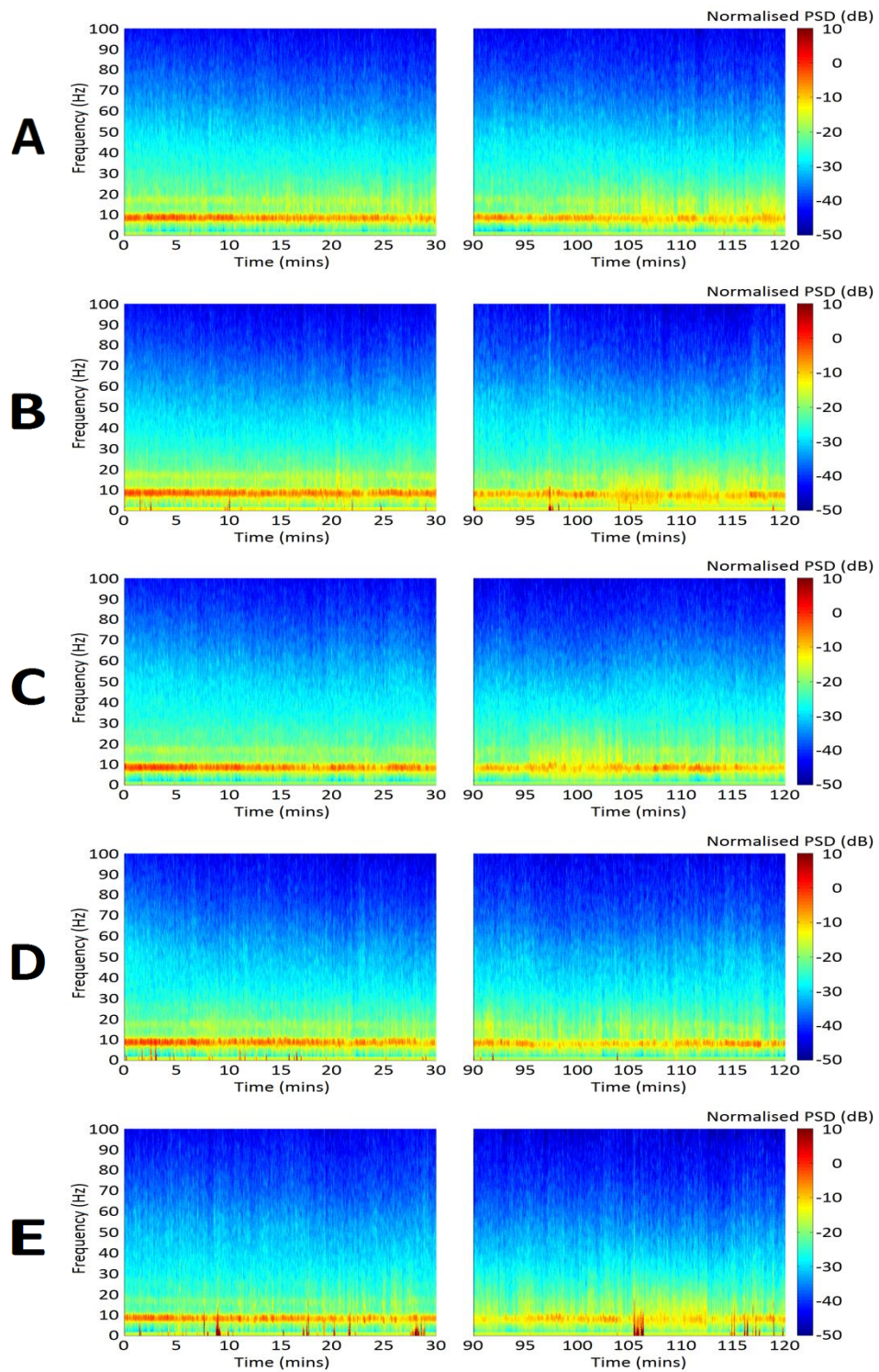


Figure 3.8 – Spectrograms of dCA1 power in each of the stimulation groups, with the pre-stimulation period shown on the left, and the post-stimulation period shown on the right. Stimulation parameters were A:  $100\mu\text{s}$ ,  $20\mu\text{A}$  ( $n=4$ ); B:  $100\mu\text{s}$ ,  $100\mu\text{A}$  ( $n=4$ ); C:  $200\mu\text{s}$ ,  $20\mu\text{A}$  ( $n=4$ ); D:  $200\mu\text{s}$ ,  $100\mu\text{A}$  ( $n=3$ ); E:  $25\mu\text{s}$ ,  $20\mu\text{A}$  ( $n=4$ ). All stimulation parameters used a stimulus frequency of  $100\text{Hz}$ . The strength of dCA1 theta-activity is seen to diminish in the post-stimulation period, as compared to the pre-stimulation period.

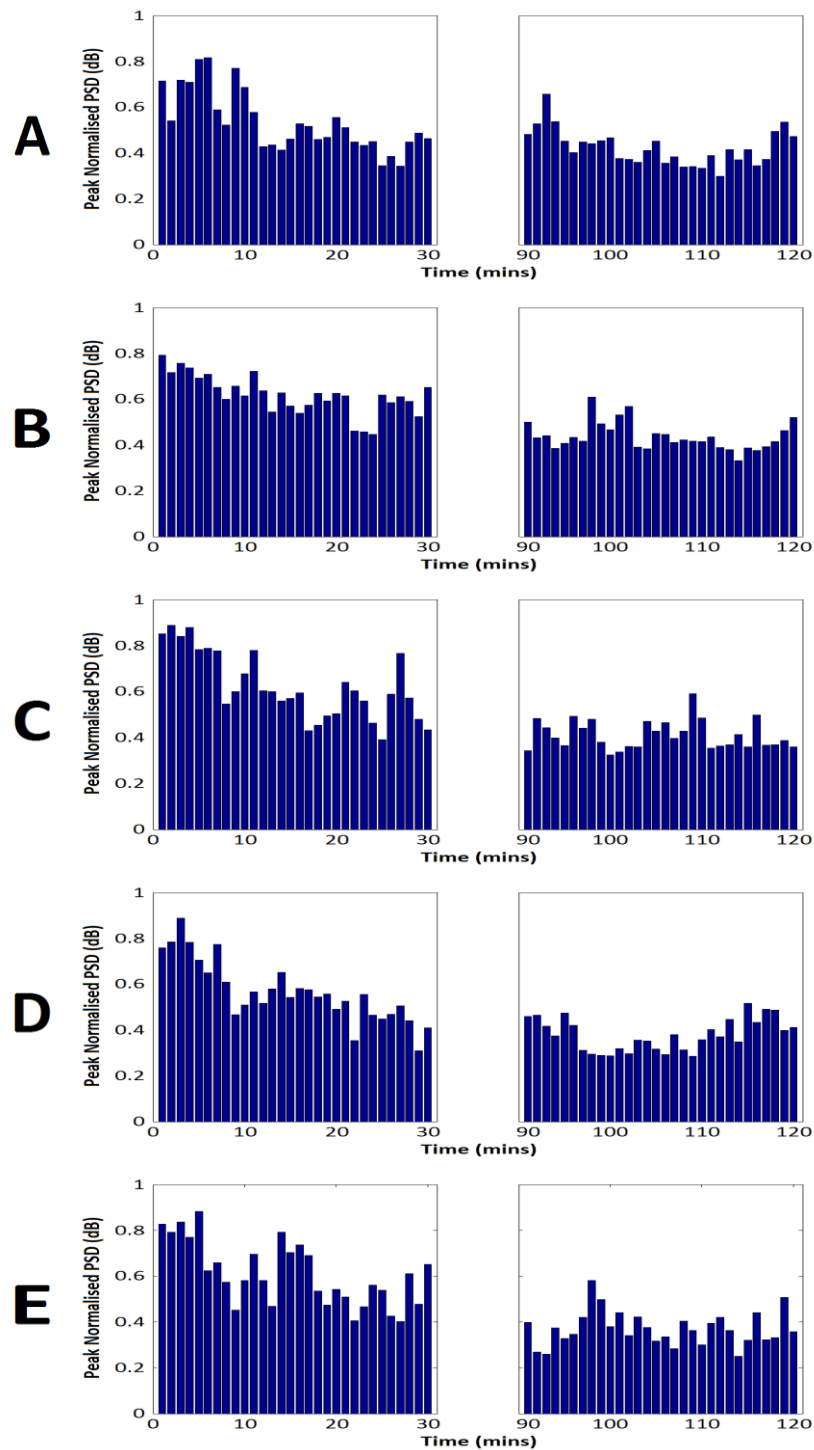


Figure 3.9 – Histograms representing normalised dCA1 theta-frequency PSD in each of the stimulus groups before and after stimulation. Histograms are shown for the pre-stimulation (0-30 minutes) and post-stimulation (90-120 minutes) recording periods. Data from each rat was extracted as the peak (normalised) theta activity and averaged into 1-minute bins with the data from the rest of the stimulus group. Stimulation parameters were A:  $100\mu\text{s}$ ,  $20\mu\text{A}$  ( $n=4$ ); B:  $100\mu\text{s}$ ,  $100\mu\text{A}$  ( $n=4$ ); C:  $200\mu\text{s}$ ,  $20\mu\text{A}$  ( $n=4$ ); D:  $200\mu\text{s}$ ,  $100\mu\text{A}$  ( $n=3$ ); E:  $25\mu\text{s}$ ,  $20\mu\text{A}$  ( $n=3$ ). All stimulation parameters used a stimulus frequency of 100Hz. Theta activity generally appears to be higher in the pre-stimulus phase, relative to the post-stimulus phase, with the largest increases occurring in the first 10 minutes of the recording session.

A major confounding feature present in the PSD plots – particularly those derived from the mPFC – are artefacts which span the duration of the pre- and post-stimulation recording periods. These artefacts mostly took the form of tooth-grinding artefacts, which produced a distinctive waveform on the mPFC electrodes, and to a lesser extent, the dCA1 electrodes (figure 3.10). These transient, high-frequency bursts were most likely associated with skull-vibrations that resulted from chewing or teeth grinding. In the working memory experiment detailed in Chapter 4, similar artefacts were present in the raw LFP recording every time the animal obtained a food reward.

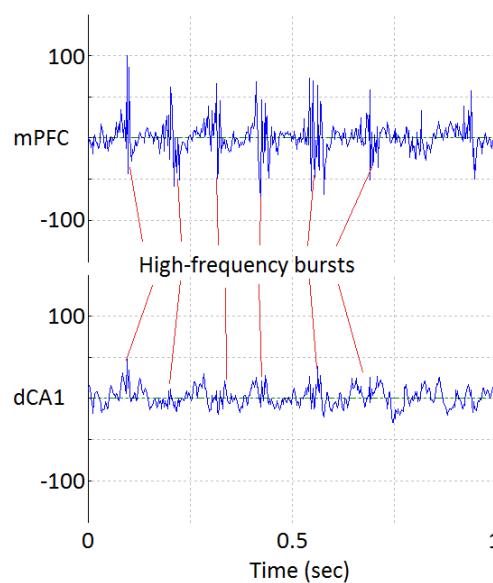


Figure 3.10 – Illustration of rat chewing artefacts on the mPFC and dCA1 recording channels. Numbers on the y-axis represent amplified voltage in mV.

### 3.4.3 Theta-Coherence between mPFC and dCA1

Similar to dCA1 theta power, the coherence between the mPFC and dCA1 is seen to gradually reduce throughout the course of the pre- and post-stimulation periods, with its largest values seen at the beginning of the session, and its lowest values at the end (figure 3.11). Again, no clear pattern can be observed between the different stimulus groups (A-E).

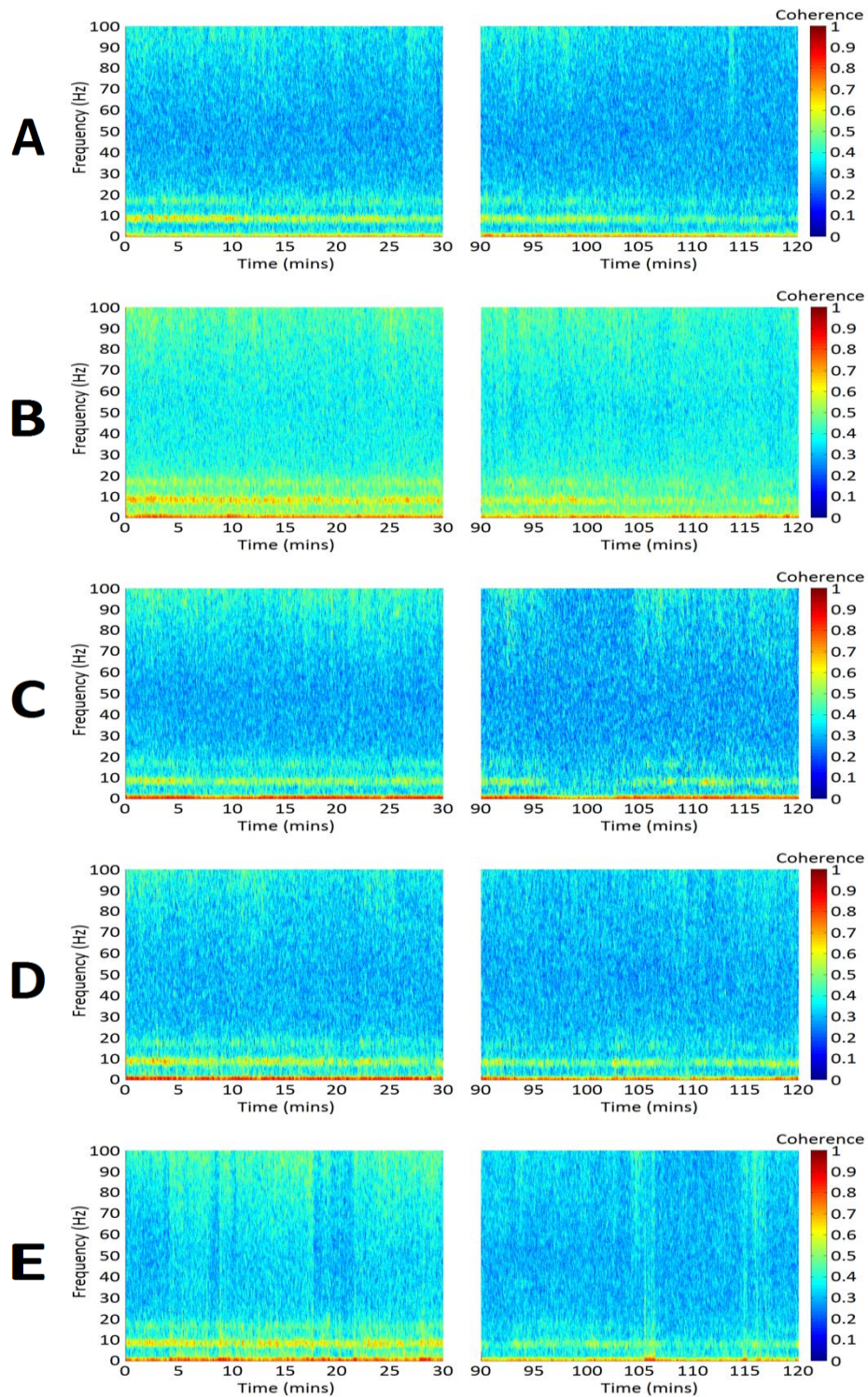


Figure 3.11 – Spectrograms of mPFC – dCA1 coherence in each of the stimulation groups, with the pre-stimulation period shown on the left, and the post-stimulation period shown on the right. Stimulation parameters were A:  $100\mu\text{s}$ ,  $20\mu\text{A}$  ( $n=4$ ); B:  $100\mu\text{s}$ ,  $100\mu\text{A}$  ( $n=4$ ); C:  $200\mu\text{s}$ ,  $20\mu\text{A}$  ( $n=3$ ); D:  $200\mu\text{s}$ ,  $100\mu\text{A}$  ( $n=4$ ); E:  $25\mu\text{s}$ ,  $20\mu\text{A}$  ( $n=4$ ). All stimulation parameters used a stimulus frequency of  $100\text{Hz}$ . Coherence between the mPFC and dCA1 regions is more prominent in the pre-stimulation period, and can be observed as a horizontal yellow band at  $\sim 10\text{Hz}$ .

### **3.4.4 Effect of Stimulation at High Currents upon Behaviour in the Open Field**

During the open-field experiments, rat mean velocity was analysed from the video-tracking data. However due to missing velocity recordings in some of the rats, data is shown for each stimulation parameter as an average of 2 (A) and 3 (B-E) sessions. Similar to theta power and coherence, rat mean velocity started off at its highest at the beginning of the test sessions, and gradually diminished towards its lowest values towards the end of the sessions (figure 3.12). This is presumably a result of the rat habituating to the open field environment. Activation of stimulation at high currents (100 $\mu$ A; parameters B and D) was seen to elicit a transient increase in rat mean velocity. From observing animal behaviour during each of the recording sessions, most stimulus activations resulted in a visual response from the rat, akin to an 'awareness' of something happening. Only at the higher current parameters did the rats begin moving around the arena. In some cases, activation of stimulation at these currents resulted in head-shaking, and circling of the arena. In this case the rats would move from corner to corner in the recording arena for several minutes.

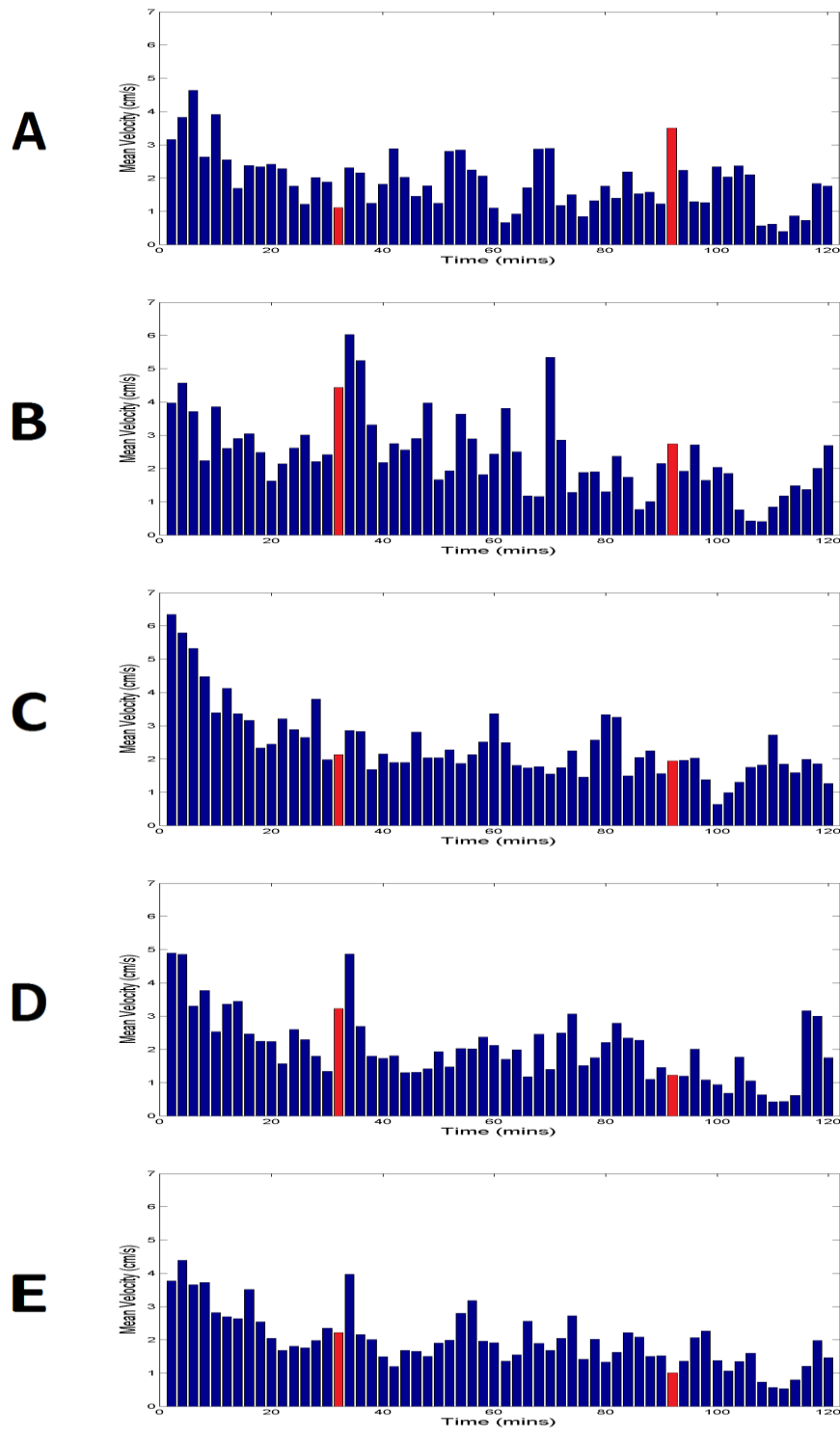


Figure 3.12 – Average velocity bar-plots for each of the stimulation groups (A-E). The mean velocity is shown for the entire duration of the session, with the activation/deactivation of stimulation represented by the first and second red bars, respectively. Each bar on the histogram represents a 2 minute time interval. Stimulation parameters were A:  $100\mu\text{s}$ ,  $20\mu\text{A}$  ( $n=2$ ); B:  $100\mu\text{s}$ ,  $100\mu\text{A}$  ( $n=3$ ); C:  $200\mu\text{s}$ ,  $20\mu\text{A}$  ( $n=3$ ); D:  $200\mu\text{s}$ ,  $100\mu\text{A}$  ( $n=3$ ); E:  $25\mu\text{s}$ ,  $20\mu\text{A}$  ( $n=3$ ). All stimulation parameters used a stimulus frequency of 100Hz. Due to missing video-tracking data with some of the rat sessions, the sample sizes used for assessing mean rat velocity were smaller than that used in the LFP PSD/coherence analysis.

### **3.4.5 Correlations Between dCA1 Theta, and Coherence/Velocity**

Rat dCA1 theta was seen to correlate with both mPFC-dCA1 theta coherence (figure 3.13 – left panel), and the rat mean velocity (figure 3.13 – right panel). In all cases, the mean velocity, theta-power and theta-coherence were seen to be lower in the post-stimulus period as compared to the pre-stimulus period, with lower correlation coefficients. Note that correlations were only made for the rat sessions which contained analogous video-tracking data (n between 2 and 3 for each of the stimulus groups). Correlations were not made with mPFC activity due to the excessive amount of artefacts contained at these recording sites.



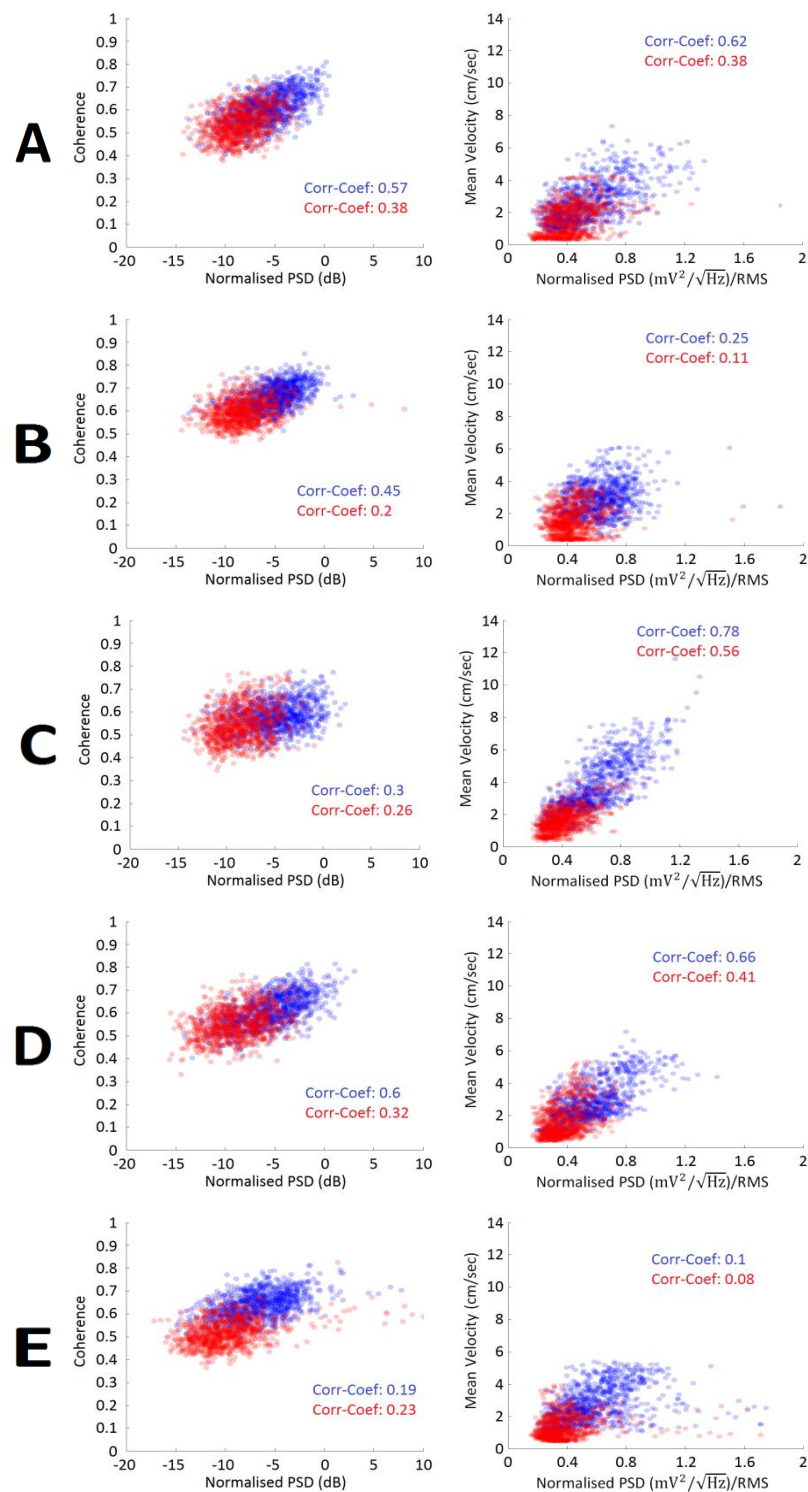


Figure 3.13 – Correlations between dCA1 peak theta power and mPFC-dCA1 peak theta-coherence for each stimulation group (left plots). Corresponding correlations between dCA1 peak theta power and rat mean velocity are shown in the right plots. Blue represents the pre-stimulation period, red represents the post-stimulation period. Stimulation parameters were A: 100 $\mu$ s, 20 $\mu$ A (n=2); B: 100 $\mu$ s, 100 $\mu$ A (n=3); C: 200 $\mu$ s, 20 $\mu$ A (n=3); D: 200 $\mu$ s, 100 $\mu$ A (n=3); E: 25 $\mu$ s, 20 $\mu$ A (n=3). All stimulation parameters used a stimulus frequency of 100Hz. Note that for correlations with coherence, the power is represented on a logarithmic scale.

### 3.5 Discussion

In this proof-of-concept study the EEG-DBS system was shown to be able to wirelessly record and stimulate *in vivo* in freely-moving rats, over a time period of 2 hours. Furthermore, basic correlations with video-tracking enriched the study with information on the rat's mean velocity in the open-field arena, allowing for correlations to be made between the LFP recording and video-tracking. A major confounding issue in this experiment was the absence of any histological verification of the implanted electrodes, due to limitations imposed by the Home Office license. As such it was impossible to verify the electrode positioning for both the recording and stimulation electrodes. In spite of the absence of electrode location verification, the recorded signals from the mPFC and dCA1 regions typically represented that which arises in these areas: large hippocampal theta-peaks in dCA1, and a broader spectrum of signals (with predominant theta-peak) in the mPFC. Whilst the system noise was not directly measured *in vivo*, 50Hz mains noise is not detectable on the raw data against the background signal at that frequency; which presents itself as a good (albeit crude) indicator of system's noise-rejection capabilities.

A summary of the findings from this study is presented in table 3.2. In almost every trial observed the theta-power in dCA1 appeared to be higher in the pre-stimulation phase as compared to the post-stimulation phase. Similarly mean theta coherence between mPFC and dCA1 also appeared to be higher during this period. The onset of stimulation in most cases elicited a visual behavioural reaction from the rats, which typically manifested as an 'awareness' of something happening (e.g. looking around after lying still for minutes, getting up and moving around, etc.). Higher current-intensity parameters often resulted in a transient but markedly increased rat movement around the arena; which sometimes including head-shaking, and a circling of the arena. In this case rats would move from corner to corner in the open-field arena for several minutes. This was seen with parameters B and D, both of which used stimulation currents of 100 $\mu$ A, rather than with 20 $\mu$ A (parameters A, C and E).

Parameter	Description
Task Period (pre- /post-stimulation)	- Reduced $\theta$ -frequency PSD and mean rat velocity in the post-stimulus phase. - Reduced correlation of $\theta$ -frequency PSD with rat velocity, and mPFC-dCA1 coherence, in the post-stimulus phase.
Stimulation Parameters	- Increase in transient mean velocity of rats observed following administration of stimulus currents at $100\mu\text{A}$ .

Table 3.2 – Overview of the main findings in rat LFP and behaviour in the proof-of-concept task.

Correlations between dCA1 theta-power and mPFC-dCA1 theta-coherence were consistent in all of the sessions recorded, with higher dCA1 amplitude being correlated with increased coherence. This was more prominently seen in the baseline recordings, given the larger presence of theta power/coherence during these periods. This fits the well-established notation of theta's role in dynamically coupling brain regions on a network level (see Chapter 1 – 1.4.4.2: Synchronisation of Brain Regions with Hippocampal Theta). In addition, correlations between rat mean velocity and hippocampal theta power were also made, and once again, were stronger in the baseline recordings. This is unsurprising given one of the fundamental associations with hippocampal theta being locomotion and spatial exploration (Green and Arduini, 1954, Vanderwolf, 1969).

Given that this was the first combined stimulation and recording study undertaken that utilised the EEG-DBS system, it highlighted some important aspects of the experimental design that affected the design of the subsequent working memory task as described in Chapter 4. Artefacts were a common occurrence most prominently featuring on the frontal electrodes, and lasted for the entire duration of the recording session. These artefacts seemed to be largely associated with the rat teeth-grinding, which gave rise to a distinctive waveform that was present throughout the task. This may potentially be related to anxiety resulting from the confinement of the animals to the box for 2 hours. The second confounding factor was the lack of a sham-stimulation control group, i.e. rats that had the electrodes implanted, but didn't receive stimulation. This was itself a result of the small rat group used. In this case the rat mean velocity, dCA1 theta power, and mPFC-dCA1 coherence were all seen

to be reduced in the post-stimulation period in almost every rat session observed. This could be a direct result of the rat becoming inactive and habituated to its environment as many observations at the end of the recording sessions shown the rats lying down and relatively docile compared to the start of the experiment. These confounding factors, along with the small group sizes could perhaps have prevented any clear differences from being highlighted in each of the post-stimulation LFP segments.

The activation of DBS resulted in prominent stimulus artefacts which prevented an analysis of the LFP between 30 and 90 minutes of the experiment. In some (but not all) cases, this would result in saturation in the analogue-digital converter input – effectively destroying any meaningful data that could otherwise be extracted with artefact removal algorithms. If such algorithms were used for non-saturated signals, the recovered signal would still be reconstructed as an “approximate” estimate of the true LFP. For these reasons LFP-recordings made during stimulation were left out of this study.

An analysis of the *in vivo* noise level was not carried out in any of the recorded LFP segments in this study. Because LFP signals inside the rat’s brain cannot simply be switched off, there exists difficulties in establishing the difference between recorded LFP and noise, without knowing *a priori* the ideal (noise-free) characteristics of the recorded LFP. A possibility towards gaining an *in vivo* noise estimate is to carry out test recordings in saline, using the same LFP electrodes and anchor screws. However this would itself be a very rough estimate, given the vast differences between a saline test chamber and the environment inside the brain of an awake rat. The noise analysis as carried out in Chapter 2 (see 2.4.17.2: Basic Noise Test) made use of a calibration signal of known characteristics, in order to provide an accurate noise estimate. However the noise as observed under these conditions are expected to be significantly larger than that present in recorded rat LFP, given that a) in the noise-test recordings the system was directly interfaced with electrical equipment, and b) in the rat the distance between the recording source and system amplifiers are much shorter, with the connections between them encapsulated in dental cement. Nonetheless it is of note that 50Hz mains noise – a problematic feature of many

wired/wireless recording systems – was not visible against the background signal at that frequency. This is encouraging, and perhaps a consequence of many of the system’s design choices which emphasised noise reduction; such as the low-noise analogue components used, and the choice to design the system in a head-mount configuration.

### **3.5.1 Implications for the Next Experiment**

Generally speaking the primary outcome of this task was to verify the performance of the EEG-DBS system *in vivo*, and to identify any issues which may be of concern when designing future experiments. The constant artefacts are likely present for two reasons: a) the experimental design which perhaps caused the rats to initiate a tooth-grinding behaviour, and b) the system-headstage connection. Design of the system-rat headstage interface presented a challenge: a tight connection minimised skull-vibrations from chewing, or large LFP-deflections from rapid movements. However a tight connection increased the system-headstage friction, resulting in increased force required when attaching/removing the system. In this study one rat (not part of the 4 analysed) was euthanized because removal of the system resulted in the headstage coming off also. In the working memory test outlined in Chapters 4 and 5, this was successfully addressed by employing a unique way of carefully attaching or removing the system, as well as the use of conductive EEG paste (Ten20; Weaver), which was applied to the system sockets prior to attachment to the headstage. This allowed the system to be quickly attached or removed with minimal friction, and greatly reduced artefacts where they would otherwise be present. In addition, the subsequent experimental design involved the rat actively engaged in a working memory task, rather than being confined to a chamber.

Based upon previous experimental data suggesting that high-current in the ATN can impair working memory (Hamani et al., 2010), and the current results which displayed a transient increase in rat movement and abnormal behaviour, the current intensity for stimulation in the subsequent experiment was kept at 30 $\mu$ A.

Furthermore, stimulation took place at transient time-periods throughout the task, allowing for stimulation-free recordings to be made at the time-points of interest.

# Chapter 4

## Investigation of DBS on Rodent Working Memory Performance

### 4.1 Introduction

This chapter explores the use of deep-brain stimulation (DBS) in freely-moving rodents as they undertake a spatial working memory task. By building upon the ideas and concepts introduced in previous chapters, the EEG-DBS system was utilised in a novel experimental design which combined bilateral DBS of the fimbria-fornix (FF) with multichannel local-field potential (LFP) recording. These recordings were synchronised with the animal's movements through a video-tracking system, which allowed the animal's position and LFP to be tightly correlated in time. In addition, this experiment allowed for DBS to be manually activated by the experimenter during discrete phases of the working memory task. In keeping with some of the core design principles of the EEG-DBS system, this experiment was designed to be simple and robust, whilst minimising the need for lengthy set-up times or maintenance. Therefore this chapter focuses on two key elements: the application of novel technology in a new type of behavioural experiment, and its use in studying the effects of DBS on learning and working memory function, with rodent task performance and LFP used as measurable outcomes. The behavioural study that is outlined in this chapter forms one part of a larger study which further includes the use of an NMDA receptor antagonist (Chapter 5).

## 4.2 Background

This section provides a brief background on spatial-working memory tasks in rodents which utilise the T-maze, including some of the effects of DBS that have previously been observed.

### 4.2.1 T-Maze Task

The working memory task used in this study is the delayed non-match to sample (DNMS) variant of the T-maze task. First used in the 1920s, the T-maze task exploits the natural inclination for rats to spontaneously alter their direction based on previous exploration. In this case rats that had travelled into one T-maze goal arm would be more inclined to travel in the opposite goal arm in the next successive trial (see Dudchenko, 2004, for a more in-depth explanation of this property). In the version of the T-maze task carried out in this study, each trial consists of two successive phases separated by a brief delay. In the first phase the rat is forced to run into one goal arm using a sliding door, in order to obtain a food reward in one of the goal arms. The second phase occurs after a brief delay, in which the rat is placed back into the starting point of the maze, with both goal arms open. The rat must then choose to visit the opposite arm to that in the first phase, in order to obtain the food reward (see Methods; figure 4.2 for further explanation). Successfully obtaining the food reward in the second task phase requires the rat to remember the direction travelled during the first (forced) phase, which requires spatial working memory. These tasks typically involve the animals being mildly food-deprived for a number of days prior to testing, as a means of reinforcing the behaviour required in this task.

Given the requirement of spatial working memory in the T-maze task, it is often used in tasks which study hippocampal function. Lesions to the hippocampus in rodents, for example have been shown to result in rats performing at chance-performance in the T-maze task (Dudchenko et al., 2000). Many of the studies discussed in Chapter 1 with regards to prefrontal-hippocampal function utilise a T-maze task in rodents (see Chapter 1 – 1.4: Working Memory).



To date there have only been a few studies in which DBS was administered to rats during a T-maze task. In a recent example Hamani et al., (2010) carried out DBS in the anterior thalamic nucleus (ATN) in rats to study its effect on spatial working memory. In this particular case they found that rat performance was impaired on the T-maze task following high-current (500 $\mu$ A) ATN stimulation, but not for a lower current of (100 $\mu$ A). Other studies of DBS inside the T-maze have been carried out to observe behaviours that aren't directly related to working memory, such as Andrade et al., (2010) who carried out low-frequency DBS in the thalamic reticular nucleus (TRN) in rats. In this case they found reductions in 8-OH-DPAT-induced preservative behaviours in rats that underwent stimulation. A number of DBS studies to assess working memory in rodents have been carried out in other types of tasks, such as that by Mair and Hembrook, (2008), who carried out rostral intralaminar thalamic nucleus (ITN) stimulation in freely-moving rats as they undertook a delayed match to position (DMTP) task. Refer to the background section of Chapter 1 (1.5.6) for an overview of the use of DBS in various other types of working memory tasks in rodents.

## 4.3 Aims and Rationale

### 4.3.1 Rationale

DBS has presented itself as a powerful treatment option for a variety of neurological disorders where pharmacological intervention has proven ineffective. However there have been relatively few DBS-related studies in freely-moving rodents that directly assess its effect on working memory – one of the core cognitive symptoms known to be disrupted in schizophrenia (Weinberger et al., 1986, Carter et al., 1998, Perlstein et al., 2001). Here, a novel type of study has taken place using the EEG-DBS system that assessed the effects of DBS on rodent learning and spatial working memory. Furthermore by building upon the concepts and techniques introduced in previous chapters, local-field potential (LFP) analysis was also utilised as a means of measuring the functional activity within and between prefrontal-hippocampal brain regions. In rodents the involvement and connectivity of these brain regions is known to be essential in working memory activities (e.g. Floresco et al., 1997, Wang and Cai, 2006, Yoon et al., 2008), and also the functional coordination between the two structures have been observed to increase during working memory tasks (Jones and Wilson, 2005, Benchenane et al., 2010, Sigurdsson et al., 2010). Thus, measurements of LFP from these brain regions can provide a valuable insight into their activity during a spatial working memory task, with and without the presence of DBS.

The fimbria-fornix (FF) has presented itself as an ideal target structure to investigate with regards to learning and memory (See Chapter 1: 1.5.6.4 – Fimbria-Fornix). Forming a vital node between the hippocampus and numerous limbic brain regions believed to be involved in learning and working memory, connectivity of the FF is known to be vital in working memory functions (e.g. Okada and Okaichi, 2006, Warburton et al., 2000b, Okada and Okaichi, 2010). Furthermore degradations to the integrity of these white matter tracts have been observed in schizophrenic patients (Kubicki et al., 2005, Kuroki et al., 2006, Nestor et al., 2007, Takei et al., 2008, Abdul-Rahman et al., 2011), which has been correlated with deficits in declarative-episodic memory (Kuroki et al., 2006), and measures of negative symptoms (Kunimatsu et al., 2012). Finally, in humans, DBS of the fornix has

previously led to significant enhancements in working memory (Hamani et al., 2008, Laxton et al., 2010, Smith et al., 2012), which have also been correlated with hippocampal activation as verified through EEG source localisation (Hamani et al., 2008) and PET analysis (Laxton et al., 2010, Smith et al., 2012). Taken together, this evidence presents a strong rationale for stimulating in the FF, as opposed to the anterior thalamic nucleus (ATN), as was carried out in the proof of concept task in Chapter 3.

### **4.3.2 Aims**

The aims of this study were as follows:

- a) Design a novel behavioural experiment based on rat spatial working memory using the EEG-DBS system, which integrates DBS, LFP recording, and video tracking in a manner which is simple to use and robust.
- b) Study the effect that fimbria-fornix (FF) DBS has on rats both during the training and testing phase of the task.
- d) Characterise any LFP differences between the different phases of the WM task, for each of the groups of rats.

In this experiment, DBS was carried out in the FF, with bilateral LFP recordings made in the medial prefrontal cortex (mPFC), and in the dCA1 region of the hippocampus (dCA1). Many of LFP observations are focussed not only on the power spectral density (PSD) changes that occur in each of the brain regions, but also on the functional cooperation between the various brain regions, as measured using coherence analysis.

The experiment as outlined in this chapter forms part of a larger study which further includes the acute effects of the NMDA receptor antagonist phencyclidine (PCP) in a similar behavioural test paradigm. Thus this chapter explores the “no-drug” condition of this study (saline is used in this experiment as a vehicle control), whereas Chapter 5 explores the “drug” condition.

## **4.4 Materials and Methods**

### **4.4.1 Experimental Outline**

The T-maze working-memory task involved real-time local-field potential (LFP) recording and deep-brain stimulation (DBS), along with video-tracking; which was used to synchronise and identify particular LFP segments relating to distinct task phases, e.g. LFP recordings at the choice-point inside the T-maze. Rats were separated into 2 groups on the basis of whether they had received DBS, or sham-DBS (with the stimulating electrodes implanted). Each rat underwent habituation, training and post-training test sessions inside the T-maze, using a reinforced, delayed non-match to sample (DNMS) spatial alternation paradigm. This section outlines the organisation and structure of the task, as well as the equipment setup and analysis techniques used on the LFP and video-tracking data. Furthermore, because this behavioural task is linked with the “drug” condition of the task as described in Chapter 5, the organisation and methodology of both tasks are described here. All procedures in this study were carried out in accordance with the Animals Scientific Procedures Act (1986).

### **4.4.2 Rat Groups and Experiment Organisation**

The two studies that are described in this chapter and in Chapter 5 differ only in their post-training test phase, in which either saline or drug was administered prior to testing inside the T-maze. Thus during training, all rats are considered to be part of either a stimulation, or a sham-stimulation treatment group (see figure 4.1). Because the experiments in these chapters are linked, the methodology and analysis techniques that are highlighted in this chapter apply also to the experiments carried out in Chapter 5. Furthermore, the training and histology data from the drug-treated rats in Chapter 5 are presented here alongside their vehicle-treated counterparts in this chapter.

Both the “drug” and “no-drug” parts of this study used in total 13 male Lister Hooded rats (Harlan UK Ltd; weighing between 350-375g at time of surgery), which

were divided into a stimulation group (n=7), and a sham-stimulation group (n=6) during training. Rats in the stimulation group received bilateral DBS in the fimbria-fornix (FF) during the intra-trial delay periods of the T-maze task (see 4.4.3: T-Maze Task), whereas rats in the sham-stimulation group received no stimulation, but still had stimulating electrodes implanted.

Post-training, rats were further sub-divided into two additional treatment groups on the basis of whether they had received an acute treatment of 0.9% saline vehicle (i.p), or the NMDA receptor antagonist phencyclidine (PCP; 3mg.kg<sup>-1</sup> i.p). The electrophysiological analysis in this chapter is based on the post-training test phase, i.e. the electrophysiological data arising from the saline-treated stimulation and sham-stimulation groups of rats. The analysis of the PCP-treated groups of rats during the post-training test phase is described in Chapter 5 (see figure 4.1).

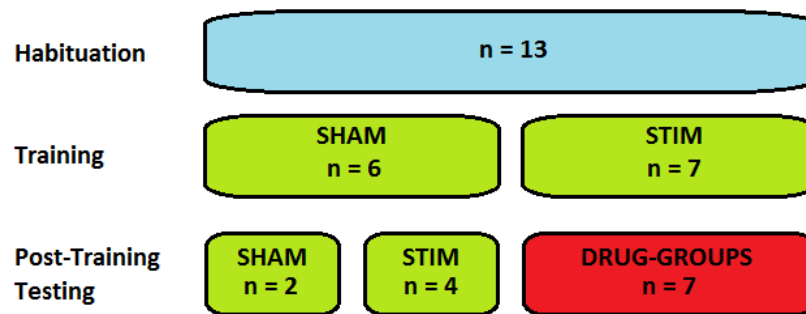


Figure 4.1 – 13 male Lister Hooded rats (Harlan UK Ltd; weighing between 350-375g at time of surgery), were allocated to either the stimulation (STIM) or sham-stimulation (SHAM) groups during the training period of the T-maze task. These rats were further divided into groups based on whether they had received an acute treatment with PCP or saline-vehicle during the post-training test sessions. In this chapter only the rats from the saline-treated vehicle group are discussed with regards to the post-training test phase, whereas the remaining (drug-group) rats are discussed in Chapter 5. Electrophysiological analysis in this chapter is based on the post-training test sessions; however an analysis of the training scores for all rats is carried out in this chapter.

Rats were pseudo-randomly assigned to their treatment groups prior to surgery (and habituation). Surgery was carried out sequentially from rat 1 to rat 16 (table 4.1).

Rat 1	SHAM	PCP	Rat 9	SHAM	VEH
Rat 2	SHAM	VEH	Rat 10	STIM	VEH
Rat 3	SHAM	VEH	Rat 11	STIM	VEH
Rat 4	STIM	PCP	Rat 12	SHAM	PCP
Rat 5	STIM	PCP	Rat 13	STIM	VEH
Rat 6	SHAM	VEH	Rat 14	STIM	PCP
Rat 7	SHAM	PCP	Rat 15	STIM	VEH
Rat 8	STIM	PCP	Rat 16	SHAM	PCP

Table 4.1 – Assignment of rats into the four treatment groups. The sham group (SHAM) had been implanted with stimulating electrodes, but received no stimulation. The stimulation group (STIM) received stimulation during the training and testing sessions (see 4.4.3: T-Maze Task). The PCP group was administered  $3\text{mg}\cdot\text{kg}^{-1}$  i.p. injections prior to their test sessions, whereas the vehicle (VEH) group received 0.9% saline i.p. injections. Each rat group had between 2 and 4 rats from a total initial count of 16. Rats highlighted in red were excluded from the study on the basis of a) incorrect placement of both DBS electrodes (Rat 5), b) failure to achieve a criterion performance during the training sessions (Rat 9), and c) infection following surgery (Rat 2). Note that the experimental design involving acute PCP administration during the post-training test sessions are detailed in Chapter 5, however all of the above rats are considered in this chapter with regards to their training performance, since PCP was introduced only during the post-training test sessions (see figure 4.1).

### 4.4.3 T-Maze Task

The T-maze task consisted of two phases: A sample (forced) phase and a choice phase, separated by delays (figure 4.2). In the sample phase the rats were directed down the central arm of the maze to one of the goal arms in order to obtain a food reward. The food reward in this case consisted of two sucrose pellets (TestDiet). The direction of the forced-run was determined by a removable sliding door positioned at the start of each goal arm. Following an intra-trial delay (refer to table 4.2 for duration), the rat was placed back into the maze with both arms removed, and was required to choose one of two goal arms, with the food reward placed in the opposite arm to that visited in the forced-run. There were 10 forced-/choice-run trials in a single training session, each of which were separated by inter-trial delays (which were always 15 seconds longer than the intra-trial delays; see table 4.2). The direction of forced runs was determined pseudo-randomly, with 5 left and 5 right

turns in each session, and no more than two consecutive trials that begin with the same forced-turn direction. This was the same for each rat, e.g. training session number 3 had the same order of left and right turns for every rat. Each rat underwent a maximum of 1 session per day, with the T-maze and holding pen cleaned and disinfected between each rat session. For rats in the stimulation group, stimulation was administered during the intra-trial delay (between forced- and choice-runs), and lasted for exactly 30 seconds.

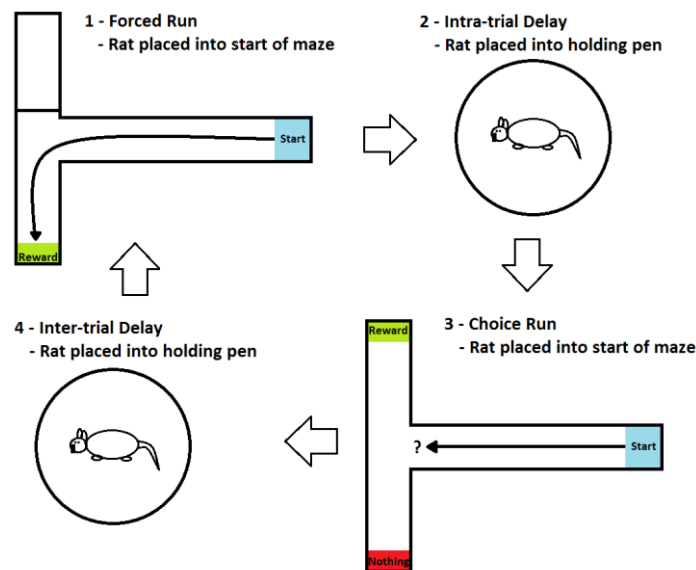


Figure 4.2 – A single trial in the T-maze task consisted of a forced- and choice-run separated by an intra-trial delay. A longer inter-trial delay separated individual trials.

#### 4.4.4 Task Summary

In the following order, all animals underwent: handling, surgery, recovery, habituation, training, and testing (figure 4.3). There were 3 different types of T-maze sessions used in this study, all of which featured simultaneous LFP recording and video-tracking (see 4.4.4.4: T-Maze Sessions).

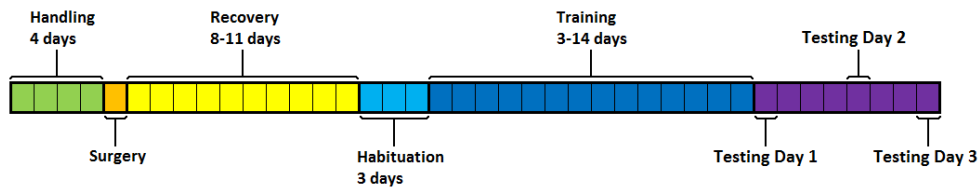


Figure 4.3 – Timeline of experimental phases, with each block representing 1 day. With exception of recovery (which varied between 8 and 11 days) and training (which varied between 3 and 14 days, depending on animal performance), everything was carried out on consecutive days. DBS was administered during the training and test phases.

#### 4.4.4.1 Handling

Handling was carried out over 4 consecutive days prior to surgery, in order to familiarise the rat with the operator, food-reward, and T-maze environment.

- Day 1 – 5 minutes manual handling of rat, 15 minutes in the T-maze – with both goal arms open and baited with 10 pellets each.
- Day 2 – 5 minutes manual handling of rat, 5 minutes alone in the holding pen, 10 minutes in the T-maze – with both goal arms open and baited with 10 pellets each.
- Day 3 – 5 minutes manual handling of rat, 5 minutes alone in the holding pen, 5 minutes in the T-maze – with both arms open and baited with 10 pellets each.
- Day 4 – 5 minutes manual handling of rat, 2 minutes in the holding pen, 5 minutes in the T-maze – with both arms open and baited with 5 pellets each.

#### 4.4.4.2 Surgery

Surgery took place for each animal on the next consecutive day following the last handling day. Animals were implanted with a headstage connector (see Chapter 2 – figure 2.25, and also Chapter 3 – figure 3.3), along with bilateral LFP electrodes targeting the mPFC, dCA1, and DBS electrodes targeting the ATN. However in this study the majority of DBS electrodes were actually positioned in the fimbria-fornix



(FF; see 4.4.6: Brain Imaging and Electrode Coordinates). For an overview of the procedure, refer to Chapter 3 – 3.3.3: Surgery.

#### 4.4.4.3 Recovery

Following surgery animals were given between 8 and 11 days to recover. Animals were placed on a restricted diet 5 days before their first habituation session, whereby 15-20g of food was given to them daily to keep their weight at or above 90% of that predicted by standard growth curves. All animals remained on a restricted diet throughout the experimental period. In the final recovery day, animals were placed into the T-maze for 5 minutes with the wireless system attached and actively recording/transmitting LFP. In this case the maze doors were removed and 5 reward pellets were placed at the ends of each of the two goal arms.

#### 4.4.4.4 T-Maze Sessions

The three types of T-maze session were given in order of habituation, training and testing. The intra- and inter-trial delay periods are both 15 seconds longer during the training and post-training test sessions (table 4.2).

	Habituation	Training	Testing
No. trials per session	10	10	10
Trial pair:	forced/forced	forced/choice	forced/choice
Intra-trial delay	15sec	30sec	30sec
Inter-trial delay	30sec	45sec	45sec
Treatment with STIM?	No	Yes	Yes

Table 4.2 -The differences in protocol between the habituation, training and testing T-maze sessions are shown. Note that during the habituation sessions there was no choice-phase, i.e. working memory was not tested during the habituation sessions. Stimulation (STIM) of the targeted area was performed during the training and testing sessions for animals in the stimulation group, during the intra-trial delay periods.

#### **4.4.4.4.1 Habituation**

Habituation to the system, T-maze and task alternation pattern was carried out over 3 consecutive days following recovery (and initial system habituation). For each habituation day, animals were placed into the T-maze to undergo 10 forced-/forced-alternation trials, meaning that a second forced-run was put in place of the choice-run, in the opposite direction. The delay period was shorter during habituation than during training and testing, with 15-seconds for the intra-trial interval and 30-seconds for the inter-trial interval. No treatment with stimulation (STIM) was given during the habituation sessions, although constant LFP recordings took place for each rat in the same way as that of the training and testing sessions.

#### **4.4.4.4.2 Acquisition of Task +/- DBS**

Training sessions began on the first consecutive day following the final habituation session. In these sessions rats were given 10 forced-/choice-trials, with an intra-/inter-trial delay of 30/45 seconds, respectively. During these sessions, stimulation was carried out during the 30-second intra-trial delay for each rat in the stimulation group. The stimulation parameters were chosen to be 130Hz, 90 $\mu$ s, 30 $\mu$ A pulses. Thus each rat in the stimulation group had obtained 10x 30-second stimulation treatments during a single training session. For each rat the criteria for passing training was to obtain a score of 70% or greater (> 7/10 correct choices) over 3 consecutive sessions. With a maximum number of 14 sessions, rats thus had between 3 and 14 days of training. Rats that successfully completed their training were advanced to the first test day, which began on the next consecutive day.

#### **4.4.4.4.3 Testing**

Post-training test sessions followed a similar protocol as that used for the training sessions, except a) the inclusion of a 20-minute baseline recording which was made prior to the first trial, and b) an injection of 0.9% saline for each rat 5 minutes prior to entering the T-maze (after 15 minutes of baseline recording). Saline injections were given to act as a control for the Chapter 5 rat groups that were treated with

acute PCP. Given that the rats were split into vehicle and drug groups, there are a reduced number of rats that participated in the test sessions ( $n=6$  for stimulation and sham-stimulation groups). Each of the three test days began with a 20-minute baseline recording, and the animals were placed into the holding pen with the EEG-DBS system attached (see figure 4.11 for a clarification of the test session timeline). During this entire period a constant LFP recording was made, and no stimulation was administered in any of the rats. The test session then proceeded with the 10 forced-/choice-trial pairs, again with an intra-/inter-trial delay of 30/45 seconds, respectively. In the final (third) test day, animals were omitted treatment saline, but a constant 20-minute LFP recording still took place.

#### **4.4.5 Perfusion, Craniotomy and Tissue Staining**

After the final day of testing, animals were given a lethal injection of  $1\text{ml.kg}^{-1}$  Euthatal (Fisher Scientific), which contained  $200\text{mg.ml}^{-1}$  of the active ingredient pentobarbital sodium. Following abolition of the hind-paw, tail and ocular reflexes, animals were secured in a fume hood, where a small incision was made along the midline of the upper abdomen. The diaphragm was removed, and the ribcage was cut down either side and pulled up, exposing the heart. A small butterfly needle was inserted into the right aortic arch, through which NaCl was pumped. The right atrium was then cut with a pair of fine scissors, allowing blood to pass out of the body. A few minutes later the line was switched to pump a 4% formaldehyde solution, which continued until the animal was rigid. Following perfusion the animal was decapitated, and the brain removed. In doing this, the headstage implant and electrodes were gently pulled upwards (after cutting round it with a pair of fine pliers), to avoid the electrodes damaging the brain upon removal. Brains were stored in a sucrose solution at  $4^{\circ}\text{C}$ , which was prepared by mixing 20g of granulated sugar with 100ml of distilled water.

When the brains were ready to be cut, they were taken out of the sucrose solution and placed onto dry ice after wrapping them in tin-foil. Once hardened a fine-tip permanent marker was used to identify the electrode locations on the dorsal side of

the brain by gently pressing it where the electrode holes were visible. This made it easier and quicker to find the electrode locations when sectioning the brain in the cryostat. Frozen brains were then coated in an embedding matrix (Shandon M-1 embedding matrix; Thermo Electron Corporation), fixed into place on a small pedestal, and mounted into a cryostat (Leica Microsystems UK Ltd). For each electrode location, three copies of sections were taken, with each section ranging from 20-30 $\mu$ m, depending on the quality of brain slices. Brain slices were then thaw-mounted onto poly-L-lysine (Sigma-Aldrich) coated microscope slides (VWR International), and stored at -80<sup>0</sup>C.

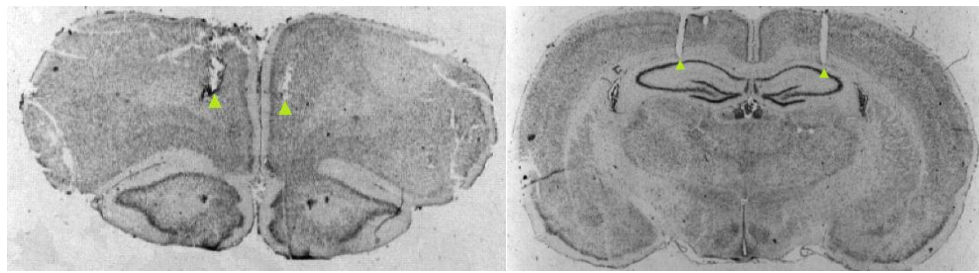
A cresyl-violet stain was prepared by dissolving 0.5g cresyl violet acetate (Sigma-Aldrich) into 25ml glacial acetic acid (Sigma-Aldrich) and 475ml distilled water, using an ultrasonic bath. Prior to staining, brains were taken out of the -80<sup>0</sup>C freezer and warmed to room temperature by placing them on top of paper towels. Slides were placed into glass racks, and fixed in a formalin gas jar for 30 minutes, to remove insoluble proteins and to ensure fixation of the sections to the slides. In the following order, slides were placed into: a xylene solution (Sigma-Aldrich) for 3 minutes, 100% ethanol (Sigma-Aldrich) for 3 minutes, 50% ethanol (in distilled water) for 3 minutes, then running tap water for 5 minutes. Following this, slides were placed into the cresyl-violet stain as prepared for 3 minutes, and then in the following order were placed into: running tap water for 5 minutes, 50% alcohol for 3 minutes, 100% alcohol for 3 minutes, and back into xylene for 3 minutes. Once dried, glass cover slips (Chance Proper Ltd) were affixed to the slides using a mounting medium (DPX; Sigma-Aldrich), and left to dry.

#### **4.4.6 Brain Imaging and Electrode Coordinates**

In order to determine the electrode locations, slides containing the cresyl-violet stained brain slices were placed onto a precision illuminator (Model R95; Imaging Research), which was placed directly below a microscope camera (micro nikkor 55mm; Nikon). The microscope-camera interfaced directly with imaging software

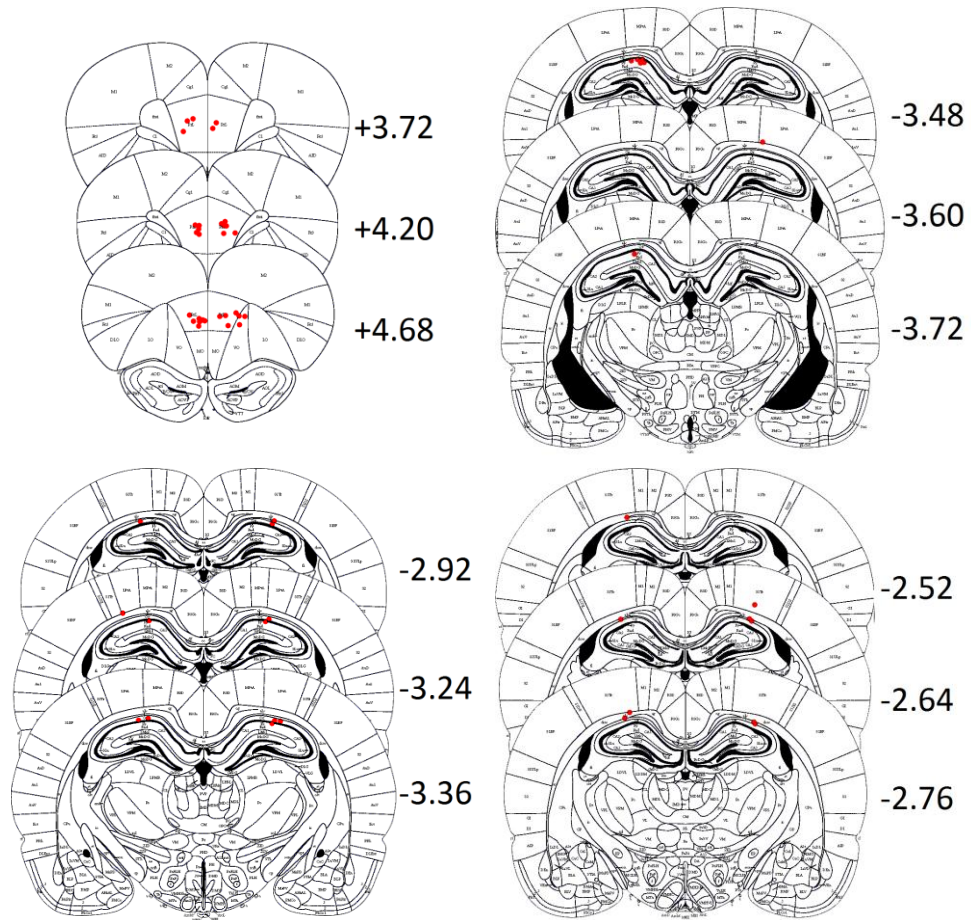
(MCID Elite 7.0; InterFocus Imaging Ltd), where pictures were saved on to the hard disk for later viewing.

Most of the implanted LFP electrodes reached their target coordinates in the mPFC and dCA1 region of the hippocampus, with every brain having at least 1 electrode correctly placed in the mPFC and dCA1 region of hippocampus (figure 4.4). The majority of dCA1 electrodes and all of the mPFC electrodes were placed at more anterior sites than their target coordinates specified. Recordings for the LFP electrodes that missed their target locations were excluded from the study (3 mPFC, 4 dCA1).



A

B



C

Figure 4.4 – Representative cresyl-violet stained brain slices are shown for the mPFC (A) and dCA1 (B), with green triangles showing the electrode positioning in each. Both photographs have been adjusted for contrast. Their corresponding locations are represented on brain maps (C) which were adapted from Paxinos and Watson, (2007). In this case the coordinates of each coronal section in mm is shown relative to bregma.

Similar to LFP electrode placement, DBS electrodes were positioned at slightly more anterior sites than that specified by their target coordinates, leading to most of the electrodes being positioned inside the fimbria-fornix (FF; figure 4.5).

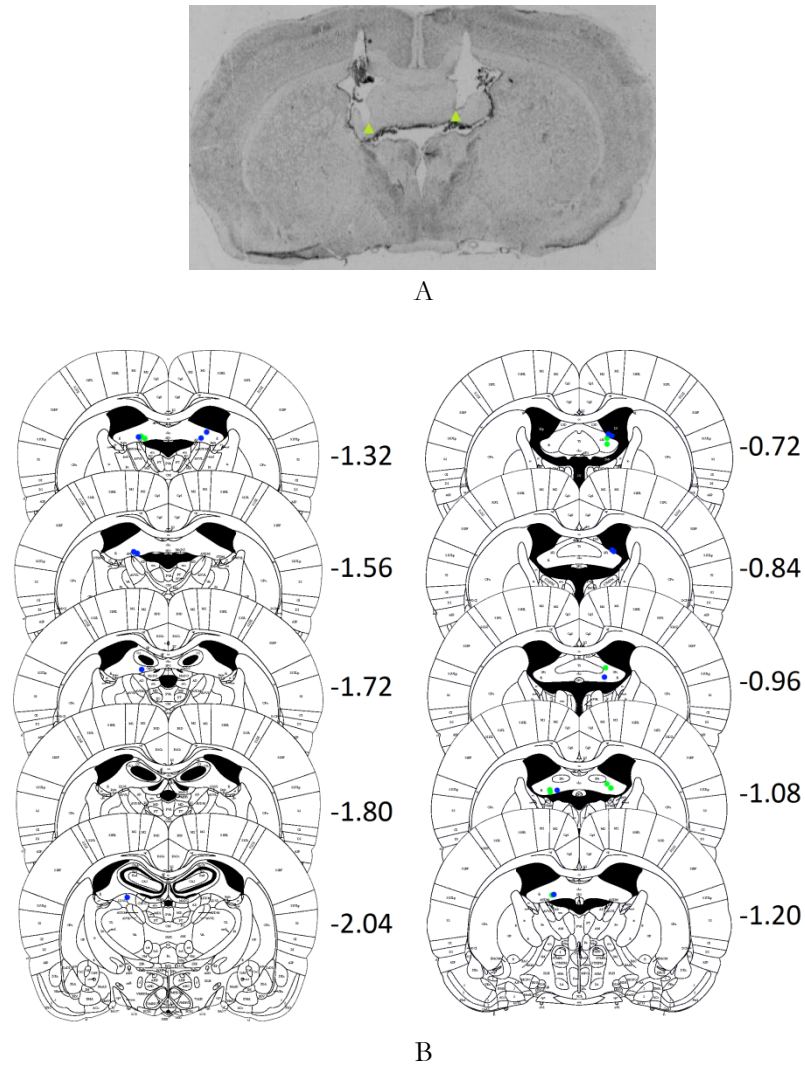


Figure 4.5 – Representative cresyl-violet stained brain slice shows bilateral DBS electrodes positioned in the FF (A), with green triangles showing the electrode tips. Photograph has been adjusted for contrast. The corresponding electrode locations are represented on brain maps (B) which were adapted from Paxinos and Watson, (2007). In this case the coordinates of each coronal section in mm is shown relative to bregma. Blue dots represent electrode positioning in rats belonging to the STIM groups, whilst green dots represent electrode positioning in rats belonging to the SHAM groups.

In this experiment, rats were included on the basis of having at least one FF electrode correctly placed (table 4.3). This resulted in one rat being excluded for not having DBS electrodes bilaterally placed in the FF (Rat 5; table 4.3). Given that there are more DBS electrodes correctly placed in the left-FF rather than the right, the subsequent results should be viewed with caution given the left-hemisphere bias on FF stimulation. Most of the electrodes that missed the FF were placed in the nearby ventricles, the ATN, or other locations which couldn't be resolved, due to missing brain slices.

	L-mPFC	R-mPFC	L-dCA1	R-dCA1	L-FF	R-FF
<b>Rat-1</b>	Y	Y	Y	Y	Y	N
<b>Rat 3</b>	Y	Y	Y	Y	Y	Y
<b>Rat 4</b>	Y	Y	Y	N	Y	Y
<b>Rat 5</b>	Y	Y	N	N	N	N
<b>Rat 6</b>	Y	Y	Y	Y	Y	Y
<b>Rat 7</b>	Y	Y	Y	Y	Y	Y
<b>Rat 8</b>	Y	Y	Y	Y	Y	Y
<b>Rat 10</b>	Y	N	Y	Y	Y	N
<b>Rat 11</b>	Y	Y	Y	Y	N	Y
<b>Rat 12</b>	Y	N	Y	N	N	Y
<b>Rat 13</b>	Y	Y	Y	Y	Y	N
<b>Rat 14</b>	Y	Y	Y	Y	Y	N
<b>Rat 15</b>	Y	N	Y	Y	Y	N
<b>Rat 16</b>	Y	Y	Y	Y	Y	Y

Table 4.3 – Electrode locations for each rat involved in the study. Most of the electrodes in the left hemisphere (LFP and DBS) reached their targets. Electrodes in the right hemisphere didn't always reach their target – particularly so with the right FF electrodes which had a tendency to be placed in the right lateral ventricle which is adjacent to the FF. This table doesn't include 2 rats which were taken out of the study due to infection (Rat-2) and for not passing training (Rat-9). Rat 5 was also excluded from the study for not having any DBS electrodes in the FF. The 6 rats highlighted in green on the left-side of the table are the saline-treated rats which are considered in the post-training test-phase as outlined in this chapter.

## 4.4.7 Equipment Setup

### 4.4.7.1 Placement of Equipment

The main equipment used in this experiment consisted of: a T-maze, holding pen, ceiling-mounted camera, laptop, EEG recorder/stimulator, and a receiver for the wireless system (figure 4.6). The T-maze was constructed of PVC with a central arm



length of approximately 160cm, a side arm length of 60cm each, a height of 30cm and a corridor width of 10cm. The central arm length was set to provide around 2 seconds of EEG recording, should the rat be running at full speed from one end to the other (estimate based on unreported pilot studies using similar equipment). The positioning of all other equipment around the T-maze was considered such that the experiment may be carried out in an easy and efficient manner. The holding pen – a 25cm diameter, 38cm tall transparent Perspex cylindrical container – was placed in close proximity to the T-maze near the goal arms. This allowed for rapid placement and recovery of the rat to and from the T-maze start and goal arms, respectively. The laptop was required during the experiments to provide information on the task timing as well as to control the stimulation/delay counters. As such it was placed in close proximity to the holding pen to allow for rapid control after the animal had been returned following a maze run. The location of the receiver was chosen based on the optimum transmission distance from the wireless system, and as such was placed near the centre of the T-maze opposite the side with the holding pen. The receiver was also placed to allow for a clear, unbroken line of sight between itself and the overhead video camera, since the receiver's built in LED was used for LFP-video synchronisation purposes. Given the height of the ceiling in the room used for the experiment, the video camera was tilted to provide coverage of the entire central arm, as well as the receiver. Finally a table opposite the goal-arms provided the food rewards and scoring sheets, which were accessed and updated during the course of the experiment. The space in-between the table and the goal arms allowed access to the rat, food-reward bowls and sliding doors without interrupting the line of sight between the overhead camera, and the central arm and receiver.

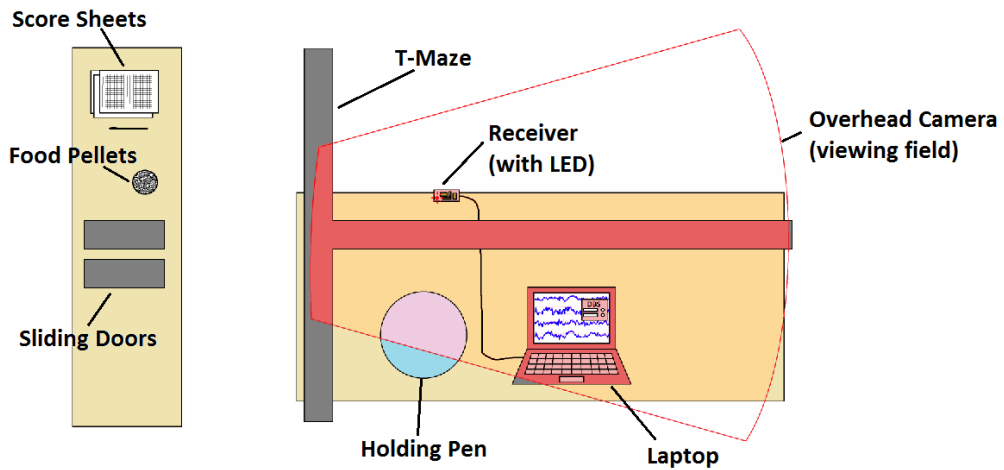


Figure 4.6 –Illustration of equipment layout for the T-maze test sessions. The camera’s field of view was set to cover the receiver, and the central-arm of the T-maze.

#### 4.4.7.2 Equipment Configuration

In this experiment the wireless EEG recorder/stimulator and its receiver were configured to facilitate synchronisation between the rat’s recorded LFP and the rat’s position data obtained through video-tracking. Whilst both were recorded independently on two different computers, both recordings featured a discrete common event that appeared on both recordings, correlated in time. In this case the video-tracking software registered a light pulse generated from the receiver, and the LFP recording registered a sync-pulse overlaid on top of the raw brain activity, and these two events co-occurred at the same-time during the experiment (figure 4.7B). Alignment of the two data-sets based on these events was carried out in the data analysis phase following testing (see 4.4.8.1: Data Organisation). In addition to synchronisation of video and LFP, the equipment was configured to provide one-button stimulation/delay commands, and to display timing information which helped to increase the accuracy of the delay periods.

#### 4.4.7.3 Video Tracking

Rat position in the central arm of the maze was tracked using an overhead video camera (Sanyo) which interfaced with commercial video-tracking software

Ethovision XT (Nodulus Information Technology), on a computer situated in the room opposite. In the video camera's field of view, there were three separate tracking points in the central arm of the T-maze, located at the beginning, middle and end (choice) sections (figure 4.7A). Whenever the rat crossed these points during the course of the experiment, the time information of this event was logged. An additional tracking point was configured to encompass the receiver, which generated the light pulses (which coincided in time with the LFP pulses).

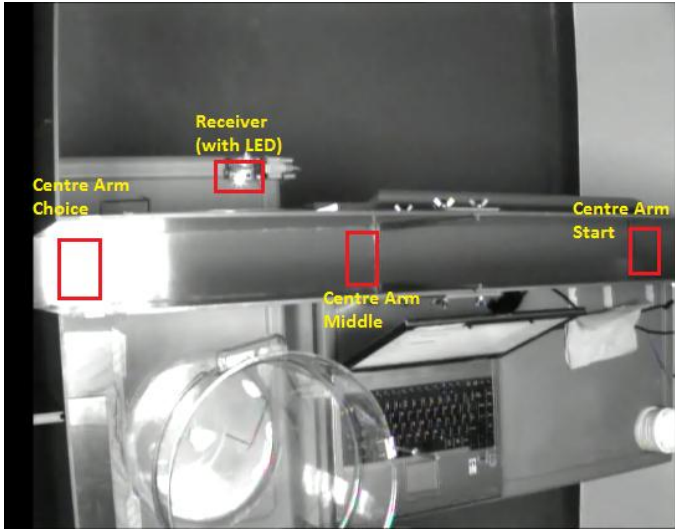
#### **4.4.7.4 LFP Recording and System Programming**

For this experiment the EEG-DBS system and its receiver were reprogrammed to satisfy the following goals:

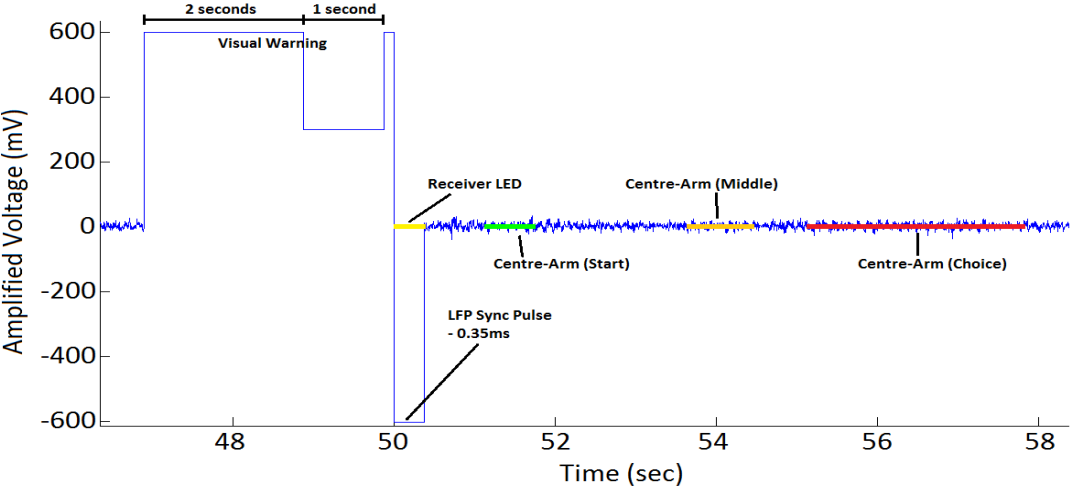
- To provide a stimulation/delay-period for a set amount of time,
- To provide a 3-second visual warning towards the end of a delay period,
- To allow for synchronisation between the LFP data and video-tracking data.

The wireless systems were pre-programmed with fixed stimulation parameters characterising a 130Hz, 90 $\mu$ S pulse train. For simplicity, control of the system was restricted to the 'DBS ON' and 'DBS OFF' commands via the WinEDR DBS control module (J. Dempster, University of Strathclyde). A flowchart in figure 4.7C illustrates the actions carried out by these commands, and where they fit in the overall sequence of events for each behavioural session. Whenever the rat was placed into the holding pen after reaching one of the goal arms, either 'DBS ON' or 'DBS OFF' was pressed in WinEDR depending on whether the rat had finished a forced- or choice-run, respectively. This action initialised a delay timer on the wireless system relating to either the intra-trial period (if DBS ON was pressed) or inter-trial period (if DBS OFF was pressed). In addition, pressing 'DBS ON' during the training and testing sessions activated DBS for animals in the stimulation group, otherwise it acted only as a delay timer. Thus in the stimulation group DBS was activated during each of the intra-trial delay periods. Three seconds prior to the end of the delay, the real-time LFP recording was replaced with a 3-second visual warning waveform, indicating to the operator that the rat had to be picked up and

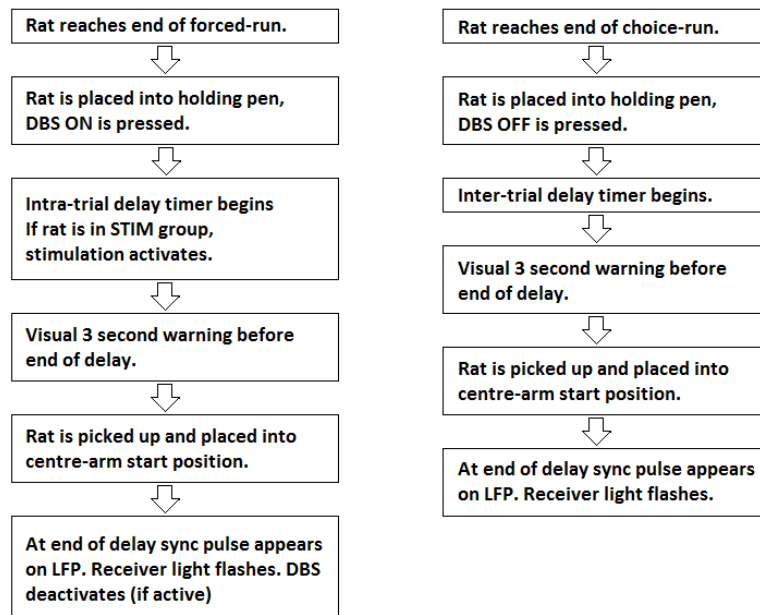
placed into the T-maze (figure 4.7B). Following this three second waveform, a 0.35 second 'SYNC' pulse signal (a -600mV, 0.35-second deflection in the LFP) was transmitted in the recorded LFP signal. The receiver was programmed to flash its LED upon receiving this synchronisation pulse waveform, which was subsequently logged in time with the video-tracking system. Thus the LFP and video-tracking data were synchronised at the beginning of each maze run, which produced 20 synchronisations per session. If DBS was active (in the stimulation rats), it deactivated immediately following the 3-second warning and prior to the SYNC pulse signal, thus ensuring that each rat had exactly 30-seconds of stimulation during the intra-trial delay periods.



A



B



C

Figure 4.7 – A video still taken from the overhead camera depicts the central arm of the maze (A), with its three tracking points situated at the start, middle and end (choice) parts. A separate tracking point encompassed the receiver, allowing its LED flashes to be tracked. The raw LFP trace shown in (B) depicts the 3-second visual warning waveform, followed by the synchronisation pulse, and the subsequent LFP recording for the animal which has just been placed into the central arm of the maze. The yellow bar represents the video-tracked LED flash, which was synchronised with the LFP SYNC pulse. The subsequent three coloured bars are the tracking data for the start, middle and end (choice) points of the T-maze central arm. Two flowcharts in (C) outline the sequence of events that occurred once the user presses either ‘DBS OFF’ or ‘DBS ON’, and how they fit in the T-maze task as a whole.

#### 4.4.8 Analysis of Results

Experimental data came from three sources: Ethovision XT video-tracking data which was exported as Excel files, WinEDR raw LFP data which was exported as tabular text files, and the rat progress/scores which were noted down by hand during each training/test session. All of this information was combined and processed in Matlab (Mathworks), where data organisation, analysis and statistics took place.

#### 4.4.8.1 Data Organisation

The first level of processing involved the data being integrated together into Matlab, and subsequently organised for further analysis. For this to happen a system was created using Matlab scripts for organising and storing information derived from three different input sources. Video-tracking data and LFP were synchronised based on the co-occurrence of the LFP and LED pulses in the LFP and video-tracking export files respectively (figure 4.7B), allowing the relevant LFP segments to be extracted based on the animal's position. For each session, LFP segments were extracted corresponding to the T-maze choice points, as well as the inter-/intra-trial delay periods when the animal is in the holding pen (figure 4.8). In this case the LFP segments extracted from the T-maze choice-point were 1-second in length, and LFP segments extracted from the holding pen during the delay periods were 20-seconds in length (5-seconds for habituation data, due to the shorter delay periods used). The T-maze choice-segments corresponded to the last time the rat passed the choice-point in a single maze run, and subsequently entered one of the goal arms (during habituation and early training the rat sometimes crossed the choice-point twice, after backtracking down the central arm). The holding-pen LFP segments were extracted 5-seconds after the start of each delay period, in order to minimise tooth-grinding artefacts from the animal chewing the reward pellets which they had recently obtained. All of this data was subsequently organised into forced and choice pen/maze segments (forced-1 and forced-2 segments for habituation). During training and testing, the choice segments were further organised into correct and incorrect responses. Whilst algorithms were written to automatically process all of the data in this way, the alignment of all data was manually checked in Matlab using automatically-generated LFP plots which overlaid the video-tracking data with LFP information (figure 4.7B). Finally, the 20-minute baseline recordings (including pre- and post-injection periods) were extracted and organised as appropriate.

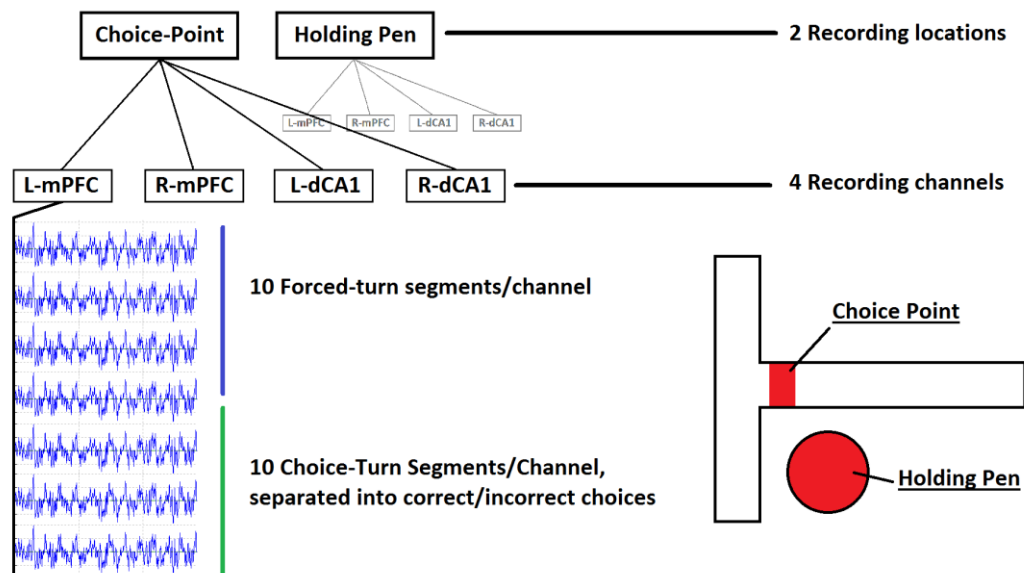


Figure 4.8 – LFP data was organised based on different recording locations, channels and task phases. In this case LFP data from the mPFC and dCA1 brain regions were taken from the inter-/intra-trial delay periods when the rat was inside the holding pen, and the T-maze, when the rat was at the choice point of the maze.

#### 4.4.8.2 Artefact Removal

Artefacts are unwanted disturbances that affect the quality of recorded data, and in this case affected the video-tracking and LFP data. Video-tracking artefacts occurred when any of the tracking points registered movement that wasn't originally intended, e.g. the experimenter accidentally putting their arm between a tracking point on the central-arm and the video camera, which would be tracked as animal movement. These artefacts were not common due to the experimental design which controlled the movement of the experimenter; and most that did occur were negated by the algorithms that were put in place when combining video-tracking and LFP data. These algorithms ensured that tracked data was only registered under certain conditions (e.g. the T-maze choice-point tracking data was only valid once preceded only by tracking data in the middle of the central arm). Further visual validation of the tracking data was achieved by visually inspecting the video-information overlaid on-top of the LFP data (figure 4.7B), and every session presented in this study was checked this way.



Artefacts in the LFP raw data were more of a concern, since they were more varied and occurred more often. These artefacts were regarded as anything on the LFP trace (besides the warning and sync-pulse) that weren't generated in the animal's brain. Animal-movement artefacts commonly included chewing or tooth-grinding, which resulted in a peculiar looking waveform mostly visible in the frontal (mPFC) electrodes (figure 4.9C), featuring high-frequency bursts of activity (see also Chapter 3 – 3.4.2: Power Spectral Density in the mPFC and dCA1 Brain Regions). Unlike the proof-of-concept task, this type of artefact was mostly present in the LFP recordings when the rat had obtained a food reward. These artefacts were almost completely negated from the subsequent analysis by careful selection of the LFP segments corresponding to the inter-/intra-trial delay periods (see 4.4.8.1: Data Organisation). The headstage connection was designed to withstand quick animal movements, and indeed the rat running at full speed through the T-maze would in nearly all instances result in artefact-free LFP signals. Sometimes however the rat would knock the system on the side of the T-maze or holding pen, resulting in an abrupt and characteristic deflection in the recorded LFP (figure 4.9B). Other LFP-related artefacts that were present took the form of voltage spikes, and 50Hz mains noise. Spikes appeared on the LFP whenever the battery was at very low levels (after several hours of use – approaching the limit of the system's battery life). This reflected a failure of adequate power supply stability in the sensitive amplification circuitry, when the battery voltage had reached a critical low point of around 2V or lower (see also Chapter 2 –2.4.17.1: EEG-DBS Battery-Life Measurements). 50Hz mains noise – which can be seen as a magnitude peak in the frequency spectrum of the recorded signal at 50Hz – was only apparent on the LFP sections of the central arm at the start-point of the T-maze. This was because this part of the central arm was in close proximity (<30cm) to a mains power outlet. 50Hz mains noise however was negligible when measured at the choice-point or the holding pen. As highlighted in the proof-of-concept task, by far the most disruptive LFP artefact was caused by activation of DBS pulses (figure 4.9D; see also Chapter 3 – 3.4.1: Raw LFP Recordings). Whilst it can be argued that good-quality mathematical algorithms can reduce this effect, comparisons between non-stimulation-contaminated data would not be easy, because it would involve a clean (non-stimulation) signal being

compared with an ‘approximate’ reconstruction, derived from a signal previously contaminated with stimulus pulses. More crucially, the stimulus artefacts in this system sometimes resulted in a saturation of the input amplification circuitry, which effectively destroyed the data. As a result all LFP data from the intra-trial intervals in stimulated animals was discarded in the subsequent analysis. With all the LFP artefacts taken together, the holding pen data was the least affected since the effects of artefacts was averaged out over 20 seconds per trial (5 seconds during habituation sessions), rather than 1 second per trial as in the central arm. The second level of processing therefore focussed on removal these LFP artefacts. Spikes were filtered away using a custom-written spike removal algorithm. Custom-written artefact-removal algorithms were written which allowed for a fast and efficient means of discarding LFP segments that contained a significant presence of artefacts.

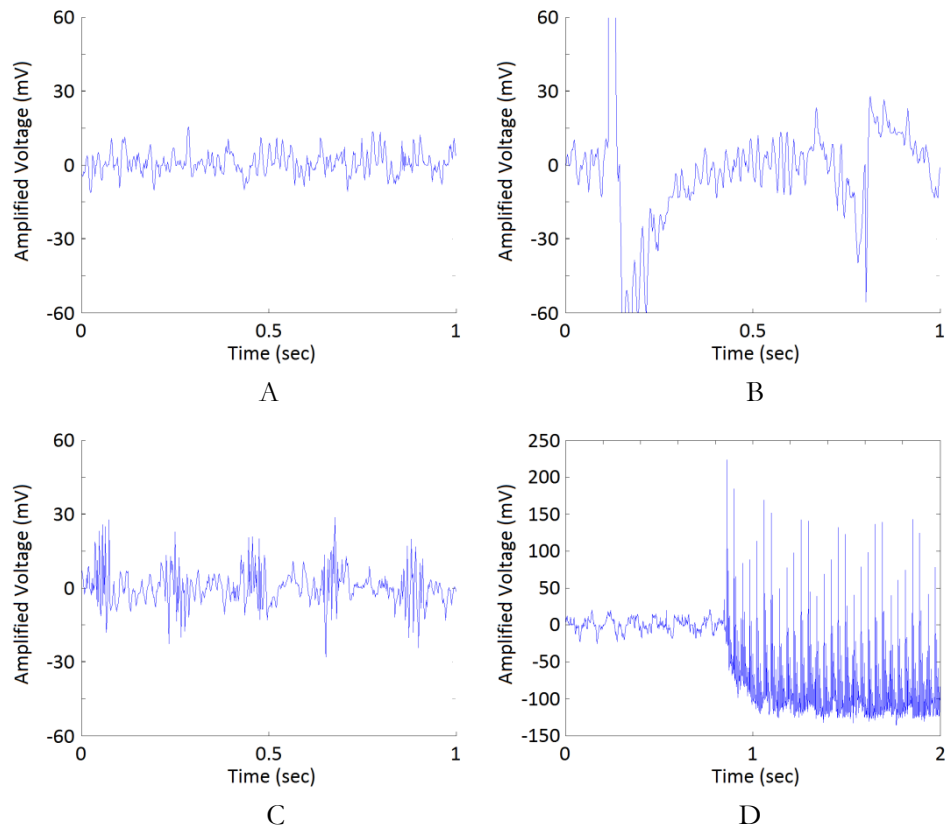


Figure 4.9 – Examples of LFP recording artefacts in the mPFC. A normal typical mPFC waveform is shown in (A). Sometimes artefacts arise from the rat hitting the system against a wall (B), resulting in an abrupt deflection in the EEG. Chewing artefacts always appeared most prominently on the mPFC electrodes (C) once the rat had obtained a food reward. Activating DBS resulted in a distinctive and prominent stimulus artefact (D) that remained as long as DBS was active. Note the altered time/voltage axis in plot D as compared to the rest of the plots.

#### 4.4.8.3 Power Spectral Density and Coherence

Power spectral density (PSD) is a traditional measure used in EEG analysis and measures the power in individual frequency bands, expressed as watts per hertz ( $\text{W}\cdot\text{Hz}^{-1}$ ). PSD calculations are based on custom-written Matlab scripts (Mathworks) using functions from software libraries provided by Chronux (<http://www.chronux.org>). Every PSD calculation carried out involved the use of 3 orthogonal leading data tapers (see Thomson, 1982), which were multiplied with the spectral power estimate to increase accuracy and to reduce ‘windowing’ artefacts. PSD calculations were used to highlight changes between the different rat groups, recording locations and task phases. All PSD estimates in this study were derived

from LFP recordings made in the mPFC and dCA1 brain regions. Bilateral channels were averaged together to produce a single mPFC and dCA1 PSD estimate for each rat.

Coherence is a measure of similarity between two different waveforms (figure 4.10), and is expressed as a ratio between 0 (waveforms are completely independent), to 1 (waveforms are the same). All coherence estimates in this study are based on the ipsilateral mPFC-dCA1 brain regions. Since up to 2 mPFC-dCA1 coherence estimates are derived from each rat (one for each hemisphere), these were averaged together to give a single mPFC-dCA1 coherence estimate.

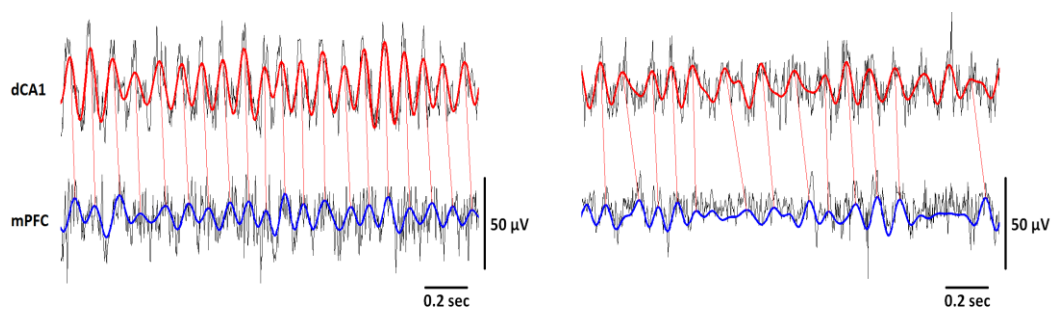


Figure 4.10 – Example of high and low theta coherence between ipsilateral mPFC and dCA1 brain regions. Raw signals for dCA1 (red/top waveforms) and mPFC (blue/bottom waveforms) are shown with its filtered theta frequency (4-12Hz) superimposed on top (thick lines). When the brain regions are synchronised the theta-peaks from dCA1 are seen to lead those in the mPFC, and both occur with a similar frequency (left). During periods of lower coherence, the theta-activity in these brain regions is more independent and less coupled to each other (right).

#### 4.4.8.4 Spectrograms/Coherograms

Spectrograms based on the PSD were derived for the mPFC and dCA1 recording locations in each rat, and were used to highlight PSD changes for each of the separate recording phases obtained from a T-maze session. PSD spectrogram estimates for each channel were calculated using a multi-taper PSD function featuring 3 leading data tapers, a 4-second sliding window with 1-second overlap, and was subsequently normalised by dividing by its baseline RMS value, which was obtained from the first 15-minutes of (pre-injection) recording. Data from each of

the rats in each of the 4 groups was then averaged together for subsequent display. Coherograms were derived in a similar manner, using a multi-taper coherence function with 3 orthogonal leading data tapers, and a 4-second sliding window with 1-second overlap.

In order to highlight changes in PSD and coherence with different task phases, spectrograms and coherograms were separated into the following phases: baseline pre-injection, baseline post-injection, inter-trial delays, intra-trial delays, and T-maze segments (as measured at the choice-point), respectively (figure 4.11). All other LFP segments, including that which contains the sync pulses are not shown. Given the short length of the individual T-maze choice-point segments (1-second each), these spectrogram/coherograms segments are stretched at 5x for display purposes. Note that in this study 0.9% saline i.p. injections were used to act as a control for the PCP-injections as discussed in the second part of the study (see Chapter 5).

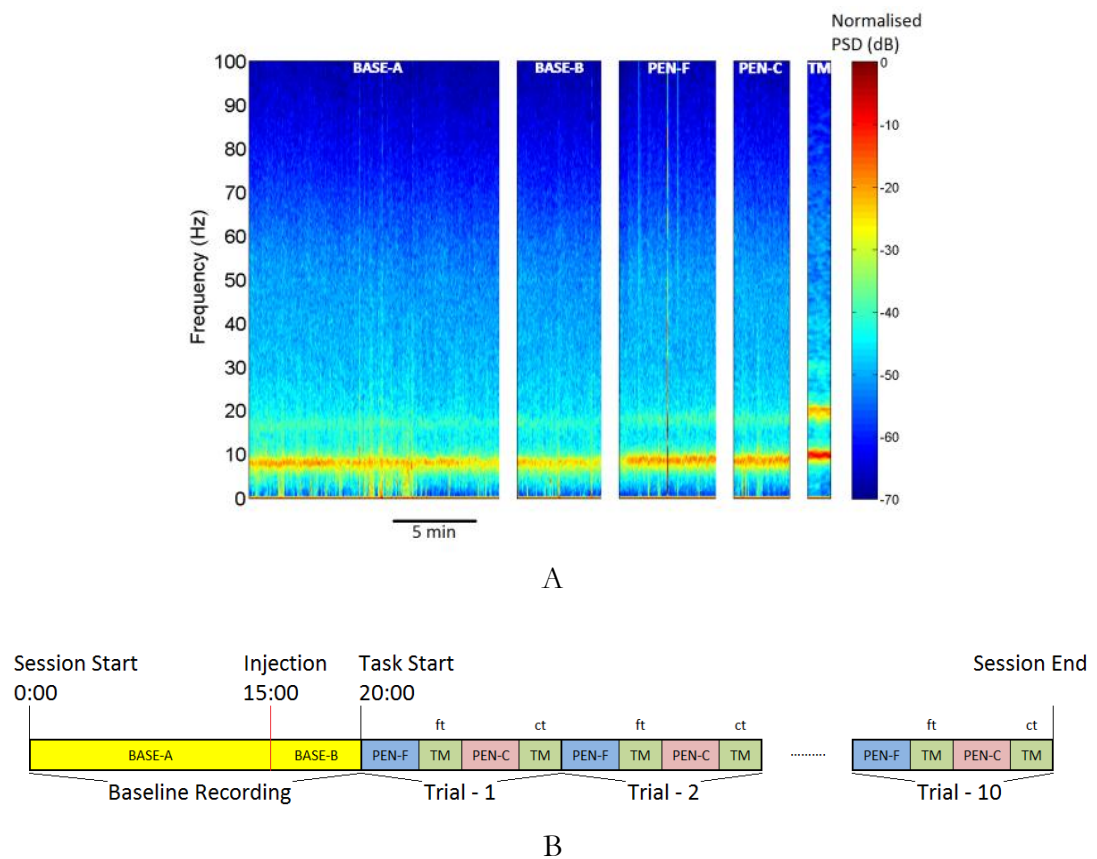


Figure 4.11 – The PSD spectrogram estimate for an entire rat session (A), containing the pre-injection (BASE-A), post-injection (BASE-B), inter-trial (PEN-F) and intra-trial (PEN-C) delays, and the T-maze choice-point segments during forced- and choice-runs (TM). Note that the T-maze spectrogram estimate (TM) has been stretched by 5x to allow for a convenient visual comparison. The sequence of events for each task is shown in (B), with the baseline recordings (BASE-A, BASE-B) immediately preceding each of the 10 trials. Each trial consists of an inter-/intra-trial delay (PEN-F/PEN-C, respectively), with T-maze sessions (TM) in-between these delays. Note that forced-turn and choice-turn segments are marked as ‘ft’, and ‘ct’, respectively.

#### 4.4.8.5 Task-Phase PSD and Coherence Changes

This type of analysis was carried out to observe differences in PSD and coherence between each of the rat groups, based on the holding-pen and T-maze recordings. For each rat session, a single mPFC and dCA1 PSD spectrum was derived from each of the task phases: baseline pre-injection (BASE-A), baseline post-injection (BASE-B), inter-trial delays (PEN-F), intra-trial delays (PEN-C; sham rats only), and the T-maze forced and choice segments (TM). In addition, mPFC-dCA1 and mPFC-mPFC coherence spectrograms were also derived for these same task phases for each rat. Data from the first two test days was averaged to produce one reading per

rat, which was subsequently combined with the rest of the rat group. All power and coherence changes were subsequently measured relative to the 15-minute pre-injection baseline period, in a manner similar to that shown by Sebban et al., (2002), by dividing the power/coherence spectra from each rat phase by its corresponding pre-injection baseline (BASE-A) power/coherence spectra:

$$[\textit{variation in mean PSD} (\%)] = \left( \frac{PSD_c}{PSD_b} \right) \times 100$$

where  $PSD_c$  = PSD observation during 5-minute post-injection, delay or maze,

$PSD_b$  = PSD estimate during 15-minute pre-injection baseline

Coherence changes are expressed in the same way:

$$[\textit{variation in mean coherence} (\%)] = \left( \frac{COH_c}{COH_b} \right) \times 100$$

where  $COH_c$  = Coherence estimate during 5-minute post-injection, delay or maze,

$COH_b$  = Coherence estimate during 15-minute pre-injection baseline

An example of these types of plots is shown in figure 4.12. Statistical analysis was based on comparisons between the peak theta (7-12 Hz) and peak gamma (45-100 Hz) activity in each rat group, for each of the brain regions. For each recording location, brain region and frequency band, one-sided t-tests were used to observe effects of stimulation. Additionally, one-sided t-tests were utilised to observe whether there were significant increases in theta/gamma PSD/coherence at the T-maze choice-point, relative to baseline. However the statistical outcome of these tests must be taken with caution given the low sample sizes per rat group (n between 2 and 4 in this case).

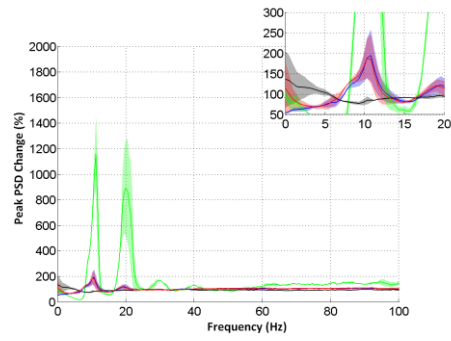


Figure 4.12 – As an example, the percentage change in dCA1 PSD is shown in the SHAM group for the following task phases: post-injection baseline (black), inter-trial delay (blue), intra-trial delay (red), and T-maze (green). Each curve is made up of the individual PSD % change estimates, as derived from each rat in the group. The inset shows a magnified waveform (between 50-300% for PSD readings) for clarifying theta-frequency changes. Subsequent statistics are based on peak theta and gamma activity in the inter-trial delay periods (blue curve), and the T-maze segments (green curve).



## 4.5 Results

This section provides an overview of the rat performance in the T-maze task, as well as the power spectral density (PSD) and coherence changes that occur in the recorded LFP obtained during different phases of the task. Whilst most of the analysis is confined to the T-maze and holding pen, baseline (pre-task) recordings are also described which provide distinctions between rat LFP at rest, and during the T-maze task under varying conditions. For additional explanation on the analysis techniques used, refer to 4.4.8: Analysis of Results. The electrophysiological analysis of the rats is based on the averaged data from the first two test days, in which they had received a saline injection. Throughout this chapter, animals which had received DBS during the intra-trial delay period are referred to as the “Stim” group, whereas animals which had DBS electrodes implanted but received no stimulation are referred to as the “Sham” group.

### 4.5.1 Rat Performance in the T-maze Task

During the training sessions all rats (from Chapters 4 and 5) were either given stimulation during the intra-trial delay period (stimulation group), or were omitted stimulation (but still had stimulating electrodes implanted; sham-stimulation group). All rats were considered for analysis during the training phase, since PCP or saline had not yet been introduced into the experiment. As such, 14 out of 16 rats reached criterion performance and were advanced to the test phase. Of the other two rats, one was taken out of the study due to an infection, and the other did not pass the performance criteria within the allocated training sessions (see table 4.4). An additional rat from the stimulation group was excluded from analysis for having both DBS electrodes incorrectly placed. As such the subsequent analysis is based on the remaining 13 rats.

Experimental Group	T1	T2	T3	T4	T5	T6	T7	T8	T9	T10	T11	T12	T13	T14
Sham	5	7	6	6	3	6	4	5	6	4	4	9	7	7
	4	7	7	7										
	8	7	9											
	5	8	6	7	6	6	9	7	7					
	7	7	3	6	5	5	6	6	6	8	9	8		
	8	7	5	8	8	9								
Stim	7	8	7											
	9	8	7											
	6	5	5	3	9	6	9	8	8					
	8	5	2	5	7	7	6	5	7	9	7			
	10	9	8											
	7	10	7											
	5	9	7	9										

Table 4.4 – Summary of scores for each of the rat training sessions. For each rat in the study, the scores for up to 14 training sessions are shown (T1-T14). All scores are shown out of 10, with yellow shading highlighting scores < 7, and green shading highlighting scores ≥ 7. During training, animals were advanced to the test phase following 3 consecutive days of achieving a score of 7/10 or greater. In this case the test phase for each rat began immediately following their final training day, which is why there is variable number of training sessions between each of the rats. As indicated by the scores, there was a variable pattern of training, as rats had taken between 3 and 14 training sessions to reach criterion performance. Note that one rat (from the sham-stimulation group) was taken out of the study due to a failure to reach criterion performance. Rats which are highlighted by a blue box were part of the saline-injection groups during the post-training test phase.

No clear pattern of learning was observed through training and the subsequent testing phase, as some rats had reached criterion in the first three sessions, whereas other rats in the same groups took over 10 sessions, and this was observed for both the stimulation and sham groups (see figure 4.13 and table 4.4). Unpaired t-tests were used to observe differences between the training scores and mean number of sessions required to reach criterion, between the stimulation and sham groups. Overall, no significant differences were found between the mean number of sessions required to reach criterion ( $p = 0.2141$ ) or the mean score ( $p = 0.1140$ ); although the latter becomes significant ( $p = 0.0320$ ) if the rat which didn't reach criterion is included in the statistics. Generally speaking there is a tendency for stimulated rats to pick up the task faster, given that 4 rats in this group learn the task in three sessions (as opposed to 1 in the sham-stimulation group).

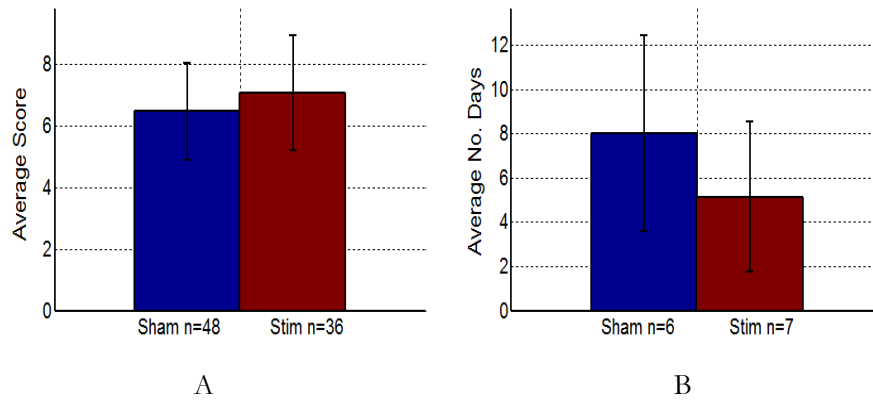


Figure 4.13 – A summary of the mean training session score (A), and the average number of training sessions required to reach criterion performance (B),  $\pm$  SEM. Sham-treated rats are shown in blue, whereas stimulation-treated rats are shown in brown.

During the post-training test phase, the sham group was made up of 2 rats, whereas the stimulation group was made up of 4 rats (see figure 4.1 for an explanation of this). No clear differences were found between these two groups during the test sessions, on either of the three test days, as analysed using unpaired t-tests (table 4.5, and figure 4.14).

	Test 1	Test 2	Test 3
Sham	8	8	10
	9	6	7
Stim	X	6	8
	6	7	4
	8	7	5
	6	7	X

Table 4.5 – Summary of rat scores during the post-training test sessions. Rat groups were sham-stimulation (Sham), and stimulation (Stim). Note that only the saline-treated rats are included in this analysis. Green shading highlights a score of 7/10 or greater, whereas yellow shading refers to scores of <7. Red shading (with a score of X) highlights sessions that were omitted from analysis due to problems regarding the rat session; in this case a) due to the rat not performing the task, and b) due to the test session not taking place.

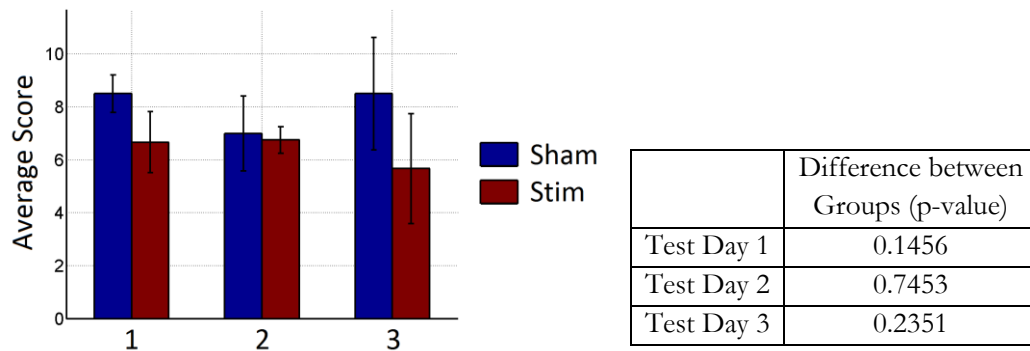


Figure 4.14 – Bar plot (left) shows the average test scores for the sham-stimulation (blue) and stimulation (brown) groups during the post-training test days 1, 2 and 3,  $\pm$  SEM. Unpaired t-tests were used to assess whether group scores were significantly different on either of the test days (right). No significant differences were found in the mean rat score between the stimulation and sham-stimulation groups on any of the post-training test days.

#### 4.5.2 PSD Changes in the mPFC

Medial prefrontal cortex (mPFC) PSD spectrograms are shown for the two groups of rats during the averaged post-training test sessions (figure 4.15). The most profound PSD changes are seen to occur to the theta and gamma amplitude in rats once they enter the T-maze, relative to that seen during baseline (figure 4.16). These increases were seen to be significant for the stimulation group ( $p=0.0001$  – theta,  $p=0.0023$  – gamma), but not for the sham-stimulation group ( $p=0.1102$  – theta,  $p=0.0927$  – gamma; see table 4.6). When rats were inside the T-maze, the mean gamma-frequency PSD is seen to reach at least twice that seen during the baseline recordings (figure 4.16-4.17). However it is of note that the sham-stimulation group had a sample size of only 2 rats. When comparing the mean theta and gamma activity of both groups of rats, no significant differences were found when measured either in the holding pen during the inter-trial delay periods, or at the T-maze choice-point (using unpaired t-tests for comparisons; figure 4.18).

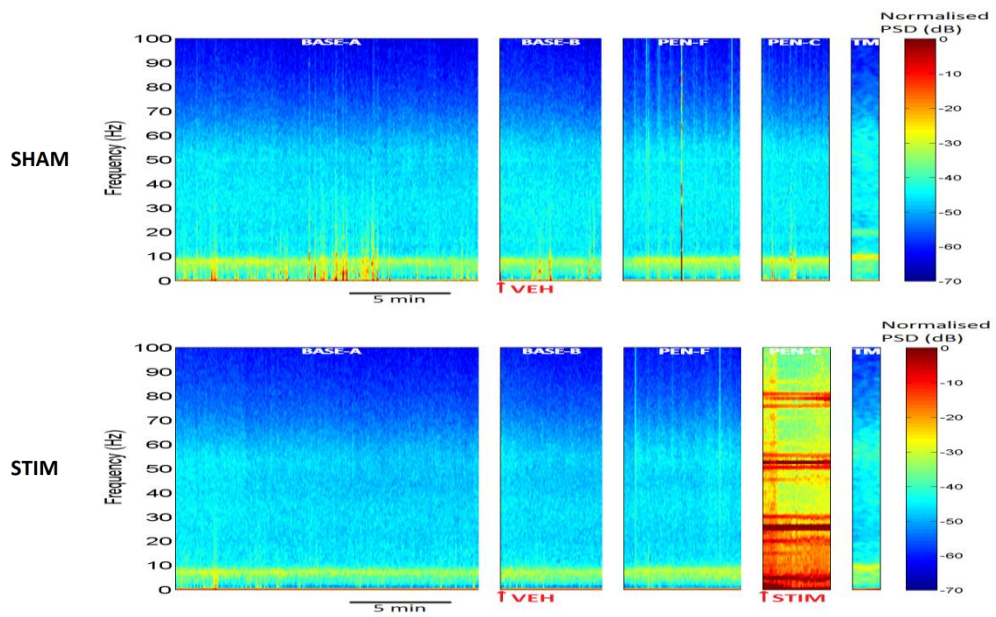


Figure 4.15 – Log spectrograms for mPFC power in each of the groups of rats during the post-training test phase. The following task phases are shown: BASE-A: baseline at 0-15 minutes, BASE B: post-saline injection (pre-test) period at 15-20 minutes, PEN-F: inter-trial delay, PEN-C: intra-trial delay, TM: T-maze choice-point. Experimental groups were sham-stimulation (SHAM) and stimulation (STIM). The application of the saline vehicle and stimulation is shown by the red arrows below the plots. Note the presence of stimulation artefacts during the intra-trial delay period (PEN-C) in the STIM rat group – a feature which is present for this rat groups in all subsequent spectrogram/coherograms plots.

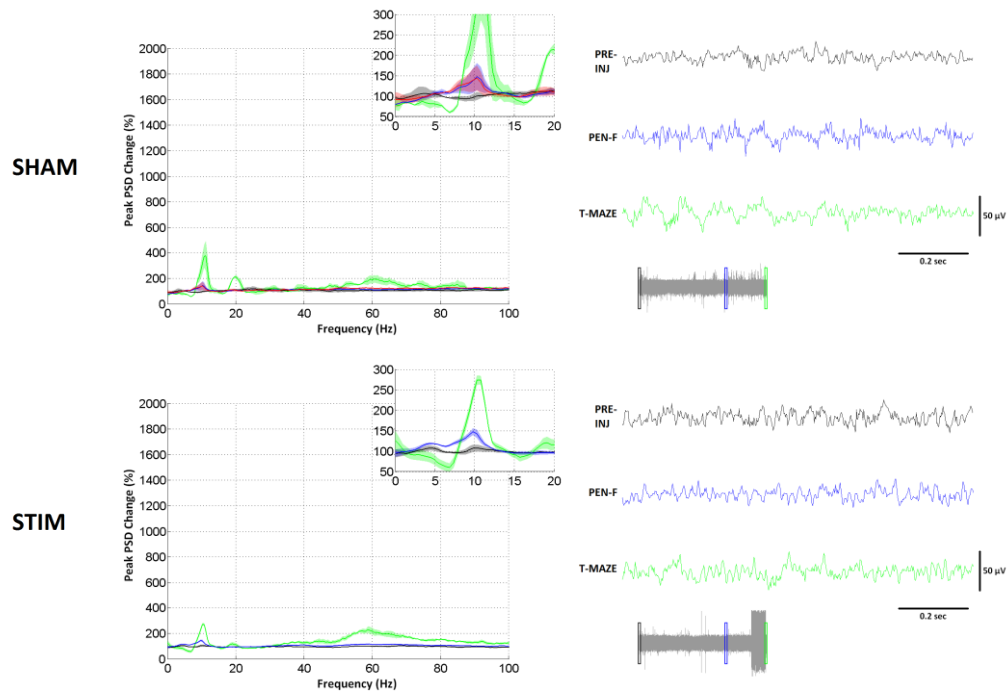


Figure 4.16 – Changes in mPFC PSD for each of the task phases during the post-training test phase, are shown as a percentage of their recorded 0-15 minute baseline value (BASE-A)  $\pm$   $\frac{1}{2}$  SEM; green = T-maze choice-point (TM), blue = inter-trial delays (PEN-F), red = intra-trial delays (PEN-C), black = post-saline injection, pre-test phase (BASE-B). A magnified part of the waveform (50-300%) is shown in the inset. The 1-second waveforms to the right depict the mPFC raw voltage signal during different phases of the task. Experimental groups were sham-stimulation (SHAM) and stimulation (STIM). Theta and gamma activity was seen to reach their maximum power in both groups during the T-maze task phases (green).

	Peak Theta Change	Peak Gamma Change	n
SHAM	0.1102	0.0927	2
STIM	0.0001	0.0023	4

Table 4.6 – T-tests were used to assess whether mPFC peak theta and gamma activity at the T-maze choice-point (TM) was significantly altered with respect to the pre-injection baseline recording (BASE-A), during the post-training test phase. Numbers in the table denote p-values corresponding to whether the observed peak theta/gamma PSD was significantly different from baseline, with green values indicating statistical significance at  $p < 0.05$ . The final column (n) indicates the sample size per t-test. Experimental groups were sham-stimulation (SHAM) and stimulation (STIM).

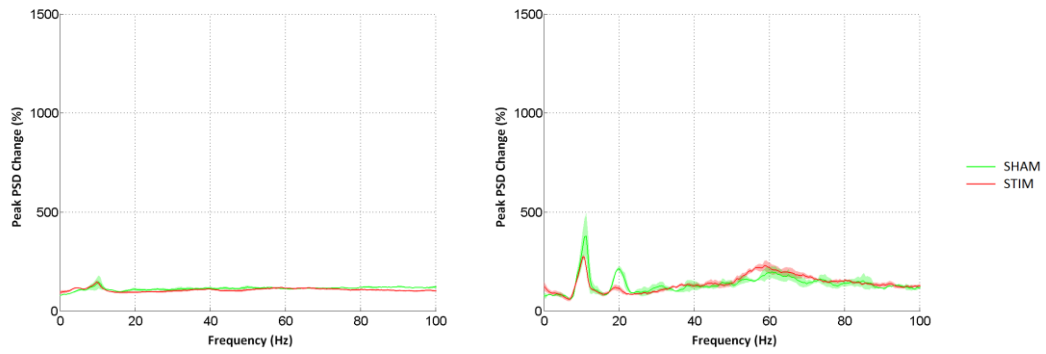
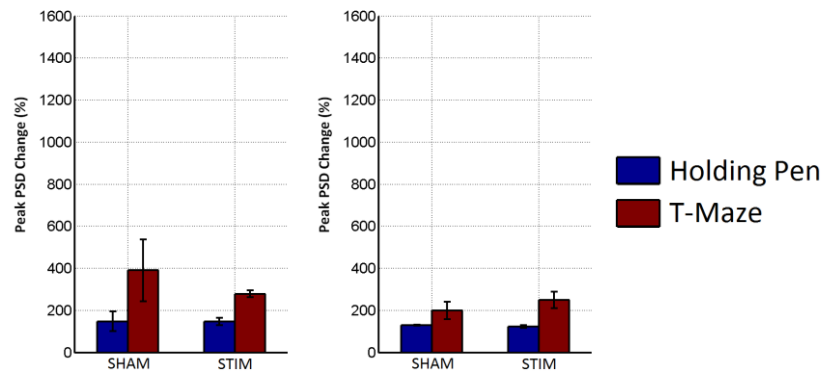


Figure 4.17 – Comparisons between inter-trial delay (PEN-F – left) and T-maze choice-point (TM – right) mPFC PSD changes in each rat group  $\pm$   $\frac{1}{2}$  SEM, during the post-training test sessions. Experimental groups were sham-stimulation (SHAM; green) and stimulation (STIM).



	Holding Pen	sig	T-Maze	sig
Theta	0.9926		0.1636	
Gamma	0.2323		0.2204	

Figure 4.18 – Bar plots denote the differences in mPFC mean theta (top-left) and gamma (top-right) PSD changes between the stimulation (STIM) and sham-stimulation (SHAM) groups of rats,  $\pm$  SEM. Blue bars indicate percentage change from baseline inside the holding pen, whilst brown bars indicate percentage change from baseline in the T-maze. Differences between the two groups were analysed using an unpaired t-test which compared the mean theta and gamma change, both inside the holding pen and T-maze (p-values given in table above). No significant differences were found between the two groups.

### 4.5.3 PSD Changes in dCA1

Hippocampal dCA1 PSD spectrograms are shown for each of the groups of rats during the averaged post-training test sessions (figure 4.19). The most profound change that is observed in dCA1 is a marked elevation in theta-frequency PSD (relative to baseline), once rats are inside the T-maze, which is visible on the spectrograms in figure 4.19. However, this increase relative to baseline is only significant for the stimulation group ( $p=0.0027$ ), and not for the sham-stimulation group ( $p=0.0858$ ). This is probably due once again to the small sample size of 2 rats in the sham-stimulation group. Mean gamma-frequency PSD is also seen to be elevated from baseline in both groups of rats when inside the T-maze, but is once again only significant for the stimulation group ( $p=0.0007$  – stim;  $p=0.0535$  – sham). Note that these gamma-frequency increases may not be apparent on the PSD spectrograms (figure 4.19) due to its logarithmic colour scale (see figures 4.20 – 4.21 instead). Interestingly the centre-frequency of this increased gamma-frequency PSD seemed to be higher in dCA1 than in the mPFC, which in this case was around 80Hz (as opposed to  $\sim 55$ Hz in the mPFC). Unpaired t-tests were used to compare the mean theta and gamma elevations between the two groups of rats, in both the holding pen and T-maze (figure 4.22). No significant differences were found in this case.



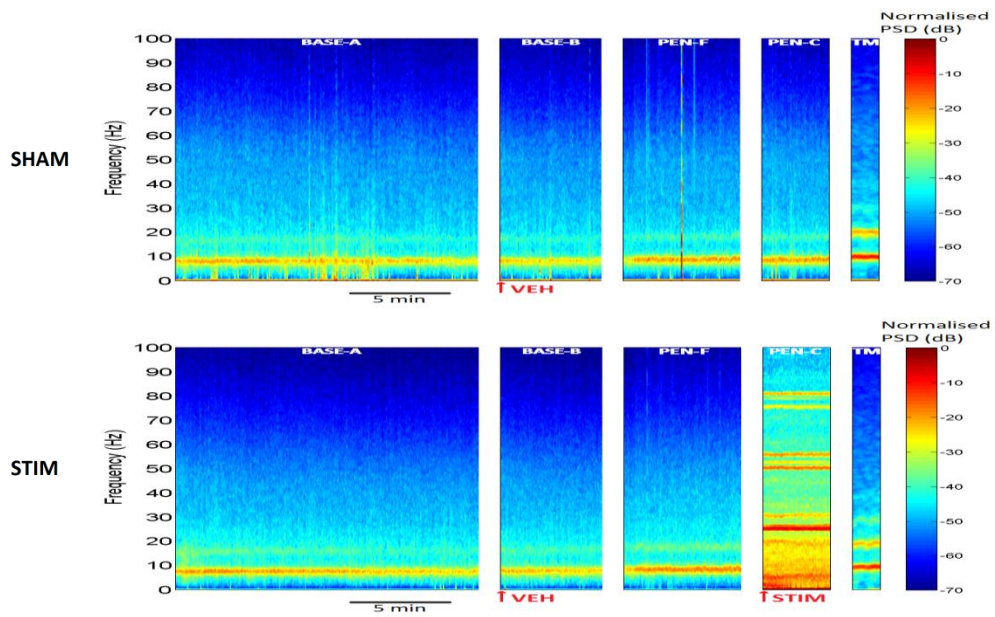


Figure 4.19 – Log spectrograms for dCA1 power in each of the groups of rats during the post-training test phase. The following task phases are shown: BASE-A: baseline at 0-15 minutes, BASE B: post-saline injection (pre-test) period at 15-20 minutes, PEN-F: inter-trial delay, PEN-C: intra-trial delay, TM: T-maze choice-point. Experimental groups were sham-stimulation (SHAM) and stimulation (STIM). The application of the saline vehicle and stimulation is shown by the red arrows below the plots. The increase in theta-activity following the 20-minute baseline recording (during the task) is visible during the inter-trial delays (PEN-F) and in particular, the T-maze (TM) recordings. In addition the increased strength of the second theta-frequency harmonic can be seen during the T-maze recordings (observed as a weaker yellow band at  $\sim 20\text{Hz}$ ) in each rat group. Note also the slight increase in the frequency of T-maze theta activity in each rat group, when observed relative to baseline (see Chapter 5: 5.5.10 – Peak Hippocampal Theta-Frequency Changes during Different Phases of the Behavioural Task; for an analysis of this).

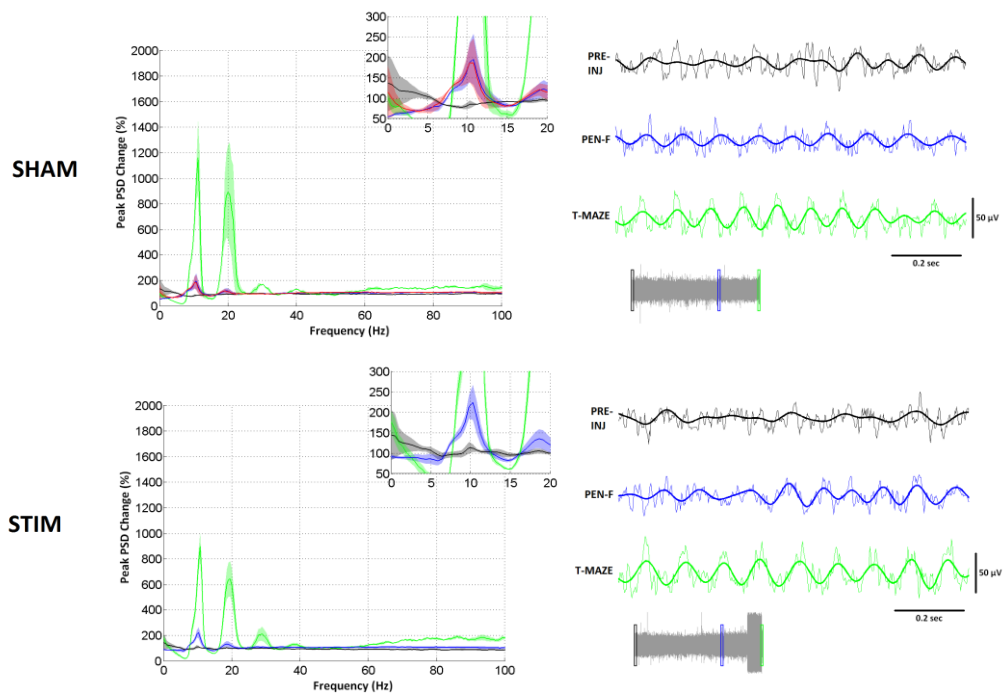


Figure 4.20 – Changes in dCA1 PSD for each of the task phases during the post-training test phase, are shown as a percentage of their recorded 0-15 minute baseline value (BASE-A)  $\pm$   $\frac{1}{2}$  SEM; green = T-maze choice-point (TM), blue = inter-trial delays (PEN-F), red = intra-trial delays (PEN-C), black = post-saline injection, pre-test phase (BASE-B). A magnified part of the waveform (50-300%) is shown in the inset. The 1-second waveforms to the right depict the dCA1 raw voltage signal during different phases of the task, with a thicker band indicating filtered theta activity (4-12 Hz). Experimental groups were sham-stimulation (SHAM) and stimulation (STIM). The mean theta-frequency PSD (as a percentage of that observed during baseline) is seen to be markedly increased in both groups of rats when inside the T-maze. Mean gamma activity appears to be increased during this period also.

	Peak Theta Change	Peak Gamma Change	n
SHAM	0.0858	0.0535	2
STIM	0.0027	0.0007	4

Table 4.7 – T-tests were used to assess whether dCA1 peak theta and gamma activity at the T-maze choice-point (TM) was significantly altered with respect to the pre-injection baseline recording (BASE-A), during the post-training test phase. Numbers in the table denote p-values corresponding to whether the observed peak theta/gamma PSD was significantly different from baseline, with green values indicating statistical significance at  $p < 0.05$ . The final column (n) indicates the sample size per t-test. Experimental groups were sham-stimulation (SHAM) and stimulation (STIM).

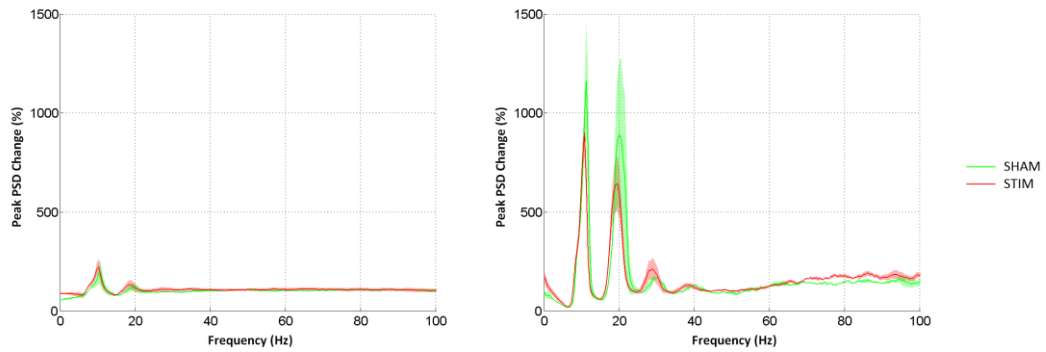
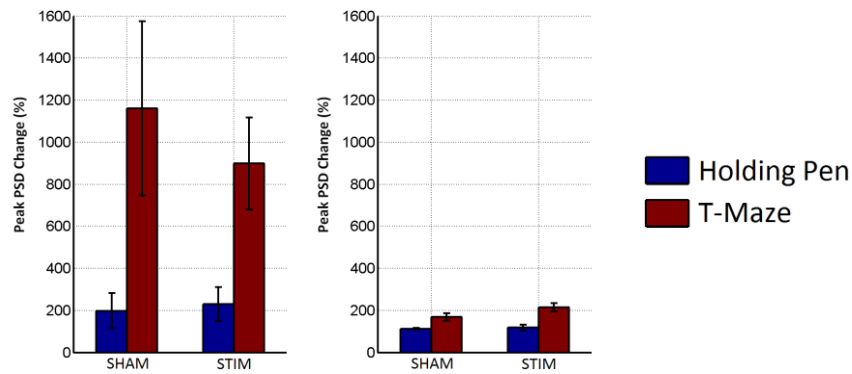


Figure 4.21 – Comparisons between inter-trial delay (PEN-F – left) and T-maze choice-point (TM – right) dCA1 PSD changes in each rat group  $\pm \frac{1}{2}$  SEM, during the post-training test sessions. Experimental groups were sham-stimulation (SHAM; green) and stimulation (STIM). Similar to previous mPFC PSD findings, mean dCA1 theta and gamma PSD is seen to be greatly elevated when rats are placed inside the T-maze (relative to baseline). However this increase is only significant in the stimulation group (see table 4.7).



	Holding Pen	sig	T-Maze	sig
Theta	0.6787		0.3431	
Gamma	0.5974		0.0507	

Figure 4.22 – Bar plots denote the differences in dCA1 mean theta (top-left) and gamma (top-right) PSD changes between the stimulation (STIM) and sham-stimulation (SHAM) groups of rats,  $\pm$  SEM. Blue bars indicate percentage change from baseline inside the holding pen, whilst brown bars indicate percentage change from baseline in the T-maze. Differences between the two groups were analysed using an unpaired t-test which compares the mean theta and gamma change, both inside the holding pen and T-maze (p-values given in table above). No significant differences were found between the two groups.

#### 4.5.4 Prefrontal-Hippocampal Coherence Changes

Coherograms depicting ipsilateral mPFC-dCA1 coherence are shown for each of the two groups of rats during the post-training test sessions (figure 4.23). Unpaired t-tests had shown significant alterations in both theta and gamma-frequency coherence in the stimulation rat group ( $p=0.008$  – theta;  $p=0.0017$  – gamma), when measured in the T-maze relative to the baseline recording. The theta-frequency coherence in particular can be seen to be elevated by  $\sim 130\%$  in both groups of rats (figure 4.24-4.25). These changes were not seen to be significant in the sham-stimulation group however ( $p=0.0559$  – theta;  $p=0.0991$  – gamma). Nonetheless these theta-frequency increases are also seen during the inter-trial delay periods, albeit at a smaller level than that observed at the T-maze choice-point. Finally, unpaired t-tests were used to assess differences in coherence changes between the stimulation and sham-stimulation groups, and found no significant differences in theta or gamma coherence either in the T-maze ( $p=0.9953$  – theta;  $p=0.5863$  – gamma) or holding pen ( $p=0.7662$  – theta;  $p=0.5597$  – gamma; see figure 4.26).

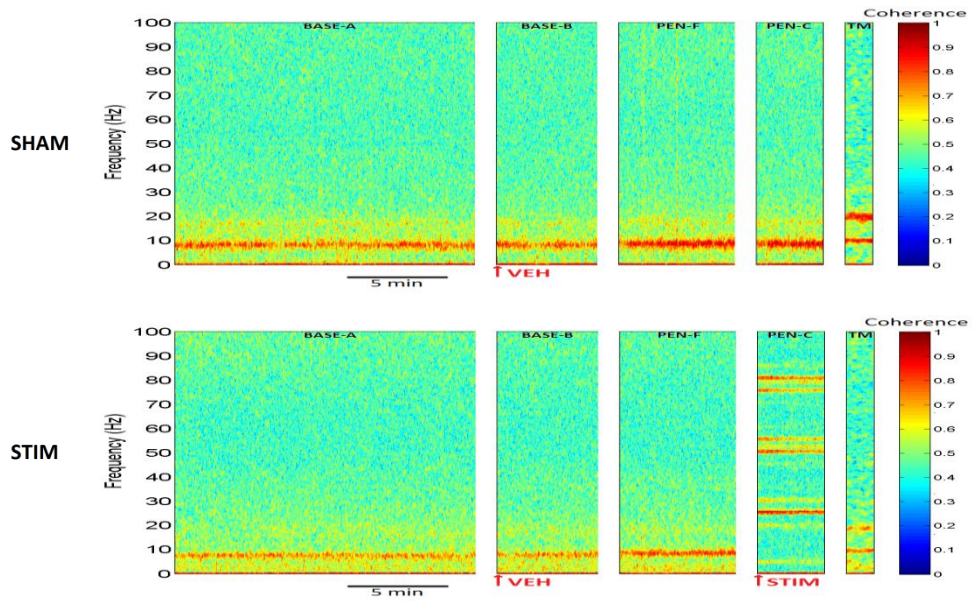


Figure 4.23 – Log coherograms for m-PFC-dCA1 coherence in each of the groups of rats during the post-training test phase. The following task phases are shown: BASE-A: baseline at 0-15 minutes, BASE B: post-saline injection (pre-test) period at 15-20 minutes, PEN-F: inter-trial delay, PEN-C: intra-trial delay, TM: T-maze choice-point. Experimental groups were sham-stimulation (SHAM) and stimulation (STIM). The application of the saline vehicle and stimulation is shown by the red arrows below the plots. The theta-frequency coherence can be seen to be slightly elevated following the baseline recording, both in the holding pen (PEN-F) and the T-maze (TM), in both groups of rats.

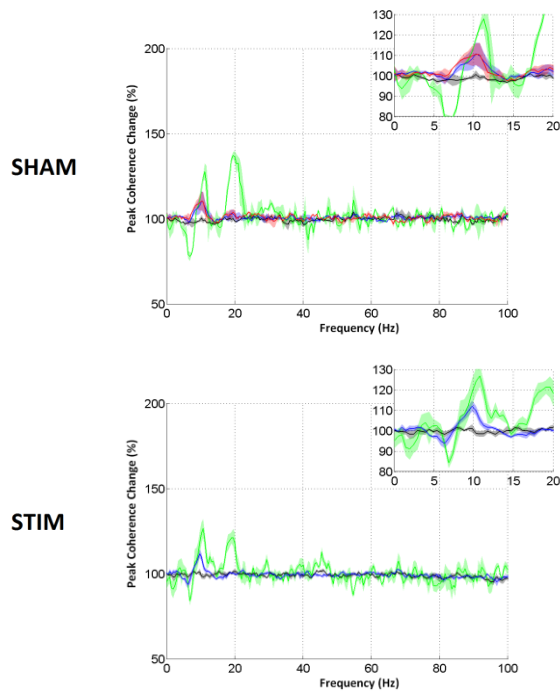


Figure 4.24 – Changes in mPFC-dCA1 coherence for each of the task phases during the post-training test phase, are shown as a percentage of their recorded 0-15 minute baseline value (BASE-A)  $\pm$   $\frac{1}{2}$  SEM; green = T-maze choice-point (TM), blue = inter-trial delays (PEN-F), red = intra-trial delays (PEN-C), black = post-saline injection, pre-test phase (BASE-B). A magnified part of the waveform (80-130%) is shown in the inset. Experimental groups were sham-stimulation (SHAM) and stimulation (STIM). The mean theta-frequency coherence change (from baseline) is seen to reach its maximum value in both groups of rats, when inside the T-maze (green curves), however this increase is only significant for the stimulation group (see table 4.8).

	Peak Theta Change	Peak Gamma Change	n
SHAM	0.0559	0.0991	2
STIM	0.0080	0.0017	4

Table 4.8 – T-tests were used to assess whether mPFC-dCA1 peak theta and gamma coherence at the T-maze choice-point (TM) was significantly altered with respect to the pre-injection baseline recording (BASE-A), during the post-training test phase. Numbers in the table denote p-values corresponding to whether the observed peak theta/gamma PSD was significantly different from baseline, with green values indicating statistical significance at  $p < 0.05$ . The final column (n) indicates the sample size per t-test. Experimental groups were sham-stimulation (SHAM) and stimulation (STIM).

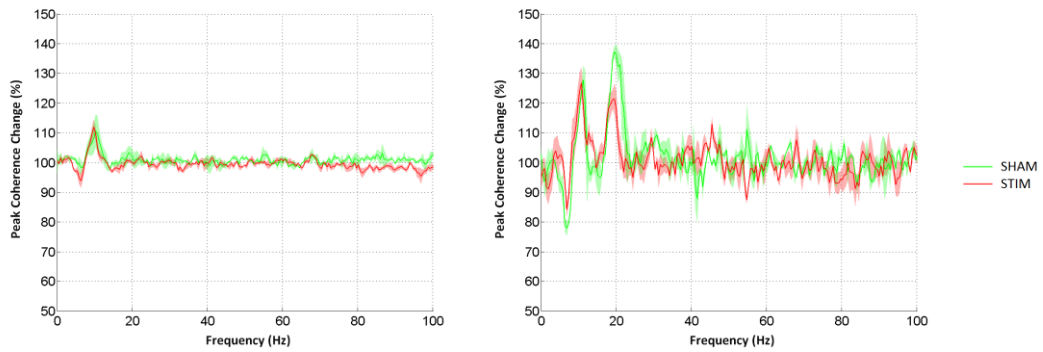
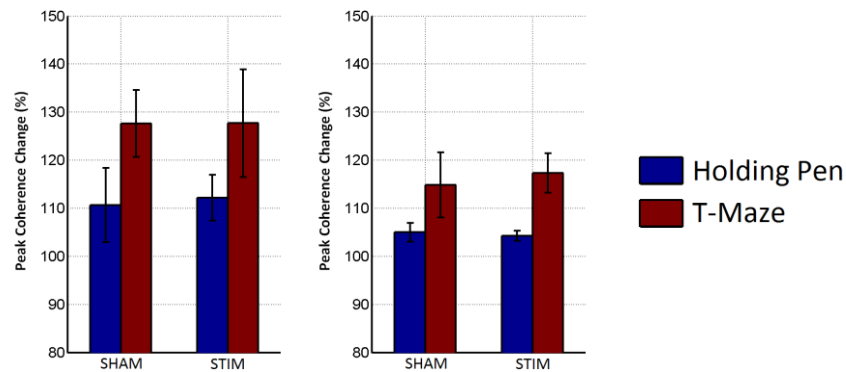


Figure 4.25 – Comparisons between inter-trial delay (PEN-F – left) and T-maze choice-point (TM – right) mPFC-dCA1 coherence changes in each rat group  $\pm \frac{1}{2}$  SEM, during the post-training test sessions. Experimental groups were sham-stimulation (SHAM; green) and stimulation (STIM).



	Holding Pen	sig	T-Maze	sig
Theta	0.7662		0.9953	
Gamma	0.5597		0.5863	

Figure 4.26 – Bar plots denote the differences in mPFC-dCA1 mean theta (top-left) and gamma (top-right) coherence changes between the stimulation (STIM) and sham-stimulation (SHAM) groups of rats,  $\pm$  SEM. Blue bars indicate percentage coherence change from baseline inside the holding pen, whilst brown bars indicate percentage coherence change from baseline inside the T-maze. Differences between the two groups were analysed using an unpaired t-test which compared the mean theta and gamma coherence changes, inside both the holding pen and T-maze (p-values given in table above). No significant differences were found between the two test groups.

#### **4.5.5 Summary of PSD and Coherence Changes**

In summary, both theta and gamma-frequency elevations were observed in the stimulation group of rats, in both the mPFC and dCA1 brain regions, when rats were placed inside the T-maze. In addition, theta and gamma-frequency elevations were also seen in the mPFC-dCA1 coherence of stimulation rats, when they were placed inside the T-maze. Whilst similar mean elevations were noted in the sham-stimulation group of rats, none of these observed elevations were significant, which is presumably because the sample size of this group is far too small to observe significant differences. In addition, there were no reported significant differences between the two groups regarding either of the PSD or coherence changes, in any of the brain regions or any of the test arenas analysed.



## 4.6 Discussion

### 4.6.1 Theta and Gamma Frequency PSD Changes

In both of the groups of rats, the largest observable LFP changes was dCA1 theta-frequency PSD, which in this case was seen to increase markedly when rats were placed inside the T-maze environment (as measured relative to the pre-task baseline recordings). Typically each of the groups of rats had displayed mean elevations in hippocampal theta-frequency PSD of between 5-10 times that of baseline under these conditions. However in a similar manner to the recordings of gamma-frequency PSD, these increases were only significant in the stimulation rat group, and not for the sham-stimulation group. As such, whilst these changes would be expected to reach statistical significance had a larger sham-stimulation group been used, a replication of this with a larger rat group is nonetheless required to confirm this prediction.

The observed T-maze related theta-power increases were to be expected in the dCA1 brain region, given the well-known presence of hippocampal theta during locomotion, spatial exploration and various learning-related behaviours (Green and Arduini, 1954, Vanderwolf, 1969); all behaviours which the T-maze environment was expected to reveal. Generally speaking for each of the rats the magnitude of theta-frequency PSD was seen to vary highly in the recordings taken inside the T-maze, often from one trial to the next. This may have been a consequence of variations in rat running speed, which was not controlled during the trial. The LFP recordings inside the T-maze were extracted as the final 1-second period from when the rat crossed the choice-point tracking area. This was done in order to obtain a fixed 1-second LFP segment from each maze run. Because of this, the rats position during the 1-second LFP segment could vary based on whether the rat was running towards the choice point, or whether the rat was standing at the choice point. Also it cannot be ruled out that some rats may have simply performed the task faster than others, leading to group differences in the profile of dCA1 PSD. Some of the largest amplitude theta-rhythms observed in the dCA1 PSD plots were obtained only from the T-maze central arm segments, and these typically also featured elevations in the

harmonic repetition of the theta peak frequency, at around 20Hz. In freely moving rats, correlations of rat running speed with both theta amplitude and frequency has long been known (Vanderwolf, 1969, McFarland et al., 1975). More recently, links between the second harmonic of the hippocampal theta frequency and locomotion have been made (Terrazas et al., 2005, Buzsaki et al., 1986).

Whilst a detailed analysis of the first harmonic component of the dCA1 theta rhythm is beyond the scope of the current study, it should be noted that virtually all comparisons between T-maze and holding-pen (whether delay-period or baseline) hippocampal recordings typically revealed the presence of larger amplitude theta-waves, along with their associated harmonic at ~20Hz. Thus it is likely that many of the theta amplitude changes in dCA1 are related to the movement speed of the animal inside the T-maze, and it is possible that this accounts for the variation in dCA1 spectral power changes as observed relative to baseline. The exact contribution of locomotor activity on hippocampal theta power cannot be elucidated here because animal movement speed was not controlled in this experiment. It should be noted however that in rats voluntary movement inherently requires the use of spatial working memory as the rat encodes information relevant to its environment (Viana Di Prisco et al., 2002), thus the two can be considered to be coupled together. A recent study attempted to separate the effects of volitional movement from the cognitive demands of a task that required rats to switch between place- and motor-response strategies (Schmidt et al., 2013). Interestingly they noted that during the choice phase of the task, not only did theta power increase in the dCA1 region of the hippocampus, but also it was uncoupled from the rats running speed during the decision-making process in this region.

In this study, gamma-frequency PSD when recorded inside the T-maze was seen to be significantly elevated in both the mPFC and dCA1 brain regions of the rats that underwent stimulation, when compared against their pre-injection baseline recordings. Whilst similar increases were also observed in the sham-stimulation group, none of these increases were statistically significant, which is perhaps due to the relatively small sample size of 2 rats. Gamma oscillations in awake mammals have traditionally been associated with sensory binding (Singer and Gray, 1995),

selective attention (Jensen et al., 2007), and more recently has been observed to be prevalent during working memory (Jensen et al., 2007, van Vugt et al., 2010, Howard et al., 2003). In human neurosurgical patients, electrocorticogram (ECoG) studies have revealed gamma-activity increases in both the cortical (Howard et al., 2003) and hippocampal (van Vugt et al., 2010) brain regions, which in both cases were correlated with working memory load. The gamma-frequency PSD increases during the T-maze LFP recordings mirrors widespread findings of increased cortical activation with working memory, as reported through various imaging studies (e.g. Callicott et al., 1999). Given the small sample sizes used in this study, it is not surprising that no significant differences were observed between the gamma-frequency PSD between the groups of rats, when compared in the holding pen and inside the T-maze.

#### **4.6.2 Coherence Changes**

In the stimulation group of rats, the mean theta-frequency coherence between the mPFC and dCA1 brain regions was seen to reach its maximum increases (relative to baseline), when measured at the T-maze choice point. Once again, whilst this increase was also seen in the sham-stimulation group, this was not found to be significant. Smaller increases relative to baseline were also noted during the inter-trial delay segments of the task in both rat groups. The functional interactions between hippocampal theta waves with various downstream targets in the brain have long been studied for various behaviours (Gordon, 2011). In particular a synchronisation between hippocampal and prefrontal theta waves has been correlated with working memory performance in both rats (Jones and Wilson, 2005, Benchenane et al., 2010) and mice (Sigurdsson et al., 2010). Jones and Wilson (2005) were able to demonstrate an enhancement of mPFC-dCA1 theta-frequency coherence in rats during the choice phase of a spatial working memory task. Later on Benchenane et al., (2010) demonstrated that the coherence at the choice-point in a Y-maze reached its maximum values after the rats had learned the task rules, and suggested that may be due in part to a reorganisation of cell ensembles in order to facilitate an enhanced coordination between these brain regions. Thus in a similar manner to that

presented in these studies, the maximum theta coherence elevations as observed at the T-maze choice point most likely reflects the functional integration of the hippocampus and prefrontal cortex for the utilisation of spatial working memory during these task phases. Whilst the t-test comparisons between the baseline and T-maze choice-point LFP revealed significant theta-frequency coherence increases only in the stimulation group, it is worth mentioning that the sample sizes were small in this type of analysis, and is perhaps the reason why these increases were not statistically significant in the sham-stimulation group. Nonetheless the coherence was visibly enhanced at the T-maze choice point in all rats which undertook the task, and given the data presented here and that by other researchers who found similar increases in theta coherence in a spatial working memory task (e.g. Jones et al., 2005), a future study featuring a larger sample size is likely to replicate the data seen here with greater certainty.

#### **4.6.3 Effect of DBS on Behavioural Performance**

During the training period each rat was given up to 14 test sessions to reach criterion performance, which was a score of 70% or greater for 3 consecutive sessions. Given that no PCP or saline was administered to any of the rats until the test phase, rat performance during training was analysed on the basis of whether they had received stimulation or not. For this reason, the stimulation/sham-stimulation groups as analysed during training are larger than the groups which were analysed during the post-training test phase. Fimbria-fornix (FF) stimulation was applied during the training sessions in order to study the effects it had on the rats ability to learn the task. As with the test sessions, DBS was applied during the 30-second intra-trial delay period for each of the 10 trials per training session. The intra-trial delay interval was selected for the stimulation period for two reasons: first it allowed for clean LFP recordings to take place inside the T-maze, which wouldn't have been the case if constant DBS were used throughout the recording session. Second, it was chosen as the optimal time to provide stimulation, since it coincided with the memory retention part of the T-maze task. The point of FF stimulation was to enhance activation in the brain regions that govern learning and memory

functions (mainly structures located in and around Papez's circuit (Papez, 1937); see also Chapter 1 – 1.5.6.4: Fimbria-Fornix; for a review), through a depolarising current on centrally-located white-matter tracts. A recent study examined the effects of rostral intralaminar thalamic nuclei DBS at different task phases in rats undergoing a delayed non-match to position task (Mair and Hembrook, 2008). They found that stimulation delivered during the delay and choice phases of the task resulted in the largest working memory improvements.

Of the 16 rats that were initially in the study, three were excluded for a) infection following surgery, b) incorrectly placed DBS electrodes, and c) failure to reach a criterion performance within 14 test sessions. During training, the rats that had received FF stimulation during the 30-second intra-trial delay had shown a non-significant increase in mean score ( $p=0.1140$ ), which became significant when the score from the excluded sham-stimulation rat (who failed to achieve criterion performance) was considered ( $p=0.0320$ ). Although the stimulation rats appeared to show a lower mean number of sessions required to reach criterion, this figure didn't reach statistical significance ( $p=0.2141$ ). Given the relatively small sample sizes used in this study, it is interesting to consider whether this may become significant if a larger sample size were used.

During testing, no significant effects of stimulation were found on the behavioural test scores between the stimulation and sham-stimulation groups, on either of the three test days. Again this may be due in part to the small sample size, since no meaningful pattern of rat performance could be discerned in either of the groups of rats through the use of stimulation.

#### **4.6.4 Experimental Design**

In this experiment the EEG-DBS system was utilised in a novel way that allowed it to be integrated into the design of the T-maze experiment. By reprogramming the EEG-DBS system and its receiver to synchronise with a video-tracking system, the LFP of relevant phases of the task could be extracted; for example LFP segments corresponding to the rat reaching the choice-point of the T-maze. Special

consideration was given to the design of this system with regards to the overall experimental complexity. Since the T-maze experiment was not automated, rat handling was an integral component in all of the recording sessions that took place. As such the rat had to be picked up and moved between the T-maze and the holding pen for every maze run. In addition the T-maze sliding doors had to be manually opened/closed, food bowls had to be manually refilled between trials, and score sheets had to be manually updated. Thus to simplify the execution of the experiment, the control of the EEG-DBS system was restricted to one-button commands in WinEDR, which were used to activate DBS and/or begin the delay timer in between maze runs. Using the EEG-DBS system to control the inter-/intra-trial delay timers allowed two things to happen; first it allowed stimulation to take place for approximately 30 seconds, and second it provided a visual 3-second warning on the LFP trace, prior to the end of the delay period. With this arrangement, the experiment was conducted in a simple and robust manner. Furthermore it allowed for the successful coordination between LFP recording and video-tracking, and the resulting recordings were subsequently integrated into the analysis stage carried out in Matlab (Mathworks).

During each recording session, special care had to be taken to avoid obscuring the line-of-sight between the overhead camera and any of the tracking points. The overhead viewing camera was positioned to capture the central arm of the T-maze, the holding pen, and the receiver (with the synchronisation LED built into it), with the tracking points located on all of these except for the holding pen. If the experimenter were to accidentally move their arm between the cameras' viewing field and the T-maze or receiver tracking points, then the Ethovision video-tracking software (Nodulus Information Technologies) would incorrectly register this as either rat movement or a synchronisation pulse, respectively. For this reason numerous algorithms were designed in Matlab to allow for a visual validation of the video-tracking data, to ensure that rat movement and the synchronisation pulses were registered correctly. Automatic 'tracking recognition' algorithms were developed to assist with the removal of unwanted tracking artefacts by placing the data through a number of checks. For example, tracking data at the choice point of

the T-maze was only valid when preceded with tracking data from the centre and start points of the T-maze central arm, respectively. Generally speaking repeated execution of this T-maze task allowed for a good working practice which resulted in over 95% of sessions recording video tracking data properly. Of those that didn't, erroneous video-tracking artefacts were either automatically or manually removed.

Owing to the simplicity of the system's design, each recording session was typically underway within 2 minutes of the rat being brought to the recording room inside their cage. Much of this time was spent attaching the EEG-DBS system to the rat, prior to pressing 'record' on the software which controlled the video-tracking camera and the EEG-DBS system. An early problem arose based on the interface between the EEG-DBS system and the animal's headstage connector. In an earlier (unreported) version of this T-maze task, there was a large amount of friction between the sockets of the EEG-DBS system, and the 10-pin headstage connector on each of the rats. This led to an excessive system insertion/removal force, which ultimately resulted in the removal of a few of the animals headstage attachments. Following this issue the sockets on the EEG-DBS system were loosened to remove the system insertion/removal friction, and a special procedure was devised for attaching and removing the system quickly and with minimal force. This involved the use of a miniature lever to pry the system away from the headstage implant, without pulling the implant upwards away from the animal's skull. However, the loosened connection between the system sockets and the headstage connector facilitated an increase in animal movement artefacts; thus whenever the animal moved quickly, a significant amount of movement-related artefacts would be displayed on the LFP trace. This was due to the movement-related vibrations incurred at the loosened pin-socket connections. A solution to this was found by treating the loosened EEG-DBS system sockets with conductive EEG paste (Ten20; Weaver), which dampened the presence of movement artefacts, whilst allowing for a minimal system insertion/removal force. With this setup, no animals in this experiment were lost due to headstage removal, and high-quality LFP recordings were produced throughout.

Future improvements to this experimental design could be based on a tighter integration between the software packages which controlled the video-tracking and the EEG-DBS system. An entirely separate system was used for video-tracking, using Ethovision XT (Nodulus Information Technologies) as the software which coordinated the video-tracking through a ceiling-mounted camera. Since this software couldn't be reprogrammed or changed, the EEG-DBS and its receiver system programming were adapted to work with the video-tracking system. An enhanced integration between LFP recording and video-tracking could be obtained if the hardware that obtained both LFP and video data were integrated together and controlled by one software program. For example, if a new type of program could be developed that perform both video-tracking and LFP recording, it could simplify both the experiment and the analysis of the data obtained.

The surgery procedure had to be adapted to work with the novel equipment and experimental design. Because the headstage implant and system was located directly on top of the skull of the animal, the electrodes had to be manufactured to allow for accurate positioning whilst allowing for adequate vertical clearance for the implant. From observing the cresyl-violet stained brain slices obtained from rats during the histology phase of the experiment, a pattern began to emerge regarding the positioning of electrodes. Generally speaking electrodes in the left hemisphere were more accurately placed than that of the right hemisphere, electrodes implanted in the mPFC were more likely to be correctly placed than that of dCA1, and the most inaccurately placed electrodes overall were the DBS electrodes. In this case most of the DBS electrodes were positioned at slightly more anterior sites than that specified by their target coordinates, leading to them being implanted in the fimbria-fornix (FF), which lies adjacent to the anterior thalamic nucleus (ATN). As discussed in Chapter 3 (see 1.5.6.4: Fimbria-Fornix), there is compelling evidence to consider this site as a candidate brain region for stimulation.

With 2 DBS electrodes, 4 LFP electrodes, and 7 skull anchors (including the reference electrode), the stereotaxic surgery was complex due to the increasingly limited space available on the skull of the animal. After each electrode was implanted, dental cement had to be applied to attach the electrode securely to the



skull, which further limited the visible skull area. Left-hemisphere electrodes were always implanted before the right hemisphere electrodes using a stereotaxic arm which was mounted on the right-hand side of the frame. This may account for the increased accuracy of electrode positioning in the left-hemisphere. In addition, electrodes were implanted from anterior to posterior positions, with the mPFC electrodes implanted first, and the dCA1 electrodes implanted last. By the time the posterior dCA1 electrodes were implanted, most of the skull was obscured with dental cement. Errors in reference coordinate measurements may therefore account for the increased accuracy of electrode positioning in the mPFC relative to the dCA1 brain region, although it should be noted that the prelimbic cortex contains more space than the region of dCA1 that was used as a site for implantation. With this in mind, there is room for improvement with the surgery procedure, to allow for easier, more accurate and more efficient implantation of the electrodes and skull anchors. A possible solution is to use a fixed ‘stencil’ implant (e.g. Chandler, 2010), which is essentially a pre-cut plastic piece that contains holes through which electrodes are implanted. This can serve the dual purpose of accurately positioning electrodes at fixed distances from each other, as well as forming a base anchor for the headstage implant.

Perhaps one of the biggest improvements that could be made to the existing experimental design is the use of larger sample sizes. Despite a small sample size of 4 rats, the stimulation group was able to display significant differences in the theta and gamma-frequency PSD and coherence, as observed between the T-maze and holding-pen task phases. However whilst similar increases were noted in the LFP of the sham-stimulation group, there were no statistically significant differences, which is not surprising given that there were only 2 rats in this group. Furthermore, the low numbers of rats in this group prevented any significant differences (if present) from being observed between the use of stimulation and sham-stimulation. This is reflected in the numerous comparisons carried out in the LFP power and coherence between these groups, which consistently revealed a lack of statistical significance.

The low sample sizes were also a problem with regards to the analysis of the task scores during the training and post-training test sessions. During the training

sessions, rats were seen to take between 3 and 14 sessions in order to reach criterion. In spite of a (non-significant) tendency for stimulated rats to reach a criterion performance quicker than their sham-stimulation counterparts, there was no clear pattern of learning observed – due to the large intra-group variation in training scores. Notably, once rats had reached the criterion performance the mean scores did not stabilize at this level, since there were 8 post-training sessions with scores of less than 7, and 8 sessions with scores of greater than or equal to 7. An interesting variation to this methodology which may be of use in future studies is that carried out by Moghaddam and Adams (1998), who studied the effects of acute phencyclidine (PCP) on rats using a delayed alternation version of the T-maze task. Instead of setting a fixed criterion performance (which in the case of the current study is 70% over three consecutive days), they established a baseline performance in each rat once their performance had stabilised during the training period. Whilst this paradigm does not require rats to reach a pre-defined percentage of correct choices, it may have been beneficial in the current study since the post-training performance of each rat would be measured in accordance with their own individual abilities, thus minimizing intra-group variation.

# Chapter 5

## Investigation of DBS in a Rodent Model Relevant to Schizophrenia

### 5.1 Introduction

This chapter aims to augment the previous experiment as detailed in Chapter 4 by introducing the NMDA receptor antagonist phencyclidine (PCP) into the behavioural task paradigm. This is done so in an attempt to model the working memory deficits that are one of the core cognitive deficits in schizophrenia. Using an almost identical paradigm to that of Chapter 4, rats are trained to criterion performance in a non-match to sample task using a T-maze, and receive either deep-brain stimulation or sham-stimulation (absence of DBS but with stimulating electrodes implanted) during the task delay periods. Following training, rats are administered acute PCP injections during the post-training test phase, and their local field potentials (LFPs) are compared between the stimulation and sham-stimulation groups. The analysis that is carried out in this chapter is subsequently extended to compare the LFP differences observed between the saline-treated rats in Chapter 4, and the PCP-treated rats in this chapter. Furthermore by combining this data, the hippocampal theta-frequency changes are analysed, as well as the power spectral density (PSD) differences between T-maze run types (i.e. forced, correct and incorrect maze runs).

## 5.2 Background

This section provides an overview of the use of PCP in behavioural experiments, including the T-maze.

### 5.2.1 PCP to Model Aspects of Schizophrenia

A number of different genetic, developmental and pharmacological options exist to model many of the schizophrenia symptoms in animals. PCP is a non-competitive *N*-methyl-D-aspartate (NMDA) receptor antagonist, and has gained popularity for its ability to mimic a wide range of schizophrenia symptoms, including the positive, negative and cognitive deficits. In humans PCP is known to induce symptoms that resemble that of schizophrenia (Luby Ed, 1959, Javitt and Zukin, 1991), as well as exacerbate symptoms in pre-existing sufferers (Luby Ed, 1959, Itil et al., 1967).

A single-dose of PCP can induce many of the positive/negative/cognitive symptoms in rats, including psychosis, delusions, thought disorder, and withdrawal (see Jentsch and Roth, 1999, for review). Acute doses have also been shown to impair prepulse-inhibition (Geyer et al., 1984) – a measure of sensorimotor gating that is known to be disrupted in schizophrenia (Ludewig et al., 2003). In addition, acute (Moghaddam and Adams, 1998) and sub-chronic (Jentsch et al., 1997; Marquis et al., 2007) administration of PCP has been shown to produce delay-dependent deficits in rat performance in a T-maze task, highlighting its ability to disrupt cognitive functions required in these tasks (see 4.2.1: T-Maze Task for a more in-depth discussion on this). Furthermore, executive function deficits have been observed in adult rats following administration of acute (Egerton et al., 2005), sub-chronic and chronic (Egerton et al., 2008) administration of PCP. These deficits were observed through an attentional set-shifting task, which identifies the rodent's ability to shift their attention from one set of stimuli to another. In addition to working memory and executive function deficits, acute PCP in adult rodents has demonstrated a hyper-locomotion behaviour, which has been suggested to be associated with the positive symptoms in schizophrenia (Adams and Moghaddam, 1998, Moghaddam and Adams, 1998). Furthermore, acute PCP has shown to cause deficits in motor

function and motivation in primates (see Jentsch and Roth, 1999, for review), as well as causing increased impulsivity (Gastambide et al., 2013; Thomson et al., 2011). In particular an acute dose of PCP has previously been found to facilitate an increase in anticipatory responding in rats as they performed a 5-choice serial reaction time test (Thomson et al., 2011). Notably, some of the effects of PCP can be blocked with antipsychotic agents (Moghaddam and Adams, 1998, Kargieman et al., 2007). Many of the effects of PCP are more persistent with subchronic or chronic administration (see Jentsch and Roth, 1999, Pratt et al., 2008, for reviews), which are believed to better model the chronic schizophrenia pathology.

Dysfunction of the NMDA receptors have increasingly been linked in the core pathology of schizophrenia (Kantrowitz and Javitt, 2010), which can help explain why PCP is able to model most of its core symptoms. Acting on a number of brain regions including the hippocampus and prefrontal cortex, PCP has previously been shown to result in increased extracellular glutamate levels (Moghaddam and Adams, 1998), presumably through a disinhibition of PFC NMDA receptors. This mirrors findings of increased immediate early gene expression (Gao et al., 1998), as well as increased neural firing (Suzuki et al., 2002) in the same region. More recently, Homayoun and Moghaddam (2007) suggested that NMDA receptor antagonists cause a disinhibition of pyramidal neurons by decreasing the activity of the inhibitory GABAergic interneurons. Furthermore they had shown that following this inhibition, the pyramidal neurons fired at a delayed rate, suggesting a disinhibitory mechanism. Indeed the signalling deficits in parvalbumin-containing GABAergic interneurons that are believed to be a major factor in many of the cognitive deficits in schizophrenia (see Chapter 1 – 1.5.2.3: Role of GABAergic Interneurons in Working Memory – and Evidence for Disruption).

Observations of rat electrocorticogram (ECoG) have revealed dose-dependent increases in EEG power at delta-frequencies (1-4Hz), along with reductions in power at higher frequencies (9-30 Hz) following acute PCP administration (Sebban et al., 2002). This pattern has been shown to shift to more positive values with higher doses ( $> 3\text{mg.kg}^{-1}$  s.c; Sebban et al., 2002). Later studies have shown gamma-activity increases in the rat following acute PCP injections; both in the mPFC

(Chandler, 2010), and following a high-dose; the hippocampus (Ma and Stan Leung, 2000). In addition, Pinault et al., (2008) noted that other NMDA antagonists ketamine and MK-801 dose-dependently increased the power of gamma-rhythms in freely-moving rats by 200-400%. Interestingly they also noted an increased intra-cortical synchronisation of gamma activity at these bands, which they associated with ataxic motor activity. This hyper-synchronisation in gamma activity (from otherwise independent gamma-networks) has been previously proposed to be associated with the positive symptoms of the disease (Spencer et al., 2004, Baldeweg et al., 1998), and recently has been demonstrated *in vitro* in rat visual cortex slices, following administration of PCP (Anver et al., 2011). At present the specific links between aberrant gamma activity and the NMDA-receptor hypofunction mediated by PCP are only vaguely understood.

### **5.2.2 PCP Administered to Rats in a T-Maze Task**

The effects of acute (Moghaddam and Adams, 1998) and sub-chronic (Jentsch et al., 1997, Marquis et al., 2007, Stefani and Moghaddam, 2002) PCP administration has been studied on rats performing either the continuous-alternation or discrete-trials delayed alternation versions of the T-maze task. Moghaddam and Adams (1998) were able to demonstrate a significant impairment in performance of rats undergoing a discrete-trials delayed alternation version of the T-maze task, following acute administration of  $1\text{mg}\cdot\text{kg}^{-1}$  and  $5\text{mg}\cdot\text{kg}^{-1}$  i.p. PCP. This performance deficit was noted as a significantly reduced percentage of correct responses relative to a baseline performance, and was significant at both the 10- and 40-second intra-trial delay periods. Interestingly these researchers noticed that co-administration of the NMDA receptor agonist LY354740 with  $5\text{mg}\cdot\text{kg}^{-1}$  PCP reversed this deficit, thus highlighting that a deregulation in glutamate is central to the PCP-mediated working memory deficits. Mixed findings have been revealed however regarding the use of sub-chronic PCP administration in rats, which are believed to be a consequence of the type of T-maze task being performed. Jentsch et al., (1997) revealed deficits in the performance of rats pre-treated with PCP for 14 days at  $10\text{mg}\cdot\text{kg}^{-1}$  i.p. PCP on a continuous alternation T-maze task, when tested 2 to 12 days following PCP

withdrawal. By contrast no significant effects of PCP pre-treatment were found on rats performing the discrete-trials version of the task, when rats were pre-treated with two daily injections of  $5\text{mg}\cdot\text{kg}^{-1}$  i.p. PCP for 5 days, and tested 9 days following the final injection (Stefani and Moghaddam, 2002). In an attempt to verify these findings, Marquis et al., (2007) pre-treated rats with 14 daily injections of  $10\text{mg}\cdot\text{kg}^{-1}$  i.p. PCP, and tested them on either the continuous or discrete version of the T-maze task after 2 days of the final injection. The results of this study corroborates both sets of earlier findings (Stefani and Moghaddam, 2002, Jentsch et al., 1997) by revealing deficits in performance of the group performing the continuous alternation version of the task, but not in the group performing the discrete-trials version of the task (as compared to saline-treated controls). Thus the effects of sub-chronic PCP were found to be sensitive to parameters used in the T-maze task.

## 5.3 Aims and Rationale

### 5.3.1 Rationale

In rodents the NMDA receptor antagonist phencyclidine (PCP) has gained popularity for its ability to model many of the core symptoms of schizophrenia (see Jentsch and Roth, 1999, Pratt et al., 2008 for reviews). In particular, an acute dose of PCP has been demonstrated to facilitate spatial working memory deficits in rodents (Moghaddam and Adams, 1998). Much can be gained by recording and analysing rodent local-field potentials (LFPs) following a dose of PCP, since it may provide a link between these reported working memory deficits, and electrophysiological correlates of working memory function that have previously been observed in rodents (e.g. Jones and Wilson, 2005, Benchenane et al., 2010, Sigurdsson et al., 2010).

To date there hasn't been a study which combines the effects of PCP and deep-brain stimulation (DBS) in a behavioural paradigm. Such a study can provide a number of interesting observations including a) the effect of PCP on rodent LFP during a behavioural task, and b) the effects of DBS on PCP-treated rodents. The fimbria-fornix (FF) is one of a number of brain regions which may provide a therapeutic benefit in cognitive disorders such as schizophrenia (see Chapter 1 - 1.5.6: Candidate Brain Regions for DBS in Schizophrenia). For now, its effects can be observed in a behavioural task involving rodent models of relevance to schizophrenia. Furthermore, by combining this with LFP recordings, a greater insight can be made into the functional interactions between brain regions, and how they correlate to behavioural performance.

### 5.3.2 Aims

The aims of this study were as follows:

- a) Characterise the behavioural performance and LFP in freely-moving, PCP-treated rodents as they undertake a working memory task; with and without the influence of FF-DBS.



b) Compare performance and LFP of PCP-treated rats, with that obtained from the saline-treated rats (from Chapter 4).

This study forms the “drug” condition of the behavioural task that was outlined in Chapter 4. As such rats are trained in a working memory task, after which they are tested under the influence of acute PCP. DBS (or sham-DBS) is administered throughout the task, and LFP recordings are made in conjunction with measures of rat behavioural performance. After characterising differences between stimulation and sham-stimulation PCP groups, this chapter then extends the results section by comparing the data between the PCP-treated rats in this chapter, and the saline-treated rats in Chapter 4, in order to build a more complete picture of the effects of FF-DBS and PCP in the working memory task.

## 5.4 Materials and Methods

This task forms the “drug” condition of the behavioural task that is described in Chapter 4. Rats were separated into two groups on the basis of whether they had received bilateral DBS during the intra-trial delay of the task, or whether they had received sham-stimulation (absence of stimulation but with DBS electrodes implanted). The difference here is that rats were given an acute injection of PCP ( $3\text{mg}\cdot\text{kg}^{-1}$  i.p) prior to the first two post-training test sessions, instead of the saline injection which was given to the stimulation and sham-stimulation experimental groups in Chapter 4. In this case the third test day is the washout day, where animals were omitted an injection of PCP. Whilst the reader is advised to refer to Chapter 4 for an overview of the experimental methodology, additional analysis techniques and differences between this and the previously described behavioural task methodology are highlighted in this chapter. The analysis in this chapter is based on the post-training test phases (Chapter 4 details the training performance in all rats from both the drug and vehicle groups). All procedures in this study were carried out in accordance with the Animals Scientific Procedures Act (1986).

### 5.4.1 Rat Groups and Experiment Overview

In the post-training test sessions involving PCP, there were 7 male Lister Hooded rats (Harlan UK Ltd; weighing between 350-375g at time of surgery) which were separated into the sham-stimulation ( $n=4$ ) and stimulation ( $n=3$ ) groups (see Chapter 4 – figure 4.1 for an illustration of the rat group organisation – rats in this chapter are highlighted in the figure as “drug groups”). All of the animal handling, surgery, training, post-training testing, perfusion, and histology procedures are the same as that described in Chapter 4, with the exception that the animals analysed in this chapter received an acute injection of PCP prior to the first two post-training test sessions of the T-maze behavioural task – instead of saline. Furthermore, the experimental timeline is as shown in Chapter 4 – figure 4.3. Once again rats in the stimulation group had received bilateral DBS during both the training and post-training test phases, which took place during the 30-second intra-trial delay period

(see Chapter 4 – 4.4.3: T-Maze Task). In this chapter the data from the third post-training test day (washout day) is also looked at in order to observe the changes that occur following a 3-day abstinence of PCP.

## **5.4.2 Analysis of Results**

The power-spectral density (PSD) and coherence analysis that is carried out between the stimulation and sham-stimulation groups have been previously described (see Chapter 4 – 4.4.8.5: Task-Phase PSD and Coherence Changes). Analysis of the PCP-treated rat groups is more comprehensive in this study, since the data from the third (washout) test day is compared with the first two (drug) test days. Data from the first two test days are averaged together in each rat, and 2-way repeated measures ANOVAs are used to compare the PSD and coherence from the stimulation and sham-stimulation groups of rats, both in the T-maze and in the holding pen (during the inter-trial delay periods). The repeated variable in this case is test day (drug or washout).

In a separate analysis, post-training electrophysiological data from the PCP-treated rats in this chapter are then compared with the saline-treated rats from Chapter 4, using a 2-way ANOVA to test for effects of stimulation (vs sham-stimulation) and PCP (vs. saline). In addition to this analysis, the PSD changes at the T-maze choice-point (between forced-/correct-/incorrect-maze runs) are observed between all 4 groups of rats, as well as the theta centre-frequency changes that occur between each of the different task phases.

### **5.4.2.1 PSD Changes at the T-maze Choice Point**

A separate analysis was carried out at the T-maze choice-point, to discern PSD differences between the forced, choice-correct, and choice-incorrect task phases in both the PCP and saline-treated groups of rats. PSD estimates were calculated for each individual 1-second choice-point segment (corresponding to individual maze-runs) using 3 leading data tapers; and the results were normalised by dividing by the

root-mean-square PSD obtained from the averaged PSD estimate obtained from all of the forced-turn segments for that particular session (figure 5.1A). For each rat, average normalised PSD estimates for mPFC and dCA1 were derived for each recording session and combined with the rest in its respective rat group based on the forced-turn, choice-correct and choice-incorrect maze runs (figure 5.1B). For statistical comparisons, two frequency bands were isolated: theta (7-12 Hz), and gamma (45-100 Hz). The peak theta and gamma activity were extracted from these frequency bands, and 3-way ANOVAs were utilised to observe effects of stimulation (vs. sham-stimulation), PCP (vs. saline), and task phase (forced/correct/incorrect maze runs) on theta and gamma activity, in each brain region.

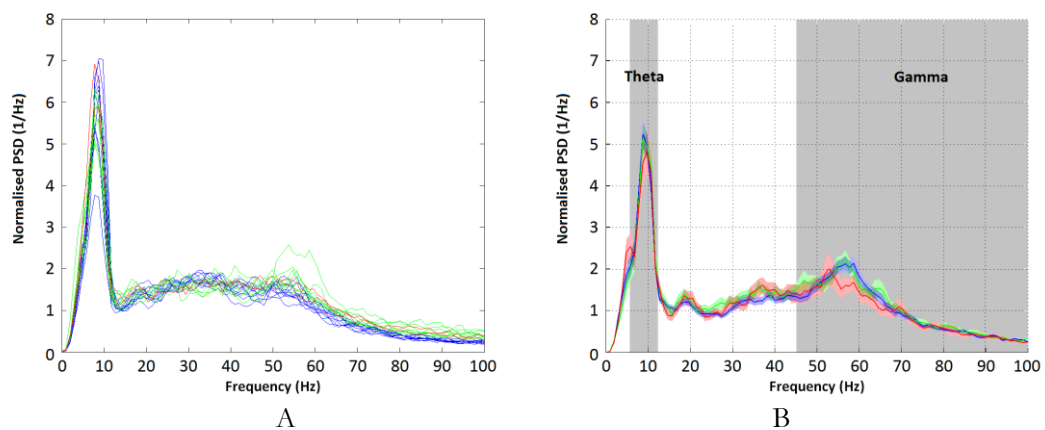


Figure 5.1 – PSD estimates are shown for a single rat session in (A), with forced-turn estimates in blue, choice-turn (correct) in green, and choice-turn (incorrect) in red. Each curve in (A) is derived from an individual maze run. An average reading for these three task phases were taken for each electrode location, and combined with the rest of the rat group to produce a group average estimate (B). The frequency range in which peak theta and peak gamma is considered is also shown in (B), as regions highlighted in grey.

#### 5.4.2.2 Hippocampal Theta-Frequency Changes

Changes in the hippocampal peak theta frequency were measured in a number of experimental situations including the baseline recordings (both pre- and post-injection), intra- and inter-trial delays, and the forced, correct and incorrect T-maze runs during habituation and testing. For each recording session, average hippocampal signals were derived for each hippocampal electrode from each of the

task phases using a 1024-point PSD function in Matlab. From this, a single average dCA1 signal was derived from each rat session, and combined with the rest of the rat group. In a manner similar to analysis looking at % change in PSD/coherence (see 5.4.2.1: PSD Changes at the T-Maze Choice Point), data from the first two days are averaged together to produce a single reading for each rat. These averaged signals were truncated between 6 – 12 Hz, and placed through a standard smoothing filter to allow the centre-frequency of the hippocampal theta peak to be extracted.

Statistics were calculated by utilising 2- and 3-way ANOVA's with factors task phase (forced-turn, choice-correct, choice-incorrect), test day (drug, washout, and habituation), delivery of drug or vehicle, and delivery of electrical stimulation or sham stimulation.

## 5.5 Results

### 5.5.1 Rat Performance in the T-Maze Task

Rats that obtained a correct training score of 7/10 in three consecutive training sessions were advanced to the post-training test phase. An acute injection of PCP ( $3\text{mg}\cdot\text{kg}^{-1}$  i.p) was administered to both groups of rats on the first two test days, but not during the washout test day. This injection was administered following the 15-minute baseline recording period (5-minutes prior to starting the T-maze task).

Generally speaking no clear differences could be observed between the stimulation and sham-stimulation groups of rats during either of the three test days (table 5.1). Unpaired t-tests were used to look for significant differences between the mean training scores between both groups of rats on each of the three test days (figure 5.2), with no significant differences found. Notably, a large variation in the post-training scores were observed, which in this case ranged from 2/10 to 10/10.

	Test 1	Test 2	Washout
Sham	5	4	7
	8	7	6
	7	5	6
	8	5	8
Stim	6	8	5
	6	6	5
	2	10	9

Table 5.1 – Summary of rat scores during the post-training test sessions. Green shading highlights a score of 7/10 or greater, whereas yellow shading refers to scores of <7. Rat groups are sham-stimulation (Sham), and stimulation (Stim). Both groups of rats were pre-treated with an acute injection of PCP ( $3\text{mg}\cdot\text{kg}^{-1}$  i.p) prior to the post-training test phase.

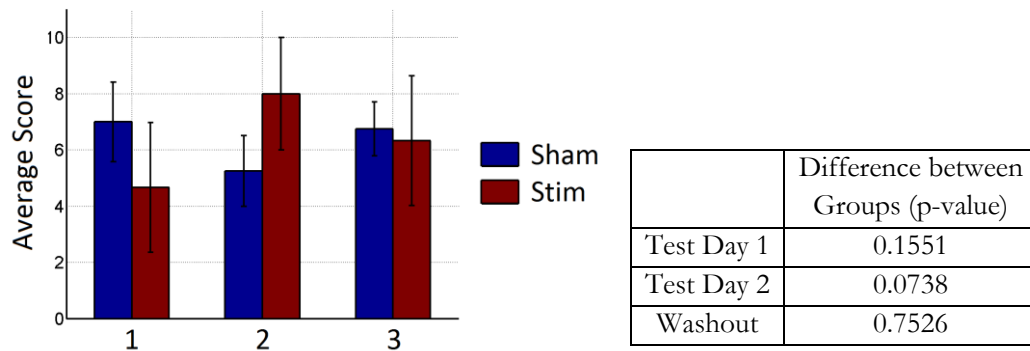
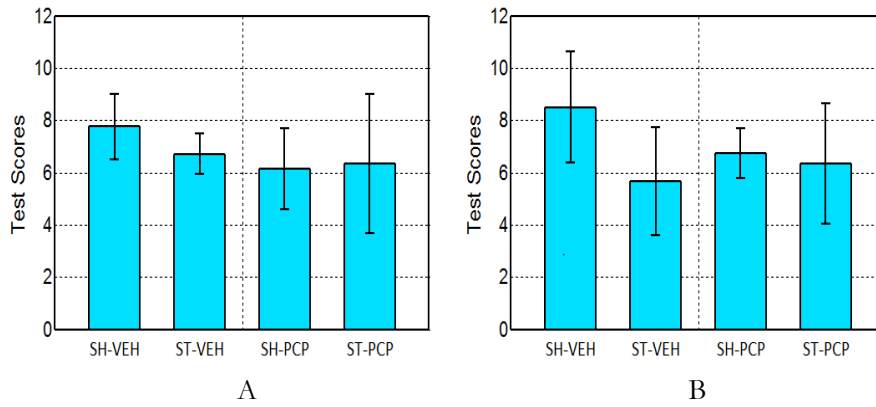


Figure 5.2 – Bar plot (left) shows the average test scores for the sham-stimulation (blue) and stimulation (brown) groups during the post-training test days 1, 2 and 3 (the latter being the washout test day),  $\pm$  SEM. Both groups of rats were pre-treated with an acute injection of PCP ( $3\text{mg}\cdot\text{kg}^{-1}$  i.p) prior to the post-training test phase. Unpaired t-tests were used to assess whether group scores were significantly different on either of the test days (right). No significant differences were found in the mean rat score between the stimulation and sham-stimulation groups on any of the post-training test days.

### 5.5.1.1 Comparison of Behavioural Performance between the Saline and PCP-Treated Groups

The behavioural performance of the PCP-treated rats in this chapter was compared with the saline-treated rats from Chapter 4. Differences between rat scores on the averaged drug/saline and washout test days were assessed using a 2-way ANOVA, which looked for effects of stimulation or PCP for each test type. No significant effects of treatment with stimulation or PCP were found in any of the rat groups, for either of the drug or washout test days (figure 5.3).



	DRUG			WASHOUT		
	F	p	sig	F	p	sig
Treat (STIM/SHAM)	0.35	0.5617		2.24	0.1725	
Drug (PCP/VEH)	2.04	0.1675		0.25	0.631	
Treat x Drug	0.79	0.3853		1.24	0.2977	

(\* p < 0.05), (\*\* p < 0.01), (\*\*\*) p < 0.001, (\*\*\*\* p < 0.0001)

C

Figure 5.3 – Rat mean scores are displayed for the drug (A) and washout (B) test days,  $\pm$  SEM. No clear difference between any of the rat groups can be observed, or a significant effect of stimulation or PCP on either the drug or washout test days (C). Experimental groups were sham-vehicle (SH-VEH), stimulation-vehicle (ST-VEH), sham-PCP (SH-PCP), and stimulation-PCP (ST-PCP).

### 5.5.2 Gamma-Power Increases in mPFC Following PCP Injection

Medial prefrontal cortex (mPFC) PSD spectrograms are shown for the PCP-treated stimulation and sham-stimulation groups of rats, during the post-training test days that included the use of PCP, and also during the washout test day (figure 5.4). A striking elevation in gamma-frequency PSD can be seen in both groups of rats, which appears to be elevated between 400-600% during the inter-trial delay periods, and 700-900% when the animals are inside the T-maze (figure 5.5). Notably this gamma-frequency increase is seen to reduce markedly during the washout test day (figure 5.5). A repeated-measures 2-way ANOVA between the groups of rats revealed a significant effect of test day (PCP vs. washout) on gamma-frequency PSD, which was observed in both the holding pen ( $p=0.0066$ ) and T-maze ( $p=0.0057$ ) recordings (figure 5.6). In addition, a significant effect of test day was seen for



mPFC theta-frequency PSD, when measured inside the holding pen ( $p=0.0475$ ), but not when measured inside the T-maze ( $p=0.208$ ). This can be observed as a slight reduction in theta-frequency PSD (relative to baseline) in the holding-pen PSD. Finally, both groups of rats had shown significant increases in theta and gamma-frequency PSD relative to baseline, on both the drug and washout test days, as measured using unpaired t-tests (table 5.2).

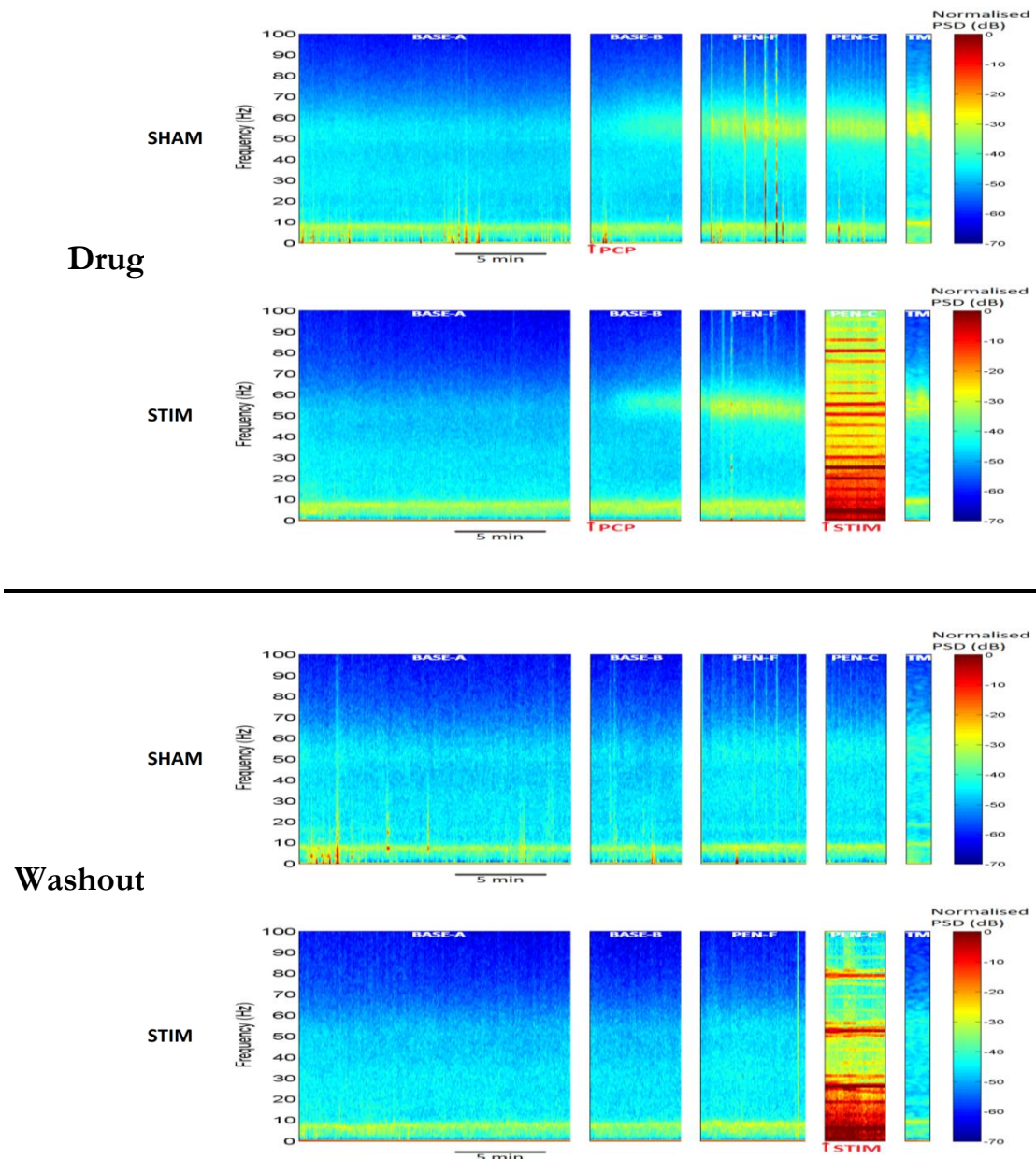


Figure 5.4 – Log spectrograms for mPFC power in each of the groups of rats during both the drug (top) and washout (bottom) post-training test days. The following task phases are shown: BASE-A: baseline at 0-15 minutes, BASE B: post-PCP injection (pre-test) period at 15-20 minutes, PEN-F: inter-trial delay, PEN-C: intra-trial delay, TM: T-maze choice-point. Experimental groups were sham-stimulation (SHAM) and stimulation (STIM). The application of PCP and stimulation is shown by the red arrows below the plots. Note the presence of stimulation artefacts during the intra-trial delay period (PEN-C) in the STIM rat group – a feature which is present for this rat groups in all subsequent spectrogram/coherograms plots. A striking feature in both PCP-treated groups is a marked increase in gamma-band activity, which appears a couple of minutes following an injection of PCP. This is seen to persist throughout the task, whereby it reaches its maximum intensity during the T-maze segments (TM). Note that these gamma-frequency increases are not present to the same extent in the washout test day spectrograms.

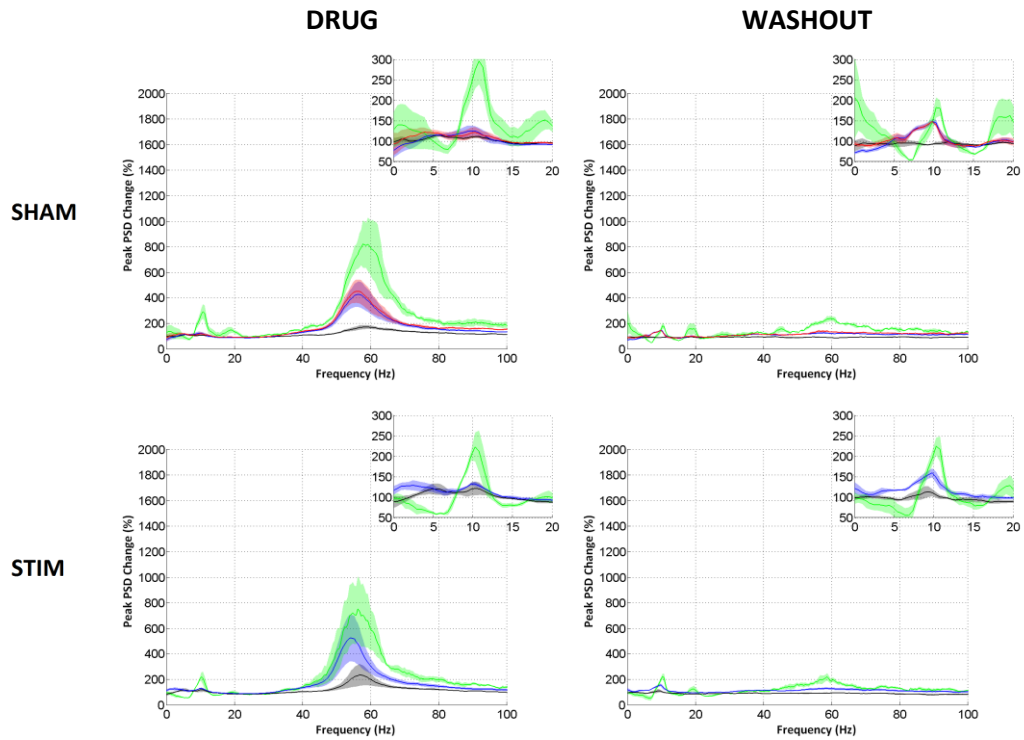


Figure 5.5 – Changes in mPFC PSD for each of the task phases during both the drug and washout post-training test days, are shown as a percentage of their recorded 0-15 minute baseline value (BASE-A)  $\pm$  1/2 SEM; green = T-maze choice-point (TM), blue = inter-trial delays (PEN-F), red = intra-trial delays (PEN-C), black = post-injection, pre-test phase (BASE-B). A magnified part of the waveform (50-300%) is shown in the inset. Experimental groups were sham-stimulation (SHAM) and stimulation (STIM). Theta and gamma activity was seen to reach their maximum power in both rat groups during the T-maze task phases (green). Note the large increases in gamma activity in both groups of rats during the drug-administration test day, as compared to the washout test day.

Drug	Peak Theta Change	Peak Gamma Change	n
SHAM	0.0181	0.0165	4
STIM	0.0437	0.0451	3

Washout	Peak Theta Change	Peak Gamma Change	n
SHAM	0.0245	0.0075	3
STIM	0.0204	0.0267	3

Table 5.2 – T-tests were used to assess whether mPFC peak theta and gamma activity at the T-maze choice-point (TM) was significantly elevated with respect to the pre-injection baseline recording (BASE-A), both the drug and washout test days. Numbers in the table denote p-values corresponding to whether the observed peak theta/gamma PSD was significantly elevated from baseline, with green values indicating statistical significance at  $p < 0.05$ . The final column (n) indicates the sample size per t-test. Experimental groups were sham-stimulation (SHAM), and stimulation (STIM).

### Peak Theta

	PEN-F			TM		
	F	p	sig	F	p	sig
Stim	0.73	0.4145		0.16	0.7	
Test Day	5.26	0.0475	*	1.84	0.208	
Stim x Day	0.05	0.8224		1.99	0.1916	

### Peak Gamma

	PEN-F			TM		
	F	p	sig	F	p	sig
Stim	0.31	0.5922		0.03	0.8715	
Test Day	12.35	0.0066	**	12.99	0.0057	**
Stim x Day	0.32	0.583		0	0.962	

(\* p < 0.05), (\*\* p < 0.01), (\*\*\*) p < 0.001, (\*\*\*\* p < 0.0001)

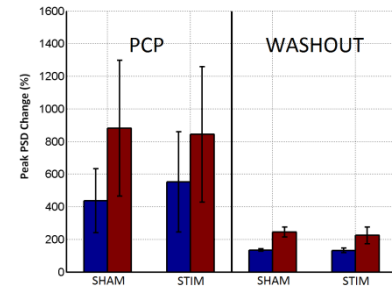
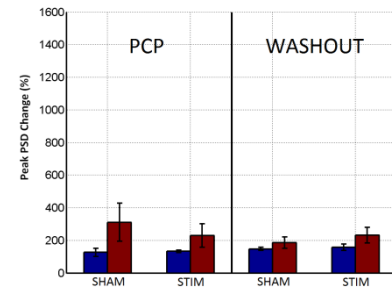


Figure 5.6 - Differences in mPFC peak theta and gamma power during the post-training test phase was analysed between the stimulation and sham-stimulation groups of rats using 2-way repeated-measures ANOVAs (with drug/washout test day as the repeated measure). Plots to the right depict the corresponding peak PSD change,  $\pm$  SEM; blue = inter-trial delay (PEN-F), brown = T-maze choice-point (TM). Experimental groups were sham-stimulation (SHAM), and stimulation (STIM). A significant effect of test day (PCP) was found for gamma-frequency PSD, which was evident both inside the holding pen and inside the T-maze. A smaller but significant effect of test day was also seen for mPFC theta PSD, when measured inside the holding pen (but not inside the T-maze).

### 5.5.3 Gamma-Power Increases in dCA1 Following PCP Injection

Hippocampal dCA1 PSD spectrograms are shown for the 2 groups of rats during the post-training test days that included the use of PCP (figure 5.7). A 2-way repeated measures ANOVA on dCA1 gamma power revealed a significant effect of test day (PCP vs. washout), both during the inter-trial delay periods inside the holding pen ( $p=0.0301$ ), and during the T-maze segments at the choice-point ( $p=0.009$ ). This can be observed as a marked elevation in gamma-frequency PSD in both groups of rats during the drug test day, when compared to the washout test day (figure 5.7). Note that these gamma-frequency changes may not be apparent on the PSD spectrograms (figure 5.7) due to its logarithmic colour scale (see figures 5.8 – 5.9 instead). These gamma-frequency elevations appear to be higher in frequency than that observed under the same conditions in the mPFC (see figure 5.5), with a centre frequency of  $\sim 80\text{Hz}$  (as opposed to  $\sim 55\text{Hz}$  in the mPFC).

In a similar manner to the findings in the mPFC, theta-frequency PSD was seen to be reduced in dCA1 in both groups of rats during the inter-trial delay periods, but not during the T-maze choice-point segments. This is reflected as a significant effect of test day on inter-trial delay period theta activity ( $p=0.001$ ), as measured using a 2-way repeated measures ANOVA.

When comparing the T-maze dCA1 PSD with that of the baseline recordings, both groups of rats had shown a significant increase in both theta and gamma-frequency activity, which was observed on both the drug and washout test days (table 5.3).

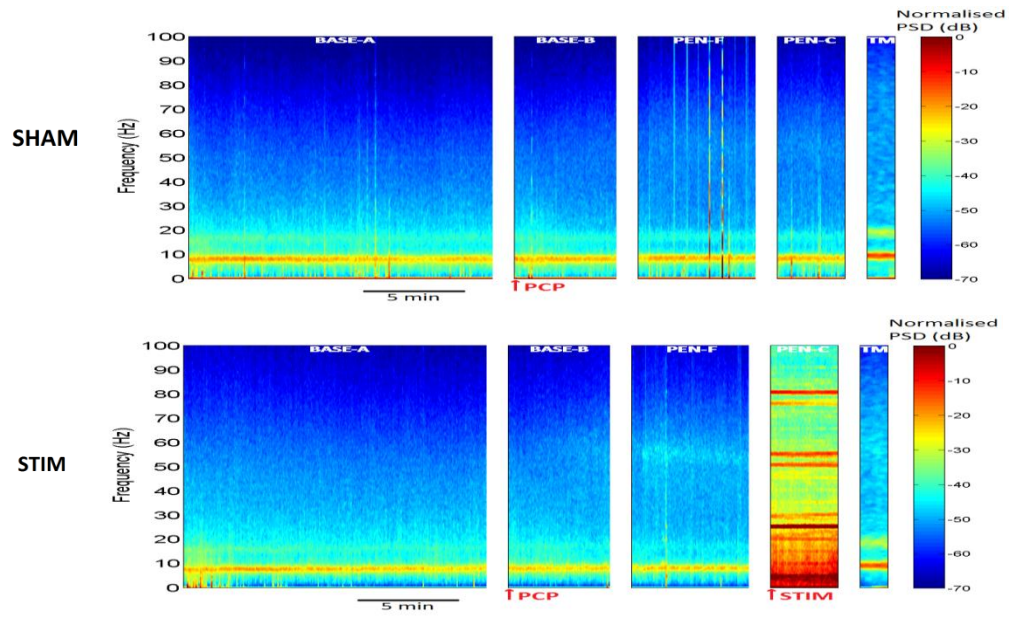


Figure 5.7 – Log spectrograms for dCA1 power in each of the groups of rats during the post-training test phase. The following task phases are shown: BASE-A: baseline at 0-15 minutes, BASE B: post-PCP injection (pre-test) period at 15-20 minutes, PEN-F: inter-trial delay, PEN-C: intra-trial delay, TM: T-maze choice-point. Experimental groups were sham-stimulation (SHAM) and stimulation (STIM). The application of PCP and stimulation is shown by the red arrows below the plots. Theta-frequency PSD appears to be elevated in both groups of rats when placed inside the T-maze (TM).

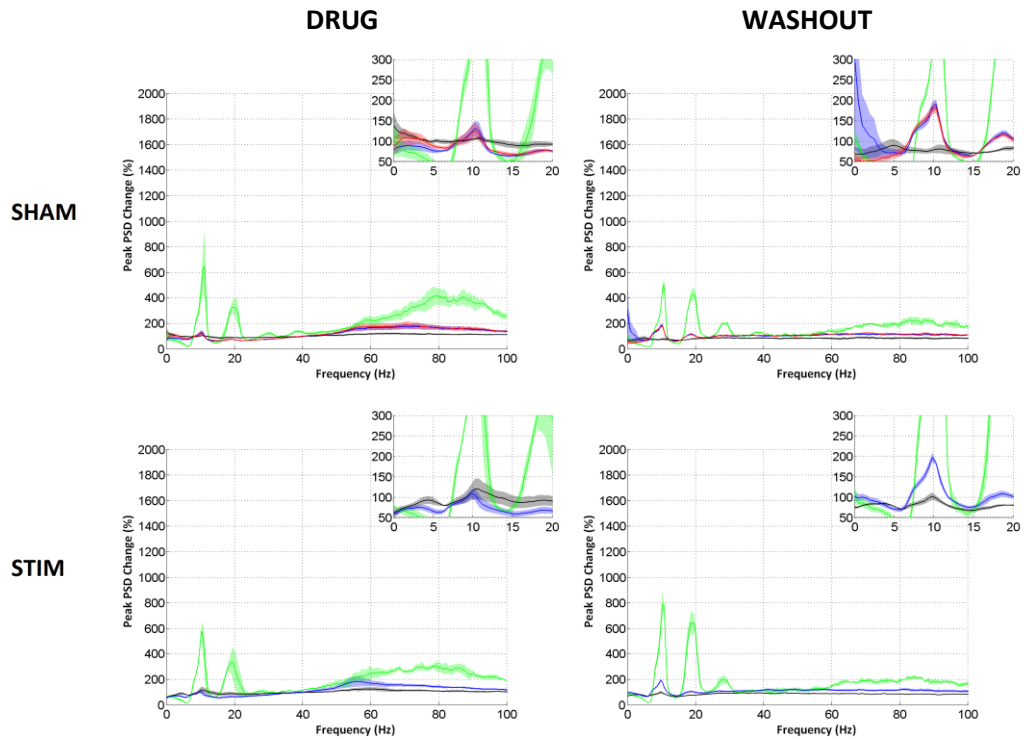


Figure 5.8 – Changes in dCA1 PSD for each of the task phases during both the drug and washout post-training test days, are shown as a percentage of their recorded 0-15 minute baseline value (BASE-A)  $\pm$  1/2 SEM; green = T-maze choice-point (TM), blue = inter-trial delays (PEN-F), red = intra-trial delays (PEN-C), black = post-injection, pre-test phase (BASE-B). A magnified part of the waveform (50-300%) is shown in the inset. Experimental groups were sham-stimulation (SHAM) and stimulation (STIM). Similar to the findings in the mPFC, theta and gamma activity was seen to reach their maximum power in both groups of rats during the T-maze task phases (green). The mean elevations in gamma-frequency activity are exacerbated in both groups during the drug-administration test days, as opposed to the washout test day.

Test	Peak Theta Change	Peak Gamma Change	n
SHAM	0.0372	0.0063	4
STIM	0.0083	0.0053	3

Washout	Peak Theta Change	Peak Gamma Change	n
SHAM	0.0084	0.0138	3
STIM	0.0030	0.0026	3

Table 5.3 – T-tests were used to assess whether dCA1 peak theta and gamma activity at the T-maze choice-point (TM) was significantly elevated with respect to the pre-injection baseline recording (BASE-A), both the drug and washout test days. Numbers in the table denote p-values corresponding to whether the observed peak theta/gamma PSD was significantly elevated from baseline, with green values indicating statistical significance at  $p < 0.05$ . The final column (n) indicates the sample size per t-test. Experimental groups were sham-stimulation (SHAM), and stimulation (STIM).

### Peak Theta

	PEN-F			TM		
	F	p	sig	F	p	sig
Stim	0.18	0.6782		0.4	0.5415	
Test Day	22.68	0.001	**	0	0.9865	
Stim x Day	1.49	0.2531		1.99	0.1922	

### Peak Gamma

	PEN-F			TM		
	F	p	sig	F	p	sig
Stim	0.06	0.8177		1.44	0.261	
Test Day	6.61	0.0301	*	10.98	0.009	**
Stim x Day	0.02	0.8817		1.32	0.2807	

(\* p < 0.05), (\*\* p < 0.01), (\*\*\*) p < 0.001, (\*\*\*\* p < 0.0001)

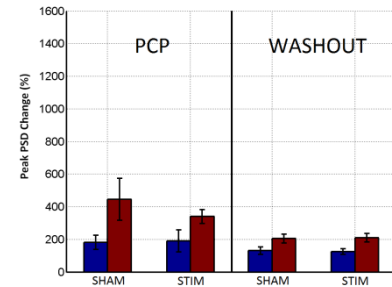
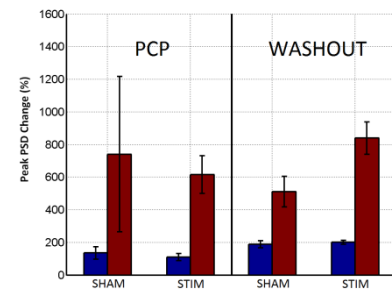


Figure 5.9 – Differences in dCA1 peak theta and gamma power during the post-training test phase was analysed between the stimulation and sham-stimulation groups of rats using 2-way repeated-measures ANOVAs (with drug/washout test day as the repeated measure). Plots to the right depict the corresponding peak PSD change,  $\pm$  SEM; blue = inter-trial delay (PEN-F), brown = T-maze choice-point (TM). Experimental groups were sham-stimulation (SHAM), and stimulation (STIM). Significant effects of test day (PCP) were observed for gamma-frequency PSD (inside the holding pen and T-maze), and also for theta-frequency PSD (inside the holding pen only).

### 5.5.4 Summary of PSD Changes

In summary, both groups of rats had demonstrated elevated theta and gamma-frequency PSD when inside the T-maze (as compared to the baseline recording), and this was apparent during both the drug and washout test days. When comparing the LFP from the drug and washout test sessions, an acute dose of PCP was seen to significantly elevate gamma-frequency PSD in both the mPFC and dCA1 brain regions. Furthermore, these increases were observed in both groups of rats during the inter-trial delay periods (with rats inside the holding pen), and during the T-maze runs (with rats at the T-maze choice-point). Interestingly, both brain regions had also displayed a marked reduction in theta-frequency PSD following PCP administration (as compared to washout), which was observed in both groups of rats during the inter-trial delay periods, but not during the T-maze segments. No effect of DBS was observed in any of the statistical tests performed, and no interactions between test day and DBS was found.



### **5.5.5 Prefrontal-Hippocampal Coherence Reductions in PCP-Treated Rats**

Coherograms depicting ipsilateral mPFC-dCA1 coherence are shown for both the sham-stimulation and stimulation groups of rats during the post-training test days that included the use of PCP (figure 5.10). Theta-frequency coherence appeared to reach its maximum in both groups of rats during the T-maze segments (figure 5.11), with no significant differences observed between the drug and washout test days. However when considering the theta-frequency coherence during the inter-trial delay periods, both groups of rats had shown a marked reduction in coherence during the drug test day, as compared to that seen during washout. This is reflected by a significant effect of test day (PCP vs. washout) on theta-frequency coherence when measured inside the holding pen ( $p=0.0027$ ; figure 5.12). A direct comparison between the T-maze theta-coherence and baseline theta-coherence had revealed significant increases in both groups during the drug test day and in the stimulation group during the washout test day (as assessed using unpaired t-tests). Finally, no effects of DBS (or interactions with DBS) were found on mPFC-dCA1 in either of the groups of rats.

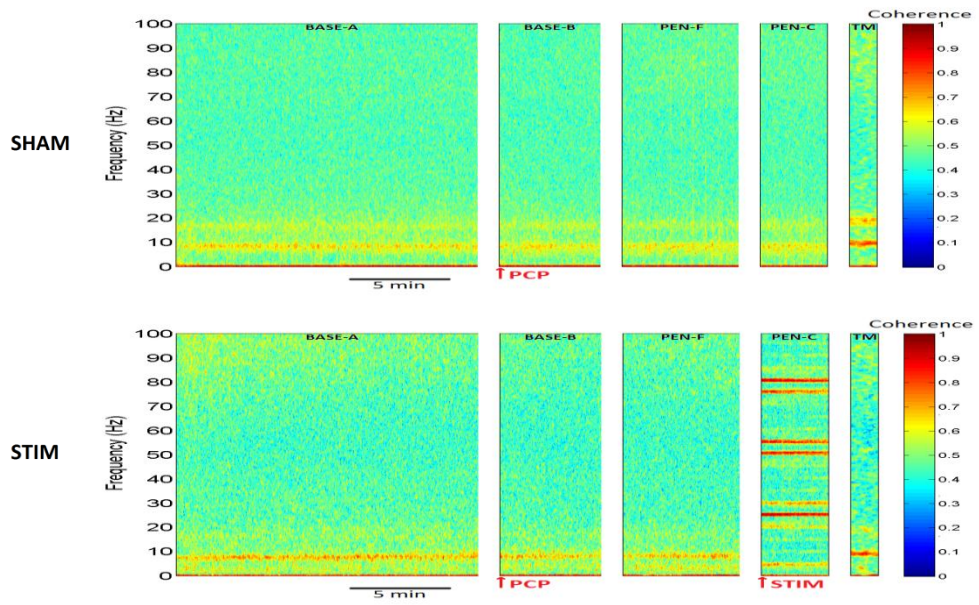


Figure 5.10 – Log coherograms for mPFC-dCA1 coherence in each of the groups of rats during the post-training test phase. The following task phases are shown: BASE-A: baseline at 0-15 minutes, BASE B: post-PCP injection (pre-test) period at 15-20 minutes, PEN-F: inter-trial delay, PEN-C: intra-trial delay, TM: T-maze choice-point. Experimental groups were sham-stimulation (SHAM) and stimulation (STIM). The application of PCP and stimulation is shown by the red arrows below the plots. Note the increase in mPFC-dCA1 theta-frequency coherence in the T-maze segments (TM).

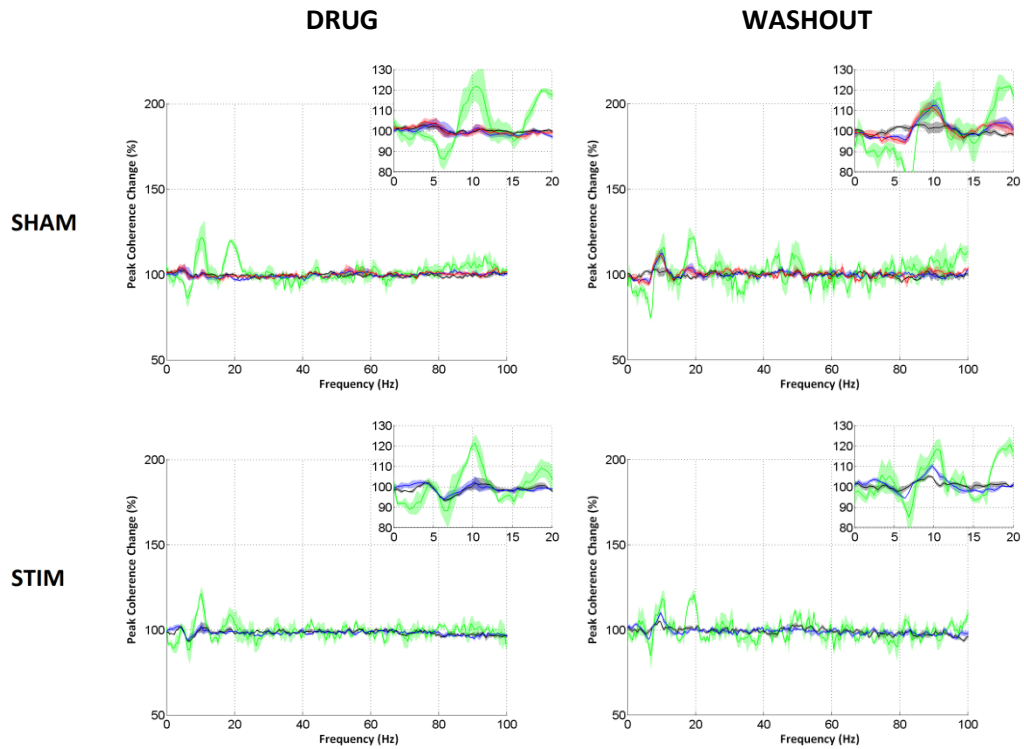


Figure 5.11 – Changes in mPFC-dCA1 coherence for each of the task phases during both the drug and washout post-training test days, are shown as a percentage of their recorded 0-15 minute baseline value (BASE-A)  $\pm$   $\frac{1}{2}$  SEM; green = T-maze choice-point (TM), blue = inter-trial delays (PEN-F), red = intra-trial delays (PEN-C), black = post-injection, pre-test phase (BASE-B). A magnified part of the waveform (80-130%) is shown in the inset. Experimental groups were sham-stimulation (SHAM) and stimulation (STIM). Similar to the findings in the mPFC, theta and gamma activity was seen to reach their maximum power in both groups of rats during the T-maze task phases (green). However theta-frequency coherence appears to be reduced following an acute dose of PCP, when measured during the task delay periods.

Test	Peak Theta Change	Peak Gamma Change	n
SHAM	0.0337	0.0158	4
STIM	0.0084	0.0204	3

Washout	Peak Theta Change	Peak Gamma Change	n
SHAM	0.0934	0.0075	3
STIM	0.0269	0.0023	3

Table 5.4 – T-tests were used to assess whether mPFC-dCA1 peak theta and gamma coherence at the T-maze choice-point (TM) was significantly elevated with respect to the pre-injection baseline recording (BASE-A), both the drug and washout test days. Numbers in the table denote p-values corresponding to whether the observed peak theta/gamma PSD was significantly elevated from baseline, with green values indicating statistical significance at  $p < 0.05$ . The final column (n) indicates the sample size per t-test. Experimental groups were sham-stimulation (SHAM), and stimulation (STIM).

### Peak Theta

	PEN-F			TM		
	F	p	sig	F	p	sig
Stim	0.55	0.4789		0	0.9726	
Test Day	16.84	0.0027	**	0.64	0.4452	
Stim x Day	0.38	0.5526		0.15	0.7088	

### Peak Gamma

	PEN-F			TM		
	F	p	sig	F	p	sig
Stim	5.07	0.0509		2.37	0.1584	
Test Day	0.71	0.4205		1.29	0.2852	
Stim x Day	1.71	0.2236		0.06	0.8177	

(\* p < 0.05), (\*\* p < 0.01), (\*\*\*) p < 0.001, (\*\*\*\* p < 0.0001)

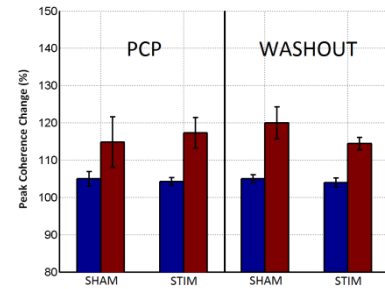
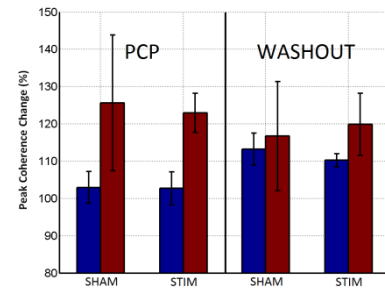


Figure 5.12 – Differences in mPFC-dCA1 peak theta and gamma coherence during the post-training test phase was analysed between the stimulation and sham-stimulation groups of rats using 2-way repeated-measures ANOVAs (with drug/washout test day as the repeated measure). Plots to the right depict the corresponding peak PSD change,  $\pm$  SEM; blue = inter-trial delay (PEN-F), brown = T-maze choice-point (TM). Experimental groups were sham-stimulation (SHAM), and stimulation (STIM). A significant effect of test day (PCP) was observed for theta-frequency coherence, for rats recorded inside the holding pen.

### 5.5.6 Cortical Gamma Hyper-Synchrony

Coherograms depicting contralateral mPFC-mPFC coherence are shown for each of the 2 groups of rats during the post-training test days that included the use of PCP (figure 5.13). Using a 2-way repeated measures ANOVA, significant effects of test day (drug vs. washout) were found both for theta-frequency ( $p=0.0374$ ) and gamma-frequency ( $p=0.0228$ ) coherence (figure 5.15). These observations were only significant for recordings made inside the holding pen, and manifested as a reduced theta-coherence, as well as increased gamma coherence; in both groups of rats. Notably the gamma-frequency coherence is markedly increased during the drug test day, as compared to that seen during the washout test day (figure 5.14). No significant differences between the test days and test groups were noted for recordings made inside the T-maze, perhaps due to the large variation in theta-/gamma-coherence observed. Also, no significant effects of test group (stimulation vs. sham-stimulation) were observed on theta-/gamma-coherence at any parts of the task. Unlike the other PSD and coherence analysis, this analysis featured a lower sample number in the sham-stimulation group ( $n=3$ ) because one rat which didn't have mPFC electrodes correctly implanted bilaterally was excluded from this analysis type. The holding-pen gamma-frequency coherence increases were seen to be diminished during the washout test day.

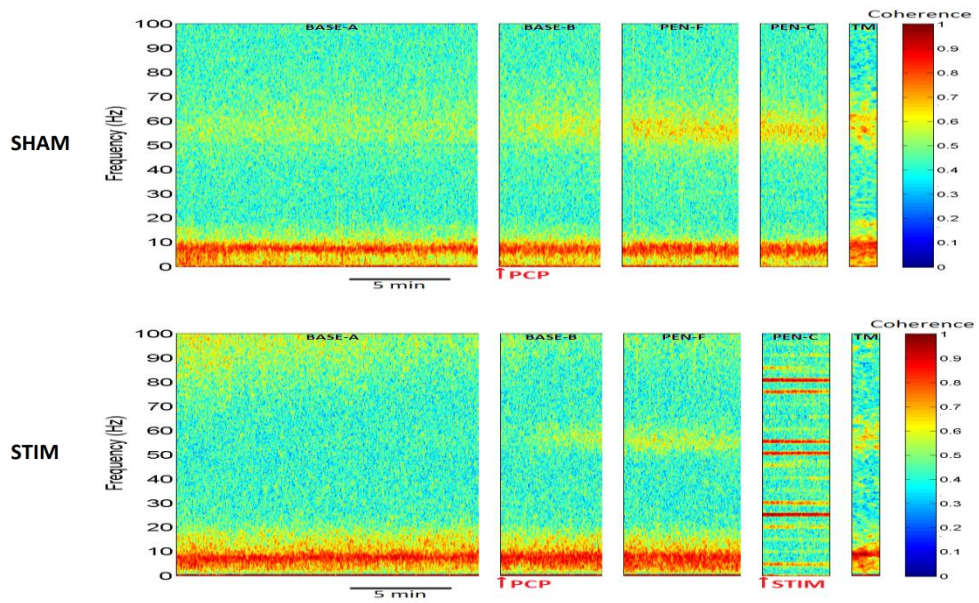


Figure 5.13 – Log coherograms for mPFC-dCA1 coherence in each of the groups of rats during the post-training test phase. The following task phases are shown: BASE-A: baseline at 0-15 minutes, BASE B: post-PCP injection (pre-test) period at 15-20 minutes, PEN-F: inter-trial delay, PEN-C: intra-trial delay, TM: T-maze choice-point. Experimental groups were sham-stimulation (SHAM) and stimulation (STIM). The application of PCP and stimulation is shown by the red arrows below the plots. Note the increased gamma-frequency coherence that occurs following the onset of PCP administration, which persists throughout the task.

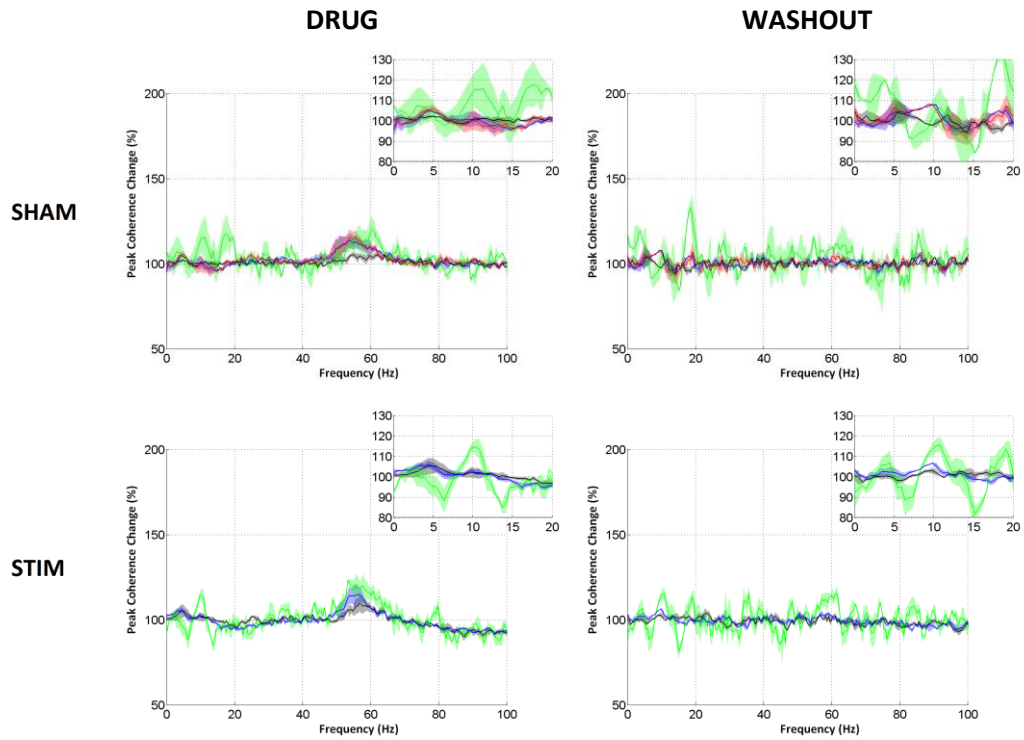


Figure 5.14 – Changes in mPFC-mPFC coherence for each of the task phases during both the drug and washout post-training test days, are shown as a percentage of their recorded 0-15 minute baseline value (BASE-A)  $\pm$   $\frac{1}{2}$  SEM; green = T-maze choice-point (TM), blue = inter-trial delays (PEN-F), red = intra-trial delays (PEN-C), black = post-injection, pre-test phase (BASE-B). A magnified part of the waveform (80-130%) is shown in the inset. Experimental groups were sham-stimulation (SHAM) and stimulation (STIM). Gamma-frequency coherence appears to be elevated during the drug-test day, but not during the washout test day.

Test	Peak Theta Change	Peak Gamma Change	n
SHAM	0.1067	0.0186	3
STIM	0.0226	0.0055	3

Washout	Peak Theta Change	Peak Gamma Change	n
SHAM	0.2010	0.0195	3
STIM	0.0084	0.0020	3

Table 5.5 – T-tests were used to assess whether mPFC-mPFC peak theta and gamma coherence at the T-maze choice-point (TM) was significantly elevated with respect to the pre-injection baseline recording (BASE-A), both the drug and washout test days. Numbers in the table denote p-values corresponding to whether the observed peak theta/gamma PSD was significantly elevated from baseline, with green values indicating statistical significance at  $p < 0.05$ . The final column (n) indicates the sample size per t-test. Experimental groups were sham-stimulation (SHAM), and stimulation (STIM).

### Peak Theta

	PEN-F			TM		
	F	p	sig	F	p	sig
Stim	0.01	0.9335		0.2	0.6669	
Test Day	6.57	0.0374	*	0.28	0.6124	
Stim x Day	0.66	0.4447		0.65	0.4462	

### Peak Gamma

	PEN-F			TM		
	F	p	sig	F	p	sig
Stim	0.08	0.7806		0.2	0.671	
Test Day	8.45	0.0228	*	1.99	0.2013	
Stim x Day	0.08	0.7898		0.45	0.5257	

(\*  $p < 0.05$ ), (\*\*  $p < 0.01$ ), (\*\*\*)  $p < 0.001$ ), (\*\*\*\*  $p < 0.0001$ )

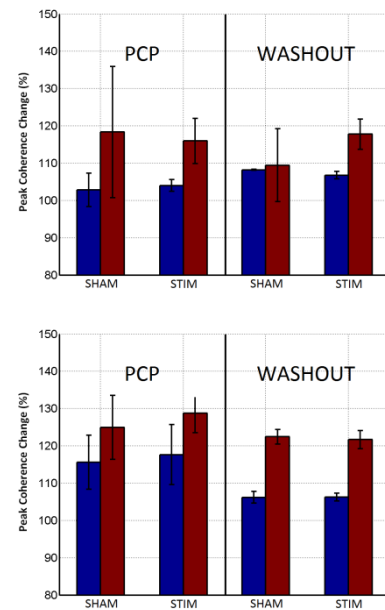


Figure 5.15 – Differences in mPFC-mPFC peak theta and gamma coherence during the post-training test phase was analysed between the stimulation and sham-stimulation groups of rats using 2-way repeated-measures ANOVAs (with drug/washout test day as the repeated measure). Plots to the right depict the corresponding peak PSD change,  $\pm$  SEM; blue = inter-trial delay (PEN-F), brown = T-maze choice-point (TM). Experimental groups were sham-stimulation (SHAM), and stimulation (STIM). A significant effect of test day (PCP) is observed for theta- and gamma-frequency coherence, for recordings made inside the T-maze.

### 5.5.7 Summary of Coherence Changes

No significant effects of stimulation were found on any of the coherence analysis carried out in this study. This reflects the lack of significant effects of stimulation in the PSD analysis carried out in the same groups of rats (see 5.5.4: Summary of PSD Changes). Interestingly, no significant effects of either stimulation or test day (drug vs. washout) were found for recordings made at the T-maze choice-point, but there were significant effects of test day on the theta and gamma-frequency coherence when measured inside the holding pen. Ipsilateral mPFC-dCA1 theta-frequency coherence was seen to be reduced in both groups of rats during the drug test day ( $p=0.0027$ ). Also, inside the holding pen both groups of rats displayed a reduced theta-frequency mPFC-mPFC coherence ( $p=0.0374$ ) and also an increased gamma-frequency coherence ( $p=0.0228$ ) during the drug test day.



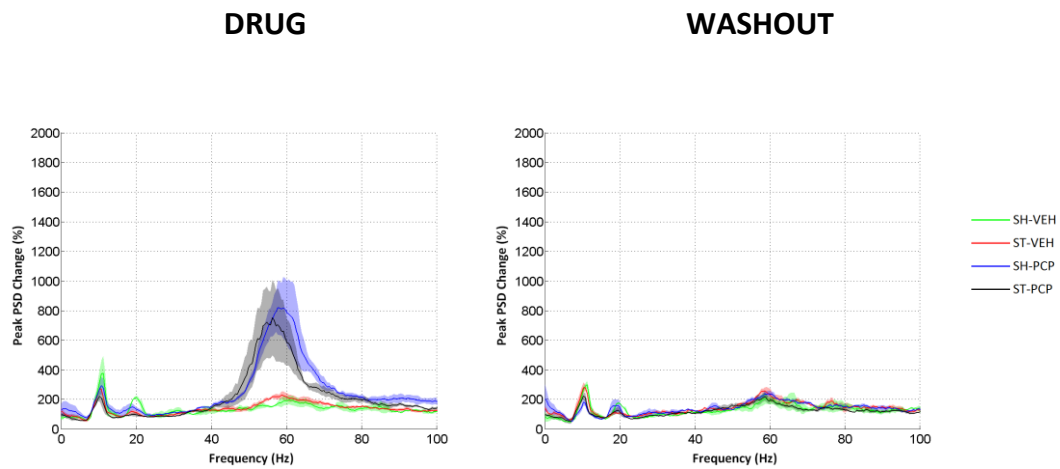
### **5.5.8 Comparison of LFP findings between the Drug- and Saline-Treated Groups of Rats**

In order to build a more complete picture of the power spectral density (PSD) and coherence changes in each of the groups of rats, this section summarises and compares some of the main LFP differences that have been observed between the saline-treated groups of rats in Chapter 4, and the PCP-treated groups of rats in this chapter. Based on the observed changes in each of the previous two analyses, comparisons between PSD are made for recordings taken at the T-maze choice-point, and comparisons between coherence are made for recordings during the inter-trial delays (inside the holding pen). Some additional comparisons are made but not displayed here, e.g. comparisons of mPFC or dCA1 PSD inside the holding pen, but are referred to in the discussion where relevant. Comparisons are made using 2-way ANOVAS, with treatment by stimulation (vs sham stimulation) and treatment by PCP (vs saline) used as the variables. Note that unlike the previous analysis in this chapter, one of the ANOVA variables used here is drug/saline treatment, i.e. not the repeated measure drug/washout (test day). For a complete picture, data from both the averaged drug/saline and washout test days are analysed this way.

#### **5.5.8.1 Comparison mPFC PSD Changes in the T-Maze**

A comparison in mPFC PSD between the drug and saline-treatment groups was made on the T-maze recordings during the drug/saline and washout test days (figure 5.16). The most striking observation that can be seen here is the large increase in gamma activity in the PCP-treated groups of rats, relative to their saline-treated counterparts. This effect is only apparent during the averaged drug/saline test days, and is accompanied by a significant effect of PCP ( $p=0.0062$ ). During the washout test day, gamma activity is seen to normalise across the rat groups, with no significant effect of PCP on gamma activity observed ( $p=0.9043$ ). During the washout test day, rats previously treated with PCP also display a slight reduction in theta-frequency PSD (relative to the saline-treated groups), which is accompanied by a significant effect of PCP ( $p=0.0088$ ). No significant effects of DBS, or significant

interactions between DBS or PCP, were observed in mPFC LFP recorded inside the T-maze during either the drug/saline or washout test days.



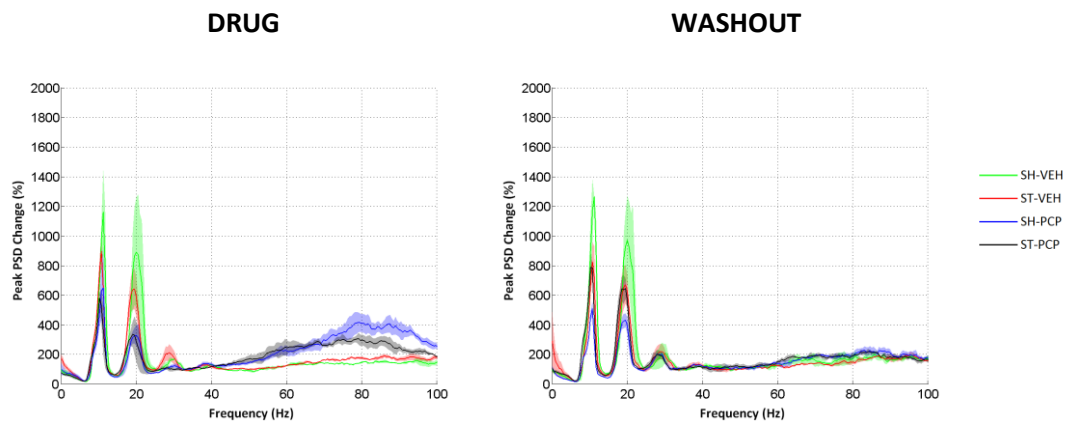
	Drug Test Days						Washout Test Day					
	Theta			Gamma			Theta			Gamma		
	F	p	sig	F	p	sig	F	p	sig	F	p	sig
Stim	3.39	0.0986		0	0.973		0.13	0.7259		0.47	0.5163	
Drug	1.5	0.2511		12.63	0.0062	**	12.93	0.0088	**	0.02	0.9043	
Stim x Drug	0.08	0.7791		0.06	0.8131		1.89	0.2115		2.13	0.1787	

(\*  $p < 0.05$ ), (\*\*  $p < 0.01$ ), (\*\*\*)  $p < 0.001$ ), (\*\*\*\*  $p < 0.0001$ )

Figure 5.16 – Comparisons between mPFC PSD changes at the choice-point of the T-maze are shown for each of the groups of rats during the post-training drug and washout test days,  $\pm$  1/2 SEM. Percentage change is relative to the 15-minute baseline recording. Experimental groups were sham-vehicle (SH-VEH; green), stimulation-vehicle (ST-VEH; red), sham-PCP (SH-PCP; blue), and stimulation-PCP (ST-PCP; black). A 2-way ANOVA was carried out for both the drug and washout test days, with effects of stimulation (vs. sham-stimulation) and drug (PCP vs. saline) looked at. Note that although the effect of drug is looked at during the washout test day, rats are not administered with PCP or saline on this day. The PCP-treated rats show profound mPFC gamma-activity increases inside the T-maze during the drug test day as accompanied by a significant effect of PCP ( $p=0.0062$ ). This effect is normalised in the washout test day, with no effect of drug observed. However during the washout test day a significant effect of previous drug administration is observed on theta-frequency PSD ( $p=0.0088$ ), which is illustrated in the above plot as a slight reduction in theta PSD in the groups previously treated with PCP.

### 5.5.8.2 Comparison of dCA1 PSD Changes in the T-Maze

The T-maze PSD recorded in the dCA1 brain regions of the PCP- and saline-treated groups of rats were compared during the drug/saline and washout test days (figure 5.17). In a similar manner to the mPFC recordings, dCA1 gamma-frequency is elevated in the PCP-treated groups (relative to the saline-treated groups) following an acute injection of PCP. This is accompanied by a significant effect of drug treatment ( $p=0.0016$ ), which is no longer present during the washout test day ( $p=0.0872$ ). During the washout test day the gamma activity in dCA1 appears to be normalised across each of the 4 groups of rats. Whilst no effect of drug or stimulation is observed on theta-frequency PSD during the drug/saline test days, there is a significant effect of drug treatment on theta-activity in the washout test day ( $p=0.0029$ ), along with a significant interaction of drug by stimulation ( $p=0.0025$ ). This can be observed as a varied size of the theta-frequency between each of the groups of rats; with lower amplitudes being attributed to the groups previously treated with PCP.



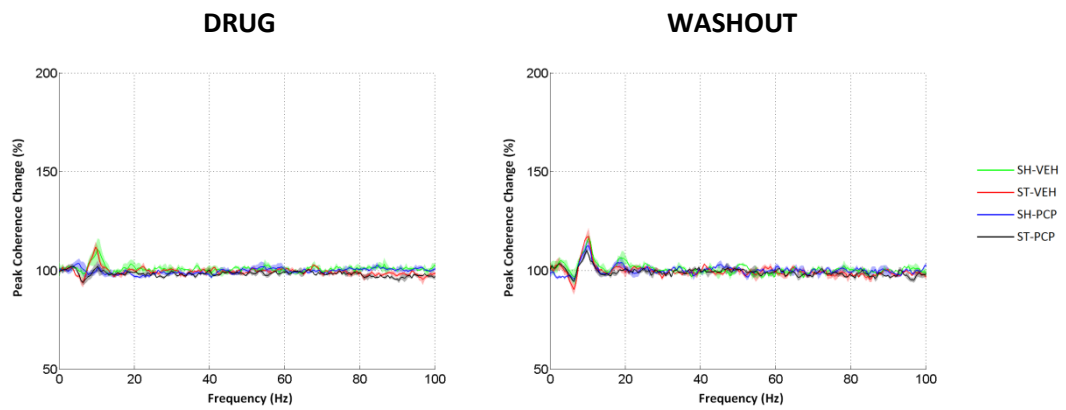
	Drug Test Days						Washout Test Day					
	Theta			Gamma			Theta			Gamma		
	F	p	sig	F	p	sig	F	p	sig	F	p	sig
Stim	0.98	0.3473		0.43	0.5279		0.89	0.3764		0	0.9597	
Drug	3.26	0.1045		19.92	0.0016	**	20.05	0.0029	**	3.95	0.0872	
Stim x Drug	0.12	0.7336		2.8	0.1284		21.15	0.0025	**	0.03	0.8638	

(\* p < 0.05), (\*\* p < 0.01), (\*\*\*) p < 0.001), (\*\*\*\* p < 0.0001)

Figure 5.17 – Comparisons between dCA1 PSD changes at the choice-point of the T-maze are shown for each of the groups of rats during the post-training drug and washout test days,  $\pm$  1/2 SEM. Percentage change is relative to the 15-minute baseline recording. Experimental groups were sham-vehicle (SH-VEH; green), stimulation-vehicle (ST-VEH; red), sham-PCP (SH-PCP; blue), and stimulation-PCP (ST-PCP; black). A 2-way ANOVA was carried out for both the drug and washout test days, with effects of stimulation (vs. sham-stimulation) and drug (PCP vs. saline) looked at. Note that although the effect of drug is looked at during the washout test day, rats are not administered with PCP or saline on this day. Similar to findings in the mPFC, there is a significant effect of drug on gamma-frequency PSD during the drug test days ( $p=0.0016$ ), which mirrors relatively increased gamma-frequency activity in the PCP-treated groups (relative to the saline-treated groups). This effect is diminished in the washout test day, with a normalisation in gamma activity between each of the 4 groups of rats. However during the washout test day, there is a significant effect of drug ( $p=0.0029$ ), and also a significant interaction between stimulation and drug ( $p=0.0025$ ).

### **5.5.8.3 Comparison of mPFC-dCA1 Coherence Changes in the Holding Pen**

Comparisons between holding-pen mPFC-dCA1 coherence can be seen for each of the 4 groups of rats during the averaged drug/saline and washout test days (figure 5.18). Compared to the saline-treated groups, the PCP-treated groups display a markedly reduced theta-frequency coherence following an administration of PCP, and this is accompanied by a significant effect of drug treatment ( $p=0.015$ ). During the washout test day, this effect appears to be reversed, with all test groups displaying normalised theta-frequency coherence, with no significant effect of drug treatment.



	Drug Test Days						Washout Test Day					
	Theta			Gamma			Theta			Gamma		
	F	p	sig	F	p	sig	F	p	sig	F	p	sig
Stim	0.05	0.826		3.97	0.0775		0.01	0.9223		1.37	0.2803	
Drug	8.99	0.015	*	0.8	0.3941		5.17	0.0572		0.03	0.859	
Stim x Drug	0.1	0.7572		1.82	0.2106		1.1	0.3289		0.22	0.6498	

(\* p < 0.05), (\*\* p < 0.01), (\*\*\*) p < 0.001), (\*\*\*\* p < 0.0001)

Figure 5.18 – Comparisons between mPFC-dCA1 coherence changes during the holding-pen task phase are shown for each of the groups of rats during the post-training drug and washout test days,  $\pm 1/2$  SEM. Percentage change is relative to the 15-minute baseline recording. Experimental groups were sham-vehicle (SH-VEH; green), stimulation-vehicle (ST-VEH; red), sham-PCP (SH-PCP; blue), and stimulation-PCP (ST-PCP; black). A 2-way ANOVA was carried out for both the drug and washout test days, with effects of stimulation (vs. sham-stimulation) and drug (PCP vs. saline) looked at. Note that although the effect of drug is looked at during the washout test day, rats are not administered with PCP or saline on this day. A significant effect of drug is observed for theta-frequency coherence during the drug test days ( $p=0.015$ ), which is accompanied by a reduction in theta-frequency coherence in the PCP-treated rats. This effect is seen to normalise on the washout test day, with all groups of rats displaying a similar level of theta-frequency coherence, with no significant differences between them.

### **5.5.9 Stimulation–Induced Theta-Power Increases**

Up until now, the analysis has looked at the differences between the LFP in each of the groups of rats, which focussed on both the T-maze and holding-pen (delay period) recordings. This analysis looked more closely at the power spectral density (PSD) changes between the different types of T-maze runs. Included in this analysis are: habituation (forced) runs, and the test runs on the averaged drug/saline and washout test days, consisting of: forced, choice-correct, and choice-incorrect runs. In this type of analysis the PSD estimates are normalised by dividing them by the root-mean square (RMS) of all of the forced-runs that make up a session, resulting in a normalised PSD estimate for each rat group with units 1/Hz (see 5.4.2.1: PSD Changes at the T-maze Choice Point). This effectively normalised the data between rat groups whilst allowing for differences between the T-maze run types to be shown. Both the saline and PCP-treated groups of rats are included in this analysis.

#### **5.5.9.1 Habituation T-maze Central Arm PSD Changes**

During habituation, each rat session consisted of 10 trials, each of which consisted of 2 consecutive forced-runs in the T-maze; in opposite directions to each other. Thus in the first part of the trial animals were forced to run into one goal arm, and in the second part of the trial animals were forced to run into the opposite goal arm. Each of the groups of rats displayed a similar normalised PSD estimate for both the mPFC and dCA1 brain regions (figure 5.19). A 2-way ANOVA was carried out to discern differences in the peak (normalised) theta- and gamma-frequency PSD between the groups, and found no significant differences (figure 5.20). This provided a baseline reading for each rat group, since the habituation sessions were carried out at the beginning of training, in the absence of treatment with DBS or PCP.

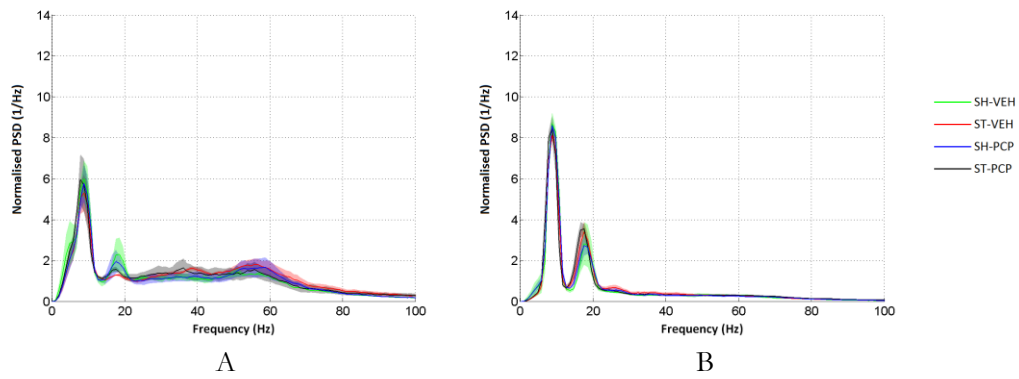
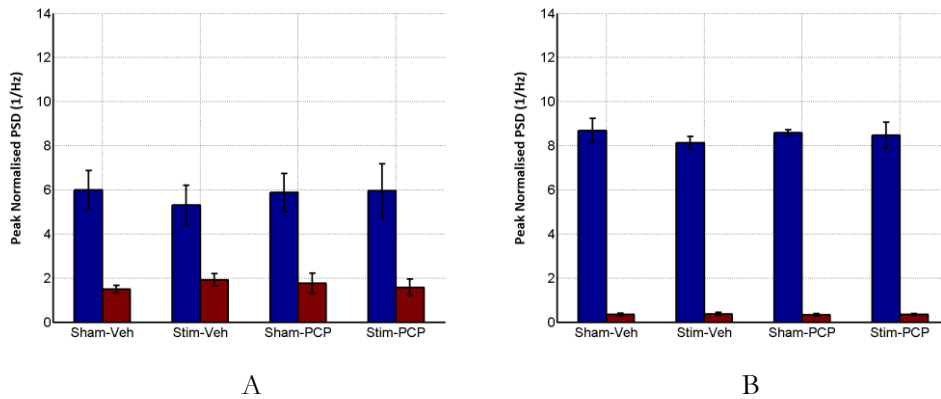


Figure 5.19 – Normalised averaged power spectral density (PSD) inside the T-maze central arm, with curves shown for each of the 4 groups of rats in the mPFC (A), and dCA1 (B),  $\pm \frac{1}{2}$  SEM. Experimental groups were sham-vehicle (SH-VEH; green), stimulation-vehicle (ST-VEH; red), sham-PCP (SH-PCP; blue), and stimulation-PCP (ST-PCP; black). No significant effects of PCP or stimulation were found for peak theta or peak gamma activity, as analysed using a 2-way ANOVA. Note that during habituation no stimulation or PCP was administered in any of the groups of rats.



	Peak Theta						Peak Gamma					
	mPFC			dCA1			mPFC			dCA1		
	F	p	sig	F	p	sig	F	p	sig	F	p	sig
Stim	0.09	0.7755		0.77	0.4039		0.09	0.7683		0.08	0.7818	
Drug	0.06	0.807		0.12	0.7394		0.01	0.9278		0.18	0.6778	
Stim x Drug	0.14	0.7191		0.31	0.5938		0.6	0.4583		0	0.9603	

(\*  $p < 0.05$ ), (\*\*  $p < 0.01$ ), (\*\*\*)  $p < 0.001$ ), (\*\*\*\*  $p < 0.0001$ )

Figure 5.20 – Bar plots represent the averaged peak PSD for each of the 4 groups of rats in the mPFC (A) and dCA1 (C) brain regions, with blue bars representing normalised peak theta, and brown bars representing normalised peak gamma. Peak values in the bar plots are derived from both forced-runs in each rat habituation session. Corresponding statistics table (below bar plots) shows the differences between each of the rat groups, with PCP and stimulation taken as separate variables in a 2-way ANOVA. Experimental groups were sham-vehicle (Sham-Veh), stimulation-vehicle (Stim-Veh), sham-PCP (Sham-PCP), and stimulation-PCP (Stim-PCP).



### **5.5.9.2 PSD Changes at the T-Maze Choice-Point during the Drug/Saline Test Days – Differences between T-Maze Run Types**

During the first two test days, animals were given an injection of either PCP or saline. Stimulation was delivered in two of the rat groups (stimulation-vehicle, and stimulation-PCP groups) for 30-seconds during the intra-trial delay period, prior to the T-maze choice run. Measurements were made at the choice-point inside the T-maze, during the forced and choice maze runs. The data from these test days were averaged together, 3-way ANOVAS were carried out on peak theta and peak gamma activity in both the mPFC and dCA1 brain regions, and the effects of stimulation, PCP, and task phase (forced-/correct-/incorrect-runs) was studied (figure 5.22). With regards to dCA1 theta activity, significant effects of stimulation ( $p=0.0202$ ) and task phase ( $p=0.0006$ ) were seen, along with a significant stimulation by task phase interaction ( $p=0.0429$ ). This can be observed as an increase in theta-activity in the stimulated rats during the choice phases of the task (green and red curves in figure 5.21), which immediately followed a 30-second treatment with DBS. In the mPFC, significant effects of PCP were seen for both peak theta ( $p=0.0007$ ) and peak gamma ( $p<0.0001$ ) activity, which mirrored earlier findings when observing T-maze PSD changes relative to baseline (see 5.5.2: Gamma-Power Increases in the mPFC Following PCP Injection).

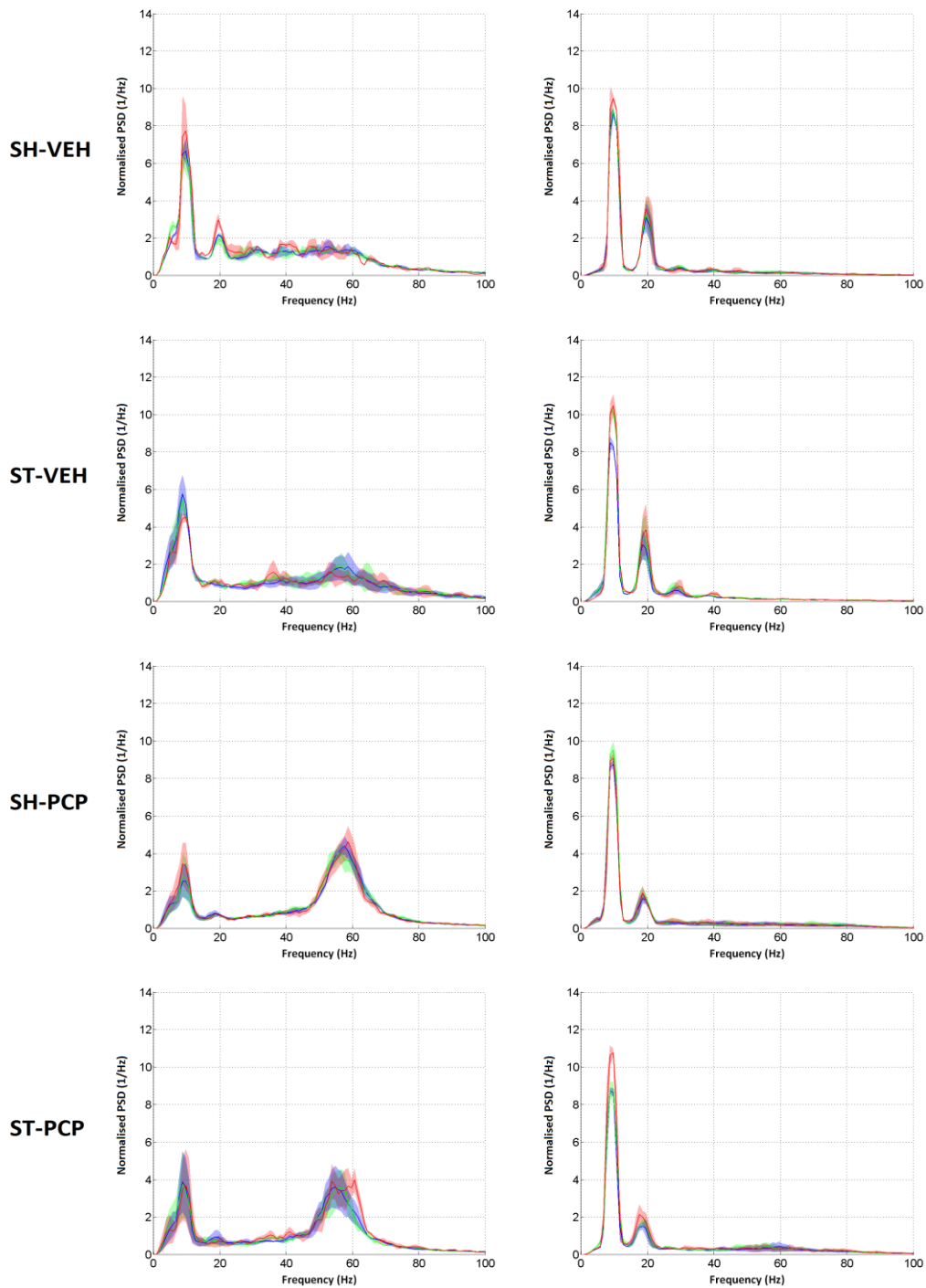
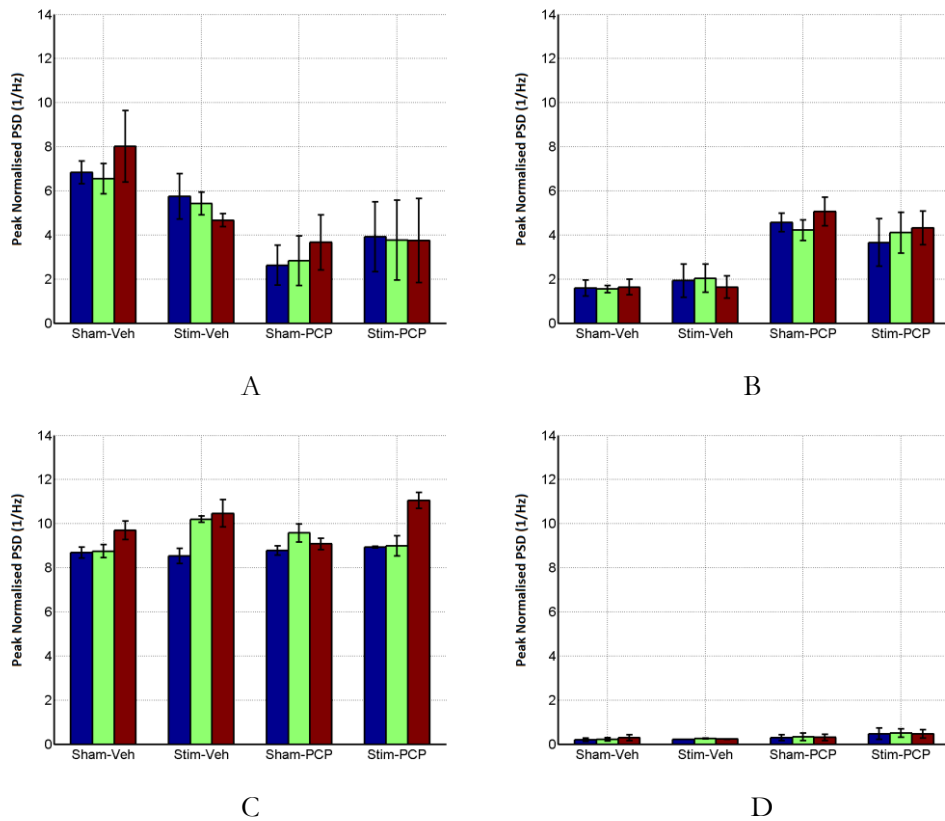


Figure 5.21 – Normalised averaged PSD changes for each of the 4 groups of rats during the averaged drug/saline test days, for the mPFC (left) and dCA1 (right) brain regions,  $\pm \frac{1}{2}$  SEM.

Blue curves represent forced-turn T-maze runs, green represents choice-correct, and red represents choice-incorrect T-maze runs. Experimental groups were sham-vehicle (SH-VEH), stimulation-vehicle (ST-VEH), sham-PCP (SH-PCP), and stimulation-PCP (ST-PCP). Notable features include increased gamma-power in the PCP-treated rats, and increased dCA1 theta-power during the choice-turn phases (red and green curves) in the stimulation rats.



	Peak Theta						Peak Gamma					
	mPFC			dCA1			mPFC			dCA1		
	F	p	sig	F	p	sig	F	p	sig	F	p	Sig
Stim	0.56	0.4609		6.12	0.0202	*	0.17	0.6873		0.89	0.3536	
Drug	14.66	0.0007	***	0	0.9582		44.13	0	****	3.3	0.0806	
Phase	0.07	0.9343		9.93	0.0006	***	0.12	0.8886		0.04	0.9622	
Stim x Drug	3.26	0.0827		0.14	0.7122		1.23	0.2783		1	0.3274	
Stim x Phase	0.52	0.6013		3.56	0.0429	*	0.23	0.7972		0.03	0.9668	
Drug x Phase	0.03	0.9721		0.37	0.6937		0.36	0.7037		0.04	0.9594	

(\*  $p < 0.05$ ), (\*\*  $p < 0.01$ ), (\*\*\*)  $p < 0.001$ ), (\*\*\*\*  $p < 0.0001$ )

Figure 5.22 – Bar plots represent the averaged peak PSD for each of the 4 groups of rats in the mPFC (A,B) and dCA1 (C,D), +/- SEM, during the averaged drug/saline test days. Data is shown for peak theta-power (A,C) and peak gamma power (B,D), with blue bars representing the forced-turn T-maze run, green representing choice-correct, and brown representing choice-incorrect. Experimental groups were sham-vehicle (Sham-Veh), stimulation-vehicle (Stim-Veh), sham-PCP (Sham-PCP), and stimulation-PCP (Stim-PCP). Corresponding statistics table (below plots) shows the effects and interactions between the use of PCP, stimulation, and variations in task phase (forced/correct/incorrect maze runs), as analysed using a 3-way ANOVA. These measurements were based on the averaged drug/saline test days, where rats were administered acute treatment with either PCP or saline vehicle.

### **5.5.9.3 Washout Test Day T-maze Central Arm PSD Changes**

During the washout test day, the PCP-induced gamma increases were seen to normalise in each of the rat groups (figure 5.23). A 3-way ANOVA on dCA1 theta activity revealed significant effects of stimulation ( $p=0.0013$ ) and task phase ( $p=0.0324$ ), but this time there was no significant interaction between stimulation and task phase ( $p=0.0853$ ; see also figure 5.24). For measurements of mPFC theta activity, a significant effect of PCP was observed ( $p=0.0049$ ), along with a significant PCP by stimulation interaction ( $p=0.0481$ ). This can be observed as a slight reduction in the theta-frequency activity of the rat groups previously treated with PCP, relative to the groups previously treated with saline.

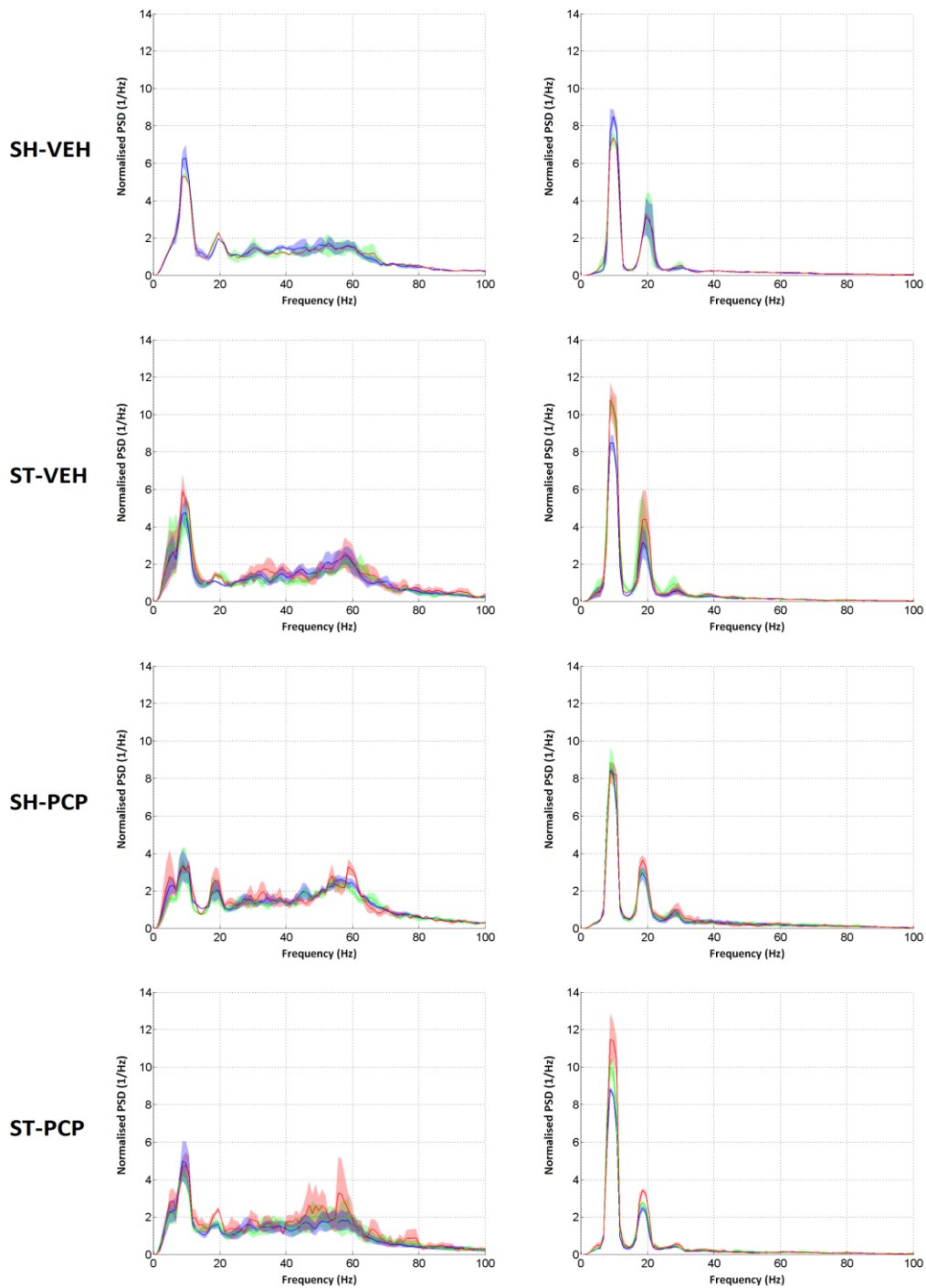
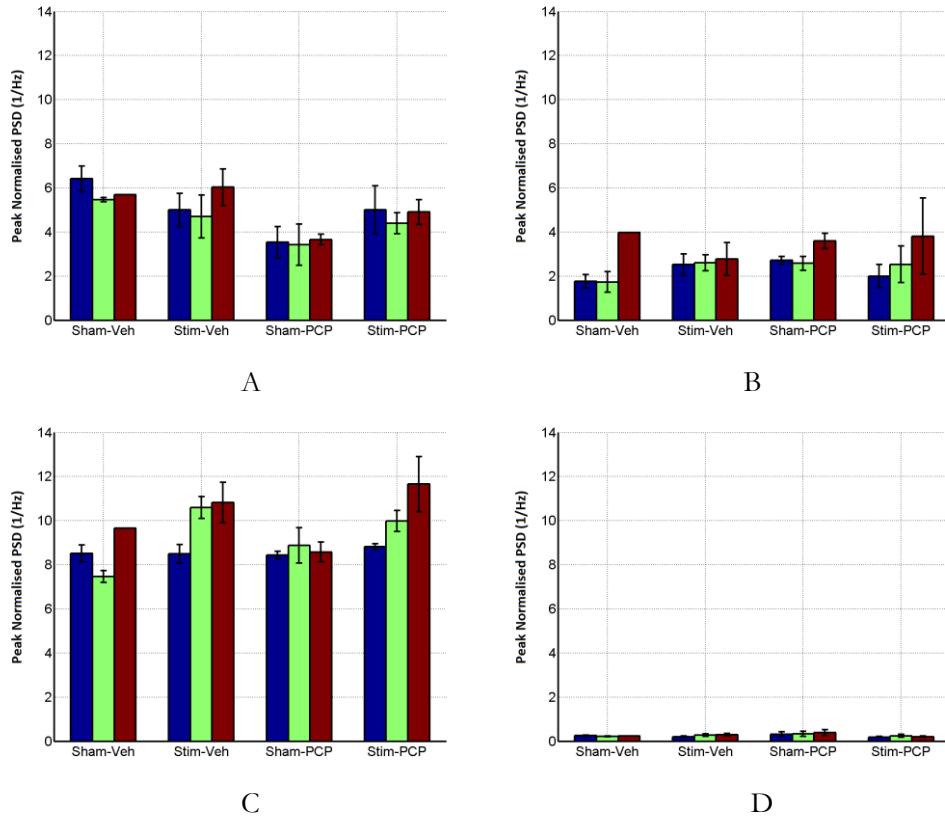


Figure 5.23 – Normalised averaged PSD changes for each of the 4 groups of rats during the PCP washout test day, for the mPFC (left) and dCA1 (right) brain regions,  $\pm \frac{1}{2}$  SEM. Blue curves represent forced-turn T-maze runs, green represents choice-correct, and red represents choice-incorrect T-maze runs. Experimental groups were sham-vehicle (SH-VEH), stimulation-vehicle (ST-VEH), sham-PCP (SH-PCP), and stimulation-PCP (ST-PCP). The PCP-induced gamma increases in the mPFC as previously seen are normalised among the rat groups, but the stimulus-induced theta-power increases remain in the stimulation rat groups.



	Peak Theta						Peak Gamma					
	mPFC			dCA1			mPFC			dCA1		
	F	p	sig	F	p	sig	F	p	sig	F	p	Sig
Stim	0.35	0.5608		13.68	0.0013	**	0.02	0.894		1.54	0.2284	
Drug	9.76	0.0049	**	0.26	0.6122		0.72	0.4052		0.43	0.5171	
Phase	0.73	0.4934		4.03	0.0324	*	2.28	0.1259		0.36	0.7007	
Stim x Drug	4.38	0.0481	*	0.01	0.9413		0.28	0.6046		2.39	0.1362	
Stim x Phase	0.14	0.8691		2.76	0.0853		0.14	0.8697		0.19	0.8317	
Drug x Phase	0.13	0.8797		0.01	0.9897		0.03	0.9119		0.03	0.9677	

(\* p < 0.05), (\*\* p < 0.01), (\*\*\*) p < 0.001, (\*\*\*\* p < 0.0001)

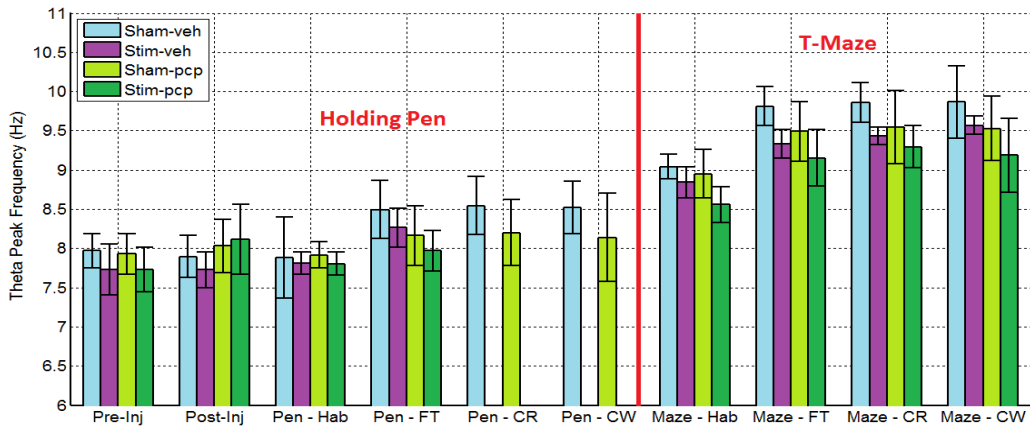
Figure 5.24 – Bar plots represent the averaged peak PSD for each of the 4 groups of rats in the mPFC (A,B) and dCA1 (C,D), +/- SEM, during the PCP washout test day. Data is shown for peak theta-power (A,C) and peak gamma power (B,D), with blue bars representing the forced-turn T-maze run, green representing choice-correct, and red representing choice-incorrect. Experimental groups were sham-vehicle (Sham-Veh), stimulation-vehicle (Stim-Veh), sham-PCP (Sham-PCP), and stimulation-PCP (Stim-PCP). Corresponding statistics table (below plots) shows the effects and interactions between the use of PCP, stimulation, and variations in task phase (forced/correct/incorrect maze runs), as analysed using a 3-way ANOVA. These measurements are based on the washout test day, where rats were not treated with PCP or saline vehicle. However rats in the stimulation group still received stimulation during the intra-trial delay periods.

#### **5.5.9.4 Summary of PSD Changes at the T-maze Choice Point**

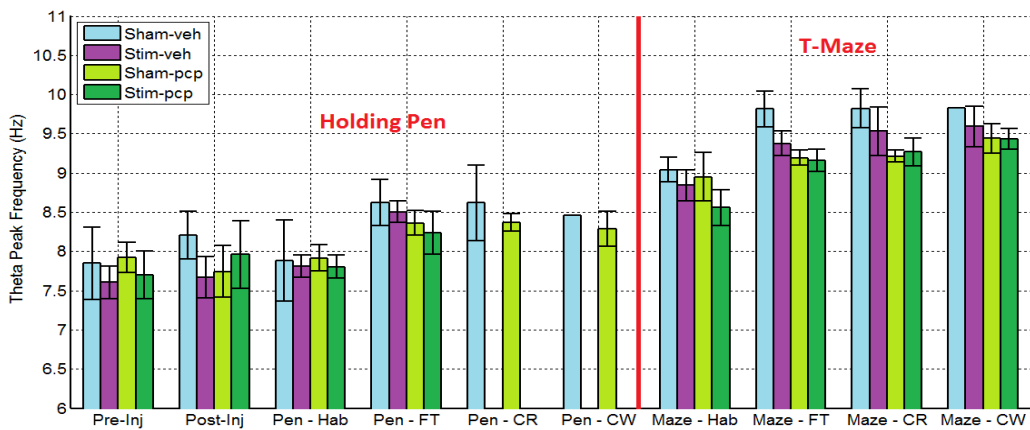
This analysis was focussed at discerning PSD changes between the forced, choice-correct and choice-incorrect T-maze runs, and how they differed between each of the 4 groups of rats. Many of the observations reflected that which arose in the previous PSD analysis of these groups, which looked at the differences between T-maze PSD (as a whole) and that from both the baseline and inter-trial delay recordings (see 5.5.2-5.5.4 in this chapter for drug-treatment groups, and 4.5.2-4.5.3 in Chapter 4 for saline-treatment groups). For example, significant effects of PCP were observed for gamma-frequency PSD during the averaged drug/saline test days. Interestingly this analysis highlighted a significant effect of DBS ( $p=0.0202$ ), along with a significant effect of task phase ( $0.0006$ ) and a significant interaction between DBS and task phase ( $p=0.0429$ ), during the averaged drug/saline test day. This was accompanied with increases in normalised dCA1 PSD during the choice-phase of the T-maze task, which implied that a stimulating current facilitated a transient increase in hippocampal theta activity.

### 5.5.10 Peak Hippocampal Theta-Frequency Changes during Different Phases of the Behavioural Task

The frequency at which peak hippocampal theta occurs was seen to change throughout the study (figure 5.25), with variations observed in each of the different session types (e.g. habituation, test), and in each of the different task phases (e.g. baseline, delays, T-maze).



A



B

Figure 5.25 – Bar plots showing average theta-frequency for each of the rat groups under a number of different task phases, for the drug test days (A) and washout test day (B). Average hippocampal theta-frequency is shown for each of the groups  $\pm$  SEM during the baseline recording (pre- and post-injection), the inter-/intra-trial delays, and during the T-maze task. Habituation data (pen and T-maze) is repeated on both plots for reference. Note that the peak-frequency during the intra-trial delays (Pen - CR, Pen - CW) is not shown for stimulation rats due to stimulus artefacts. Pre-inj = pre-injection baseline; Post-inj = post-injection baseline; Pen-Hab = habituation delay periods; Pen-FT = test inter-trial delays; Pen-CR = test intra-trial delays (prior to correct run); Pen-CW = test inter-trial delays (prior to incorrect run); Maze-Hab = habituation T-maze; Maze-FT = T-maze forced-turn; Maze-CR = T-maze choice-correct; Maze-CW = T-maze choice-incorrect.



For animals tested inside the T-maze during habituation, a 2-way ANOVA revealed no significant effects of prior stimulation ( $p=0.0651$ ) or drug ( $p=0.213$ ), and no significant interactions between the two ( $p=0.4949$ ; table 5.6). During the averaged drug/saline test days as well as during washout, 3-way ANOVAs revealed significant effects of stimulation ( $p=0.0023$  during the averaged drug/saline test days;  $p=0.024$  during washout; see also table 5.7) and PCP ( $p=0.0141$  during the averaged drug/saline test days;  $p<0.0001$  during washout). Additionally a stimulation by PCP interaction was also found during washout ( $p=0.0213$ ). Thus, whilst no significant differences were observed in dCA1 theta-frequency between the rat groups during habituation, the differences between the rat groups were varied during the drug/saline and washout test days.

	F	p	sig
Stim	4.41	0.0651	
Drug	1.8	0.213	
Stim x Drug	0.51	0.4949	

(\*  $p < 0.05$ ), (\*\*  $p < 0.01$ ), (\*\*\*)  $p < 0.001$ ), (\*\*\*\*  $p < 0.0001$ )

Table 5.6 – A 2-way ANOVA on the habituation T-maze data revealed no significant effects of PCP or stimulation on the theta peak frequency, between any of the rat groups. Note that no PCP or stimulation was administered during the habituation baseline.

	Drug/Saline Test Days			Washout		
	F	p	sig	F	p	sig
Stim	11.12	0.0023	**	5.88	0.024	*
Drug	6.83	0.0141	*	31.41	0	****
Phase	0.35	0.7062		2.88	0.0774	
Stim x Drug	0.18	0.6748		6.14	0.0213	*
Stim x Phase	0.06	0.9459		0.31	0.7394	
Drug x Phase	0.18	0.8388		0.41	0.6676	

(\*  $p < 0.05$ ), (\*\*  $p < 0.01$ ), (\*\*\*)  $p < 0.001$ ), (\*\*\*\*  $p < 0.0001$ )

Table 5.7 – A 3-way ANOVA on the test T-maze data revealed significant effects of stimulation and PCP on both the averaged drug/saline and washout test days, along with a significant stimulation x drug interaction during washout. Note that ‘Phase’ refers to the T-maze choice-point during forced, choice-correct and choice-incorrect runs.

The significant effects of PCP and stimulation as highlighted in table 5.7 revealed that each group has its own characteristic variation in dCA1 peak theta-frequency. This was to be expected since each rat had their own minor variations in peak theta frequency for each of the different task phases. To illustrate this, figure 5.26 depicts the recorded PSD from dCA1 in three rats from the stimulation-vehicle group. These PSD estimates are derived from the T-maze (figure 5.26A) and holding pen during the delay periods (figure 5.26B) over the same test days, and have been smoothed for clarity. Whilst all rats display a mean theta-frequency increase when placed inside the T-maze, the variance in theta-frequency for each given task phase for individual rats is small when compared to that of the group. This helps to explain why many of the mean frequency values are similar for both drug and washout test days within a rat group, in spite of variance between the rat groups. As such, the subsequent analysis focuses on assessing the theta-frequency changes that are present within individual rat groups.

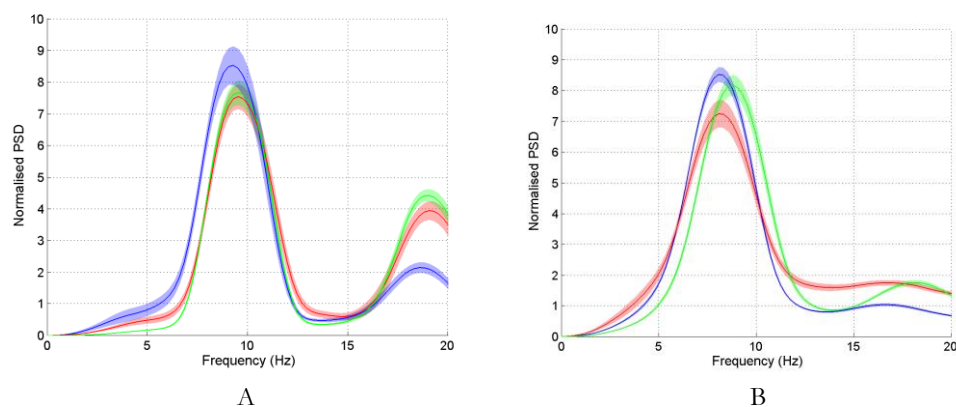


Figure 5.26 – An example of the subtle difference in hippocampal peak frequency is seen between three rats in the stimulation-vehicle (ST-VEH) group, at the choice point inside the T-maze (A) and during the inter-trial delay (B). Each curve is derived from up to 40 dCA1 PSD measurements made over the first 2 test sessions, and smoothed so that its peak frequency can be extracted. PSD for each signal is normalised by dividing by its root-mean square voltage.

Individual rat groups were analysed using a 1-way ANOVA to determine effects of task phase (forced-/correct-/incorrect-runs) on dCA1 peak theta frequency. No

significant differences were noted in any of the rat groups tested on either drug or washout test days (table 5.8).

Drug				Washout			
	F	p	sig		F	p	sig
SH-VEH	0.02	0.9847		SH-VEH	0	0.9991	
ST-VEH	2.8	0.1131		ST-VEH	0.62	0.5705	
SH-PCP	0.01	0.9862		SH-PCP	3.3	0.1081	
ST-PCP	0.11	0.8957		ST-PCP	2.39	0.1722	

Table 5.8 – Tests for differences between task phases on drug and washout days, using a 1-way ANOVA looking for effects of task phase (forced-/correct-/incorrect-runs in the T-maze). Experimental groups were sham-vehicle (SH-VEH), stimulation-vehicle (ST-VEH), sham-PCP (SH-PCP), and stimulation-PCP (ST-PCP).

To examine differences between peak theta frequency during the drug and washout test days, 1-way ANOVAS were used for each rat group on the forced, correct and incorrect maze runs (table 5.9). No significant differences were found between the two test days for any of the rat groups or task phases.

	Forced Turn			Choice Correct			Choice Incorrect		
	F	p	sig	F	p	sig	F	p	sig
SH-VEH	0	0.9908		0.03	0.8885		0	0.9573	
ST-VEH	0.09	0.7773		0.36	0.5757		0.03	0.8679	
SH-PCP	1.69	0.2503		1.38	0.2934		0.12	0.7443	
ST-PCP	0	0.9798		0.02	0.9066		0.76	0.4322	

Table 5.9 – Tests for group differences between the drug and washout days for the three task phases, as analysed using a 1-way ANOVA, which looked for differences between the drug and washout test days. Experimental groups were sham-vehicle (SH-VEH), stimulation-vehicle (ST-VEH), sham-PCP (SH-PCP), and stimulation-PCP (ST-PCP).

Peak hippocampal frequency differences were studied in the dCA1 brain region between the T-maze forced-runs (at the choice-point) and the baseline recordings made inside the holding pen, using 1-way ANOVAS. In all rat groups, hippocampal theta-frequency was shown to be significantly higher at the T-maze choice-point

than that of its corresponding baseline recording inside the holding pen, and this was found during both the averaged drug/saline and washout test days (table 5.10).

	Baseline – Drug/Saline T-Maze			Baseline – Washout T-Maze		
	F	p	sig	F	p	sig
SH-VEH	62.93	0.0155	*	69.68	0.014	*
ST-VEH	75.18	0.0001	***	63.73	0.0005	***
SH-PCP	46.02	0.0002	***	61.44	0.0005	**
ST-PCP	28.66	0.0059	**	60.1	0.0015	**

Table 5.10 – Tests for differences between baseline and T-maze choice-point (forced-run) dCA1 theta frequency, using 1-way ANOVAS. Experimental groups were sham-vehicle (SH-VEH), stimulation-vehicle (ST-VEH), sham-PCP (SH-PCP), and stimulation-PCP (ST-PCP). Hippocampal theta-frequency was found to be significantly elevated at the T-maze choice-point (during forced-runs) as compared to the session’s corresponding baseline recording, on both the drug/saline (centre column) and washout (right column) test days.

A similar test was carried out to assess differences between hippocampal centre-frequency of theta between the T-maze choice-point data recorded during the habituation sessions, and the T-maze choice-point data recorded during the averaged drug/saline and washout test days (forced-runs only). In this case the results were mixed, with only the stimulation rat groups showing significance over the two test days, and most of the remaining groups showing p-values close to a statistical significance of 0.05 (table 5.11).

	T-Maze: Habituation – Drug/Saline			T-Maze: Habituation – Washout		
	F	p	sig	F	p	sig
SHVEH	14.05	0.0644		16.08	0.0569	
STVEH	13.44	0.0105	*	14.38	0.0127	*
SHPCP	4.96	0.0675		1.71	0.2474	
STPCP	5.78	0.0741		14.63	0.0187	*

Table 5.11 – Tests for differences in dCA1 theta frequency at the T-maze choice point, between the habituation and test data, as analysed using 1-way ANOVAS. Experimental groups were sham-vehicle (SH-VEH), stimulation-vehicle (ST-VEH), sham-PCP (SH-PCP), and stimulation-PCP (ST-PCP). T-maze data obtained during habituation was compared with that from the averaged drug/saline test days (centre column), and the washout test day (right column).

In summary, the frequency of dCA1 theta activity was seen to increase significantly for all rat groups from the baseline recording, to the theta activity recorded at the T-maze choice-point. Increases in hippocampal theta frequency were also observed between the T-maze segments reported during habituation, and that observed during the test sessions, but this didn't reach significance in many of rat groups. No significant differences were found in the T-maze recordings between any of the rat groups when the data from the averaged drug/saline test days were compared with data from washout. Finally, no significant differences in dCA1 theta frequency were found between any of the T-maze run types (forced/correct/incorrect), when analysis was carried out on both the averaged drug/saline and washout test days.

## 5.6 Discussion

### 5.6.1 Gamma Frequency PSD Increases at the T-Maze Choice-Point, and with Acute PCP Treatment

In both of the PCP-treated groups of rats, gamma-frequency power spectral density (PSD) was observed to reach its maximum value for recordings made inside the T-maze (relative to the pre-task, pre-injection baseline recording). Increases in gamma-activity were also noted during the inter-trial delay periods when the rats were inside the holding pen (as compared to baseline), albeit at a smaller increase than that seen in the T-maze. These changes were noted in both the mPFC and dCA1 brain regions on all test days, and they reflect similar findings with the increased gamma activity that were observed in the saline-treated groups of rats in Chapter 4. In the PCP-treated groups of rats, this increase in gamma activity seemed to augment the large increases that were already apparent from an acute injection of PCP (as explained later in this section).

As explained in the discussion in Chapter 4 (4.6.1: Theta and Gamma Frequency PSD Changes), the observation of maximum gamma-frequency PSD at the choice-point of the T-maze is likely a result of processes that are related to the working memory task. Gamma activity is known to be prevalent during working memory processes (Jensen et al., 2007, van Vugt et al., 2010, Howard et al., 2003) and have been correlated with working memory load (van Vugt et al., 2010, Howard et al., 2003). In spite of this when the drug and vehicle-treated groups were analysed together, there were no observable effects of T-maze run-type (forced/correct/incorrect) on normalised gamma-frequency PSD, either in the mPFC ( $p=0.8886$  during the averaged drug/saline test days;  $p=0.1259$  during washout) or dCA1 brain regions ( $p=0.9622$  during the averaged drug/saline test days;  $p=0.7007$  during washout). Thus the gamma-frequency PSD was not observed to differ between T-maze run types in each of the groups of rats. This may imply that during the forced-run T-maze segments, some kind of cognitive process is still taking place that is accompanied by gamma-activity increases, e.g. an updating of task rules.

Whilst PCP was not observed to produce behavioural deficits in the T-maze task, it was seen to have a profound effect on both mPFC and dCA1 LFP. The most noticeable of these effects were large gamma-frequency increases following an acute injection of PCP (at  $3\text{mg}\cdot\text{kg}^{-1}$  i.p). From observing the LFP in the PCP-treated groups derived from the averaged drug-injection test days, a visual inspection of the mPFC log PSD spectrograms revealed these gamma-frequency PSD increases to occur within a few minutes of the rats receiving an injection of PCP, and lasted throughout the entire duration of the recording session (which typically lasted 20-25 minutes following an acute injection). When comparing the drug and washout test days for each of the two PCP test groups, a significant effect of test day (drug vs. washout) on gamma-frequency PSD was found for recordings inside the T-maze ( $p=0.0057$  – mPFC;  $p=0.009$  – dCA1) and also inside the holding pen during the inter-trial delay periods ( $p=0.0066$  – mPFC;  $p=0.0301$  – dCA1). This shows that the gamma activity had changed significantly in both PCP groups between the drug and washout test days. Later, when comparing the results from the PCP and saline-treated groups of rats during the averaged drug/saline test days, a significant effect of drug/saline treatment was observed during the test days in which PCP/saline was administered, for recordings at the T-maze choice point ( $p=0.0062$  – mPFC;  $p=0.0016$  – dCA1) and also for recordings made inside the holding pen ( $p=0.007$  – mPFC;  $p=0.0143$  – dCA1 – data not shown). All of these gamma-frequency PSD increases were seen to normalise during the washout test day, with all rat groups displaying a similar level of gamma-frequency PSD in both brain regions, and no significant effect of drug/saline treatment on gamma-frequency PSD.

What these results suggest is that PCP is having a profound effect on the amplitude of gamma-frequency signals in the rats, and is apparent not only at the T-maze choice-point, but also in the holding pen during the inter-trial delay periods. Increases in cortical and hippocampal gamma activity has previously been observed through the use of NMDA receptor antagonists ketamine and MK-801 (Pinault, 2008, Hakami et al., 2009, Lazarewicz et al., 2010, Kittelberger et al., 2012), and more recently, through the use of acute and sub-chronic doses of PCP (Chandler, 2010). NMDA receptor antagonists have gained widespread acceptance in modelling

many of the pathological and behavioural deficits present in schizophrenia, and their use was considered based on the widespread evidence linking NMDA receptor dysfunction to the core pathology of schizophrenia (Moghaddam, 2003, Kantrowitz and Javitt, 2010). Activations in the prefrontal cortex have previously been demonstrated through the use of various NMDA receptor antagonists. Pinault and colleagues (2008) noticed a dose-dependent increase in gamma-frequency power in freely-moving rats by 200-400% following administration of ketamine and MK-801. Furthermore, administration of MK-801 and PCP have been demonstrated to result in an increase in the spontaneous firing rate of mPFC neurons (Jackson et al., 2004, Suzuki et al., 2002, Homayoun and Moghaddam, 2007). This mechanism has been proposed to result in an increase in gamma-frequency activity, as predicted through computer modelling (Spencer, 2009). Notably, *in vitro* recordings of mouse hippocampal slices had demonstrated an enhanced level of kainate-induced gamma oscillations for animals pre-treated with MK-801, and this also had coincided with a significantly more depolarized pyramidal cell resting membrane potential (Kehrer et al., 2007), which may contribute to an increased firing frequency of these cells following NMDA receptor blockade. As such the authors suggested that differences in the Na<sup>+</sup>-K<sup>+</sup> pump activity may have underlined the differences in the resting membrane potentials of mice pretreated with MK-801 (Kehrer et al., 2007). Interestingly, in anaesthetized rats PCP was observed to result in increased mPFC spontaneous activity when applied systemically, and not when applied directly to the mPFC neurons via micro-ionophoretic injections (Suzuki et al., 2002). This finding suggests that PCP is modulating the mPFC principal neuron firing rate through some other means. Through the use of NMDA receptor antagonists, these PFC firing rate increases have been mirrored by increased expression of the immediate early gene *c-fos* (Gao et al., 1998), as well as increases in the levels of extracellular glutamate (Moghaddam and Adams, 1998). Notably the extracellular glutamate increases have been mentioned to agree with the spontaneous discharge rate of mPFC neurons (Suzuki et al., 2002).

Given that PCP itself is an NMDA receptor antagonist (Javitt and Zukkin, 1991), one would expect an acute injection to have a suppressive effect on mPFC neurons,



and hence a reduction in the gamma frequencies – contrary to the results that was observed in the present study. NMDA receptors are known to mediate excitation of inhibitory interneurons (Grunze et al., 1996, Goldberg et al., 2003), of which they are thought to preferentially act. Notably, GABAergic interneurons are tenfold more sensitive to NMDA receptor antagonists than pyramidal neurons (Grunze et al., 1996), thus NMDA receptor antagonists would be expected to act primarily on these cell types. An insight into the mechanisms of action of NMDA receptor antagonists have been suggested, based on a possible disinhibitory action of the GABAergic interneurons on pyramidal cell firing (Homayoun and Moghaddam, 2007). In the prefrontal cortex, fast-spiking parvalbumin-containing GABAergic interneurons provide a powerful perisomatic inhibitory control over widespread cortical pyramidal neurons (Wilson et al., 1994). By administering i.p. injections of MK-801 in freely-moving rats, Homayoun and Moghaddam (2007) were able to demonstrate not only an increase in cortical pyramidal cell spiking activity, but this increased activity was preceded by an increased electrical activity measured in the GABAergic inhibitory interneurons, thus further suggesting a preceding effect on the GABAergic interneurons.

In the current study the findings of increased gamma-frequency PSD mirror that which have previously been seen through the use of NMDA receptor antagonists (e.g. Pinault, 2008, Hakami et al., 2009, Lazarewicz et al., 2010, Chandler, 2010, Ma and Stan Leung, 2000, Ehrlichman et al., 2009). Notably GABAergic interneurons that express the calcium-binding protein parvalbumin are known to be crucial for generating and maintaining gamma-frequency oscillations (Bartos et al., 2007). As such whilst a disinhibitory mechanism of interneuron control over pyramidal cell output is likely taking place, it doesn't fully explain why gamma activity reaches such high levels relative to that observed in the baseline (pre-injection) recordings. NMDA-receptor signalling is known to be critical for the generation and maintenance of baseline gamma activity. For example, Carlen et al., (2012) and Korotkova (2010) had both demonstrated an augmented basal gamma activity in mice which featured a selective deletion in NMDA-receptors in parvalbumin cells (PV-Cre/NR1f/f mice), which in both cases were associated with cognitive

impairments from various behavioural indices including learning and spatial working memory. One possible mechanism taking place, is glutamate-mediated activation of the fast-spiking parvalbumin interneurons, in which the increased extracellular glutamate binds to AMPA ( $\alpha$ -amino-3-hydroxy-5-methyl-4-isoxazolepropionic acid) receptors on the fast-spiking cells, thus giving rise to the increased gamma rhythmicity seen (see Chandler, 2010). Activation of these interneurons through their AMPA receptors is known to cause these cells to oscillate in the gamma-frequency range (Pike et al., 2000). Previously, the loss of NMDA-receptor miniature-signalling in rat hippocampal slices (using tetrodotoxin) has been demonstrated to result in a rapid increase in GluR1 permeable AMPA channels, as well as a resulting increase in miniature post-synaptic currents (Sutton et al., 2006), which may serve as a fast-acting homeostatic process as well as an explanation for the increased cortical activity following NMDA receptor blockade. Indeed, *in vitro* studies using AMPA-receptor knockout mice (via reduction of the GluR-D or the GluR-A subunit on parvalbumin interneurons) have revealed a disruption in the gamma-frequency inhibitory drive to pyramidal cells, which was accompanied by a selective reduction in the AMPA-mediated current, as well as a reduced cell firing rate (Fuchs et al., 2007). Interestingly, these observations were associated with a deficit in performance of working memory (but not spatial reference memory), which suggests that an activation of fast-spiking neurons via NMDA-receptor signalling is required for these behaviours. Furthermore, these results have been mirrored by *in vivo* studies in rats, in which the AMPA receptor antagonist 6,7-dinitroquinoxaline-2,3,dione (DNQX; at 5-10 $\mu$ g) was shown to decrease the amplitude of hippocampal EEG, leading the authors to conclude that both AMPA and NMDA receptors in the hippocampus are involved in the generation of theta and gamma frequencies (Leung and Shen, 2004). If the gamma activity increases in the current study are indeed mediated (at least in part) by activation of the fast-spiking interneurons through their AMPA receptors, then this could serve to reduce the signal-noise ratio of gamma rhythms which would otherwise be required in behaviours relevant to cognitive demand. Gamma rhythms are known to be coupled to the underlying theta rhythm in various regions including the hippocampus (Bragin et al., 1995, Belluscio et al., 2012), and between the hippocampus and prefrontal

cortex (Dzirasa et al., 2009, Adhikari et al., 2010, Sirota et al., 2008), and the strength of coupling has been observed to increase with decision-making epochs of a behavioural task (Tort et al., 2008). The NMDA receptor antagonist PCP has been shown previously to decouple theta from gamma in the hippocampus (Chandler, 2010), a finding which has also been observed through ablation of the NMDA receptors on parvalbumin-containing interneurons in PV-Cre/NR1f/f knockout mice (Korotkova et al., 2010). Notably this latter study found a reduction in the spatial and temporal precision of pyramidal cells. Taken together, this data highlights the possibility of NMDA receptor blockade increasing gamma noise whilst reducing its coordination with other rhythms, which are required for successful working memory performance (Jensen, 2006).

### **5.6.2 Coherence Changes in the T-Maze Task**

As observed with the saline-treated groups of rats in Chapter 4, the PCP-treated groups had displayed maximal increases in mPFC-dCA1 theta-frequency coherence when placed inside the T-maze environment. In spite of rats having an acute PCP injection, these T-maze coherence increases were seen to match those observed in the saline-treated groups. A different scenario had emerged in the PCP-treated rats, for recordings made inside the holding pen (during the inter-trial delay periods). Rats treated with PCP displayed significant reductions in theta-frequency coherence, relative to the measurements made during washout ( $p=0.0027$ ), and also relative to comparisons made with the saline-treated rats during the drug/saline test days ( $p=0.015$ ). Visibly the theta-frequency coherence in the PCP-treated rats remained at baseline levels during the task delay periods (unlike the increases observed in the saline-treated rats), and was seen to normalise during the washout test day.

Theta activity has been studied in rodents with regards to its role in synchronising the electrical activity of separate brain regions. For instance, mPFC and dCA1 theta activity have been shown to synchronise in tasks that require spatial working memory (Jones and Wilson, 2005, Benchenane et al., 2010, Sigurdsson et al., 2010; see also Chapter 4 – 4.6.2: Coherence Changes), which presumably occurs through

the monosynaptic hippocampo-PFC glutamatergic pathway (Jay et al., 1992). In a PCP-treated rodent, one would expect to find deficits in hippocampal-prefrontal synchrony, given the crucial role that GABAergic interneurons play in synchronising the activity of these brain regions. The monosynaptic hippocampo-prefrontal pathway is known to synapse not only on pyramidal cells in the prelimbic cortex (Carr and Sesack, 1996), but also onto parvalbumin-containing interneurons (Gabbott et al., 2002). Numerous studies have probed this connection using single-pulse stimulation in the hippocampus, only to consistently reveal complex activation patterns in the prefrontal cortex which involves the engagement of pyramidal and non-pyramidal cells (Degenetais et al., 2003, Buzsaki, 1984, Tierney et al., 2004). Crucially Tierney et al., (2004) noticed that hippocampal stimulation resulted in interneurons becoming active before the pyramidal cells in most cases, which can be explained by the increased excitability of the interneurons as compared to the pyramidal cells (e.g. the differential expression of K<sup>+</sup> channels and increased density of Na<sup>+</sup> channels on these cells; Du et al., 1996, Martina et al., 2000). Furthermore, the hippocampo-prefrontal pathway is known to synapse exclusively onto the parvalbumin-containing interneurons, rather than the calbindin or calretinin interneurons (Gabbott et al., 2002). The preferential activation of inhibitory interneurons in this pathway is believed to mediate a feed-forward inhibition mechanism which ultimately results in a precise and widespread synchrony of inhibitory control in this network (Swadlow, 2003), which in turn is believed to underlie the generation and synchronisation of the hippocampo-prefrontal theta rhythm (Tierney et al., 2004).

In schizophrenia patients, numerous functional imaging and EEG studies have revealed a diminished coordination of information between neural networks (e.g. Koenig et al., 2001, Koukkou et al., 1993; Saito et al., 1998, Liddle, 1996), which collectively may be attributed to dysfunctional glutamatergic signalling. In a transgenic mouse model relevant to schizophrenia, reductions in the theta-frequency coherence between the mPFC and dCA1 brain regions have been observed (Sigurdsson et al., 2010), which in this case was correlated with working memory deficits. In addition, a low dose of ketamine (2.5 mg.kg<sup>-1</sup>) has been shown to reduce

theta-frequency coherence across the long axis of the septotemporal CA1 network (Hinman et al., 2013), which decreased further with increasing distance. In the current study, the lack of a significant coherence reduction in the theta band for PCP-treated rats when tested inside the T-maze is surprising, given the critical role played by GABAergic interneurons in mediating functional coordination between the hippocampal and mPFC brain regions. Working memory has been shown to correlate with theta-frequency hippocampo-prefrontal coherence (Jones and Wilson, 2005, Benchenane et al., 2010, Sigurdsson et al., 2010), and in addition working memory is known to be disrupted following an acute dose of PCP (Verma and Moghaddam, 1996). It is worth noting that in this experiment no significant effect of PCP was found on behavioural performance on either the drug or washout test days, although this may indeed be attributed to the relatively small sample size of each rat group. One rat in particular had obtained a perfect score of 10/10 following an acute administration of PCP.

In the current study, it was observed that the non-PCP treated rats were much more active during the inter- and intra-trial delays than the PCP-treated rats, which by comparison appeared to be less physically active with docile behaviours such as lying down until the next trial. Furthermore, in contrast to the holding-pen recordings, theta-frequency PSD and coherence were always at their maximum values when rats were inside the T-maze, with no significant differences observed between the PCP- and saline-treated groups. Whether the PCP-mediated coherence reductions in the holding pen are linked to the corresponding holding-pen theta-frequency PSD reductions (see 5.6.3: Theta Frequency PSD Observations during Drug and Washout Test Days) cannot be fully elucidated here, because a) rat movement speed may have played a part in shaping the amplitude of the theta rhythm (which was reduced inside the holding pen; particularly so for the PCP-treated rats), and b) the coherence reductions were only noticeable during the task delay periods, when it is expected that the rat would require less of a coordination between the recorded brain regions that are involved in working memory. Indeed, Benchenane and colleagues (2010) had noticed theta-frequency amplitude reductions in rats during periods of high theta-frequency coherence between these brain regions. Nonetheless, despite these

coherence reductions only being visible inside the holding pen, they are present only in the PCP-treated groups of rats. Whether this effect is secondary to a PCP-mediated behavioural change, or whether the observed behavioural change is a result of the PCP-mediated coherence reduction is yet to be determined. As such, a future experiment can be carried out to probe the behaviour and LFP of PCP-treated rats during a task that measures different levels of cognitive demand using varied PCP-dosage groups.

When measuring the coherence between bilateral mPFC brain regions, gamma-frequency coherence was found to be elevated in the PCP-treated groups of rats. Similar to the previous coherence findings, these gamma-coherence increases were only significant in the holding-pen recordings when comparing the data between the drug and washout test days. A significant effect of test day (drug vs. washout) was observed for gamma-frequency coherence ( $p=0.0228$ ) during the holding-pen recordings, but not inside the T-maze ( $p=0.2013$ ). Whilst these changes are still striking when observing the comparisons between the PCP and saline-treated groups, it did not reach statistical significance in this case, which is perhaps due to the sample numbers being even lower than normal for this particular measurement. The sample numbers were smaller here because measurements of inter-hemispheric coherence required both mPFC electrodes to be correctly positioned, thus rats with only one mPFC electrode correctly positioned were excluded from this analysis. Nonetheless the mPFC gamma-coherence increases can be clearly seen on the relevant coherograms, and also they appear to diminish in the same groups during the washout test day.

The positive symptoms of schizophrenia have previously been associated not only with transient increases in gamma-frequency power (Lee et al., 2003), but also with a hypersynchrony of prefrontal gamma power (Spencer et al., 2004, Baldeweg et al., 1998, Herrmann and Demiralp, 2005). Furthermore, an acute dose of the NMDA antagonists ketamine and MK-801 has revealed an increased synchronisation of gamma oscillations *in vivo* (Pinault, 2008), which in this case was associated with ataxic motor activity. Interestingly, Caixeta (2013) noticed that the phase coherence of gamma and high-frequency oscillations increased immediately following an

injection of ketamine in rats, which had only subsequently returned to baseline levels after cessation of the resultant hyperlocomotion; which is a well-known behaviour associated with NMDA receptor blockade in rodents (Adell et al., 2012). In humans, an increased excitability of neurons in the association and sensory cortices have previously been linked to hallucinations (e.g. Hoffman et al., 2003), and also the acute administration of NMDA receptor antagonists in rodents are known to lead to principal cell hyper-excitability (Jackson et al., 2004, Suzuki et al., 2002, Homayoun and Moghaddam, 2007). As suggested by Caixeta (2013), this may lead to an over-processing of information through functionally connected brain regions which experiences this hyper-synchronicity; which may subsequently be in part responsible for the psychotic symptoms experienced in schizophrenia patients and through NMDA receptor blockade. In an *in vitro* study using visual cortex slices from a rat, Anver et al., (2011) were able to demonstrate an enhanced synchronisation of gamma-frequency signals, following administration of PCP and ketamine. This was found to occur through a selective deceleration of the high-frequency gamma activity in layer 3, which subsequently matched the gamma-frequency in layer 5 thus causing a synchronisation. This effect presumably occurred due to a reduction in the firing of the fast-spiking parvalbumin interneurons; which in turn arose from the NMDA receptor antagonism. Interestingly, they hypothesised that aberrant perceptions may result from the matching of gamma activity in two different networks, i.e. the gamma activity in layer 5 with the “decelerated” gamma activity in layer 3, which has the possible functional implications of matching memory-based top-down with stimulus-driven bottom-up information (Anver et al., 2011). Ultimately, if the observed gamma-frequency coherence increases are indeed a consequence of acute PCP administration, it could provide another link between the relevancy of PCP as an effective model for schizophrenia, and some of the EEG changes in humans that have been associated with the positive symptoms of the disease.

### 5.6.3 Theta-Frequency PSD Observations during Drug and Washout Test Days

As with the saline-treated groups of rats in Chapter 4, both the stimulation and sham-stimulation PCP-treated groups had shown large and significant elevations in theta-frequency activity when placed inside the T-maze environment. This was particularly evident in dCA1, which had shown the largest increases. As discussed in Chapter 4 (see 4.6.1: Theta and Gamma Frequency PSD Changes), this may be related to a number of behaviours including spatial exploration and rat locomotion (Green and Arduini, 1954, Vanderwolf, 1969). When this theta activity was compared between the drug and washout test days within the PCP-treated groups, a significant effect of test day was observed both in the mPFC ( $p=0.0475$ ) and dCA1 ( $p=0.001$ ) brain regions. Interestingly this was only noted during the inter-trial delay periods (inside the holding pen), and manifested as a slight reduction in theta-frequency PSD, relative to that seen during washout. No significant effects of test day were found on theta-frequency PSD at the T-maze choice-point, hence these reductions were confined only to the task delay periods. This finding mirrors some of the observations that were made when comparing the PCP and saline-treated rats, also. For instance, a significant effect of drug/saline was observed for holding-pen theta activity in dCA1 ( $p=0.0271$ ; data not presented), but not in mPFC ( $p=0.243$ ; data not presented).

Several *in vivo* studies have reported reductions in hippocampal theta activity following an acute administration of NMDA receptor antagonists (Caixeta et al., 2013, Leung and Shen, 2004, Kittelberger et al., 2012, Lazarewicz et al., 2010, Ehrlichman et al., 2009). Interestingly in a recent study, acute administration of ketamine was found to reduce theta-frequency power in the stratum pyramidale layer, which reversed further down to theta-frequency increases in the hippocampal fissure (Caixeta, 2013). Similarly Kittelberger (2012) noted decreases in theta power in the dCA1 region following an acute administration of ketamine or MK-801, but no change in the dentate gyrus region. Finally, in addition to reducing the power of background theta activity in the hippocampus, acute administration of ketamine has



also shown to diminish stimulus evoked theta in mice, in a paired click auditory gating paradigm (Lazarewicz et al., 2010, Ehrlichman et al., 2009).

The theta signal that propagates throughout the hippocampus is thought to be driven by the interplay between principal cells and GABAergic interneurons, with major inputs arising from the entorhinal cortex (Leung, 1984) via the perforant pathway, and the medial septum (Bland, 1986, Hasselmo et al., 2002). A blockade of glutamate through NMDA receptor antagonists can serve to disrupt these pathways by reducing the phasic inhibitory feedback control between the hippocampus and these brain regions, which may have the effect of attenuating theta activity. A blockade of glutamate is known to inhibit also the excitation of interneurons in CA1 by pyramidal cells from both CA1 and CA3 (Grunze et al., 1996), which may further contribute to a disruption in theta-frequency activity. Although several types of interneurons involved in the generation of theta activity are affected by NMDA receptor antagonists (Grunze et al., 1996), hippocampal interneurons located in the lacunosum-moleculare layer (OLM cells) in particular are known to play a critical role in generating theta (Gillies et al., 2002, Klausberger et al., 2003), and contain an abundance of NMDA receptors which are highly susceptible to NMDA receptor blockade (Hajos et al., 2002). Ultimately, disruption of NMDA receptor signalling by antagonism of NMDA receptors may result in theta-frequency disruption in the hippocampus through a number of inter-related mechanisms. Given the complexity of the various factors that are proposed to generate and maintain hippocampal theta, the exact effect that NMDA receptor antagonists have on theta-frequency activity is currently not fully understood.

In the current study a PCP-mediated reduction in hippocampal theta was only noticeable for recordings made inside the holding pen, and not during the T-maze task. This may indeed be a consequence of rat movement speed, which is known to be correlated with the amplitude and characteristics of hippocampal theta (e.g. Vanderwolf, 1969, McFarland et al., 1975; see also 4.6: Chapter 4 Discussion). During the inter-trial delay periods rats that had been given an acute injection of PCP were noticeably less active; however without a quantifiable record of holding-pen locomotor activity this correlation between rat movement and theta-frequency is

at present only speculative. Nonetheless it is of note that the inter-trial delay periods are the only time-points in the experiment in which dCA1-mPFC theta-frequency coherence was seen to be significantly reduced in the PCP-treated rats. Furthermore, the periods of greatest theta-frequency coherence (inside the T-maze) had also coincided with the largest-amplitude hippocampal theta waves. One would expect this correlation, given that theta-frequency coherence between these regions is mediated by monosynaptic hippocampo-prefrontal pathway (Jones and Wilson, 2005, Jay et al., 1992), in which dCA1 theta activity is seen to lead that in the mPFC (Jones and Wilson, 2005).

It is expected that during the T-maze recording segments, a higher-frequency atropine-resistant theta rhythm would have been more predominant in the LFP, as opposed to a lower-frequency atropine-sensitive theta rhythm (Kramis et al., 1975). The lower-frequency atropine-sensitive theta rhythm is known to be predominant during a resting state, and reflects sensory processing (Bland, 1986), whereas the higher-frequency atropine-resistant rhythm is associated with voluntary motor behaviours (Kramis et al., 1975, Vanderwolf and Baker, 1986, Olvera-Cortes et al., 2004). Whilst this was apparent given the amplitude and frequency increases (see 5.6.6: Hippocampal Theta-Frequency Changes), there are numerous lines of evidence which suggest that this component of the theta rhythm should be diminished through NMDA receptor blockade. Selective ablation of NMDA receptors on parvalbumin positive interneurons using NR1(PVCre-/-) knockout mice have been shown to specifically reduce the atropine-resistant theta rhythm (Korotkova et al., 2010). This is supported by *in vitro* data in which NMDA receptor antagonists were shown to block atropine-resistant theta in rat hippocampal slices (Gillies et al., 2002). As such one would expect the PCP-related deficits in theta activity to be more predominant in the recordings made inside the T-maze. One possible explanation for this discrepancy is that the T-maze recordings were 1-second in length, as opposed to the recordings made inside the holding pen which were each 20-seconds, allowing for a greater probability of a robust theta-amplitude change to be detected. Furthermore, the variation in the theta-frequency inside the T-maze was large, and probably dependent on the running speed of the rat (see 4.6:

Chapter 4 Discussion). Nonetheless, whether the observed docile behaviour in the PCP-treated animals is a result of reductions in hippocampal theta, or vice versa, would have to be established through a future study that quantified rat movement alongside the LFP recordings.

#### **5.6.4 Effect of Deep-Brain Stimulation**

In this study, the effect of deep-brain stimulation (DBS) only became apparent when comparing the different T-maze run types between both the saline- and drug-treated groups of rats. When dCA1 peak (normalised) theta-frequency PSD was analysed during the post-training test days, significant effects were found for stimulation ( $p=0.0202$  during drug/saline test days,  $p=0.0013$  during washout day) and task phase ( $p=0.0006$  during drug/saline test days,  $p=0.0324$  during washout day). In addition a significant stimulation by task-phase interaction was found for the drug test day ( $p=0.0429$ ); although this was not significant for the washout test day ( $p=0.0853$ ). Observation of the relevant dCA1-PSD plots (see 5.5.9: Stimulation Induced Theta-Power Increases) indeed revealed an increased (normalised) theta-power PSD in the choice-turn T-maze segments, relative to that shown during the forced-turn segments. These observations imply that FF-DBS is either directly or indirectly responsible for the increased theta-frequency PSD observed in dCA1, which is interesting given that these observations are made within a few seconds of the rats receiving 30 seconds of stimulation.

Activation of the hippocampus has been consistently observed in humans following DBS of the ventral hypothalamus/fornix region (Hamani et al., 2008, Laxton et al., 2010, Smith et al., 2012), which in turn has been correlated with working memory improvements in each of these studies. Hamani et al., (2008) was the first to notice hippocampal activation in a patient undergoing bilateral hypothalamus/fornix DBS for the treatment of morbid obesity; which was verified using EEG source localisation. Similarly Laxton et al., (2010) performed bilateral DBS at the same site in Alzheimer's patients, and noted an increased neural activity in the entorhinal and hippocampal areas, as verified using positron emission tomography (PET). In both

of these cases the increased hippocampal activity was accompanied with improvements in cognitive performance as assessed using standard tests such as tests for verbal learning (Hamani et al., 2008) and the Alzheimer's Disease Assessment Scale – cognitive subscale (ADAS-cog; Laxton et al., 2010; Smith et al., 2010). The FF is known to be a major conduit of information between the hippocampus and various limbic structures known to be involved in learning and memory, and stimulation of these adjacent white matter tracts could indeed be directly responsible for the increased theta-frequency PSD observed in the rats that had received stimulation. Large myelinated axons have a higher conductivity than that of grey matter (Ranck, 1975, Nowak and Bullier, 1998), and are known to generate excitatory responses upon stimulation (Ranck, 1975). As such one would expect DBS to result in orthodromic synaptic responses in efferent axons, as well as antidromic spikes which collide with spontaneously generated spikes from afferent axons (Hammond et al., 2008). Given the widespread connectivity of the FF with various limbic structures including the hippocampus, anterior thalamic nucleus (ATN), medial septum and mammillary bodies (Andersen, 2007, Amaral and Witter, 1995), it is of no surprise that widespread metabolism increases in the ectorhinal, hippocampal and parahippocampal regions have been observed through previous studies which utilize fornix-DBS in humans (Hamani et al., 2008, Laxton et al., 2010, Smith et al., 2012).

Should there be a widespread activation of brain regions through DBS, what effect would this have on learning and memory functions? The hippocampal theta rhythm in rats is known to be predominantly active during locomotion, spatial exploration, and various learning-related behaviours (Green and Arduini, 1954, Vanderwolf, 1969), and is known to synchronise with various LFP signals from local and distal networks such as hippocampal gamma oscillations (Tort et al., 2008) and mPFC theta oscillations (Jones et al., 2005, Sigurdsson et al., 2010) during spatial working memory functions. Inactivation of the medial septum – an area where hippocampal theta activity is thought to originate – has been shown to abolish the hippocampal theta rhythm (Stumpf et al., 1962). More recent findings have shown that disconnection of the medial septum and hippocampus (via the FF) in rats has

revealed deficits in working memory performance in rats (Okada and Okaichi, 2010). Furthermore a recent study highlighted that theta-frequency stimulation in the medial septum of brain-injured rats could restore an otherwise diminished spatial working memory (Lee et al., 2013). Interestingly this study also highlighted a transient increase in hippocampal theta activity directly following stimulation. Given that the medial septum connects to the hippocampus via the white matter tracts of the FF, direct stimulation of these tracks may also contribute to an increased hippocampal theta activity in rodents, in a manner similar to that demonstrated through hypothalamus/fornix stimulation in humans (Hamani et al., 2008, Laxton et al., 2010, Smith et al., 2012).

Whilst the current study does not provide direct evidence to support that FF stimulation in rodents contributes to working memory improvements, the (non-significant) tendency for the stimulated rats to learn the task faster may highlight an intriguing consequence of the transient hippocampal activation observed, following FF stimulation (see Chapter 4 - **Error! Reference source not found.** Rat Performance in the T-Maze Task). A recent study by Suthana and colleagues (2012) demonstrated that stimulation of the perforant pathway in epileptic patients (via entorhinal cortex DBS) had shown a significant increase in spatial working memory performance, when it was applied during the learning phase of the task. Interestingly measurements of local-field potentials in the same subjects had revealed a significant increase in the power of hippocampal theta-power in the period directly following entorhinal stimulation (as compared to the period prior to stimulation). Should FF stimulation indeed be mediating an enhancement in the ability of the rats to learn the task, then numerous possibilities could exist to explain this, beyond simply an activation of the relevant circuits involved in learning and memory.

One possible mechanism involved is that stimulus pulses could be resetting the phase of the theta-frequency waveforms. Phase-resetting of the theta-rhythm is a stimulus-evoked mechanism by which the theta activity is reset and becomes phase-locked to arriving stimuli. (McCartney et al., 2004, Givens, 1996). This has been observed across a variety of sensory modalities, and has been proposed to improve cognitive functioning and memory by allowing for an enhanced encoding of novel

stimuli (Givens, 1996, Vinogradova et al., 1996). In rodents, DBS of both the fornix and the perforant pathway have been demonstrated to induce phase-resetting of the hippocampal theta rhythm (Williams and Givens, 2003). This has suggested to occur via a stimulation-induced GABA-dependent inhibition of the pacemaker neurons in the medial septal area (via the fornix descending fibres), which subsequently results in a reset of their theta-frequency rhythmic-bursting properties (Williams and Givens, 2003, Buno et al., 1978).

Another possible mechanism that results from DBS is long-term potentiation (LTP). This is a lasting enhancement of synaptic potentials resulting from a strengthened connectivity between neurons, and is widely believed to be one of the core mechanisms by which learning and memory works. The hippocampus, dentate gyrus and various brain regions involved in learning and memory have long been known for their high degree of plasticity. Tetanic or high-frequency stimulation has been previously shown to induce LTP in both anaesthetised (Bliss and Lomo, 1973, Laroche et al., 1990) and freely-moving rodents (Degenetais et al., 2003). Early on, Bliss (1975) noticed that repetitive stimulation in the perforant pathway of anaesthetised rabbits had resulted in potentiated responses in the dentate gyrus region, with time-scales between 30 minutes to 10-hours. In anaesthetised rats, Laroche and colleagues (1990) discovered a sustained potentiation of field potentials recorded in the mPFC following high-frequency stimulation of the CA1-subicular hippocampal region (Laroche et al., 1990). A similar experiment to this was carried out in freely-moving rats, in which tetanic stimulation was also seen to produce LTP in this same monosynaptic pathway (Degenetais et al., 2003). This is interesting given the requirement of this glutamatergic white matter tract in successful working memory performance (see 1.4.3: Working Memory Relies on Connectivity of Hippocampus and Prefrontal Cortex). Indeed following a year of DBS in the fornix of Alzheimer's patients (Laxton et al., 2010), Smith et al., (2012) noted an enhancement in the functional connectivity of multiple brain regions connecting to the hippocampus, as verified through PET functional connectivity analysis. In this case an enhanced connectivity was found in the fronto-temporal-occipital-hippocampal network, and the frontal-temporal-parietal-striatal-thalamic network, as

observed a year after the onset of fornix DBS. Notably these connectivity increases were correlated with not only an increased baseline metabolism in these regions, but also with improved cognition and memory performance (Smith et al., 2012).

As such one of the possible consequences of high-frequency stimulation of the FF could be plastic changes in the hippocampal region which links to various structures involved with learning and memory. In the hippocampus, activation of postsynaptic NMDA receptors is known to be a requirement for LTP (Nicoll and Malenka, 1995). In rat subthalamic nucleus (STN) slices *in vitro*, Shen et al., (2003) demonstrated both short and long-lasting increases in excitatory post-synaptic current amplitude following high-frequency stimulation, which as the authors suggested, may be due to an stimulation-induced increase in calcium within the presynaptic nerve terminals, which leads to an increased probability of glutamate release (Shen et al., 2003, Zucker et al., 1991). However it is of note that long-term depression (LTD) was also observed in this same study (in a comparatively smaller number of neurons recorded). Whilst the current study used a 30-second train of stimulus pulses at 130Hz, the optimal conditions for inducing LTP between neurons is when discrete bursts of high-frequency pulses are delivered at a theta-frequency (Larson et al., 1986). Furthermore, in the CA1 region of the hippocampus it has been shown that LTP or LTD can be induced, depending on whether these pulses are delivered at the peak or the trough of the theta waveform, respectively (Hyman et al., 2003). With this in mind, it may be of interest to attempt to facilitate LTP in the hippocampoprefrontal pathway by applying stimulus pulses at the peak of hippocampal theta – and to study its effects on learning and memory. Given the widespread connectivity of the FF, it is difficult to pinpoint the exact effects of DBS without studying the electrophysiology and metabolism in a myriad of the connected brain regions.

Finally, another possible mechanism of action of DBS involves the neurogenesis of cells. High-frequency DBS of the entorhinal cortex in mice has been demonstrated to result in a transient neurogenesis of cells in the dentate gyrus region of the hippocampus, which in turn was associated with an enhancement in spatial working memory (Stone et al., 2011). Furthermore, a neurogenesis of cells has also been observed in the hippocampus of rats, which underwent high-frequency DBS in the

anterior thalamic nucleus (ATN; Toda et al., 2008). Without the use of relevant immunohistochemical techniques to complement the data obtained in this study, the neurogenesis mechanism remains a possible outcome of DBS which may warrant future study.

Taken together, the information presented in the current study regarding the effects of FF stimulation should be taken with caution given a) the small sample sizes used, and b) the inconsistency in FF electrode placement; in that some rats only had one of the two electrodes correctly placed inside the FF (see Chapter 4 - 4.4.6: Brain Imaging and Electrode Coordinates). Nonetheless an intriguing future study could probe deeper into the mechanisms by which FF stimulation causes enhancements in hippocampal theta rhythm, and how it may cause an enhancement in spatial learning in rats. A future study featuring a larger number of rats can probe the mechanisms of action of FF-DBS better if it featured post-mortem immunohistochemical techniques such as staining for cell activity markers such as *c-fos*. Such a study could highlight activation patterns in the brain following an acute administration of DBS.

### **5.6.5 Effect of PCP on Behavioural Performance**

In this study, PCP was not found to produce significant behavioural deficits in the T-maze task, as measured by observing the rat mean score during test days. This may have been a consequence of the relatively small sample sizes used; as each of the two PCP-treatment groups had only 3-4 rats. Furthermore PCP was only administered on 2 test days, leading to a relatively small number of observations per rat tested. To contrast with this, Moghaddam and Adams (1998) were able to demonstrate a significant impairment in performance of rats which underwent a discrete-trials delayed alternation version of the T-maze task, following acute administration of  $1\text{mg}\cdot\text{kg}^{-1}$  and  $5\text{mg}\cdot\text{kg}^{-1}$  i.p. PCP. This performance deficit was noted as a significantly reduced percentage of correct responses relative to a baseline performance, and was significant at both the 10- and 40-second intra-trial delay periods. As discussed in Chapter 4 (see 4.6.4: Experimental Design), the design of this study by Moghaddam and Adams had required rats to reach a “stable baseline”



performance during training, and their test scores would later be measured relative to this. This particular design may have been beneficial to the current study given the small sample size and the large variation in test scores observed. For instance, one rat in particular (from the stimulation-PCP test group) had obtained a score of 2/10 on the first test day, followed by a perfect score of 10/10 on the next test day.

### **5.6.6 Hippocampal Theta-Frequency Changes**

Throughout the course of the experiment the frequency of peak hippocampal theta was seen to vary depending on the level of rat training and on the phase of the T-maze task (e.g. baseline, T-maze central arm, etc.). This effect was therefore studied to investigate a) how theta-frequency changes in behavioural experiments have been interpreted by other researchers, and b) if it was affected by the use of PCP, or DBS of the FF. In this experiment the centre-frequency of hippocampal theta was found to be significantly elevated from baseline in all groups of rats when they were placed inside the T-maze. These increases were found during both the drug and washout test days. When the T-maze data from both the drug and washout test days was compared with the T-maze data obtained during habituation however, there were mixed results regarding the differences in the centre-frequency of hippocampal theta. In this case the centre-frequency was found to be significantly elevated in the stimulation-vehicle group on all test days ( $p=0.0105$  – drug,  $p=0.0127$  – washout), and also in the stimulation-PCP group during the washout test day ( $p=0.0187$ ). All other groups displayed non-significant mean increases in the theta centre-frequency between the habituation and test T-maze recordings. These mixed results may be due to the small sample sizes used. Given the sample sizes used the frequency elevations between that recorded during the pre-test baseline and at the T-maze choice-point were large enough to show statistical significance in all rat groups; although the varied results between habituation T-maze data and testing T-maze data is still intriguing. Given the relatively small sample size used in these tests, as well as the slight variation in hippocampal frequency between each of the rats, these mixed results were to be expected. A repeated study featuring a larger sample size is required to properly determine whether the centre-frequency of hippocampal theta

had increased in each of the experimental groups following a period of training. Finally, no significant differences in theta centre frequency were found between the data obtained during the drug test day and the washout test day, and no significant effects of T-maze run type (forced, correct and incorrect turns) were found in each of the groups of rats.

Similar to measurements of hippocampal theta power, theta frequency changes has been previously associated with rat movement. An early study found that during locomotion the frequency at which hippocampal power was elevated became constant (Vanderwolf, 1969), and this has more recently been correlated with rat movement speed (Hyman et al., 2003, Bouwman et al., 2005, Slawinska and Kasicki, 1998). More recent attempts to discern the nature of hippocampal frequency changes have resulted in various sub-bands of theta power being proposed, such as the cholinergic-independent low-frequency theta, as well as a higher-frequency cholinergic rhythm associated with voluntary motor behaviours (Kramis et al., 1975, Vanderwolf and Baker, 1986, Olvera-Cortes et al., 2004). In this sense the power of each sub-band of hippocampal theta would determine the overall centre-frequency observed during a particular behavioural task. A recent experiment attempted to control the speed of rat running by utilising a running wheel with regular velocity measurements, and through this the authors were able to observe changes in the various sub-bands of hippocampal theta (Li et al., 2012). They indeed noted a positive correlation between rat running speed and the high-frequency (>6.5 Hz) component of theta, but this correlation was only valid during the onset of running, and subsequent speed changes had no effect on theta. An interesting recent study examined the effects of environmental novelty on hippocampal theta frequency (Jeewajee et al., 2008), and noticed a mean drop in theta-frequency of 0.6Hz when rats were recorded in a novel environment rather than a familiar one. This was based on the hypothesis that cholinergic input to the hippocampus – which contributes to a slow theta rhythm (Kramis et al., 1975) is triggered by environmental novelty, as previously observed by Thiel et al., (1998). These results have recently come under scrutiny however (see Sambeth et al., 2009), due in part to the design of the study which may have induced a low-frequency hippocampal rhythm due to the foraging

activity of the rats (as they used food-deprived animals in environments with food placed inside), rather than environmental novelty.

The increased hippocampal centre-frequency observed in the T-maze recordings relative to baseline makes sense when considered in tandem with many of the findings that positively correlate hippocampal frequency with rat movement speed. Indeed if the centre-frequency of the test-sessions are elevated with respect to that obtained during habituation, then this may too reflect an increased rat speed through the T-maze central arm following the training process. Should environmental novelty play a part in shaping this theta rhythm, it cannot be elucidated in the present study because the speed at which the rat moved through the T-maze was not controlled. Nonetheless by this theory the theta centre-frequency reductions would be expected during habituation and in the earlier stages of training, and may thus provide a useful tool to assess familiarity of the rat to its environment. Furthermore it is intriguing that the centre-frequency of hippocampal theta remained unchanged between the drug and washout test days for the PCP-treated rats. Of particular note is that the PCP-treated rats were observed to move much more slowly through the T-maze than their saline-treated counterparts. Again, without a robust measurement of rat velocity this will require replication in a new type of experiment, but nonetheless raises the intriguing possibility that the centre-frequency of rat theta activity may be largely determined by some behavioural measure related to the task that isn't solely based on the mean velocity of the rats.

### **5.6.7 Summary of Results**

This experiment augments the previous one by introducing the effects of PCP into DBS and sham-treated rats, as they undertake a working memory task. Furthermore, it offers a more in-depth analysis by comparing the results from the PCP-treated rats in this chapter, with the saline-treated rats in Chapter 4.

The most robust observations made during this experiment revolved around the use of PCP. Following an acute injection, PCP was shown to significantly increase the gamma-frequency activity in both the mPFC (700% – 900%) and in dCA1 (300% –

400%), relative to both the washout test day LFP, and also to the saline-treated controls. This effect can be in part explained by a disinhibition of pyramidal cell activity resulting from a blockade of NMDA receptors located on the GABAergic parvalbumin-containing interneurons (Homayoun and Moghaddam, 2007). Accompanied by this were increases in cortical gamma synchronisation in the PCP-treated rats. Whilst this particular analysis was confounded by a small sample size (and only significant when comparing drug and washout LFP within the PCP-treated groups), these striking observations are interesting because they hint at the ability of acute PCP to mimic some of the functional deficits that have previously been associated with the positive symptoms of schizophrenia (Spencer et al., 2004, Baldeweg et al., 1998, Herrmann and Demiralp, 2005). Indeed these observations have also been through the use of other NMDA receptor antagonists such as MK-801 and ketamine in humans (Pinault, 2008). Theta coherence between the prefrontal cortex and hippocampus has been correlated numerous times with spatial working memory in rodents (Jones and Wilson, 2005, Sigurdsson et al., 2010), and this mechanism has been shown to rely on the monosynaptic connections between these structures. As expected theta coherence reached its maximum increase for rats tested in the T-maze, however PCP only resulted in significant reductions during the inter-trial delay period, and no significant effect of PCP was found in the T-maze recordings.

Deep brain stimulation was applied throughout the training and test period, and its use hinted at the possibility of an increased ability for rats to learn the T-maze task. Whilst no significant increases in rat score or task acquisition time were found, this may have been due again, to the small sample sizes used. Notably 4 rats in the stimulation groups learned the task in 3 sessions, as compared to 1 rat in the two sham groups. Stimulation of the FF was found to result in a significant increase in the mean (normalised) theta-frequency PSD as observed in the hippocampal region, and this was seen to occur in the T-maze choice-runs that directly followed a 30-second period of stimulation. This is intriguing because the fimbria-fornix (FF) contains white-matter tracts that form one of the major sources of hippocampal input from various limbic structures including the medial septum.

Finally, significant increases in the mean frequency of hippocampal peak theta activity were observed between the T-maze runs during testing, and its corresponding baseline recording. This may be due to rat locomotion, which has seen various positive correlations with rat running speed in the past (Hyman et al., 2003, Bouwman et al., 2005, Slawinska and Kasicki, 1998). Interestingly non-significant increases were observed between the centre-frequency recorded in the T-maze during testing, as compared to that seen in the T-maze during habituation. If these increases are valid, it may be due to a) increased rat running speed during testing, or b) a reduction in the cholinergic-mediated low-frequency component of theta following familiarity to the T-maze environment.

	Power Spectral Density				
	mPFC		dCA1		dCA1 Theta Frequency
	Theta	Gamma	Theta	Gamma	
DBS Effects	↔	↔	↑ following transient stimulation	↔	↔
Acute PCP Effect	↔	↑	↔	↑	↔
PCP x T-Maze Interaction	↔	↔	yes	↔	↔
PCP Washout Effect	↓	↔	↓	↔	↔
T-Maze vs. Baseline	↑	↑	↑	↑	↑

	Coherence			
	mPFC-dCA1		mPFC-mPFC	
	Theta	Gamma	Theta	Gamma
Acute PCP Effect	↓ during inter-trial delay	↔	↔	↔ non-significant increase
PCP Washout Effect	↔	↔	↔	↔
T-Maze vs. Baseline	↑	↔	↔	↔

Table 5.12 – Summary of LFP findings in the behavioural experiment. Most of the LFP changes were apparent through the use of PCP, which included increased gamma activity following an acute injection, and reduced theta activity during washout. When animals were placed into the T-maze widespread increases were seen in theta and gamma frequencies in both brain regions, as well as increases in theta coherence between mPFC-dCA1 brain regions. Finally an enhanced theta activity was noted in the T-maze choice-point recordings following a 30-second treatment with FF stimulation.

# Chapter 6

## Conclusions

This study has detailed the design and development of novel electrophysiological devices for performing neural recording and stimulation in freely-moving rodents. In doing so, it has paved the way for entirely new types of experiments to take place that previously would have been impossible or impractical, given the currently available technology. Subsequently, these systems were utilised in a novel type of behavioural experiment which allowed local-field potential (LFP) recording, video-tracking, and deep-brain stimulation (DBS) to take place in a rodent model of relevance to schizophrenia.

The EEG-DBS system and its receiver were developed for the purpose of augmenting existing behavioural studies that involve DBS in freely-moving rodents, with multichannel LFP recordings. Previously, a miniature wireless DBS device has been used to study the effects of thalamic stimulation in a rodent model relevant to schizophrenia (Ewing et al., 2009). However the same researcher was only able to carry out a combined DBS and EEG-recording study in anaesthetised rodents, since two separate systems were required to carry out the functions of recording and stimulation (Ewing et al., 2009). This reflects a common problem in studies of this type, in that the experimental design is often limited by the equipment that is available. As the application areas surrounding DBS expands into neuropsychiatric disorders, novel solutions are required to increase the range of experiments that can be made in the research setting. This is essential because DBS itself – as well as the disorders they are used to treat – are not fully understood. At present there is a large variety of wireless commercial and non-commercial systems that have been developed to perform either DBS or LFP recording in freely-moving rodents (see

Chapter 2 Background for a review). However there are only several such devices capable of combining these two modalities, and these are either too large for the current study, or simply lack the required functionality such as channel count or battery life. To the author's knowledge, the EEG-DBS system that has been developed is the smallest device currently available that is capable of multichannel DBS and LFP recording in freely-moving rodents; weighing at 8.5g including the battery. Furthermore, it is able to outperform all of the other systems in its class in many of their design specifications; such as battery life, voltage resolution as well as the amount of controllable features, parameters and operating modes it has (see Chapter - 2.2: Background; for a detailed review of the current technologies and systems). Designed for portability and simplicity, the EEG-DBS system has demonstrated its ability to be set up for rapid use, and utilised in a variety of recording arenas. Furthermore, the system is adaptable enough to synchronise its activities with existing systems, such as systems that mediate animal video-tracking.

The second system to be developed was the M-DBS system, and was adapted from the design of the EEG-DBS system. This was developed to allow for 4-channel DBS to take place in a chronic rodent study, involving multichannel DBS of the pedunculopontine nucleus (PPN) and its implications in Parkinson's disease (Gut and Winn, 2012). This system featured two independently controllable channel pairs, as well as more advanced pulse-mode control including the option for biphasic pulses on each of the channel pairs. Weighing less than 8.5g (including battery), this system was easily carried by the rodents and was subsequently used over a period of several weeks.

Following device development, the EEG-DBS system was utilised in a series of experiments to a) validate its ability to perform the functions for which it was designed, and b) study the effects of DBS in a rodent model of relevance to schizophrenia. In the proof-of-concept study, bilateral stimulation to the anterior thalamic nucleus (ATN) was shown to facilitate a transient increase in rat velocity, when current was delivered at the highest intensity (100 $\mu$ A). Furthermore, correlations were made between theta-frequency power spectral density (PSD) in the hippocampus, and both theta-frequency intra-hemispheric coherence and rat mean



velocity. Ultimately the ideas and concepts introduced in this study enabled appropriate boundaries of the working memory task to be set; mainly involving the experimental design. For example, the current intensity of stimulation was set at 30 $\mu$ A, due in part to the transient locomotor activity increases observed through application of 100 $\mu$ A DBS of the ATN.

The novel experimental design introduced in Chapter 4 described how the EEG-DBS system was modified to incorporate synchronised video-tracking into a behavioural task, which already featured LFP recording and DBS in freely-moving rodents. The system was able to successfully integrate these modalities, allowing for a complex and varied cross-analysis of the data which was obtained. In this experiment, DBS of the fimbria-fornix (FF) was carried out in rodents as they undertook a working-memory task. This experiment was subsequently expanded in Chapter 5 to include the acute effects of the NMDA receptor antagonist PCP.

Generally speaking many of the findings from these experiments revolved around the use of PCP. Gamma-frequency brain waves were seen to be significantly elevated in all of the rats that was administered acute PCP (at 3mg.kg<sup>-1</sup>), and these increases were significant for both the mPFC and dCA1 brain regions. The main mechanism surrounding this increase is most likely due to a disinhibition of GABAergic interneuron inhibitory control on its connecting pyramidal neurons. Non-significant increases in cortical gamma synchrony were also observed, which may provide a link between acute PCP and the positive symptoms of schizophrenia. Finally, a reduction in mPFC-dCA1 theta-frequency coherence was also observed through the use of acute PCP, but this was only significant during the inter-trial delay periods of the task. In this case the loss of coordination between these brain regions is most likely a result of a reduced ability of GABAergic interneurons to synchronise and coordinate the activity of neural networks.

Stimulation in the FF was observed to correlate with an increase in hippocampal activity, presumably via direct activation of its connecting white-matter tracts. In this case significant effects of stimulation were seen for dCA1 theta-frequency PSD, which were accompanied by significant effects of task-phase

(forced/correct/incorrect turns), as well as a significant stimulation by task-phase interaction. This suggests that hippocampal activity is increased directly following a 30-second period of FF DBS. Interestingly an increased activity in the hippocampus has previously been observed through stimulation of various brain regions in and around Papez's circuit, including the fornix (Hamani et al., 2008, Laxton et al., 2010, Smith et al., 2012), medial septum (Lee et al., 2013), and entorhinal cortex (Suthana et al., 2012). Furthermore, these increases in activity as previously seen have all been correlated with working memory enhancements in the studies in which they were performed. Whilst no significant increase in rat score or learning rate was observed during the training period, this may have been due to lower sample numbers, given the intriguing (non-significant) tendency for stimulated rats to learn the task faster. Thus one of the main mechanisms of FF stimulation may be an enhancement in the rat's ability to learn the working memory task; however a repeated study with a larger sample size will have to take place to probe these observations further.

A large number of possibilities exist to further the findings discussed in the present study, and are related to the wireless devices, the experimental design, and the direction for future research involving DBS and its implications for the treatment of schizophrenia. For a comprehensive overview of these possible expansions to the current research, refer to the discussion sections in Chapter 2 - 2.5, Chapter 4 - 4.6, and Chapter 5 - 5.6).

Numerous improvements can be made to the wireless devices for the purposes of reducing their size, increasing their functionality, or increasing their battery life. Battery life and system size are largely coupled together because the size of the system's battery size ultimately dictates the battery life of the system. For considering a device small enough for mouse studies, significant reductions in system size will have to be made. This can be achieved in a number of ways, one of which is to consider the use of application-specific integrated circuit (ASIC) or field-gate programmable array (FGPA) technology. FPGA's in particular provides the functionality and performance of ASIC systems albeit on a much smaller budget, and in general is more accessible to the designer. Further enhancements to the system can be considered by replacing the wireless data transmission functionality

with an in-built memory module – effectively turning the system into a wireless neuro-logging device. This can circumvent many of the power-consumption problems inherent with the transmission of wireless EEG, and can also reduce the overall size of the system. Numerous enhancements can be made to the experimental design, for example by using software which controls the action of both the EEG-DBS and video-tracking systems. Perhaps an even more ambitious idea is to develop an automated test maze, which is integrated into a computer-controlled system which also mediates the actions of the video-tracking and EEG-DBS systems. Not only could this increase the accuracy of the working memory tasks, but it could also make the studies more controlled by removing the human influence, as well as save the operator literally hundreds of hours of manual rat handling. Furthermore, this would simplify analysis since the multiple types of data obtained in the study would automatically be synchronised together.

The behavioural experiment outlined in Chapters 4 and 5 provided a number of interesting findings with regards to the workings of both PCP, and the use of FF-DBS. Many of the observations however did not reach significance, perhaps due to the small sample sizes used. A replication in this study using a larger sample group can serve to provide a more robust insight into many of the changes seen. For example, a study featuring more rats can be used to study the effects of acute and sub-chronic PCP in a working-memory task, using video-tracking to monitor the animal's position and speed, and LFP recording to assess the functional changes in fronto-hippocampal brain regions. In addition to future studies which probe deeper into the use of FF-DBS, various other limbic brain regions can be investigated such as the entorhinal cortex and medial septum, and the effect that DBS of these structures has on learning and memory.

# References

- ABDUL-RAHMAN, M. F., QIU, A. Q. & SIM, K. 2011. Regionally Specific White Matter Disruptions of Fornix and Cingulum in Schizophrenia. *PLoS One*, 6.
- ABELSON, J. L., CURTIS, G. C., SAGHER, O., ALBUCHER, R. C., HARRIGAN, M., TAYLOR, S. F., MARTIS, B. & GIORDANI, B. 2005. Deep brain stimulation for refractory obsessive-compulsive disorder. *Biol Psychiatry*, 57, 510-6.
- ACKERMANS, L., TEMEL, Y., CATH, D., VAN DER LINDEN, C., BRUGGEMAN, R., KLEIJER, M., NEDERVEEN, P., SCHRUERS, K., COLLE, H., TIJSEN, M. A. & VISSER-VANDEWALLE, V. 2006. Deep brain stimulation in Tourette's syndrome: two targets? *Mov Disord*, 21, 709-13.
- ADAMS, B. & MOGHADDAM, B. 1998. Corticolimbic dopamine neurotransmission is temporally dissociated from the cognitive and locomotor effects of phencyclidine. *J Neurosci*, 18, 5545-54.
- ADELL, A., JIMENEZ-SANCHEZ, L., LOPEZ-GIL, X. & ROMON, T. 2012. Is the Acute NMDA Receptor Hypofunction a Valid Model of Schizophrenia? *Schizophrenia Bulletin*, 38, 9-14.
- ADHIKARI, A., TOPIWALA, M. A. & GORDON, J. A. 2010. Synchronized activity between the ventral hippocampus and the medial prefrontal cortex during anxiety. *Neuron*, 65, 257-69.
- AGGLETON, J. P., HUNT, P. R., NAGLE, S. & NEAVE, N. 1996. The effects of selective lesions within the anterior thalamic nuclei on spatial memory in the rat. *Behav Brain Res*, 81, 189-98.
- AGGLETON, J. P., NEAVE, N., NAGLE, S. & HUNT, P. R. 1995. A comparison of the effects of anterior thalamic, mamillary body and fornix lesions on reinforced spatial alternation. *Behav Brain Res*, 68, 91-101.
- AGGLETON, J. P., O'MARA, S. M., VANN, S. D., WRIGHT, N. F., TSANOV, M. & ERICHSEN, J. T. 2010. Hippocampal-anterior thalamic pathways for memory: uncovering a network of direct and indirect actions. *Eur J Neurosci*, 31, 2292-307.
- AKBARIAN, S., HUNTSMAN, M. M., KIM, J. J., TAFAZZOLI, A., POTKIN, S. G., BUNNEY, W. E., JR. & JONES, E. G. 1995a. GABAA receptor subunit gene expression in human prefrontal cortex: comparison of schizophrenics and controls. *Cereb Cortex*, 5, 550-60.
- AKBARIAN, S., KIM, J. J., POTKIN, S. G., HAGMAN, J. O., TAFAZZOLI, A., BUNNEY, W. E., JR. & JONES, E. G. 1995b. Gene expression for glutamic acid decarboxylase is

- reduced without loss of neurons in prefrontal cortex of schizophrenics. *Arch Gen Psychiatry*, 52, 258-66.
- AKERT, K. & HARTMANN-VON MONAKOW, K. 1980. Relationships of precentral premotor and prefrontal cortex to the mediodorsal and intralaminar nuclei of the monkey thalamus. *Acta Neurobiol Exp (Wars)*, 40, 7-25.
- ALELU-PAZ, R. & GIMENEZ-AMAYA, J. M. 2008. The mediodorsal thalamic nucleus and schizophrenia. *J Psychiatry Neurosci*, 33, 489-98.
- AMARAL, D. G. & COWAN, W. M. 1980. Subcortical afferents to the hippocampal formation in the monkey. *J Comp Neurol*, 189, 573-91.
- AMARAL, D.G., WITTER, M.P. 1995. Hippocampal formation. In: Paxinos G, editor. The rat nervous system. 2nd ed. San Diego: Academic Press, 443-93.
- ANDERSEN, P. 2007. *The hippocampus book*, Oxford ; New York, Oxford University Press.
- ANDO, N., SHIMOYAMA, I. & KANZAKI, R. 2002. A dual-channel FM transmitter for acquisition of flight muscle activities from the freely flying hawkmoth, *Agrius convolvuli*. *J Neurosci Methods*, 115, 181-7.
- ANDRADE, P., CARRILLO-RUIZ, J. D., RAMIREZ, Y. & JIMENEZ, F. 2010. Effects of Thalamic Reticular Nucleus Electrical Stimulation in Rats in a T-maze Perseverative Behavior Model Induced by 8-OH-DPAT. *Neuromodulation*, 13, 2-9.
- ANDREASEN, N. C. 1997. Linking mind and brain in the study of mental illnesses: a project for a scientific psychopathology. *Science*, 275, 1586-93.
- ANDREASEN, N. C., ARNDT, S., SWAYZE, V., 2ND, CIZADLO, T., FLAUM, M., O'LEARY, D., EHRHARDT, J. C. & YUH, W. T. 1994. Thalamic abnormalities in schizophrenia visualized through magnetic resonance image averaging. *Science*, 266, 294-8.
- ANDREWS, J., WANG, L., CSERNANSKY, J. G., GADO, M. H. & BARCH, D. M. 2006. Abnormalities of thalamic activation and cognition in schizophrenia. *Am J Psychiatry*, 163, 463-9.
- ANVER, H., WARD, P. D., MAGONY, A. & VREUGDENHIL, M. 2011. NMDA receptor hypofunction phase couples independent gamma-oscillations in the rat visual cortex. *Neuropsychopharmacology*, 36, 519-28.
- AOUIZERATE, B., CUNY, E., MARTIN-GUEHL, C., GUEHL, D., AMIEVA, H., BENAZZOUZ, A., FABRIGOULE, C., ALLARD, M., ROUGIER, A., BIOULAC, B., TIGNOL, J. & BURBAUD, P. 2004. Deep brain stimulation of the ventral caudate nucleus in the treatment of obsessive-compulsive disorder and major depression. Case report. *J Neurosurg*, 101, 682-6.
- ARNOLD, S. E., FRANZ, B. R., GUR, R. C., GUR, R. E., SHAPIRO, R. M., MOBERG, P. J. & TROJANOWSKI, J. Q. 1995. Smaller neuron size in schizophrenia in hippocampal subfields that mediate cortical-hippocampal interactions. *Am J Psychiatry*, 152, 738-48.
- ASTON-JONES, G., RAJKOWSKI, J. & KUBIAK, P. 1997. Conditioned responses of monkey locus coeruleus neurons anticipate acquisition of discriminative behavior in a vigilance task. *Neuroscience*, 80, 697-715.

- ATIVANICHAYAPHONG, T., HE, J. W., HAGAINS, C. E., PENG, Y. B. & CHIAO, J. C. 2008. A combined wireless neural stimulating and recording system for study of pain processing. *J Neurosci Methods*, 170, 25-34.
- AUGUSTINACK, J. C., HELMER, K., HUBER, K. E., KAKUNOORI, S., ZOLLEI, L. & FISCHL, B. 2010. Direct visualization of the perforant pathway in the human brain with ex vivo diffusion tensor imaging. *Front Hum Neurosci*, 4, 42.
- AURA, J. & RIEKKINEN, P., JR. 1999. Blockade of NMDA receptors located at the dorsomedial prefrontal cortex impairs spatial working memory in rats. *Neuroreport*, 10, 243-8.
- BADDELEY, A. 1992. Working memory. *Science*, 255, 556-9.
- BADDELEY, A. 2003. Working memory: looking back and looking forward. *Nat Rev Neurosci*, 4, 829-39.
- BALDEWEG, T., SPENCE, S., HIRSCH, S. R. & GRUZELIER, J. 1998. Gamma-band electroencephalographic oscillations in a patient with somatic hallucinations. *Lancet*, 352, 620-1.
- BARBAS, H. 1995. Anatomic basis of cognitive-emotional interactions in the primate prefrontal cortex. *Neurosci Biobehav Rev*, 19, 499-510.
- BARCH, D. M. 2005. The cognitive neuroscience of schizophrenia. *Annu Rev Clin Psychol*, 1, 321-53.
- BARCH, D. M. & CEASER, A. 2012. Cognition in schizophrenia: core psychological and neural mechanisms. *Trends Cogn Sci*, 16, 27-34.
- BARCH, D. M., CARTER, C. S., BRAVER, T. S., SABB, F. W., MACDONALD, A., 3RD, NOLL, D. C. & COHEN, J. D. 2001. Selective deficits in prefrontal cortex function in medication-naïve patients with schizophrenia. *Arch Gen Psychiatry*, 58, 280-8.
- BARTOS, M., VIDA, I., FROTSCHER, M., MEYER, A., MONYER, H., GEIGER, J. R. & JONAS, P. 2002. Fast synaptic inhibition promotes synchronized gamma oscillations in hippocampal interneuron networks. *Proc Natl Acad Sci U S A*, 99, 13222-7.
- BARTOS, M., VIDA, I. & JONAS, P. 2007. Synaptic mechanisms of synchronized gamma oscillations in inhibitory interneuron networks. *Nat Rev Neurosci*, 8, 45-56.
- BASSER, P.J. 1995. Inferring microstructural features and the physiological state of tissues from diffusion-weighted images. *NMR Biomed*, 8, 333-344.
- BAUP, N., GRABLI, D., KARACHI, C., MOUNAYAR, S., FRANCOIS, C., YELNIK, J., FEGER, J. & TREMBLAY, L. 2008. High-frequency stimulation of the anterior subthalamic nucleus reduces stereotyped behaviors in primates. *J Neurosci*, 28, 8785-8.
- BEASLEY, C. L. & REYNOLDS, G. P. 1997. Parvalbumin-immunoreactive neurons are reduced in the prefrontal cortex of schizophrenics. *Schizophr Res*, 24, 349-55.
- BEAULIEU, C. 2002. The basis of anisotropic water diffusion in the nervous system – a technical review. *NMR Biomed*, 15, 435-455.

- BELLUSCIO, M. A., MIZUSEKI, K., SCHMIDT, R., KEMPTER, R. & BUZSAKI, G. 2012. Cross-frequency phase-phase coupling between theta and gamma oscillations in the hippocampus. *J Neurosci*, 32, 423-35.
- BENABID, A. L., BENAZZOUS, A. & POLLAK, P. 2002. Mechanisms of deep brain stimulation. *Mov Disord*, 17 Suppl 3, S73-4.
- BENABID, A. L., POLLAK, P., LOUVEAU, A., HENRY, S. & DE ROUGEMONT, J. 1987. Combined (thalamotomy and stimulation) stereotactic surgery of the VIM thalamic nucleus for bilateral Parkinson disease. *Appl Neurophysiol*, 50, 344-6.
- BENAZZOZ, A., GAO, D. M., NI, Z. G., PIALLAT, B., BOUALI-BENAZZOZ, R. & BENABID, A. L. 2000. Effect of high-frequency stimulation of the subthalamic nucleus on the neuronal activities of the substantia nigra pars reticulata and ventrolateral nucleus of the thalamus in the rat. *Neuroscience*, 99, 289-95.
- BENAZZOZ, A. & HALLETT, M. 2000. Mechanism of action of deep brain stimulation. *Neurology*, 55, S13-6.
- BENAZZOZ, A., PIALLAT, B., POLLAK, P. & BENABID, A. L. 1995. Responses of substantia nigra pars reticulata and globus pallidus complex to high frequency stimulation of the subthalamic nucleus in rats: electrophysiological data. *Neurosci Lett*, 189, 77-80.
- BENCHENANE, K., PEYRACHE, A., KHAMASSI, M., TIERNEY, P. L., GIOANNI, Y., BATTAGLIA, F. P. & WIENER, S. I. 2010. Coherent theta oscillations and reorganization of spike timing in the hippocampal- prefrontal network upon learning. *Neuron*, 66, 921-36.
- BENES, F. M., SORENSEN, I. & BIRD, E. D. 1991. Reduced neuronal size in posterior hippocampus of schizophrenic patients. *Schizophr Bull*, 17, 597-608.
- BENES, F. M., VINCENT, S. L., MARIE, A. & KHAN, Y. 1996. Up-regulation of GABAA receptor binding on neurons of the prefrontal cortex in schizophrenic subjects. *Neuroscience*, 75, 1021-31.
- BERKE, J. D., OKATAN, M., SKURSKI, J. & EICHENBAUM, H. B. 2004. Oscillatory entrainment of striatal neurons in freely moving rats. *Neuron*, 43, 883-96.
- BERTRAM, E. H., WILLIAMSON, J. M., CORNETT, J. F., SPRADLIN, S. & CHEN, Z. F. 1997. Design and construction of a long-term continuous video-EEG monitoring unit for simultaneous recording of multiple small animals. *Brain Res Brain Res Protoc*, 2, 85-97.
- BEURRIER, C., BIOULAC, B., AUDIN, J. & HAMMOND, C. 2001. High-frequency stimulation produces a transient blockade of voltage-gated currents in subthalamic neurons. *J Neurophysiol*, 85, 1351-6.
- BI, G. Q. & POO, M. M. 1998. Synaptic modifications in cultured hippocampal neurons: dependence on spike timing, synaptic strength, and postsynaptic cell type. *J Neurosci*, 18, 10464-72.
- BIKSON, M., LIAN, J., HAHN, P. J., STACEY, W. C., SCIORTINO, C. & DURAND, D. M. 2001. Suppression of epileptiform activity by high frequency sinusoidal fields in rat hippocampal slices. *J Physiol*, 531, 181-91.

- BIRDNO, M. J., COOPER, S. E., REZAI, A. R. & GRILL, W. M. 2007. Pulse-to-pulse changes in the frequency of deep brain stimulation affect tremor and modeled neuronal activity. *J Neurophysiol*, 98, 1675-84.
- BIRDNO, M. J. & GRILL, W. M. 2008. Mechanisms of deep brain stimulation in movement disorders as revealed by changes in stimulus frequency. *Neurotherapeutics*, 5, 14-25.
- BIRDNO, M. J., KUNCEL, A. M., DORVAL, A. D., TURNER, D. A. & GRILL, W. M. 2008. Tremor varies as a function of the temporal regularity of deep brain stimulation. *Neuroreport*, 19, 599-602.
- BJORGVINSSON, T., HART, J. & HEFFELFINGER, S. 2007. Obsessive-compulsive disorder: update on assessment and treatment. *J Psychiatr Pract*, 13, 362-72.
- BLAIR, H. T. & SHARP, P. E. 1995. Anticipatory head direction signals in anterior thalamus: evidence for a thalamocortical circuit that integrates angular head motion to compute head direction. *J Neurosci*, 15, 6260-70.
- BLAND, B. H. 1986. The physiology and pharmacology of hippocampal formation theta rhythms. *Prog Neurobiol*, 26, 1-54.
- BLAND, B. H., ANDERSON, P. & GANES, T. 1975. Two generators of hippocampal theta activity in rabbits. *Brain Res*, 94, 199-218.
- BLISS, T. V. & LOMO, T. 1973. Long-lasting potentiation of synaptic transmission in the dentate area of the anaesthetized rabbit following stimulation of the perforant path. *J Physiol*, 232, 331-56.
- BOOSTANI, R., SADATNEZHAD, K. & SABETI, M. 2009. An efficient classifier to diagnose of schizophrenia based on the EEG signals. *Expert Syst. Appl.*, 36, 6492-6499.
- BORAUD, T., BEZARD, E., BIOULAC, B. & GROSS, C. 1996. High frequency stimulation of the internal Globus Pallidus (GPi) simultaneously improves parkinsonian symptoms and reduces the firing frequency of GPi neurons in the MPTP-treated monkey. *Neurosci Lett*, 215, 17-20.
- BOULET, S., LACOMBE, E., CARCENAC, C., FEUERSTEIN, C., SGAMBATO-FAURE, V., POUPARD, A. & SAVASTA, M. 2006. Subthalamic stimulation-induced forelimb dyskinesias are linked to an increase in glutamate levels in the substantia nigra pars reticulata. *J Neurosci*, 26, 10768-76.
- BOUTROS, N. N., ARFKEN, C., GALDERISI, S., WARRICK, J., PRATT, G. & IACONO, W. 2008. The status of spectral EEG abnormality as a diagnostic test for schizophrenia. *Schizophr Res*, 99, 225-37.
- BOUWMAN, B. M., VAN LIER, H., NITERT, H. E. J., DRINKENBURG, W. H. I. M., COENEN, A. M. L. & VAN RIJN, C. M. 2005. The relationship between hippocampal EEG theta activity and locomotor behaviour in freely moving rats: effects of vigabatrin. *Brain Research Bulletin*, 64, 505-509.
- BRAGIN, A., JANDO, G., NADASDY, Z., HETKE, J., WISE, K. & BUZSAKI, G. 1995. Gamma (40-100 Hz) oscillation in the hippocampus of the behaving rat. *J Neurosci*, 15, 47-60.



- BRAMON, E., RABE-HESKETH, S., SHAM, P., MURRAY, R. M. & FRANGOU, S. 2004. Meta-analysis of the P300 and P50 waveforms in schizophrenia. *Schizophr Res*, 70, 315-29.
- BREIT, S., SCHULZ, J. B. & BENABID, A. L. 2004. Deep brain stimulation. *Cell Tissue Res*, 318, 275-88.
- BRITTAİN, J. S., GREEN, A. L., JENKINSON, N., RAY, N. J., HOLLAND, P., STEIN, J. F., AZIZ, T. Z. & DAVIES, P. 2009. Local field potentials reveal a distinctive neural signature of cluster headache in the hypothalamus. *Cephalalgia*, 29, 1165-73.
- BROADBELT, K., BYNE, W. & JONES, L. B. 2002. Evidence for a decrease in basilar dendrites of pyramidal cells in schizophrenic medial prefrontal cortex. *Schizophr Res*, 58, 75-81.
- BUBSER, M., DE BRABANDER, J. M., TIMMERMAN, W., FEENSTRA, M. G., ERDTSIECK-ERNSTE, E. B., RINKENS, A., VAN UUM, J. F. & WESTERINK, B. H. 1998. Disinhibition of the mediodorsal thalamus induces fos-like immunoreactivity in both pyramidal and GABA-containing neurons in the medial prefrontal cortex of rats, but does not affect prefrontal extracellular GABA levels. *Synapse*, 30, 156-65.
- BUCHSBAUM, M. S., SOMEYA, T., TENG, C. Y., ABEL, L., CHIN, S., NAJAFI, A., HAIER, R. J., WU, J. & BUNNEY, W. E., JR. 1996. PET and MRI of the thalamus in never-medicated patients with schizophrenia. *Am J Psychiatry*, 153, 191-9.
- BUNO, W., JR., GARCIA-SANCHEZ, J. L. & GARCIA-AUSTT, E. 1978. Reset of hippocampal rhythmical activities by afferent stimulation. *Brain Res Bull*, 3, 21-8.
- BURGESS, N., MAGUIRE, E. A. & O'KEEFE, J. 2002. The human hippocampus and spatial and episodic memory. *Neuron*, 35, 625-41.
- BURGESS, P. W., SCOTT, S. K. & FRITH, C. D. 2003. The role of the rostral frontal cortex (area 10) in prospective memory: a lateral versus medial dissociation. *Neuropsychologia*, 41, 906-18.
- BUZSAKI, G. 1984. Feed-forward inhibition in the hippocampal formation. *Prog Neurobiol*, 22, 131-53.
- BUZSAKI, G. 1991. The thalamic clock: emergent network properties. *Neuroscience*, 41, 351-64.
- BUZSAKI, G. 2002. Theta oscillations in the hippocampus. *Neuron*, 33, 325-40.
- BUZSAKI, G. 2004. Large-scale recording of neuronal ensembles. *Nat Neurosci*, 7, 446-51.
- BUZSÁKI, G. 2006. *Rhythms of the brain*, Oxford ; New York, Oxford University Press.
- BUZSAKI, G., BORS, L., NAGY, F. & EIDELBERG, E. 1982. Spatial mapping, working memory, and the fimbria-fornix system. *J Comp Physiol Psychol*, 96, 26-34.
- BUZSAKI, G., CZOPF, J., KONDAKOR, I. & KELLENYI, L. 1986. Laminar distribution of hippocampal rhythmic slow activity (RSA) in the behaving rat: current-source density analysis, effects of urethane and atropine. *Brain Res*, 365, 125-37.
- BUZSAKI, G., LEUNG, L. W. & VANDERWOLF, C. H. 1983. Cellular bases of hippocampal EEG in the behaving rat. *Brain Res*, 287, 139-71.

- BYATT, G. & DALRYMPLE-ALFORD, J. C. 1996. Both anteromedial and anteroventral thalamic lesions impair radial-maze learning in rats. *Behav Neurosci*, 110, 1335-48.
- BYNE, W., BUCHSBAUM, M. S., KEMETHER, E., HAZLETT, E. A., SHINWARI, A., MITROPOULOU, V. & SIEVER, L. J. 2001. Magnetic resonance imaging of the thalamic mediodorsal nucleus and pulvinar in schizophrenia and schizotypal personality disorder. *Arch Gen Psychiatry*, 58, 133-40.
- BYNE, W., BUCHSBAUM, M. S., MATTIACE, L. A., HAZLETT, E. A., KEMETHER, E., ELHAKEM, S. L., PUROHIT, D. P., HAROUTUNIAN, V. & JONES, L. 2002. Postmortem assessment of thalamic nuclear volumes in subjects with schizophrenia. *Am J Psychiatry*, 159, 59-65.
- BYNE, W., HAZLETT, E. A., BUCHSBAUM, M. S. & KEMETHER, E. 2009. The thalamus and schizophrenia: current status of research. *Acta Neuropathol*, 117, 347-68.
- CAIXETA, F. V., CORNELIO, A. M., SCHEFFER-TEIXEIRA, R., RIBEIRO, S. & TORT, A. B. 2013. Ketamine alters oscillatory coupling in the hippocampus. *Sci Rep*, 3, 2348.
- CALLICOTT, J. H., MATTAY, V. S., BERTOLINO, A., FINN, K., COPPOLA, R., FRANK, J. A., GOLDBERG, T. E. & WEINBERGER, D. R. 1999. Physiological characteristics of capacity constraints in working memory as revealed by functional MRI. *Cereb Cortex*, 9, 20-6.
- CALLICOTT, J. H., MATTAY, V. S., VERCHINSKI, B. A., MARENCO, S., EGAN, M. F. & WEINBERGER, D. R. 2003. Complexity of prefrontal cortical dysfunction in schizophrenia: more than up or down. *Am J Psychiatry*, 160, 2209-15.
- CARLEN, M., MELETIS, K., SIEGLE, J. H., CARDIN, J. A., FUTAI, K., VIERLING-CLAASSEN, D., RUHLMANN, C., JONES, S. R., DEISSEROTH, K., SHENG, M., MOORE, C. I. & TSAI, L. H. 2012. A critical role for NMDA receptors in parvalbumin interneurons for gamma rhythm induction and behavior. *Mol Psychiatry*, 17, 537-48.
- CARR, D. B. & SESACK, S. R. 1996. Hippocampal afferents to the rat prefrontal cortex: synaptic targets and relation to dopamine terminals. *J Comp Neurol*, 369, 1-15.
- CARTER, C. S., PERLSTEIN, W., GANGULI, R., BRAR, J., MINTUN, M. & COHEN, J. D. 1998. Functional hypofrontality and working memory dysfunction in schizophrenia. *Am J Psychiatry*, 155, 1285-7.
- CHANDLER, H. 2010. Rat models of abnormal hippocampal-cortical network activity associated with schizophrenia. PhD. University of Bristol.
- CHEN, H. Y., WU, J. S., HYLAND, B., LU, X. D. & CHEN, J. J. 2008. A low noise remotely controllable wireless telemetry system for single-unit recording in rats navigating in a vertical maze. *Med Biol Eng Comput*, 46, 833-9.
- CHESTEK, C. A., GILJA, V., NUYUJUKIAN, P., KIER, R. J., SOLZBACHER, F., RYU, S. I., HARRISON, R. R. & SHENOY, K. V. 2009. HermesC: low-power wireless neural recording system for freely moving primates. *IEEE Trans Neural Syst Rehabil Eng*, 17, 330-8.
- CHEUNG, T. & TAGLIATI, M. 2010. Deep brain stimulation: can we do it better? *Clin Neurophysiol*, 121, 1979-80.

- CHIEN, C. N. & JAW, F. S. 2005. Miniature telemetry system for the recording of action and field potentials. *J Neurosci Methods*, 147, 68-73.
- CHO, R. Y., KONECKY, R. O. & CARTER, C. S. 2006. Impairments in frontal cortical gamma synchrony and cognitive control in schizophrenia. *Proc Natl Acad Sci U S A*, 103, 19878-83.
- CHUA, S. E., CHEUNG, C., CHEUNG, V., TSANG, J. T., CHEN, E. Y., WONG, J. C., CHEUNG, J. P., YIP, L., TAI, K. S., SUCKLING, J. & MCALONAN, G. M. 2007. Cerebral grey, white matter and csf in never-medicated, first-episode schizophrenia. *Schizophr Res*, 89, 12-21.
- CHUNG-CHIUN, L., O'CONNOR, E. & STROHL, K. P. 2006. A multichannel, wireless telemetric microsystem for small animal studies. *Sensors Journal, IEEE*, 6, 187-202.
- CIESLEWSKI, G., CHENEY, D., GUGEL, K., SANCHEZ, J. C. & PRINCIPE, J. C. 2006. Neural signal sampling via the low power wireless pico system. *Conf Proc IEEE Eng Med Biol Soc*, 1, 5904-7.
- CLARK, C., KOPALA, L., LI, D. K. & HURWITZ, T. 2001. Regional cerebral glucose metabolism in never-medicated patients with schizophrenia. *Can J Psychiatry*, 46, 340-5.
- COBB, S. R., BUHL, E. H., HALASY, K., PAULSEN, O. & SOMOGYI, P. 1995. Synchronization of neuronal activity in hippocampus by individual GABAergic interneurons. *Nature*, 378, 75-8.
- COCHRAN, S. M., FUJIMURA, M., MORRIS, B. J. & PRATT, J. A. 2002. Acute and delayed effects of phencyclidine upon mRNA levels of markers of glutamatergic and GABAergic neurotransmitter function in the rat brain. *Synapse*, 46, 206-14.
- COCHRAN, S. M., KENNEDY, M., MCKERCHAR, C. E., STEWARD, L. J., PRATT, J. A. & MORRIS, B. J. 2003. Induction of metabolic hypofunction and neurochemical deficits after chronic intermittent exposure to phencyclidine: differential modulation by antipsychotic drugs. *Neuropsychopharmacology*, 28, 265-75.
- COLGIN, L. L., DENNINGER, T., FYHN, M., HAFTING, T., BONNEVIE, T., JENSEN, O., MOSER, M. B. & MOSER, E. I. 2009. Frequency of gamma oscillations routes flow of information in the hippocampus. *Nature*, 462, 353-7.
- COLOM, L. V., CHRISTIE, B. R. & BLAND, B. H. 1988. Cingulate cell discharge patterns related to hippocampal EEG and their modulation by muscarinic and nicotinic agents. *Brain Res*, 460, 329-38.
- CONDE, F., LUND, J. S., JACOBOWITZ, D. M., BAIMBRIDGE, K. G. & LEWIS, D. A. 1994. Local circuit neurons immunoreactive for calretinin, calbindin D-28k or parvalbumin in monkey prefrontal cortex: distribution and morphology. *J Comp Neurol*, 341, 95-116.
- CONRAD, A. J., ABEBE, T., AUSTIN, R., FORSYTHE, S. & SCHEIBEL, A. B. 1991. Hippocampal pyramidal cell disarray in schizophrenia as a bilateral phenomenon. *Arch Gen Psychiatry*, 48, 413-7.
- CONSTANTINIDIS, C. & WANG, X. J. 2004. A neural circuit basis for spatial working memory. *Neuroscientist*, 10, 553-65.

- COREY-BLOOM, J., JERNIGAN, T., ARCHIBALD, S., HARRIS, M. J. & JESTE, D. V. 1995. Quantitative magnetic resonance imaging of the brain in late-life schizophrenia. *Am J Psychiatry*, 152, 447-9.
- CRICK, F. 1984. Function of the thalamic reticular complex: the searchlight hypothesis. *Proc Natl Acad Sci U S A*, 81, 4586-90.
- CRONENWETT, W. J. & CSERNANSKY, J. 2010. Thalamic pathology in schizophrenia. *Curr Top Behav Neurosci*, 4, 509-28.
- CSERNANSKY, J. G., WANG, L., JONES, D., RASTOGI-CRUZ, D., POSENER, J. A., HEYDEBRAND, G., MILLER, J. P. & MILLER, M. I. 2002. Hippocampal deformities in schizophrenia characterized by high dimensional brain mapping. *Am J Psychiatry*, 159, 2000-6.
- CULLEN, T. J., WALKER, M. A., PARKINSON, N., CRAVEN, R., CROW, T. J., ESIRI, M. M. & HARRISON, P. J. 2003. A postmortem study of the mediodorsal nucleus of the thalamus in schizophrenia. *Schizophr Res*, 60, 157-66.
- CUMMINGS, J. L. 1995. Anatomic and Behavioral Aspects of Frontal-Subcortical Circuits. *Annals of the New York Academy of Sciences*, 769, 1-14.
- DANOS, P., BAUMANN, B., BERNSTEIN, H. G., FRANZ, M., STAUCH, R., NORTHOFF, G., KRELL, D., FALKAI, P. & BOGERTS, B. 1998. Schizophrenia and anteroventral thalamic nucleus: selective decrease of parvalbumin-immunoreactive thalamocortical projection neurons. *Psychiatry Res*, 82, 1-10.
- DANOS, P., BAUMANN, B., KRAMER, A., BERNSTEIN, H. G., STAUCH, R., KRELL, D., FALKAI, P. & BOGERTS, B. 2003. Volumes of association thalamic nuclei in schizophrenia: a postmortem study. *Schizophr Res*, 60, 141-55.
- DANOS, P., SCHMIDT, A., BAUMANN, B., BERNSTEIN, H. G., NORTHOFF, G., STAUCH, R., KRELL, D. & BOGERTS, B. 2005. Volume and neuron number of the mediodorsal thalamic nucleus in schizophrenia: a replication study. *Psychiatry Res*, 140, 281-9.
- DAVIDSON, M., REICHENBERG, A., RABINOWITZ, J., WEISER, M., KAPLAN, Z. & MARK, M. 1999. Behavioral and intellectual markers for schizophrenia in apparently healthy male adolescents. *Am J Psychiatry*, 156, 1328-35.
- DE HAAS, R., STRUIKMANS, R., VAN DER PLASSE, G., VAN KERKHOF, L., BRAKKEE, J. H., KAS, M. J. & WESTENBERG, H. G. 2012. Wireless implantable micro-stimulation device for high frequency bilateral deep brain stimulation in freely moving mice. *J Neurosci Methods*, 209, 113-9.
- DEFELIPE, J. 1997. Types of neurons, synaptic connections and chemical characteristics of cells immunoreactive for calbindin-D28K, parvalbumin and calretinin in the neocortex. *J Chem Neuroanat*, 14, 1-19.
- DEFELIPE, J. & FARINAS, I. 1992. The pyramidal neuron of the cerebral cortex: morphological and chemical characteristics of the synaptic inputs. *Prog Neurobiol*, 39, 563-607.

- DEGENETAIS, E., THIERRY, A. M., GLOWINSKI, J. & GIOANNI, Y. 2003. Synaptic influence of hippocampus on pyramidal cells of the rat prefrontal cortex: an in vivo intracellular recording study. *Cereb Cortex*, 13, 782-92.
- DENIAU, J. M., DEGOS, B., BOSCH, C. & MAURICE, N. 2010. Deep brain stimulation mechanisms: beyond the concept of local functional inhibition. *Eur J Neurosci*, 32, 1080-91.
- DESCHENES, M., TIMOFEEVA, E., LAVALLEE, P. & DUFRESNE, C. 2005. The vibrissal system as a model of thalamic operations. *Prog Brain Res*, 149, 31-40.
- DICKSON, C. T., KIRK, I. J., ODDIE, S. D. & BLAND, B. H. 1995. Classification of theta-related cells in the entorhinal cortex: cell discharges are controlled by the ascending brainstem synchronizing pathway in parallel with hippocampal theta-related cells. *Hippocampus*, 5, 306-19.
- DIEDERICH, N. J., KALTEIS, K., STAMENKOVIC, M., PIERI, V. & ALESCH, F. 2005. Efficient internal pallidal stimulation in Gilles de la Tourette syndrome: a case report. *Mov Disord*, 20, 1496-9.
- DIXON, G. & HARPER, C. G. 2004. No evidence for selective GABAergic interneuron deficits in the anterior thalamic complex of patients with schizophrenia. *Prog Neuropsychopharmacol Biol Psychiatry*, 28, 1045-51.
- DORPH-PETERSEN, K. A., PIERRI, J. N., SUN, Z., SAMPSON, A. R. & LEWIS, D. A. 2004. Stereological analysis of the mediodorsal thalamic nucleus in schizophrenia: volume, neuron number, and cell types. *J Comp Neurol*, 472, 449-62.
- DOSTROVSKY, J. O., LEVY, R., WU, J. P., HUTCHISON, W. D., TASKER, R. R. & LOZANO, A. M. 2000. Microstimulation-induced inhibition of neuronal firing in human globus pallidus. *J Neurophysiol*, 84, 570-4.
- DOSTROVSKY, J. O. & LOZANO, A. M. 2002. Mechanisms of deep brain stimulation. *Mov Disord*, 17 Suppl 3, S63-8.
- DOYERE, V., ERRINGTON, M. L., LAROCHE, S. & BLISS, T. V. 1996. Low-frequency trains of paired stimuli induce long-term depression in area CA1 but not in dentate gyrus of the intact rat. *Hippocampus*, 6, 52-7.
- DU, J., ZHANG, L., WEISER, M., RUDY, B. & MCBAIN, C. J. 1996. Developmental expression and functional characterization of the potassium-channel subunit Kv3.1b in parvalbumin-containing interneurons of the rat hippocampus. *J Neurosci*, 16, 506-18.
- DUDCHENKO, P. A. 2004. An overview of the tasks used to test working memory in rodents. *Neurosci Biobehav Rev*, 28, 699-709.
- DUDCHENKO, P. A., WOOD, E. R. & EICHENBAUM, H. 2000. Neurotoxic hippocampal lesions have no effect on odor span and little effect on odor recognition memory but produce significant impairments on spatial span, recognition, and alternation. *J Neurosci*, 20, 2964-77.
- DZIRASA, K., RAMSEY, A. J., TAKAHASHI, D. Y., STAPLETON, J., POTES, J. M., WILLIAMS, J. K., GAINETDINOV, R. R., SAMESHIMA, K., CARON, M. G. & NICOLELIS, M. A. 2009. Hyperdopaminergia and NMDA receptor hypofunction disrupt neural phase signaling. *J Neurosci*, 29, 8215-24.

- EGERTON, A., REID, L., MCGREGOR, S., COCHRAN, S. M., MORRIS, B. J. & PRATT, J. A. 2008. Subchronic and chronic PCP treatment produces temporally distinct deficits in attentional set shifting and prepulse inhibition in rats. *Psychopharmacology (Berl)*, 198, 37-49.
- EGERTON, A., REID, L., MCKERCHAR, C. E., MORRIS, B. J. & PRATT, J. A. 2005. Impairment in perceptual attentional set-shifting following PCP administration: a rodent model of set-shifting deficits in schizophrenia. *Psychopharmacology (Berl)*, 179, 77-84.
- EHRlichMAN, R. S., GANDAL, M. J., MAXWELL, C. R., LAZAREWICZ, M. T., FINKEL, L. H., CONTRERAS, D., TURETSKY, B. I. & SIEGEL, S. J. 2009. N-methyl-D-aspartic acid receptor antagonist-induced frequency oscillations in mice recreate pattern of electrophysiological deficits in schizophrenia. *Neuroscience*, 158, 705-12.
- EICHENBAUM, H. 2004. Hippocampus: cognitive processes and neural representations that underlie declarative memory. *Neuron*, 44, 109-20.
- ELVEVAG, B. & GOLDBERG, T. E. 2000. Cognitive impairment in schizophrenia is the core of the disorder. *Crit Rev Neurobiol*, 14, 1-21.
- ERDTSIECK-ERNSTE, E. B., FEENSTRA, M. G., BOTTERBLOM, M. H., VAN UUM, H. F., SLUITER, A. A. & HEINSBROEK, R. P. 1995. C-Fos expression in the rat brain after pharmacological stimulation of the rat "mediodorsal" thalamus by means of microdialysis. *Neuroscience*, 66, 115-31.
- EWING, S. G. & GRACE, A. A. 2013a. Deep brain stimulation of the ventral hippocampus restores deficits in processing of auditory evoked potentials in a rodent developmental disruption model of schizophrenia. *Schizophr Res*, 143, 377-83.
- EWING, S.G., PORR, B. & PRATT, J.A. 2013b. Deep brain stimulation of the mediodorsal thalamic nucleus yields increases in the expression of *zif-268* but not *c-fos* in the frontal cortex. *Journal of Chemical Neuroanatomy* [online], In Press. Available from: <http://www.sciencedirect.com/science/article/pii/S0891061813000495> [Accessed 2 September 2013].
- EWING, S. G., PORR, B., RIDDELL, J., WINTER, C. & GRACE, A. A. 2013. SaBer DBS: A fully programmable, rechargeable, bilateral, charge-balanced preclinical microstimulator for long-term neural stimulation. *Journal of Neuroscience Methods*, 213, 228-235.
- EYLES, D. W., MCGRATH, J. J. & REYNOLDS, G. P. 2002. Neuronal calcium-binding proteins and schizophrenia. *Schizophr Res*, 57, 27-34.
- FAN, D., RICH, D., HOLTZMAN, T., RUTHER, P., DALLEY, J. W., LOPEZ, A., ROSSI, M. A., BARTER, J. W., SALAS-MEZA, D., HERWIK, S., HOLZHAMMER, T., MORIZIO, J. & YIN, H. H. 2011. A wireless multi-channel recording system for freely behaving mice and rats. *PLoS One*, 6, e22033.
- FANG-REN, L., CHI-AN, C., SHEY-SHI, L., NAN-FU, C., CHII-WANN, L., JEN-YU, L., CHIA-NAN, C., FU-SHAN, J., JIUN-MIN, W., LUNG-JIEH, Y., TZU-CHIEN, H. & LEE, C.-K. Year. An implantable integrated SiGe FM transmitter for HRV biotelemetry. *In: Biomedical Circuits and Systems, 2004 IEEE International Workshop on*, 1-3 Dec. 2004 2004. S1/8-9-11.

- FERINO, F., THIERRY, A. M. & GLOWINSKI, J. 1987. Anatomical and electrophysiological evidence for a direct projection from Ammon's horn to the medial prefrontal cortex in the rat. *Exp Brain Res*, 65, 421-6.
- FERRARELLI, F. & TONONI, G. 2011. The thalamic reticular nucleus and schizophrenia. *Schizophr Bull*, 37, 306-15.
- FERRON, A., THIERRY, A. M., LE DOUARIN, C. & GLOWINSKI, J. 1984. Inhibitory influence of the mesocortical dopaminergic system on spontaneous activity or excitatory response induced from the thalamic mediodorsal nucleus in the rat medial prefrontal cortex. *Brain Res*, 302, 257-65.
- FILALI, M., HUTCHISON, W. D., PALTER, V. N., LOZANO, A. M. & DOSTROVSKY, J. O. 2004. Stimulation-induced inhibition of neuronal firing in human subthalamic nucleus. *Exp Brain Res*, 156, 274-81.
- FISCHER, H., KAUTZ, H. & KUTSCH, W. 1996. A radiotelemetric 2-channel unit for transmission of muscle potentials during free flight of the desert locust, *Schistocerca gregaria*. *J Neurosci Methods*, 64, 39-45.
- FISHER, R., SALANOVA, V., WITT, T., WORTH, R., HENRY, T., GROSS, R., OOMMEN, K., OSORIO, I., NAZZARO, J., LABAR, D., KAPLITT, M., SPERLING, M., SANDOK, E., NEAL, J., HANDFORTH, A., STERN, J., DESALLES, A., CHUNG, S., SHETTER, A., BERGEN, D., BAKAY, R., HENDERSON, J., FRENCH, J., BALTUCH, G., ROSENFELD, W., YOUKILIS, A., MARKS, W., GARCIA, P., BARBARO, N., FOUNTAIN, N., BAZIL, C., GOODMAN, R., MCKHANN, G., BABU KRISHNAMURTHY, K., PAPAVALASSILIOU, S., EPSTEIN, C., POLLARD, J., TONDER, L., GREBIN, J., COFFEY, R. & GRAVES, N. 2010. Electrical stimulation of the anterior nucleus of thalamus for treatment of refractory epilepsy. *Epilepsia*, 51, 899-908.
- FLORESCO, S. B., SEAMANS, J. K. & PHILLIPS, A. G. 1997. Selective roles for hippocampal, prefrontal cortical, and ventral striatal circuits in radial-arm maze tasks with or without a delay. *J Neurosci*, 17, 1880-90.
- FONTAINE, D., MATTEI, V., BORG, M., VON LANGSDORFF, D., MAGNIE, M. N., CHANALET, S., ROBERT, P. & PAQUIS, P. 2004. Effect of subthalamic nucleus stimulation on obsessive-compulsive disorder in a patient with Parkinson disease. Case report. *J Neurosurg*, 100, 1084-6.
- FORBES, N. F., CARRICK, L. A., MCINTOSH, A. M. & LAWRIE, S. M. 2009. Working memory in schizophrenia: a meta-analysis. *Psychol Med*, 39, 889-905.
- FORD, J. M. 1999. Schizophrenia: the broken P300 and beyond. *Psychophysiology*, 36, 667-82.
- FREUND, T. F. 1989. GABAergic septohippocampal neurons contain parvalbumin. *Brain Res*, 478, 375-81.
- FREUND, T. F. & ANTAL, M. 1988. GABA-containing neurons in the septum control inhibitory interneurons in the hippocampus. *Nature*, 336, 170-3.
- FRIES, P., NIKOLIC, D. & SINGER, W. 2007. The gamma cycle. *Trends Neurosci*, 30, 309-16.
- FRISTON, K. J. & FRITH, C. D. 1995. Schizophrenia: a disconnection syndrome? *Clin Neurosci*, 3, 89-97.

- FUCHS, E. C., ZIVKOVIC, A. R., CUNNINGHAM, M. O., MIDDLETON, S., LEBEAU, F. E., BANNERMAN, D. M., ROZOV, A., WHITTINGTON, M. A., TRAUB, R. D., RAWLINS, J. N. & MONYER, H. 2007. Recruitment of parvalbumin-positive interneurons determines hippocampal function and associated behavior. *Neuron*, 53, 591-604.
- FUENTEALBA, P. & STERIADE, M. 2005. The reticular nucleus revisited: intrinsic and network properties of a thalamic pacemaker. *Prog Neurobiol*, 75, 125-41.
- FUNG, S. H., BURSTEIN, D. & BORN, R. T. 1998. In vivo microelectrode track reconstruction using magnetic resonance imaging. *J Neurosci Methods*, 80, 215-24.
- FUSTER, J. M. 1997. Network memory. *Trends Neurosci*, 20, 451-9.
- GABBOTT, P., HEADLAM, A. & BUSBY, S. 2002. Morphological evidence that CA1 hippocampal afferents monosynaptically innervate PV-containing neurons and NADPH-diaphorase reactive cells in the medial prefrontal cortex (Areas 25/32) of the rat. *Brain Res*, 946, 314-22.
- GABRIELS, L., COSYNS, P., NUTTIN, B., DEMEULEMEESTER, H. & GYBELS, J. 2003. Deep brain stimulation for treatment-refractory obsessive-compulsive disorder: psychopathological and neuropsychological outcome in three cases. *Acta Psychiatr Scand*, 107, 275-82.
- GALANI, R., OBIS, S., COUTUREAU, E., JARRARD, L. & CASSEL, J. C. 2002. A comparison of the effects of fimbria-fornix, hippocampal, or entorhinal cortex lesions on spatial reference and working memory in rats: short versus long postsurgical recovery period. *Neurobiol Learn Mem*, 77, 1-16.
- GAO, F., GUO, Y., ZHANG, H., WANG, S., WANG, J., WU, J. M., CHEN, Z. & DING, M. P. 2009. Anterior thalamic nucleus stimulation modulates regional cerebral metabolism: an FDG-MicroPET study in rats. *Neurobiol Dis*, 34, 477-83.
- GAO, X. M., HASHIMOTO, T. & TAMMINGA, C. A. 1998. Phencyclidine (PCP) and dizocilpine (MK801) exert time-dependent effects on the expression of immediate early genes in rat brain. *Synapse*, 29, 14-28.
- GARCIA, L., AUDIN, J., D'ALESSANDRO, G., BIOULAC, B. & HAMMOND, C. 2003. Dual effect of high-frequency stimulation on subthalamic neuron activity. *J Neurosci*, 23, 8743-51.
- GARCIA, L., D'ALESSANDRO, G., BIOULAC, B. & HAMMOND, C. 2005a. High-frequency stimulation in Parkinson's disease: more or less? *Trends Neurosci*, 28, 209-16.
- GARCIA, L., D'ALESSANDRO, G., FERNAGUT, P. O., BIOULAC, B. & HAMMOND, C. 2005b. Impact of high-frequency stimulation parameters on the pattern of discharge of subthalamic neurons. *J Neurophysiol*, 94, 3662-9.
- GAREY, L. J., ONG, W. Y., PATEL, T. S., KANANI, M., DAVIS, A., MORTIMER, A. M., BARNES, T. R. & HIRSCH, S. R. 1998. Reduced dendritic spine density on cerebral cortical pyramidal neurons in schizophrenia. *J Neurol Neurosurg Psychiatry*, 65, 446-53.



- GASTAMBIDE, F., MITCHELL, S. N., ROBBINS, T. W., TRICKLEBANK, M. D. & GILMOUR, G. 2013. Temporally distinct cognitive effects following acute administration of ketamine and phencyclidine in the rat. *Eur Neuropsychopharmacol*.
- GEYER, M. A., SEGAL, D. S. & GREENBERG, B. D. 1984. Increased startle responding in rats treated with phencyclidine. *Neurobehav Toxicol Teratol*, 6, 161-4.
- GIACINO, J. T., ASHWAL, S., CHILDS, N., CRANFORD, R., JENNETT, B., KATZ, D. I., KELLY, J. P., ROSENBERG, J. H., WHYTE, J., ZAFONTE, R. D. & ZASLER, N. D. 2002. The minimally conscious state: definition and diagnostic criteria. *Neurology*, 58, 349-53.
- GIGG, J., TAN, A. M. & FINCH, D. M. 1992. Glutamatergic excitatory responses of anterior cingulate neurons to stimulation of the mediodorsal thalamus and their regulation by GABA: an in vivo iontophoretic study. *Cereb Cortex*, 2, 477-84.
- GIGUERE, M. & GOLDMAN-RAKIC, P. S. 1988. Mediodorsal nucleus: areal, laminar, and tangential distribution of afferents and efferents in the frontal lobe of rhesus monkeys. *J Comp Neurol*, 277, 195-213.
- GILLIES, M. J., TRAUB, R. D., LEBEAU, F. E., DAVIES, C. H., GLOVELI, T., BUHL, E. H. & WHITTINGTON, M. A. 2002. A model of atropine-resistant theta oscillations in rat hippocampal area CA1. *J Physiol*, 543, 779-93.
- GIMSA, J., HABEL, B., SCHREIBER, U., VAN RIENEN, U., STRAUSS, U. & GIMSA, U. 2005. Choosing electrodes for deep brain stimulation experiments--electrochemical considerations. *J Neurosci Methods*, 142, 251-65.
- GIVENS, B. 1996. Stimulus-evoked resetting of the dentate theta rhythm: relation to working memory. *Neuroreport*, 8, 159-63.
- GLANTZ, L. A. & LEWIS, D. A. 2000. Decreased dendritic spine density on prefrontal cortical pyramidal neurons in schizophrenia. *Arch Gen Psychiatry*, 57, 65-73.
- GOLDBERG, J. H., YUSTE, R. & TAMAS, G. 2003. Ca<sup>2+</sup> imaging of mouse neocortical interneurone dendrites: contribution of Ca<sup>2+</sup>-permeable AMPA and NMDA receptors to subthreshold Ca<sup>2+</sup>dynamics. *J Physiol*, 551, 67-78.
- GOLDMAN-RAKIC, P. S. 1996. Regional and cellular fractionation of working memory. *Proc Natl Acad Sci U S A*, 93, 13473-80.
- GOLDMAN-RAKIC, P. S. 1994. Working memory dysfunction in schizophrenia. *J Neuropsychiatry Clin Neurosci*, 6, 348-57.
- GOLDMAN-RAKIC, P. S., SELEMON, L. D. & SCHWARTZ, M. L. 1984. Dual pathways connecting the dorsolateral prefrontal cortex with the hippocampal formation and parahippocampal cortex in the rhesus monkey. *Neuroscience*, 12, 719-43.
- GOLDMAN, P. S. & ROSVOLD, H. E. 1970. Localization of function within the dorsolateral prefrontal cortex of the rhesus monkey. *Exp Neurol*, 27, 291-304.
- GONZALEZ-BURGOS, G., KRIMER, L. S., POVYSHEVA, N. V., BARRIONUEVO, G. & LEWIS, D. A. 2005. Functional properties of fast spiking interneurons and their synaptic

- connections with pyramidal cells in primate dorsolateral prefrontal cortex. *J Neurophysiol*, 93, 942-53.
- GONZALEZ-BURGOS, G. & LEWIS, D. A. 2008. GABA neurons and the mechanisms of network oscillations: implications for understanding cortical dysfunction in schizophrenia. *Schizophr Bull*, 34, 944-61.
- GORDON, J. A. 2011. Oscillations and hippocampal-prefrontal synchrony. *Curr Opin Neurobiol*, 21, 486-91.
- GORMAN, P. H. & MORTIMER, J. T. 1983. The effect of stimulus parameters on the recruitment characteristics of direct nerve stimulation. *IEEE Trans Biomed Eng*, 30, 407-14.
- GREEN, J. D. & ARDUINI, A. A. 1954. Hippocampal electrical activity in arousal. *J Neurophysiol*, 17, 533-57.
- GREENBERG, B. D., MALONE, D. A., FRIEHS, G. M., REZAI, A. R., KUBU, C. S., MALLOY, P. F., SALLOWAY, S. P., OKUN, M. S., GOODMAN, W. K. & RASMUSSEN, S. A. 2006. Three-year outcomes in deep brain stimulation for highly resistant obsessive-compulsive disorder. *Neuropsychopharmacology*, 31, 2384-93.
- GRIFFITH, R. W. & HUMPHREY, D. R. 2006. Long-term gliosis around chronically implanted platinum electrodes in the Rhesus macaque motor cortex. *Neurosci Lett*, 406, 81-6.
- GROENEWEGEN, H. J., BERENDSE, H. W., WOLTERS, J. G. & LOHMAN, A. H. 1990. The anatomical relationship of the prefrontal cortex with the striatopallidal system, the thalamus and the amygdala: evidence for a parallel organization. *Prog Brain Res*, 85, 95-116; discussion 116-8.
- GROHROCK, P., HAUSLER, U. & JURGENS, U. 1997. Dual-channel telemetry system for recording vocalization-correlated neuronal activity in freely moving squirrel monkeys. *J Neurosci Methods*, 76, 7-13.
- GRUNZE, H. C., RAINNIE, D. G., HASSELMO, M. E., BARKAI, E., HEARN, E. F., MCCARLEY, R. W. & GREENE, R. W. 1996. NMDA-dependent modulation of CA1 local circuit inhibition. *J Neurosci*, 16, 2034-43.
- GUBELLINI, P., SALIN, P., KERKERIAN-LE GOFF, L. & BAUNEZ, C. 2009. Deep brain stimulation in neurological diseases and experimental models: from molecule to complex behavior. *Prog Neurobiol*, 89, 79-123.
- GUIDOTTI, A., AUTA, J., DAVIS, J. M., DI-GIORGI-GEREVINI, V., DWIVEDI, Y., GRAYSON, D. R., IMPAGNATIELLO, F., PANDEY, G., PESOLD, C., SHARMA, R., UZUNOV, D. & COSTA, E. 2000. Decrease in reelin and glutamic acid decarboxylase67 (GAD67) expression in schizophrenia and bipolar disorder: a postmortem brain study. *Arch Gen Psychiatry*, 57, 1061-9.
- GUILLERY, R. W., FEIG, S. L. & LOZSADI, D. A. 1998. Paying attention to the thalamic reticular nucleus. *Trends Neurosci*, 21, 28-32.
- GUILLERY, R. W. & HARTING, J. K. 2003. Structure and connections of the thalamic reticular nucleus: Advancing views over half a century. *J Comp Neurol*, 463, 360-71.

- GUILLERY, R. W. & SHERMAN, S. M. 2002. Thalamic Relay Functions and Their Role in Corticocortical Communication: Generalizations from the Visual System. *Neuron*, 33, 163-175.
- GULYAS, A. I., SZABO, G. G., ULBERT, I., HOLDERITH, N., MONYER, H., ERDELYI, F., SZABO, G., FREUND, T. F. & HAJOS, N. 2010. Parvalbumin-containing fast-spiking basket cells generate the field potential oscillations induced by cholinergic receptor activation in the hippocampus. *J Neurosci*, 30, 15134-45.
- GUT, N.K., WINN, P. 2012. Wireless deep brain stimulation of the pedunculopontine tegmental nucleus in a novel rodent model of Parkinson's disease. *Program No. 761.09. 2012 Neuroscience Meeting Planner. New Orleans, LA: Society for Neuroscience*. Online.
- HAENSCHEL, C., BITTNER, R. A., WALTZ, J., HAERTLING, F., WIBRAL, M., SINGER, W., LINDEN, D. E. & RODRIGUEZ, E. 2009. Cortical oscillatory activity is critical for working memory as revealed by deficits in early-onset schizophrenia. *J Neurosci*, 29, 9481-9.
- HAJOS, N., FREUND, T. F. & MODY, I. 2002. Comparison of single NMDA receptor channels recorded on hippocampal principal cells and oriens/alveus interneurons projecting to stratum lacunosum-moleculare (O-LM cells). *Acta Biol Hung*, 53, 465-72.
- HAKAMI, T., JONES, N. C., TOLMACHEVA, E. A., GAUDIAS, J., CHAUMONT, J., SALZBERG, M., O'BRIEN, T. J. & PINAULT, D. 2009. NMDA receptor hypofunction leads to generalized and persistent aberrant gamma oscillations independent of hyperlocomotion and the state of consciousness. *PLoS One*, 4, e6755.
- HALLANGER, A. E., LEVEY, A. I., LEE, H. J., RYE, D. B. & WAINER, B. H. 1987. The origins of cholinergic and other subcortical afferents to the thalamus in the rat. *J Comp Neurol*, 262, 105-24.
- HAMANI, C., DUBIELA, F. P., SOARES, J. C., SHIN, D., BITTENCOURT, S., COVOLAN, L., CARLEN, P. L., LAXTON, A. W., HODAIE, M., STONE, S. S., HA, Y., HUTCHISON, W. D., LOZANO, A. M., MELLO, L. E. & OLIVEIRA, M. G. 2010. Anterior thalamus deep brain stimulation at high current impairs memory in rats. *Exp Neurol*, 225, 154-62.
- HAMANI, C., MCANDREWS, M. P., COHN, M., OH, M., ZUMSTEG, D., SHAPIRO, C. M., WENNBERG, R. A. & LOZANO, A. M. 2008. Memory enhancement induced by hypothalamic/fornix deep brain stimulation. *Ann Neurol*, 63, 119-23.
- HAMMOND, C., AMMARI, R., BIOULAC, B. & GARCIA, L. 2008. Latest view on the mechanism of action of deep brain stimulation. *Mov Disord*, 23, 2111-21.
- HAMPSON, R. E., COLLINS, V. & DEADWYLER, S. A. 2009. A wireless recording system that utilizes Bluetooth technology to transmit neural activity in freely moving animals. *J Neurosci Methods*, 182, 195-204.
- HARNACK, D., WINTER, C., MEISSNER, W., REUM, T., KUPSCH, A. & MORGENSTERN, R. 2004. The effects of electrode material, charge density and stimulation duration on the safety of high-frequency stimulation of the subthalamic nucleus in rats. *J Neurosci Methods*, 138, 207-16.
- HARRIS, K. D., CSICSVARI, J., HIRASE, H., DRAGOI, G. & BUZSAKI, G. 2003. Organization of cell assemblies in the hippocampus. *Nature*, 424, 552-6.

- HARRISON, R. R., WATKINS, P. T., KIER, R. J., LOVEJOY, R. O., BLACK, D. J., GREGER, B. & SOLZBACHER, F. 2007. A Low-Power Integrated Circuit for a Wireless 100-Electrode Neural Recording System. *Solid-State Circuits, IEEE Journal of*, 42, 123-133.
- HARTWICH, K., POLLAK, T. & KLAUSBERGER, T. 2009. Distinct firing patterns of identified basket and dendrite-targeting interneurons in the prefrontal cortex during hippocampal theta and local spindle oscillations. *J Neurosci*, 29, 9563-74.
- HASHIMOTO, T., ELDER, C. M., OKUN, M. S., PATRICK, S. K. & VITEK, J. L. 2003a. Stimulation of the subthalamic nucleus changes the firing pattern of pallidal neurons. *J Neurosci*, 23, 1916-23.
- HASHIMOTO, T., VOLK, D. W., EGGAN, S. M., MIRNICS, K., PIERRI, J. N., SUN, Z., SAMPSON, A. R. & LEWIS, D. A. 2003b. Gene expression deficits in a subclass of GABA neurons in the prefrontal cortex of subjects with schizophrenia. *J Neurosci*, 23, 6315-26.
- HASSELMO, M. E., BODELON, C. & WYBLE, B. P. 2002. A proposed function for hippocampal theta rhythm: separate phases of encoding and retrieval enhance reversal of prior learning. *Neural Comput*, 14, 793-817.
- HAWLEY, E. S., HARGREAVES, E. L., KUBIE, J. L., RIVARD, B. & MULLER, R. U. 2002. Telemetry system for reliable recording of action potentials from freely moving rats. *Hippocampus*, 12, 505-13.
- HAZLETT, E. A., BUCHSBAUM, M. S., BYNE, W., WEI, T. C., SPIEGEL-COHEN, J., GENEVE, C., KINDERLEHRER, R., HAZNEDAR, M. M., SHIHABUDDIN, L. & SIEVER, L. J. 1999. Three-dimensional analysis with MRI and PET of the size, shape, and function of the thalamus in the schizophrenia spectrum. *Am J Psychiatry*, 156, 1190-9.
- HAZLETT, E. A., BUCHSBAUM, M. S., KEMETHER, E., BLOOM, R., PLATHOLI, J., BRICKMAN, A. M., SHIHABUDDIN, L., TANG, C. & BYNE, W. 2004. Abnormal glucose metabolism in the mediodorsal nucleus of the thalamus in schizophrenia. *Am J Psychiatry*, 161, 305-14.
- HE, J., YAMADA, K. & NABESHIMA, T. 2002. A role of Fos expression in the CA3 region of the hippocampus in spatial memory formation in rats. *Neuropsychopharmacology*, 26, 259-68.
- HEIDBREDE, C. A. & GROENEWEGEN, H. J. 2003. The medial prefrontal cortex in the rat: evidence for a dorso-ventral distinction based upon functional and anatomical characteristics. *Neurosci Biobehav Rev*, 27, 555-79.
- HENRY, J., PETRIDES, M., ST-LAURENT, M. & SZIKLAS, V. 2004. Spatial conditional associative learning: effects of thalamo-hippocampal disconnection in rats. *Neuroreport*, 15, 2427-31.
- HERRMANN, C. S. & DEMIRALP, T. 2005. Human EEG gamma oscillations in neuropsychiatric disorders. *Clin Neurophysiol*, 116, 2719-33.
- HINMAN, J. R., PENLEY, S. C., ESCABI, M. A. & CHROBAK, J. J. 2013. Ketamine disrupts theta synchrony across the septotemporal axis of the CA1 region of hippocampus. *J Neurophysiol*, 109, 570-9.

- HIRSCH, J. C. & CREPEL, F. 1990. Use-dependent changes in synaptic efficacy in rat prefrontal neurons in vitro. *J Physiol*, 427, 31-49.
- HODAIE, M., WENNERBERG, R. A., DOSTROVSKY, J. O. & LOZANO, A. M. 2002. Chronic anterior thalamus stimulation for intractable epilepsy. *Epilepsia*, 43, 603-8.
- HOFFMAN, R. E., HAWKINS, K. A., GUEORGUIEVA, R., BOUTROS, N. N., RACHID, F., CARROLL, K. & KRYSTAL, J. H. 2003. Transcranial magnetic stimulation of left temporoparietal cortex and medication-resistant auditory hallucinations. *Arch Gen Psychiatry*, 60, 49-56.
- HOMAYOUN, H. & MOGHADDAM, B. 2007. NMDA receptor hypofunction produces opposite effects on prefrontal cortex interneurons and pyramidal neurons. *J Neurosci*, 27, 11496-500.
- HOUETO, J. L., KARACHI, C., MALLET, L., PILLON, B., YELNIK, J., MESNAGE, V., WELTER, M. L., NAVARRO, S., PELISSOLO, A., DAMIER, P., PIDOUX, B., DORMONT, D., CORNU, P. & AGID, Y. 2005. Tourette's syndrome and deep brain stimulation. *J Neurol Neurosurg Psychiatry*, 76, 992-5.
- HOWARD, M. W., RIZZUTO, D. S., CAPLAN, J. B., MADSEN, J. R., LISMAN, J., ASCHENBRENNER-SCHEIBE, R., SCHULZE-BONHAGE, A. & KAHANA, M. J. 2003. Gamma oscillations correlate with working memory load in humans. *Cereb Cortex*, 13, 1369-74.
- HUANG, Y. Y. & KANDEL, E. R. 2005. Theta frequency stimulation up-regulates the synaptic strength of the pathway from CA1 to subiculum region of hippocampus. *Proc Natl Acad Sci U S A*, 102, 232-7.
- HUNT, P. R. & AGGLETON, J. P. 1998. An examination of the spatial working memory deficit following neurotoxic medial dorsal thalamic lesions in rats. *Behav Brain Res*, 97, 129-41.
- HYMAN, J. M., WYBLE, B. P., GOYAL, V., ROSSI, C. A. & HASSELMO, M. E. 2003. Stimulation in hippocampal region CA1 in behaving rats yields long-term potentiation when delivered to the peak of theta and long-term depression when delivered to the trough. *J Neurosci*, 23, 11725-31.
- HYMAN, J. M., ZILLI, E. A., PALEY, A. M. & HASSELMO, M. E. 2005. Medial prefrontal cortex cells show dynamic modulation with the hippocampal theta rhythm dependent on behavior. *Hippocampus*, 15, 739-49.
- HYMAN, J. M., ZILLI, E. A., PALEY, A. M. & HASSELMO, M. E. 2010. Working Memory Performance Correlates with Prefrontal-Hippocampal Theta Interactions but not with Prefrontal Neuron Firing Rates. *Front Integr Neurosci*, 4, 2.
- IRAZOQUI-PASTOR, P., MODY, I. & JUDY, J. W. Year. In-vivo EEG recording using a wireless implantable neural transceiver. *In: Neural Engineering, 2003. Conference Proceedings. First International IEEE EMBS Conference on, 20-22 March 2003* 2003. 622-625.
- ITIL, T., KESKINER, A., KIREMITCI, N. & HOLDEN, J. M. 1967. Effect of phencyclidine in chronic schizophrenics. *Can Psychiatr Assoc J*, 12, 209-12.

- IZAKI, Y., TAKITA, M., JAY, T. M., KANEKO, H., SUZUKI, S. S. & NOMURA, M. 2001. Effect of long-term potentiation induction on gamma-band electroencephalograms in prefrontal cortex following stimulation of rat hippocampus in vivo. *Neurosci Lett*, 305, 57-60.
- JACKSON, M. E., HOMAYOUN, H. & MOGHADDAM, B. 2004. NMDA receptor hypofunction produces concomitant firing rate potentiation and burst activity reduction in the prefrontal cortex. *Proc Natl Acad Sci U S A*, 101, 8467-72.
- JACOBS, B., DRISCOLL, L. & SCHALL, M. 1997. Life-span dendritic and spine changes in areas 10 and 18 of human cortex: a quantitative Golgi study. *J Comp Neurol*, 386, 661-80.
- JAVITT, D. C. & ZUKIN, S. R. 1991. Recent advances in the phencyclidine model of schizophrenia. *Am J Psychiatry*, 148, 1301-8.
- JAY, T. M., GLOWINSKI, J. & THIERRY, A. M. 1989. Selectivity of the hippocampal projection to the prelimbic area of the prefrontal cortex in the rat. *Brain Res*, 505, 337-40.
- JAY, T. M., THIERRY, A. M., WIKLUND, L. & GLOWINSKI, J. 1992. Excitatory Amino Acid Pathway from the Hippocampus to the Prefrontal Cortex. Contribution of AMPA Receptors in Hippocampo-prefrontal Cortex Transmission. *Eur J Neurosci*, 4, 1285-1295.
- JAY, T. M. & WITTER, M. P. 1991. Distribution of hippocampal CA1 and subicular efferents in the prefrontal cortex of the rat studied by means of anterograde transport of Phaseolus vulgaris-leucoagglutinin. *J Comp Neurol*, 313, 574-86.
- JEEWAJEE, A., LEVER, C., BURTON, S., O'KEEFE, J. & BURGESS, N. 2008. Environmental novelty is signaled by reduction of the hippocampal theta frequency. *Hippocampus*, 18, 340-348.
- JENKINS, T. A., DIAS, R., AMIN, E., BROWN, M. W. & AGGLETON, J. P. 2002. Fos imaging reveals that lesions of the anterior thalamic nuclei produce widespread limbic hypoactivity in rats. *J Neurosci*, 22, 5230-8.
- JENSEN, O. 2006. Maintenance of multiple working memory items by temporal segmentation. *Neuroscience*, 139, 237-49.
- JENSEN, O., KAISER, J. & LACHAUX, J. P. 2007. Human gamma-frequency oscillations associated with attention and memory. *Trends Neurosci*, 30, 317-24.
- JENTSCH, J. D. & ROTH, R. H. 1999. The neuropsychopharmacology of phencyclidine: from NMDA receptor hypofunction to the dopamine hypothesis of schizophrenia. *Neuropsychopharmacology*, 20, 201-25.
- JENTSCH, J. D., TRAN, A., LE, D., YOUNGREN, K. D. & ROTH, R. H. 1997. Subchronic phencyclidine administration reduces mesoprefrontal dopamine utilization and impairs prefrontal cortical-dependent cognition in the rat. *Neuropsychopharmacology*, 17, 92-9.
- JEON, Y. W. & POLICH, J. 2003. Meta-analysis of P300 and schizophrenia: patients, paradigms, and practical implications. *Psychophysiology*, 40, 684-701.
- JONES, E. G. 2007. *The thalamus*, Cambridge ; New York, Cambridge University Press.

- JONES, M. W. & WILSON, M. A. 2005. Theta rhythms coordinate hippocampal-prefrontal interactions in a spatial memory task. *PLoS Biol*, 3, e402.
- JUNG, M. W., QIN, Y., MCNAUGHTON, B. L. & BARNES, C. A. 1998. Firing characteristics of deep layer neurons in prefrontal cortex in rats performing spatial working memory tasks. *Cereb Cortex*, 8, 437-50.
- JÜRGENS, U. & HAGE, S. R. 2006. Telemetric recording of neuronal activity. *Methods*, 38, 195-201.
- KALIA, S. K., SANKAR, T. & LOZANO, A. M. 2013. Deep brain stimulation for Parkinson's disease and other movement disorders. *Curr Opin Neurol*, 26, 374-80.
- KANTROWITZ, J. T. & JAVITT, D. C. 2010. N-methyl-d-aspartate (NMDA) receptor dysfunction or dysregulation: the final common pathway on the road to schizophrenia? *Brain Res Bull*, 83, 108-21.
- KARGIEMAN, L., SANTANA, N., MENGOD, G., CELADA, P. & ARTIGAS, F. 2007. Antipsychotic drugs reverse the disruption in prefrontal cortex function produced by NMDA receptor blockade with phencyclidine. *Proc Natl Acad Sci U S A*, 104, 14843-8.
- KATZ, M., BUCHSBAUM, M. S., SIEGEL, B. V., JR., WU, J., HAIER, R. J. & BUNNEY, W. E., JR. 1996. Correlational patterns of cerebral glucose metabolism in never-medicated schizophrenics. *Neuropsychobiology*, 33, 1-11.
- KEHRER, C., DUGLADZE, T., MAZIASHVILI, N., WOJTOWICZ, A., SCHMITZ, D., HEINEMANN, U. & GLOVELI, T. 2007. Increased inhibitory input to CA1 pyramidal cells alters hippocampal gamma frequency oscillations in the MK-801 model of acute psychosis. *Neurobiol Dis*, 25, 545-52.
- KEMETHER, E. M., BUCHSBAUM, M. S., BYNE, W., HAZLETT, E. A., HAZNEDAR, M., BRICKMAN, A. M., PLATHOLI, J. & BLOOM, R. 2003. Magnetic resonance imaging of mediodorsal, pulvinar, and centromedian nuclei of the thalamus in patients with schizophrenia. *Arch Gen Psychiatry*, 60, 983-91.
- KIM, U., SANCHEZ-VIVES, M. V. & MCCORMICK, D. A. 1997. Functional dynamics of GABAergic inhibition in the thalamus. *Science*, 278, 130-4.
- KITO, S., JUNG, J., KOBAYASHI, T. & KOGA, Y. 2009. Fiber tracking of white matter integrity connecting the mediodorsal nucleus of the thalamus and the prefrontal cortex in schizophrenia: a diffusion tensor imaging study. *Eur Psychiatry*, 24, 269-74.
- KITTELBERGER, K., HUR, E. E., SAZEGAR, S., KESHAVAN, V. & KOCSIS, B. 2012. Comparison of the effects of acute and chronic administration of ketamine on hippocampal oscillations: relevance for the NMDA receptor hypofunction model of schizophrenia. *Brain Struct Funct*, 217, 395-409.
- KLAUSBERGER, T., MAGILL, P. J., MARTON, L. F., ROBERTS, J. D., COBDEN, P. M., BUZSAKI, G. & SOMOGYI, P. 2003. Brain-state- and cell-type-specific firing of hippocampal interneurons in vivo. *Nature*, 421, 844-8.
- KLEIN, J., HADAR, R., GÖTZ, T., MÄNNER, A., EBERHARDT, C., BALDASSARRI, J., SCHMIDT, T. T., KUPSCH, A., HEINZ, A., MORGENSTERN, R., SCHNEIDER, M.,

- WEINER, I. & WINTER, C. 2012. Mapping brain regions in which deep brain stimulation affects schizophrenia-like behavior in two rat models of schizophrenia. *Brain Stimulation*.
- KOENIG, T., LEHMANN, D., SAITO, N., KUGINUKI, T., KINOSHITA, T. & KOUKKOU, M. 2001. Decreased functional connectivity of EEG theta-frequency activity in first-episode, neuroleptic-naïve patients with schizophrenia: preliminary results. *Schizophr Res*, 50, 55-60.
- KOJIMA, S. & GOLDMAN-RAKIC, P. S. 1982. Delay-related activity of prefrontal neurons in rhesus monkeys performing delayed response. *Brain Res*, 248, 43-9.
- KOLB, B. 1990. Animal models for human PFC-related disorders. *Prog Brain Res*, 85, 501-19.
- KOLLER, W., PAHWA, R., BUSENBARK, K., HUBBLE, J., WILKINSON, S., LANG, A., TUITTE, P., SIME, E., LAZANO, A., HAUSER, R., MALAPIRA, T., SMITH, D., TARSY, D., MIYAWAKI, E., NORREGAARD, T., KORMOS, T. & OLANOW, C. W. 1997. High-frequency unilateral thalamic stimulation in the treatment of essential and parkinsonian tremor. *Ann Neurol*, 42, 292-9.
- KONRADI, C., YANG, C. K., ZIMMERMAN, E. I., LOHMANN, K. M., GRESCH, P., PANTAZOPOULOS, H., BERRETTA, S. & HECKERS, S. 2011. Hippocampal interneurons are abnormal in schizophrenia. *Schizophr Res*, 131, 165-73.
- KOROTKOVA, T., FUCHS, E. C., PONOMARENKO, A., VON ENGELHARDT, J. & MONYER, H. 2010. NMDA receptor ablation on parvalbumin-positive interneurons impairs hippocampal synchrony, spatial representations, and working memory. *Neuron*, 68, 557-69.
- KRAMIS, R., VANDERWOLF, C. H. & BLAND, B. H. 1975. Two types of hippocampal rhythmic slow activity in both the rabbit and the rat: relations to behavior and effects of atropine, diethyl ether, urethane, and pentobarbital. *Exp Neurol*, 49, 58-85.
- KRASNOW, B., TAMM, L., GREICIUS, M. D., YANG, T. T., GLOVER, G. H., REISS, A. L. & MENON, V. 2003. Comparison of fMRI activation at 3 and 1.5 T during perceptual, cognitive, and affective processing. *Neuroimage*, 18, 813-26.
- KRETTEK, J. E. & PRICE, J. L. 1977. The cortical projections of the mediodorsal nucleus and adjacent thalamic nuclei in the rat. *J Comp Neurol*, 171, 157-91.
- KRITZER, M. F. & GOLDMAN-RAKIC, P. S. 1995. Intrinsic circuit organization of the major layers and sublayers of the dorsolateral prefrontal cortex in the rhesus monkey. *J Comp Neurol*, 359, 131-43.
- KUBICKI, M., PARK, H., WESTIN, C. F., NESTOR, P. G., MULKERN, R. V., MAIER, S. E., NIZNIKIEWICZ, M., CONNOR, E. E., LEVITT, J. J., FRUMIN, M., KIKINIS, R., JOLESZ, F. A., MCCARLEY, R. W. & SHENTON, M. E. 2005. DTI and MTR abnormalities in schizophrenia: Analysis of white matter integrity. *Neuroimage*, 26, 1109-1118.
- KUNCEL, A. M., COOPER, S. E. & GRILL, W. M. 2008. A method to estimate the spatial extent of activation in thalamic deep brain stimulation. *Clin Neurophysiol*, 119, 2148-58.



- KUNIMATSU, N., AOKI, S., KUNIMATSU, A., ABE, O., YAMADA, H., MASUTANI, Y., KASAI, K., YAMASUE, H. & OHTOMO, K. 2012. Tract-specific analysis of white matter integrity disruption in schizophrenia. *Psychiatry Research-Neuroimaging*, 201, 136-143.
- KUROKI, N., KUBICKI, M., NESTOR, P. G., SALISBURY, D. F., PARK, H. J., LEVITT, J. J., WOOLSTON, S., FRUMIN, M., NIZNIKIEWICZ, M., WESTIN, C. F., MAIER, S. E., MCCARLEY, R. W. & SHENTON, M. E. 2006. Fornix integrity and hippocampal volume in male schizophrenic patients. *Biological Psychiatry*, 60, 22-31.
- LAPRAY, D., BERGELER, J., DUPONT, E., THEWS, O. & LUHMANN, H. J. 2008. A novel miniature telemetric system for recording EEG activity in freely moving rats. *J Neurosci Methods*, 168, 119-26.
- LAROCHE, S., DAVIS, S. & JAY, T. M. 2000. Plasticity at hippocampal to prefrontal cortex synapses: dual roles in working memory and consolidation. *Hippocampus*, 10, 438-46.
- LAROCHE, S., JAY, T. M. & THIERRY, A. M. 1990. Long-Term Potentiation in the Prefrontal Cortex Following Stimulation of the Hippocampal Ca1/Subicular Region. *Neuroscience Letters*, 114, 184-190.
- LARSON, P. S. 2008. Deep brain stimulation for psychiatric disorders. *Neurotherapeutics*, 5, 50-8.
- LARSON, J., WONG, D. & LYNCH, G. 1986. Patterned Stimulation at the Theta-Frequency Is Optimal for the Induction of Hippocampal Long-Term Potentiation. *Brain Research*, 368, 347-350.
- LAXTON, A. W., TANG-WAI, D. F., MCANDREWS, M. P., ZUMSTEG, D., WENNBERG, R., KEREN, R., WHERRETT, J., NAGLIE, G., HAMANI, C., SMITH, G. S. & LOZANO, A. M. 2010. A Phase I Trial of Deep Brain Stimulation of Memory Circuits in Alzheimer's Disease. *Annals of Neurology*, 68, 521-534.
- LAZAREWICZ, M. T., EHRLICHMAN, R. S., MAXWELL, C. R., GANDAL, M. J., FINKEL, L. H. & SIEGEL, S. J. 2010. Ketamine modulates theta and gamma oscillations. *J Cogn Neurosci*, 22, 1452-64.
- LEE, D. J., GURKOFF, G. G., IZADI, A., BERMAN, R. F., EKSTROM, A. D., MUIZELAAR, J. P., LYETH, B. G. & SHAHLAIE, K. 2013. Medial septal nucleus theta frequency deep brain stimulation improves spatial working memory after traumatic brain injury. *J Neurotrauma*, 30, 131-9.
- LEE, I. & KESNER, R. P. 2003. Time-dependent relationship between the dorsal hippocampus and the prefrontal cortex in spatial memory. *J Neurosci*, 23, 1517-23.
- LEE, K. H., CHANG, S. Y., ROBERTS, D. W. & KIM, U. 2004. Neurotransmitter release from high-frequency stimulation of the subthalamic nucleus. *J Neurosurg*, 101, 511-7.
- LEE, K. H., WILLIAMS, L. M., BREAKSPEAR, M. & GORDON, E. 2003. Synchronous gamma activity: a review and contribution to an integrative neuroscience model of schizophrenia. *Brain Res Brain Res Rev*, 41, 57-78.
- LEE, K. J., JANG, K. S. & SHON, Y. M. 2006. Chronic deep brain stimulation of subthalamic and anterior thalamic nuclei for controlling refractory partial epilepsy. *Acta Neurochir Suppl*, 99, 87-91.

- LEE, M. G., CHROBAK, J. J., SIK, A., WILEY, R. G. & BUZSAKI, G. 1994. Hippocampal Theta-Activity Following Selective Lesion of the Septal Cholinergic System. *Neuroscience*, 62, 1033-1047.
- LEE, J. & PARK, S. 2005. Working memory impairments in schizophrenia: a meta-analysis. *J Abnorm Psychol*, 114, 599-611.
- LEE, S. H., WYNN, J. K., GREEN, M. F., KIM, H., LEE, K. J., NAM, M., PARK, J. K. & CHUNG, Y. C. 2006. Quantitative EEG and low resolution electromagnetic tomography (LORETA) imaging of patients with persistent auditory hallucinations. *Schizophr Res*, 83, 111-9.
- LEICHNETZ, G. R. 1989. The prefrontal cortex: Anatomy, physiology, and neuropsychology of the frontal lobe, Second Edition, by Joaquin M. Fuster; Raven Press, 1989, 255 pp. *Synapse*, 4, 96-97.
- LEMPKA, S. F., JOHNSON, M. D., MIOCINOVIC, S., VITEK, J. L. & MCINTYRE, C. C. 2010. Current-controlled deep brain stimulation reduces in vivo voltage fluctuations observed during voltage-controlled stimulation. *Clin Neurophysiol*, 121, 2128-33.
- LEONE, M., FRANZINI, A., BROGGI, G., MAY, A. & BUSSONE, G. 2004. Long-term follow-up of bilateral hypothalamic stimulation for intractable cluster headache. *Brain*, 127, 2259-64.
- LEONE, M., FRANZINI, A. & BUSSONE, G. 2001. Stereotactic stimulation of posterior hypothalamic gray matter in a patient with intractable cluster headache. *N Engl J Med*, 345, 1428-9.
- LEONE, M., FRANZINI, A., CECCHINI, A. P., BROGGI, G. & BUSSONE, G. 2010. Hypothalamic deep brain stimulation in the treatment of chronic cluster headache. *Ther Adv Neurol Disord*, 3, 187-95.
- LEUNG, L. S. & SHEN, B. 2004. Glutamatergic synaptic transmission participates in generating the hippocampal EEG. *Hippocampus*, 14, 510-25.
- LEUNG, L. W. 1984. Model of gradual phase shift of theta rhythm in the rat. *J Neurophysiol*, 52, 1051-65.
- LEVITT, J. B., LEWIS, D. A., YOSHIOKA, T. & LUND, J. S. 1993. Topography of pyramidal neuron intrinsic connections in macaque monkey prefrontal cortex (areas 9 and 46). *J Comp Neurol*, 338, 360-76.
- LEWIS, D. A. 1998. Chandelier cells: shedding light on altered cortical circuitry in schizophrenia. *Mol Psychiatry*, 3, 468-71, 466-7.
- LEWIS, D. A. 2000. GABAergic local circuit neurons and prefrontal cortical dysfunction in schizophrenia. *Brain Res Brain Res Rev*, 31, 270-6.
- LEWIS, D. A. & LIEBERMAN, J. A. 2000. Catching up on schizophrenia: natural history and neurobiology. *Neuron*, 28, 325-34.
- LEWIS, D. A. & LUND, J. S. 1990. Heterogeneity of chandelier neurons in monkey neocortex: corticotropin-releasing factor- and parvalbumin-immunoreactive populations. *J Comp Neurol*, 293, 599-615.

- LI, J. Y., KUO, T. B. J., HSIEH, I. T. & YANG, C. C. H. 2012. Changes in hippocampal theta rhythm and their correlations with speed during different phases of voluntary wheel running in rats. *Neuroscience*, 213, 54-61.
- LIDDLE, P. F. 1996. Functional imaging--schizophrenia. *Br Med Bull*, 52, 486-94.
- LIN, D. C., BUCHER, B. P., DAVIS, H. P. & SPRUNGER, L. K. 2008. A low-cost telemetry system suitable for measuring mouse biopotentials. *Med Eng Phys*, 30, 199-205.
- LIN, L., CHEN, G., XIE, K., ZAIA, K. A., ZHANG, S. & TSIEN, J. Z. 2006. Large-scale neural ensemble recording in the brains of freely behaving mice. *J Neurosci Methods*, 155, 28-38.
- LIPPITZ, B. E., MINDUS, P., MEYERSON, B. A., KIHLLSTROM, L. & LINDQUIST, C. 1999. Lesion topography and outcome after thermocapsulotomy or gamma knife capsulotomy for obsessive-compulsive disorder: relevance of the right hemisphere. *Neurosurgery*, 44, 452-8; discussion 458-60.
- LISMAN, J. E. & IDIART, M. A. 1995. Storage of 7 +/- 2 short-term memories in oscillatory subcycles. *Science*, 267, 1512-5.
- LODGE, D. J. & GRACE, A. A. 2007. Aberrant hippocampal activity underlies the dopamine dysregulation in an animal model of schizophrenia. *J Neurosci*, 27, 11424-30.
- LOMBARDI, F., TARICCO, M., DE TANTI, A., TELARO, E. & LIBERATI, A. 2002. Sensory stimulation for brain injured individuals in coma or vegetative state. *Cochrane Database Syst Rev*, CD001427.
- LUBY ED, C. B. R. G. G. J. K. R. 1959. Study of a new schizophrenomimetic drug—sernyl. *A.M.A. Archives of Neurology & Psychiatry*, 81, 363-369.
- LUCK, D., MALLA, A. K., JOOBER, R. & LEPAGE, M. 2010. Disrupted integrity of the fornix in first-episode schizophrenia. *Schizophrenia research*, 119, 61-64.
- LUDEWIG, K., GEYER, M. A. & VOLLENWEIDER, F. X. 2003. Deficits in prepulse inhibition and habituation in never-medicated, first-episode schizophrenia. *Biol Psychiatry*, 54, 121-8.
- LUDVIG, N., BOTERO, J. M., TANG, H. M., GOHIL, B. & KRAL, J. G. 2001. Single-cell recording from the brain of freely moving monkeys. *J Neurosci Methods*, 106, 179-87.
- LUJAN, J. L., CHATURVEDI, A., CHOI, K. S., HOLTZHEIMER, P. E., GROSS, R. E., MAYBERG, H. S. & MCINTYRE, C. C. 2013. Tractography-Activation Models Applied to Subcallosal Cingulate Deep Brain Stimulation. *Brain Stimulation*.
- LUND, J. S. & LEWIS, D. A. 1993. Local circuit neurons of developing and mature macaque prefrontal cortex: Golgi and immunocytochemical characteristics. *J Comp Neurol*, 328, 282-312.
- MA, J. & STAN LEUNG, L.-W. 2000. Relation between hippocampal  $\gamma$  waves and behavioral disturbances induced by phencyclidine and methamphetamine. *Behavioural Brain Research*, 111, 1-11.

- MACIUNAS, R. J., MADDUX, B. N., RILEY, D. E., WHITNEY, C. M., SCHOENBERG, M. R., OGRÖCKI, P. J., ALBERT, J. M. & GOULD, D. J. 2007. Prospective randomized double-blind trial of bilateral thalamic deep brain stimulation in adults with Tourette syndrome. *J Neurosurg*, 107, 1004-14.
- MAGARINOS-ASCONE, C., PAZO, J. H., MACADAR, O. & BUNO, W. 2002. High-frequency stimulation of the subthalamic nucleus silences subthalamic neurons: a possible cellular mechanism in Parkinson's disease. *Neuroscience*, 115, 1109-17.
- MAIR, R. G. & HEMBROOK, J. R. 2008. Memory enhancement with event-related stimulation of the rostral intralaminar thalamic nuclei. *J Neurosci*, 28, 14293-300.
- MAIR, R. G., ONOS, K. D. & HEMBROOK, J. R. 2011. Cognitive activation by central thalamic stimulation: the yerkes-dodson law revisited. *Dose Response*, 9, 313-31.
- MALLET, L., MESNAGE, V., HOUETO, J. L., PELISSOLO, A., YELNIK, J., BEHAR, C., GARGIULO, M., WELTER, M. L., BONNET, A. M., PILLON, B., CORNU, P., DORMONT, D., PIDOUX, B., ALLILAIRE, J. F. & AGID, Y. 2002. Compulsions, Parkinson's disease, and stimulation. *Lancet*, 360, 1302-4.
- MALLET, L., POLOSAN, M., JAAFARI, N., BAUP, N., WELTER, M. L., FONTAINE, D., DU MONTCEL, S. T., YELNIK, J., CHEREAU, I., ARBUS, C., RAOUL, S., AOUIZERATE, B., DAMIER, P., CHABARDES, S., CZERNECKI, V., ARDOUIN, C., KREBS, M. O., BARDINET, E., CHAYNES, P., BURBAUD, P., CORNU, P., DEROST, P., BOUGEROL, T., BATAILLE, B., MATTEI, V., DORMONT, D., DEVAUX, B., VERIN, M., HOUETO, J. L., POLLAK, P., BENABID, A. L., AGID, Y., KRACK, P., MILLET, B. & PELISSOLO, A. 2008. Subthalamic nucleus stimulation in severe obsessive-compulsive disorder. *N Engl J Med*, 359, 2121-34.
- MALONE, D. A., JR., DOUGHERTY, D. D., REZAI, A. R., CARPENTER, L. L., FRIEHS, G. M., ESKANDAR, E. N., RAUCH, S. L., RASMUSSEN, S. A., MACHADO, A. G., KUBU, C. S., TYRKA, A. R., PRICE, L. H., STYPULKOWSKI, P. H., GIFTAKIS, J. E., RISE, M. T., MALLOY, P. F., SALLOWAY, S. P. & GREENBERG, B. D. 2009. Deep brain stimulation of the ventral capsule/ventral striatum for treatment-resistant depression. *Biol Psychiatry*, 65, 267-75.
- MANOACH, D. S., GOLLUB, R. L., BENSON, E. S., SEARL, M. M., GOFF, D. C., HALPERN, E., SAPER, C. B. & RAUCH, S. L. 2000. Schizophrenic subjects show aberrant fMRI activation of dorsolateral prefrontal cortex and basal ganglia during working memory performance. *Biol Psychiatry*, 48, 99-109.
- MANOACH, D. S., PRESS, D. Z., THANGARAJ, V., SEARL, M. M., GOFF, D. C., HALPERN, E., SAPER, C. B. & WARACH, S. 1999. Schizophrenic subjects activate dorsolateral prefrontal cortex during a working memory task, as measured by fMRI. *Biol Psychiatry*, 45, 1128-37.
- MARKRAM, H., LUBKE, J., FROTSCHER, M. & SAKMANN, B. 1997. Regulation of synaptic efficacy by coincidence of postsynaptic APs and EPSPs. *Science*, 275, 213-5.
- MARQUIS, J. P., AUDET, M. C., DORE, F. Y. & GOULET, S. 2007. Delayed alternation performance following subchronic phencyclidine administration in rats depends on task parameters. *Prog Neuropsychopharmacol Biol Psychiatry*, 31, 1108-12.

- MARTINA, M., VIDA, I. & JONAS, P. 2000. Distal initiation and active propagation of action potentials in interneuron dendrites. *Science*, 287, 295-300.
- MAURICE, N., THIERRY, A. M., GLOWINSKI, J. & DENIAU, J. M. 2003. Spontaneous and evoked activity of substantia nigra pars reticulata neurons during high-frequency stimulation of the subthalamic nucleus. *J Neurosci*, 23, 9929-36.
- MAVOORI, J., JACKSON, A., DIORIO, C. & FETZ, E. 2005. An autonomous implantable computer for neural recording and stimulation in unrestrained primates. *J Neurosci Methods*, 148, 71-7.
- MAY, A., BAHRA, A., BUCHEL, C., FRACKOWIAK, R. S. & GOADSBY, P. J. 1998. Hypothalamic activation in cluster headache attacks. *Lancet*, 352, 275-8.
- MAYBERG, H. S., LOZANO, A. M., VOON, V., MCNEELY, H. E., SEMINOWICZ, D., HAMANI, C., SCHWALB, J. M. & KENNEDY, S. H. 2005. Deep brain stimulation for treatment-resistant depression. *Neuron*, 45, 651-60.
- MAYO, J. P. 2009. Intrathalamic mechanisms of visual attention. *J Neurophysiol*, 101, 1123-5.
- MCALONAN, K., CAVANAUGH, J. & WURTZ, R. H. 2008. Guarding the gateway to cortex with attention in visual thalamus. *Nature*, 456, 391-4.
- MCCARTNEY, H., JOHNSON, A. D., WEIL, Z. M. & GIVENS, B. 2004. Theta reset produces optimal conditions for long-term potentiation. *Hippocampus*, 14, 684-7.
- MCFARLAND, N. R. & HABER, S. N. 2002. Thalamic relay nuclei of the basal ganglia form both reciprocal and nonreciprocal cortical connections, linking multiple frontal cortical areas. *J Neurosci*, 22, 8117-32.
- MCFARLAND, W. L., TEITELBAUM, H. & HEDGES, E. K. 1975. Relationship between hippocampal theta activity and running speed in the rat. *J Comp Physiol Psychol*, 88, 324-8.
- MCINTYRE, C. C. & GRILL, W. M. 2000. Selective microstimulation of central nervous system neurons. *Ann Biomed Eng*, 28, 219-33.
- MCINTYRE, C. C. & HAHN, P. J. 2010. Network perspectives on the mechanisms of deep brain stimulation. *Neurobiol Dis*, 38, 329-37.
- MCINTYRE, C. C., MORI, S., SHERMAN, D. L., THAKOR, N. V. & VITEK, J. L. 2004a. Electric field and stimulating influence generated by deep brain stimulation of the subthalamic nucleus. *Clin Neurophysiol*, 115, 589-95.
- MCINTYRE, C. C., SAVASTA, M., KERKERIAN-LE GOFF, L. & VITEK, J. L. 2004b. Uncovering the mechanism(s) of action of deep brain stimulation: activation, inhibition, or both. *Clin Neurophysiol*, 115, 1239-48.
- MEISSNER, W., HARNACK, D., PAUL, G., REUM, T., SOHR, R., MORGENSTERN, R. & KUPSCH, A. 2002. Deep brain stimulation of subthalamic neurons increases striatal dopamine metabolism and induces contralateral circling in freely moving 6-hydroxydopamine-lesioned rats. *Neurosci Lett*, 328, 105-8.

- MEISSNER, W., LEBLOIS, A., HANSEL, D., BIOULAC, B., GROSS, C. E., BENAZZOUZ, A. & BORAUD, T. 2005. Subthalamic high frequency stimulation resets subthalamic firing and reduces abnormal oscillations. *Brain*, 128, 2372-82.
- MELCHITZKY, D. S., GONZALEZ-BURGOS, G., BARRIONUEVO, G. & LEWIS, D. A. 2001. Synaptic targets of the intrinsic axon collaterals of supragranular pyramidal neurons in monkey prefrontal cortex. *J Comp Neurol*, 430, 209-21.
- MERRILL, D. R., BIKSON, M. & JEFFERYS, J. G. 2005. Electrical stimulation of excitable tissue: design of efficacious and safe protocols. *J Neurosci Methods*, 141, 171-98.
- MIKELL, C. B., MCKHANN, G. M., SEGAL, S., MCGOVERN, R. A., WALLENSTEIN, M. B. & MOORE, H. 2009. The hippocampus and nucleus accumbens as potential therapeutic targets for neurosurgical intervention in schizophrenia. *Stereotact Funct Neurosurg*, 87, 256-65.
- MINK, J. W. 2001. Basal ganglia dysfunction in Tourette's syndrome: a new hypothesis. *Pediatr Neurol*, 25, 190-8.
- MITELMAN, S. A., BYNE, W., KEMETHER, E. M., HAZLETT, E. A. & BUCHSBAUM, M. S. 2005. Metabolic disconnection between the mediodorsal nucleus of the thalamus and cortical Brodmann's areas of the left hemisphere in schizophrenia. *Am J Psychiatry*, 162, 1733-5.
- MOGHADDAM, B. 2003. Bringing order to the glutamate chaos in schizophrenia. *Neuron*, 40, 881-4.
- MOGHADDAM, B. & ADAMS, B. W. 1998. Reversal of phencyclidine effects by a group II metabotropic glutamate receptor agonist in rats. *Science*, 281, 1349-52.
- MOHSENI, P., NAJAFI, K., ELIADES, S. J. & XIAOQIN, W. 2005. Wireless multichannel biopotential recording using an integrated FM telemetry circuit. *Neural Systems and Rehabilitation Engineering, IEEE Transactions on*, 13, 263-271.
- MOJARRADI, M., BINKLEY, D., BLALOCK, B., ANDERSEN, R., ULSHOEFER, N., JOHNSON, T. & DEL CASTILLO, L. 2003. A miniaturized neuroprosthesis suitable for implantation into the brain. *IEEE Trans Neural Syst Rehabil Eng*, 11, 38-42.
- MOLLAZADEH, M., MURARI, K., CAUWENBERGHS, G. & THAKOR, N. 2008a. From spikes to EEG: integrated multichannel and selective acquisition of neuropotentials. *Conf Proc IEEE Eng Med Biol Soc*, 2008, 2741-4.
- MOLLAZADEH, M., MURARI, K., SCHWERDT, H., XING, W., THAKOR, N. & CAUWENBERGHS, G. Year. Wireless multichannel acquisition of neuropotentials. *In: Biomedical Circuits and Systems Conference, 2008. BioCAS 2008. IEEE*, 20-22 Nov. 2008 2008b. 49-52.
- MONTGOMERY, E. B., JR., BAKER, K. B., KINKEL, R. P. & BARNETT, G. 1999. Chronic thalamic stimulation for the tremor of multiple sclerosis. *Neurology*, 53, 625-8.
- MONTGOMERY, E. B., JR. & GALE, J. T. 2008. Mechanisms of action of deep brain stimulation(DBS). *Neurosci Biobehav Rev*, 32, 388-407.

- MOOSUNG, C., WENTAI, L., YANG, Z., TUNGCHIEN, C., JUNGSUK, K., SIVAPRAKASAM, M. & YUCE, M. Year. A 128-Channel 6mW Wireless Neural Recording IC with On-the-Fly Spike Sorting and UWB Tansmitter. *In: Solid-State Circuits Conference, 2008. ISSCC 2008. Digest of Technical Papers. IEEE International, 3-7 Feb. 2008 2008.* 146-603.
- MORMANN, F., FELL, J., AXMACHER, N., WEBER, B., LEHNERTZ, K., ELGER, C. E. & FERNANDEZ, G. 2005. Phase/amplitude reset and theta-gamma interaction in the human medial temporal lobe during a continuous word recognition memory task. *Hippocampus*, 15, 890-900.
- MORO, E., ESSELINK, R. J., XIE, J., HOMMEL, M., BENABID, A. L. & POLLAK, P. 2002. The impact on Parkinson's disease of electrical parameter settings in STN stimulation. *Neurology*, 59, 706-13.
- MORRISON, J. H. & FOOTE, S. L. 1986. Noradrenergic and serotonergic innervation of cortical, thalamic, and tectal visual structures in Old and New World monkeys. *J Comp Neurol*, 243, 117-38.
- MOSER, E., MOSER, M. B. & ANDERSEN, P. 1993. Spatial learning impairment parallels the magnitude of dorsal hippocampal lesions, but is hardly present following ventral lesions. *J Neurosci*, 13, 3916-25.
- NEAFSEY, E. J. 1990. Prefrontal cortical control of the autonomic nervous system: anatomical and physiological observations. *Prog Brain Res*, 85, 147-65; discussion 165-6.
- NELSON, M. D., SAYKIN, A. J., FLASHMAN, L. A. & RIORDAN, H. J. 1998. Hippocampal volume reduction in schizophrenia as assessed by magnetic resonance imaging: a meta-analytic study. *Arch Gen Psychiatry*, 55, 433-40.
- NESTOR, P. G., KUBICKI, M., KUROKI, N., GURRERA, R. J., NIMIKIEWICZ, M., SHENTON, M. E. & MCCARLEY, R. W. 2007. Episodic memory and neuroimaging of hippocampus and fornix in chronic schizophrenia. *Psychiatry Research-Neuroimaging*, 155, 21-28.
- NICHOLSON, P. W. 1965. Specific impedance of cerebral white matter. *Exp Neurol*, 13, 386-401.
- NICOLL, R. A. & MALENKA, R. C. 1995. Contrasting properties of two forms of long-term potentiation in the hippocampus. *Nature*, 377, 115-8.
- NIEDER, A. 2000. Miniature stereo radio transmitter for simultaneous recording of multiple single-neuron signals from behaving owls. *J Neurosci Methods*, 101, 157-64.
- NOWAK, L. G. & BULLIER, J. 1998. Axons, but not cell bodies, are activated by electrical stimulation in cortical gray matter. I. Evidence from chronaxie measurements. *Exp Brain Res*, 118, 477-88.
- NUTTIN, B., COSYNS, P., DEMEULEMEESTER, H., GYBELS, J. & MEYERSON, B. 1999. Electrical stimulation in anterior limbs of internal capsules in patients with obsessive-compulsive disorder. *Lancet*, 354, 1526.
- O'KEEFE, J. & CONWAY, D. H. 1978. Hippocampal place units in the freely moving rat: why they fire where they fire. *Exp Brain Res*, 31, 573-90.

- O'KEEFE, J. & RECCE, M. L. 1993. Phase relationship between hippocampal place units and the EEG theta rhythm. *Hippocampus*, 3, 317-30.
- OBEID, I., NICOLELIS, M. A. & WOLF, P. D. 2004. A low power multichannel analog front end for portable neural signal recordings. *J Neurosci Methods*, 133, 27-32.
- OH, Y. S., KIM, H. J., LEE, K. J., KIM, Y. I., LIM, S. C. & SHON, Y. M. 2012. Cognitive improvement after long-term electrical stimulation of bilateral anterior thalamic nucleus in refractory epilepsy patients. *Seizure*, 21, 183-7.
- OKADA, K. & OKAICHI, H. 2006. [The functional cooperation of the hippocampus and anterior thalamus via the fimbria-fornix in spatial memory in rats]. *Shinrigaku Kenkyu*, 77, 261-70.
- OKADA, K. & OKAICHI, H. 2010. Functional cooperation between the hippocampal subregions and the medial septum in unreinforced and reinforced spatial memory tasks. *Behavioural Brain Research*, 209, 295-304.
- OKUN, M. S., GALLO, B. V., MANDYBUR, G., JAGID, J., FOOTE, K. D., REVILLA, F. J., ALTERMAN, R., JANKOVIC, J., SIMPSON, R., JUNN, F., VERHAGEN, L., ARLE, J. E., FORD, B., GOODMAN, R. R., STEWART, R. M., HORN, S., BALTUCH, G. H., KOPELL, B. H., MARSHALL, F., PEICHEL, D., PAHWA, R., LYONS, K. E., TROSTER, A. I., VITEK, J. L. & TAGLIATI, M. 2012. Subthalamic deep brain stimulation with a constant-current device in Parkinson's disease: an open-label randomised controlled trial. *Lancet Neurol*, 11, 140-9.
- OLNEY, J. W., LABRUYERE, J., WANG, G., WOZNIAK, D. F., PRICE, M. T. & SESMA, M. A. 1991. NMDA antagonist neurotoxicity: mechanism and prevention. *Science*, 254, 1515-8.
- OLVERA-CORTES, E., GUEVARA, M. A. & GONZALEZ-BURGOS, I. 2004. Increase of the hippocampal theta activity in the Morris water maze reflects learning rather than motor activity. *Brain Research Bulletin*, 62, 379-384.
- PAHAPILL, P. A., LEVY, R., DOSTROVSKY, J. O., DAVIS, K. D., REZAI, A. R., TASKER, R. R. & LOZANO, A. M. 1999. Tremor arrest with thalamic microinjections of muscimol in patients with essential tremor. *Ann Neurol*, 46, 249-52.
- PAKKENBERG, B. 1990. Pronounced reduction of total neuron number in mediodorsal thalamic nucleus and nucleus accumbens in schizophrenics. *Arch Gen Psychiatry*, 47, 1023-8.
- PAKKENBERG, B. 1992. The volume of the mediodorsal thalamic nucleus in treated and untreated schizophrenics. *Schizophr Res*, 7, 95-100.
- PAKKENBERG, B., SCHEEL-KRUGER, J. & KRISTIANSEN, L. V. 2009. Schizophrenia; from structure to function with special focus on the mediodorsal thalamic prefrontal loop. *Acta Psychiatr Scand*, 120, 345-54.
- PAPEZ, J. W. 1937. A proposed mechanism of emotion. 1937. *Arch. Neurol. Psychiatr.* 38, 725-743.
- PARTHASARATHY, J., HOGENSON, J., ERDMAN, A. G., REDISH, A. D. & ZIAIE, B. 2006. Battery-operated high-bandwidth multi-channel wireless neural recording system using 802.11b. *Conf Proc IEEE Eng Med Biol Soc*, 1, 5989-92.



- PAXINOS, G. & WATSON, C. 2007. *The rat brain in stereotaxic coordinates*, Amsterdam ; Boston ; Academic Press/Elsevier.
- PENG, C.-W., CHEN, J.-J. J., LIN, C.-C. K., POON, P. W.-F., LIANG, C.-K. & LIN, K.-P. 2004. High frequency block of selected axons using an implantable microstimulator. *Journal of Neuroscience Methods*, 134, 81-90.
- PERELMAN, Y. & GINOSAR, R. 2007. An integrated system for multichannel neuronal recording with spike/LFP separation, integrated A/D conversion and threshold detection. *IEEE Trans Biomed Eng*, 54, 130-7.
- PEREZ, S. M., SHAH, A., ASHER, A. & LODGE, D. J. 2012. Hippocampal deep brain stimulation reverses physiological and behavioural deficits in a rodent model of schizophrenia. *Int J Neuropsychopharmacol*, 1-9.
- PERLSTEIN, W. M., CARTER, C. S., NOLL, D. C. & COHEN, J. D. 2001. Relation of prefrontal cortex dysfunction to working memory and symptoms in schizophrenia. *Am J Psychiatry*, 158, 1105-13.
- PICTON, T. W. 1992. The P300 wave of the human event-related potential. *J Clin Neurophysiol*, 9, 456-79.
- PIERRI, J. N., VOLK, C. L., AUH, S., SAMPSON, A. & LEWIS, D. A. 2001. Decreased somal size of deep layer 3 pyramidal neurons in the prefrontal cortex of subjects with schizophrenia. *Arch Gen Psychiatry*, 58, 466-73.
- PIKE, F. G., GODDARD, R. S., SUCKLING, J. M., GANTER, P., KASTHURI, N. & PAULSEN, O. 2000. Distinct frequency preferences of different types of rat hippocampal neurones in response to oscillatory input currents. *J Physiol*, 529 Pt 1, 205-13.
- PINAULT, D. 2004. The thalamic reticular nucleus: structure, function and concept. *Brain Res Brain Res Rev*, 46, 1-31.
- PINAULT, D. 2008. N-methyl d-aspartate receptor antagonists ketamine and MK-801 induce wake-related aberrant gamma oscillations in the rat neocortex. *Biol Psychiatry*, 63, 730-5.
- PINAULT, D. 2011. Dysfunctional thalamus-related networks in schizophrenia. *Schizophr Bull*, 37, 238-43.
- PIROT, S., GLOWINSKI, J. & THIERRY, A. M. 1995. Excitatory responses evoked in prefrontal cortex by mediodorsal thalamic nucleus stimulation: influence of anaesthesia. *European Journal of Pharmacology*, 285, 45-54.
- POLICH, J. 1998. P300 clinical utility and control of variability. *J Clin Neurophysiol*, 15, 14-33.
- PORTER, M. C., BURK, J. A. & MAIR, R. G. 2000. A comparison of the effects of hippocampal or prefrontal cortical lesions on three versions of delayed non-matching-to-sample based on positional or spatial cues. *Behav Brain Res*, 109, 69-81.
- POTKIN, S. G., ALVA, G., FLEMING, K., ANAND, R., KEATOR, D., CARREON, D., DOO, M., JIN, Y., WU, J. C. & FALLON, J. H. 2002. A PET study of the pathophysiology of negative symptoms in schizophrenia. Positron emission tomography. *Am J Psychiatry*, 159, 227-37.

- PRATT, J. A., WINCHESTER, C., EGERTON, A., COCHRAN, S. M. & MORRIS, B. J. 2008. Modelling prefrontal cortex deficits in schizophrenia: implications for treatment. *Br J Pharmacol*, 153 Suppl 1, S465-70.
- RAJKOWSKA, G., SELEMON, L. D. & GOLDMAN-RAKIC, P. S. 1998. Neuronal and glial somal size in the prefrontal cortex: a postmortem morphometric study of schizophrenia and Huntington disease. *Arch Gen Psychiatry*, 55, 215-24.
- RANCK, J. B., JR. 1963. Specific impedance of rabbit cerebral cortex. *Exp Neurol*, 7, 144-52.
- RANCK, J. B., JR. 1975. Which elements are excited in electrical stimulation of mammalian central nervous system: a review. *Brain Res*, 98, 417-40.
- RAO, S. G., WILLIAMS, G. V. & GOLDMAN-RAKIC, P. S. 2000. Destruction and creation of spatial tuning by disinhibition: GABA(A) blockade of prefrontal cortical neurons engaged by working memory. *J Neurosci*, 20, 485-94.
- RATTAY, F. 1998. Analysis of the electrical excitation of CNS neurons. *IEEE Trans Biomed Eng*, 45, 766-72.
- RAUCH, S. L., DOUGHERTY, D. D., MALONE, D., REZAI, A., FRIEHS, G., FISCHMAN, A. J., ALPERT, N. M., HABER, S. N., STYPULKOWSKI, P. H., RISE, M. T., RASMUSSEN, S. A. & GREENBERG, B. D. 2006. A functional neuroimaging investigation of deep brain stimulation in patients with obsessive-compulsive disorder. *J Neurosurg*, 104, 558-65.
- REES, G. 2009. Visual attention: the thalamus at the centre? *Curr Biol*, 19, R213-4.
- REYNOLDS, G. P. & BEASLEY, C. L. 2001. GABAergic neuronal subtypes in the human frontal cortex--development and deficits in schizophrenia. *J Chem Neuroanat*, 22, 95-100.
- RIZZONE, M., LANOTTE, M., BERGAMASCO, B., TAVELLA, A., TORRE, E., FACCANI, G., MELCARNE, A. & LOPIANO, L. 2001. Deep brain stimulation of the subthalamic nucleus in Parkinson's disease: effects of variation in stimulation parameters. *J Neurol Neurosurg Psychiatry*, 71, 215-9.
- ROSE, S. E., CHALK, J. B., JANKE, A. L., STRUDWICK, M. W., WINDUS, L. C., HANNAH, D. E., MCGRATH, J. J., PANTELIS, C., WOOD, S. J. & MOWRY, B. J. 2006. Evidence of altered prefrontal-thalamic circuitry in schizophrenia: an optimized diffusion MRI study. *Neuroimage*, 32, 16-22.
- ROY, S. & WANG, X. 2012. Wireless multi-channel single unit recording in freely moving and vocalizing primates. *J Neurosci Methods*, 203, 28-40.
- RUTTER, L., CARVER, F. W., HOLROYD, T., NADAR, S. R., MITCHELL-FRANCIS, J., APUD, J., WEINBERGER, D. R. & COPPOLA, R. 2009. Magnetoencephalographic gamma power reduction in patients with schizophrenia during resting condition. *Hum Brain Mapp*, 30, 3254-64.
- SAHA, S., CHANT, D. & MCGRATH, J. 2007. A systematic review of mortality in schizophrenia: is the differential mortality gap worsening over time? *Arch Gen Psychiatry*, 64, 1123-31.

- SAMBETH, A., MEETER, M. & BLOKLAND, A. 2009. Hippocampal theta frequency and novelty. *Hippocampus*, 19, 407-8; author reply 409-10.
- SAUSENG, P., KLIMESCH, W., DOPPELMAYR, M., HANSLMAYR, S., SCHABUS, M. & GRUBER, W. R. 2004. Theta coupling in the human electroencephalogram during a working memory task. *Neurosci Lett*, 354, 123-6.
- SAWAGUCHI, T., MATSUMURA, M. & KUBOTA, K. 1989. Delayed response deficits produced by local injection of bicuculline into the dorsolateral prefrontal cortex in Japanese macaque monkeys. *Exp Brain Res*, 75, 457-69.
- SAYKIN, A. J., SHTASEL, D. L., GUR, R. E., KESTER, D. B., MOZLEY, L. H., STAFINIAC, P. & GUR, R. C. 1994. Neuropsychological deficits in neuroleptic naive patients with first-episode schizophrenia. *Arch Gen Psychiatry*, 51, 124-31.
- SCHIFF, N. D., GIACINO, J. T., KALMAR, K., VICTOR, J. D., BAKER, K., GERBER, M., FRITZ, B., EISENBERG, B., BIONDI, T., O'CONNOR, J., KOBYLARZ, E. J., FARRIS, S., MACHADO, A., MCCAGG, C., PLUM, F., FINS, J. J. & REZAI, A. R. 2007. Behavioural improvements with thalamic stimulation after severe traumatic brain injury. *Nature*, 448, 600-3.
- SCHLAEPFER, T. E., COHEN, M. X., FRICK, C., KOSEL, M., BRODESSER, D., AXMACHER, N., JOE, A. Y., KREFT, M., LENARTZ, D. & STURM, V. 2008. Deep brain stimulation to reward circuitry alleviates anhedonia in refractory major depression. *Neuropsychopharmacology*, 33, 368-77.
- SCHMIDT, B., HINMAN, J. R., JACOBSON, T. K., SZKUDLAREK, E., ARGRAVES, M., ESCABÍ, M. A. & MARKUS, E. J. 2013. Dissociation between Dorsal and Ventral Hippocampal Theta Oscillations during Decision-Making. *The Journal of Neuroscience*, 33, 6212-6224.
- SCHMIEDT, C., BRAND, A., HILDEBRANDT, H. & BASAR-EROGLU, C. 2005. Event-related theta oscillations during working memory tasks in patients with schizophrenia and healthy controls. *Brain Res Cogn Brain Res*, 25, 936-47.
- SCHOENEN, J., DI CLEMENTE, L., VANDENHEEDE, M., FUMAL, A., DE PASQUA, V., MOUCHAMPS, M., REMACLE, J. M. & DE NOORDHOUT, A. M. 2005. Hypothalamic stimulation in chronic cluster headache: a pilot study of efficacy and mode of action. *Brain*, 128, 940-7.
- SCHON, K., TINAZ, S., SOMERS, D. C. & STERN, C. E. 2008. Delayed match to object or place: an event-related fMRI study of short-term stimulus maintenance and the role of stimulus pre-exposure. *Neuroimage*, 39, 857-72.
- SCHREGARDUS, D. S., PIENEMAN, A. W., TER MAAT, A., JANSEN, R. F., BROUWER, T. J. & GAHR, M. L. 2006. A lightweight telemetry system for recording neuronal activity in freely behaving small animals. *J Neurosci Methods*, 155, 62-71.
- SCHRODER, J., BUCHSBAUM, M. S., SIEGEL, B. V., GEIDER, F. J., LOHR, J., TANG, C., WU, J. & POTKIN, S. G. 1996. Cerebral metabolic activity correlates of subsyndromes in chronic schizophrenia. *Schizophr Res*, 19, 41-53.
- SCOVILLE, W. B. & MILNER, B. 1957. Loss of recent memory after bilateral hippocampal lesions. *J Neurol Neurosurg Psychiatry*, 20, 11-21.

- SEBBAN, C., TESOLIN-DECROS, B., CIPRIAN-OLLIVIER, J., PERRET, L. & SPEDDING, M. 2002. Effects of phencyclidine (PCP) and MK 801 on the EEGq in the prefrontal cortex of conscious rats; antagonism by clozapine, and antagonists of AMPA-, alpha(1)- and 5-HT(2A)-receptors. *Br J Pharmacol*, 135, 65-78.
- SEIDENBECHER, T., LAXMI, T. R., STORK, O. & PAPE, H. C. 2003. Amygdalar and hippocampal theta rhythm synchronization during fear memory retrieval. *Science*, 301, 846-50.
- SESACK, S. R., DEUTCH, A. Y., ROTH, R. H. & BUNNEY, B. S. 1989. Topographical organization of the efferent projections of the medial prefrontal cortex in the rat: an anterograde tract-tracing study with Phaseolus vulgaris leucoagglutinin. *J Comp Neurol*, 290, 213-42.
- SHARP, F. R., TOMITAKA, M., BERNAUDIN, M. & TOMITAKA, S. 2001. Psychosis: pathological activation of limbic thalamocortical circuits by psychomimetics and schizophrenia? *Trends Neurosci*, 24, 330-4.
- SHEN, K. Z., ZHU, Z. T., MUNHALL, A. & JOHNSON, S. W. 2003. Synaptic plasticity in rat subthalamic nucleus induced by high-frequency stimulation. *Synapse*, 50, 314-9.
- SHENG-FU, L., FU-ZEN, S., CHUNG-PING, Y., DA-WEI, C. & YI-CHENG, L. Year. A closed-loop brain computer interface for real-time seizure detection and control. *In: Engineering in Medicine and Biology Society (EMBC), 2010 Annual International Conference of the IEEE*, Aug. 31 2010-Sept. 4 2010 2010. 4950-4953.
- SHERK, H. & WILKINSON, E. J. 2008. A novel system for recording from single neurons in unrestrained animals. *J Neurosci Methods*, 173, 201-7.
- SHIMIZU, M., FUJIWARA, H., HIRAO, K., NAMIKI, C., FUKUYAMA, H., HAYASHI, T. & MURAI, T. 2008. Structural abnormalities of the adhesio interthalamica and mediodorsal nuclei of the thalamus in schizophrenia. *Schizophr Res*, 101, 331-8.
- SIAPAS, A. G., LUBENOV, E. V. & WILSON, M. A. 2005. Prefrontal phase locking to hippocampal theta oscillations. *Neuron*, 46, 141-51.
- SIGURDSSON, T., STARK, K. L., KARAYIORGOU, M., GOGOS, J. A. & GORDON, J. A. 2010. Impaired hippocampal-prefrontal synchrony in a genetic mouse model of schizophrenia. *Nature*, 464, 763-7.
- SILLAY, K. A., SANI, S. & STARR, P. A. 2010. Deep brain stimulation for medically intractable cluster headache. *Neurobiol Dis*, 38, 361-8.
- SINGER, W. & GRAY, C. M. 1995. Visual feature integration and the temporal correlation hypothesis. *Annu Rev Neurosci*, 18, 555-86.
- SIROTA, A., MONTGOMERY, S., FUJISAWA, S., ISOMURA, Y., ZUGARO, M. & BUZSAKI, G. 2008. Entrainment of neocortical neurons and gamma oscillations by the hippocampal theta rhythm. *Neuron*, 60, 683-97.
- SLAWINSKA, U. & KASICKI, S. 1998. The frequency of rat's hippocampal theta rhythm is related to the speed of locomotion. *Brain Research*, 796, 327-331.

- SLOAN, H. L., GOOD, M. & DUNNETT, S. B. 2006. Double dissociation between hippocampal and prefrontal lesions on an operant delayed matching task and a water maze reference memory task. *Behav Brain Res*, 171, 116-26.
- SMITH, G. S., LAXTON, A. W., TANG-WAI, D. F., MCANDREWS, M. P., DIACONESCU, A. O., WORKMAN, C. I. & LOZANO, A. M. 2012. Increased Cerebral Metabolism After 1 Year of Deep Brain Stimulation in Alzheimer Disease. *Archives of Neurology*, 69, 1141-1148.
- SMITH, I. D. & GRACE, A. A. 1992. Role of the subthalamic nucleus in the regulation of nigral dopamine neuron activity. *Synapse*, 12, 287-303.
- SMITH, T., WESTON, C. & LIEBERMAN, J. 2010. Schizophrenia (maintenance treatment). *Am Fam Physician*, 82, 338-9.
- SOHAL, V. S., ZHANG, F., YIZHAR, O. & DEISSEROTH, K. 2009. Parvalbumin neurons and gamma rhythms enhance cortical circuit performance. *Nature*, 459, 698-702.
- SOMOGYI, P. 1977. A specific 'axo-axonal' interneuron in the visual cortex of the rat. *Brain Res*, 136, 345-50.
- SONG, W., WANG, Y., CHAI, J., LI, Q., YUAN, K. & HAN, T. 2006a. A Wireless Miniature Device for Neural Stimulating and Recording in Small Animals. In: JIAO, L., WANG, L., GAO, X., LIU, J. & WU, F. (eds.) *Advances in Natural Computation*. Springer Berlin Heidelberg.
- SONG, W. G., CHAI, J., HAN, T. Z. & YUAN, K. 2006b. A remote controlled multimode micro-stimulator for freely moving animals. *Sheng Li Xue Bao*, 58, 183-8.
- SPENCER, K. M. 2011. Baseline gamma power during auditory steady-state stimulation in schizophrenia. *Front Hum Neurosci*, 5, 190.
- SPENCER, K. M. 2009. The functional consequences of cortical circuit abnormalities on gamma oscillations in schizophrenia: insights from computational modeling. *Front Hum Neurosci*, 3, 33.
- SPENCER, K. M., NESTOR, P. G., PERLMUTTER, R., NIZNIKIEWICZ, M. A., KLUMP, M. C., FRUMIN, M., SHENTON, M. E. & MCCARLEY, R. W. 2004. Neural synchrony indexes disordered perception and cognition in schizophrenia. *Proc Natl Acad Sci U S A*, 101, 17288-93.
- SQUIRE, L. R. 1992. Memory and the hippocampus: a synthesis from findings with rats, monkeys, and humans. *Psychol Rev*, 99, 195-231.
- STEFANI, A., LOZANO, A. M., PEPPE, A., STANZIONE, P., GALATI, S., TROPEPI, D., PIERANTOZZI, M., BRUSA, L., SCARNATI, E. & MAZZONE, P. 2007. Bilateral deep brain stimulation of the pedunculopontine and subthalamic nuclei in severe Parkinson's disease. *Brain*, 130, 1596-607.
- STERIADE, M., GLOOR, P., LLINAS, R. R., LOPES DE SILVA, F. H. & MESULAM, M. M. 1990. Report of IFCN Committee on Basic Mechanisms. Basic mechanisms of cerebral rhythmic activities. *Electroencephalogr Clin Neurophysiol*, 76, 481-508.

- STOKES, K. A. & BEST, P. J. 1988. Mediodorsal thalamic lesions impair radial maze performance in the rat. *Behav Neurosci*, 102, 294-300.
- STOKES, K. A. & BEST, P. J. 1990. Mediodorsal thalamic lesions impair "reference" and "working" memory in rats. *Physiol Behav*, 47, 471-6.
- STONE, S. S., TEIXEIRA, C. M., DEVITO, L. M., ZASLAVSKY, K., JOSSELYN, S. A., LOZANO, A. M. & FRANKLAND, P. W. 2011. Stimulation of entorhinal cortex promotes adult neurogenesis and facilitates spatial memory. *J Neurosci*, 31, 13469-84.
- STUMPF, C., PETSCHKE, H. & GOGOLAK, G. 1962. The significance of the rabbit's septum as a relay station between the midbrain and the hippocampus. II. The differential influence of drugs upon both the septal cell firing pattern and the hippocampus theta activity. *Electroencephalogr Clin Neurophysiol*, 14, 212-9.
- STURM, V., LENARTZ, D., KOULOUSAKIS, A., TREUER, H., HERHOLZ, K., KLEIN, J. C. & KLOSTERKOTTER, J. 2003. The nucleus accumbens: a target for deep brain stimulation in obsessive-compulsive- and anxiety-disorders. *J Chem Neuroanat*, 26, 293-9.
- STUSS, D. T. & ALEXANDER, M. P. 2000. Executive functions and the frontal lobes: a conceptual view. *Psychol Res*, 63, 289-98.
- STYNER, M., LIEBERMAN, J. A., PANTAZIS, D. & GERIG, G. 2004. Boundary and medial shape analysis of the hippocampus in schizophrenia. *Med Image Anal*, 8, 197-203.
- SUSSMANN, J. E., LYMER, G. K., MCKIRDY, J., MOORHEAD, T. W., MUNOZ MANIEGA, S., JOB, D., HALL, J., BASTIN, M. E., JOHNSTONE, E. C., LAWRIE, S. M. & MCINTOSH, A. M. 2009. White matter abnormalities in bipolar disorder and schizophrenia detected using diffusion tensor magnetic resonance imaging. *Bipolar Disord*, 11, 11-8.
- SUTHANA, N., HANEEF, Z., STERN, J., MUKAMEL, R., BEHNKE, E., KNOWLTON, B. & FRIED, I. 2012. Memory Enhancement and Deep-Brain Stimulation of the Entorhinal Area. *New England Journal of Medicine*, 366, 502-510.
- SUTTON, M. A., ITO, H. T., CRESSY, P., KEMPF, C., WOO, J. C. & SCHUMAN, E. M. 2006. Miniature neurotransmission stabilizes synaptic function via tonic suppression of local dendritic protein synthesis. *Cell*, 125, 785-99.
- SUZUKI, Y., JODO, E., TAKEUCHI, S., NIWA, S. & KAYAMA, Y. 2002. Acute administration of phencyclidine induces tonic activation of medial prefrontal cortex neurons in freely moving rats. *Neuroscience*, 114, 769-79.
- SWADLOW, H. A. 2003. Fast-spike interneurons and feedforward inhibition in awake sensory neocortex. *Cereb Cortex*, 13, 25-32.
- SZIKLAS, V. & PETRIDES, M. 1999. The effects of lesions to the anterior thalamic nuclei on object-place associations in rats. *Eur J Neurosci*, 11, 559-66.
- TAI, C. H., BORAUD, T., BEZARD, E., BIOULAC, B., GROSS, C. & BENAZZOUZ, A. 2003. Electrophysiological and metabolic evidence that high-frequency stimulation of the subthalamic nucleus bridles neuronal activity in the subthalamic nucleus and the substantia nigra reticulata. *FASEB J*, 17, 1820-30.

- TAKASE, K., SHIGETO, H., KAMADA, T., OHYAGI, Y. & KIRA, J. 2009. Efficacy of mediodorsal thalamic nucleus stimulation in a rat model of cortical seizure. *Fukuoka Igaku Zasshi*, 100, 274-80.
- TAKEI, K., YAMASUE, H., ABE, O., YAMADA, H., INOUE, H., SUGA, M., SEKITA, K., SASAKI, H., ROGERS, M., AOKI, S. & KASAI, K. 2008. Disrupted integrity of the fornix is associated with impaired memory organization in schizophrenia. *Schizophrenia research*, 103, 52-61.
- TAKEUCHI, S. & SHIMOYAMA, I. 2004. A radio-telemetry system with a shape memory alloy microelectrode for neural recording of freely moving insects. *IEEE Trans Biomed Eng*, 51, 133-7.
- TAUBE, J. S. 1995. Head direction cells recorded in the anterior thalamic nuclei of freely moving rats. *J Neurosci*, 15, 70-86.
- TAUBE, J. S., GOODRIDGE, J. P., GOLOB, E. J., DUDCHENKO, P. A. & STACKMAN, R. W. 1996. Processing the head direction cell signal: a review and commentary. *Brain Res Bull*, 40, 477-84; discussion 484-6.
- TAUBE, J. S., MULLER, R. U. & RANCK, J. B., JR. 1990. Head-direction cells recorded from the postsubiculum in freely moving rats. I. Description and quantitative analysis. *J Neurosci*, 10, 420-35.
- TEMEL, Y. & VISSER-VANDEWALLE, V. 2004. Surgery in Tourette syndrome. *Mov Disord*, 19, 3-14.
- TERRAZAS, A., KRAUSE, M., LIPA, P., GOTHARD, K. M., BARNES, C. A. & MCNAUGHTON, B. L. 2005. Self-motion and the hippocampal spatial metric. *J Neurosci*, 25, 8085-96.
- TESCHE, C. D. & KARHU, J. 2000. Theta oscillations index human hippocampal activation during a working memory task. *Proc Natl Acad Sci U S A*, 97, 919-24.
- Texas Instruments Incorporated, 2007. *MSP430x20x1, MSP430x20x2, MSP430x20x3 Mixed Signal Microcontroller*. [online] Place: Texas Instruments Incorporated. Available at: <http://www.ti.com/product/msp430f2013> [Accessed 6th March 2010].
- Texas Instruments Incorporated, 2010. *CC2500 Low-Cost Low-Power 2.4GHz RF Transceiver*. [online] Place: Texas Instruments Incorporated. Available at: <http://www.ti.com/product/cc2500> [Accessed 12th March 2010].
- THIEL, C. M., HUSTON, J. P. & SCHWARTING, R. K. 1998. Hippocampal acetylcholine and habituation learning. *Neuroscience*, 85, 1253-62.
- THIELS, E., BARRIONUEVO, G. & BERGER, T. W. 1994. Excitatory stimulation during postsynaptic inhibition induces long-term depression in hippocampus in vivo. *J Neurophysiol*, 72, 3009-16.
- THOMSON, D. J. 1982. Spectrum estimation and harmonic analysis. *Proceedings of the IEEE*, 70, 1055-1096.
- THOMSON, D. M., MCVIE, A., MORRIS, B.J. & PRATT, J.A. 2011. Dissociation of acute and chronic intermittent phencyclidine-induced performance deficits in the 5-choice serial reaction time task: influence of clozapine. *Psychopharmacology (Berl)*, 213, 681-95.

- TIERNEY, P. L., DEGENETAIS, E., THIERRY, A. M., GLOWINSKI, J. & GIOANNI, Y. 2004. Influence of the hippocampus on interneurons of the rat prefrontal cortex. *Eur J Neurosci*, 20, 514-24.
- TODA, H., HAMANI, C., FAWCETT, A. P., HUTCHISON, W. D. & LOZANO, A. M. 2008. The regulation of adult rodent hippocampal neurogenesis by deep brain stimulation. *J Neurosurg*, 108, 132-8.
- TORREY, E. F., BARCI, B. M., WEBSTER, M. J., BARTKO, J. J., MEADOR-WOODRUFF, J. H. & KNABLE, M. B. 2005. Neurochemical markers for schizophrenia, bipolar disorder, and major depression in postmortem brains. *Biol Psychiatry*, 57, 252-60.
- TORT, A. B., KRAMER, M. A., THORN, C., GIBSON, D. J., KUBOTA, Y., GRAYBIEL, A. M. & KOPELL, N. J. 2008. Dynamic cross-frequency couplings of local field potential oscillations in rat striatum and hippocampus during performance of a T-maze task. *Proc Natl Acad Sci U S A*, 105, 20517-22.
- TOTH, K., BORHEGYI, Z. & FREUND, T. F. 1993. Postsynaptic targets of GABAergic hippocampal neurons in the medial septum-diagonal band of Broca complex. *J Neurosci*, 13, 3712-24.
- TRENDELENBURG, G. & DIRNAGL, U. 2005. Neuroprotective role of astrocytes in cerebral ischemia: focus on ischemic preconditioning. *Glia*, 50, 307-20.
- TSANOV, M., CHAH, E., VANN, S. D., REILLY, R. B., ERICHSEN, J. T., AGGLETON, J. P. & O'MARA, S. M. 2011a. Theta-modulated head direction cells in the rat anterior thalamus. *J Neurosci*, 31, 9489-502.
- TSANOV, M., WRIGHT, N., VANN, S. D., ERICHSEN, J. T., AGGLETON, J. P. & O'MARA, S. M. 2011b. Hippocampal inputs mediate theta-related plasticity in anterior thalamus. *Neuroscience*, 187, 52-62.
- TSUCHIDA, Y., HAMA, N. & TAKAHATA, M. 2004. An optical telemetry system for underwater recording of electromyogram and neuronal activity from non-tethered crayfish. *J Neurosci Methods*, 137, 103-9.
- VAN DER STAAY, F. J., RAAIJMAKERS, W. G., LAMMERS, A. J. & TONNAER, J. A. 1989. Selective fimbria lesions impair acquisition of working and reference memory of rats in a complex spatial discrimination task. *Behav Brain Res*, 32, 151-61.
- VAN DER WERF, Y. D., WITTER, M. P. & GROENEWEGEN, H. J. 2002. The intralaminar and midline nuclei of the thalamus. Anatomical and functional evidence for participation in processes of arousal and awareness. *Brain Res Brain Res Rev*, 39, 107-40.
- VAN KUYCK, K., BRAK, K., DAS, J., RIZOPOULOS, D. & NUTTIN, B. 2008. Comparative study of the effects of electrical stimulation in the nucleus accumbens, the mediodorsal thalamic nucleus and the bed nucleus of the stria terminalis in rats with schedule-induced polydipsia. *Brain Res*, 1201, 93-9.
- VAN KUYCK, K., DEMEULEMEESTER, H., FEYS, H., DE WEERDT, W., DEWIL, M., TOUSSEYN, T., DE SUTTER, P., GYBELS, J., BOGAERTS, K., DOM, R. & NUTTIN, B. 2003. Effects of electrical stimulation or lesion in nucleus accumbens on the behaviour of rats in a T-maze after administration of 8-OH-DPAT or vehicle. *Behav Brain Res*, 140, 165-73.



- VAN OS, J. & KAPUR, S. 2009. Schizophrenia. *Lancet*, 374, 635-45.
- VAN VUGT, M. K., SCHULZE-BONHAGE, A., LITT, B., BRANDT, A. & KAHANA, M. J. 2010. Hippocampal gamma oscillations increase with memory load. *J Neurosci*, 30, 2694-9.
- VANDERWOLF, C. H. 1969. Hippocampal electrical activity and voluntary movement in the rat. *Electroencephalogr Clin Neurophysiol*, 26, 407-18.
- VANDERWOLF, C. H. & BAKER, G. B. 1986. Evidence that serotonin mediates non-cholinergic neocortical low voltage fast activity, non-cholinergic hippocampal rhythmical slow activity and contributes to intelligent behavior. *Brain Res*, 374, 342-56.
- VANDEWALLE, V., VAN DER LINDEN, C., GROENEWEGEN, H. J. & CAEMAERT, J. 1999. Stereotactic treatment of Gilles de la Tourette syndrome by high frequency stimulation of thalamus. *Lancet*, 353, 724.
- VANN, S. D., BROWN, M. W. & AGGLETON, J. P. 2000. Fos expression in the rostral thalamic nuclei and associated cortical regions in response to different spatial memory tests. *Neuroscience*, 101, 983-91.
- VELAKOULIS, D., WOOD, S. J., WONG, M. T., MCGORRY, P. D., YUNG, A., PHILLIPS, L., SMITH, D., BREWER, W., PROFFITT, T., DESMOND, P. & PANTELIS, C. 2006. Hippocampal and amygdala volumes according to psychosis stage and diagnosis: a magnetic resonance imaging study of chronic schizophrenia, first-episode psychosis, and ultra-high-risk individuals. *Arch Gen Psychiatry*, 63, 139-49.
- VERMA, A. & MOGHADDAM, B. 1996. NMDA receptor antagonists impair prefrontal cortex function as assessed via spatial delayed alternation performance in rats: modulation by dopamine. *The Journal of Neuroscience*, 16, 373-379.
- VERTES, R. P. 2004. Differential projections of the infralimbic and prelimbic cortex in the rat. *Synapse*, 51, 32-58.
- VERTES, R. P., ALBO, Z. & VIANA DI PRISCO, G. 2001. Theta-rhythmically firing neurons in the anterior thalamus: implications for mnemonic functions of Papez's circuit. *Neuroscience*, 104, 619-25.
- VERTES, R. P. & KOCSIS, B. 1997. Brainstem-diencephalo-septohippocampal systems controlling the theta rhythm of the hippocampus. *Neuroscience*, 81, 893-926.
- VIANA DI PRISCO, G., ALBO, Z., VERTES, R. P. & KOCSIS, B. 2002. Discharge properties of neurons of the median raphe nucleus during hippocampal theta rhythm in the rat. *Exp Brain Res*, 145, 383-94.
- VINOGRADOVA, O. S., BRAZHNIK, E. S., KICHIGINA, V. F. & STAFEKHINA, V. S. 1996. Modulation of the reaction of hippocampal neurons to sensory stimuli by cholinergic substances. *Neurosci Behav Physiol*, 26, 113-24.
- VISSER-VANDEWALLE, V., TEMEL, Y., BOON, P., VREELING, F., COLLE, H., HOOGLAND, G., GROENEWEGEN, H. J. & VAN DER LINDEN, C. 2003. Chronic bilateral thalamic stimulation: a new therapeutic approach in intractable Tourette syndrome. Report of three cases. *J Neurosurg*, 99, 1094-100.

- VOLK, D. W., AUSTIN, M. C., PIERRI, J. N., SAMPSON, A. R. & LEWIS, D. A. 2000. Decreased glutamic acid decarboxylase67 messenger RNA expression in a subset of prefrontal cortical gamma-aminobutyric acid neurons in subjects with schizophrenia. *Arch Gen Psychiatry*, 57, 237-45.
- VYSSOTSKI, A. L., SERKOV, A. N., ITSKOV, P. M., DELL'OMO, G., LATANOV, A. V., WOLFER, D. P. & LIPP, H. P. 2006. Miniature neurologgers for flying pigeons: multichannel EEG and action and field potentials in combination with GPS recording. *J Neurophysiol*, 95, 1263-73.
- WAGER, T. D. & SMITH, E. E. 2003. Neuroimaging studies of working memory: a meta-analysis. *Cogn Affect Behav Neurosci*, 3, 255-74.
- WALKER, M. A., HIGHLEY, J. R., ESIRI, M. M., MCDONALD, B., ROBERTS, H. C., EVANS, S. P. & CROW, T. J. 2002. Estimated neuronal populations and volumes of the hippocampus and its subfields in schizophrenia. *Am J Psychiatry*, 159, 821-8.
- WANG, G. W. & CAI, J. X. 2006. Disconnection of the hippocampal-prefrontal cortical circuits impairs spatial working memory performance in rats. *Behav Brain Res*, 175, 329-36.
- WARBURTON, E. C. & AGGLETON, J. P. 1999. Differential deficits in the Morris water maze following cytotoxic lesions of the anterior thalamus and fornix transection. *Behav Brain Res*, 98, 27-38.
- WARBURTON, E. C., BAIRD, A. L. & AGGLETON, J. P. 1997. Assessing the magnitude of the allocentric spatial deficit associated with complete loss of the anterior thalamic nuclei in rats. *Behav Brain Res*, 87, 223-32.
- WARBURTON, E. C., BAIRD, A. L., MORGAN, A., MUIR, J. L. & AGGLETON, J. P. 2000a. Disconnecting hippocampal projections to the anterior thalamus produces deficits on tests of spatial memory in rats. *Eur J Neurosci*, 12, 1714-26.
- WARBURTON, E. C., BAIRD, A. L., MORGAN, A., MUIR, J. L. & AGGLETON, J. P. 2000b. Disconnecting hippocampal projections to the anterior thalamus produces deficits on tests of spatial memory in rats. *European Journal of Neuroscience*, 12, 1714-1726.
- WARD-ROBINSON, J., WILTON, L. A., MUIR, J. L., HONEY, R. C., VANN, S. D. & AGGLETON, J. P. 2002. Sensory preconditioning in rats with lesions of the anterior thalamic nuclei: evidence for intact nonspatial 'relational' processing. *Behav Brain Res*, 133, 125-33.
- WEINBERGER, D. R., BERMAN, K. F. & ZEC, R. F. 1986. Physiologic dysfunction of dorsolateral prefrontal cortex in schizophrenia. I. Regional cerebral blood flow evidence. *Arch Gen Psychiatry*, 43, 114-24.
- WELTER, M. L., HOUETO, J. L., BONNET, A. M., BEJJANI, P. B., MESNAGE, V., DORMONT, D., NAVARRO, S., CORNU, P., AGID, Y. & PIDOUX, B. 2004. Effects of high-frequency stimulation on subthalamic neuronal activity in parkinsonian patients. *Arch Neurol*, 61, 89-96.
- WELTER, M. L., MALLET, L., HOUETO, J. L., KARACHI, C., CZERNECKI, V., CORNU, P., NAVARRO, S., PIDOUX, B., DORMONT, D., BARDINET, E., YELNIK, J., DAMIER, P. & AGID, Y. 2008. Internal pallidal and thalamic stimulation in patients with Tourette syndrome. *Arch Neurol*, 65, 952-7.

- WHITTINGTON, M. A., TRAUB, R. D. & JEFFERYS, J. G. 1995. Synchronized oscillations in interneuron networks driven by metabotropic glutamate receptor activation. *Nature*, 373, 612-5.
- WILLIAMS, P., WHITE, A., FERRARO, D., CLARK, S., STALEY, K. & DUDEK, F. E. 2006. The use of radiotelemetry to evaluate electrographic seizures in rats with kainate-induced epilepsy. *J Neurosci Methods*, 155, 39-48.
- WILLIAMS, J. M. & GIVENS, B. 2003. Stimulation-induced reset of hippocampal theta in the freely performing rat. *Hippocampus*, 13, 109-16.
- WILSON, F. A., O'SCALAIDHE, S. P. & GOLDMAN-RAKIC, P. S. 1994. Functional synergism between putative gamma-aminobutyrate-containing neurons and pyramidal neurons in prefrontal cortex. *Proc Natl Acad Sci U S A*, 91, 4009-13.
- WINDELS, F., BRUET, N., POUPARD, A., FEUERSTEIN, C., BERTRAND, A. & SAVASTA, M. 2003. Influence of the frequency parameter on extracellular glutamate and gamma-aminobutyric acid in substantia nigra and globus pallidus during electrical stimulation of subthalamic nucleus in rats. *J Neurosci Res*, 72, 259-67.
- WINDELS, F., BRUET, N., POUPARD, A., URBAIN, N., CHOUVET, G., FEUERSTEIN, C. & SAVASTA, M. 2000. Effects of high frequency stimulation of subthalamic nucleus on extracellular glutamate and GABA in substantia nigra and globus pallidus in the normal rat. *Eur J Neurosci*, 12, 4141-6.
- WINTER, K. F., HARTMANN, R. & KLINKE, R. 1998. A stimulator with wireless power and signal transmission for implantation in animal experiments and other applications. *J Neurosci Methods*, 79, 79-85.
- WOO, T. U., KIM, A. M. & VISCIDI, E. 2008. Disease-specific alterations in glutamatergic neurotransmission on inhibitory interneurons in the prefrontal cortex in schizophrenia. *Brain Res*, 1218, 267-77.
- WOO, T. U., MILLER, J. L. & LEWIS, D. A. 1997. Schizophrenia and the parvalbumin-containing class of cortical local circuit neurons. *Am J Psychiatry*, 154, 1013-5.
- WU, Y. R., LEVY, R., ASHBY, P., TASKER, R. R. & DOSTROVSKY, J. O. 2001. Does stimulation of the GPi control dyskinesia by activating inhibitory axons? *Mov Disord*, 16, 208-16.
- XIN, J. & XIAO GUANG, W. Year. Development of ultra small two-channel system of EEG radio telemetry. *In: Neural Interface and Control*, 2005. Proceedings. 2005 First International Conference on, 26-28 May 2005 2005. 60-63.
- XING, Q., HONGWEI, H., BOZHI, M., XIONGWEI, W. & LUMING, L. Year. Study on DBS device for small animals. *In: Engineering in Medicine and Biology Society, EMBC, 2011 Annual International Conference of the IEEE*, Aug. 30 2011-Sept. 3 2011 2011. 6773-6776.
- XU, S., TALWAR, S. K., HAWLEY, E. S., LI, L. & CHAPIN, J. K. 2004. A multi-channel telemetry system for brain microstimulation in freely roaming animals. *J Neurosci Methods*, 133, 57-63.

- YAMAMOTO, J. 1997. Cortical and hippocampal EEG power spectra in animal models of schizophrenia produced with methamphetamine, cocaine, and phencyclidine. *Psychopharmacology (Berl)*, 131, 379-87.
- YE, X., WANG, P., LIU, J., ZHANG, S., JIANG, J., WANG, Q., CHEN, W. & ZHENG, X. 2008. A portable telemetry system for brain stimulation and neuronal activity recording in freely behaving small animals. *J Neurosci Methods*, 174, 186-93.
- YIANNI, J., BAIN, P., GILADI, N., AUCA, M., GREGORY, R., JOINT, C., NANDI, D., STEIN, J., SCOTT, R. & AZIZ, T. 2003. Globus pallidus internus deep brain stimulation for dystonic conditions: a prospective audit. *Mov Disord*, 18, 436-42.
- YOON, T., OKADA, J., JUNG, M. W. & KIM, J. J. 2008. Prefrontal cortex and hippocampus subserve different components of working memory in rats. *Learn Mem*, 15, 97-105.
- YOUNG, K. A., MANAYE, K. F., LIANG, C., HICKS, P. B. & GERMAN, D. C. 2000. Reduced number of mediodorsal and anterior thalamic neurons in schizophrenia. *Biol Psychiatry*, 47, 944-53.
- ZANOS, S., RICHARDSON, A. G., SHUPE, L., MILES, F. P. & FETZ, E. E. 2011. The Neurochip-2: an autonomous head-fixed computer for recording and stimulating in freely behaving monkeys. *IEEE Trans Neural Syst Rehabil Eng*, 19, 427-35.
- ZIKOPOULOS, B. & BARBAS, H. 2006. Prefrontal projections to the thalamic reticular nucleus form a unique circuit for attentional mechanisms. *J Neurosci*, 26, 7348-61.
- ZIKOPOULOS, B. & BARBAS, H. 2007. Circuits formultisensory integration and attentional modulation through the prefrontal cortex and the thalamic reticular nucleus in primates. *Rev Neurosci*, 18, 417-38.
- ZOLA-MORGAN, S. & SQUIRE, L. R. 1985. Medial temporal lesions in monkeys impair memory on a variety of tasks sensitive to human amnesia. *Behav Neurosci*, 99, 22-34.
- ZUCKER, R. S., DELANEY, K. R., MULKEY, R. & TANK, D. W. 1991. Presynaptic calcium in transmitter release and posttetanic potentiation. *Ann N Y Acad Sci*, 635, 191-207.
- ZUO, C., YANG, X., WANG, Y., HAGAINS, C. E., LI, A. L., PENG, Y. B. & CHIAO, J. C. 2012. A digital wireless system for closed-loop inhibition of nociceptive signals. *J Neural Eng*, 9, 056010.

# Suppliers

**Abbott Animal Health** – Abbott Laboratories Ltd, Queensborough, Kent, ME11 5EL, U.K.

**A-M Systems Inc** – 131 Business Park Loop, Sequim, WA 98382, U.S.A.

**Analog Devices** – Analog Devices LTD, No 3 Horizon Business Village, 1 Brooklands Road, Weybridge, Surrey, KT13 0TJ, U.K.

**Antex Electronics** – Antex (Electronics) Limited, 2 Westbridge Industrial Estate, Tavistock, Devon, PL19 8DE, U.K.

CadSoft – support@cadsoft.de.

**Chance Proper Ltd** – Cooper Parry Llp, The Crescent, King Street, Leicester, LE1 6RX, U.K.

**Chronux** – <http://www.chronux.org>.

**David Kopf Instruments** – 7324 Elmo Street, Tujunga, California, 91042.

**Farnell** – Canal Road, Leeds, LS12 2TU.

**Fisher Scientific** – Fisher Scientific UK Ltd, Bishop Meadow Road, Loughborough, LE11 5RG, U.K.

**Harlan UK Limited** – Shaw's Farm, Blackthorn, Bicester, Oxon, OX25 1TP.

**IAR Systems** – [www.iar.com](http://www.iar.com).

**Imaging Research** – Imaging Research Inc, St. Catharines, Canada.

**InterFocus Imaging Ltd** – Interfocus Imaging Ltd. Cambridge Road, Linton, Cambridge, CB21 4NN.

**Kemdent** – Associated Dental Products Ltd, Purton, Swindon, Wiltshire, SN5 4HT.

**Leica Microsystems UK Ltd** – Leica Microsystems (UK) Ltd, Davy Avenue, Knowlhill, Milton Keynes, MK5 8LB.

**Maplin** – 30 St Enoch Square, Glasgow, G1 4DB.

**Mathworks** – Matrix House, Cambridge Business Park, Cambridge, CB4 0HH, U.K.

**Maxim Integrated Products** – Maxim Integrated, 160 Rio Robles, San Jose, CA 95134, U.S.A.

**National Instruments** – 11500 N Mopac Expwy, Austin, TX 78759-3504, USA.

**Nikkon** – Nikon UK Limited, 380 Richmond Road, Kingston upon Thames, Surrey, KT2 5PR, U.K.

**Nodus Information Technology** – Unit 15, Faraday Building, Nottingham Science & Technology Park, University Boulevard, Nottingham, NG7 2QP, U.K.

**PCB-Pool** – Beta Layout Ltd, Bay 98, Shannon Free Zone, Kiltrush, Co Clare, Ireland.

**Pfizer** – Pfizer Ltd, Ramsgate Road, Sandwich, Kent, CT13 9NJ.

**Plastics One** – 6591 Merriman Road, Roanoke, VA 24018, U.S.A.

**Quasar UK** – sales@quasaruk.co.uk.

**Royem Scientific Limited** – PO Box 961, Luton, Bedfordshire, LU2 0WB.

**RS Components** – PO Box 99, Corby, Northants, NN17 9RS.

**Sanyo** – Sales & Marketing Europe GmbH, 18 Colonial Way, Watford, Herts, WD24 4PT.

**Schott** – Schott UK Ltd, Drummond Road, Stafford, ST16 3EL, U.K.

**Sigma-Aldrich** – Sigma-Aldrich Company Ltd, The Old Brickyard, New Road, Gillingham, Dorset, SP8 4XT.

**Smallparts USA (now part of Amazon Supply)** – www.amazonsupply.com.

**Strathclyde University** – The Strathclyde Institute of Pharmacy and Biomedical Sciences, University of Strathclyde, The John Arbuthnott Building, 27 Taylor Street, Glasgow, G4 ONR.

**Tektronix** – Tektronix Inc., 14150 SW Karl Braun Drive, P.O. Box 500,  
Beaverton, OR 97077, U.S.A.

**TestDiet** – TestDiet, P.O. Box 19798, St. Louis, MO 63144, U.S.A.

**Texas Instruments** – 12500 TI Boulevard, Dallas, Texas, 75243, U.S.A.

**Thermo Electron Corporation** – Anatomical Pathology International, 93/96  
Chadwick Rd, Runcorn, Cheshire, WA7 1PR.

**TPS Healthcare** – 27-35 Napier Place, Wardpark North, Cumbernauld, G68 0LL,  
U.K.

**VWR International** – VWR International Ltd, Poole, BH15 1TD.

**Weaver** – Weaver and Company, 565 Nucla Way, Unit B, Aurora, Colorado 80011,  
U.S.A.

# Appendix

The attached CD contains all of the hardware and software design files for each of the systems developed in this study. Refer to the README.txt file located on the CD for instructions of use.